'91 HIGH ENERGY HADRONIC INTERACTIONS

XXVIth Rencontre de Moriond
Les Arcs, Savoie, France - March 17-23, 1991

'91 HIGH ENERGY HADRONIC INTERACTIONS
Series : Moriond Particle Physics Meetings - Hadronic Session

ISBN 2-86332-103-X

EDITIONS FRONTIERES
B. P. 33
91192 Gif-sur-Yvette Cedex - France

Printed in Singapore by Fong & Sons Printers Pte Ltd

Proceedings of the XXVIth RENCONTRE DE MORIOND
Series : Moriond Particle Physics Meetings
Les Arcs, Savoie, France March 17-23, 1991

'91 HIGH ENERGY HADRONIC INTERACTIONS

edited by

J. Trân Thanh Vân

EDITIONS
FRONTIERES

The Hadronic Session of the Twenty-sixth Rencontre de Moriond

was organized by

J. Trân Thanh Vân

with the active collaboration of :

Capella A.
Berger E.
Denegri D.
Fontannaz M.
Le Bellac M.
Montanet L.
Pietrzyk B.
Voltolini C.

FOREWORD

The XXVIth Rencontre de Moriond was held in 1991 in Les Arcs, Savoie (France).

The first such meeting took place at Moriond in the French Alps in 1966. There, experimental as well as theoretical physicists, not only shared their scientific preoccupations but also the household chores. The participants in the first meeting were mainly French physicists interested in electromagnetic interactions. In subsequent years, a session on high energy strong interactions was also added.

The main purpose of these meetings is to discuss recent developments in contemporary physics and also to promote effective collaboration between experimentalists and theorists in the field of elementary particle physics. By bringing together a relatively small number of participants, the meeting helps to develop better human relations as well as a more thorough and detailed discussion of the contributions.

This concern of research and experimentation of new channels of communication and dialogue which from the start animated the Moriond meetings, inspired us to organize a simultaneous meeting of biologists on Cell Differentiation and to create the Moriond Astrophysics meeting. Common meetings between biologists, astrophysicists and high energy physicists are organized to study the implications of the advances in one field into the others. I hope that these conferences and lively discussions may give birth to new analytical methods or new mathematical languages.

At the XXVIth Rencontre de Moriond in 1991, 3 physics sessions, one astrophysics session and one biology session were organized :

* January 26-February 2	"Tests of Fundamental Laws in Physics"
* March 11-17	"Electroweak Interactions and Unified Theories"
	"Early Observable Universe from Diffuse Backgrounds"
* March 17-23	"High Energy Hadronic Interactions"
	"Cell differentiation"

I thank the organizers of the XXVIth Rencontre de Moriond :

A. Aspect, F. Boehm, G. Chardin, O. Fackler, J. Faller, E. Fischbach, G. Fontaine, E. Gerbier, G. Greene, B. Kayser, M. Mugge, R. Pain, S. Petcov, M. Spiro, J. Wilkerson, J.-P. Wuthrick for the session on Tests of Fundamental Laws in Physics,

- A. Billoire, A. Binetruy, A. Blondel, A. Bouquet, J. Ernwein, P. Fayet, J.-M. Frère, G. Goldhaber, J. F. Grivaz and L. Oliver for the Leptonic Session,

- J. Audouze, F. Bouchet, S. Bowyer, B. J. Carr, P. Crane, M. Davis, J. M. Deharveng, G. Efstathiou, A. C. Fabian, R. E. Griffiths, B. Guiderdoni, M. Lachièze-Rey, S. Lilly, M. Longair, F. Melchiorri, C. Norman, J. P. Ostriker, P. J. E. Peebles, J. L. Puget, M. J. Rees, B. Rocca-Volmerange, R. Schaeffer, D. Sciama, G. Setti, J. Silk and G. F. Smoot for the Astrophysics meeting,

- A. Capella, E. Berger, D. Denegri, M. Fontannaz, M. Le Bellac, L. Montanet, B. Pietrzyk and C. Voltolini for the Hadronic Session.

- A. Adoutte, G. Belliard, M. Fellous, J.-C. Kader, P. Rouzé and K. Trân Thanh Vân for the Biology meeting,

and the conference secretaries G. Ambonati, M. Albera, V. Boas, L. Besson, S. Decaux, V. Demailly, C. Douillet, F. Eschenbrenner, C. Jouanen Lucas, F. Macek, N. Mathieu, L. Norry, N. Osswald and I. Paresys who have devoted much of their time and energy to the success of this Rencontre.

I am also grateful to MM. E. Rocca-Serra, D. Touraille, Director of Hotel La Cachette, and to Ms. Rocca-Serra who contributed through their hospitality and cooperation to the well-being of the participants enabling them to work in a relaxed atmosphere.

This Rencontre was sponsored by the Centre National de la Recherche Scientifique (IN2P3 and MPB) and by the Commissariat à l'Energie Atomique (DPhPE and SAP). The Workshop on Tests of Fundamental Laws was also sponsored by the National Science Foundation. I would like to express my thanks to their encouraging support.

I sincerely wish that a fruitful exchange and an efficient collaboration between the physicists, the astrophysicists and the biologists will arise from this Rencontre as from the previous ones.

J. Trân Thanh Vân

Contents

V. QCD STRONG COUPLING CONSTANT

VI. STRUCTURE FUNCTIONS

VII. HADRON-NUCLEUS AND NUCLEUS-NUCLEUS COLLISIONS

VIII. SOFT PHYSICS AND FRAGMENTATION

HEAVY FLAVOUR PHYSICS

DELPHI results on Z^0 decays into heavy flavours

DELPHI Collaboration

presented by :

Achille Stocchi
Laboratoire de l'Accélérateur Linéaire, IN2P3 - CNRS
et Université de Paris-Sud, F-91405 ORSAY Cedex, FRANCE

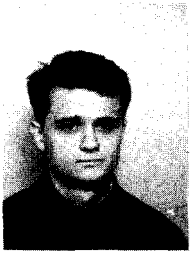

Abstract :

DELPHI results on Z^0 decays into heavy flavours using data collected during 1989 and 1990 (130K hadronic Z^0 in total) are presented. They concern : the partial width of the Z^0 into charm and bottom pairs and the lifetime of B hadrons.

INTRODUCTION

In the Born approximation the partial width of the Z^0 into heavy quark pairs is given by

$$\Gamma(Z^0 \to q\bar{q}) = \beta\frac{3-\beta^2}{2}\Gamma_0^V + \beta^3\Gamma_0^A$$

where

$$\Gamma_0^{V(A)} = \frac{G_\mu m_z^3}{8\sqrt{2}\pi}v^2(a^2)$$

and $\beta = \sqrt{1-\mu^2}$ with $\mu^2 = 4\frac{m_Q^2}{s}$. Even for b quarks $\beta \simeq 1$ and we can write

$$\Gamma(Z^0 \to q\bar{q}) = \Gamma_0(v^2 + a^2) \tag{1}$$

G_F is the Fermi constant, m_z the mass of the Z^0 and v and a are the electroweak vector and axial couplings defined as :

$$v = 2T^{3L} - 4e\sin^2\vartheta_W \quad ; \quad a = 2T^{3L}$$

$2T^{3L} = \pm 1$ where T^{3L} is the third component of the weak isospin, e_q is the electric charge and ϑ_W is the Weinberg angle. Due to the fact that $\sin^2\vartheta_W$ is very close to $\frac{1}{4}$, with respect to the "low" energy region, at the Z^0 resonance, the production rate imbalance between c and b quarks is reversed. This shift occurs because the electric charge of c and b are $\frac{2}{3}$ and $-\frac{1}{3}$ respectively whereas the weak vector charge are (approximatively) $\frac{1}{3}$ and $-\frac{2}{3}$. Quantitatively we have

$$\frac{\Gamma_{b\bar{b}}}{\Gamma_{c\bar{c}}}\,|_{Z^0} \simeq \frac{v_b^2 + a_b^2}{v_c^2 + a_c^2} \simeq 1.28$$

$$\frac{\Gamma_{b\bar{b}}}{\Gamma_{c\bar{c}}}\,|_{low\ energy} \simeq \frac{e_b^2}{e_c^2} = 0.25$$

Putting the right values in formula (1) (taking into account QED,QCD and genuine electroweak corrections) we obtain:

$$\Gamma(Z^0 \to b\bar{b}) \simeq 380MeV \quad R_{b\bar{b}} = \frac{\Gamma(Z^0 \to b\bar{b})}{\Gamma(Z^0 \to had)} \simeq 0.217 \tag{2a}$$

$$\Gamma(Z^0 \to c\bar{c}) \simeq 280MeV \quad R_{c\bar{c}} = \frac{\Gamma(Z^0 \to c\bar{c})}{\Gamma(Z^0 \to had)} \simeq 0.171 \tag{2b}$$

THE DELPHI APPARATUS

DELPHI (Detector with Lepton Photon and Hadron Identification) is a 4π detector operating at LEP (Large Electron and Positron Collider) the e^+e^- collider at CERN. It has been already described in details elsewhere[1] . We would like to present here only the most important features of the apparatus which are relevant for the following analysis. The tracks are measured in a 1.2 Tesla magnetic field by using three cylindrical tracking detectors

- a drift chamber : ID (Inner Detector) 12 $cm < r < 28$ cm and $29^o < \vartheta < 151^o$
- a time projection chamber : TPC 28 $cm < r < 122$ cm and $21^o < \vartheta < 159^o$

- five layers of drift tubes : OD (Outer Detector) r$\simeq$ 2m and $50^o < \vartheta < 130^o$

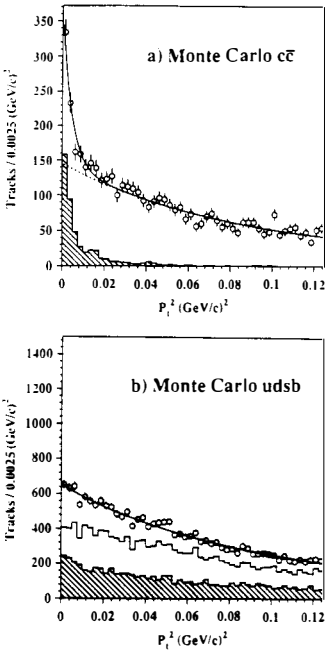

Fig. 1 : Monte Carlo p_t^2 distribution. The curves are the results of the fit using the equation (3). The simulation is performed a) for $c\bar{c}$ events only (the $D^* - D^0\pi$ is presented in hatched histogram) b) for all the other flavours where the light quarks and the $b\bar{b}$ events are presented in the upper and in the hatched histogram respectively

The average momentum resolution is $\Delta p/p \simeq (0.005 - 0.01)p$ [p *in GeV*] Two concentric shells of Si-strips detector VD (Vertex Detector) situated at 9cm ($47^o < \vartheta < 133^o$) and 11cm ($53^o < \vartheta < 127^o$) provide a very high Rϕ resolution : $\simeq 8\mu$m for a single hit and $\simeq 100\mu$m for the double track separation. The muon identification is performed using a set of muon chambers both in the barrel (MUB) and in the forward (MUF) region. The Hadron Calorimeter (HCAL) is a sampling gas detector incorporated in the magnet yoke, its energy resolution is $120\%/\sqrt{E}$. In the following analysis we consider only charged tracks.

THE Z^0 PARTIAL WIDTHS INTO HEAVY FLAVOURS

The partial width $\Gamma(Z^0 \to c\bar{c})$[2]

A relevant part of the c quarks fragments into a D^* which keeps in memory the initial direction of the parent quark[3,4,5,6] . In about 50% of the cases the D^* decays into $D^o\,\pi^{\pm}$. This decay, due to the small $(D^* - D^o)$ mass difference, has a very small Q value $\simeq$ 6 MeV which implies a very small transverse momentum for the π with respect to the D^* direction : $\simeq$ 40 MeV/c. Taking into account the relative p_t of the D^* with respect to the c quark axis and the smearing in the jet axis reconstruction, the average p_t of the π with respect to the jet axis is $\simeq$ 65 Mev/c. This value has to be compared with the p_t for ordinary hadrons in a jet which is $\simeq$ 300 MeV/c. So, without using the normal techniques relying on the reconstruction of their decay products, the charm events should

Table 1: *Systematic contribution to the $c\bar{c}$ width*

Systematic source	error
Ratio of global efficiencies $\varepsilon_h/\varepsilon_{c\bar{c}}$	$\pm$ 0.001
Probability ($c \to D^{*+}$ with $D^{*+} \to D^0\pi^+$)	$\pm$ 0.026
Reconstruction and selection of π^+ mesons	$\pm$ 0.012
Shape of the signal in fitting procedure	$\pm$ 0.010
Choice of the background shape	$\pm$ 0.027
Background from other quark flavours	$\pm$ 0.029
Electron background	$\pm$ 0.002
Total	$\pm$ 0.050

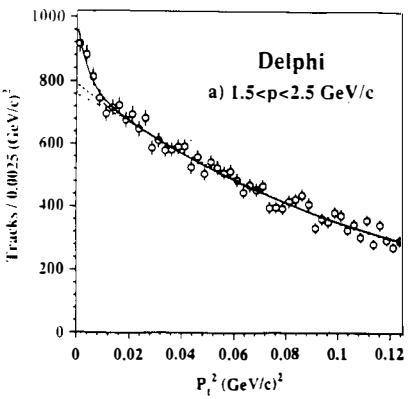

Fig. 2 : Data p_t^2 distribution in the range $1.5 < p < 2.5$ *GeV/c*, $p_t^2 <$ 0.25 *(GeV/c)*^{2}. The curve is the results of the fit in the equation (3)

manifest themselves in an excess of pions having a small p_t with respect to the jet axis[3,7] . The Monte Carlo results for $c\bar{c}$ and non $c\bar{c}$ events are shown in Fig. 1. The analysis is based on 10100 $Z^0(from\ \ 1989) + 26800\ Z^0(up\ \ to\ \ May\ \ 1990) = 36900\ Z^0$ we fit the p_t^2 distribution in the range $p_t^2 < 0.25(GeV/c)^2$ and $1.5GeV/c < p < 2.5GeV/c$ (Fig. 2) with a function

$$S + F_i \tag{3}$$

where :

$$S = \left(\frac{N_S^0}{B^2}\right) \times \exp\frac{-p_t^2}{B^2} \tag{3a}$$

accounts for the signal and F_1,F_2 correspond to two different parametrizations of the background :

$$F_1 = a + b\exp\frac{-p_t^2}{c^2} \quad ; \quad F_2 = \frac{a'}{1 + b'p_t^2 + c'p_t^4} \tag{3b}$$

The parameter B was found to be equal to 65 $\pm$ 3 MeV/c by fitting an analogous distribution on the Monte Carlo data for the studied channel $c \rightarrow D^* \rightarrow D^0\pi$. The results of this fit is a measurement of :

$$P_1(Z^0 \rightarrow c\bar{c}) \times P_2(c \rightarrow D^*) \times P_3(D^* \rightarrow D^0\pi)$$

assuming P_2 and P_3 to be the same as those measured at CLEO[4] and assuming that these probabilities do not vary with the center of mass energy (this assumption is in agreement with measurements at $\sqrt{s}$ = 29 GeV/c)[6] , we obtain

$$\frac{\Gamma_{c\bar{c}}}{\Gamma_{had}} = 0.162 \ \pm \ 0.030(stat) \ \pm \ 0.050(syst) \tag{4}$$

to be compared with the value 0.171 given by the Standard Model (2a). The accuracy of this measurement is dominated by the systematic error (30 %). The different contributions to the total systematic error are listed in Table I. The most important contributions are the choice of the background shape (17 %) and the contributions to the observed accumulation of tracks at low p_t^2 coming from other sources (18 %) (the defined cuts, in fact, reduce the background contribution from the channel $\pi^0 \rightarrow \gamma\gamma$, where one γ converts into a low p_t electron, at a negligeable value, but not the b contribution). Another important contribution is the error on $P_2(c \rightarrow D^*) \times P_3(D^* \rightarrow D^0\pi)$ taken from low energy experiments (18 %) Using $\Gamma_{had} = 1756 \ \pm \ 32MeV$[8] we obtain

$$\Gamma_{c\bar{c}} = 282 \ \pm \ 53(syst) \ \pm \ 88(syst)\ MeV \tag{5}$$

The partial width $\Gamma(Z^0 \rightarrow b\bar{b})$[9]

We measure $\Gamma(Z^0 \rightarrow b\bar{b})$ by using as discriminator an event shape parameter : the Boosted Sphericity Product (BSP)[10] . Due to the large mass of B hadrons and due to the fact that they take a large fraction of the jet energy, the jet's sphericity, computed in a frame boosted along the jet direction, is larger for b jets than for other quark flavours. So, choosen a value

for the boost β (near to the β of the B production) the two jets are separately boosted and the two sphericities S_1 and S_2 are calculated, obtaining

$$BSP = S_1 \times S_2$$

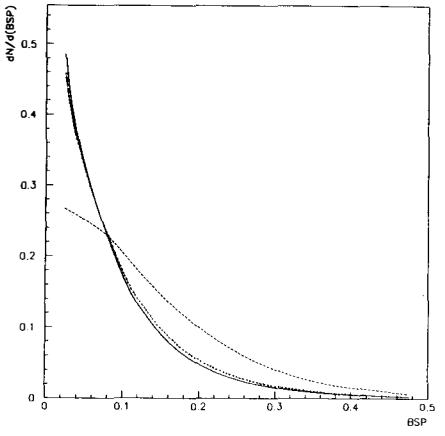

Fig. 3 : $S_1 \times S_2$ distribution for bottom (dashed line) charm (dotted line) and light events (solid line), β=0.96. Simulation with JETSET PS.

The value β =0.96 gives the maximum separation between $b\bar{b}$ and non-$b\bar{b}$ events (Fig. 3). At LEP energies an event selection based only on the BSP cannot provide $b\bar{b}$ samples of high purity with a large efficiency (the maximum enrichement is of the order of 40% with a loss of 85%). To determine the content in $b\bar{b}$ of all hadronic events, we consider that the experimental distribution of the BSP variable is the combination of two distributions : one corresponding to pure $b\bar{b}$ events and the other corresponding to non-$b\bar{b}$ events. These individual distributions have been obtained from a Monte Carlo simulation (Fig. 3).

Table 2: *Systematic contribution to the $b\,\bar{b}$ width*

Systematic source	error
b fragmentation	±0.006
c fragmentaion	±0.002
$Br(Z^0 \to c\bar{c})$	±0.004
Modelling	±0.010

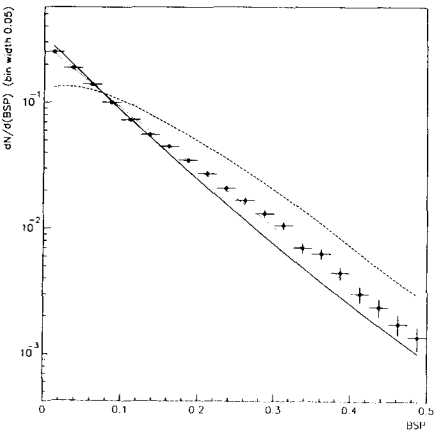

Fig. 4 : $S_1 \times S_2$ differential distribution for DATA, for β=0.96. The lines superimposed correspond to the predictions of JETSET PS for a branching fraction of 1. (dashed line), 0.217 (dotted line), 0. (solid line).

We fit all the 1990 data sample ($\simeq$ 120000 hadronic Z^0 decays) (Fig. 4) with

$$(S_1 \times S_2)_{data} = \alpha(S_1 \times S_2)_{b\bar{b}} + (1-\alpha)(S_1 \times S_2)_{non-b\bar{b}} \qquad (6)$$

obtaining

$$\frac{\Gamma_{b\bar{b}}}{\Gamma_{had}} = 0.222 \pm 0.015(stat) \pm 0.013(syst) \qquad (7)$$

where the Standard Model predicts 0.217 (2b). The contributions to the systematic uncertainties are listed in Table II. The two largest contributions are coming from the modelling of the transverse momentum distribution of the hadrons relative to the jet axis (4.5%) and from the uncertainty on the value of ε_b, the parameter of the b fragmentation function in the Peterson scheeme. We consider a large domain of variation for ε_b corresponding to $\varepsilon_b = (5.0 \pm 3.0 \times 10^{-3})$; it gives a 3% relative error contribution. Using $\Gamma_{had} = 1756 \pm 32 MeV$ [8] we get

$$\Gamma(Z^0 \rightarrow b\bar{b}) = 390 \pm 35 MeV \tag{8}$$

From the two measured widths (5, 8) and using the Delphi measurement of $\Gamma_{\mu\mu} = 87.2 \pm 2.7 \pm 2.2\ MeV/c^2$ [8] we can extract

$$v_c^2 + a_c^2 = 1.08 \pm 0.40 \quad (Standard\ \ Model\ \ 1.19) \tag{9a}$$

$$v_b^2 + a_b^2 = 1.49 \pm 0.16 \quad (Standard\ \ Model\ \ 1.49) \tag{9b}$$

In (Fig. 5) we resume in a pictorial way these results using also the DELPHI Γ_{had} measurement [8]

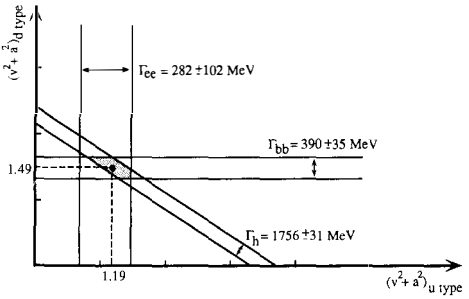

Fig. 5 : Constraints on the $(v^2+a^2)_{d-type}/(v^2+a^2)_{u-type}$ from the $\Gamma_{b\bar{b}}, \Gamma_{c\bar{c}}$ and Γ_{had} measurements

Therefore using the LEP average [13,14,15,16] for

$$Br(c \rightarrow lX) \times \frac{\Gamma(Z^0 \rightarrow c\bar{c})}{\Gamma(Z^0 \rightarrow had)} = 0.0172 \pm 0.002 \tag{10a}$$

$$Br(b \rightarrow lX) \times \frac{\Gamma(Z^0 \rightarrow b\bar{b})}{\Gamma(Z^0 \rightarrow had)} = 0.0246 \pm 0.0006 \tag{10b}$$

we can extract

$$Br(c \rightarrow lX) = 10.6\% \pm 3.9\% \tag{11a}$$

$$Br(b \rightarrow lX) = 11.1\% \pm 1\% \tag{11b}$$

THE B HADRON LIFETIME

The lifetime of the B hadrons is given by the formula

$$\tau_B = \frac{192\pi^3}{G_F^2 m_b^5} Br(b \to lX) \frac{1}{\mid V_{bu} \mid^2 + 0.48 \mid V_{bc} \mid^2} \tag{12}$$

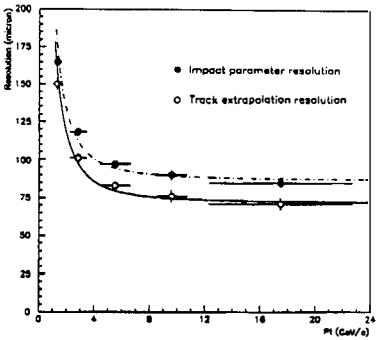

Fig. 6 : Impact parameter and track extrapolation resolution vs momentum in the $R\phi$ plane for the hadronic tracks with 2 hits on the MicroVertex Detector. The primary vertex reconstruction error is $\sigma_{VTX}=\sqrt{\sigma^2_{IMP}-\sigma^2_{ext}}$ (the σ_{ext} to be used has to be computed unfolding the residual contribution from the horizontal beam width and from the error on the beam position).

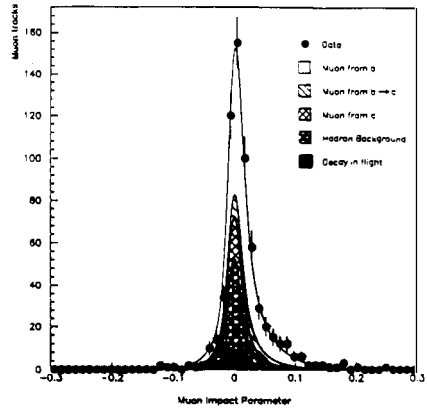

Fig. 7 : Impact parameter of high p_t muons. The curve is a result of the fit[17]. Also the single fits for all the five different components of the muon sample are shown.

Table 3: Systematic error evaluation for the muon sample.

Source	Systematic error [ps]
Muon sample composition	0.080
Physics functions	0.030
Hadronic background parametrization	0.020
Decay background parametrization	0.040
Resolution function	0.050
Average τ_C	0.015
Fragmentation	0.010
Total	0.110

where G_F is the Fermi constant, m_b the mass of the b quark and $Br(b \to lX)$ is the b semileptonic branching ratio. V_{bu} and V_{bc} are the two elements of the Cabibbo-Kobayashi-Maskawa matrix governing the b decay into u and c quark respectively. We would like to stress that the long b lifetime ($\sim$ 1 psec) and thus its actual observability ($< c\tau > \simeq 300\mu\ m$) is due to the fact that the mixing between the second and the third family is smaller than the one between the first and the second. The lifetime in this analysis is measured from the impact parameter distribution of muons produced in semileptonic decays[12]

In fact it can be easily derived that for large values of $\gamma\ \beta$ the relation $< \delta >=< c\ \tau >$ is valid. For this analysis we use all the 1990 data sample requiring that the candidate muon tracks have at least 2 hits measured in the MicroVertex. The impact parameter distribution is given by $\sigma^2_{impact} = \sigma^2_{extrap} + \sigma^2_{vertex}$. In Fig. 6 we show the impact parameter distribution and the extrapolation error distribution vs the track momentum. This attained accuracy is the result of a deep work and careful understanding of the MicroVertex alignment. From Fig. 6, we can quote 85μm for the asymptotic impact parameter resolution, resulting from $\simeq$ 60μm extrapolation accuracy and $\simeq$ 60μm primary vertex reconstruction error. The impact parameter distribution of 610 muon candidates, remaining after the cuts, is fitted (Fig. 7) by means of a Likelihood function[17] . The lifetime comes out to be the statistical

$$\tau_b = 1.31 \pm 0.12 \pm 0.11 psec \quad (13)$$

error is a consequence of the number of muons that survive the cuts, of the purity of the muon sample itself and of the accuracy on the impact parameter. The systematic contributions are listed in Table IV. This analysis permits the measurement of the B hadrons lifetime with a 15% relative error. Using this determination of the B lifetime,taking $m_b = 5.00 \pm 0.2$[18] and $Br(b \to lX) = 11.1\% \pm 1\%$ (11b) and neglecting V_{bu} (in fact $V_{bu} = \simeq 0.1\ V_{bc}$)[11] we obtain.

$$V_{bc} = 0.040 \pm 0.0025 \pm 0.0043 \quad (14)$$

where the first error is coming from the τ_b lifetime measurement while the second is coming from the uncertainties on m_b and on the knowledge of $Br(b \to lX)$.

ACKNOWLEDGEMENTS

I would like to thank P. Roudeau for his patient and precious help both in the preparation of the conference and of this proceeding and for all the stimulating discussions. Thank to J. Brosselard for the help in the redaction of this proceeding

References.

1. P. Aarnio et al. (DELPHI Collaboration), The DELPHI Detector at LEP CERN/EF 90-5, CERN-PPE/90-128 13 September 1990, submitted to Nucl. Instr. and Meth.
2. P.Abreu et al. (DELPHI Collaboration), CERN-PPE/90-123
3. W. Braunschweig et al. (TASSO Collaboration), Z. Phys. C44(1989) 365.
4. D. Bortoletto et al. (CLEO Collaboration), Phys. ReV. D37(1988) 1719; D39(1989) 1471.
5. J.M Yelton et al. (MARKII Collaboration), Phys Rev. Lett. 49(1982) 430.
   W. Bartel et al. (JADE Collaboration), Phys Lett. B146(1984) 121.
   H. Albrecht et al. (ARGUS Collaboration), Phys. Lett. B150(1985) 235.
   H. Yamamoto et al. (DELCO Collaboration), Phys. Rev. Lett. 54(1985) 522.
   H. Aihara et al. (TPC/Two-Gamma Collaboration), Phys. Rev. D34(1986) 1945.
6. P. Baringer et al. (HSR Collaboration), Phys. Lett. B206(1988) 551
7. S. Abachi et al. (HSR Collaboration), Phys. Lett. B205(1988) 411.
8. P. Abreu et al. (DELPHI Collaboration), CERN-PPE/90-119 16 August 1990 contribut ed to the Singapore Conference
9. P. Abreu et al. (DELPHI Collaboration),CERN-PPE/90-118 16 August 1990 contribut ed to the Singapore Conference
10. W. Braunschweig et al. (TASSO Collaboration), DESY 88-159(1988)
11. A. Albrecht et al. (ARGUS Collaboration), Phys. Lett. B254(1990) 409.
    Fulton et al. (CLEO Collaboartion), Phys. ReV. Lett. 64(1990) 16.
12. J.M Brom et al. (HSR Collaboration), Phys. Lett. B195(1987) 301.
    W.W. Ash et al. (MAC Collaboration), Phys. ReV. Lett. 58 (1987) 640.
    D.A. Klem et al. (DELCO Collaboration), Phys. ReV. D37(1988) 41.
    R.A. Ong et al. (MARKII Collaboration), Phys. ReV. Lett. 62(1989) 1236.
    J. Hagenmann et al. (JADE Collaboration), Z. Phys. C48 (1990) 401.
13. DELPHI Collaboration, in preparation
    $Br(b \to lX) \times \frac{\Gamma(Z^0 \to b\bar{b})}{\Gamma(Z^0 \to hadrons)} = 0.0224 \pm 0.0013(stat)$
    $\epsilon_b = (4.5 \pm \frac{3}{2}(stat)) \times 10^{-3}$
14. D. Decamp et al. (ALEPH Collaboration), Phys. Lett. B244 (1990) 551.
15. B. Adeva et al. (L3 Collaboration), Phys. Lett. B241 (1990) 416.
16. M.Z.Akrawy et al. (OPAL Collaboration) CERN-PPE/91-48 14 March 1991 , submitted to Phys. Lett. B.)
17. XXVIth Rencontre de Moriond 1991 "Electroweak Interactions and Unified Theories", 10-17 March, talk given by C. Troncon
18. D.B. Lichtemberg et al.,IUHET 175 (1989)

NEW RESULTS ON CHARM HADROPRODUCTION

The WA82 Collaboration

M. Adamovich[6], Y. Alexandrov[6], F. Antinori[3], D.P. Barberis[2], W. Beusch[2], A. Buys[5], M. Dameri[3], M. Davenport[2], J.P. Dufey[2], A. Forino[1], B.R. French[2], S. Gerasimov[6], R. Gessaroli[1], F. Grard[5], R. Hurst[3], A. Jacholkowski[2], A. Kirk[2], S. Kharlamov[6], J.C. Lassalle[2], P. Legros[5], L. Malinina[6], P. Mazzanti[1], C. Meroni[4], F. Muller[2†], B. Osculati[3], A. Quareni[1], N. Redaelli[4], L. Rossi[3], G. Tomasini[3], F. Viaggi[1] and M. Zavertyaev[6]

Presented by: A. Kirk, CERN

1 Dipartimento di Fisica and INFN, Bologna, Italy.
2 CERN, European Organization for Nuclear Research, Geneva, Switzerland.
3 Dipartimento di Fisica and INFN, Genova, Italy.
4 Dipartimento di Fisica and INFN, Milano, Italy.
5 Université de l'Etat, Mons, Belgium.
6 Lebedev Physical Institute, Moscow, USSR.
† Deceased.

Abstract

Experiment WA82 has measured charm production by 340 GeV pions and 370 GeV protons on a target made of silicon and tungsten. Clean, high statistics charmed meson and baryon mass peaks have been obtained. These signals have been used to measure the charm differential cross section and its dependence on nucleon number. The semileptonic decay of charm to $K\pi e\nu_e$ has been studied. The ratio of branching ratios $B(D^+ \rightarrow \overline{K}^{*0} e^+ \nu_e)/B(D^+ \rightarrow K^- \pi^+ \pi^+) = 0.7 \pm 0.2$ and the $\overline{K}^{*0}$ mesons have a ratio of longitudinal to transverse polarisation of 0.6 ± 0.4.

The aim of experiment WA82 is to study the production and decay properties of charmed particles produced in hadronic interactions. These properties contribute to the understanding of perturbative and non-perturbative QCD and through a study of semileptonic decays give information on the Cabibbo-Kobayashi-Maskawa (CKM) matrix elements.

A major problem in the study of charmed particles is to select the events including charm from the 1000 times more abundant background. This has been achieved, in part, by triggering on events having a high impact parameter track using silicon microstrip detectors. This trigger [1] increases the charm content of the recorded data by a factor of $\sim$ 15. The accuracy with which the tracks are measured using the microstrips enables the separation of the charmed vertices from the main vertex in a good fraction of the events in which charm is produced The data come from experiment WA82 that was performed using the CERN Omega Spectrometer. Details of the layout of the apparatus, the trigger conditions and the data processing have been given in a previous publication [2].

The charm events presented in this paper have been selected from data samples consisting of 1.8×10^7 and 1×10^7 triggers from π^- and p beams respectively. Events are selected with the following characteristics: (1) a primary vertex reconstructed in the target; (2) a secondary vertex separated from the primary vertex by $> 6\sigma$ and located outside the thin target (1-2 mm); (3) total momentum vector of the secondary vertex tracks pointing back to the primary vertex within $60\mu m$.

Fig. 1(a) shows the effective mass spectra for the events compatible with being $D^+ \rightarrow K^-\pi^+\pi^+$, $D^0 \rightarrow K^-\pi^+$, $D^0 \rightarrow K^-\pi^+\pi^+\pi^-$ and charge conjugate states. A clear D signal is seen with 991 events above background. In this figure RICH information is not used. Use of the RICH information decreases the background by a factor of 3. The ratio of the number of D^-/D^+ is found to be 1.4 ± 0.2 and 1.4 ± 0.4 for π^- and p beams respectively. Fig. 1(b) shows the $K^+K^-\pi^\pm$ effective mass spectrum requiring that the K^+K^- mass is consistent with being a ϕ. Clear $D^\pm$ and $D_S^\pm$ signals are observed. Fig. 1(c) shows the $pK\pi$ effective mass spectrum where the p and K have been identified using the RICH a clear Λ_C signal is observed.

Figs. 2 (a) and (b) show the acceptance corrected x_F distributions for the incident

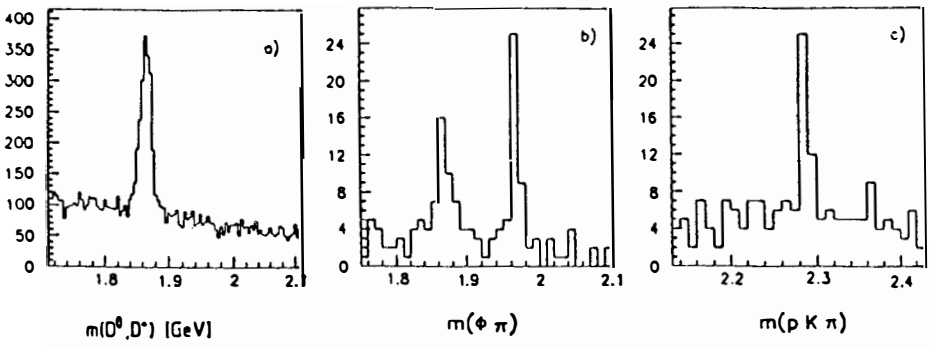

Figure 1: Invariant masses of secondary vertex tracks for the assumptions (a)$K\pi\pi$,$K\pi$ and $K\pi\pi\pi$, (b)$\phi\pi$ and (c) $pk\pi$.

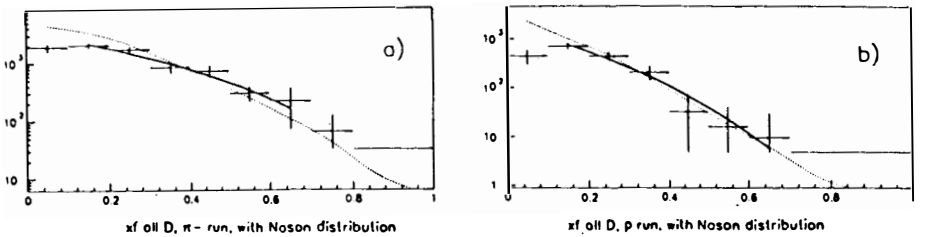

Figure 2: Acceptance corrected x_F distributions for D mesons from (a) π^- and (b) p incident data with fit described in the text (solid) and QCD prediction (dotted).

π^- and p beams respectively. The data has been fitted to the form

$$\frac{d\sigma}{dx_F} \propto (1 - x_F)^n$$

for $0.1 \leq x_F \leq 0.7$. For the π^- incident beam we find $n = 2.9 \pm 0.3$ and for the proton beam we find $n = 5.5 \pm 0.8$. The distributions give information on the structure functions of the incident particles. If charm production is dominated by gluon-gluon fusion the x_F distribution for the π^- data should be harder than that of the p data as observed. Also shown in figs. 2 (a) and (b) are the prediction from next to leading order QCD calculations [3] in both cases there is moderate agreement with the data but the experimental distributions are harder.

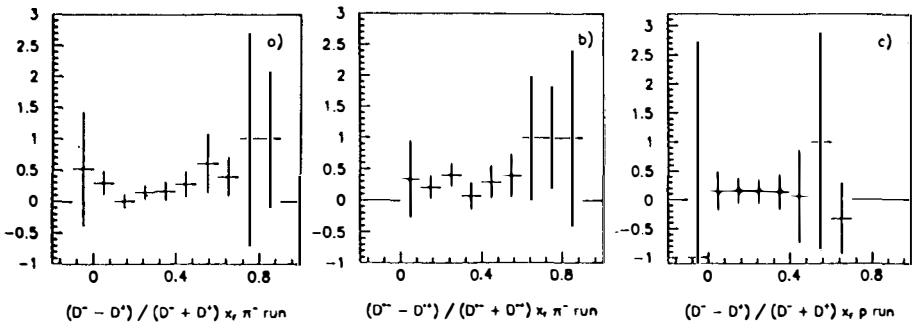

Figure 3: x_F distributions for (a) $(D^- - D^+)/(D^- + D^+)$ (b) $(D^{*-} - D^{*+})/(D^{*-} + D^{*+})$ for the π^- beam and (c) $(D^- - D^+)/(D^- + D^+)$ for the p beam.

Since a π^- beam is composed of $(d\bar{u})$ quarks it could be possible that $D^-(d\bar{c})$ mesons would be produced more forward than $D^+(c\bar{d})$ mesons. In fact a leading particle effect, as this is called, has been claimed by NA27 [4] but has yet to be confirmed. Figs. 3 (a) and (b) show for the π^- beam data the x_F distributions for $(D^- - D^+)/(D^- + D^+)$ and $(D^{*-} - D^{*+})/(D^{*-} + D^{*+})$ respectively. Although there is some slight indication of a rise the effect is not as strong as that indicated by the NA27 data. Fig. 3(c) shows the x_F distribution for $(D^- - D^+)/(D^- + D^+)$ for the p beam, no rise is observed in this data.

The dependence on the atomic number (A) of the target is usually parameterised as

$$\sigma(A) = \sigma_0 A^\alpha$$

where theoretically $\alpha = 2/3$ for a purely geometrical cross section and $\alpha = 1$ for a pure point like process. Therefore by determining α for charm the applicability of QCD in the case of charm can be established. In order to measure α WA82 has used a target split vertically into two equal sections of tungsten and silicon. This allows a simultaneous measurement of σ_W/σ_{Si} both for ordinary interactions and for charm production. A control measurement has been made using the K^0_S signal and for $< x_F >= 0.06$ we find

$$\alpha_{K^0_S} = 0.74 \pm 0.01$$

which is in good agreement with previous measurements [5]. For D mesons for

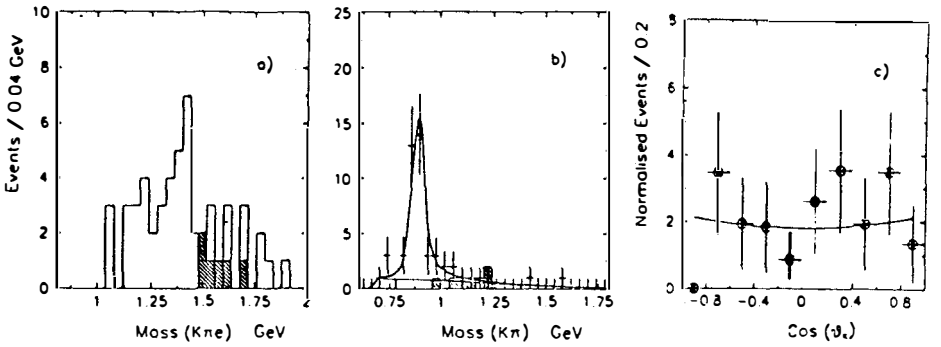

Figure 4: (a) the $K\pi e$ effective mass spectrum, (b) the corresponding $K\pi$ spectrum and (c) the $\cos\theta_K$ distribution with fit described in the text.

$< x_F >= 0.24$ we find

$$\alpha_D = 0.88^{+0.04}_{-0.05}$$

which is in good agreement from the latest value from E772 for J/ψ production of $\alpha_{J/\psi} = 0.92 \pm 0.008$ [6].

A preliminary analysis of the semileptonic decay $D^+ \rightarrow \overline{K}^- \pi^+ e^+ \nu_e$ plus c.c. has been performed. The candidate events are selected with the following characteristics: (1) a primary vertex reconstructed in the target; (2) a 3 prong secondary vertex separated from the primary vertex by $> 6\sigma$ and outside the target with one of the like signed particles identified as an electron by the electromagnetic calorimeter; (3) one of the other two particles was required to be identified as a K by the RICH; (4) require that the maximum missing p_T relative to the D line of flight be less than the maximum p_T of the ν_e. If the K and e have opposite (same) charge then they are considered to be a signal (background) event. Fig. 4 (a) shows the resulting $K\pi e$ effective mass spectrum for the 50 signal events and the 6 background events shown shaded. The $K\pi$ effective mass spectrum for the signal and background events is shown in fig. 4(b) where it can be seen that the decay is dominated by the K^* resonance. A fit to fig. 4 (b) using a relativistic P-wave Breit-Wigner plus an S-wave background yields a resonance fraction of 0.7 ± 0.2 which is consistent with the K^* domination found by E691

[7] and Mark III [8]. We find

$$\frac{B(D^+ \rightarrow \overline{K}^{*0} e^+ \nu_e)}{B(D^+ \rightarrow K^- \pi^+ \pi^+)} = 0.7 \pm 0.2$$

The acceptance corrected normalised cos θ_K distribution, where θ_K is the helicity angle of the kaon in the K^* centre of mass is shown in fig. 4(c). It has been fitted to the form

$$\frac{dN}{d(cos\theta_K)} \propto (1 + (2\frac{\Gamma_L}{\Gamma_T} - 1)\cos^2\theta_K)$$

and gives $\frac{\Gamma_L}{\Gamma_T} = 0.6 \pm 0.4$. This measurement is in agreement with the value obtained by Mark III [8] of $(0.5^{+1.0}_{-0.1}{}^{+0.1}_{-0.2})$ and is consistent with theoretical predictions which range from 0.9 to 1.2 but is smaller than the value of $(1.8^{+0.6}_{-0.4} \pm 0.3)$ found by E691 [7].

In summary good charm signals have been extracted from the WA82 data. The x_F distributions for π^- and p are harder than next to leading order QCD calculations. At present there is no clear positive evidence for a leading particle effect. For $< x_F >= 0.24$, a measurement of the A dependence of the open charm cross section gives $\alpha = 0.88^{+0.04}_{-0.05}$. The semileptonic decay of charm to $K\pi e\nu_e$ has been studied. The ratio of branching ratios $B(D^+ \rightarrow \overline{K}^{*0} e^+ \nu_e)/B(D^+ \rightarrow K^- \pi^+ \pi^+) = 0.7 \pm 0.2$ and the $\overline{K}^{*0}$ mesons have a ratio of longitudinal to transverse polarisation of 0.6 ± 0.4.

References

[1] M. Adamovich et al., IEEE Trans. Nucl. Sci. 37 (1990) 236.

[2] M. Adamovich et al., Submitted to Nucl. Instr. Method.

[3] P. Nason et al., ETH-PT/89/2 (1989).

[4] M. Aguilar-Benitez et al., Phys Lett. 168B (1986) 170;
M. Aguilar-Benitez et al., Zeitschr. fur Phys. C31 (1986) 491.

[5] C. S. Barton et al., Phys. Rev. D27 (1983) 2580.

[6] D. M. Alde et al., Fermilab-Pub-90/156-E.

[7] J. C. Anjos et al., Phys. Rev. Lett 65 (1990) 2630.

[8] Z. Bai et al., Phys. Rev. Lett. 66 (1991) 1011.

PRODUCTION AND DECAY OF CHARM IN E687

L.Perasso
I.N.F.N Milano - Italy

ABSTRACT:
E687 is an experiment to study charm and beauty photoproduction using the highest energy (350 Gev) photon beam now available: the Wide Band photon beam at Fermilab (Illinois). More than 10000 charmed decays have been reconstructed so far: very precise measuraments of the D^+, D^0, D_S^+ and Λ_c^+ lifetime are presented, together with some detected decays and brancing ratios of particular interest. Preliminary results on the total cross section of the D^+ and D^{*+} will also be presented.

*The E687 Collaboration:
Bologna, Colorado, Fermilab, Frascati, Urbana-Champaign, Milano, Northwestern, Notre Dame, Pavia, Puerto Rico

Introduction.

The purpose of the E687 experiment is to study the production and decay of charm and beauty particles using the highest enrgy photon beam available, the Wide Band Photon Beam at Fermilab, and taking full advantage of its characteristics: 350 *Gev* maximum energy (221 *Gev* average energy) with a 13 % momentum spread, 10^7 photon/burst and an hadronic contamination below 1 %.

A two magnet spectrometer [1] with an acceptance of ±100 mrad (hor.) and ±170 mrad (vert.) provides excellent particle identification for hadrons, leptons and photons and a mass resolution below $2Mev/c^2$.

After the 2 Interaction Lengths Be target and before the first magnet there is the vertex detector: 12 planes of Si microstrips which allow the recontruction of the charmed particle production and decay vertices for each event, thus providing the *direct* measurament of the decay path length and a reduction of the combinatorial background.

The results presented here are from the jan-feb 1988 running period: just before that we had a fire which completely destroyed the original Inner e.m. calorimeter, soon replaced by part of the Outer e.m. calorimeter, and damaged the Outer muon detector and the Hadronic calorimeter; still, even with a "degraded" apparatus, we could get very competitive results: this makes us confident to get extremely interesting results when the 1990 (300 million events on tapes) and the 1991 (hopefully 300 millions again) data will be fully analyzed.

The 1988 data sample, 60 million events, was obtained with the trigger:

(number of charged particles > 2) (photon energy > 150 *Gev*) (hadronic energy > 35 *Gev*) (e.m. pairs rejection).

Here are presented the final results on: $D^{\pm}$, D^0, Λ_c^+ and D_S^+ lifetimes, and the preliminary results on some rare decays, some branching fractions, and on the photoproduction cross section values for D^+ and D^{*+} at our energies.

The charge conjugate state is implied when a decay mode of a specific charge is stated.

Data Analysis.

Two independent event selection analyses [2)-3)] are available, each using a different algorithm for the vertexing: a "stand alone" (s.a.) algorithm, using only the track information from the microstrips to recontruct the primary and the (one or more) secondaries; and a "candidate driven" (c.d.) algorithm, selecting a particular decay channel, finding the decay vertex from the particles identified by the spectrometer and using the candidate $\vec{p}$ as seed track to find

the primary vertex. The former has a better signal/noise ratio but has lower efficency for shorter lifetimes; the latter is good when the decay channel is already known but cannot be used for decays with neutrals. An example of the different data samples obtained by the two analyses is shown in Fig.1-2, which show also the high statistics already reached by E687 with the 1988 data.

Charmed Particle Lifetimes.

For the D^+ the decay channel $D^+ \to K(2\pi)$ has been selected by both analyses, see the two mass plots in fig.1-e and 2-b.

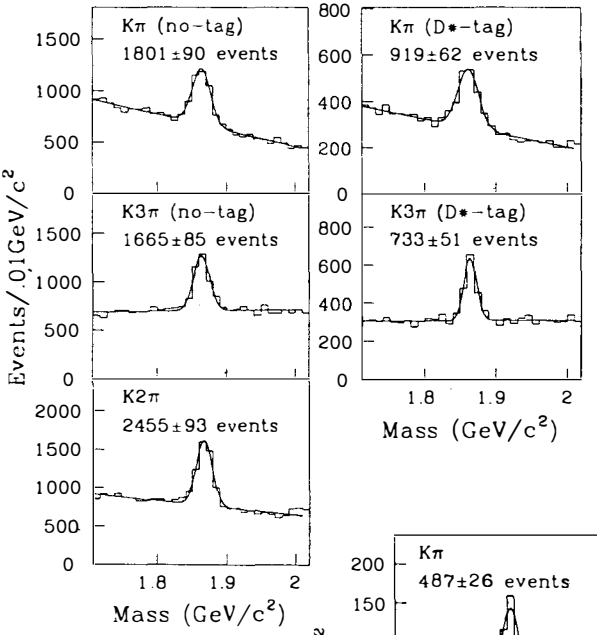

Fig.1: Mass plots of the D samples used in the c. d. analysis; the four top plots (a,b,c,d) are the D^0 samples: the "tagged" D^0 on the right, the "non-tagged" on the left; the bottom plot is the D^+ sample.

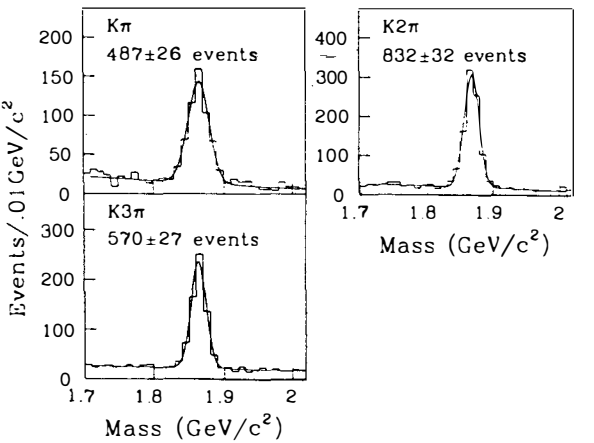

Fig.2: Mass plots of the D samples used in the s. a. analysis; a, c: D^0 sample; b: D^+ sample

For the D^0 lifetime measurament, the two analyses used different data samples: the s.a. used the $D^0 \rightarrow K^-\pi^+$ and the $D^0 \rightarrow K^-\pi^+\pi^+\pi^-$ decays (see Fig.2 a-c); the c.d. used four samples: the $D^0 \rightarrow K^-\pi^+$ and the $D^0 \rightarrow K^-(3\pi)$ decays with the D^0 coming (or not) from the $D^{*+} \rightarrow D^0\pi^+$ decay; if the request: $M(D^*\pi^+)$- $M(D^0)$= (known mass difference $\pm 2 Mev/c^2$) was satisfied, the event was classified as "tagged" (or "not tagged"). The mass plots for these four samples are shown in Fig.1 a-b-c-d. The final lifetime values are [2]: $\tau(D^+) = 1.075 \pm 0.040 \pm 0.018 psec$, $\tau(D^0) = 0.424 \pm .011 \pm 0.007 psec$, for the c.d. analysis, and $\tau(D^+) = 1.095 \pm 0.05 \pm 0.018 psec$, $\tau(D^0) = 0.460 \pm .014 \pm 0.029 psec$, for the s.a. analysis. The present world average is $1.062 \pm 0.28 psec$ for the D^+ and 0.421 ± 0.010 for the D^0.

For the Λ_c^+ and D_S^+ lifetime measuraments, the c.d. analysis has been applied to the decays: $\Lambda_c^+ \rightarrow pK^-\pi^+$ and $D_S^+ \rightarrow \phi\pi^+$. The final Λ_c sample had 90 ± 19 events at a mass of 2283 ± 4 Mev/c^2; fits to individual particle and antiparticle plots yield 50 ± 12 and 51 ± 17 event signals respectively. The final sample of 104 ± 15 D_S events was selected from 100000 candidates with K^+ K^- masses of 1020 ± 10 Mev/c^2.

The results are [3]: $\tau(\Lambda_c^+) = 0.20 \pm 0.03 \pm 0.03 psec$, and $\tau(D_S^+) = 0.50 \pm 0.06 \pm 0.03 psec$, to be compared with the other high statistics experiment (E691) values: $0.22 \pm 0.03 \pm 0.02 psec$ and $0.47 \pm 0.04 \pm 0.02 psec$ respectively.

Branching Ratios.

These still preliminary results are quite interesting because they show the E687 capability to detect Cabibbo suppressed decays: see for example in Fig.3 the mass plot for the decay $D \rightarrow 4\pi$. Combining the s.a. and the c.d. results, we obtain: $Br(D \rightarrow 4\pi)/Br(D \rightarrow K3\pi) = 0.10 \pm 0.02 \pm 0.02$. From the s.a. analysis alone, we obtain: $Br(D \rightarrow KK\pi)/Br(D \rightarrow K2\pi) = 0.114 \pm 0.010 \pm 0.031$.

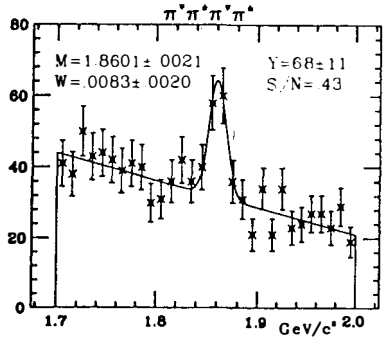

Fig.3: Mass plot of the $D^0 \rightarrow 4\pi$, as obtained from the s. a. algorithm.

The E687 capability to detect also the decays with K_S^0 is being used in the determination of the $Br(D^0 \rightarrow \overline{K_S^0}\phi)/Br(D^0 \rightarrow \overline{K_S^0}\pi^+\pi^-) = 0.16 \pm 0.06$, very important as a test of for the presence of non-spectator decay, and the $Br(D^0 \rightarrow \overline{K_S^0}K^+K-)/Br(D^0 \rightarrow \overline{K_S^0}\pi^+\pi^-) = 0.20 \pm 0.06$.

Associate Production.

The number of D^+ produced compared to the number of D^- and of D^{*+} compared to D^{*-} has been measured to test the hypothesis of the associate production of meson-barion states, which predicts an excess of D^- and D^{*-} respectively. From 2500 $D^{\pm}$ we obtain (see Fig.4): $N(D^+)/N(D^-) = 1.060 \pm 0.063$ considering the $D \rightarrow K2\pi$ decay, and $(N(D^{*-}) - N(D^{*+}))/N(D^{*-}) = -0.074 \pm 0.088 \pm 0.035$, considering the $D^{*+} \rightarrow D^0\pi^+$ decay with $D^0 \rightarrow K\pi, K3\pi$.

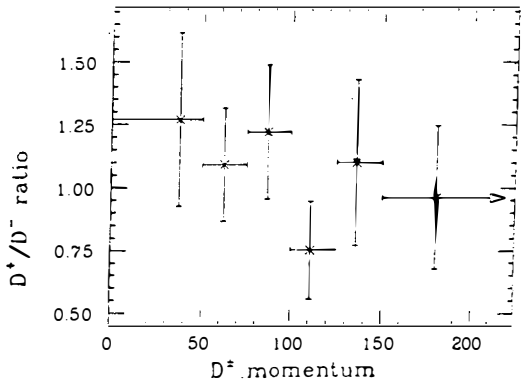

Fig.4: The values of the D^+/D^- for different momentum values.

Cross Sections

Other preliminary results are the values of the photoproduction cross-sections of D^+ and D^{*+} on Be nucleus, very important because measured for the first time at these energies. The $\sigma(D^+)$ values shown in Fig.5-a have been obtained from a sample of 1757 ± 70 D^+ coming from the $D^+ \rightarrow K2\pi$ decay.

For the D^{*+} two independent samples have been obtained from the $D^{*+} \rightarrow D^0\pi^+$ decay, with $D^0 \rightarrow K\pi, K3\pi$: the first one (of 293 ± 32 events) was selected exploiting the narrow $M(D^{*+}) - M(D^0)$ value and looking for a low momentum π; the second one (of 1154 ± 59 events) was selected using both the ΔM cut and the finite lifetime cut in the c.d. analysis. The preliminary $\sigma(D^{*+})$ values on Be are shown in Fig.5-b.

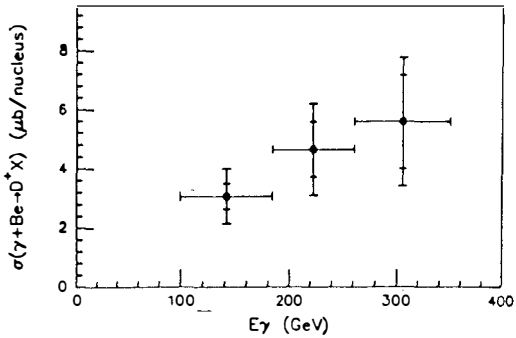

Fig.5-a: The E_γ dependence of the cross-section on Be for $D^+ \to K^-\pi^+\pi^+$ with $x_F > 0$. The inner error is statistical only and the outer error includes the systematic error in quadrature.

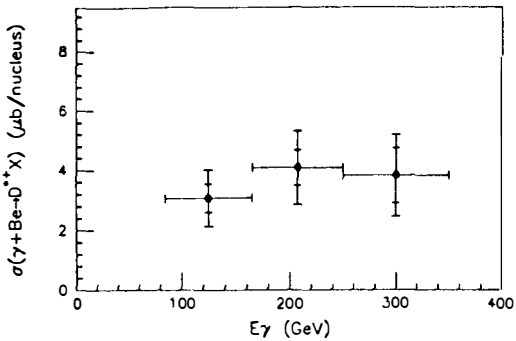

Fig.5-b: The E_γ dependence of the cross-section on Be for $D^{*+} \to D^0\pi^+$; with $D^0 \to K^-\pi^+$ and $D^0 \to K^-\pi^+\pi^+\pi^-$ with $x_F > 0.2$. The inner error is statistical only and the outer error includes the systematic error in quadrature.

REFERENCES.

1) Description and Performance of the E687 Spectrometer, P.L.Frabetti et al., Fermilab PUB-90/258-E.

2) A Measurament of the D° and D^+ Lifetimes, P.L.Frabetti et al., accepted for pubblication in Phis. Lett. B.

3) Measurament of the Λ_c^+ and D_s^+ Lifetimes, P.L.Frabetti et al., Fermilab PUB-90/158-E; Phys.Lett. B 251, 639 (1990).

B QUARK PHYSICS : RECENT RESULTS FROM UA1

Jeffrey B. Gronberg
University of California, Los Angeles
405 Hilgard Ave, Los Angeles, CA, 90024, USA

for the UA1 Collaboration,* CERN
Geneva, Switzerland

ABSTRACT

We present the results of the b-quark analysis of the UA1 '88 and '89 physics runs ($4.7 pb^{-1}$). We measure inclusive b-quark production over a wide range of p_t^b and find good agreement with $O(\alpha_s^3)$ predictions over 5 orders of magnitude. The rate of $B^0 \bar{B}^0$ mixing is measured to be $\chi = 0.145^{+0.040}_{-0.036}$. We use measurements of B_d^0 mixing from ARGUS and CLEO to determine the rate of B_s^0 mixing in our data to be $\chi_s = 0.50 \pm 0.20$. Finally, we present the results of a search for the rare B-hadron decays $B^0 \rightarrow \mu^+\mu^-$, $B \rightarrow \mu^+\mu^- X$, $B_d \rightarrow \mu^+\mu^- K^{0*}$. The new results allow us to put a limit on $M_{top} < 400\, GeV/c^2$ at 90% C.L.

*Aachen - Amsterdam (NIKHEF) - Annecy (LAPP) - Birmingham - Boston - CERN - Helsinki - Kiel - Imperial College, London - Queen Mary College, London - Madrid (CIEMAT) - MIT - Padua - Paris (College de France) - Rome - Rutherford Appleton Lab - Saclay (CEN) - UCLA - Vienna Collaboration

1 Introduction

Presuming a $b\bar{b}$ production cross section of $10\mu b$ at $\sqrt{s} = 630 GeV$, there should be $\sim 5 \cdot 10^7$ $b\bar{b}$ pairs in our sample of $4.7\ pb^{-1}$. The potential for studying $b\bar{b}$ physics with this sample is good. We observe b-quarks by their decays into high p_t muons. A detailed description of the detector has been given in previous papers.[1] Detailed discussion of the work presented here has been published elsewhere. [2, 3, 4]

2 b-Quark Production

We have used four independent data samples to measure b-quark production:

- Muon-Jet - an inclusive single muon + jet sample
- $B \rightarrow J/\psi$ - a sample of high p_t J/ψ's from decays of B-Hadrons
- Low-Mass Dimuons - a dimuon sample with the invariant mass of the two muons ($M_{\mu\mu}$) less than $6\ GeV/c^2$
- High-Mass Dimuons - a dimuon sample with $6 < M_{\mu\mu} < 35\ GeV/c^2$

For each sample we measure a muon-level cross section $\sigma(p\bar{p} \rightarrow b \rightarrow \mu's)$. We then use a Monte Carlo simulation of the $b \rightarrow \mu$ process to extrapolate to the b-level cross section. Since we have information only on p_t^μ and not p_t^b, we choose to quote a p_t^b dependent cross section for each sample

$$\sigma(p\bar{p} \rightarrow bX; p_t^b > p_t^{min}, |\ y_b\ | < 1.5) = \int_{-1.5}^{1.5} dy_b \int_{p_t^{min}}^{\infty} dp_t^b \frac{d^2\sigma(p\bar{p} \rightarrow bX)}{dy_b\, dp_t^b} \qquad (1)$$

where p_t^{min} is chosen such that of all Monte Carlo b-quark events which pass the cuts for the sample, 90% have $p_t^b > p_t^{min}$. The b-level cross section can then be compared with the recently calculated $O(\alpha_s^3)$ QCD prediction.[5]

The major sources of systematic error on the cross section are the luminosity (8%), acceptance (~10%) and p_t^μ resolution (2% at 10 GeV/c to 50% at 40 GeV/c). Furthermore the Muon-Jet sample has a jet energy scale error (12%). The extrapolation from muon level to b-level cross section includes three more systematic errors. The uncertainties due to the b-quark fragmentation function, the semi-leptonic branching ratio and decay kinematics of the B-hadron, and the shape of the b-quark p_t spectrum in our Monte Carlo.[6]

We have used recent ALEPH data for $Z^0 \rightarrow b\bar{b}$ [7] (see Figure 1) to tune the ε_b parameter in the Peterson fragmentation function.[8] We find $\varepsilon_b \sim 0.02 \pm 0.01$ which leads to a 6% error in the cross section. We have averaged the recent results of ARGUS and CLEO [9] to determine the semileptonic branching fraction of B-hadrons $Br(b \rightarrow \mu) = 10.2\% \pm 1.0\%$. We have also checked that the V-A, spectator model used in ISAJET for semileptonic B-meson decays gives good agreement with recent $\Upsilon(4S)$ measurements from ARGUS and CLEO [10]. For the Low-Mass Dimuons there is uncertainty on the mixture of charmed hadrons produced in B-decays. We include a 20% error on the average $c \rightarrow \mu$ branching ratio to take this into account. Finally we assume a 20% uncertainty on the ISAJET shape of $d\sigma/dp_t^b$. Overall, the shape agrees well with the $O(\alpha_s^3)$ prediction of Nason, *et al* .[5]

2.1 *The Muon-Jet Sample*

The Muon-Jet data sample comes from single muon data ($p_t^{\mu} > 10\ GeV/c$) with an accompanying jet ($E_t^{jet} > 10\ GeV$). The jet requirement reduces W/Z decay background.

Events from b-quarks can be separated from background on a statistical basis by using the quantity (p_t^{rel}) *, since the distribution of p_t^{rel} peaks higher with higher hadron mass. Using this technique we fit a $b\bar{b}$ fraction of $0.33 \pm 0.03(stat) \pm 0.03(syst)$ in the Muon-Jet data. The cross section, separated into bins of different p_t^{μ}, is given in Table 1.

2.2 *The $B \rightarrow J/\psi$ Sample*

High p_t J/ψ's are produced at the collider primarily through two processes: either directly via gluon-gluon fusion to χ states which tend to give Isolated J/ψ's, or through the decay of B-Hadrons where the J/ψ's are accompanied by other B decay products and hence are Non-Isolated.

$$\begin{array}{lll} gg \rightarrow \chi g & & gg \dashrightarrow b\bar{b} \dashrightarrow BX \\ \quad \hookrightarrow J/\psi\gamma & & \quad \hookrightarrow J/\psi X \\ \quad\quad \hookrightarrow \mu^+\mu^- & & \quad\quad \hookrightarrow \mu^+\mu^- \end{array}$$

The difference in the Monte Carlo isolation distributions for these two processes is used to separate them on a statistical basis. We find the fraction of $B \rightarrow J/\psi$ events in the sample to be $0.31 \pm 0.02(stat) \pm 0.12(syst)$ where the systematic error is primarily from the uncertainty in the fragmentation process.

We use $Br(b \rightarrow J/\psi) = (1.12 \pm 0.18)\%$, $Br(J/\psi \rightarrow \mu^+\mu^-) = (6.9 \pm 0.9)\%$ and the measured J/ψ production cross section to find the muon level and b-quark level cross sections (see Table 1).

2.3 *The Low-Mass Dimuon Sample*

The Low-Mass Dimuon sample ($p_t^{\mu} > 3\ GeV/c$, $M_{\mu\mu} < 6\ GeV/c^2$) is chosen to be sensitive to b-chain decays.

$$\begin{array}{lll} b & \rightarrow & c\mu\nu \\ & & \hookrightarrow s\mu\nu \end{array}$$

For this sample we determine the fraction of b-quarks by a fit to the dimuon mass distribution ($M_{\mu\mu}$). We separate out low mass mesons, decay background, Drell-Yan, and heavy flavor decays. The result of the fit is a b-fraction of 0.14 ± 0.04.

From this fraction we estimate the cross-section for muons from b-chain decays, $\sigma(p\bar{p} \dashrightarrow b \rightarrow \mu\mu X;\ p_t^{\mu} > 3GeV/c, |\eta_{\mu}| < 1.5, M_{\mu\mu} < 6\ GeV/c^2)$ and extrapolate to b-quark and hadron-level results (see Table 1).

2.4 *The High-Mass Dimuon Sample*

The cut $M_{\mu\mu} > 6\ GeV/c^2$ insures that the muons in this sample come from separate b-quarks and excludes low mass mesons. We also cut on $M_{\mu\mu} < 35\ GeV/c^2$ in order to eliminate

*p_t^{rel} is defined as the momentum of the muon transverse to the jet axis.

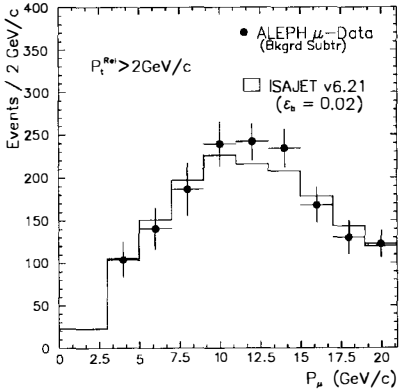

Figure 1: Comparison of ALEPH data for $Z \rightarrow b\bar{b} \rightarrow \mu$ (background subtracted) with the prediction of ISAJET for the same process using $\epsilon_b = 0.02$

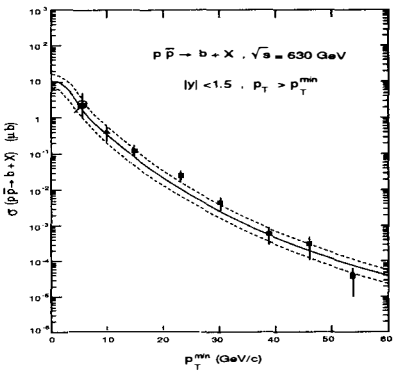

Figure 2: The b-quark cross-section for $| y_b | < 1.5$ versus p_t^{min}. The solid curve is the $O(\alpha_s^3)$ prediction of Nason *et al* . The dashed curve is the error band on this prediction from varying m_b, μ, and Λ

$Z \rightarrow \mu^+\mu^-$ decays. As in the Muon-Jet sample we use p_t^{rel} to separate $b\bar{b}$ events from backgrounds. We find fractions of $b\bar{b}$ events in the like and unlike-sign data of $0.63 \pm 0.08(stat) \pm 0.01(syst)$ and $0.55 \pm 0.04(stat) \pm 0.01(syst)$ respectively.

Combining the like and unlike-sign results we find a cross-section for dimuons from different b-quarks, $\sigma(p\bar{p} \rightarrow b\bar{b} \rightarrow \mu\mu X;\ p_t^\mu > 3GeV/c, |\ \eta_\mu\ | < 1.5, 6 < M_{\mu\mu} < 35\, GeV/c^2)$ which is extrapolated to a b-quark and hadron-level result (see Table 1).

2.5 Total Cross-Sections

In Figure 2 we plot the inclusive b-level cross-section as a function of p_t^{min} for the quark measurements of each sample. Also shown on this plot is the prediction of Nason, *et al* for $d\sigma/dp_t^{min}$. The error bands on the prediction are due to uncertainties on the renormalization scale μ, the b-quark mass, and the mass scale Λ.

Using the Nason curve normalized to our data to extrapolate back to $p_t^{min} = 0$, we find the total inclusive b-quark production cross-section $\sigma(p\bar{p} \rightarrow bX\ ;\ |\ y_b\ | < 1.5) = 12.8^{+7}_{-5.4}\ \mu b$. This agrees with the absolute prediction of the theory $(10.2^{+5.8}_{-3.8}\ \mu b)$.

3 $B^0\bar{B}^0$ Mixing

Oscillation of neutral particles into their anti-particles is allowed in the Standard Model by 2nd order diagrams. We define a quantity χ that is the probability that a B^0 meson will oscillate into it's anti-particle before decaying.

$$\chi = \frac{BR(B^0 \rightarrow \bar{B}^0 \rightarrow \mu^- \nu_\mu X)}{BR(B^0 \rightarrow \mu^\pm \nu_\mu X)}$$

Since different CKM matrix elements appear in the theoretical calculations for B_d^0 and B_s^0, χ_d and χ_s will not be identical. At the $Sp\bar{p}S$ collider energies a mixture of both types of B^0

Table 1: Results of muon-level and b-level cross-section calculations

Sample	Muon		b-Quark	
	p_t^μ Range $[GeV/c]$	$\sigma(\mu - level)$ $[nb]$	p_t^{min} $[GeV/c]$	$\sigma(b - level)$ $[nb]$
$B \rightarrow J/\psi$	$p_t^{J/\psi} > 5, \mid y \mid < 2$	1.92 ± 0.80	6.0	2360 ± 1215
High-Mass Dimuons	> 3	2.12 ± 0.39	6.0	2660 ± 1330
Low-Mass Dimuons	> 3	0.31 ± 0.08	10	390 ± 170
Muon-Jet	10-15	1283 ± 269	15	120 ± 38
	15-20	180 ± 140	23	24 ± 8
	20-25	24.3 ± 6.5	30	4.1 ± 1.4
	25-30	3.2 ± 1.4	39	0.55 ± 0.3
	30-35	1.1 ± 0.6	46	0.32 ± 0.2
	35-40	0.14 ± 0.09	54	0.04 ± 0.03

mesons are produced, thus our measured χ will be a linear combination of χ_d and χ_s.

3.1 Data sample

We measure mixing in the high mass dimuon sample. We use a cut on $M_{\mu\mu} > 6GeV/c^2$ to remove dimuons from low-mass mesons and from b-chain decays. The muons are also required to be non-isolated in order to remove Drell-Yan and Υ events. Since the flavor quantum number of the decaying meson determines the sign of the muon, in $b\bar{b}$ events with no mixing we expect the two muons to be unlike-sign. In the presence of mixing there is a probability that one of the mesons will oscillate before decaying. In this case a like-sign event would be observed. From this we can see that it is possible to measure mixing by comparing the number

Table 2: Probability of $b\bar{b}$ events producing unlike-sign and like-sign dimuons

$p\bar{p} \rightarrow b\bar{b} \rightarrow$	$B^0\bar{B}^0 \rightarrow \mu^- \nu_\mu X$ $\hookrightarrow \mu^+ \nu_\mu X$	$\chi^2 + (1-\chi)^2$	unlike-sign
$p\bar{p} \rightarrow b\bar{b} \rightarrow$	$B^0\bar{B}^0 \rightarrow \mu^- \nu_\mu X$ $\hookrightarrow \bar{B}^0 \rightarrow \mu^- \nu_\mu X$	$2\chi(1-\chi)$	like-sign

of unlike-sign and like-sign dimuon events in the data to the monte carlo prediction.

3.2 Separation of $b\bar{b}$ events from background

The dimuon events are produced by the sources listed below; only the first two yield information on $B^0\bar{B}^0$ mixing.

1st generation $b\bar{b}$	–	These are events in which both B-mesons decay directly into muons.
2nd generation $b\bar{b}$	–	These are events in which one B-meson decays directly into a muon while the other decays to a muon via a C-Meson.
$c\bar{c}$	–	Events in which both C-mesons decay directly into muons.
Decay Background	–	Dimuon events where one or both muons come from decays in flight of π or K mesons.
Drell-Yan	–	$p\bar{p} \rightarrow \gamma, Z \rightarrow \mu^+\mu^-$
Υ	–	$p\bar{p} \rightarrow \Upsilon \rightarrow \mu^+\mu^-$

We separate the $b\bar{b}$ events from background events on a statistical basis by fitting Monte Carlo p_t^{rel} distributions for each process to the data. Each distribution is made by fitting a parameterized curve to the Monte Carlo events. The p_t^{rel} distributions of the $b\bar{b}$ events peak at a higher value than the distributions for Decay background and $c\bar{c}$. The muons in each dimuon event are separated into muons of higher and lower p_t, and p_t^{rel} distributions are made for each ($p_t^{rel}hi$ and $p_t^{rel}lo$ respectively). The data, separated into unlike-sign and like-sign samples, is shown in Figure 3.

3.3 Mixing measurements and B_s^0 limits

The minimum of the fit occurs at $\chi = 0.145^{+0.040}_{-0.036}$, where the uncertainty derived from the fit includes both statistical and systematic uncertainties. The $\chi = 0.0$ region is excluded at about the 4σ level. The systematic uncertainties are included in the fit as variables and allowed to vary within a Gaussian constraint. By fixing these variables to their best fit value and observing the decrease in the total error on χ the error can be separated into statistical and systematic parts. In order to separate them we assume a symmetrical error of ± 0.038 on χ.

New result: $\chi = 0.145 \pm 0.035(stat) \pm 0.014(syst)$
Previous result: $\chi = 0.158 \pm 0.052(stat) \pm 0.026(syst)$

Combining these results assuming fully correlated systematic errors we get
Combined result: $\chi = 0.148 \pm 0.029(stat) \pm 0.017(syst)$

The measured value of χ is a combination of χ_d and χ_s, namely $\chi = f_{dd}\chi_d + f_{ss}\chi_s$ where f_{qq} is the probability of a b-quark forming a $b\bar{q}$ meson during hadronization. We use $f_{dd} = 0.36$ and $f_{ss} = 0.18$. [11] By combining the UA1 measurement of χ with a measurement of χ_d from ARGUS and CLEO [12] ($\chi_d = 0.162 \pm 0.039$) we can determine χ_s as shown in Figure 4. When these two measurements are combined we determine $\chi_s = 0.50 \pm 0.20$. The $\pm 1\sigma$ region extends into a non-physical region. In order to set a one dimensional limit on χ_s we cut away the non-physical region and renormalize the remaining probability density to one. We find $\chi_s > 0.17(0.12)$ at 90% (95%)C.L. and we show the two dimensional 90% and 95% C.L. ellipses in Figure 5 We can also include in the fit the measurements of χ from Aleph [13] ($\chi = 0.132 \pm 0.027$) and L3 [14] ($\chi = 0.178 \pm 0.045$). Repeating the analysis including the LEP measurements we find $\chi_s = 0.53 \pm 0.15$ and $\chi_s > 0.27(0.23)$ at 90% (95%)C.L.

4 Rare B-Decays

We present branching ratio limits for three different rare B-hadron decay modes: $B^0 \rightarrow \mu^+\mu^-$, $B \rightarrow \mu^+\mu^- X$, $B_d \rightarrow \mu^+\mu^- K^{0*}$. These decays measure the relative strength of Flavor Changing Neutral Currents (FCNC) which are forbidden by the Standard Model at the tree-level, but expected due to loop diagrams. The presence of these quark loops make the branching ratios sensitive to the top-quark mass. In Table 3 we compare several theoretical predictions with our measurements and results from other experiments.

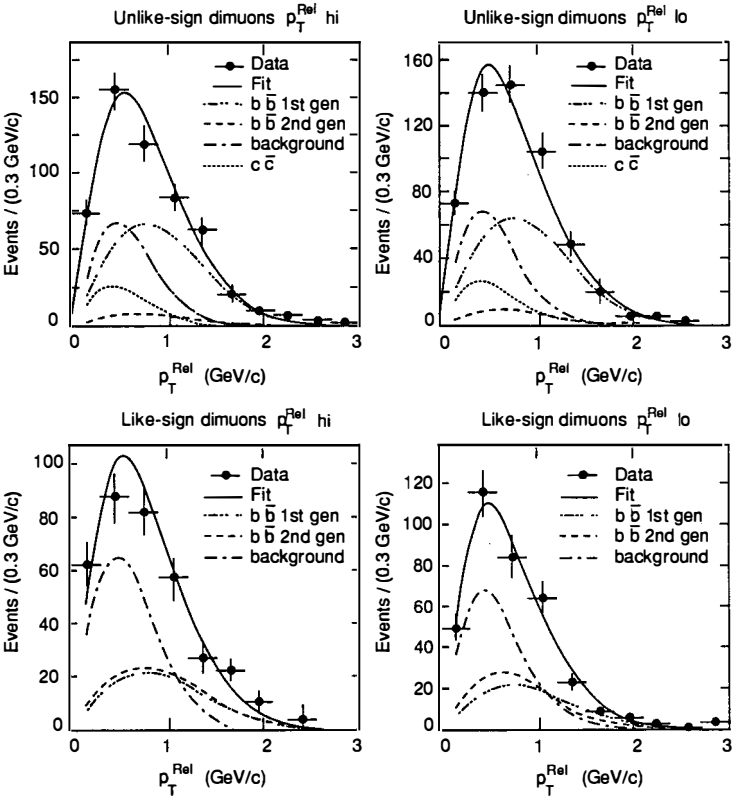

Figure 3: p_t^{rel} for unlike-sign and like-sign events with the fitted curves

4.1 Branching Ratio Limits

The data sample for the $B^0 \to \mu^+\mu^-$ and $B \to \mu^+\mu^- X$ searches is unlike-sign dimuons of $p_t^{\mu\mu} \geq 7\, GeV/c^2$. The search region in dimuon mass for the $B^0 \to \mu^+\mu^-$ decay, $5.1 < M_{\mu\mu} < 5.5\, GeV/c^2$, is centered on the B_d mass with a width given by the detector dimuon mass resolution, $\sim 200\, MeV/c^2$. For $B \to \mu^+\mu^- X$ decays we choose a mass region for $B \to \mu^+\mu^- X$ candidates of $3.9 < M_{\mu\mu} < 4.4\, GeV/c^2$, to avoid interference from J/ψ and ψ' decays.[17]

In these analyses we use $M(B_d) = 5.28\, GeV/c^2$,[18] and assume $M(B_s) = 5.38\, GeV/c^2$. The B-hadronization ratio is assumed to be $B^{\pm} : B_d : B_s : B - baryon = 36 : 36 : 18 : 10$.

A plot of the data in and around the regions of interest is shown in Figure 6. We determine the background for our searches by a fit to the data outside of the search regions. This fit contains Gaussians centered at the J/ψ and ψ' masses and a term linear in $M_{\mu\mu}$. As can be seen from Figure 6 there are no significant excesses of events in either search region. This allows us to place upper limits on these branching ratios which are given in Table 3.

In the search for $B_d \to \mu^+\mu^- K^{0*}$ we relax the $p_t^{\mu\mu}$ cut since we ultimately demand a

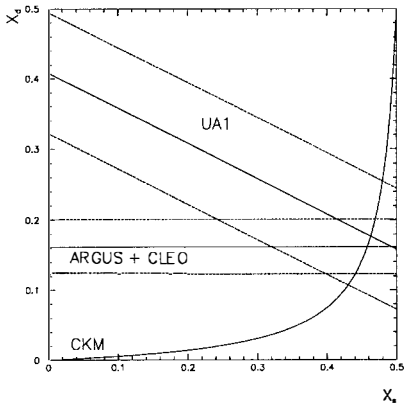

Figure 4: Relationship of χ_d versus χ_s for the UA1 combined result. The central value and $\pm 1\sigma$ lines are drawn. The combined ARGUS and CLEO results for χ_d are also drawn.

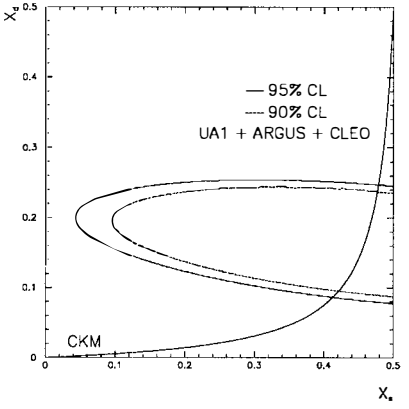

Figure 5: Confidence ellipses for χ_d versus χ_s using the UA1 measurement and the ARGUS and CLEO measurement.

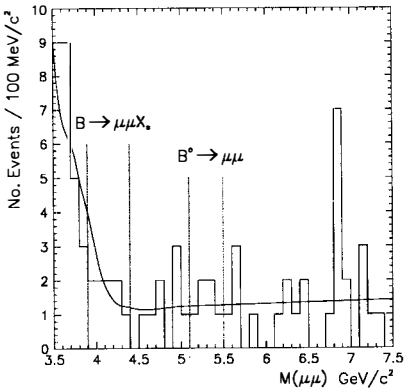

Figure 6: The dimuon invariant mass distribution in the $B^0 \to \mu^+\mu^-$ and $B \to \mu^+\mu^- X$ search regions. The solid line represents the fit to the background

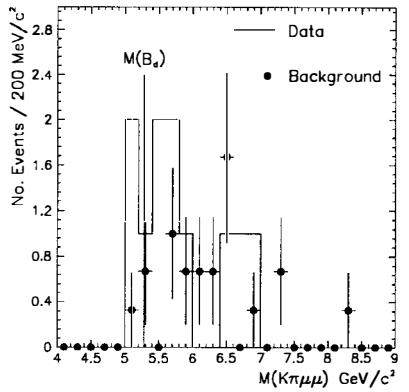

Figure 7: The $K\pi\mu\mu$ mass distribution for events near the $B_d \to \mu^+\mu^- K^{0*}$ search region with background estimate

Table 3: Predicted branching ratios (for $100 < M_{top} < 200\ GeV/c^2$) and experimental limits for rare B-decays

Process	Branching Ratios		
	Theoretical Prediction	UA1 Limit (90%C.L.)	Other Limits (90%C.L.)
$B_{s,d} \to \mu^+\mu^-$	$4 \cdot 10^{-10} - 4 \cdot 10^{-9}$ [16]	$8.3 \cdot 10^{-6}$	
$B_s \to \mu^+\mu^-$		$2.5 \cdot 10^{-5}$	
$B_d \to \mu^+\mu^-$		$1.2 \cdot 10^{-5}$	$5 \cdot 10^{-5}$ ARGUS[19] CLEO[20]
			$3.2 \cdot 10^{-6}$ CDF [21]
$B \to \mu^+\mu^- X$	$3 \cdot 10^{-5} - 7 \cdot 10^{-5}$ [22]	$5 \cdot 10^{-5}$	$2.4 \cdot 10^{-3}$ CLEO [23]
$B_d \to \mu^+\mu^- K^{0*}$	$2 \cdot 10^{-7} - 8 \cdot 10^{-7}$ [15]	$1.1 \cdot 10^{-5}$	$1.9 \cdot 10^{-4}$ CLEO [20]

$K^{0*} \to K^+\pi^-$ candidate in the event. The background to this sample is estimated by loosening the cuts on the $K\pi$ system.

The data and background estimation are plotted in Figure 7. Again we see no significant excess of data events in a region of $\pm 200\ MeV/c^2$ around the B_d mass. The branching ratio upper limit we derive is given in Table 3.

4.2 Top Mass Limit

Grigjanis *et al* [22] have calculated the branching ratio $\mathrm{Br}(b \to l^+l^-s)$ as a function of M_{top}. This quark level calculation can be compared to our measured $\mathrm{Br}(B \to \mu^+\mu^- X)$ upper limit. Comparing the calculation with our upper limit we find $M_{top} < 400\ GeV/c^2$ at 90% C.L. This limit is independent of the possible decay modes of the top-quark.

5 Conclusions

We have studied several aspects of heavy quark physics at UA1 ranging from production to decay modes and mixing. We find excellent agreement between our measurements of b-quark production and $O(\alpha_s^3)$ QCD predictions over a wide range of transverse momentum . We find B_s^0 mixing to be maximal, consistent with Standard Model predictions, and exclude the region of zero mixing. We have also improved branching ratio limits for loop-induced B-hadron decays by an order of magnitude over previous results from e^+e^- experiments.

Acknowledgements

I would like to thank all of my colleagues at UA1 who made this work possible.

References

[1] C. Albajar *et al* (UA1 Collab.), *Z. Phys.* **C48** (1990) 1.

[2] C. Albajar *et al* (UA1 Collab.), *CERN-PPE/90-155.*

[3] C. Albajar *et al* (UA1 Collab.), *CERN-PPE/91-55.*

[4] C. Albajar *et al* (UA1 Collab.), *CERN-PPE/91-54.*

[5] P. Nason, S. Dawson, R.K. Ellis, *Nucl. Phys.* **B303** (1988) 607, *Nucl. Phys.* **B327** (1989) 49.
W. Beenakker *et al* , *DESY 90-064, ITP-SB-90-46* (1990).

[6] F. Paige, S.D. Protopopescu, *BNL-38034* (1986).

[7] R. Johnson, talk given at *XXV Int. Conf. on High Energy Physics, Singapore 1990.*

[8] C. Peterson *et al* , *Phys. Rev.* **D27** (1986) 105.

[9] H. Albrecht *et al* (ARGUS Collab.), *DESY 90-088* (1990).
R. Fulton *et al* (CLEO Collab.), *Phys. Rev. Lett.* **64** (1990) 16.

[10] M. Danilov (for the ARGUS Collab.), *DESY 89-147* (1989).
M. Artuso *et al* (CLEO Collab.), *Phys. Lett.* **62** (1989) 2233.

[11] M. Banner *et al* (UA2 Collab.), *Phys. Lett.* **B122** (1983) 322;
A. Breakstone *et al* , *Phys. Lett.* **B135** (1984) 510;
G.J. Alner *et al* (UA5 Collab.), *Nucl. Phys.* **B258** (1985) 505.

[12] H. Albrecht *et al* (ARGUS Collab.), *Phys. Lett.* **B192** (1987) 246;
A. Bean *et al* (CLEO Collab.), *Phys. Rev. Lett.* **58** (1987) 183.

[13] D. Decamp *et al* (ALEPH Collab.), *CERN-PPE 90-194*, submitted to Phys. Lett. B.

[14] B. Adeva *et al* (L3 Collab.), *L3 preprint #20*, submitted to Phys. Lett. B.

[15] W. Jaus and D. Wyler, *Phys. Rev.* **D41** (1990) 3705.

[16] J.L. Hewett *et al* , *Phys. Rev.* **D39** (1989) 250.

[17] C.S. Lim *et al* , *Phys. Lett.* **B218** (1989) 343.

[18] Particle Data Group, *Phys. Lett.* **B239** (1990).

[19] H. Albrecht *et al* (ARGUS Collab.), *Phys. Lett.* **B199** (1987) 451.

[20] P. Avery *et al* (CLEO Collab.), *Phys. Lett.* **B223** (1989) 470.

[21] T.F. Rohaly, talk given at *XXV Int. Conf. on High Energy Physics, Singapore 1990.*

[22] R. Grigjanis *et al* , *UTPT-89-32* (1989).
P. O'Donnell, private communications.

[23] A. Bean *et al* (CLEO Collab.), *Phys. Rev.* **D35** (1987) 3533.

[24] E.W.N. Glover, A.D. Martin, W.J. Stirling, *Z. Phys.* **C38** (1988) 473, and private communications with E.W.N. Glover.

B Physics at CDF

The CDF Collaboration [1]

Presented by A. Sansoni

INFN,Laboratori Nazionali di Frascati

00044 Frascati (RM), Italy

Abstract

An overview of the B physics results obtained by CDF is presented. During the 1988-1989 run we have collected 4.4pb^{-1} of $p\bar{p}$ collisions at $\sqrt{s}$ =1.8Tev. Using the $J/\psi \rightarrow \mu^+\mu^-$ sample the first reconstruction of exclusive B mesons decays at a hadron collider was obtained. From the inclusive electron sample and the exclusive B decays a measurement of the b quark production cross section was made and compared with the theory prediction. The $e\mu$ sample was used to study $B\bar{B}$ mixing and the χ parameter,averaged over B_d and B_s mesons, was measured to be $\chi = 0.176 \pm 0.028(\text{stat}) \pm 0.041(\text{sys})$.

1 Introduction

B mesons have been extensively studied at e^+e^- colliders in the past ten years [2]. At the machines running at the $Y(4S)$ the masses of the B^0 and $B^\pm$ mesons, their branching ratios and decay kinematics were measured while the B lifetime was measured at the higher energy colliders.

At the Fermilab $p\bar{p}$ collider the b production cross section is large but the identification of the B decay products in presence of the high background characteristic of the hadronic interactions poses a challenging experimental problem. The measurement of the $p\bar{p} \rightarrow b + X$ production cross section is important as the uncertanties involved in its calculation are large. The high center of mass energy allows for the production and study of all kinds of B hadrons if the background can be reduced. At CDF we have achieved a favorable signal to background ratio in three data samples: the $J/\psi \rightarrow \mu^+\mu^-$ sample, the inclusive electron and the $e\mu$ sample.

2 The $J/\psi \rightarrow \mu^+\mu^-$ sample

The decay of B mesons into $J/\psi X$, where $J/\psi \rightarrow \mu^+\mu^-$, is particulary suited for the reconstruction of final states. Due to the large mass of the J/ψ the exclusive branching ratios of the two body decays are a big fraction of the inclusive $B \rightarrow J/\psi X$ rate. By mass constraining the muons of the $J/\psi \rightarrow \mu^+\mu^-$ decay, the B mass resolution is greatly improved. Furthermore the fraction of J/ψ from B decays is expected to be large in the high p_t and large angle region explored by CDF [3].

Muon identification at CDF [4] is obtained in the central region $|\eta|$ <0.6 by means of muons chambers surrounding the central calorimeter, each chamber consists of four drift planes. Stubs in the muon chambers are matched to tracks in the central tracking chamber (CTC) to define good muons. The dimuon trigger required a loose matching cut and a p_t cut on the muon tracks; the majority of the data was collected with a p_t cut of 3 GeV on both muons. The invariant mass distribution of the opposite signed dimuons corresponding to 4.0 pb^{-1} of integrated luminosity is shown in Fig. 1. The J/ψ sample is defined by requiring the dimuon invariant mass to be whithin $\pm$ 50 MeV of the J/ψ mass of 3097 MeV. This sample consists of 2500 J/ψ events above background.

Due to the trigger p_t cut on the muons the average p_t of the reconstructed J/ψ is $\approx$ 8 GeV . If these J/ψ come from B decays the momentum of the parent B meson must be even higher and its decay products are boosted forward and close to the J/ψ flight direction. The momentum of the K and π coming from the $B^\pm \rightarrow J/\psi K^\pm$ and $B^0 \rightarrow J/\psi K^{*0}$ decays is therefore expected to be larger than the average momentum of the particles associated with the underlying event.

To reconstruct a given decay final state the J/ψ legs are first constrained to the J/ψ mass. Combinations of the reconstructed J/ψ and the other tracks in a 60 degree cone around the J/ψ flight direction are formed with the relevant mass assignment. To search for $B^\pm \rightarrow J/\psi K^\pm$ combinations are formed with tracks with momentum above 3 GeV and the K mass assignment. The resulting invariant mass spectrum is shown in Fig. 2 where an excess of events is observed at the B mass. The search for $B^0 \rightarrow J/\psi K^{*0}$ is affected by a large combinatorial background. Due to the lack of particle identification at CDF for every pair of tracks, candidate $K^{*0} \rightarrow K^\pm\pi^\mp$, both $K\ \pi$ and $\pi\ K$ mass assignment must be given to the pair. To reduce this combinatorial

background only the three highest momentum tracks in the 60 degree cone are used to form K π pairs. If the K π mass is whithin $\pm$ 50 MeV of the K^{*0} mass (896MeV) the $J/\psi K^{\pm}\pi^{\mp}$ combination is formed and the resulting invariant mass distribution is shown in Fig. 3 where a clear peak at the B mass is visible. Fig. 4 shows the sum of the $J/\psi K^{\pm}$ and the $J/\psi K^{*0}$ mass spectra. This demonstrates that the $J/\psi \rightarrow \mu^+\mu^-$ is a very good tag for B production at hadron colliders and can be employed to search for the yet undiscovered heavier B hadrons.

The $B^{\pm} \rightarrow J/\psi K^{\pm}$ reconstructed decays are used to measure the b quark production cross section. To relate the number of reconstructed B mesons in the $J/\psi K^{\pm}$ channel to the number of produced b quarks we use the following monte carlo method: b quarks are produced according to the p_t spectrum predicted by QCD [5], flat in rapidity for $|y^b|$ <1 and then fragmented in B hadrons according to the Peterson model [6]. We assume that a b quark fragments in a B^- meson 40% of the times. After the kinematics of the $B^{\pm} \rightarrow J/\psi K^{\pm}$ and $J/\psi \rightarrow \mu^+\mu^-$ decays is simulated and the analysis cuts applied we find that 90% of the reconstructed B mesons come from b quarks with p_t^b >10GeV. Therefore we choose to quote the b quark production cross section integrated for p_t^b >10GeV . Using the $B^{\pm} \rightarrow J/\psi K^{\pm}$ branching ratio measured at e^+e^- [7] and the calculated reconstruction efficiency our result for the cross section is:

$$\sigma(p\bar{p} \rightarrow b + X \ , \ p_t^b > 10\text{GeV}, \ |y^b| < 1) = (8.2 \pm 2.9(\text{stat}) \pm 3.3(\text{sys}))\mu b$$

3 The inclusive electron sample

Electron identification in CDF relys on the finely segmented central calorimeter, the proportional gas chamber embedded in the electromagnetic section of the calorimeter at shower maximum and the central tracking chamber. Good electrons are defined requiring that:

- only one track points to the calorimeter cluster,
- the ratio of the calorimeter energy to the track momentum be $0.75 < E/P < 1.4$,
- the ratio of the energy deposition in the hadronic and in the electromagnetic compartment be $HAD/EM < 0.04$,
- the energy sharing with adjacent towers must be in agreement with the expected electron lateral shower shape,
- in the proportional chamber the shower position must match the extrapolated CTC track and the shower shape must be compatible with a single electron as measured in the test beam.

Conversion electrons from interacting $\gamma \rightarrow e^+e^-$ and $\pi^0 \rightarrow \gamma e^+e^-$ are removed with 50% efficiency looking for a partner track with small opening angle with the candidate electron. The contribution of electrons from W decays is removed by the requirement that the missing E_t in the event be less than $8\sqrt{E_t}$ and electrons from Z decays are removed searching for a second electromagnetic cluster and requiring an invariant mass with the candidate electron less than 80 GeV. The p_t distribution of this prompt electron sample

before and after the W and Z removal is shown in Fig. 5. This corresponds to 4.4pb^{-1} of data collected with an electron trigger threshold of p_t^e >12GeV and 200nb^{-1} (prescaled) with a trigger threshold of p_t^e >7GeV . We estimate a residual background of (20±5)% due to unidentified conversions and (15±15)% due to misidentified charged hadrons.

After background subtraction the source of prompt electrons is the heavy quarks semileptonic decay. At CDF b and c quarks are expected to be produced at similar rates but the harder fragmentation and the heavier b quark mass combined with the trigger p_t cut results in an enhancement of electrons from b decays in our sample. Using the Isajet monte carlo [8] we estimate a 10% charm fraction in our sample.

We have measured the b quark production cross section following the method employed by UA1 [9]. The monte carlo is used to relate the b production cross section to the observed electron rate. The b quark p_t^b spectrum is generated according to QCD [5], the Peterson model [6] is used for the fragmentation and the semileptonic B decay is generated with the kinematics measured at e^+e^- [10]. We choose to use three different region of the electron p_t^e spectrum and quote a b quark production cross section integrated for $p_t^b > p_t^{min}$ where p_t^{min} is chosen such that 90% of the electrons in the given region come from b quarks with p_t^b above p_t^{min} . The b cross section for the three kinematical regions is:

$p\bar{p} \rightarrow b + X$,$p_t^b > p_t^{min}$,$\lvert y^b \rvert < 1$		
p_t^e (GeV)	p_t^{min} (GeV)	$\sigma(nb)$
10-15	15	1220±390
15-20	23	220±70
20-25	32	56±18

Fig. 6 shows the experimental points obtained using the inclusive electrons together with the measurement form the B exclusive decays compared with the theory prediction [5]. The shape of the curve agrees well with the data while the absolute normalization of the theoretical calculation seams to underestimate the observed cross section.

4 The $e\mu$ sample

The phenomenon of mixing, or flavor oscillation, consists in the transformation of a neutral meson into its antiparticle through a second order weak transition. This phenomenon, well known in the $K^0\bar{K}^0$ system, has been studied recently in the $B^0\bar{B}^0$ system at $p\bar{p}$ and e^+e^- colliders [11] . The amount of mixing is sensitive to some of the yet unmeasured parameters of the standard model: the top mass and elements of the CKM matrix.

$B\bar{B}$ production followed by the semileptonic decay of the B hadrons is a source of dilepton events: ee,$\mu\mu$ and $e\mu$. First generation B decays produce unlike sign pairs while a second generation $b \rightarrow c \rightarrow lepton$ decay of one B hadron produces a pair with the same sign. The oscillation of one neutral B meson into its antiparticle also produces a like sign dilepton pair, therefore the signature of mixing is an excess of same sign dilepton events.

At a $p\bar{p}$ collider the ratio R of like sign to unlike sign lepton pairs is:

$$R = \frac{2\chi(1-\chi) + [(1-\chi)^2 + \chi^2]f_*}{[(1-\chi)^2 + \chi^2] + 2\chi(1-\chi)f_* + f_c}$$

where f_s is the fraction of second generation b decays and f_c the fraction of charm decays with respect the the first generation b decays. The mixing parameter χ is the probability that a B^0 meson oscillates into a $\bar{B}^0$ meson averaged over B_d and B_s mesons: $\chi = P_d\chi_d + P_s\chi_s$ where P_d and P_s are the fraction of B_d and B_s mesons produced.

To measure R we use the $e\mu$ events, in this channel there is no contribution from Drell-Yan, J/ψ and Y production and the only background is due to fake electrons or muons. Electrons and muons candidates are required to have $E_t^e > 5$ GeV and $p_t^\mu > 3$ GeV. Electrons from conversions and from W decays are removed. Fig. 7 and Fig. 8 show the invariant mass of the like sign and unlike sign $e\mu$ pairs respectively. The peak at low mass for the unlike sign pairs is due to events from a single $b \rightarrow ce\nu_e$ followed by $c \rightarrow s\mu\nu_\mu$, we cut these events requiring M($e\mu$)>5 GeV. After these cuts we are left with 346 like sign events and 554 opposite sign events.

We estimate that the background due to fake electrons and muons is (20±10)% of the sample. After the mass cut the contribution to the background from the same sign and the opposite sign events is the same and the background subtracted value of R is :

$$R = 256/464 = 0.552 \pm 0.049(\text{stat})^{+0.039}_{-0.048}(\text{sys})$$

To extract the mixing parameter χ we estimate the fraction of secondary generation b decays to first generation b decays f_s and the fraction of charm decays to first generation b decays f_c using the monte carlo. At first order f_s and f_c depend on the relative c and b production cross section and the semileptonic branching ratios. Due to the analysis cuts f_s and f_c are also sensitive, to a lesser extent, to the c and b production mechanism. Taking into account the uncertaintes associated with these quantities and with the production mechanism we find that $f_s = (0.248 \pm 0.055)$ and $f_c = (0.066 \pm 0.066)$. The epected ratio of like sign to unlike sign lepton pair R_0 in absence of mixing is $R_0 = f_s/(1 + f_c) = 0.233 \pm 0.051$ significantly lower than the observed ratio. From the measured R value we extract the χ parameter :

$$\chi = 0.176 \pm 0.028(\text{stat}) \pm 0.041(\text{sys})$$

in good agreement with the other measurements [11].

5 Conclusions

During the 1988-1989 run $\approx 10^7$ high p_t b hadrons were produced at CDF. We have shown that samples of data useful for b studies can be obtained at $p\bar{p}$ collisions.

Thanks to the excellent momentum resolution the $B^\pm \rightarrow J/\psi K^\pm$ and $B^0 \rightarrow J/\psi K^{*0}$ decays were fully reconstructed in the $J/\psi \rightarrow \mu^+\mu^-$ sample. Good lepton identification is essential to obtain b rich samples in the inclusive electron and $e\mu$ data. From the inclusive electron sample the b quark production cross section was measured and $B\bar{B}$ mixing was studied with the $e\mu$ data. In the next run, with higher luminosity, extended muon coverage and a silicon vertex detector the sample of reconstructed decays should be much larger and our B physics capabilities increased.

References

[1] The CDF Collaboration : Argonne National Laboratory, Brandeis University, University of Chicago, Fermi National Accelerator Laboratory, Istituto Nazionale di Fisica Nucleare (LNF) Frascati, Harvard University, University of Illinois, The Johns Hopkins University, National Laboratory for High Energy Physics (KEK), Lawrence Berkeley Laboratory, University of Pennsylvania, Istituto Nazionale di Fisica Nucleare Pisa, Purdue University, University of Rochester, Rockefeller University, Rutgers University, Texas A&M University, University of Tsukuba, Tufts University, University of Wisconsin.

[2] E.H.Thorndike and R.A.Poling Phys.Rep.157,183(1988)

[3] N.Glover et al.,Z.Phys.C38,473(1988)

[4] CDF,F.Abe et al.,Nucl.Instr.Meth.A271,387(1988)

[5] P.Nason et al.,Nucl.Phys.B327,49(1989)

[6] C.Peterson et al.,Phys.Rev.D27,105(1983)

[7] ARGUS,H.Albrecht et al.Phys.Lett.B199,451(1987), DESY 90-046 (1990)
CLEO,C.Bebek et al.Phys.Rev.D36,1289(1987), D.H.Miller Proc. EPS Int.Conf. Madrid 1989

[8] F.E.Paige,S.D.Protopopescu,BNL-38034(1986)

[9] UA1,C.Albajar et al.Phys.Lett.B213,405(1988)

[10] CLEO monte carlo,P.Avery et al.,CSN-212(1985)

[11] UA1,C.Albajar et al.Phys.Lett.B186,247(1987)
ARGUS,H.Albrecht et al.Phys.Lett.B192,245(1987)
CLEO,M.Artuso et al.Phys.Rev.Lett.62,2233(1989)
ALEPH,D.Decamp et al.CERN-PPE/90-194(1990)
L3,L3 preprint n.20(1990)

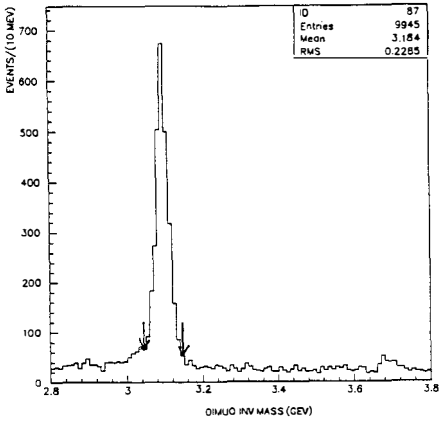

Fig.1

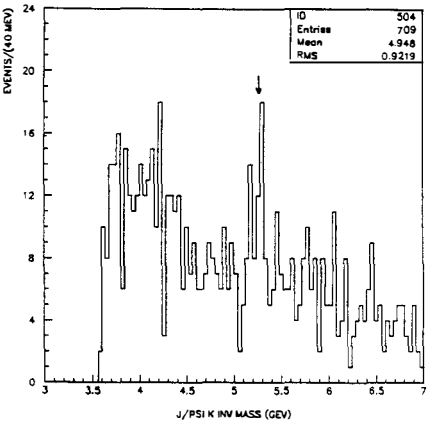

Fig.2

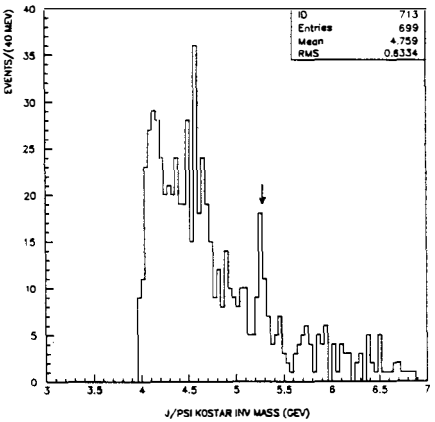

Fig.3

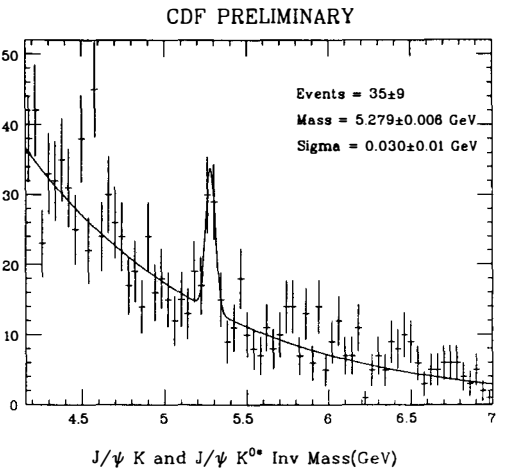

Fig.4

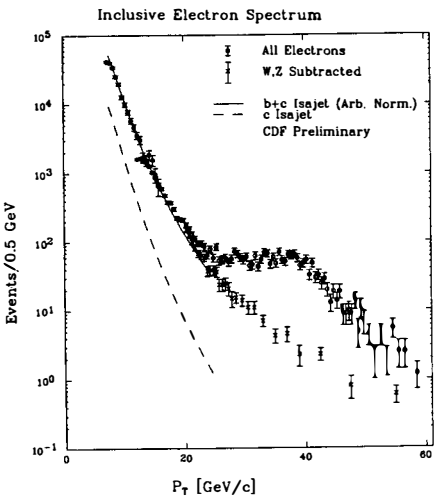

Fig.5

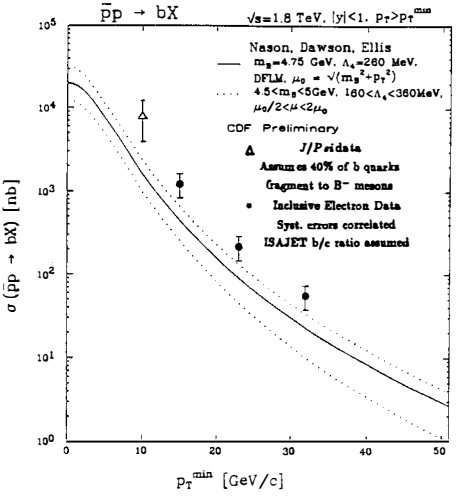

Fig.6

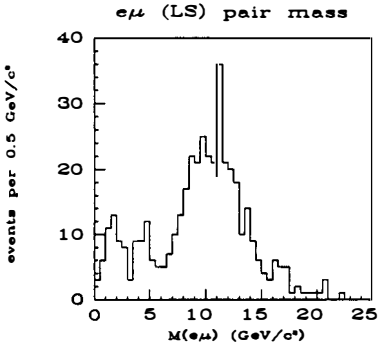

Fig.7

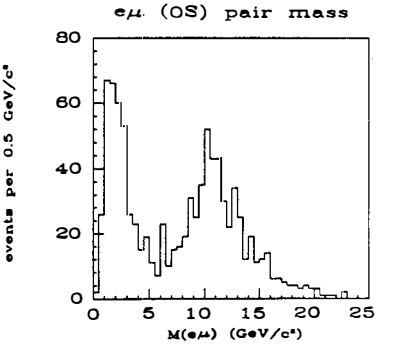

Fig.8

HEAVY QUARK PRODUCTION IN NUCLEON COLLISIONS

Presented by Yuly Shabelski
Leningrad Nuclear Physics Institute
Gatchina, Leningrad 188350. USSR

Abstract

We compare the results of calculations of heavy quark production cross section in leading log QCD to those parton model. The formulae of parton model are obtained from QCD via several subsequent simplifications. The cross section of b-quark production in LLA QCD is predicted to be $2-3$ times larger than the parton model predictions.

The presented results were obtained together with E.M.Levin, M.G.Ryskin and A.G.Shuvaev.

In this paper we compare two approaches to the production of the heavy quarks in high energy hadron-hadron collisions. One of them employs the parton model, another one is based on the theory of semihard processes [1]. The heavy pair production is described in the lowest order of QCD as an elementary process given by the sum of three graphs in Fig.1 in both approaches. In the parton model all particles involved are assumed to be on mass shell and the cross section is averaged over two transverse polarizations of the gluons. The virtualities q^2 of the initial partons are taken into account through their densities. The latter are calculated in leading logarithm approximation (LLA) collecting the terms of the form $(\alpha_s \ln q^2)^n$ and resulting in the well-known Gribov-Lipatov-Altarelli-Parisi evolution equation. The probabilistic picture of noninteracting partons underlies this way of proceeding.

The theory of semihard processes deals with the region where the values of Bjorken variables x are very small. It is just the region that dominates in the heavy quark production at high energies $\sqrt{s}$ since the characteristic value of x is $x \sim 2m_T/\sqrt{s}$ ($m_T^2 = m^2 + p_T^2$ is transverse mass of the quark). The drastical growth of the parton density in this domain makes the effects of parton-parton interaction very significant. For the correct description of these phenomena it is necessary to sum up in Feynman diagrams not only the terms of the form $(\alpha_s \ln q^2)^n$ but also the terms $(\alpha_s \ln 1/x)^n$ and $(\alpha_s \ln q^2 \ln 1/x)^n$. Another problem that appeared at $x \sim 0$ is that of the screening (absorption) corrections which stop the growth of the cross section and restore the unitary. As a result the gluon structure function $xG(x, q^2)$ becomes proportional to q^2R^2 at relatively small virtuality $q^2 \leq q_0^2(x)$ and the cross section is $\sigma \sim (1/q^2)xG(x, q^2) \sim R^2$. Here $R = const$ is a new phenomenological parameter with dimension of $(\text{mass})^{-1}$ and the value of $q_0(x)$ can be considered as a new typical transverse momentum of partons in the parton cascade of the hadron which leads to natural infrared cut-off in semihard processes (see ref. [1] for details).

The main contribution to the cross section at small x is known to come from gluons. Their distribution over x and transverse momenta q_T in hadron is given in semihard theory by function $\varphi(x, q^2)$. It differs from the usual function $G(x, q^2)$:

$$xG(x, q^2) = \frac{1}{4\sqrt{2}\,\pi^3} \int_0^{q^2} \varphi(x, q_1^2) dq_1^2. \qquad (1)$$

Such definition of $\varphi(x, q^2)$ makes possible to treat correctly the effects arising from gluons virtualities. The exact expression for this function can be obtained

as a solution of the evolution equation which, contrary to the parton model case, is nonlinear due to interactions between the partons in small x region.

The differential cross section of heavy quark production has the form

$$\frac{d\sigma}{dy_1^* dy_2^* d^2p_{1T} d^2p_{2T}} = \frac{1}{(2\pi)^8}\frac{1}{(s)^2}\int d^2q_{1T}d^2q_{2T}\delta(q_{1T}+q_{2T}-p_{1T}-p_{2T})$$

$$\times \frac{\alpha_s(q_1^2)}{q_1^2}\frac{\alpha_s(q_2^2)}{q_2^2}\varphi(q_1^2,y)\varphi(q_2^2,x)|M|^2. \qquad (2)$$

Here $s = 2p_A p_B$, $y_{1,2}^*$ are the quarks' rapidities in c.m.s.,

$$x_1 = \frac{m_{1T}}{\sqrt{s'}}e^{-y_1^*}, \quad x_2 = \frac{m_{2T}}{\sqrt{s'}}e^{-y_2^*}, \quad x = x_1 + x_2$$

$$y_1 = \frac{m_{1T}}{\sqrt{s'}}e^{y_1^*}, \quad y_2 = \frac{m_{2T}}{\sqrt{s'}}e^{y_2^*}, \quad y = y_1 + y_2. \qquad (3)$$

$q_{1,2T}$ are the gluons' transverse momenta. $|M|^2$ is the square of the matrix element. The explicit expression for $|M|^2$ is rather bulky and we do not present it here (one can find it in ref. [2]).

There is a certain limit case in which our formulas can be transformed into parton model ones. Introducing the polar coordinates

$$d^2q_{1\perp} = \frac{1}{2}dq_{1\perp}^2 d\theta_1 \qquad (4)$$

we obtain

$$\int_0^{2\pi} d\theta_1 q_{1T}^\mu q_{1T}^\nu = \pi\, q_{1T}^2\, \delta_T^{\mu\nu} \qquad (5)$$

$$\int d\theta_1 \int d\theta_2 |M|^2 = 2\pi^2 \frac{q_{1T}^2 q_{2T}^2}{(x\,y)^2}|M_{part}|^2 \qquad (6)$$

Here M_{part} is just the matrix element in the parton model since the result is the same as that calculated for the real (mass shell) gluons and averaged over transverse polarizations. Then we obtain the cross section (2) in the form

$$\frac{d\,\sigma}{dy_1^* dy_2^* d^2p_{1T}} = \int |M|^2 \frac{d\theta_1 d\theta_2}{2\pi^2 q_1^2 q_2^2 (s)^2}\int \frac{\alpha_s(q_1^2)\varphi(y,q_{1T}^2)}{4\sqrt{2}\pi^3}\frac{\alpha_s(q_2^2)\varphi(x,q_{2T}^2)}{4\sqrt{2}\pi^3}dq_{1T}^2 dq_{2T}^2$$

$$= |M_{part}|^2 \frac{1}{(\hat{s})^2}\int \frac{\alpha_s(q_1^2)\varphi(y,q_{1T}^2)}{4\sqrt{2}\,\pi^3}\frac{\alpha_s(q_2^2)\varphi(x,q_{2T}^2)}{4\sqrt{2}\,\pi^3}dq_{1T}^2 dq_{2T}^2 \qquad (7)$$

where $s = xys$ is the mass square of $\bar{Q}Q$ pair.

The difference between eqs. (2) and (7) is caused by change of the matrix element square $|M|^2$ in (2) by $q_{1T}^2 q_{2T}^2 [M/(q_{1T}^2 q_{2T}^2)]_{q_{1T}=q_{2T}=0}$. In order to show this we present in Fig. 2 the values of $|M|^2$ averaged over gluon polarizations, as the functions of $q_{1T} = q_{2T} = \Delta q$ at three values of b-quark ($m_b = 4.7\,GeV$) transverse momenta, $\sqrt{s} = 1.8\,TeV$, $y_1^* = 0.5$, $y_2^* = 0$. Here we integrate $|M|^2$ over transverse momentum of the second b-quark. The values of $\Delta q \geq 10\,GeV/c$ don't contribute really to eq.(2) because of fast decrease of the gluon distributions. The value of $|M|^2$ decrease with Δq at small p_{1T}. Thus eq. (7) overestimates the cross section in this region. But with the growth of p_{1T} the minimum of $|M|^2$ appears at $\Delta q = 0$ and the maximum of $|M|^2$ moves away (it is in the region $\Delta q \simeq p_{1T}/2$). The numerical calculations show that the cross sections given by eqs.(2) and (7) coincide approximately at $p_{1T} = 5 - 7\ GeV/c$. At larger values of p_t the cross section of eq.(7) becomes smaller. The difference is, however, not so large and does not vary with p_{1T} (see fig.3). The reason is that the maximum value of $|M|^2$ at high p_T is achieved at large values of Δq which give very small contribution to the cross section. The most important is the different p_T dependence of the two eqs. (2) and (7). For example, the cross section ratios at $p_{1T} = 0$ to $p_{1T} = 10\,GeV/c$ are about 1.5 times different.

The next step to the well-known parton model is changing of the argument in α_s QCD constant. As it was discussed earlier (see, e.g., refs.[3, 4]) the theory cannot fix the value of this argument. Eq.(6) corresponds to the direct calculation of the diagrams of Fig.1 and here it seems to be the most natural to use $\alpha_s(q_1^2) \cdot \alpha_s(q_2^2)$. The essential values of q_1^2 and q_2^2 in eq. (2) are of the order of $q_0^2(x)$, which is equal to several GeV^2 and increase very slowly with initial energy [1]. Thus the essential values of α_s are of the order of $\alpha_s \sim 0.2$. In the parton model the value of mass of heavy quark is used usually as an argument of α_s, with the possible variation of numerical factor. In this case the results of calculations of heavy quark production cross section or these of the distributions $d\sigma/dp_{1T}^2$ should differ by the numerical factor (which can depends on the value of initial energy). However, it seems to be more natural to use the transverse mass of heavy quark, $m_T^2 = m_Q^2 + p_{1T}^2$

The results of calculations of cross section

$$\frac{d\sigma}{dy_1^* dy_2^* d^2 p_{1T}} = |M_{part}|^2 \left[\frac{\alpha_s(4m_T^2)}{\hat{s}}\right]^2 \int \frac{\varphi(y, q_{1T}^2)}{4\sqrt{2}\,\pi^3} \frac{\varphi(x, q_{2T}^2)}{4\sqrt{2}\,\pi^3} dq_{1T}^2 dq_{2T}^2 \qquad (8)$$

are shown in Fig. 3 by dotted curve.

The factorization of gluon distributions in eq. (8) is one more distinguish from parton model. It connects with accounting for the dependence of x and y distributions on the transverse momentum, see eqs.(3). Nevertheless, if we

rewrite eq.(8) in the form

$$\frac{d\sigma}{dy_1^* dy_2^* d^2p_{2T}} = |M_{part}|^2 \left[\frac{\alpha_s(4m_T^2)}{\hat{s}}\right]^2 \int \frac{\varphi(y, q_{1T}^2)}{4\sqrt{2}\,\pi^3} dq_{1T}^2 \int \frac{\varphi(x, q_{2T}^2)}{4\sqrt{2}\,\pi^3} dq_{2T}^2$$

$$= |M_{part}|^2 \left[\frac{\alpha_s(4m_T^2)}{\hat{s}}\right]^2 xG(x, 4m_T^2) \cdot yG(y, 4m_T^2) \qquad (9)$$

the distributions $d\sigma/dp_{1T}^2$ change at small transverse momenta and the differences depend on the initial energy. The cross section of b-quark production, $d\sigma/dp_{1T}^2$ increase in the region $p_{1T}^2 \ll m_b^2$ about 20% at $\sqrt{s} = 1.8\,TeV$ and by $1.5 - 2$ times at $\sqrt{s} = 18\,TeV$.

In practical calculations we need in the explicit form of gluon distribution function $\varphi(x, q_T^2)$. It was obtained in ref.[1] that $\varphi(x, q_T^2) \sim q_T^{-2}$ at $q_T^2 \to \infty$. At not so large q_T^2 it is necessary to account for preexponent factor, so the approximation $\varphi(x, q_T^2) \sim q_T^{-4}$ seems to be better. As a function of x $\varphi(x, q_T^2)$ should decrease at $x \to 1$ at least as $\sim (1 - x)^3$. The values of $\varphi(x, q_T^2)$ at $x \to 0$ and large q_T^2 should determine also the cross section of high p_T jet production that allow one to normalize $\varphi(x, q_T^2)$ in this region. It is possible to select the most consistent parametrization with the help of the data on J/Ψ production in pp and $\bar{p}p$ collisions. In the first case the gluons and sea antiquarks contribute only, whereas in the case of $\bar{p}p$ collisions there is the valence quark-antiquark contribution also. So we can normalize our gluon distribution to the valence quark structure functions.

The result of calculation of the ratio

$$R = \frac{\sigma(pp \to J/\Psi)}{\sigma(\bar{p}p \to J/\Psi)} \qquad (10)$$

is shown together with existing experimental data [5, 6] in Fig.4. We used Duke-Owens quark structure function [7] (set 1) and the gluon distribution in the form

$$\varphi(x, q_T^2) = \varphi(1 - x)^3 \frac{0.05}{0.05 + x} f(x, q_T^2), \qquad (11)$$

$$f(x, q_T^2) = \begin{cases} 1 & q_T^2 < q_0^2(x) \\ [q_0^2(x)/q_T^2]^2 & q_T^2 > q_0^2(x) \end{cases} \qquad (12)$$

$$q_0^2(x) = Q_0^2 + \Lambda^2 \exp\left(3.56\sqrt{\ln x/x_0}\right) \qquad (13)$$

$\varphi_0 = 170\,mb$, $Q_0^2 = 2\,GeV^2$, $\Lambda = 52\,MeV$, $x_0 = 1/3$. The reasonable agreement allows us to use this parametrization in the further calculations.

In Figs. 5 and 6 we compare the results of our calculations [2] (solid curves) with new experimental data presented in this Rencontres de Moriond. Parton

model predictions are shown by dashed curves. The $S\bar{p}pS$ collider data at $\sqrt{s} = 630\ GeV$ are in agreement with the parton model calculations. The results of calculations of eq. (2) don't contradict the data also. The Tevatron-collider data at $\sqrt{s} = 1800\ GeV$ lay significantly higher than the parton model curve and agree with our predictions. It can be connected with the specific behaviour of the gluon distribution function at small x.

Figure Captions

Fig.1. The diagrams, taking into account in calculation of heavy quark production via gluon-gluon collision.

Fig.2. Dependences of the matrix element square of $gg \to \bar{Q}Q$ reaction on the gluon transverse momenta Δq at different values of the heavy quark transverse momentum p_{1T}. The values of another variables are $\sqrt{s} = 1.8\ TeV$, $y_1^* = 0.5$, $y_2^* = 0$, $m_Q = 4.7\ GeV$.

Fig.3. The calculated dependences of heavy quark production cross section on its transverse momenta in the LLA QCD, eq.(2) (solid curve), in the approximations of eq. (7) (dashed curve) and eq.(8) (dotted curves). The values of another variables are $\sqrt{s} = 1.8\ TeV$, $m_Q = 4.7\ GeV$, $y_1^* = 0.5$.

Fig.4. Comparison of calculated values of $\sigma(pp \to J/\Psi)/\psi(\bar{p}p \to J/\Psi)$ ratios with the data of refs [5, 6].

Fig.5 Calculated cross sections of b-quark production in $\bar{p}p$ collisions at $\sqrt{s} = 630\ GeV$ in LLA QCD (solid curve) and parton model (dashed curve).

Fig.6 Calculated cross section of b-quark production in $\bar{p}p$ collisions at $\sqrt{s} = 1800\ GeV$ in LLA QCD (solid curve) and parton model (dashed curve)

References

[1] Gribov L.V., Levin E.M., Ryskin M.G. Phys.Rep., 1983, v.100, p.1.

[2] Levin E.M. et al. Preprint LNPI-1643, Leningrad (1990).

[3] Nason P., Dawson S., Ellis R.K. Nucl.Phys., 1988, v.B303, p.607.

[4] Altarelli G. et al. Nucl.Phys., 1988, v.B308, p.724.

[5] Morel C. et al. UA6-Coll. Preprint CERN-PPE/90-127 (1990).

[6] Badier J. et al. Z.Phys 1983, v.C20, p.101

[7] Duke D., Owens J. Phys.Rev. 1984, v D30, p.49.

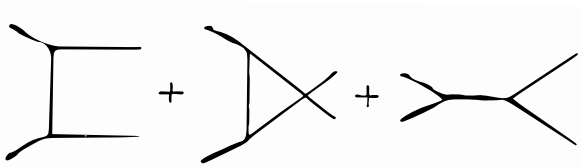

Fig. 1

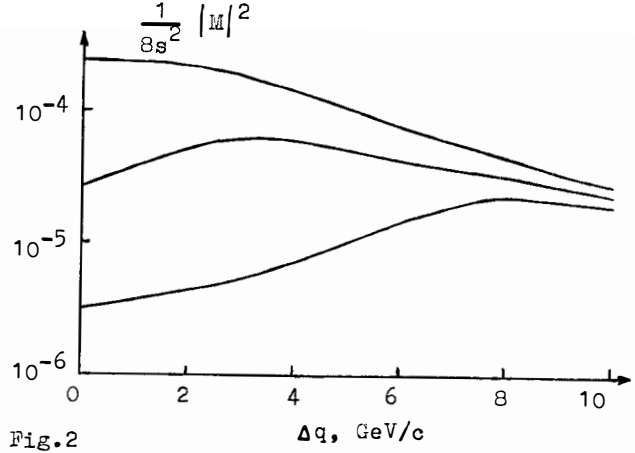

Fig.2

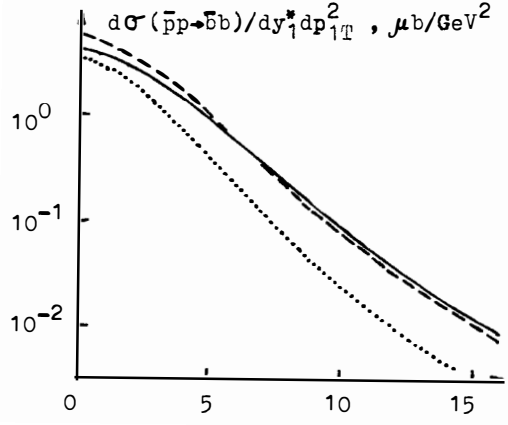

Fig.3

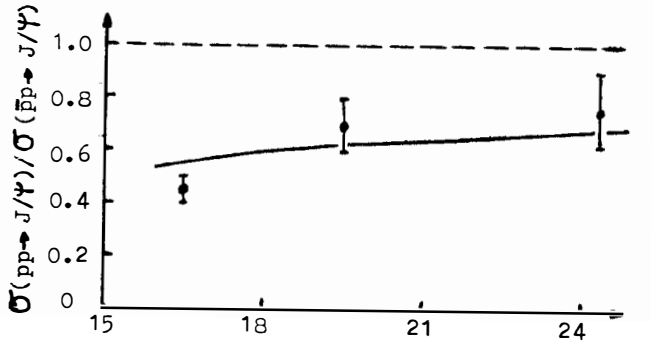

Fig.4

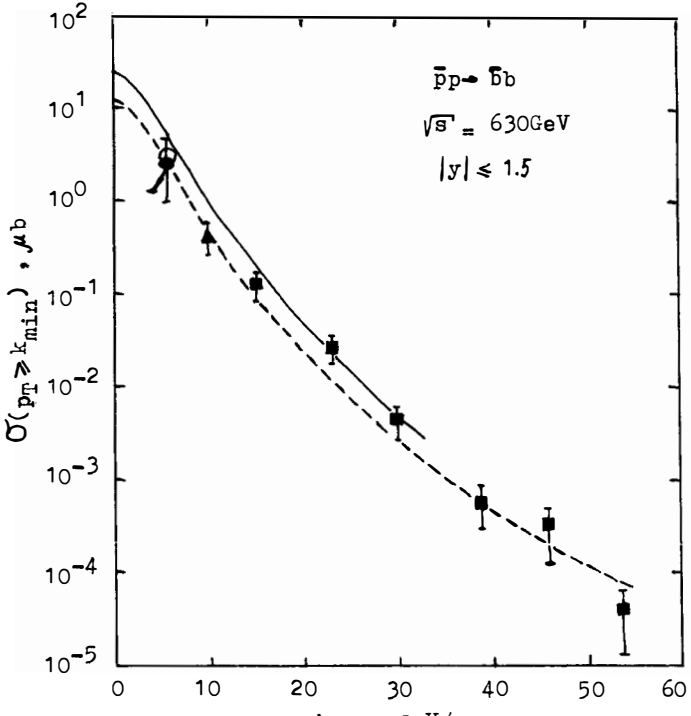
$\bar{p}p \to \bar{b}b$
$\sqrt{s}$ = 630GeV
$|y| \leq 1.5$
$\sigma(p_T \geq k_{min})$, μb
k_{min}, GeV/c

Fig.5

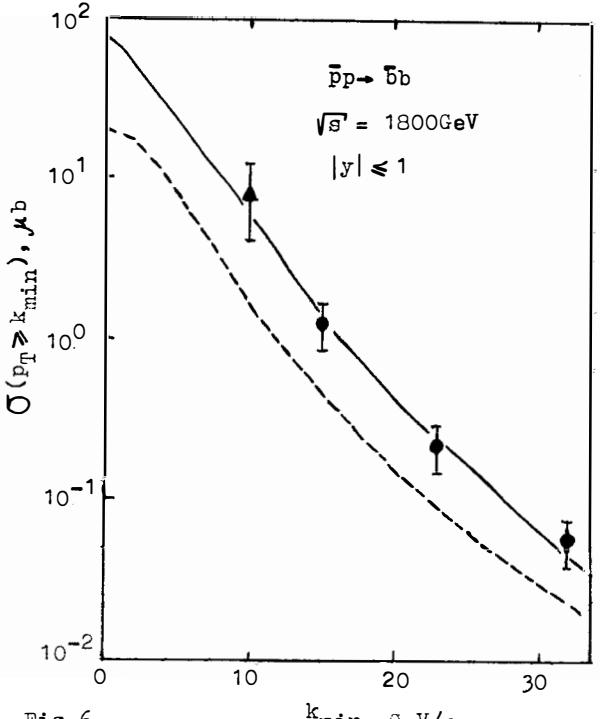
$\bar{p}p \to \bar{b}b$
$\sqrt{s}$ = 1800GeV
$|y| \leq 1$
$\sigma(p_T \geq k_{min})$, μb
k_{min}, GeV/c

Fig.6

SINGLE HEAVY QUARK PRODUCTION AT HADRON COLLIDERS

G. Bordes

Lab. de Physique Corpusculaire,

College de France, Paris, France

Abstract

In the case of top quarks or members of families appearing in extensions of the minimal Standard Model, the weak coupling of these particles may give rise to non-negligible contributions from weak current processes. We present an alternative calculation of the matrix element for the process of heavy flavour production through the W-gluon fusion mechanism in hard hadronic interactions. The expression for the matrix element squared has been implemented in the Eurojet Monte Carlo event generator providing a flexible tool to study event distributions for both partonic and hadronic fir al states.The formula we use in the Eurojet Monte Carlo involves the substraction of the collinear singularity of the W gluon process in the case of a doublet of heavy quarks .We present some results for the production of the Top at the Tevatron and LHC colliders.

1. Introduction

In the standard model, the expected mass of the t-quark lies in the mass range between 89[1] - 244 GeV/c^2 [2]. The electroweak measurements lead to the following value: $m_t = 135 \pm 40$ GeV/c^2 [2].

As the mass difference between the two members of the yet incomplete third generation of quarks increases, the production of top quarks through W gluon fusion becomes competitive with QCD pair production and even dominant for very large top quark masses ($m_t \sim 300$ GeV/c^2) [3]

The interest of a precise study of the various possible production mechanisms of heavy quarks is twofold: Obviously the discovery of the Top and of other heavy quarks either belonging to a fourth family with or without heavy neutrinos or exotic (E_6) and a possible precise determination of the mass of the top quark It has indeed been claimed by Yuan [4] that the weak process W gluon $\rightarrow t\bar{b}$ may lead to a precision of 5 GeV/c^2 for the top mass.

The LHC workshop at Aachen has performed a study of the W gluon $\rightarrow t\bar{b}$ process for the LHC collider.using the Pythia 5.4 Monte Carlo [5]. Motivated by the need of having a comparison between different simulations we have implemented [6] the W gluon process into the Eurojet event generator [7]. This paper describes the comparison between QCD and weak production of the top and a comparison between the results of Pythia and Eurojet where the parton shower program uses the W bottom process as an approximation to W gluon. This comparison leads us to establish a formula taking into account the W gluon and W bottom terms avoiding double counting by properly sustracting the singularity of the W gluon process.

2 Production mechanisms

Figure 1 shows the dependance in the top mass of the top production cross sections. A similar comparison was performed by Zerwas et al. [3]. THe flat dependance of the W gluon process with respect to the strong decrease of the QCD one leads to a ratio $R = \frac{\sigma_{Wg}}{\sigma_{QCD}} < \frac{1}{10}$ for $M_{top} \sim 100$ GeV/c^2 $R \sim 1$ for $M_{top} \sim 250$ GeV/c^2 and $R \sim 100$ for $M_Q \sim 500$ GeV/c^2

Figure 1. comparison between QCD and W-gluon production of the Top quark

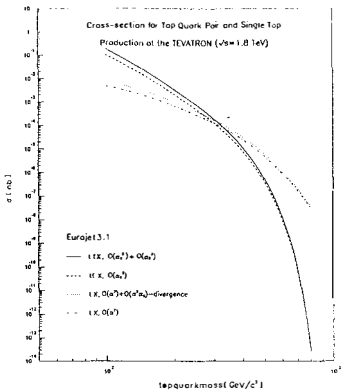

3 W Gluon process

The application of QCD for the heavy quark processes is based on the formula:

$$d\sigma = \sum_{i\,j} \int dx_1\, dx_2\; f_i(x_1,Q^2)\, f_j(x_2,Q^2)\, d\hat{\sigma} \qquad (3.1)$$

where the functions fi are the number densities of partons evaluated at the scale μ. The symbol $\hat{\sigma}$ denotes the short distance cross section from which the mass singularities have been factorized, . The scale μ is a priori only determined to be of the order of the mass of the produced heavy flavour. The Feynman graphs we are dealing with are depicted in figure 2:

Fig.2a: Order α^2 quark-bottom scattering contributions to heavy flavour top production via W-gluon fusion in hadronic interactions. To obtain the complete set of diagrams, the charge conjugates and additional Cabibbo Kobayashi Maskawa mixings are to be included as well.

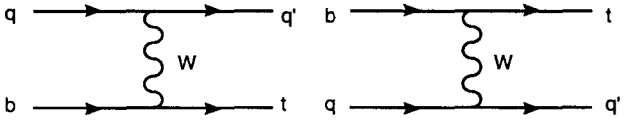

Fig. 2b: Order $\alpha^2 \alpha_s$ (anti)quark-gluon scattering contributions to heavy flavour production via W-gluon fusion in hadronic interactions Same remarks apply as for figure 1a.

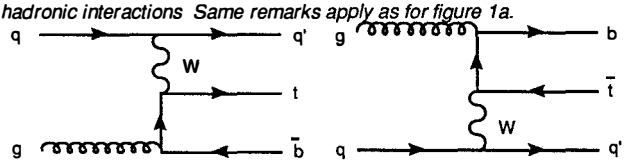

The Cabibbo Kobayashi Maskawa coupling between the top quark and d, s-quarks beeing small compared to the one with the b-quark, can savely be neglected.The canonical QCD approach is then as far as the b quark is considered as an heavy quark to compute the partonic cross section of the processes in fig 2b and insert it in formula 3.1. But the ratio (M_{top}/M_{bottom}) > 20 and it is one of the reasons why the contribution of this process becomes increasingly important with the top mass [8]. The Monte Carlo Pythia 5.4 uses the 0^{th} order in α_s process W b $\rightarrow t\bar{b}$ to simulate the single top production . Table 1 gives a comparison between the results of Pythia and the ones of Eurojet .The results were obtained with the same distribution functions ($EHLQ_1$) [9] and α_{em} running .

Table 1: Top quark cross-sections for pp $\rightarrow$ t X at the LHC ($\sqrt{s}$ = 16 TeV).

m_t	Eurojet 3.1	Pythia 5.4
100	0.54±0.06	0.39
200	0.23±0.02	0.20
300	0.12±0.01	0.11
400	0.068±0.007	$0.79 * 10^{-1}$

4 W gluon versus W bottom

.As stressed in [8] [3] the computation of the graphs of fig 2a with a distribution function of the bottom quark leads to results believed to well approximate the computation of the W gluon fusion process ; in addition , when the ratio between the masses of the two heavy quarks becomes too large not only the first order in α_s diagram is dominated by the singularity of the b quark propagator but the following orders in perturbation theory can not be neglected anymore and the use of the bottom quark

distribution approach is becoming the right one. In view of the fact that the range of masses available for the top quark at future colliders will extent on several hundreds of GeV/c^2 , it appears that we will cross the edge of the domain of applicability of the two approaches. We have then found useful to include in the Monte Carlo the full contribution of the graphes of figure 2a and 2b , but adding the contributions in figures 2a and 2b raises the question of double counting. The graphs in figure 2b partially overlap with the b-quark structure function, already included at lowest order. This occurs when the intermediate b-quark becomes on-shell and collinear with the gluon. An essential feature of the factorisation theorem in Eq. (3.1) is that hard parton-parton cross section is free from mass singularities. It will then appear that a correct formulation of the computation excluding the mass singularity also avoids the double counting.[10) 11)]

We then use the formulae of Ref 11) in which we isolate the singular term at the limit mb=0 and the outgoing bottom quark collinear with the incoming gluon; and we obtain a formula for the singular term (see Ref [12)] see also [13)])

5 factorisation

In this section we establish the factorisation of the singular term [3.1] under the form of the zeroth order cross section times the first order in α_s distribution function of the bottom quark This first order in α_s bottom distribution function will be identical with the distribution function until the full QCD evolution takes effect at an energy which is order of magnitude larger than mb. Then when mb ≤ Q with Q of the order of the top mass the substraction of the singular term in the W gluon fusion process compensates the inclusion of the zeroth order in α_s process. When Q increases the compensation between the two lowest order terms remains but the contribution of the resummed α_s logQ2 terms is no more negligeable.

We define by z_1 the part of the gluon taken by the b quark and the cross section takes the form:

$$d\sigma = \frac{\pi\alpha_s g_w^2}{(2\pi)^5 \hat{s}} \frac{1}{(q^2-M_w^2)^2+M_w^2\Gamma_w^2} \hat{s}(\hat{s}-M_t^2)[z_1^2+(z_1-1)^2]\frac{16}{z}\delta^4(p_a+p_z-k_1-k_2)\,d\Omega^3 \qquad (5.1)$$

where we recognized the Altarelli Parisi splitting function of the gluon P_{qg} and the contribution of the graph in fig 2a

6 Single Top production cross sections

Table 2 gives the numerical values of the cross section σ_{wg} as obtained with Eurojet 3.1.

Table 2[a] *Top quark cross-sections for $p\bar{p} \rightarrow t\,X$ at the Tevatron collider ($\sqrt{s}$ = 1.8 TeV).*

m_t	$O(\alpha^2\alpha_s)$	$O(\alpha^2)$	$O(\alpha^2\alpha_s)$ - div.	$O(\alpha^2) + O(\alpha^2\alpha_s)$ - div.
100	$0.5 * 10^{-2}$	$0.47 * 10^{-2}$	$0.32 * 10^{-2}$	$0.79 * 10^{-2}$
200	$0.6 * 10^{-3}$	$0.70 * 10^{-3}$	$0.33 * 10^{-3}$	$1.04 * 10^{-3}$
300	$0.10 * 10^{-3}$	$0.128 * 10^{-3}$	$0.46 * 10^{-4}$	$0.174 * 10^{-3}$
400	$0.18 * 10^{-4}$	$0.249 * 10^{-4}$	$0.73 * 10^{-5}$	$0.322 * 10^{-4}$
500	$0.32 * 10^{-5}$	$0.50 * 10^{-5}$	$0.12 * 10^{-5}$	$0.62 * 10^{-5}$
600	$0.6 * 10^{-6}$	$0.96 * 10^{-6}$	$0.20 * 10^{-6}$	$1.16 * 10^{-5}$

7 Conclusion

The W-Gluon process seems promising . Nevertheless the Aachen workshop has shown how to exploit its interesting properties needs to face the difficulty of disentangling the events from the important background W + n jets . We think that with our formula we provide a needed tool to improve this study . Besides the case of the top quark our computation may find applications for the exotic isosinglet quarks whose mass may reach several hundred of GeV/c^2 where the W gluon process is definitively dominant.

References

[1] CDF collaboration 26st Rencontre de Moriond, Les Arcs , France , Mar. 1991, this Proceedings
[2] K.Tiittel, 26st Rencontres de Moriond, Les Arcs, France, Mar. 1991, this Proceedings.
[3] E. Reya et al., Proceedings of the ECFA Workshop on the Large Hadron Collider, Vol II p. 295 (ed. G. Jarlskog and D. Rein) Aachen 4-9 Oct. 1990.
[4] C.Yuan, Phys. Rev.D41(1990)42.
[5] Pythia 5.4 H.U. Bengtsson and T.Sjostrand,Comp. Phys. Comm.46 (1987) 43.
[6] F. Anselmo, G.Bordes and B. van Eijk, College de France Report LPC 9054, submitted to Nucl.Phys. B.
[7] Eurojet Version 3.1, F. Anselmo and B. van Eijk, Cern Program Library Long Write-Up W5048 (in preparation),
A.Ali,B.van Eijk and I. ten Have, Nucl. Phys. B292 (1987) 1.
[8] S.D.Willenbrock and P.A. Dicus Phys.Rev. D34 (1986) 155
[9] E.Eichten, I.Hinchliffe, K.Lane, C.Quigg, Rev.Mod.Phys.56(1984) 579,58(1985)1065,
[10] F.I.Olness and W.K.Tung Nucl.Phys.B308 (1988)813,
[11] J.C. Collins and D.E.Soper Ann. Rev. Nucl. Part.Sci. 37(1987) 383..
[12] F.Anselmo, G. Bordes and B.van Eijk , (in preparation)
[13] G.Schuler Nucl. Phys. B229 [1988] 21

W, Z AND JETS

Jet Physics with the UA2 Detector

The UA2 Collaboration
Bern - Cambridge - CERN - Dortmund - Heidelberg - Melbourne
Milano - Orsay (LAL) - Pavia - Perugia - Pisa - Saclay (CEN)

Presented by
Patrizia Cenci
INFN Sezione di Perugia - Perugia - Italy

Abstract

In this paper we present results on jet physics obtained with the UA2 detector at the CERN $\bar{p}p$ Collider, using data taken in the 1988 and 1989 runs at 630 GeV and corresponding to an integrated luminosity of 7.8 pb^{-1}. The single inclusive jet cross-section has been measured and compared to the absolute prediction of leading order QCD. A study of multi-jet events has been done. Comparison with leading order QCD have been perfomed on four–jet and five–jet event samples. A search for additional production mechanisms of four–jet events has been performed. In all cases QCD has been found to describe well the data.

1 Introduction

Jet physics has become an important field of study at hadron colliders since the earlier observations of two–jet production dominance [1] in high transverse energy events at the CERN $\bar{p}p$ Collider. The dynamics of the jet production processes, the inclusive cross–section and the parton fragmentation properties have been extensively studied and found to be in good agreement with perturbative QCD predictions.

In this paper we report results on the measurement of the inclusive jet cross–section (Section 3) and on the study of events with at least four high transverse momentum (p_T) jets in the final state (Section 4) from a data sample collected during the 1988–89 Collider running period ($\sqrt{s}$=630 GeV) corresponding to an integrated luminosity of 7.8 pb^{-1}. The following section briefly describes the detector elements relevant to jet studies and jet identification criteria.

2 The UA2 Detector

The UA2 detector has been substantially upgraded [2] between 1985 and 1987 to improve the calorimeter hermeticity and the electron identification.

Jet identification and energy measurement are provided by a lead– and iron–scintillator calorimeter divided into a central part (CC) within the range $|\eta| < 1$, and two end cap regions (EC) reaching $|\eta| = 3$. Both regions have full azimuthal coverage and a high granularity structure segmented into 624 cells pointing towards the interaction region. The cell size is $\Delta\eta \cdot \Delta\phi = 0.2 \cdot 15°$ in the range $|\eta| < 2.2$ while the two cells closest to the beam axis ($2.2 < |\eta| < 2.5$ and $2.5 < |\eta| < 3.0$) cover 30° in azimuth. Each cell is divided into an electromagnetic section (EM) and an hadronic section. The EM section has a total thickness of 17 radiation lenghts (x_0) in the CC and between 17.1 and 24.4 x_0 in the EC depending on the polar angle; the hadronic section is 4 absorption lenghts (λ) deep in the CC and 6.5 λ deep in the EC. Typical resolutions are $\sigma(E)/E \sim 17\%/\sqrt{E}$ for the EM compartments and $\sigma(E)/E \sim 32\% \cdot E^{-1/4}$ for the hadronic ones (E in GeV). The initial calibration of all the cells has been done with e^-, π and μ beams. The calibration stability has been monitored by using ^{60}Co sources, by measuring the energy distribution in minimum bias events and by recalibrating individual modules on a test beam. In this way we are able to achieve a systematic uncertainty on the energy scale of $\leq 1\%$ for the EM compartments and of $\leq 2\%$ for the hadronic ones.

The central detector is situated inside the calorimeter and consists of several cylindrical sub–detectors providing charged particle tracking and electron identification. A more complete description can be found in ref. [3].

Jets are defined through their energy deposition pattern in the calorimeter by joining into clusters all the cells with an energy above 400 MeV and sharing a common edge. Due to the high trigger rate no track reconstruction is performed in jet events, hence the

position of the interaction vertex is measured by two time–of–flight hodoscopes covering the range $2.3 < |\eta| < 4.1$ on each side of the beam crossing point.

3 Inclusive Jet Cross Section

In order to take into account final state gluon radiation, in this analysis jets are defined by merging clusters within a cone of radius $r = \sqrt{\Delta\phi^2 + \Delta\eta^2} = 1.3$ around the highest energy one. The jet axis is given by the direction between the interaction vertex and the energy centroid of all the clusters in the cone and the jet transverse energy is the scalar sum of all their transverse energies.

The results [4] for the acceptance–corrected inclusive jet cross section $d^2\sigma/dp_T\,d\eta$ are shown in Fig. 1, where the data have been subdivided into five equidistant $|\eta|$ intervals. The error bars include statistic and p_T–dependent systematic errors added in quadrature which are dominated by the uncertainties on the underlying event contribution. The overall systematic uncertainty is 32%, with contributions, added in quadrature, from the limited knowledge of the fragmentation processes (25%), the analysis parameters (15%), the absolute calorimeter energy scale (11%) and the luminosity measurement (5%). These results are compared to a leading–order calculation, where the momentum transfer scale is chosen as $Q^2 = (p_T/2)^2$ and the structure functions of ref. [5] are used. Good agreement is observed between data and prediction, especially for central values of pseudorapidity. The same conclusion is reached using other parametrizations of the parton distribution functions.

A hypothetical superstrong interaction binding preons inside quarks is expected to appear as a deviation from pure QCD behavior at large p_T. In the model presented in ref. [6] the strength of the new interaction is described through a characteristic energy scale Λ_C. Finite values of Λ_C would produce an excess of events at large p_T with respect to the standard QCD predictions corresponding to $\Lambda_C = \infty$. Such an effect has been searched for in the CC data which extend to the highest p_T values. The calculations have been normalized to the data between 69 and 79 GeV, where only QCD is expected to contribute to the cross section. Different structure function sets have been used, and the Q^2 scale has been varied in the range $p_T^2/12 < Q^2 < p_T^2/2$, compatible with the overall scale uncertainty on the data. Only the choice yielding the most pessimistic bound on Λ_C has been retained, which corresponds to the structure functions of ref. [5] and $Q^2 = p_T^2/4$.

The results of the fit are shown in Fig. 2, where the ratio between the data and the QCD calculation is compared to the predicted behaviour for different values of Λ_C. The best fit is obtained for a pure QCD behavior ($\Lambda_C = \infty$). A lower limit of 845 GeV for Λ_c is obtained at 95% CL, including statistical and p_T–dependent systematic errors into the comparison. Distortions to the cross section shape due to systematic effects have been investigated. The most important one is the calorimeter energy scale uncertainty which reduces the 95% CL limit to the final result $\Lambda_C > 825$ GeV.

4 Multijet Physics

Multijet events are selected by defining as a jet any cluster with transverse energy above 15 GeV and within the pseudorapidity range $|\eta| < 2$. For each event the jets are sorted in order of decreasing transverse energy and exclusive topologies are then defined. In addition to the kinematical cuts, a further selection is required to reduce a luminosity dependent background characterized by events with large unclustered energy depositions and cluster radii, mainly due to multiple $\overline{p}p$ collisions within the same bunch crossing.

A sample of 9947 four–jet, 281 five–jet and 7 six–jet events is obtained. Their distributions have been compared to QCD predictions obtained by implementing the matrix element calculations of Kunszt and Stirling (KS) [7] and of Kuijf and Berends (KB) [8] into a Monte Carlo simulation. The KS calculation provides matrix elements up to four–jet production, and the KB one extends the exact calculation up to five–jet production. All the calculations have been performed using the structure functions of ref. [9] with Λ_{QCD} = 200 MeV and a Q^2 scale given by the maximum transverse energy among the final state partons. To avoid the divergences due to the bremsstrahlung nature of gluon radiation only final state partons well separated in phase–space and above a transverse energy threshold are considered. The Field–Feynman fragmentation model [10], modified in order to allow gluon radiation from the original partons, has been used to describe hadronization. To obtain a Monte Carlo sample directly comparable to the data a full simulation of the UA2 calorimeter acceptance has been performed including the trigger algorithms used for event selection, the detector response as measured from test beam data and superimposing real minimum bias events to simulate the underlying energy deposition.

In Fig. 3 the inclusive p_T spectra, not corrected for acceptance, for four, five and six–jet events are compared with leading order QCD predictions. The data points represent the observed spectra, the solid curve represent KB calculations for four and five–jet production, the dashed curve is the KS calculation for four–jet events. The errors include statistical and p_T–dependent systematic uncertainties (23%, due to the calorimeter energy scale uncertainty) added in quadrature. The overall p_T independent systematic uncertainty on the p_T spectrum is 51%, with contributions, added in quadrature, from the limited knowledge of the calorimeter response to low energy hadrons (28%), of the underlying event structure (20%) and of the fragmentation processes (40%). The observed shapes are well reproduced by the QCD calculations.

Fig. 4 compares four–jet data and predictions for two distributions: (a) the *sphericity* distribution, which describes the general topology of an event; (b) the invariant mass M_{4j} distribution of the four–jet system. No significant deviation from the QCD calculations are observed.

An additional mechanism for multijet production in which multiple independent hard parton interactions occur within the same $\overline{p}p$ collision has also been considered [12]. Due to the dominance of the two–jet cross–section these multiparton interactions should be

observed in four–jet final state (Double Parton Scattering DPS). The good description of the four–jet data sample in term of standard QCD double bremsstrahlung process suggests that very little room is left for other multijet production mechanisms. The main feature of DPS events is the presence of two jet pairs, each with jets balanced in transverse momentum and back–to–back in azimuth. These considerations lead to the definition of a variable S particulary sensitive to the presence of jet pairs in this configuration:

$$S^2 = \frac{1}{2} \cdot min\left[\frac{|\vec{p}_{t,i} + \vec{p}_{t,j}|^2}{|\vec{p}_{t,i}| + |\vec{p}_{t,j}|} + \frac{|\vec{p}_{t,k} + \vec{p}_{t,l}|^2}{|\vec{p}_{t,k}| + |\vec{p}_{t,l}|}\right]$$

where minimization is performed over the three possible jet pairs. For a DPS event S should be close to zero, because of the transverse momentum balance of the two jet pairs. A modified version of the PYTHIA generator [11], in which two hard scattering are forced to occur within the same $\overline{p}p$ collision, has been used to simulate DPS events. The acceptance of the calorimeter and the details of its response have also been simulated. Fig. 5 shows the $Log(S)$ distributions for the data, together with QCD and DPS Monte Carlo predictions: to emphasize the different shapes all the distributions have been normalized to the same area and $Log(S)$ rather than S itself has been used.

The DPS fraction of the four–jet sample is determined in the following way. Monte Carlo simulation of QCD and DPS events are used to predict the shapes of the $Log(S)$ distributions.These distributions are then weighted with factors N_{QCD} and N_{DPS}, whose sum is kept equal to the observed number of four–jet events, and then compared to the measured distribution using a minimum χ^2 method. The reliability of this fitting procedure has been verified using Monte Carlo event samples consisting of known amounts of DPS and QCD events. The same Monte Carlo study ensures that $Log(S)$ is the most sensitive variable for detecting a possible DPS signal. The best fit, including DPS and QCD contributions, is compared to the data in Fig. 6.

The number of events found by the fit has been converted into a cross–section after correcting for efficiency factors and systematic effects associated with the detector modelling. Distortions of the $Log(S)$ distribution shape due to systematic effects have been studied by varying the calorimeter response, the energy scale, the simulation of the underlying event and by repeating the fit. They are found to vary the final result by 14.4%. The overall efficiency is $18.8 \pm 5.5\%$ with contributions from the combined efficiency of the analysis cuts, the trigger efficiency and the geometrical acceptance for DPS events. A non–negligible source of background to DPS events comes from multiple $\overline{p}p$ interactions within the same bunch crossing. At present Collider luminosities the average probability for having two interactions in the same bunch crossing is $\sim$ 10%. The class of events where both interactions result into two–jet pairs is indistinguishable from the DPS signal and this contribution has been subtracted in the cross–section calculation. Using the total integrated luminosity of 7.8 pb^{-1} the value $\sigma_{DPS} = 0.49 \pm 0.20\ nb$ is obtained for the DPS production cross–section, which gives the 95% CL limit $\sigma_{DPS} < 0.82\ nb$.

References

[1] UA2 Collaboration, M. Banner *et al.*, Phys.Lett. **B 118** (1982) 203;
UA1 Collaboration, G. Arnison *et al.*, Phys. Lett. **B 123** (1983) 115;

[2] UA2 Collaboration, C. N. Booth, Proc. 6th Topical Workshop on $\bar{p}p$ Collider Physics (Aachen, 1986), eds. K. Eggert et al. (World Scientific, Singapore, 1987) p. 381;

[3] M. Primavera (UA2 Collaboration), these Proceedings;

[4] UA2 Collaboration, J. Alitti *et al.*, Phys. Lett. **B 257** (1991) 232;

[5] E. Eichten *et al.*, Rev. Mod. Phys. **56** (1984) 579; Rev. Mod. Phys. **58** (1986) 1065(E);

[6] E. Eichten *et al.*, Phys. Rev. Lett. **50** (1983) 811;

[7] Z. Kunszt and W. J. Stirling, Phys. Lett. **B 171** (1986) 307;

[8] H. Kuijf *et al.*, Nucl. Phys. **B 333** (1990) 120; Phys. Lett. **B 232** (1990) 266;

[9] D. W. Duke and J. F. Owens, Phys. Rev. **D 30** (1984) 49;

[10] R. D. Field and R. P. Feynman, Nucl. Phys. **B 136** (1978) 1;

[11] H.U Bengtsson, T. Sjostrand, PYTHIA, Comput. Phys. Comm. **46** (1987) 43;

[12] UA2 Collaboration, J. Alitti *et al.*, 'A study of multi-jet events ...', to be submitted to Phys. Lett. **B**.

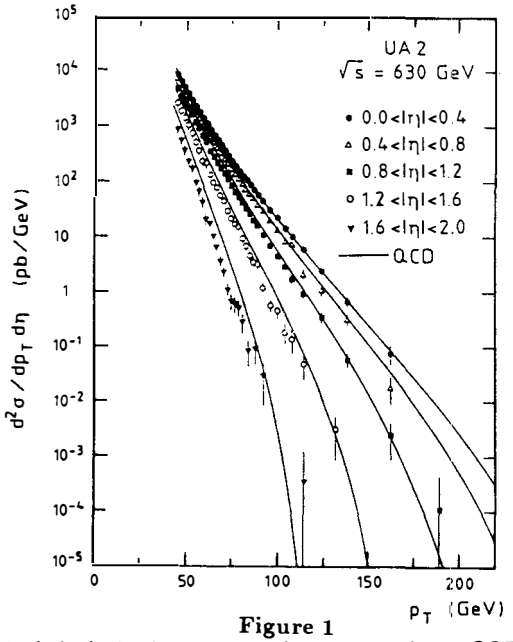

Figure 1
The single inclusive jet cross-section compared to a QCD prediction.

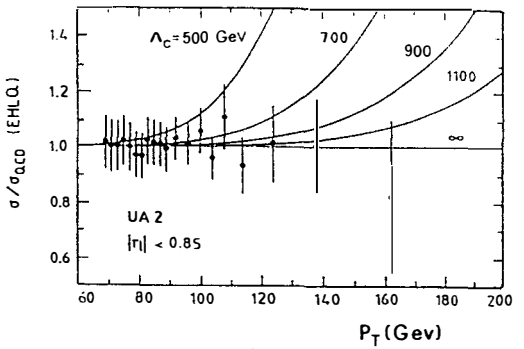

Figure 2
Inclusive jet cross-section data and predictions for different values of Λ_C normalized to the theoretical calculations.

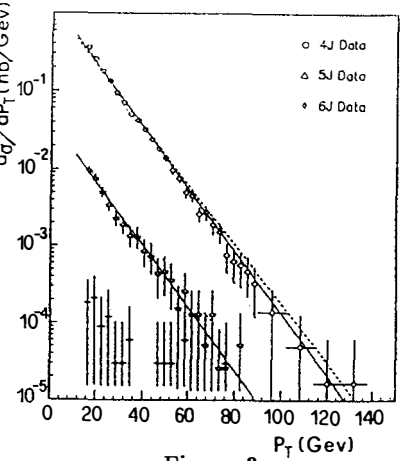

Figure 3
Inclusive p_T spectra for multijet events compared to QCD predictions.

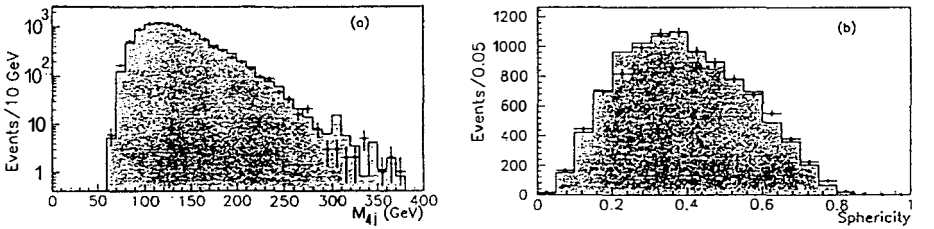

Figure 4
Sphericity (a) and invariant mass (b) distributions for four-jet data compared to QCD predictions.

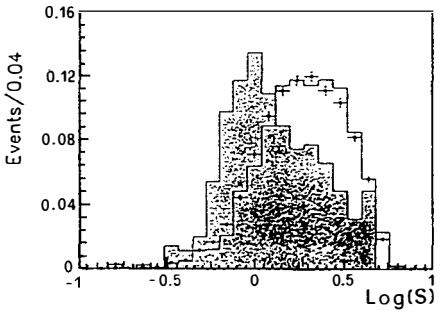

Figure 5
Log(S) distribution for four-jet data compared to predictions.

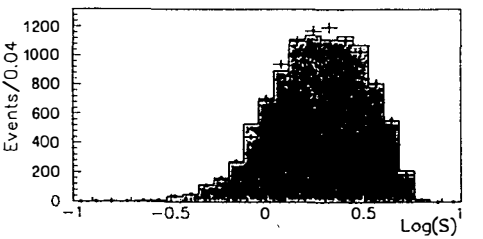

Figure 6
Best fit to the Log(S) distribution.

Jet Results from CDF

Naor Wainer
Fermilab
(Representing the CDF Collaboration)

Abstract

Recent results from CDF in jet physics are presented. Tests of leading order and next to leading order QCD are performed by measuring the dijet invariant mass spectrum, jet shapes and three jet events. Tests the leading logarithm approximation in QCD are made by comparing the highest energy events at CDF with the Herwig Monte Carlo.

Introduction

CDF has collected approximately 4.5 pb^{-1} of integrated luminosity at $\sqrt{s}$ = 1800 GeV of $p\bar{p}$ collisions. This high statistics sample allows more accurate tests of QCD. Fortunately, significant theoretical progress is being made in parallel, either through calculating hard scattering at Next to Leading Order (NLO), or by modeling higher order contributions in the Leading Log Approximation through shower Monte Carlos.

In this paper comparisons of data and QCD calculations are done in three different levels:

1. Tests of Leading Order (LO) QCD. When a higher order calculation is not available, the data was compared with LO QCD. This allows us to understand which features of the data are not well described by theory, and need higher order calculations. In this note the differential cross section $d\sigma/dM_{JJ}$ is measured where M_{JJ} is the invariant mass of a 2 jet system. Also 3-jet distributions are compared with α_s^3 tree level calculations.

2. Tests of Next to Leading Order QCD. In this note we describe a measurement of Jet Shape, a process which is not existent in LO calculations and is obtained when calculating in NLO $d\sigma/dE_t$.

3. Tests of the Leading Log approximation as implemented by the Monte Carlo program Herwig[1]. A comparison is performed between this Monte Carlo and the most energetic events in CDF (measured by the total transverse energy in the calorimeter).

Data Selection

The CDF detector has been described in detail elsewhere [2]. For these measurements, jets in the central, wall and plug calorimeter were used(See fig. 1). For the jet shapes measurement three dimensional tracks in the central tracking chamber were used.

For the dijet analysis, online triggers in which a single jet is required to have transverse energy in the calorimeter above specific threshold were used. The minimum energy required were 20, 40 and 60 GeV. The 20 and 40 GeV triggers were prescaled, in order to maintain a manageable trigger rate.

The jet shape analysis was done using only the jet trigger data which required 60 GeV or more transverse energy. The jets were required to be in the central calorimeter.

The 3-jet analysis and the comparison of high energy events with Herwig were performed with data from a total transverse energy trigger. The trigger required the total transverse energy in the calorimeter to be greater than 120 GeV.

Jet Algorithm

In order to compare theory with data a common jet definition has to be adopted both by experimentalists and theoreticians. A serious attempt to reach a standard is the Snowmass accord [3], in which a common definition was specified. One of the main outcomes is that a jet should be defined by its transverse energy (E_t) and cone size (R).

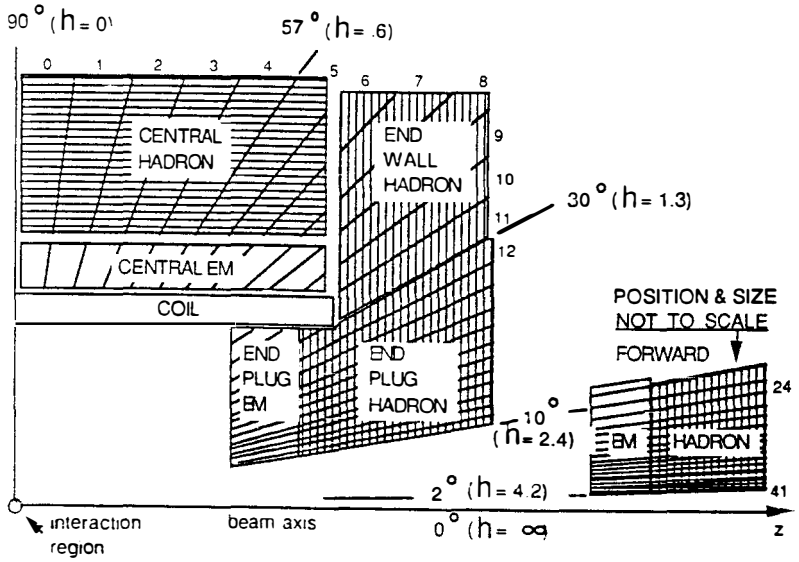

Figure 1: The CDF Calorimeter.

The cone size R is defined as $R = \sqrt{\Delta\eta^2 + \Delta\phi^2}$ where $\eta = \log\cot(\theta/2)$, ϕ is the azimuthal angle difference and θ is the polar angle difference between a tower/particle/parton and the jet axis. One then defines:

$$E_t^{jet} = \sum_{R_i \le R_0} E_{ti} \qquad \eta^{jet} = \frac{1}{E_t^{jet}} \sum_{R_i \le R_0} E_{ti}\eta_i \qquad \phi^{jet} = \frac{1}{E_t^{jet}} \sum_{R_i \le R_0} E_{ti}\phi_i$$

Where, again, the sums can be over partons, particles or towers within R_0.

Clearly, the chosen cone size of the jet does not affect LO QCD calculations, but it is important for higher order calculations, where more than one parton can be within the cone.

In order to avoid biases, we do not correct for the two processes that change slightly the jet energy in the cone: particles that due to fluctuations or magnetic field effects slipped out of the cone, and underlying event particles, created by soft processes among the debris of the nucleons, that may fall into the cone. Although predictions of the magnitude of the Jet E_t change due to these processes are model dependent, they tend to be small and negligible at high energies and large cone sizes.

Two Jet Invariant Mass

We measured the dijet invariant mass spectrum. In the center of mass system, the two jets are back to back and, after integration over the azimuthal angle ϕ, the cross section is dependent on the dijet invariant mass M_{JJ} and the azimuthal angle θ.

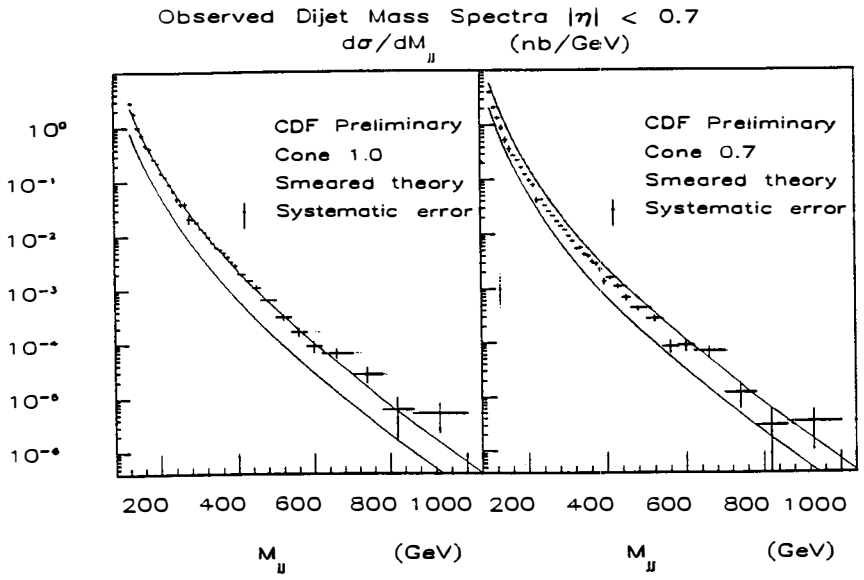

Figure 2: The dijet mass distribution.

As a NLO calculation is not available for M_{JJ}, the data will be compared to the LO QCD calculation. As described above, no out of cone or underlying event correction are applied. The mass is calculated in the usual way $M_{JJ} = \sqrt{(E_1 + E_2)^2 - (\vec{P}_1 + \vec{P}_2)^2}$, where E_j is the energy of jet j, obtained by summing tower energies, and $\vec{P}_j$ is the momentum of the jet, calculated by assigning a vector to each tower and then performing a vector sum within the cone.

Instead of correcting the data for detector response, the theory was smeared, i.e. corrected for the combined effect of the detector response with a rapidly falling M_{JJ} spectrum. The corrections were estimated with the Herwig Monte Carlo and a detector simulation.

In Fig 2 measurements of the cross section $d\sigma/dM_{JJ}$ are shown for 2 different cone sizes, $R = 1$, and $R = 0.7$, integrated in the pseudorapidity range $|\eta| \leq 0.7$. The data are represented by crosses, including systematic errors. The band defined by the two curves represent the theoretical uncertainty, obtained by varying the scale Q^2 within $0.5P_t^2 < Q^2 < 2P_t^2$ and using the following parametrizations of structure functions: EHLQ [4], DO [5], DFLM [6], HMRS [7], and MT [8]. These are absolute scale comparisons.

In order to test the agreement between data and theory on the shape of the distributions, data and theory were normalized. Table 1 shows χ^2 confidence levels for fits using different structure functions, scales and cone sizes. The fitting procedure took into account all system-

Confidence Levels (%)						
$Q^2/P_t^2 =$	1	2	$\frac{1}{2}$	1	2	$\frac{1}{2}$
Structure Functions	Cone 1.0			Cone 0.7		
DFLM101	48	46	47	1	1	< 1
DFLM173	54	52	54	1	1	2
DFLM250	50	52	53	2	2	2
DO1	51	51	47	2	1	< 1
DO2	49	48	48	2	2	2
EHLQ1	40	38	40	< 1	< 1	< 1
EHLQ2	24	21	25	< 1	< 1	< 1
HMRSB	46	48	47	2	1	1
HMRSE	46	46	39	3	4	4
MT155	57	58	54	3	3	2
MT187	56	56	56	2	2	1
MT191	66	65	64	5	6	6
MT212	62	61	59	3	4	3

Table 1: L0 QCD vs. M_{JJ} spectrum χ^2 confidence levels in percent.

atic uncertainties. Basically the main difference found is the dependence on the jet cone size. There is not much difference between various structure function parametrizations and energy scales. The cone 1.0 distribution is steeper than the cone 0.7 one. The data with cone of 1.0 agrees well with theory while a cone of 0.7 is disfavored. This effect can occur if higher order diagrams change the energy within the smaller cone size, mainly through bremsstrahlung out of the cone. Another possible effect will be initial state radiation falling within the larger jet cone, increasing its energy. It will be interesting to see if NLO calculations can describe this effect.

Three Jet Events

Another method of testing NLO QCD calculations is to study 3-jet distributions. In this case only tree diagrams were evaluated. The main motivation is the that the calculation shows different angular and energy distributions for the different subprocesses, e.g. $gg \rightarrow ggg$ is more singular than $q\bar{q} \rightarrow ggg$. Based on these distributions, it is interesting to measure the amount of $q\bar{q}$ initiated processes in our 3-jet events sample.

The conventions adopted here are relatively simple: the initial partons are labeled 1 and 2 and the outgoing partons (jets) are labeled 3, 4 and 5, ordered by energy. Two important kinematical angles are defined in the CM frame, namely θ, the angle between jet 3 and the beam axis, and the angle ψ defined as the angle between the plane defined by the 3-jet system (3,4 and 5) and the plane defined by the beam and the hardest jet (1,2 and 3). The scaled energy variables are defined $x_i = 2E_i/M_{3J}$, where M_{3J} is the invariant mass of the 3-jet system.

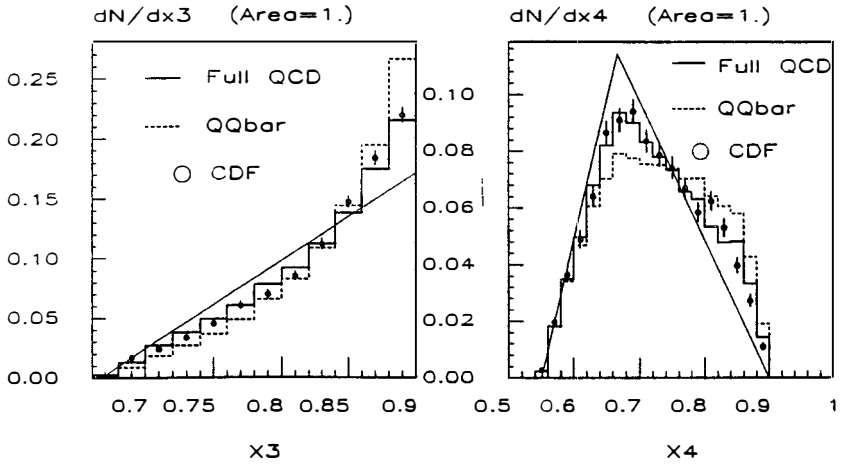

Figure 3: Jet energy fractions in three jet events.

The selection of events reflects the needs of having both well separated jets in the detector and events kinematically away from infrared and collinear divergencies. Events are selected by requiring at least 3 jets with uncorrected $E_t \geq 10$ GeV in the region $|\eta| < 3.5$, separated by $\Delta R \geq 0.85$. Additional cuts avoid trigger biases and divergencies: $M_{3J} > 250$ GeV, $|\cos(\theta)| < 0.6$, $30^0 < \psi < 150^0$ and $x_1 < 0.9$.

The theoretical distributions [10] were obtained by generating 3 partons in the final state away from the infrared or collinear divergencies (cuts similar to those applied on data are applied at parton level) and then fragmenting the partons and processing the event through a detector simulation. Identical cuts as in the data are applied to the generated sample.

The measured cross section is 1.2 ± 0.6 to be compared with the one obtained from theory, 1.8 ± 0.9. The main uncertainty in the data is energy scale and in the theory is structure functions and renormalization scale used in α_s evaluation.

In Fig. 3 the distributions for x_3 and x_4 are shown. The histograms represent full QCD and a QCD calculation involving only $q\bar{q}$ in the initial state. The linear curves are the phase space predictions. The data clearly prefers the full QCD prediction. The same is observed for the angular distributions, shown in fig. 4. The full QCD distribution is more singular than the $q\bar{q}$ originated distribution, as it shows more prominent peaks when $\cos\theta$ approaches 1, and when ψ approaches 0 or 180 degrees.

The 4 distributions of figs. 3,4 are used to estimate the fraction of $q\bar{q}$ in the initial state. The result of the combined fit is $3^{+12}_{-3}\%$, to be compared to $11 \pm 4\%$, the theoretical prediction.

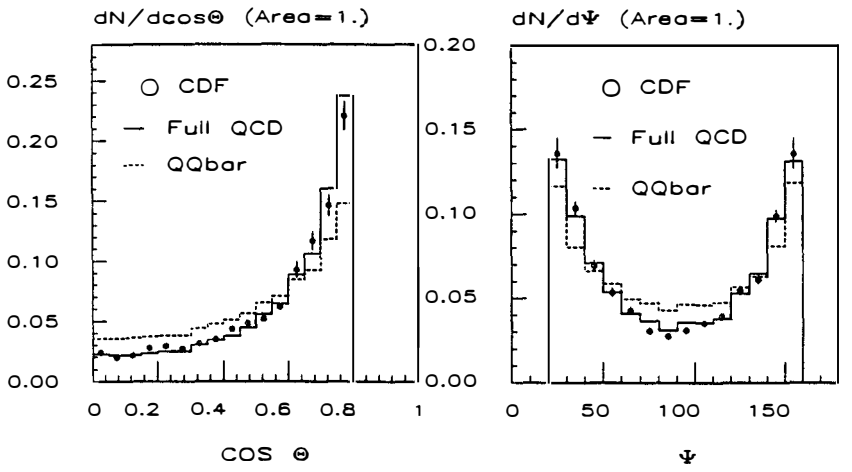

Figure 4: Angular distributions in three jet events.

Jet Shapes

Within the framework of NLO QCD calculations it is possible to obtain more than one parton inside the cone. The jet energy is shared between these two partons. This effect produces an energy distribution inside the jet cone. At high enough energies, where fragmentation effects become negligible, this distribution should be measurable.

To experimentally study the jet shapes, it was decided to use tracks. Tracks have a better spatial resolution than calorimeter towers, which have spatial resolutions on the order of their size. The use of tracks also avoids dealing with calorimeter non-linearities which are large in the P_t range of interest.

To measure the jet shape we define the average P_t density:

$$\rho(r) = \frac{1}{N} \sum_{jets} \frac{1}{P_t^{jet}(R_0)} \sum_{towers} dP_t$$

where dP_t is the the P_t measured in the annular domain between r and $r + dr$. By definition $\int_0^{R_0} \rho(r)dr = 1$, so that P_t^{jet} is also calculated with the tracks. The integral shape variable $\Psi(r) = \int_0^r \rho(r')dr'$ is used to compare data with theory.

In fig. 5 we show both the definition of the variables and the comparison between data and theory. The theory points were calculated for 100 Gev E_t jets. The jets in the data were required to be central, namely $|\eta| \leq 0.7$, and to pass the cut $95 < E_t < 120$ GeV, when the jet E_t was corrected for detector effects. The shape distribution was corrected for tracking

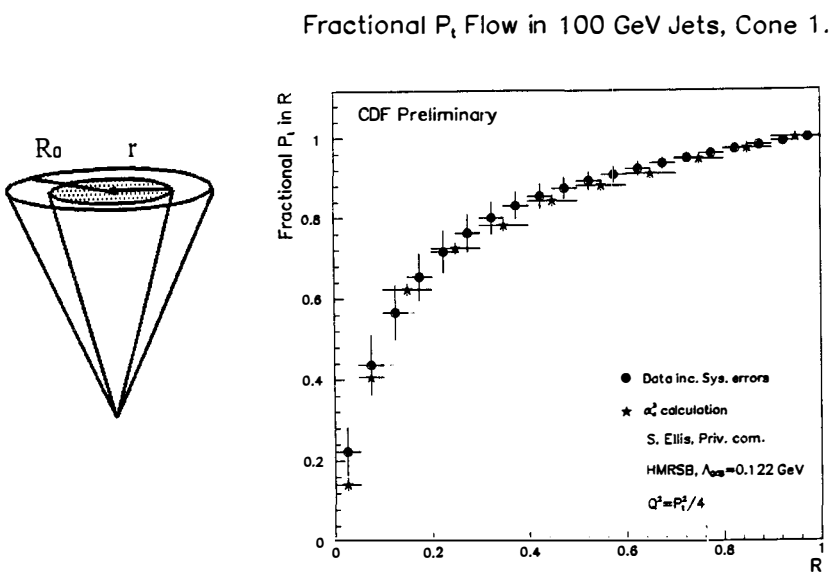

Figure 5: Variables and the integral shape of 100 GeV jets.

efficiency effects.

The data show a surprisingly good agreement with theory [9] for a cone $R = 1.0$. The agreement is not as good for other cone sizes (not shown). This effect is under study, as well as the evolution of the shape with jet E_t.

High Total Transverse Energy Events

Events with high total transverse energy ($\sum E_t$) are selected and compared to the parton shower Monte Carlo Herwig version 4.3 with DO1 structure function and $\Lambda_{QCD} = 200$ MeV. The main motivation was to try to detect deviations from QCD in this new energy regime. As a byproduct, this analysis serves as a test of the leading log approximation in this energy regime.

The events were selected by requiring uncorrected $\sum E_t > 400$ GeV, where the sum is over calorimeter towers with $E_t > 500$ MeV. Cosmic rays and events with more than one vertex are rejected.

In Fig 6 the total transverse energy and the missing transverse energy (defined by summing vectorially the E_t of the towers) are shown. The Herwig [1] Monte Carlo describe relatively well the distributions.

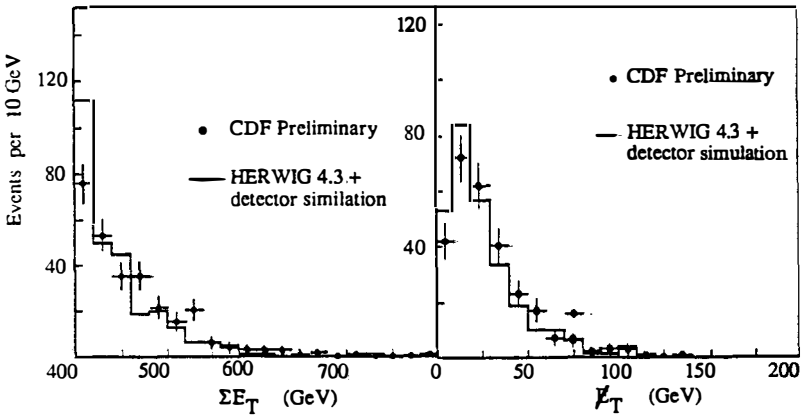

Figure 6: Total and Missing Transverse Energy for the high E_t data sample.

To study how well the Monte Carlo describe the data we study both intra-jet and inter-jet variables. As an example of inter-jet properties of the event, the jet multiplicity, as a function of a jet P_t cut is plotted in fig. 7, for $|\eta| < 2$. The Monte Carlo describe well the data, including the intermediate P_t range (not shown), showing that the leading log approximation describes well the additional creation of soft jets, expected at higher orders.

To probe how well the intra-jet properties are calculate the E_t flow about the Jet axis is calculated. In fig. 7 the E_t flow in ϕ-space is also shown for jets in different P_t ranges. The agreement is very good. The different curves represent different Monte Carlo samples which have the same sizes as the data, and are an estimate of the statistical error in these plots. Similar agreement is found also in η space and for the intermediate P_t range.

Summary

We are probing QCD in all possible levels. A good description of the two jet invariant mass is obtained when one compare and LO QCD calculation with data consisting of cone 1.0 jets. The same cone size is used to compare the shape of 100 GeV jets with a NLO calculations and , again, good agreement is found. Using tree level 3-jet matrix elements we showed that full QCD is needed to describe the data, and estimated the amount of $q\bar{q}$ initiated processes in the data. At the highest energy regime, our events are well described by the Herwig Monte Carlo.

References

[1] Marchesini and Webber, Nucl. Phys. **B310** 1988 461.

[2] Abe et al., CDF Collab., Nucl. Instr. Meth. **A271** (1988) 387.

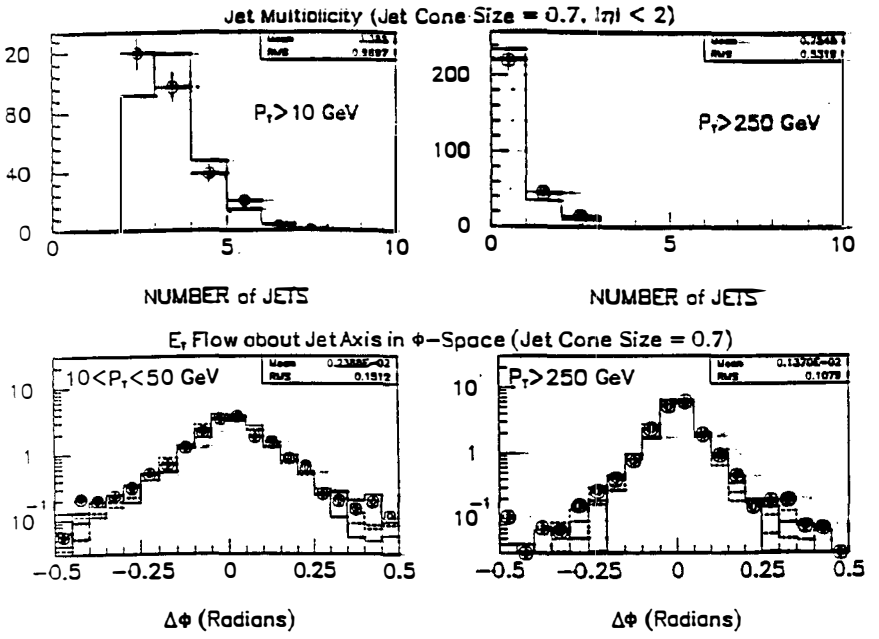

Figure 7: Jet multiplicity and ϕ jet shape in the high Et data sample for different P_t's.

[3] Huth et al., Fermilab-CONF-90/249-E and Proceed. of the Snowmass Summer Study on High Energy Physics (1990).

[4] Eichten et al., Rev. Mod. Phys. **56** (1984) 579.

[5] Duke and Owens, Phys. Rev. **D30** (1984) 49.

[6] Diemoz et al., Z Phys. **C39** (1988) 21.

[7] Harriman et al., RAL preprint 90-007 (1990).

[8] Tung and Morfin, Fermilab-PUB-90/74, IIT-PUB-90/11 (1990).

[9] S.D. Ellis, private communication, based on Ellis, Kunszt and Soper, Phys. Rev. Lett. **64** (1990) 2121.

[10] Kunszt and Pietarinen, Nucl. Phys. **B164** (1980) 45; Gottschalk and Sivers, Phys. Rev. **D21** (1980) 102; Berends et al., Phys. Lett. 124 (1981) 124.

RECENT RESULTS ON W, Z PRODUCTION AT $\sqrt{s} = 1.8$ TeV

The CDF Collaboration

Presented by Johnny S.T. Ng
Harvard University, High Energy Physics Laboratory
42 Oxford St., Cambridge, MA. 02138, U.S.A.

Abstract

Some recent results on W, Z production from CDF are presented. We have measured the W, Z production differential cross section as a function of transverse momentum, using data from $\bar{p}p$ collisions at $\sqrt{s} = 1.8$ TeV. The results agree with a next-to-leading order QCD calculation over the range $0 < p_T < 180\,\mathrm{GeV}/c$ available from this data sample. We have also measured the charge asymmetry in the W lepton rapidity. Comparison with Standard Model prediction shows good agreement for most available parametrizations of parton distributions.

1 Introduction

A large number of W and Z events were collected by the CDF experiment during the 1988-89 run. These events have a clean signature among QCD jet production processes typical at high energy hadron colliders. The measured quantities can also be easily interpreted. In this paper, we present some results on the W and Z gauge boson production properties.[1]

The boson transverse momentum (p_T) distribution provides a detailed test of Standard Model predictions. In QCD, the W, Z p_T results from the the associated production of quarks or gluons with the gauge boson. At high p_T, $\mathcal{O}(\alpha_s^2)$ QCD calculation of the boson $d\sigma/dp_T$ exists.[2] At low p_T, however, soft gluon resummation procedures are needed to handle large logarithmic terms. Recently, the prediction for the low p_T region has been matched to the $\mathcal{O}(\alpha_s^2)$ prediction for the high p_T region, to obtain a result valid to next-to-leading order at all p_T.[3]

The gauge boson longitudinal momentum, on the other hand, is sensitive to the proton structure function.[4] At $\sqrt{s}$ = 1.8 TeV, W production is dominated by valence-valence and valence-sea quark-antiquark interactions. Because u quarks have a harder momentum distribution than d quarks, the W^+ is produced preferentially in the proton direction. Conversely, the W^- is produced preferentially in the anti-proton direction. Thus, the charge asymmetry in the W rapidity distribution can be used to probe the parton distributions at the small x and high Q^2 where the bosons are produced.

2 The Data Sample

The W and Z bosons are observed in CDF in their leptonic decays. These events are characterized by the presence of a high transverse momentum charged lepton. Electrons can be identified in the electromagnetic calorimeters covering three pseudo-rapidity regions: the central region ($|\eta| < 1.1$), the plug region ($1.1 < |\eta| < 2.4$), and the forward region ($2.4 < |\eta| < 4.2$). Muons are detected in drift chambers located behind the central calorimeters in the region $|\eta| < 0.6$. The central tracking chamber measures charged particle momentum in a 1.4 Tesla magnetic field. It is important for both electron and muon identifications.

The electron sample consists of events passing an electron trigger. The central electron must be isolated, with a transverse shower shape and a hadronic energy deposition consistent with a test beam electron. We also require a charge track pointing at the electron cluster, with momentum matching the energy. The muon sample consists of events passing the central muon trigger. The central muon is identified as a track segment in the muon drift chamber matching an extrapolated CTC track. The energy deposited in the calorimeter tower traversed by the muon must be consistent with that for a minimum ionizing particle.

3 The Z $d\sigma/dp_T$ Measurement

The $Z \rightarrow ee$ sample is selected by requiring one well measured, isolated electron with $E_T > 20$ GeV in the central region, and a second isolated electron in the region $|\eta| < 4.2$

with $E_T > 10$ GeV. The $Z \rightarrow \mu\mu$ sample is selected by requiring one muon identified by a muon track segment with $p_T > 20\,\mathrm{GeV}/c$, and a second muon in the region $|\eta| < 1.0$ identified by its minimum ionizing property with $p_T > 10\,\mathrm{GeV}/c$. There are 235 $Z \rightarrow ee$ and 103 $Z \rightarrow \mu\mu$ candidate events with invariant mass in the range 75 to 105 Gev/c^2. The events outside the mass peak is consistent with the Drell-Yan continuum. Residual backgrounds from QCD jet production are negligible.

The muon momentum is determined by the central tracking. The electron energy is measured by the calorimeter, with energy response map and nonlinearity corrections. The electron direction is given by the track in the central region, and the shower position in the plug and forward regions. The Z p_T is the vector sum of the $ee, \mu\mu$ transverse momenta with respect to the beam axis. We correct for the effect of resolution smearing on the shape of the spectrum. A smearing matrix is derived from a Monte Carlo simulation. This matrix describes the probability that a given p_T is measured to have a different value due to resolution smearing. We use the inverse of this matrix to unfold the resolution smearing in the observed p_T spectrum.

The observed Z p_T spectrum, after being corrected for acceptance, resolution smearing, and the Drell-Yan continuum contribution to the Z peak, is normalized to the integrated luminosity and the $Z \rightarrow ee, \mu\mu$ branching ratio. The result is shown in Figure 1. It is compared to a prediction from the next-to-leading order calculation which is plotted as a band, where the width of the band indicates the theoretical uncertainties.[3] There is good agreement.

4 The W $d\sigma/dp_T$ Measurement

The $W \rightarrow e\nu$ sample is selected by requiring one well measured electron with $E_T > 20$ GeV in the central region. The neutrino transverse energy is inferred from the energy imbalance: $\not\!\!E_T = -\sum_i E_T^i \cdot \hat{n}_i$, a vector sum of the transverse energy in calorimeter towers in the region $|\eta| < 3.6$. The magnitude of the missing E_T must be at least 20 GeV. There are 2496 candidate events. QCD backgrounds are determined from studying the rate of isolated and non-isolated electrons in both the background and the W samples. The background shape is determined from data. Remaining backgrounds from $W \rightarrow \tau\nu$ and Zs where one electron escaped detection are estimated using a Monte Carlo simulation.

The $\not\!\!E_T$ is corrected for measurement errors due to cracks in the detector and calorimeter nonlinear response to low energy particles. The electron energy correction is relatively small. The correction to energy measured by the calorimeter, other than the electron energy, is obtained with a Monte Carlo simulation tuned to reproduce the jet fragmentation observed in the data, and the nonlinear energy response studied at the test beam. The $\not\!\!E_T$ correction is checked with a $Z \rightarrow ee$ sample. The energy recoiling against the Z is subjected to the same measurement error as that in W events. The W p_T is the vector sum of the electron transverse momentum and the corrected $\not\!\!\vec{E}_T$.

The observed W p_T spectrum, after being corrected for acceptance and the distortion in the shape of the spectrum due to resolution smearing, is normalized to the integrated

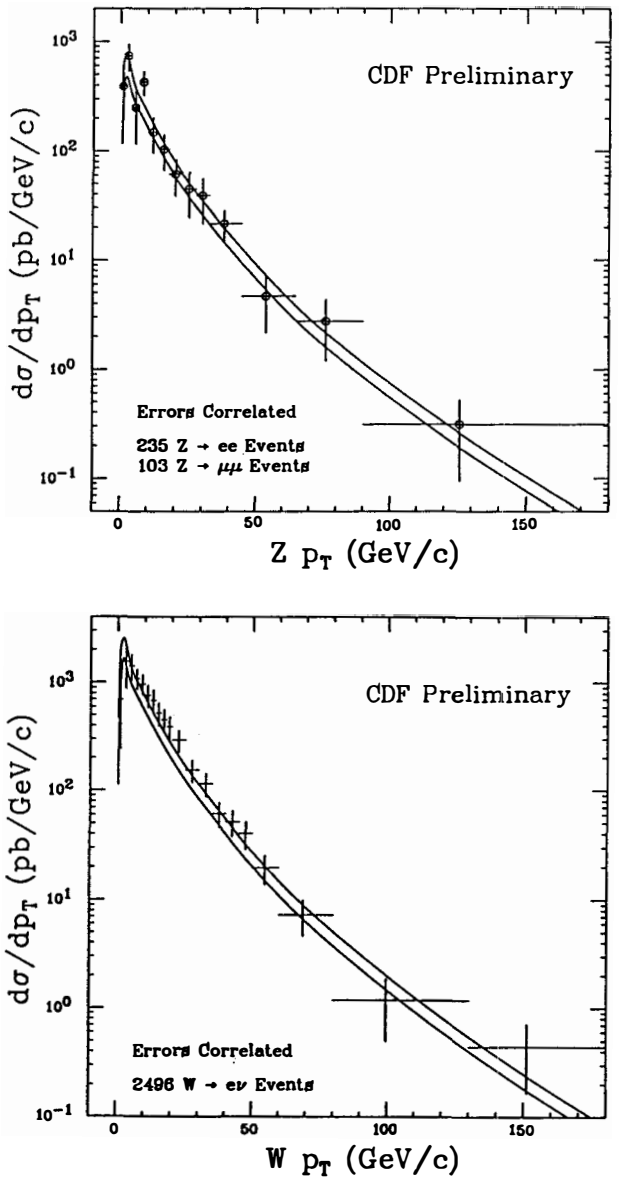

Figure 1: The W,Z p_T distributions corrected for acceptance and resolution smearing. The uncertainties are systematic and statistical combined, and are correlated due to correction for resolution smearing. The QCD prediction is shown a band, the width of the band indicates uncertainty in the calculation.

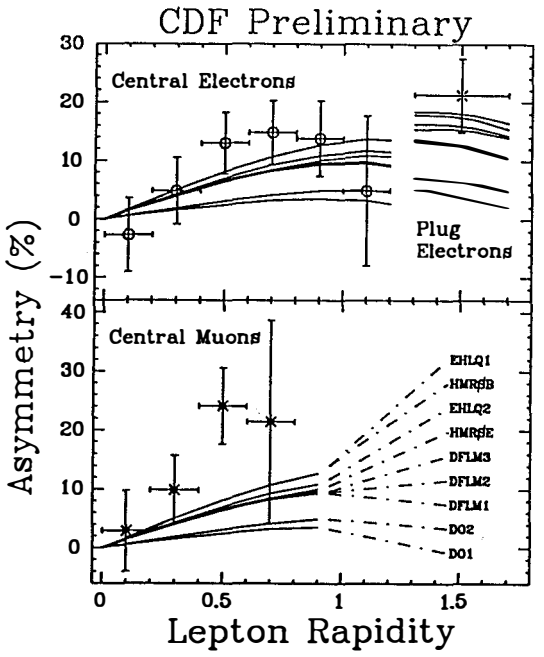

Figure 2: The lepton rapidity charge asymmetries in W decays. The curves are leading order calculations using various parton distributions.

luminosity and the assumed $W \to e\nu$ branching ratio of $\frac{1}{9}$. The result is shown in Figure 1. The comparison with QCD next-to-leading order calculation shows good agreement.

5 The W Decay Lepton Charge Asymmetry

The central electron $W \to e\nu$ events are selected as in the W p_T measurement. The central muon $W \to \mu\nu$ events are selected by requiring a muon with at least 20 GeV/c of transverse momentum, and 20 GeV of $\not\!\!E_T$. The trigger E_T threshold is 23 GeV for plug electrons. So for W events where the electron is in the plug region, we require the electron $E_T > 25$ GeV, and $\not\!\!E_T > 25$ GeV. To reduce backgrounds, we require that there be no jet clusters with observed $E_T > 10$ GeV. There are 1605 central electron, 800 central muon, and 262 plug electron events.

Because only the electron momentum and the $\not\!\!E_T$ are measured, the W rapidity cannot be obtained directly for each event. But the lepton rapidity distribution depends not only on V–A couplings, but also on the W longitudinal motion. Thus, the lepton charge asymmetry as a function of rapidity $A(y) = (\sigma^+(y) - \sigma^-(y))/(\sigma^+(y) + \sigma^-(y))$ can be used to probe the

parton distributions.

Backgrounds from QCD events that dilute the asymmetry, and $W \rightarrow \tau\nu$ sequential decays that enhance the asymmetry affect the observed asymmetry by less than 1%. Charge dependence in the acceptance can also affect the observed asymmetry. But lepton efficiencies are found to be charge independent to the 1% level, and the plug electron charge assignment error is found to be negligible. The observed asymmetries are shown in Figure 2. Also shown as curves are leading-order calculations with various parametrizations of parton distributions.[5] Except for DO1 and DO2, all sets of parton distribution parametrizations are in satisfactory agreement with our data.

6 Conclusion

In summary, the W and Z p_T distributions are in good agreement with QCD predictions. A more quantitative test of QCD require improved measurements and theoretical calculations. We also show that the charge asymmetry in W lepton rapidity distribution is sensitive to the parton distributions.

References

[1] CDF Collaboration,F. Abe *et. al.*,"Measurement of the Z p_T Distribution in $\bar{p}p$ Collisions at $\sqrt{s} = 1.8$ TeV". To be submitted to the Phys. Rev. Lett.
CDF Collaboration,F. Abe *et. al.*,"Measurement of the W p_T Distribution in $\bar{p}p$ Collisions at $\sqrt{s} = 1.8$ TeV". To be submitted to the Phys. Rev. Lett.
CDF Collaboration,F. Abe *et. al.*,"Lepton Asymmetry in W decays from $\bar{p}p$ Collisions at $\sqrt{s} = 1.8$ TeV". To be submitted to the Phys. Rev. Lett.

[2] P .B. Arnold, M. H. Reno, Nucl. Phys. **B319**, (1989)37.

[3] P. B. Arnold and R. P. Kauffman, Nucl. Phys. **B349**, (1991)381.

[4] E. L. Berger *et. al.*, Phys. Rev. **D40**, (1989)83; F.Halzen and S.Keller, in Proceedings of Workshop on Hadron Structure Functions and Parton Distributions, 1990, Fermilab.

[5] P.N. Harriman *et. al.* (HMRS), DTP/90/04 and RAL/90/007 (1990);E. Eichten *et. al.* (EHLQ), Rev. Mod. Phys,**56**,(1984)579; M. Diemoz *et. al.* (DFLM), Z. Phys. **C39**,(1988)21; D. Duke *et. al.* (DO), Phys. Rev. **D30**, (1984)49.

Decay-Lepton Distribution of high q_T Gauge Bosons at NLO in Hadronic Collisions

E. Mirkes

Institut für theoretische Kernphysik
Universität Karlsruhe
Kaiserstr. 12, Postfach 6980
7500 Karlsruhe 1, Germany

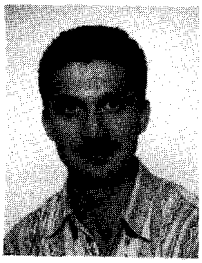

Abstract

We calculate the parity conserving part of the angular distribution for dileptons arising from the decay of high-q_T gauge bosons (W, Z, γ^*) produced in hadronic collisions in next-to-leading (NLO) order of perturbative QCD. It is shown that the general structure of the decay lepton distribution is controlled by nine helicity structure functions. A brief outline is given on the complete $O(\alpha_s^2)$ calculation of these structure functions. We present numerical results for W^+ production at the Tevatron collider including all the subprocesses up to $O(\alpha_s^2)$. The results are given both in the Gottfried-Jackson and the Collins-Soper frame.

Introduction

The measurement of the angular distribution of the lepton pair provides a test of the production mechanism (Drell-Yan process including QCD corrections) and the decay properties of high q_T polarized gauge bosons.

The lowest order QCD processes which contribute to large q_T gauge boson ($V \equiv W^{\pm}, Z, \gamma^*$) production with the subsequent decay into a lepton (or jet) pair are [1]:

$$\begin{array}{llll} q + \bar{q} & \to V + G & \to l_1 + l_2 + G \\ q + G & \to V + q & \to l_1 + l_2 + q \end{array} \tag{1}$$

In this work, we investigate the NLO QCD effects on the angular distribution of the high q_T leptons l_1 and l_2. Recently the complete NLO $O(\alpha_s^2)$ corrections to the production rate of high q_T gauge bosons ($V = W, Z, \gamma^*$) at hadron colliders have been completed [2]. In this paper we extend the calculation of [2] to the polarization of the produced high-q_T gauge bosons at $O(\alpha_s^2)$.

The polarization of the gauge boson determines the angular distribution of the decay leptons (or jets) in the gauge boson rest frame. Since the NLO corrections to the rate are sizeable it is important that the complete NLO $O(\alpha_s^2)$ corrections to the polarization of high-q_T gauge bosons produced in hadronic collisions are available. In addition, the inclusion of the $O(\alpha_s^2)$ corrections reduces the renormalization and factorization scale dependence of the $O(\alpha_s)$ results. First numerical results for the dominant $O(\alpha_s^2)$ contributions are given in [3].

The $O(\alpha_s^2)$ corrections to the angular distribution

High q_T lepton pair production in hadronic collisions proceeds through the following reaction chain:

$$h_1(P_1) + h_2(P_2) \to V(Q) + X \to l_1 + l_2 + X \tag{2}$$

Here h_1 and h_2 are unpolarized hadrons with momenta P_i, V is a gauge bosons ($V = W, Z, \gamma^*$) with transverse momentum q_T which subsequently decays into a lepton pair $l_1 + l_2$.

In the parton model the hadronic cross section is obtained by folding the hard parton level cross section with the respective parton densities. One has

$$\frac{d\sigma^{h_1 h_2}}{dq_T^2\, dy\, d\Omega^*} = \sum_{ab} \int dx_1 dx_2 f_a^{h_1}(x_1, M^2) f_b^{h_2}(x_2, M^2) \frac{s\, d\tilde{\sigma}_{ab}}{dt\, du\, d\Omega^*} \left(x_1 P_1, x_2 P_2, \alpha_s(\mu^2)\right) \tag{3}$$

where one sums over $a, b = q, \bar{q}, G$. $f_a^h(x, M^2)$ is the probability density to find parton a with momentum fraction x in hadron h if it is probed at scale M^2. The parton cross section is denoted by $d\tilde{\sigma}_{ab}$ and s, t and u are the partonic Mandelstam variables. We denote the rapidity of the gauge boson by y. The angles θ and ϕ in $d\Omega^* = d\cos\theta\, d\phi$ are the polar and azimuthal decay angles of the leptons in the gauge boson rest frame with respect to coordinate systems described below.

The partonic cross sections $d\tilde{\sigma}_{ab}$ are proportional to $H_{ab}^{\mu\nu} L_{\mu\nu}$, where $L_{\mu\nu}$ is the well-known lepton tensor and $H_{ab}^{\mu\nu}$ is the hadron tensor at the partonic level for parton a, b in the initial state. The lowest order QCD processes contributing to $H_{ab}^{\mu\nu}$ are given in eq. (1). At $O(\alpha_s^2)$ we have the following tree and loop processes that contribute to high q_T gauge

boson production:

$$H^{\mu\nu}(\text{tree}): \begin{array}{lcl} q+\bar{q} & \to & V+G+G \\ q+\bar{q} & \to & V+q+\bar{q} \\ q+G & \to & V+q+G \\ q+q & \to & V+q+q \\ G+G & \to & V+q+\bar{q} \end{array} \tag{4}$$

$$H^{\mu\nu}(\text{loop}): \begin{array}{lcl} q+\bar{q} & \to & V+G \\ q+G & \to & V+q \end{array} \tag{5}$$

The $O(\alpha_s^2)$ tree contributions, after integrating over the solid angle $d\Omega_{k_1k_2}$ of the two final state partons in (4) with the gauge boson held fixed at a given q_T, have the same structure as the partonic cross sections in (3). For notational convenience we introduce the following definition:

$$\hat{H}_{ab}^{\mu\nu} \equiv \begin{cases} H_{ab}^{\mu\nu}\,[\text{Born}, O(\alpha_s)] \\ H_{ab}^{\mu\nu}\,[\text{loop}, O(\alpha_s^2)] \\ \int H_{ab}^{\mu\nu}\,[\text{tree}, O(\alpha_s^2)]\; d\Omega_{k_1k_2} \end{cases} \tag{6}$$

It is understood that $\hat{H}_{ab}^{\mu\nu}$ stands for one of the three possibilities depending on the case under consideration. We can construct the helicity projections $H^{\sigma\sigma'}$ defined by:

$$H_{ab}^{\sigma\sigma'} = \epsilon_\mu(\sigma)\hat{H}_{ab}^{\mu\nu}\epsilon_\nu^*(\sigma') \tag{7}$$

where $\epsilon_\mu(\sigma)$, $\sigma = +1, 0, -1$, are the polarization vectors for the gauge boson defined with respect to some coordinate axis in its rest frame (see below).

The angular dependence in eq. (3) can be extracted by introducing nine helicity cross sections corresponding to the nine polarization density matrix elements in eq. (7).

One has:

$$\frac{d\sigma^{h_1h_2}}{dq_T^2\,dy\,d\Omega^*} = \sum_{\alpha\in\mathcal{M}} g_\alpha(\theta,\phi)\,\frac{3}{16\pi}\,\frac{d\sigma^\alpha}{dq_T^2\,dy} \qquad \mathcal{M} := \{U+L, L, T, I, P, A, 7, 8, 9\} \tag{8}$$

where the hadronic helicity cross sections $d\sigma^\alpha$ ($\alpha \in \mathcal{M}$) are defined by:

$$\frac{d\sigma^\alpha}{dq_T^2\,dy} = \sum_{ab}\int dx_1dx_2 f_a(x_1,M^2)f_b(x_2,M^2)\frac{s\,d\tilde{\sigma}_{ab}^\alpha}{dt\,du}(x_1P_1, x_2P_2) \tag{9}$$

The partonic helicity cross sections $d\tilde{\sigma}_{ab}^\alpha$ are proportional to helicity structure functions[1] H_{ab}^α

$$\frac{s\,d\tilde{\sigma}_{ab}^\alpha}{dt\,du} = K_{ab}^V\,H_{ab}^\alpha \tag{10}$$

K_{ab}^V contains all the electroweak and strong couplings, phase space, statistical factors and the gauge boson propagators. H_{ab}^α are simply linearly combinations of $H^{\sigma\sigma'}$ defined in

[1] Equivalently we can decompose the hadron tensor $\hat{H}^{\mu\nu}(p_1, p_2, q)$ into nine invariant structure functions F_i [4].

eq. (7) (the indices ab have been suppressed in the following):

$$\begin{aligned}
H^{U+L} &= H^{00} + H^{++} + H^{--} & H^{A} &= \tfrac{1}{4}(H^{+0} + H^{0+} + H^{-0} + H^{0-}) \\
H^{L} &= H^{00} & H^{7} &= -\tfrac{i}{2}(H^{+-} - H^{-+}) \\
H^{T} &= \tfrac{1}{2}(H^{+-} + H^{-+}) & H^{8} &= -\tfrac{i}{4}(H^{+0} - H^{0+} + H^{-0} - H^{0-}) \\
H^{I} &= \tfrac{1}{4}(H^{+0} + H^{0+} - H^{-0} - H^{0-}) & H^{9} &= -\tfrac{i}{4}(H^{+0} - H^{0+} - H^{-0} + H^{0-}) \\
H^{P} &= H^{++} - H^{--}
\end{aligned} \tag{11}$$

Each of the helicity cross section carries a definite θ and ϕ dependence which is given by the coefficients $g_\alpha(\theta,\phi)$:

$$\begin{aligned}
g_{U+L}(\theta,\phi) &= 1 + \cos^2\theta & g_A(\theta,\phi) &= 4\sqrt{2}\sin\theta\cos\phi \\
g_L(\theta,\phi) &= 1 - 3\cos^2\theta & g_7(\theta,\phi) &= 2\sin^2\theta\sin 2\phi \\
g_T(\theta,\phi) &= 2\sin^2\theta\cos 2\phi & g_8(\theta,\phi) &= 2\sqrt{2}\sin 2\theta\sin\phi \\
g_I(\theta,\phi) &= 2\sqrt{2}\sin 2\theta\cos\phi & g_9(\theta,\phi) &= 4\sqrt{2}\sin\theta\sin\phi \\
g_P(\theta,\phi) &= 2\cos\theta
\end{aligned} \tag{12}$$

For $\alpha = U+L$, $d\sigma^\alpha$ denotes the unpolarized differential production cross section (already calculated in [2]), whereas for all other values of $\alpha \in \mathcal{M}$ it denotes the different contributions to the cross section for polarized gauge bosons. The cross section contribution of the longitudinal polarization is given by $d\sigma^L$, the transverse longitudinal interference by $d\sigma^I$ and the transverse interference by $d\sigma^T$. $d\sigma^{7,8,9}$ receive only contributions from the absorptive $O(\alpha_s^2)$ one loop contributions. They have already been calculated in [5] and will not be discussed here further.

Here we shall concentrate on the $O(\alpha_s^2)$ corrections to the parity conserving (p.c.) helicity cross sections $d\sigma^\alpha$ ($\alpha \in \{U+L, L, T, I\}$) that get contributions from the dispersive part of the hadron tensors in eqs. (4) and (5). The finiteness of the partonic helicity cross sections is arrived at the following manner:

i) Ultraviolet-(UV)-divergencies are removed by UV renormalization which introduces a renormalization scale dependence into the strong coupling constant $\alpha_s(\mu^2)$.

ii) Infrared and collinear divergencies associated with final partons cancel among loop and tree diagrams.

iii) Collinear initial state divergencies are absorbed into the parton densities ("removed by renormalizing the parton densities") introducing a factorization scale dependence into the parton densities $f(x_i, M^2)$.

The corresponding analytical $O(\alpha_s^2)$ expressions for the partonic cross sections $d\bar{\sigma}^\alpha_{ab}$ in eq. (9) are quite lengthy. The complete set of the analytical results are given in [7] and will be published in a sequel to this paper. Introducing standard angular coefficients [6]:

$$A_0 = \frac{2\,d\sigma^L/dq_T^2}{d\sigma^{U+L}/dq_T^2} \qquad A_1 = \frac{2\sqrt{2}\,d\sigma^I/dq_T^2}{d\sigma^{U+L}/dq_T^2} \qquad A_2 = \frac{4\,d\sigma^T/dq_T^2}{d\sigma^{U+L}/dq_T^2} \tag{13}$$

the angular distribution of the lepton pair for the p.c. dispersive contributions is conventionally written as:

$$\frac{d\sigma^{h_1 h_2}}{dq_T^2\, dy\, d\Omega^*} = \frac{3}{16\pi}\frac{d\sigma^{U+L}}{dq_T^2\, dy}\Big\{1+\cos^2\theta+\frac{1}{2}A_0\,(1-3\cos^2\theta) + A_1\,\sin 2\theta\cos\phi+\frac{1}{2}A_2\,\sin^2\theta\cos 2\phi\Big\} \tag{14}$$

Numerical results

At this point it is necessary to discuss the choise of the z-axis in the rest frame of the lepton pair. We will give numerical results for A_0, A_1 and A_2 in the Collins-Soper frame (CS) where the z-axis bisects the angle between $\vec{P}_1$ and $\vec{P}_2$

$$\begin{aligned} CS: \quad \vec{P}_1 &= E_1/\sqrt{1+r^2}\ (-r,0,1) \\ \vec{P}_2 &= E_2/\sqrt{1+r^2}\ (-r,0,-1) \end{aligned} \tag{15}$$

and the Gottfried-Jackson frame (GJ, also known as t-channel helicity frame)

$$\begin{aligned} GJ: \quad \vec{P}_1 &= E_1\ (0,0,1) \\ \vec{P}_2 &= E_2/(1+r^2)\ (-2r,0,1-r^2) \end{aligned} \tag{16}$$

with $r = q_T/\sqrt{Q^2}, E_1 = (\sqrt{S}/2)\sqrt{1+r^2}e^{-y}$, $E_2 = (\sqrt{S}/2)\sqrt{1+r^2}e^{+y}$ and $S = (P_1+P_2)^2$. To be specific we shall evaluate the q_T distribution for the angular coefficients A_0, A_1 and A_2 for W^+ production at $\sqrt{S} = 1.8\,\text{TeV}$ for all contributing parton subprocesses in eqs. (1)(4)(5) in these frames. We use the parton density parametrization set 2 of DFLM [8] with $\Lambda_{QCD} = 175\,\text{MeV}$ for five flavours and work in the DIS factorization scheme, where one substracts the non-pole terms found in the parton structure function in DIS. We identify the scales used in the coupling constant and in the parton distribution function and set them equal to $\mu^2 = (m_W^2+q_T^2)/2$ where m_W is the W-mass.

Figs. 1a and 1b show the q_T-distribution of A_0, A_1 and A_2 for the $q\bar{q}$ (fig. 1a) and the qG (fig. 1b) initial states separately at $O(\alpha_s)$ (dashed lines) and at NLO ($O(\alpha_s)$+ $O(\alpha_s^2)$) in the CS frame. Note that at NLO two different classes of processes contribute to the $q\bar{q}$ intitial state (see eq. (4)). A_0 and A_2 are increasing functions of q_T reaching about 0.9 at high q_T. As has been emphasized by Tung et. al. [9] these coefficients are simply related by $A_0 = A_2$ at the Born level. The result $A_0 = A_2$ at $O(\alpha_s)$ is valid for any choise of axis in the lepton-pair rest frame, as long the z-axis lies in the hadronic event plane.

Turning now to the NLO corrections to A_0 and A_2 we find that $A_0 = A_2$ is no longer true at $O(\alpha_s^2)$. For the $q\bar{q}$ initial state (fig. 1a), the dominant corrections are to A_0 and they are positive, whereas the $O(\alpha_s^2)$ contributions for the qG initial state (fig. 1b) leads mainly to negative corrections to A_2. A_1 is very small in the CS frame. The NLO corrections are too small to be visible in the plots of fig. 1.

In figs. 2a and 2b, we show the q_T dependence of A_0, A_1 and A_2 up to $O(\alpha_s^2)$ including all partonic subprocesses in eqs. (1)(4) and (5) in both the CS and GJ frame. The numerical size of the qq and GG initiated $O(\alpha_s^2)$ tree diagrams in (4) are very small (less than 1%) in both frames.

Note that in the limit $q_T \to 0$ all coefficients A_i vanish implying that the polar angle distributions reduce to the well-known $1+\cos^2\theta$ prediction of the Drell Yan mechanism in all frames.

Finally, to give a feeling for the numerical contributions of different processes, we show their relative contribution to $d\sigma^{U+L}$ and $d\sigma^{L}$ in the CS frame at $\sqrt{S} = 1.8$ TeV in fig. 3a,b.

In summary, the deviations for the angular coefficients A_i from the LO $O(\alpha_s)$ expections are less than 10 % at Tevatron energies when they are normalized to the NLO rate $d\sigma^{U+L}$ as was done in eq. (13). It is clear that the $O(\alpha_s^2)$ results are more reliable than the $O(\alpha_s)$ results as they are less dependent on the renormalization and factorization scales.

I am grateful to J.G. Körner and G.A. Schuler for interesting collaboration in this study.

References

[1] K. Kajantie, J. Lindfors and R. Raito, Phys. Lett. B74 (1978) 384; Nucl. Phys. B144 (1978) 422;
P. Aurenche and J. Lindfors, Nucl. Phys. B185 (1981) 274; ibid. 301;
M. Chaichian, M. Hayashi and K. Yamagishi, Phys. Rev. D25 (1982) 130.

[2] P. B. Arnold and M. H. Reno, Nucl. Phys. B319 (1989) 37.
R. J. Gonsalves, J. Pawlowski, Chung-Fai Wai, Phys. Rev. D40 (1989) 2245.

[3] E.Mirkes, J.G.Körner and G.A.Schuler, Phys. Lett. B259 (1991) 151

[4] J.G. Körner and E. Mirkes, Mainz-preprint MZ-TH/90-32 (1990)

[5] K. Hagiwara, K. Hikasa and N. Kai, Phys. Rev. Lett. 52 (1984) 1076.

[6] J. C. Collins and D. E. Soper, Phys. Rev. D16 (1977) 2219.

[7] E. Mirkes, thesis Universität Mainz (1990)

[8] M. Diemoz, F. Ferroni, E. Longo and G. Martinelli, Z. Phys. C39 (1988) 472.

[9] C. S. Lam and Wu-Ki Tung, Phys. Rev. D18 (1978) 2447; ibid D21 (1980) 2712; Phys. Lett. 80B (1979) 228.

Figure Captions

Fig. 1a,b:
Angular coefficients A_0, A_1 and A_2 as a function of q_T for $p\bar{p} \to W^+ + X$ at $\sqrt{s} = 1.8$ TeV. Shown are the contributions from the $q\bar{q}$ initiated subprocesses (fig 1a.: $[q\bar{q} \to G\,(G)W^+]$ + $[q\bar{q} \to q\bar{q}W^+]$) and the qG initiated subprocesses (fig 1b.: $[qG \to q\,(G)W^+]$) up to $O(\alpha_s^2)$. Dashed lines are the corresponding $O(\alpha_s)$ results.

Fig. 2a,b:
q_T dependence of A_0, A_1 and A_2 at NLO including all parton processes of eqs. (1)(4)(5) in the Collins Soper (fig. 2a) and Gottfried Jackson (fig.2b) frame.

Fig. 3a,b:
Relative contributions to $d\sigma^{U+L}$ and $d\sigma^{L}$ for W^+ production at $\sqrt{S} = 1.8$TeV and $\mu^2 = (m_W^2 + q_T^2)/2$.
At LO: (A) $[q\bar{q} \to GW^+]$ and (B) $[qG \to qW^+] + [\bar{q}G \to \bar{q}W^+]$.
At NLO: (C+F) $[q\bar{q} \to GW^+ + GGW^+] + [q\bar{q} \to q\bar{q}W^+]$, (D) $[qG \to qW^+ + qGW^+] +$ $[\bar{q}G \to \bar{q}W^+ + \bar{q}GW^+]$, (E) $[GG \to q\bar{q}W^+]$, (G)$[qq \to qqW^+] + [\bar{q}\bar{q} \to \bar{q}\bar{q}W^+]$.

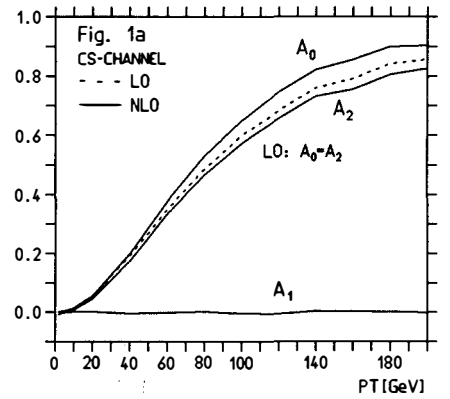
Fig. 1a
CS-CHANNEL
- - - LO
NLO
A_0
A_2
LO: A_0=A_2
A_1
PT [GeV]

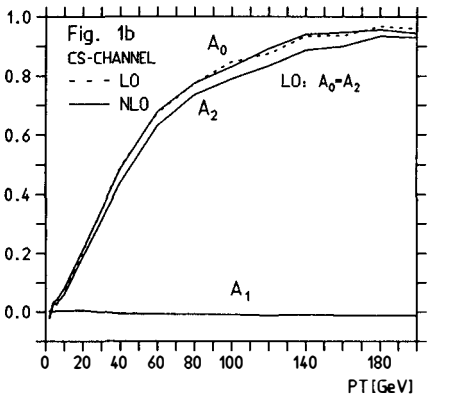
Fig. 1b
CS-CHANNEL
- - - LO
NLO
A_0
A_2
LO: A_0=A_2
A_1
PT [GeV]

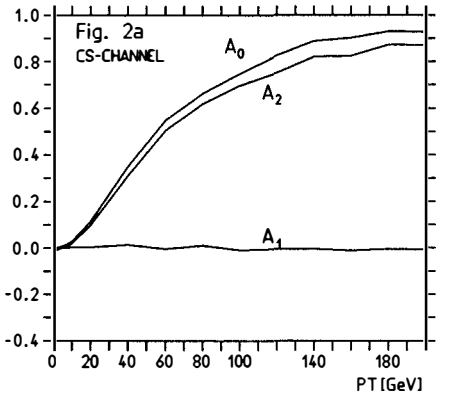
Fig. 2a
CS-CHANNEL
A_0
A_2
A_1
PT [GeV]

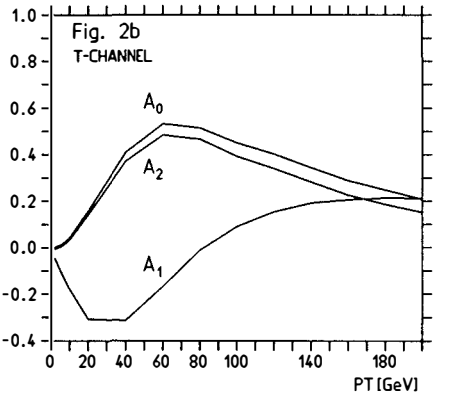
Fig. 2b
T-CHANNEL
A_0
A_2
A_1
PT [GeV]

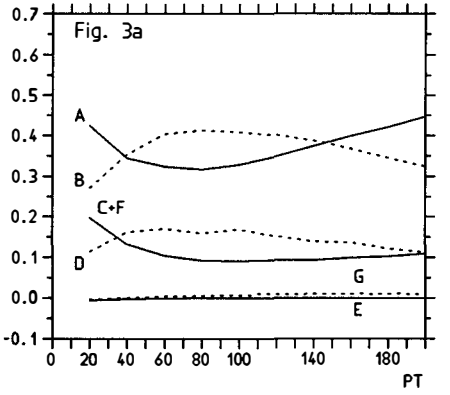
Fig. 3a
A
B
C+F
D
G
E
PT

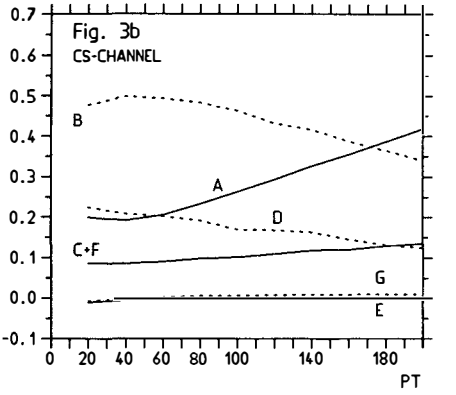
Fig. 3b
CS-CHANNEL
B
A
D
C+F
G
E
PT

DIRECT PHOTONS AND JETS

Measurement of Isolated Photon Production in Hadronic Z Decays

presented by Patrice Perez

DPhPE, C.E.N Saclay

on behalf of the ALEPH Collaboration

Abstract

The production of high energy isolated photons in hadronic Z decays is measured with the ALEPH detector at LEP using a sample of 172391 hadronic events. The observed rate is compared with a QCD calculation of final state radiation from quarks.

1 Introduction

In this talk, a measurement of the production of high energy isolated photons in hadronic Z decays is presented.

The decay of hadrons, mainly π^0 and η^0, produces a copious rate of photons ("non-prompt" photons). In the Standard Model, prompt photons are mainly produced by final state radiation (FSR) from the quarks, with a small contribution from initial state radiation (ISR), which is suppressed at the Z pole. Hard photons emitted from the quarks are the only "partons" produced in the primary interaction that are detectable free of fragmentation effects, thus providing a test of the theoretical understanding of the early hadronic shower development.

Since the electric charge of u-type quarks is twice the electric charge of d-type quarks, a sample of hadronic events with a FSR photon is enriched in u-type quarks by a factor 4. This fact could be used to extract the couplings of the quarks to the Z [1, 2]. However, this can only be done provided the dynamics of photon radiation from quarks is well understood.

Prompt-photons are also a signature for new physics (excited quarks, composite models, exotic Higgs, exotic decays of the b′ etc...). A search for these new processes requires a good knowledge of FSR photons which form the main background.

A display of one prompt photon candidate with $E_\gamma = 29$ GeV is shown in figure 1. As described in ref [5], events with such a striking topology have been used as a control sample in the search for the standard Higgs boson.

This measurement is based on data collected in 1989 and 1990 at centre of mass energies between 88 and 95 GeV.

2 Hadronic Event Selection

Hadronic events are selected offline using charged tracks [3]. Charged particle tracking is provided by a drift chamber (ITC), surrounded by a large cylindrical time projection chamber (TPC), both inside a 1.5 T superconducting solenoid [4]. Tracks are required to originate in a cylinder centred on the interaction point, with a 2.5 cm radius in the plane transverse to the beam direction, and a ± 7 cm length along the beam direction, to have a polar angle $\theta > 18.2^0$ and a minimum of 4 reconstructed TPC coordinates.

An event must have at least 5 such "good" tracks and the sum of the energies of the tracks must be greater than 10% of the centre of mass energy. This selection has an efficiency of $97.4 \pm 0.2\%$. The background from τ pairs and two-photon production is less than 0.25% [3]. A total of 186040 events satisfy this selection.

The polar angle of the thrust axis, θ_{Thrust}, determined with charged tracks must lie in the range $25^0 \leq \theta_{Thrust} \leq 155^0$. After this cut, the sample reduces to 172391 events.

3 Photon Identification

Photons are detected in the electromagnetic calorimeter (ECAL) surrounding the TPC and placed inside the coil. The calorimeter is instrumented down to 11^0 from the beam. Each module consists of 45 lead plates interspersed with proportional tubes filled with a mixture of Xe(80%) and CO_2(20%). Charges are collected on segmented cathode

planes ("pads"). The pads from consecutive planes are connected to form projective towers covering an angular region of approximately $1^0 \times 1^0$ each. Each tower is read out in three successive storeys in depth, corresponding to 4, 9 and 9 radiation lengths.

Photons are searched for among clusters of connected storeys that are not linked to a reconstructed charged track and whose barycentre positions are in the range $18^0 < \theta < 162^0$ and are not near a crack between two ECAL modules.

Neutral hadrons are rejected by requiring that the fraction of energy deposited in the third stack be less than 40%. The efficiency for this cut to retain photons of more than 10 GeV is 97.0 ± 0.2% for such "electromagnetic neutral" clusters, independent of energy.

The lateral spread of the cluster is used to separate single photons from π^0s : the transverse shape of a cluster is characterized by the fraction F_4 of its total energy that is contained in the subcluster of 2×2 adjacent towers whose energy is maximum (leading subcluster). A single photon of more than 5 GeV deposits on average 86% of its energy in the leading subcluster, with an r.m.s spread of 4%. In contrast, a high energy π^0 materializes as a cluster whose width depends on its energy.

Photon candidates are defined by the cut $F_4 > 0.75$. The measured efficiency for this cut is 99.5 ± 0.4% for photons, independent of energy. The efficiency for π^0s is 20% at 10 GeV, 50% at 15 GeV and reaches 95% at 30 GeV.

For hadronic Z decays, the bulk of the photons in the final state come from π^0 decay. This is illustrated in figure 2a, which shows the distribution of F_4 for neutral electromagnetic clusters of energy greater than 10 GeV.

4 Isolated Photon Selection

The production of π^0s or ηs results from a series of cascades in the hadronization of quarks and gluons. Consequently their energy spectrum is much softer than that of photons from FSR and they are less isolated from other fragmentation remnants. Therefore events are selected with a high energy isolated neutral electromagnetic cluster.

The isolation condition is defined in terms of a cone with a 20^0 half opening angle around the direction of the candidate photon. It is required that no charged track with momentum greater than 500 MeV/c is found inside the cone, nor any other neutral electromagnetic cluster with an energy above 500 MeV.

A total of 735 events have a neutral electromagnetic cluster with energy greater than 10 GeV which satisfies the above isolation criteria. After the final photon identification cut ($F_4 > 0.75$) 474 candidates remain.

5 Test of Isolation with Random Vectors

This definition of isolation is sensitive to the distribution of low energy fragments around jets and to the presence of noise in the ECAL. This effect has been studied in the following way. Randomly oriented vectors were inserted into hadronic events and the fraction of events with isolated such vectors in the data and in the simulation were compared. Figure 3 shows the fraction of isolated random vectors in the data and in the simulation as a function of their angle θ_{jet} to the nearest jet. Jets are defined using

the jet finding algorithm of JADE [9], using charged tracks only, with a scaled invariant mass cut of $y_{cut} = 0.02$. Data and simulation agree to better than 2% for $\theta_{jet} > 30^0$. However the fraction of isolated vectors in the data exceeds that of the simulation by 15% for $\theta_{jet} < 20^0$.

As a result of this systematic check the analysis of isolated neutral clusters has been restricted to the region $\theta_{jet} > 30^0$. Figure 2b shows the F_4 distribution of the selected clusters . One can see from this figure that the isolation plays an important role in reducing the background. After all cuts the number of isolated prompt photon candidates is reduced to 421.

Other definitions for the isolation criterion have been considered. Each definition has been tested using random vectors. From the differences between data and the simulation the systematic error on the acceptance due to the isolation is estimated to be 6%.

6 Background Subtraction

With the same isolation criteria, a Monte Carlo simulation of hadronic events with the JETSET 6.3 generator [6] predicts 71 ± 7 events from background sources in the signal region ($F_4 > 0.75$) of which 15 are from ISR.

In order to verify the rate of non-prompt background using the data the following checks have been performed.

The number of isolated clusters from non-FSR sources has been monitored in the region $F_4 < 0.75$. Comparison with the simulation (fig. 2b) shows an excess of data of $29 \pm 10\%$, independent of energy within errors. This excess could be due to an underestimate of the number of isolated π^0s or ηs in the fragmentation model. This was checked for π^0 energies less than 20 GeV, where the two photons from a π^0 can be resolved with an efficiency of 25% at 15 GeV. The number of resolved and isolated π^0s in the data exceeds that from the simulation by $43 \pm 15\%$.

The numbers of events with isolated charged tracks also provides a test of the validity of the fragmentation model. For the same isolation criteria as described in section 4, but replacing the ECAL cluster by a charged track, the yield of isolated charged tracks of more than 10 GeV/c momentum is 14 ± 5 % greater than predicted by the Monte Carlo simulation.

These comparisons indicate an underestimate of the π^0 background from the simulation in the signal region $F_4 > 0.75$. Therefore the Monte Carlo prediction for the background from non ISR sources in this signal region is rescaled by 30% leading to an increase of the total background from 17% to 21%.

From the above mentioned checks of the predicted background a systematic error of $\pm 15\%$ is assigned to the background level.

7 Systematic Errors

The experimental systematic errors are summarized in table 1. The total systematic error is 7%, mainly due to uncertainties in the isolation and the background subtraction.

The calculation of FSR given by the JETSET 7.3 program is used [7]. At present, this is the only available calculation of final state radiation from quarks in the frame-

work of QCD. Photons are produced in the parton shower in the same way as gluons. This prediction depends on the values of the parameters driving the parton shower: the QCD scale parameter Λ_{QCD} and the minimum parton invariant masses allowed during the showering, M^g_{min} for a QCD shower and M^γ_{min} for photon radiation. The assumed values for these parameters are given in table 1 together with the effect of a change within the range allowed by measurements for Λ_{QCD} and M^g_{min} ([8]). A change of M^γ_{min} over a large range does not affect the rate of high energy isolated FSR photons. The total theoretical uncertainty within the JETSET 7.3 model is estimated to be 3%.

8 Result

The number of events with $E_\gamma > 10$ GeV is $333 \pm 22(stat.) \pm 23(syst.)$, after background subtraction. A clear signal of prompt photons is observed. The JETSET 7.3 prediction is $279 \pm 6(stat.) \pm 8(theor.)$, and the ratio of data divided by the prediction is : $1.20 \pm 0.12(exp.) \pm 0.04(theor.)$. The distributions of the photon energy (figure 4a) and of the transverse momentum $p_\perp$ of the photon with respect to the thrust axis (figure 4b) follow qualitatively the JETSET 7.3 prediction. At the present level of statistics, a possible excess cannot be assigned to a particular region of phase space.

As a final systematic check, the θ_{jet} cut is increased to 50^0 and the observed number of final state prompt photons becomes $260 \pm 19(stat.) \pm 13(syst.)$ while the JETSET 7.3 prediction is $218 \pm 5(stat.) \pm 7(theor.)$, giving a ratio of 1.19 ± 0.11. This indicates that the systematic uncertainties due to the definition of the isolation are under control.

9 Conclusion

Using a sample of 172391 hadronic events collected by the ALEPH collaboration in 1989 and 1990, a clear signal of

$$333 \pm 22(stat.) \pm 23(syst.)$$

isolated final state prompt photons has been observed for $E_\gamma > 10$ GeV.

The expected number of FSR photons in the framework of the JETSET 7.3 model is:

$$279 \pm 6(stat.) \pm 8(theor.)$$

The observed rate is larger than the prediction by $20 \pm 13\%$.

The extraction of quark couplings requires a knowledge of the acceptance for FSR photons which has not yet reached a sufficient understanding.

However, this study shows that we are starting to probe quarks in the parton shower, and the 1991 run statistics will hopefully provide a nice sample of events for an insight into the colour world.

Table 1: Summary of errors for the isolated photon sample with $E_\gamma > 10$ GeV. For the theoretical errors, the changes in the yield of FSR isolated photons correspond to the changes of the parameters of the model in the quoted ranges. The 1σ total error corresponds to half of the parameter ranges.

Experimental Errors	Photon identification	1%
	ECAL energy calibration	1%
	Isolation	6%
	Background subtraction	3%
	Total systematic error	7%
	Statistical error	7%
	Total experimental error	10%
Theoretical Errors on the prediction for FSR (JETSET7.3)	$\Lambda_{QCD} = 300$ MeV (tuned, see [8]) range 260 $\rightarrow$ 400 MeV	-2%
	Invariant mass cut-off for gluons: $M^g_{min} = 1.5$ GeV (tuned, see [8]) range 1 $\rightarrow$ 2 GeV	$+5\%$
	Invariant mass cut-off for photons: $M^\gamma_{min} = 1$ GeV (default) range 100 MeV $\rightarrow$ 5 GeV	$<1\%$
	Total theoretical error ($\pm 1\sigma$)	$\pm 3\%$

References

[1] T.F. Walsh and P. Zerwas, Phys. Lett. B 44 (1973) 195; S.J. Brodsky, C.E Carlson and R. Suaya, Phys. Rev. D 14 (1976) 2264.

[2] M.Z. Akrawy et al., OPAL collaboration, Phys. Lett. B 246 (1990) 285.

[3] D. Decamp et al., ALEPH Collaboration, Phys. Lett. B 231 (1989) 519; Z. Phys. C 48 (1990) 365.

[4] D. Decamp et al., ALEPH Collaboration, Nucl. Inst. and Meth. A 294 (1990) 121.

[5] D. Decamp et al., ALEPH Collaboration, Phys. Lett. B 246 (1990) 306.

[6] T. Sjöstrand and M. Bengtsson, Comput. Phys. Commun. 43 (1987) 367.

[7] T. Sjöstrand. JETSET, version 7.3.

[8] D. Decamp et al., ALEPH Collaboration, Measurement of Charge Asymmetry in Hadronic Z decays. Preprint CERN-PPE-91/27, Submitted to Phys. Lett. B.

[9] W. Bartel et al., JADE Collaboration, Z. Phys. C 33 (1986) 23; S. Bethke et al., JADE Collaboration, Phys. Lett. B 213 (1988) 235.

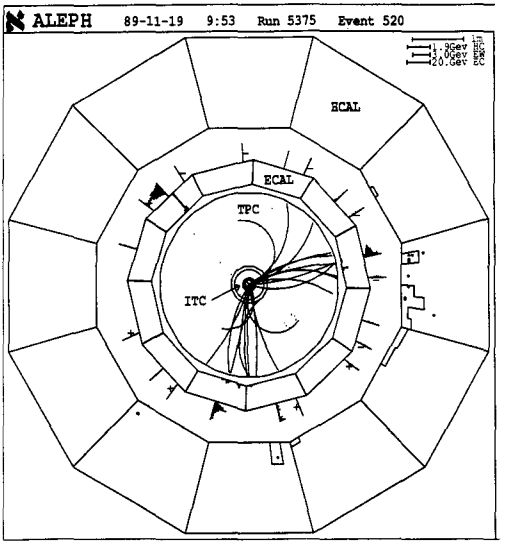

Figure 1: A display of an event with a prompt photon candidate with $E_\gamma = 29$ GeV.

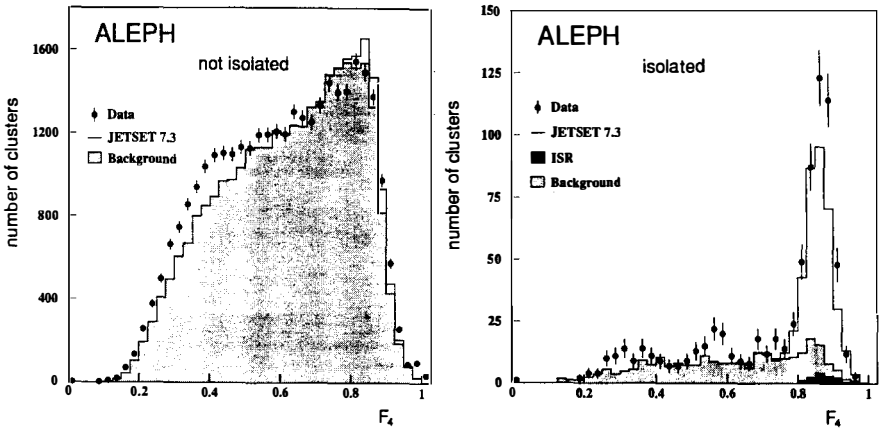

Figure 2: Fraction F_4 of cluster energy, for neutral electromagnetic clusters of energy greater than 10 GeV in hadronic events (a) not isolated (b) isolated. The shaded area represents the background. The black area represents the ISR contribution. The histogram represents the total simulation including FSR.

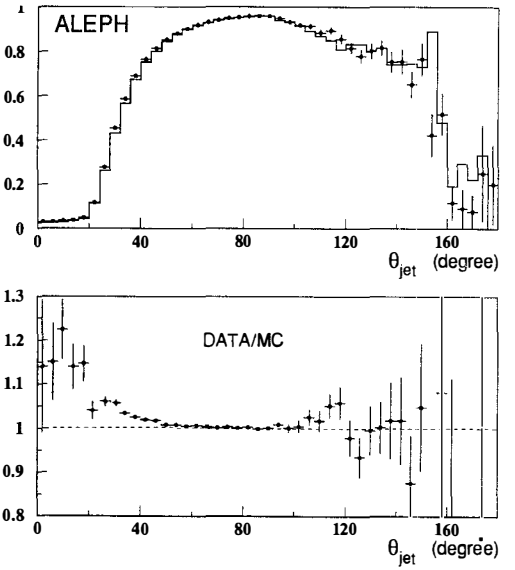

Figure 3: (a) Fraction of isolated random vectors as a function of the angle to the nearest jet θ_{jet} for data (full circles) and simulation (histogram). (b) Ratio of the fraction of isolated random vectors in the data divided by the same fraction in the simulation.

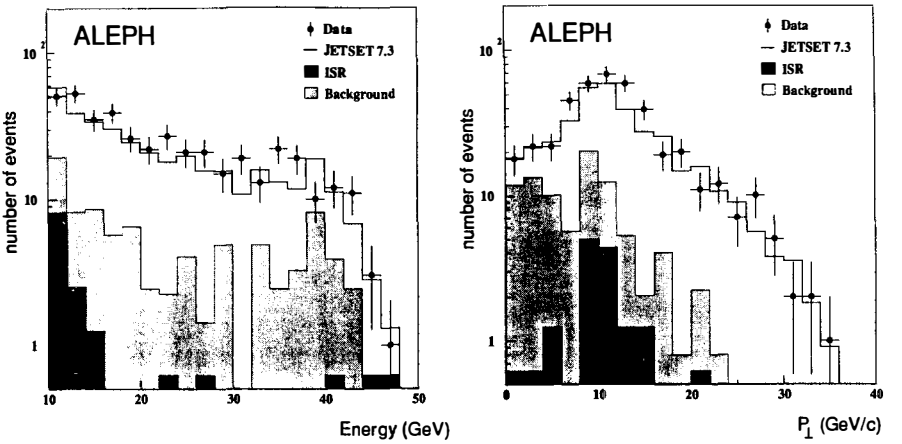

Figure 4: Prompt photon candidates (a) energy spectrum (b) $p_\perp$ with respect to the thrust axis. The shaded area represents the corrected background. The black area represents the ISR contribution.The histogram represents the total simulation including FSR.

RECENT RESULTS ON DIRECT PHOTON PHYSICS FROM UA2

The UA2 Collaboration
Bern — Cambridge — CERN — Dortmund — Heidelberg — Melbourne
Milano — Orsay (LAL) — Pavia — Perugia — Pisa — Saclay (CEN)

presented by M. Primavera
now at University of Calabria
and
I.N.F.N. Cosenza, Italy

Abstract

New results on direct photon production from the UA2 experiment are presented. The data were collected during the '88 and '89 Collider runs and correspond to a total integrated luminosity of 7.8 pb^{-1}.

1 — Introduction

The direct production of high p_T photons from $\bar{p}p$ collisions is described in the Born approximation by $q\bar{q}$ annihilation and the Compton process $gq \rightarrow \gamma q (or\ g\bar{q} \rightarrow \gamma\bar{q})$. It is a good test of QCD, because the theoretical calculations exist at the order α_s^2 [1] and the photon transverse momentum (p_T) is not affected by fragmentation effects, thus reducing the size of experimental uncertainties.

The UA2 detector has been upgraded between 1985 and 1987. The calorimeter [2] provides full coverage in the azimuthal angle over the polar angle interval $5° < \theta < 175°$ and consists of a central part (CC, $|\eta| < 1.$) and two forward/backward parts (EC, $1. < |\eta| < 3.$). There are in total 624 cells and each cell is segmented in electromagnetic and hadronic compartments.

The central detector, used for tracking and electron identification, consists, in order of increasing radius, of: an inner silicon hodoscope [3] (ISI), placed at 2.9 cm from the beam axis; a cylindrical drift chamber with jet geometry (JVD) [4]; an outer silicon hodoscope (OSI) at 14.8 cm radius; two transition radiation detectors (TRD) [5] for electron/pion separation and a scintillating fibre detector (SFD) [6] with a tracking part (18 layers of fibres) and a preshower part (lead converter of 1.5 r.l. followed by 6 layers of fibres).

In the forward/backward region, two stereo triplets of proportional tubes (ECPT) [7], placed in front of the EC calorimeters, are used for tracking and a 2 r.l. lead converter followed by another stereo triplet as a preshower detector.

The event selection is performed by a three level trigger system [8], based on calorimeter informations.

In this report the results from a study of direct photon production will be presented. The photon identification criteria and the background estimate will be described and the measured inclusive γ cross- section will be compared to a next to leading order QCD calculation and to cross-sections from other processes; finally, a brief study of the event associated to photon production will be presented.

2 — Photon identification

This study has been performed only in the central region of the detector. We have required events with an electromagnetic cluster fully contained in the CC ($|\eta| < 0.76$) and with only one vertex within 250 mm from the centre of the detector. The lateral and longitudinal profile of the electromagnetic cluster had to be consistent with that expected from an isolated photon.

Isolation cuts on tracks and preshower signals have been applied to reduce the contamination of hadronic jets and of photons coming from quark bremsstrahlung:

- no charged track in a region $\Delta\eta < 0.2$ and $\Delta\phi < 15°$ around the direction defined by the vertex and the cluster centroid;
- at most one preshower signal in a cone $\sqrt{\Delta\eta^2 + \Delta\phi^2} < 0.265$ (approximately the size of one calorimeter cell) around the same direction.

A total of 26086 photon candidates with $p_T > 15$ GeV have been found for a total integrated luminosity $\mathcal{L} = 7.4\ pb^{-1}$. The global efficiency for detecting photon events, excluding preshower detector effects, has been computed to be $\varepsilon_c = 0.44$.

3 — Background evaluation

The residual background of unresolved γ pairs from $\pi°$ and η decays has been estimated using a statistical method, which uses the measured fraction α of events in which the photon has begun showering in the lead converter of the preshower detector:

$$\alpha = \frac{N_c}{N_c + N_u} \tag{1}$$

where N_c and N_u are the numbers of converted and unconverted photons corrected for preshower efficiencies.

The conversion probability of an incident photon in the preshower, ε_γ, has been computed using the EGS [9] shower simulation, tuned to reproduce the results obtained from test beam electrons of 10 and 40 GeV and from W decay electrons. The calculation takes into account the geometry and the material placed in front of the preshower detector, the light output of the scintillating fibres and the effects of the online and offline cuts applied to reconstruct the preshower signal.

Finally, the conversion probability ε_π of the backgrond from single $\pi°$ and η decays has been calculated by a Monte Carlo simulation using the values of ε_γ for each photon and assuming the ratio $\eta/\pi°$ equal to 0.6 and p_T independent, as measured by UA2 [10]. Fig. 1 shows the measured values of α together with the computed ε_γ and ε_π as a function of the photon energy. The systematic error on ε_γ has been estimated to be of the order of 2% and that on ε_π, coming essentially from the uncertainty on the two photon angular resolving power (20 ± 7 mrad), between 3% and 2% and decreasing with energy. From the $\alpha, \varepsilon_\gamma, \varepsilon_\pi$ values, the background fraction in the sample of γ candidates due to $\pi°$ and η is

given by:

$$b(p_T) = \frac{(\alpha - \varepsilon_\gamma)}{(\varepsilon_\pi - \varepsilon_\gamma)} \tag{2}$$

The background from multi π° events has been reduced to a negligible level by the preshower isolation cut. This has been checked by measuring the conversion probability of a background data sample, which has been selected by requiring large lateral shower profile and rejecting the residual single photon fraction. The results are close to the computed ε_π when preshower isolation is required. Other contaminations caused by beam - halo particles and by $W \rightarrow e\nu$ decays in which an electron was identified as a photon because of track inefficiency, have been estimated to be smaller than 1% and have been neglected.

4 — Inclusive cross - section

The invariant inclusive cross - section $\bar{p}p \rightarrow \gamma X$ at $\eta = 0$ is given by

$$E\frac{d^3\sigma}{dp^3} = \frac{N_\gamma(p_T)[1 - b(p_T)]}{2\pi p_T \Delta p_T \mathcal{L} \varepsilon_c A(p_T)} \tag{3}$$

where $N_\gamma(p_T)$ is the number of photon candidates in the p_T bin of Δp_T width, $b(p_T)$ is the background fraction in the same bin, $\mathcal{L}$ is the integrated luminosity of the data sample ($7.4 \pm 0.4\ pb^{-1}$), ε_c is the efficiency of the cuts and $A(p_T)$ is the geometrical acceptance, computed by a Monte Carlo simulation.

This cross-section has been compared to the next-to-leading order QCD calculation [1]), where the predictions take into account the effect of the isolation cut on the contribution from quark bremsstrahlung . The comparison is shown in fig. 2 using different sets of parton distributions ($Q^2 = p_T^2$). We can observe that the experimental points agree well with the theoretical curves, but we cannot discriminate between the various sets of structure functions. The results are also compared in fig. 3 with the inclusive jet cross-section [11]) and with the double γ cross - section (preliminary). Integrating the γ and the jet cross - sections over the p_T range we find a ratio $\sigma_\gamma/\sigma_{jet} \approx 10^{-4}$. The errors shown in figures 2 and 3 represent only the statistical and p_T dependent systematic uncertainties, which take into account the errors on ε_γ, ε_π and on the detection efficiency of converted and unconverted γ. An overall p_T independent systematic error of 9% comes from the uncertainties on the energy scale (6.4%), on the luminosity measurement (5.4%), on the acceptance determination (1%), and on the efficiencies of the selection criteria (2%).

5 — Structure of direct γ events

In the parton model, direct photon production at high p_T results from the hard collision of two high energy partons. As a conseguence, a jet should be observed at opposite azimuth from the photon.

A γ - jet sample has been selected by requiring $p_T^{\gamma} > 20\ GeV$, $p_T^{jet} > 15\ GeV$ and $|\eta_{\gamma}| < 0.76$, $|\eta_{jet}| < 2.$. Nearby jets have been merged to take into account final state radiation and no other jet with $p_T > 6\ GeV$ has been allowed in the event. This γ - jet sample has been compared with a "symmetric" 2 - jet sample, selected requiring $p_T^{jet1} > 20\ GeV$, $p_T^{jet2} > 15\ GeV$ (jets are ordered in decreasing energy), with both jets in the pseudorapidity interval $|\eta| < 2.$ and one of the two jets having $|\eta| < 0.76$. As in the previous case, events with a third jet having $p_T > 6\ GeV$ have been rejected and other nearby jets have been merged with the two leading ones.

The features of the $\gamma - jet$ final state have been compared with those of the two jet sample. To this purpose, the distributions of $\Delta\phi(\gamma - jet)$, $\Delta\phi(jet - jet)$ and of the components [12] of the total transverse momentum of the 2 - jets system, parallel (p_T^{η}) and perpendicular (p_T^{ξ}) to the bisector of the $p_T^1 - p_T^2$ angle, have been used. One should notice that the p_T^{η} distribution is less affected than p_T^{ξ} by instrumental effects, because it depends mainly on the angular resolution, whereas p_T^{ξ} depends strongly on the energy measurement errors. We observe that these distributions are wider in the case of the two jet events than in the $\gamma - jet$ sample. This can be seen in fig. 4, where the r.m.s. of the p_T^{η} component, as a function of the invariant mass of the two - body system, is plotted for $\gamma - jet$, jet - jet and $Z \rightarrow e^+e^-$ [13] events. These results can be qualitatively explained considering the different behaviour of quarks and gluons. Incoming gluons are expected to radiate more than incoming quarks and this would imply larger transverse momenta [14] of the final system. In the kinematical region studied, gluon - gluon collisions are dominant in the jet - jet production, gluon - quark in the $\gamma - jet$ production, while Z bosons are produced from $q\bar{q}$ annihilations. Thus, the results are consistent with this qualitative QCD picture.

6 — Conclusions

The UA2 experiment has collected an integrated luminosity of 7.8 pb^{-1} during the 1988 and 1989 runs. New results have been obtained on the cross-sections for direct and double high p_T photons (the latter one is preliminary). Good agreement with next-to-leading order QCD calculations has been found. This analysis is being extended to include

the 1990 data which correspond to an integrated luminosity of 5.7 pb^{-1}.

REFERENCES

[1] P. Aurenche et al., Phys. Lett. 140B (1984) 87
P. Aurenche et al., Nucl. Phys. B297 (1988) 661
[2] A. Beer et al., Nucl. Instrum. Methods A224 (1984) 360
[3] R. Ansari et al., Nucl. Instrum. Methods A279 (1989) 388
[4] F. Bosi et al., Nucl. Instrum. Methods A283 (1989) 532
[5] R. Ansari et al., Nucl. Instrum. Methods A263 (1988) 51
[6] R.E. Ansorge et al., Nucl. Instrum. Methods A265 (1988) 33
J. Alitti et al., Nucl. Instrum. Methods A279 (1989) 364
[7] K. Borer et al., Nucl. Instrum. Methods A286 (1990) 128
[8] G. Blaylock et al., Proc. Intern. Conf. on the Impact of Digital Microelectronics and Microprocessor on Particle Physics, eds. M. Budinich et al. (World Scientific, Singapore, 1988) 247
P. Baehler et al., Proc. Intern. Conf. on the Impact of Digital Microelectronics and Microprocessor on Particle Physics, eds. M. Budinich et al. (World Scientific, Singapore, 1988) 254
[9] R. Ford and W. Nelson, SLAC - 210 (1978)
[10] UA2 Collaboration, M. Banner et al., Z. Phys. C27 (1985) 329
[11] UA2 Collaboration, J. Alitti et al., CERN - PPE/90-188, submitted to Physics Letters
[12] UA2 Collaboration, P. Bagnaia et al., Phys. Lett 144B (1984) 283
[13] UA2 Collaboration, J. Alitti et al., Phys. Lett 241B (1990) 150
[14] M. Greco, Z. Phys. C26 (1985) 567

Figures

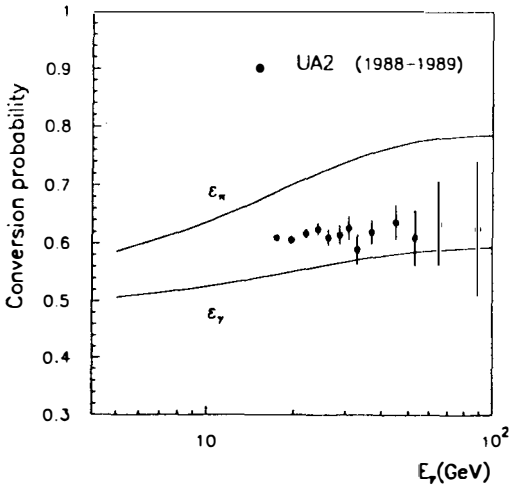

fig. 1 - Fraction of events with converted γ. ε_γ and ε_π are the conversion probabilities for single γ and multi γ background, respectively.

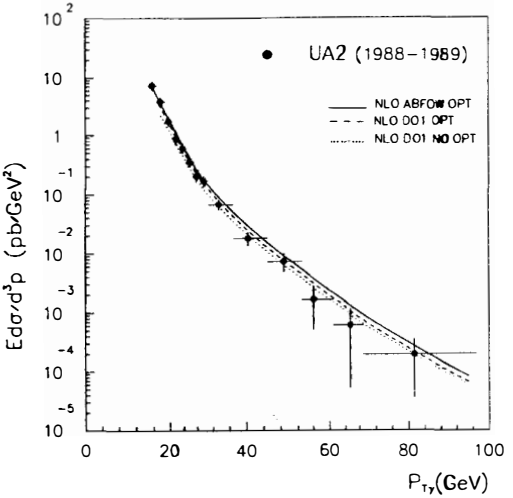

fig. 2 - Inclusive differential cross-section for direct photon production compared with the QCD next-to-leading order calculation [1] *with different sets of structure functions.*

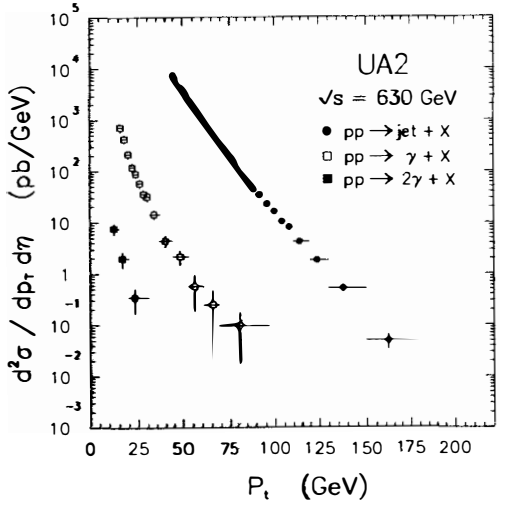

fig. 3 - Differential cross-sections for direct photon, jet and double photons production (preliminary) at $\eta = 0$.

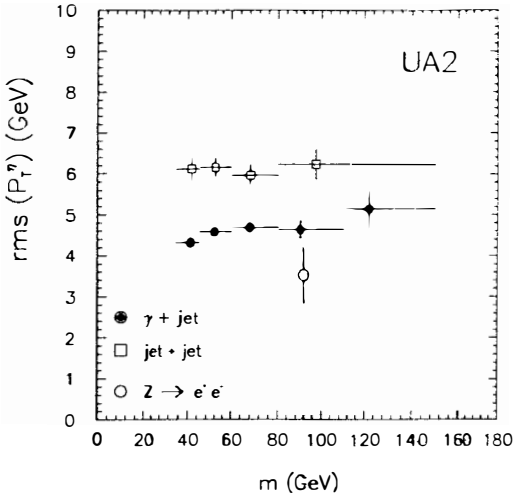

fig. 4 - The r.m.s. values of p_T^η distributions for two-jets, $\gamma - jet$ and $Z \rightarrow e^+e^-$ systems.

HADRONIC PRODUCTION OF DIRECT PHOTONS AT LARGE TRANSVERSE MOMENTUM

K. Hartman
(for the E706 Collaboration)
Department of Physics
Pennsylvania State University
University Park, Pennsylvania 16802

We report results from Fermilab fixed target experiment E706, a large acceptance study of direct photons produced in hadronic interactions. During its first run in 1987-88 the experiment accumulated ≈ 1 pb^{-1} of data that includes samples of large p_T single photons, as well as π° and η mesons. The experiment triggered on high transverse momentum showers detected in the electromagnetic part of a large liquid argon calorimeter. The present analysis utilizes data induced by proton and negative pion beams at 530 GeV, incident on Be and Cu targets. The kinematic range of the data extends in p_T from 3 to 10 GeV, and in center-of-mass rapidity from -0.7 to 0.7. In addition to discussing the unique scheme employed to determine the energy scale, inclusive cross sections for direct photon production will be presented. The E706 results will be compared to theoretical predictions.

1 Introduction

The hadronic production of direct photons provides a unique method for testing perturbative QCD[1]. To leading order in the strong coupling constant, α_s, only two processes contribute to the yield: quark-antiquark annihilation ($q + \bar{q} \rightarrow \gamma + g$) and Compton scattering ($g + q \rightarrow \gamma + q$). The annihilation mechanism provides an opportunity for the study of gluon fragmentation while the Compton contribution is well-suited to investigating the gluon distribution in the nucleon and the pion. Next-to-leading-log calculations for direct photon and direct photon plus jet production are now available[2] and E706 will provide an accurate test of this recent work, in addition to a new measure of the gluon content of the nucleon.

In this paper we will briefly discuss the current state of our analysis including the scheme employed to determine the energy scale of the electromagnetic liquid argon calorimeter (EMLAC) and we will present recent results from our direct photon analysis.

2 Data Analysis

As a second generation direct photon experiment, E706 will provide the most precise measurement of photons originating from hard hadronic collisions of positive and negative beams with nuclear targets. The photons and π^0s produced in these collisions generate triggers in the EMLAC. The accompanying charged particles are reconstructed in a charged particle spectrometer consisting of a silicon microstrip system upstream and a PWC system downstream of a large dipole magnet.

Since the direct photon signal is determined by subtracting all known sources of background, it is essential to have a thorough understanding of these background sources. The primary component of the background arises from π^0s and ηs decaying into two photons which are subsequently not fully reconstructed in our detector. A sensitive test of the level of one's understanding of the background is found in the energy asymmetry of the two photons from the meson decay. The asymmetry, defined as $A = |E_1 - E_2|/(E_1 + E_2)$, is shown in Figure 1a where the E_i are the photon energies. As a pseudoscalar meson, the π^0 decays isotropically in its rest frame; this directly corresponds to a flat energy asymmetry distribution. The dotted line indicates to the same quantity as determined in our Monte Carlo. The losses at high asymmetry are due to reconstruction efficiency, geometrical acceptance and insensitivity to low energy photons. The $\gamma\gamma$ mass spectrum is shown in Figure 1b for diphoton $p_T \geq 3.5$ GeV; note the logarithmic scale of ordinate. The dotted line shows the effect of the asymmetry cut: $A \leq 0.75$.

3 Energy Scale

In the E706 spectrometer, about 10% of the photons arising from the decay of π^0s, ηs and other sources will convert to e^+e^- pairs in the target. In addition to leaving a

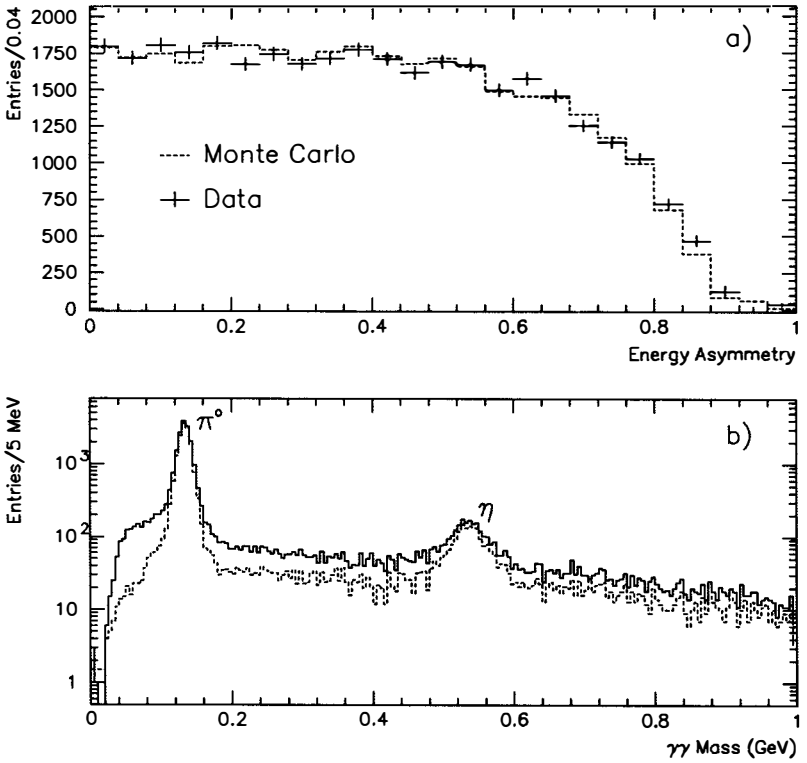

Figure 1: a) Two photon asymmetry; the points are from the data and the line corresponds to our Monte Carlo result; b) $\gamma\gamma$ mass spectrum for diphotons; the dashed curve shows the result of the asymmetry cut: A $\leq$ 0.75. In both plots, the photon pairs have $p_T \geq$ 3.5 GeV.

clear signal in the charged particle spectrometer, the electron pair will deposit showers in the EMLAC. The other photon from the π° will typically not convert and will also shower in the electromagnetic calorimeter. With this sample of γe^+e^- events, we can establish the energy scale of the EMLAC. We measure the e^+e^- component with the tracking system and the γ energy with the EMLAC. We have established the scale of the tracking system by tuning to the $J/\psi \rightarrow \mu^+\mu^-$ signal and verifying with the double conversion π° (i.e. $\pi^\circ \rightarrow e^+e^-e^+e^-$), $J/\psi \rightarrow e^+e^-$ and $K^\circ \rightarrow \pi^+\pi^-$.

In Figure 2a we show the γe^+e^- mass spectrum where both the π° and η signals are visible. Fits to these distributions give 134.5 $\pm$ 0.6 MeV and 550 $\pm$ 4 MeV for the π° and η signals, respectively. For the electrons, we also compare directly the shower energy (E) and the tracking momentum (P) in Figure 2b, where the fit gives 1.003 $\pm$ 0.008. Shown in Figure 2c is the dependence of the π° ($\rightarrow \gamma e^+e^-$) mass on the γ energy. All points are within $\pm 1\sigma$ of the nominal π° mass (dotted line) over the entire range. Similarly, Figure 2d shows the EMLAC energy dependence of the E/P distribution for the electrons. Again, nearly all points are within $\pm 1\sigma$ of perfect agreement throughout the energy region.

Additionally, a Gaussian fit to the signal for $J/\psi \rightarrow e^+e^-$ gives a mean value of 3.07 $\pm$ 0.04 GeV and the $\gamma\gamma$ decay mode of the η is 546 MeV, about 0.5% below its nominal value. Using this scale definition, our mean two-photon π° mass is about 1.5% high. The source of this discrepancy is not yet understood and can be taken as an upper limit on the uncertainty in our energy scale. This corresponds roughly to an uncertainty in our photon cross sections of about 20%.

4 Direct Photon Results

In Figure 3 we show our direct photon cross sections. In Figure 3a our proton data are compared directly with the next-to-leading log QCD calculations of Aurenche, et. al.[2] using three different values of the scale, q^2. It is clear that the curves follow the data in the higher p_T region but it is not possible, at this level of statistics, to distinguish between the various scale parameters. The negative data, shown in Figure 3b, display the same trend when comparing to the QCD curves.

We are preparing to analyze the data from our 1990 run which has more than fifteen times the negative data shown here. We are also in position to accumulate more than ten times our current positive data sample during the latter half of 1991.

Acknowledgements – This research is supported by the US Department of Energy, the National Science Foundation and UGC (India).

References

1. J. F. Owens, *Rev. Mod. Phys.* **59** (1987) 465, and references therein.
2. P. Aurrenche, et. al., *Phys. Rev.* **D39** (1989) 3275.

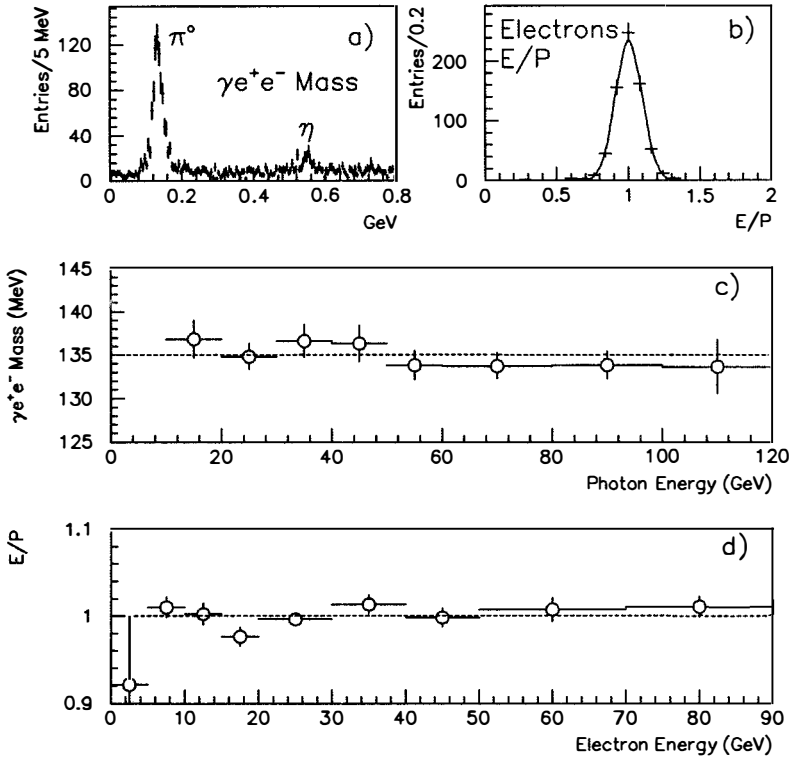

Figure 2: a) γe^+e^- mass distribution; b) E/P from electrons; c) γ energy dependence of the π° signal; d) energy dependence of E/P for the electrons.

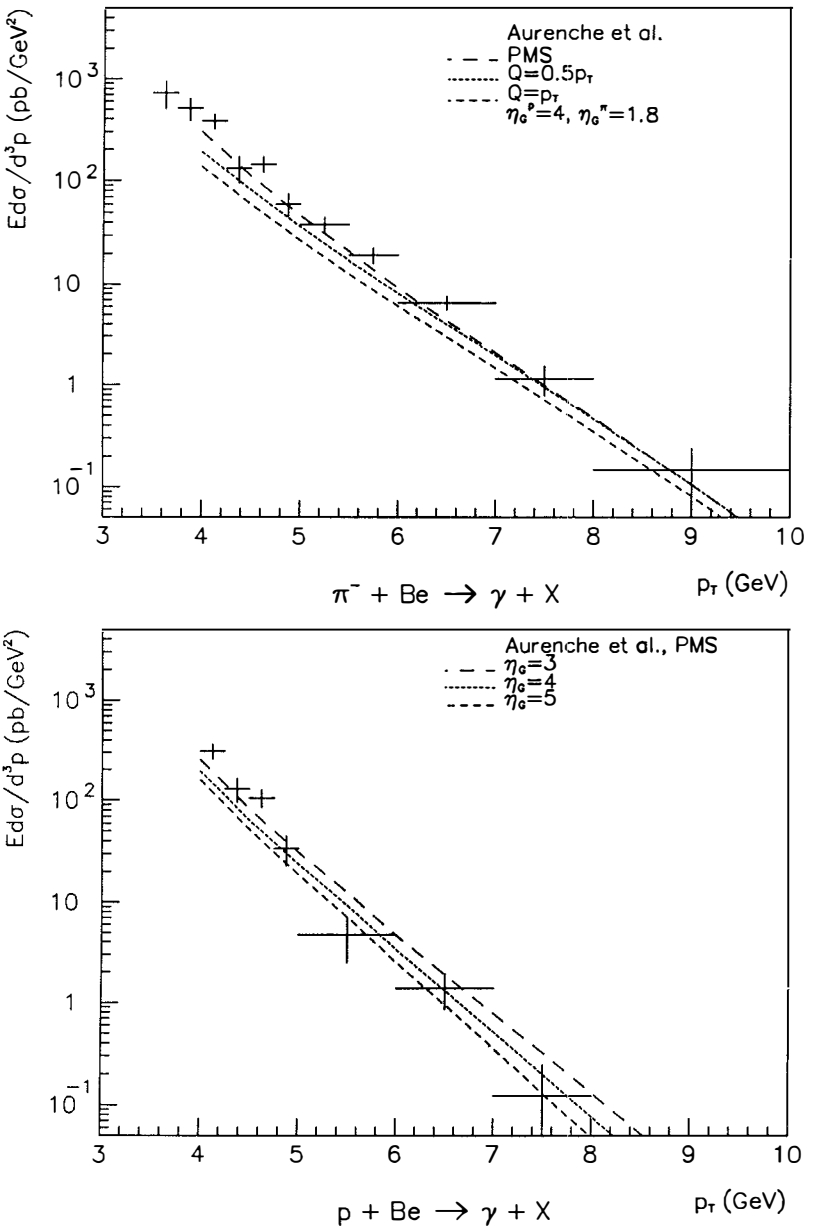

Figure 3: Invariant direct photon cross section produced in the reactions: a) $p + Be \rightarrow \gamma + X$ and b) $\pi^- + Be \rightarrow \gamma + X$. The overlaying curves represent the QCD calculations of Aurenche, et. al.[2)]

BREMSSTRAHLUNG CONTRIBUTION TO LARGE P_T PHOTON PRODUCTION AT NEXT TO LEADING ORDER

E. PILON
Laboratoire de Physique Théorique et Hautes Energies*
Université de Paris-Sud, Bât.211, 91405 Orsay Cédex, France

Abstract :

We consider the production of high p_T direct photons in hadronic collisions at high energies. In the region where the transverse momentum of the photon is small compared to the hadronic center of mass energy, $2p_T/\sqrt{s} << 1$, the bremsstrahlung "anomalous" contribution is important. We calculate the $0(\alpha\alpha_s^2)$ corrections to the leading $(\alpha\alpha_s)$ anomalous contribution.

---

* Laboratoire associé au Centre National de la Recherche Scientifique

Direct photon production has been and is still extensively studied [1] since it provides a nice test of QCD at short distances and allows the measurement of the gluon content of hadrons, which will be probed down to $x \simeq 10^{-3} - 10^{-4}$ at the future LHC and SSC colliders.

Basically two mechanisms are responsible for the emission of direct photons :

- Production of what we can call an "internal" photon, that is, a photon which takes part directly to the hard subprocess as illustrated on Figs (1.a), (1.b) ;

- Production of a bremsstrahlung, or anomalous, photon, which is radiated quasi-colinearly by a parton, itself produced at high p_T by the hard subprocess as pictured on Fig.(1.c). Here the phase space integration near the colinear pole yields a term proportional to $\mathrm{Log}(p_T^2/\Lambda^2)$ behaving as $1/\alpha_s(p_T^2)$, so that the diagrams of Fig. (1.c) are effectively $0(\alpha\alpha_s)$ that is, leading order (LO).

Indeed higher order calculations already performed [2] include only $0(\alpha\alpha_s)$ anomalous photon contributions.

As one sees on Fig.(2), for $x_T = 2p_T/\sqrt{s}$ high enough (where p_T is the transverse momentum of the photon and $\sqrt{s}$ the center of mass energy of the incoming hadrons) the anomalous contribution is small compared to the so called internal one, so a LO estimate of the anomalous contribution is sufficient.

But at small x_T, $x_T \leq 0(10^{-2})$ the anomalous mechanism dominates : at $\sqrt{s} = 1.8$ TeV, $p_T = 15$ GeV, and a photon rapidity $y=0$ it represents 60% of the theoretical prediction for the fully inclusive cross section. Thus a LO estimate is not sufficient in principle since the correction of such a large term may be large.

Moreover as shown [3] on Fig.(3) there is a clear disagreement in this small x_T-region between the theoretical predictions and the experimental data, the latter being well above the former.

We are thus led to perform the calculation of the next to leading order (NTLO) contribution to the anomalous mechanism. To do this, we have to convolute the hard partonic subprocesses which are of order $0(\alpha_s^2) + 0(\alpha_s^3)$ with the NTLO anomalous fragmentation functions of partons into a high p_T photon, which are of order $0(\alpha/\alpha_s) + 0(\alpha)$. This yields two $0(\alpha\alpha_s^2)$ contributions.

One contribution is given by the convolution of the fragmentation functions with the finite $0(\alpha_s^3)$ terms of the hard partonic subprocesses that remain after the factorization of the colinear singularities. These $0(\alpha_s^3)$ terms are independant of the fragmentation and have been calculated by [3] in the case of hadro-production of high p_T hadrons.

The other one comes from the $0(\alpha)$ contribution of the NTLO anomalous fragmentation functions which are obtained by solving the NTLO inhomogeneous Altarelli Parisi equations :

$$M^2 \frac{\partial D_{NS}}{\partial M^2} = K_{NS} + P_{NS} \otimes D_{NS} \qquad \text{(non singlet case)} \qquad (1)$$

$$M^2 \frac{\partial D_{\gamma/q}}{\partial M^2} = K_{q\gamma} + P_{qq} \otimes D_{\gamma/q} + P_{qg} \otimes D_{\gamma/g} \qquad \text{(singlet case)} \qquad (2)$$

$$M^2 \frac{\partial D_{g/q}}{\partial M^2} = K_{g\gamma} + P_{gq} \otimes D_{\gamma/q} + P_{gg} \otimes D_{\gamma/g}$$

where the time-like NTLO splitting kernels

$$P_{ij} = \frac{\alpha_s(M^2)}{2\pi} \cdot P_{ij}^{(o)}(z) + \left(\frac{\alpha_s(M^2)}{2\pi}\right)^2 \cdot P_{ij}^{(1)}(z) \qquad (3)$$

are calculated in [5]. The NTLO terms $K_{ij}^{(1)}$ appearing in the inhomogeneous terms

$$K_{q\gamma} = \frac{\alpha}{2\pi}\ 2N_F \langle e^2 \rangle \left[\frac{1+(1-z)^2}{z} + \frac{\alpha_s(M^2)}{2\pi} C_F\ K_{q\gamma}^{(1)}(z) \right] \qquad (4)$$

$$K_{g\gamma} = \frac{\alpha}{2\pi}\ \frac{\alpha_s(M^2)}{2\pi}\ N_F T_R \langle e^2 \rangle\ K_{g\gamma}^{(1)}(z) \qquad (5)$$

are extracted from the time-like $P_{ig}^{(1)}$ by identifying the proper group factors.

As a preliminary and partial estimate of the effect of the corrections, we use the LO distribution and fragmentation functions from [1, 8] and we perform the convolution of these with the $0(\alpha_s^3)$ partonic cross section given in [4] . The ratio of this result over the higher order fully inclusive calculation of [2] is plotted on Fig.(4). At low x_T, e.g. for $\sqrt{s}$ = 1.8 TeV, p_T = 15 GeV, the NTLO anomalous correction becomes as large as 40% to 90% of the fully inclusive prediction, which means that in this x_T region the total anomalous contribution is about twice its LO estimate[1] . We have not calculated the isolated photon cross section yet but we expect a similar result because of the dominance of the bremsstrahlung mechanism.

As a byproduct of our investigation, let us correct a mistake in the litterature concerning the space-like photon splitting kernels. In the expression of the inhomogeneous term $K_{\gamma g}^{(1)}$ that describes the anomalous gluonic content of the photon, the following expression has been used [6],[7] (ref. [6] gives the moments of the inhomogeneous terms) :

$$K_{\gamma g}^{(1)} = k_{\gamma g}^{(1)}(x) - \delta(1-x) \qquad (6)$$

where the function

$$k_{\gamma g}^{(1)}(x) = -16 + 8x + \frac{20}{3}x^2 + \frac{4}{3x} - (6+10x)\ln x - 2(1+x)\ln^2 x \qquad (7)$$

---

1 This is obviously to be taken only as a promising hint for the complete final result, which requires the full NTLO corrections and the study of the dependance of the predictions on the scales used.

is picked up by identifying in the space-like $P_{gg}^{(1)}$ the term proportional to $T_R N_F C_F$ (Fig. (5-a)), replacing this group factor by $N_C C_F N_F < e^2 >$ when incoming gluons are replaced by photons (Fig. (5-b))

The $\delta(1-x)$ term corresponds to disconnected diagrams (Fig.(5.c)). But since there is no mixing between a gluon and a photon no such term appears at this order. So the $\delta(1-x)$ must be suppressed. The phenomenological consequences of this mistake, which generates a contribution to the gluonic content of the photon proportionnal to $\delta(1-x)$, are worthwhile to be investigated.

This work has been done in collaboration with P. Aurenche, M. Fontannaz and J. Ph. Guillet.

REFERENCES

[1] J.F. Owens, Rev.Mod. Phys. 59 (1987) 465.

[2] P. Aurenche et al Nucl. Phys. B 297 (1988) 661
P. Aurenche et al Phys. Rev. D 42 (1990) 1440.

[3] CDF preprint Fermilab-conf. 90/118-E [E-741/CDF]
Proceeding of the workshop on hadron structure functions and parton distributions, Batavia Illinois April 26-28, 1990, rapported by R. Harris.

[4] F. Aversa et Al, Nucl. Phys. B327 (1989) 105.

[5] G. Curci, W.Furmanski, R. Petronzio Nucl. Phys. B 175 (1980) 27
W. Furmanski, R. Petronzio Phys. Lett. 97B (1980) 437.

[6] W.A. Bardeen, A.J. Buras Phys. Rev. D20 (1979) 166

[7] M. Glück, E. Reya Phys. Rev. D28 (1983) 2749.

[8] D.W. Duke, J. F. Owens Phys. Rev. D30 (1984) 49

FIGURE CAPTIONS

Fig. (1) : examples of diagrams contributing at
(1-a) : LO to the internal mechanism
(1-b) : NTLO to the internal mechanism
(1-c) : LO to the bremsstrahlung mechanism

Fig. (2) : the dependance of the theoretical inclusive single photon corss section on the anomalous component. The dashed curve is obtained with $F_{\gamma/q} = F_{\gamma/g} = 0$ and the solid curve with the parametrization of [1], given by

$$F_{\gamma/q}(z) = \frac{1}{2\pi}\left[e_q^2 \frac{2.21 - 1.28z + 1.29z^2}{1-1.631n(1-z)} z^{0.049} + 0.002(1-z)^2 z^{-1.54}\right],$$

$$F_{\gamma/g}(z) = \frac{1}{2\pi}\, 0.0243(1-z)z^{-0.97}.$$

Fig. (3) : Comparison of the CDF data on inclusive photons and QCD predictions.

Fig. (4) : Ratio Δ of the $0(\alpha_s^3)$ partonic cross section convoluted with the LO distributions D.O.1 [8] and fragmentation functions [1], over the fully inclusive cross section $d\sigma/dp_T\, dy$ of [2]. Both factorization scale M and renormalization scale μ are taken to be $p_T/4$. The fragmentation scale M_F is $\sqrt{\hat{s}}$.

Fig. (5) : NTLO diagrams contributing to $P_{gg}^{(1)}$ and their counterparts for $K_{\gamma g}^{(1)}$.

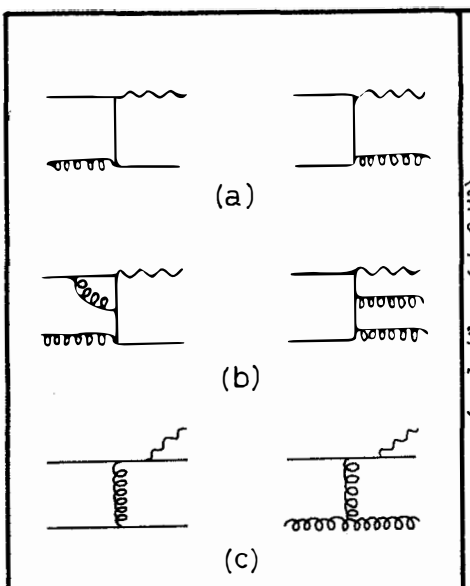

Fig.(1)

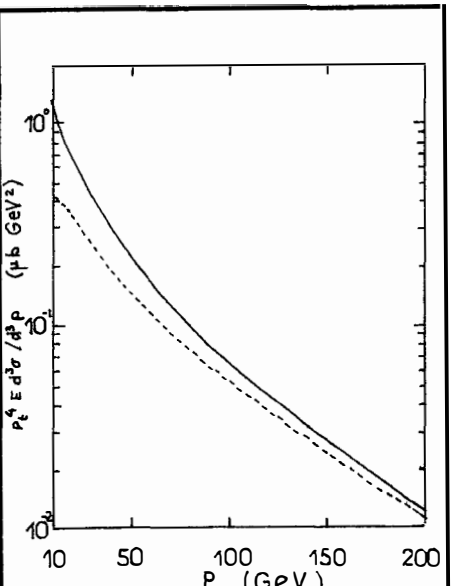

Fig. (2)

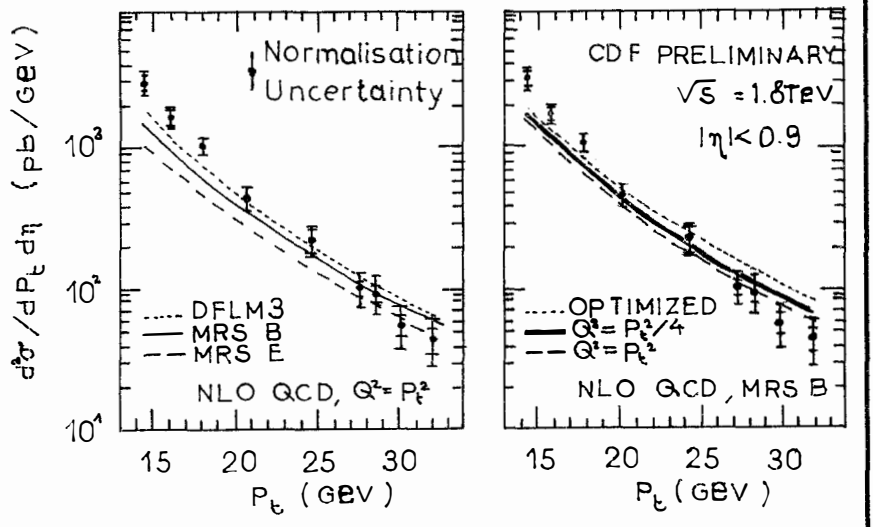

Fig. (3)

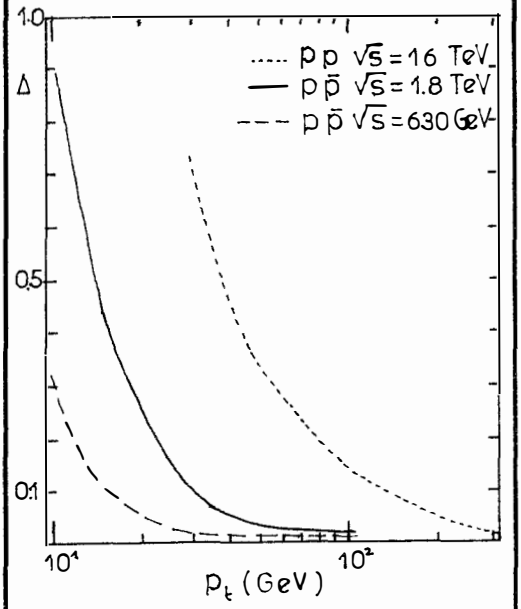

Fig. (4)

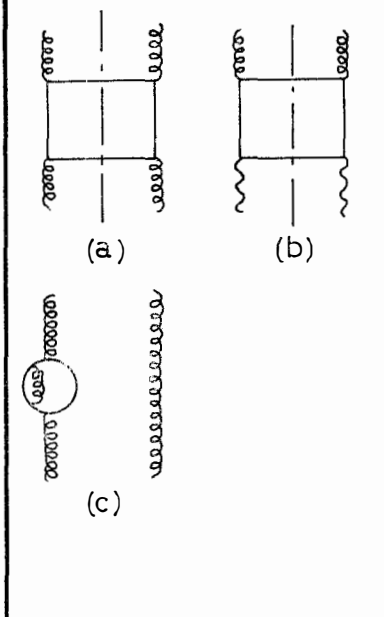

Fig. (5)

HIGGS SECTOR

LABORATORI NAZIONALI DI FRASCATI DELL'INFN

Searching for a Light Intermediate Mass Higgs at the Large Hadron Collider

Giulia Pancheri

INFN, Laboratori Nazionali di Frascati
P.O.Box 13, I00044 Frascati (Rome)
PANCHERI@IRMLNF

Abstract

Decay channels and event signatures for a light intermediate Higgs boson of mass $m_Z \leq m_H \leq 2m_W$ are reviewed in light of recent CDF limits on the top quark mass . At hadron colliders, LHC and SSC, rare decay channels like $H \rightarrow Z^*Z^*$ and $H \rightarrow \gamma\gamma$ are necessary in order to disentagle the signal from the background. It is noticed that the very rare process in which a Higgs boson is produced in association with a Z boson could be used to detect a Higgs boson in the 80-100 Gev/c^2 mass range, but only if a very high luminosity option were available.

1 Introduction

The question of the existence of at least one neutral Higgs particle (H^0) is a central problem of electro-weak unification. As well known, although the properties of the Higgs field are rather well constrained, the expectations on its mass, which are crucial when it comes to detecting it, are widely open.

A first systematic search for H^0 is on its way at LEP and it is amongst the main motivations for a further increase of its energy (LEP200). Present measurements [1] have established that the Higgs mass is larger than 48 GeV/c^2. In the next few years it is expected [2] that either H^0 will be found at LEP or such limits will be raised to $80 \div 85$ GeV/c^2.

Any further extensions of this search will require energies and luminosities which are beyond the possibility of the present LEP project and would then need new colliders[3]. It should be pointed out that the energy domain next to the one of LEP, i.e. $80\ GeV/c^2 \leq M_H \leq 2m_Z$ is crucial, since there are many theoretical indications, from minimal supersymmetry [4, 5] to lattice simulations [6], which point to its possible existence in this mass range. In addition, recent studies on radiative corrections to W and Z-boson masses [7] have shown that the most probable value for the top mass is given by $m_{top} = 127 \pm 30\ GeV/c^2$ and that for such value, the minimum of the χ^2 relative to all existing data on the electroweak parameters falls in the region $M_H \approx 100 - 130\ GeV/c^2$. The detection of such an "intermediate mass" H^0 is considered as very difficult and perhaps even impossible [8] with the hadronic colliders presently planned (LHC,SSC) in view of the presence of severe QCD-related backgrounds and in the absence of an appropriate signature. This observation has prompted the interest for an e^+e^- collider of energy beyond the one of LEP - in the range $0.5 \div 1\ TeV$ - in order to extend the search for H^0 to about $200 \div 300\ GeV/c^2$ [9].

In the present paper we would like to show that if a sufficiently high luminosity ($5 \times 10^{34} cm^{-2} sec^{-1}$) is made available at a hadron collider, one can find signatures which make such an intermediate Higgs detectable with an appropriate specialized detector, thus closing the mass gap with respect to LEP200 and removing - so to say - the "necessity" of an additional e^+e^- collider. In particular, in this note, we shall address the possibility of detecting a "light intermediate" Higgs boson , in the mass range $80 - 130\ GeV/c^2$, i.e. in a range which is not accessible to the so called "gold plated" signature, $H \rightarrow ZZ^* \rightarrow 4\ leptons$.

We shall start presenting width and production cross-sections for a Higgs boson in this mass range. Next we shall discuss event rates and comparison with the expected background.

2 Decay widths and Branching Fractions

Since the coupling to fermion pairs is proportional to their mass, the physics of the Higgs sector is strongly dominated by the top quark for which there is an upper bound to the mass, m_{top}, from radiative corrections [7], $m_{top} \leq 200\ GeV/c^2$ since $\rho \approx 1$. The present experimental limit reported by the CDF collaboration [10] at FermiLab is $m_{top} \geq 89\ GeV/c^2$.

The fact that m_{top} has exceeded m_W has profund consequences on the H^0 phenomenology :

- the decay channel into $b-\bar{b}$ pairs dominates below the W-pair threshold ($M_H \leq 2m_W$) and correspondingly the decay width of a light Higgs is extremely narrow. Rare decay channels become experimentally accessible, in particular those with one or both IVB propagators off-the-mass-shell, and decay into two photons . The branching fractions into these rare channels become sensitive to higher order QCD corrections[11] to the b-quark mass, a QCD enhancement effect, which may be crucial for detecting a light intermediate Higgs.

- The production of $t-\bar{t}$ pairs is now a QCD driven process of large cross-section in hadronic collisions of sufficiently high energy (many TeV). The new limit on the top mass [10] implies that the dominant decay will be $t \rightarrow Wb$. Hence production of W-pairs occurs at a rate typical of strong interactions, an overwhelming background to the electroweakly produced W-particles from H^0 decay. Fortunately Z^0 channels are free of such background at least in the absence of flavour changing neutral currents in t-decays. Relying on Z^0 leptonic decays introduces a reduction of event rate (with corresponding luminosity requirement) of about one order of magnitude with respect to previous estimates, since (i) the production of Z^0 is less frequent than the one for $W^{\pm}$ and (ii) its leptonic branching ratio is smaller.

We shall now look in detail into the Higgs boson decay processes. Since the Higgs boson couples to all the known elementary particles, its branching ratioes are many and varied. In Table 1 we write the expressions for the decay probability in various channels and in **Fig. 1** we show some of the decay widths in the mass range $50 \leq M_H \leq 300\ GeV/c^2$. We have chosen $m_{top} = 90\ GeV/c^2$ and $m_b = 3\ GeV/c^2$, the latter so as to take into account higher order QCD corrections to the direct $H \rightarrow f\bar{f}$ coupling. The choice for the top mass , once it exceeds the W-mass, does not influence appreciably neither the widths nor the branching fractions if , as we do , one is interested in signals for $M_H \leq 2m_W$. Not so , as already mentioned, for the choice of the b-quark mass. Indeed choosing a running quark mass, rather than the value $m_b = 5\ GeV$, roughly doubles all the branching ratioes in this region.

For an accurate prediction, it also very important to include decays into Intermediate Vector Bosons off-the-mass-shell . The Higgs decay width into two lepton pairs

Process	Partial Width
$q\bar{q}$	$\frac{3G_F m_q^2 m_H}{4\pi\sqrt{2}}\left(1-4\lambda_q^2\right)^{\frac{3}{2}}$
l^+l^-	$\frac{G_F m_l^2 m_H}{4\pi\sqrt{2}}\left(1-4\lambda_l m_l\right)^{\frac{3}{2}}$
W^+W^-	$\frac{G_F}{8\pi\sqrt{2}} m_H^3 \left(1-4\lambda_W)\right)^{\frac{1}{2}}\left(12\lambda_W^2-4\lambda_W+1\right)$
Z^0Z^0	$\frac{G_F}{16\pi\sqrt{2}} m_H^3 \left(1-4\lambda_Z)\right)^{\frac{1}{2}}\left(12\lambda_Z^2-4\lambda_Z+1\right)$
gluon gluon	$\frac{G_F}{36\pi\sqrt{2}} m_H^3 \left(\frac{\alpha_s(m_H^2)}{\pi}\right)^2 \left\|\sum_q 3I_q\right\|^2$
$\gamma\gamma$	$\frac{G_F}{8\pi\sqrt{2}} m_h^3 \left(\frac{\alpha}{\pi}\right) \left\|3\sum_q Q_q^2 I_q+\sum_l Q_l^2 I_l-\left\|(3I_W+6\lambda_W)\frac{1-2\lambda_W}{1-4\lambda_W}+3\lambda_W+\frac{1}{2}\right\|\right\|^2$

Table 1: Partial Widths of the Higgs decay with $\lambda_k = \left(\frac{m_k}{m_H}\right)^2$ and $I_k = \int_0^1 dx \int_0^{1-x} dy \frac{1-4xy}{1-\frac{xy}{\lambda_q}-i\epsilon}$

through real or virtual Z^0 exchange can be written as follows[12, 13] :

$$\Gamma(H^0 \to 4\mu) = \int_0^{m_H^2} dQ_1^2 \int_0^{(m_H-Q_1)^2} dQ_2^2 \Gamma(H \to Z^*Z^*)\cdot \tag{1}$$

$$\cdot \frac{Q_1\Gamma(Z^* \to \mu^+\mu^-)}{\pi\left[(Q_1^2-m_Z^2)^2+(m_Z\Gamma_Z^*)^2\right]} \frac{Q_2\Gamma(Z^* \to \mu^+\mu^-)}{\pi\left[(Q_2^2-m_Z^2)^2+(m_Z\Gamma_Z^*)^2\right]} \tag{2}$$

where Γ_Z^* is the total width of a Z_0 of mass Q and $\Gamma(H \to Z^*Z^*)$ represents the decay of the Higgs boson into a pair of Z_0's of masses Q_1 and Q_2 and it is given by

$$\Gamma(H \to Z^*Z^*) = \frac{G_F m_H^3}{16\pi\sqrt{2}}\sqrt{1+\lambda_1^2+\lambda_2^2-2\lambda_1\lambda_2-2\lambda_1-2\lambda_2} \tag{3}$$

$$\cdot\left[1+\lambda_1^2+\lambda_2^2+10\lambda_1\lambda_2-2\lambda_1-2\lambda_2\right] \tag{4}$$

with $\lambda_i = \frac{Q_i^2}{m_H^2}$. It can easily be checked that the above equation reproduces the known expression for $H^0 \to Z^0Z^0$ when $Q_1 = Q_2 = m_Z$. For Higgs masses near or above the 2 Z^0 threshold , the narrow width approximation in eq.(1) thus reproduces the decay probability of Higgs into 4 muons. Notice that although the above expression has been written for both Z^0's off the mass shell, the favourite kinematical configuration is one in which one Z^0 is on shell. This is the decay configuration which appears in Fig. 1. A formula similar to the above holds also for W-pairs (with a extra factor 2, to compensate for non-identical final state particles) and enters into the calculation for the total width.

In **Fig. 2** we show the branching fractions for a Higgs boson in this mass range, for some purely electromagnetic and leptonic channels : $H^0 \to \gamma\gamma$, $H^0 \to \mu^+\mu^-$ and $H^0 \to Z^*Z^* \to e^+e^-e^+e^-$. Notice that in Fig.2 , we have used eq.(1) for the width,

with both Z^0's off-the-mass shell, as appropriate. To evidentiate the dependence upon the running b-quark mass, we have plotted the BR for two different values of m_b.

3 Production of H^0

The production of H^0 is significant in high energy hadron collisions and it is primarily mediated either through its (predicted) coupling to the heaviest quark (top) or the IVB's. The first production mechanism leads to production of an isolated H^0, while the latter implies the production of either a pair $H^0 - Z^0$ or of a pair $H^0 - W^{\pm}$. Cross-sections for direct or associated production are shown in **Fig.3** together with some typical cross-sections for processes which produce Z^0's. These cross-sections are calculated using parton densities from EHLQ[14], set 2, except for Z^0 inclusive production, for which we have followed the calculation by Altarelli et al. [15].

One can see that the reduction of about a factor 10^2 between direct and associated production cross-section may be compensated by

- the signature of the presence of the Z^0 in the debris of the event and perhaps also
- the more reliable estimate of the cross-section since the properties of the Z^0 (mass, couplings, etc.) are better known than the ones of the top and more immediately related to H^0.

Although higher by about a factor 2 (and more , if branching fractions of the IVB into leptonic channels are taken into account), the cross-section for $H^0 - W^{\pm}$ has not been shown, since the process $H^0 - Z^0$ is free of t-quark associated backgrounds and thus highly preferable.

The inclusive selection of a Z^0 is an excellent precursory signature toward $H^0 - Z^0$ events as shown in Fig.3 , where one can see that typically $10^{-4} \div 10^{-5}$ of Z^0 events [15] may contain an H^0 depending on its mass. As a comparison, if the isolated H^0 production (in this mass range the cross-section is of the order of few tenths of a nanobarn) is related to the inelastic cross-section, the corresponding ratio is $10^{-8} \div 10^{-9}$!

The production of Z^0 pairs has a cross-section which is approximately ten times larger than the one for $H^0 - Z^0$ events. It therefore follows that this production mode can be useful for H^0 detection only if one where to observe the Higgs boson in a decay mode inaccessible to the Z^0. Such is the decay of Higgs into two photons, since due to Yang's theorem [16] , the mode $Z^0 \to \gamma\gamma$ is forbidden.

4 Event Rates and Background

We can now compare cross-sections for direct Higgs production and decay into two lepton pairs , with and without cuts on the lepton invariant masses, with the cross-section for associated Higgs-Z^0 production and decay into one pair of photons and one lepton pair, respectively. This comparison is shown in **Fig.4**. In this figure we also show cross-section for direct Higgs production and decay into $\gamma\gamma$. From this figure, one can see that the intermediate mass H^0 ($M_H \leq 2M_Z$) can be detected by two partially overlapping methods :

- In the alternative that the mass of H^0 falls below threshold for a pair of real particles, it is possible to attempt detection - still based on inclusive H^0 production - with the reaction $H \rightarrow Z_1^0 + Z_2^* \rightarrow e_1^+ + e_1^- + e_2^+ + e_2^-$ but with Z_2^* off-the-mass-shell. An appropriate cut ($M_2 \geq 0.6M_Z$) must be introduced in the invariant mass of M_2 of the $e_2^+ + e_2^-$ pair in order to remove events in which a virtual photon γ_2^* is exchanged in the place of Z_2^* [17, 18, 19]. On the other hand, the presence of the Z^0 propagator makes the distribution of M_2 peak sharply toward its highest possible value. This is method is valid, but it runs out of rate when $M_H \leq 140\ GeV/c^2$.

- The decay channel $H \rightarrow \gamma\gamma$ is of considerable interest since (i) it is sizeable for all H^0-masses below the IVB threshold (ii) it cannot be masked by Z^0's. However, unless an extraordinarily sharp mass resolution is ensured, the H^0-mass peak from inclusive production will remain buried within the QCD continuum primarily due to $q\bar{q} \rightarrow \gamma\gamma$.

From the above considerations we conclude that in order to have a clearly identifiable signal for a Higgs boson in the Z^0mass region, one must make use of the associated $H^0 - Z^0$ production, because of the far greater probability of finding an $H \rightarrow \gamma\gamma$ event when in coincidence with a $Z^0 \rightarrow e^+ + e^-$ signature. However, in order to be able to collect an acceptable number of events, the integrated luminosity must be correspondingly larger. In addition, use must be made of events from $Z^0 \rightarrow \mu^+\mu^-$. In Table 2, we show the expected number of events for this production channel, assuming an integrated luminosity of $5\text{x}10^5\ pb^{-1}$ at the LHC, for all Higgs bosons produced within $\pm$ 2.5 units of rapidity, and with two different cuts on the photon transverse momentum (see later discussion).

Before concluding that the number of events, although not large, could be adequate, we must examine resolution and intrinsic background problems. There is in fact a potentially dangerous background constituted by γ pairs emitted,through QED bremsstrahlung, from the initial quark-antiquark legs. To eliminate some of this background, one must introduce appropriate cuts on the photon transverse momentum. One can impose a generic cut $p_t^\gamma \geq 30\ GeV$ on the photons , and assume that a

M_{Higgs}	# Events $p_t^\gamma \geq 30GeV$	# Events $p_t^\gamma \geq 20GeV$
80 GeV	19	31
100 GeV	25	34
120 GeV	25	30
140 GeV	16	17

Table 2: **Table 2 : HZ→ $\gamma\gamma l^+l^-$**

resolution $\Delta M = 1\ GeV/c^2$ can be achieved. With these values of the parameters, we see from **Fig.5a** that the signal is well visible above the background[20]. To increase the statistical significance, one might try to adopt a less stringent cut. This was done in **Fig. 5b** where the cut on the photon transverse momentum is $p_t^\gamma \geq 20\ GeV/c^2$. The number of events from the signal increases , as shown in Table 2, and so does the background[20]. The signal however remains well visible.

5 Conclusions

We have examined the rare decay processes $H^0 \rightarrow Z^*Z^*$ and $H \rightarrow \gamma\gamma$ for an intermediate mass Higgs produced directly and in association with a Z^0 . Upon imposing some reasonable cuts to eliminate part of the intrinsic background from $Z\gamma^*$ for one process and $Z^0\gamma\gamma$ for the other, it appears that for a Higgs boson such that $M_H \approx m_Z$, the process $pp \rightarrow Z^0H \rightarrow l^+l^-\gamma\gamma + X$ has a good signal to noise ratio and a number of events which is rather small, but adequate provided a very high luminosity is available, i.e. L=5x10$^{34}cm^{-2}sec^{-1}$. We notice that the cross-section for direct Higgs production and decay into $\gamma\gamma$ is much larger (and so it is for the event rate), but given the large background which accompanis this process, we believe the signature discusses here to be, if not competitive, at least complementary with $H \rightarrow \gamma\gamma$. We think that the process $pp \rightarrow Z^0H \rightarrow l^+l^-\gamma\gamma + X$ should be seriously considered at the LHC, as a mean to discover the Higgs boson or to exclude its existence in the mass range just above the region accessible to LEP200, i.e . $80 \leq M_H \leq 130GeV/c^2$.

References

[1] ALEPH Collaboration, Phys. Letters 236 (1990) 233.
OPAL Collaboration, Phys. Lett. 236 (1990) 225 .

[2] S.L.Wu et al., ECFA Workshop on LEP200, eds A.Bohm and W.Hoogland, Vol. ii (1987).

[3] C.Rubbia, "Perspectives for a Hadron Collider in the LEP Tunnel", CERN Seminar, November 6th, 1989.

[4] R. Barbieri and S.Ferrara, "Supersymmetry and Fundamental Interactions in the Region of the Fermi Scale", in Surveys in High Energy Physics, Vol. 4, pag.33 (1983).

[5] H.P.Nilles, Physics Reports C110, 1 (1984).

[6] I. Montvay, Nuclear Physics B293, 479 (1987) ; Rev. Mod. Physics 59, (1987).

[7] J.Ellis and G.L.Fogli,, CERN-TH.5817/90, "New Bounds on M_H from Precision Electroweak Data" and references therein ; Physics Lett. 232B, 139 (1989).

[8] B.Cox and F.Gilman, p.87, Proc. 1984 Summer Study on Design and Utilization at SSC, eds. R.Donaldson and J.Morfin, American Physical Society.

[9] D. Froidevaux in Proceedings of the Workshop on Physics at Future Accelerators, ed. J.Mulvey, CERN 87-07 (1987).

[10] CDF Collaboration, F.Abe et al., Phys. Rev. Letters 64, 142 (1990); ibid. 147 (1990).

[11] J.Gasser and H.Leutwyler, Physics reports 87, 77 (1990).

[12] R.Cahn, Reports on Progr. in Physics 52, 389 (1989).

[13] A.Grau, G.Pancheri and R.J.N.Phillips, Phys.Lett.B251 ((1990) 293.

[14] Eichten, Hinchcliffe, K,Lane and C. Quigg, Rev. of Modern Phys. 54 (1984) 579.

[15] G.Altarelli, K.Ellis and G. Martinelli, Zeit Phys. C 27, 617 (1985).

[16] C.N.Yang, Phys.Rev. D77, 242(1950).

[17] J.[AF.Gunion, P.Kalyniak, M.Soldate and P.Galison, Phys. Rev.D34, 101 (1986). J.F.Gunion, G.L.Kane and J.Wudka, Nucl.Phys. B299, 231 (1988).

[18] J.F.Gunion, H.H.Haber, G.L.Kane and S.Dawson, "The Higgs Hunter's Guide",UCD-89-4.

[19] A.Grau, G.Pancheri and Y.N. Srivastava, "$Z^0\gamma^*$ Production at Hadron Colliders", LNF-91/026(P), May 1991. Submitted to Phys.Rev.D.

[20] A.Grau, G. Pancheri and T.Han, in Proceedings of the ECFA Large Hadron Collider Workshop, Aachen, 4-9 October 1990.

Figure Captions

Fig.1 Decay width for an intermediate mass Higgs boson decaying into : WW^* and ZZ^* with both charges included for the W's (dot-dashes), W^+W^- and Z^0Z^0 pairs (dashes), $b\bar{b}$-pairs of mass $m_b = 3\ GeV$ (dots), two photons (dashes) with $m_{top} = 90\ GeV$, $\mu^+\mu^-$-pairs (dots). Full line is the total width.

Fig. 2 Decay fractions for an intermediate mass Higgs into two photons (dots), $\mu^+\mu^-$pairs (dashes) and 4 electrons (full line) from all , on and off-shell, Z^0Z^0 pairs, with $m_{top} = 90\ GeV/c^2$ and $m_b = 3$ and $5\ GeV/c^2$.

Fig. 3 Total cross-section in proton-proton collisions at $\sqrt{s} = 16\ TeV$ for the following processes : (1) inclusive Z^0 production to order α_s as from ref. 15, varying between indicated limits (dots) because of theoretical errors from QCD,(3) production of an isolated Higgs boson from gluon-gluon fusion with different top mass values (full line) and $|y_{Higgs}| \leq 2.5$, (4) production of Z^0 pairs from quark-antiquark annihilation (dashes) with $|y_Z| \leq 2.5$, (5) associated production of Higgs and Z^0 boson (full line) with $|y_{H,z}| \leq 2.5$.Parton densities are from ref.14, mode 2.

Fig.4 Total production cross-section for the processes :

$pp \rightarrow HZ + X \rightarrow \gamma\gamma e^+e^- + X$ (full line)

$pp \rightarrow H + X \rightarrow \gamma\gamma + X$ (dots)

$pp \rightarrow Z^*Z^* + X \rightarrow e_1^+e_1^- + e_2^+e_2^- + X$ with

(i) no special selection (dashes)

(ii) one lepton pair such that $|M_{e^+e^-} - m_Z| \leq \Gamma_Z$ and the other such that $M_{e^+e^-} \geq 20\ GEV$ (dotdashes)

(iii) one lepton pair such that $|M_{e^+e^-} - m_Z| \leq \Gamma_Z$ and the other such that $M_{e^+e^-} \geq 50\ GeV$ (dotdashes).

Everywhere is $|y_Z| \leq 2.5$

Fig.5 Differential cross-section for $pp \rightarrow Z\gamma\gamma + X$ vs. the invariant mass of the $\gamma\gamma$ system at $\sqrt{s} = 16\ GeV$. Histograms are for the purely QED process, i.e. Z^0 production and double bremsstrahlung from initial quark legs , and for production of a Higgs boson of mass $M_{Higgs} = 80, 100, 120, 140\ GeV/C^2$. In Fig.5a the cut on each single photon is $p_t^\gamma \geq 30\ GeV$, while in Fig.5b is $p_t^\gamma \geq 20\ GeV$.In both figures, $|y_Z| \leq 2.5$.

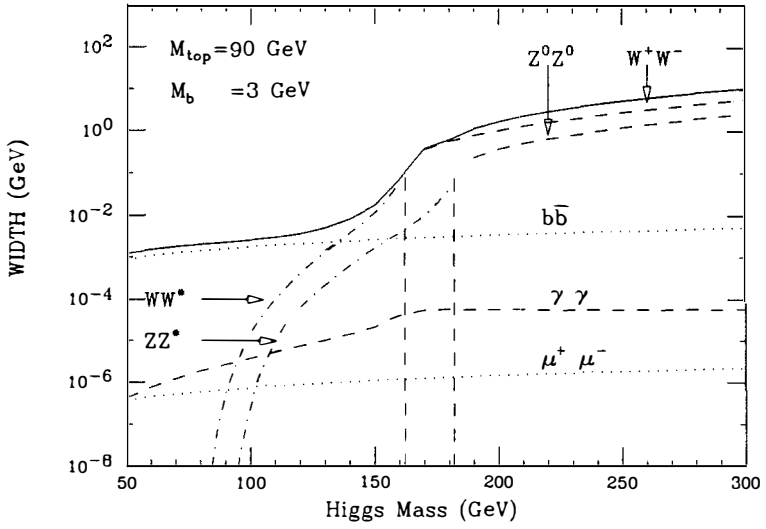
M_{top}=90 GeV
M_b =3 GeV
Z^0Z^0
W^+W^-
$b\bar{b}$
WW*
ZZ*
$\gamma\gamma$
$\mu^+\mu^-$
WIDTH (GeV)
Higgs Mass (GeV)

Fig. 1

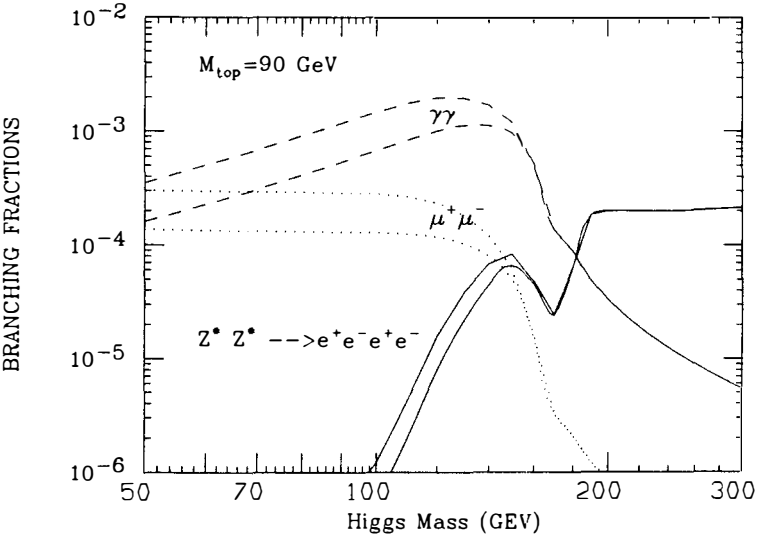
M_{top}=90 GeV
$\gamma\gamma$
$\mu^+\mu^-$
Z* Z* -->$e^+e^-e^+e^-$
BRANCHING FRACTIONS
Higgs Mass (GEV)

Fig. 2

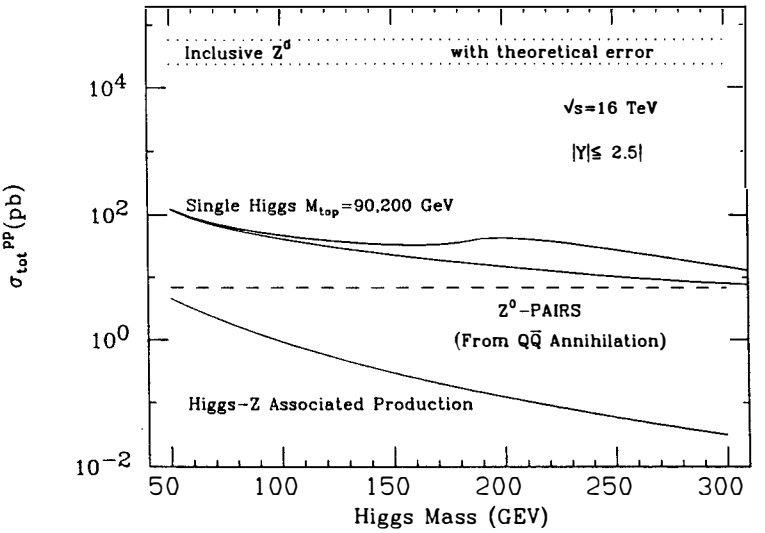
Inclusive Z⁰ with theoretical error
√s=16 TeV
|Y|≤ 2.5|
Single Higgs M_top=90,200 GeV
Z⁰-PAIRS
(From QQ̄ Annihilation)
Higgs-Z Associated Production
σ_tot^PP(pb)
10⁴
10²
10⁰
10⁻²
50
100
150
200
250
300
Higgs Mass (GEV)

Fig. 3

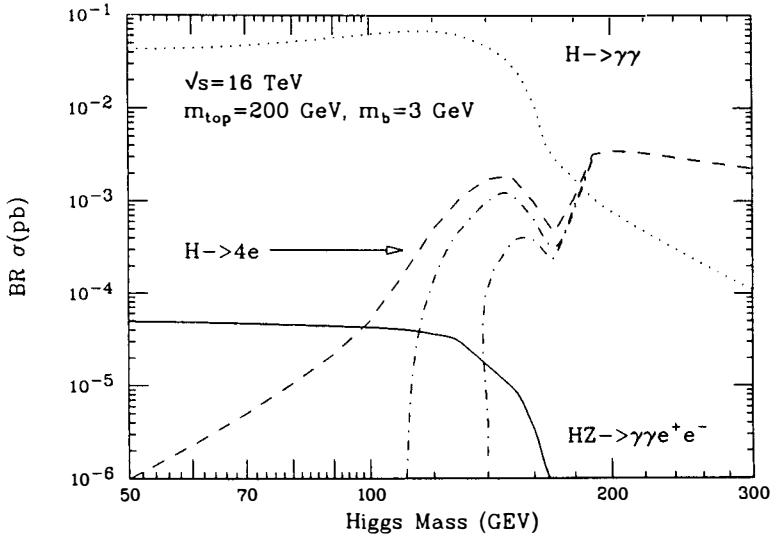
H->γγ
√s=16 TeV
m_top=200 GeV, m_b=3 GeV
H->4e
HZ->γγe⁺e⁻
BR σ(pb)
10⁻¹
10⁻²
10⁻³
10⁻⁴
10⁻⁵
10⁻⁶
50
70
100
200
300
Higgs Mass (GEV)

Fig. 4

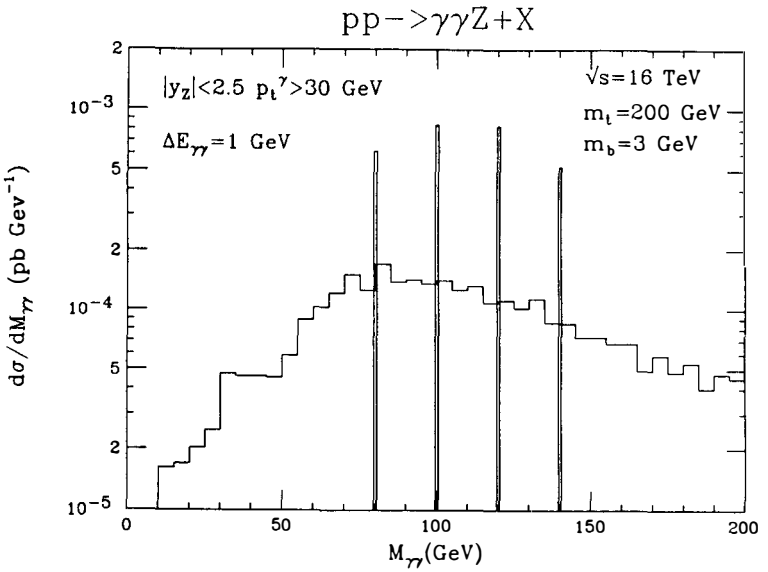
pp->γγZ+X
|y_Z|<2.5 p_t^γ>30 GeV
ΔE_γγ=1 GeV
√s=16 TeV
m_t=200 GeV
m_b=3 GeV
dσ/dM_γγ (pb Gev^-1)
M_γγ(GeV)

Fig.5A

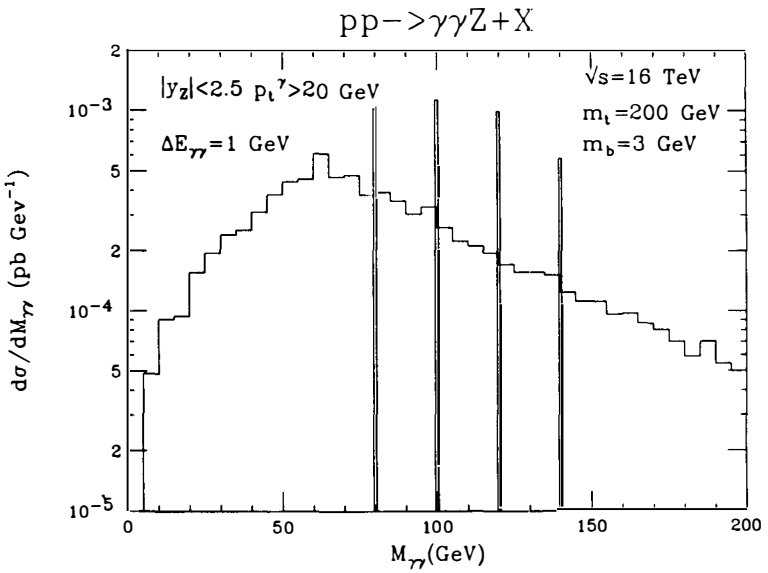
pp->γγZ+X
|y_Z|<2.5 p_t^γ>20 GeV
ΔE_γγ=1 GeV
√s=16 TeV
m_t=200 GeV
m_b=3 GeV
dσ/dM_γγ (pb Gev^-1)
M_γγ(GeV)

Fig.5B

PROSPECTS OF CHARGED HIGGS SEARCH IN TOP QUARK DECAY AT TEVATRON COLLIDER ENERGY

D.P. Roy*
Theory Division, CERN
CH-1211 Geneva 23, Switzerland

ABSTRACT

Assuming a top quark mass of about 150 GeV, we analyze the prospect of charged Higgs search in top quark decay at the Tevatron upgrade. Universality predicts the relative size of the top decay signal via the W boson in different decay channels; and a sizeable excess over this prediction constitutes a viable signature for charged Higgs production. The effect of QCD corrections on the charged Higgs signature is considered in detail. In the charged Higgs-fermion coupling scheme suggested by minimal SUSY or E_6 string-inspired models, one expects to see an observable signal up to a charged Higgs mass of $\simeq$ 100 GeV throughout the allowed range of the coupling parameter $\tan\beta$. This is not true, however, for the alternative coupling schemes of two Higgs doublet models.

The direct top search experiment by CDF as well as the $B_d - \bar{B}_d$ mixing data suggest a heavy top quark of mass > 80 GeV. Furthermore, the radiative corrections to W, Z masses suggest a fairly definitive mass range for the top[1], i.e., $m_t = 150 \pm 30$ GeV. It is reasonably certain that a top quark in this mass range will have an observable signal at the Tevatron upgrade[2], with an expected annual luminosity of several hundred pb^{-1}. Besides providing the first direct evidence for the top, this will enable one to probe for new particles in the top quark decay; the large mass of the top offers the possibility of carrying on this probe to a hitherto unexplored mass range. In particular there has been a great deal of current interest in one such new particle[3], i.e., the charged Higgs boson of the two-Higgs-doublet model[4]. This talk is devoted to a systematic study of the prospect of charged Higgs search at the Tevatron collider energy, based on Refs. 5) and 6). In particular we shall address ourselves to the following questions. (1) Assuming a top quark mass of 150 GeV, what range of the charged Higgs mass can be probed unambiguously, in the sense that one expects an observable signal throughout the

* On sabbatical leave from TIFR, Bombay 5, India

allowed range of the coupling parameter ($\tan\beta$)? (2) What are the most promising $t\bar{t}$ decay channels for the charged Higgs signal? (3) What is the effect of QCD corrections on this signal?

Two -- Higgs – Doublet Model: It contains two $SU(2)$ doublets of complex scalar fields

$$\begin{pmatrix} \phi_1^0 \\ \phi_1^- \end{pmatrix} \quad \begin{pmatrix} \phi_2^+ \\ \phi_2^0 \end{pmatrix}$$

with vacuum expectation values

$$< \phi_1^0 > = \frac{v_1}{\sqrt{2}}, \quad < \phi_2^0 > = \frac{v_2}{\sqrt{2}} \tag{1}$$

satisfying the W mass constraint

$$v_1^2 + v_2^2 = v^2 = (246 \text{ GeV})^2 \tag{2}$$

A key parameter of the model is the ratio of the v.e.v's

$$\tan\beta = \frac{v_2}{v_1} \tag{3}$$

After absorbing the three Goldstone bosons one is left with five physical Higgs particles - the neutral scalars h^0, H^0 and pseudo-scalar A^0 along with the charged states $H^\pm$. We shall be concerned here only with the charged states, i.e.,

$$H^\pm = \phi_2^\pm \cos\beta - \phi_1^\pm \sin\beta \tag{4}$$

The two-Higgs-doublet model is a minimal extension of the Standard Model with the following attractive features. It naturally satisfies the constraints of $\rho = 1$ and the absence of a flavour charging neutral current at the tree level. While the first is guaranteed by the doublet structure of the Higgs, the second is ensured by choosing the Higgs-fermion couplings according to the Glashow-Weinberg theorem[7], which states that the tree-level FCNC will be absent if all the fermions of a given charge have Yukawa couplings to only one Higgs doublet. A very important model automatically satisfying this theorem is the minimal SUSY extension of the standard model, where the up-type quarks have Yukawa couplings to one Higgs doublet (ϕ_2, say) while the down-type quarks and charged leptons couple to the other. There is considerable theoretical interest in this two-Higgs-doublet model[4] since it provides the most economical solution

to the hierarchy problem of the Standard Model. Moreover it offers the possibility of explaining the quark mass hierarchy $m_c \gg m_b$ and $m_t \gg m_b$ in terms of that of the v.e.v.'s $v_2 \gg v_1$. In this model the Yukawa couplings of the physical charged Higgs fields of Eq. (4) to fermions are given by

$$\alpha = \frac{g}{\sqrt{2}m_W} H^+\{\cot\beta\ m_{ui}\ \bar{u}_i\ d_{iL} + \tan\beta\ m_{d_i}\ \bar{u}_i\ d_{iR} + \tan\beta\ m_{\ell i}\ \bar{\nu}_i\ \ell_{iR}\} + \text{h.c.} \quad (5)$$

in the approximation of the diagonal KM matrix. Identical charged Higgs couplings to fermions hold in the E_6 superstring-inspired models[8] as well. The main phenomenological difference between the minimal SUSY and the E_6 models is that while the former predicts $m_H > m_W$ the latter gives a less restrictive bound $m_H > 53$ GeV.

We shall concentrate on the coupling scheme of Eq. (5) above in view of the wide theoretical interest behind it. Let us note, however, that there are three alternative schemes allowed by the Glashow-Weinberg theorem - i.e., where the down-type quarks or the charged leptons or both have Yukawa couplings to ϕ_2 instead of ϕ_1. They correspond to replacing either of the two $\tan\beta$ factors or both by $\cot\beta$ in Eq. (5). We shall see how the result changes when one goes to these alternative schemes.

The present constraints on the charged Higgs mass and coupling parameters are as follows. (1) The LEP experiments[9] give a lower mass bound $m_H > 40$ GeV. (2) Validity of perturbation theory requires the Yukawa coupling proportional to m_t in Eq. (5) to be $< g_s(\simeq 1)$. This implies $\tan\beta > m_t/600$ GeV ($\simeq 1/4$). A somewhat stranger bound of $\tan\beta > 0.3$-0.4 has been obtained from the H^+ exchange loop contribution to $b \to s\gamma$ decay and the ϵ'/ϵ ratio[10]. (3) Applying the analogous perturbative limit for the Yukawa coupling proportional to m_b, appearing in the second term of Eq. (5), given $\tan\beta < 600\ \text{GeV}/m_b(\simeq 120)$. Thus the region of phenomenological interest is $m_H > 40$ GeV and $\tan\beta = 0.5$-100.

<u>$H^\pm$ signal v. s. $W^\pm$ background in t quark decay</u>

We have

$$\Gamma_{t\to bW} = \frac{g^2}{64\pi m_W^2 m_t}\lambda^{1/2}\left(1, \frac{m_b^2}{m_t^2}, \frac{m_W^2}{m_t^2}\right)\left[m_W^2(m_t^2+m_b^2) + (m_t^2-m_b^2)^2 - 2m_W^4\right] \quad (6)$$

while from Eq. (5) one gets the partial width

$$\Gamma_{t\to bH} = \frac{g^2}{64\pi m_W^2 m_t}\lambda^{1/2}\left(1, \frac{m_b^2}{m_t^2}, \frac{m_H^2}{m_t^2}\right)\left[(m_t^2\cot^2\beta + m_b^2\tan^2\beta)(m_t^2+m_b^2-m_H^2) + 4m_t^2m_b^2\right] \quad (7)$$

and the corresponding branching fraction

$$B_{t\to bH} = \Gamma_{t\to bH}/(\Gamma_{t\to bH} + \Gamma_{t\to bW}) \tag{8}$$

From Eq. (5) one can also get the dominant H decay widths

$$\Gamma_{H\to\tau\nu} = \frac{g^2 m_H}{32\pi m_W^2} \cdot m_\tau^2 \tan^2\beta \tag{9}$$

$$\Gamma_{H\to c\bar{s}} = \frac{3g^2 m_H}{32\pi m_W^2}(m_c^2 \cot^2\beta + m_s^2 \tan^2\beta) \tag{10}$$

and the branching fraction

$$B_{H\to\tau\nu} = 1 - B_{H\to c\bar{s}} = \frac{m_\tau^2 \tan^2\beta}{m_\tau^2 \tan^2\beta + 3(m_c^2 \cot^2\beta + m_s^2 \tan^2\beta)} \tag{11}$$

This is in striking contrast to the branching fractions of W decay as given by universality, i.e., 1/9 into each lepton species and 2/3 into hadrons (with a small QCD correction factor of $\simeq 4\%$). This difference will be exploited below to separate the H signal from the W background in top quark decay.

Figure 1 shows the branching fractions $t \to bH$ and $H \to \tau\nu$ as functions of $\tan\beta$ for m_H = 60-100 GeV [5,6]. The $t \to bH$ branching fraction is large at the two ends of the $\tan\beta$ space where the Yukawa coupling terms proportional to m_t and m_b approach the perturbative limit. But it is small around

$$\tan\beta = \sqrt{m_t/m_b} \simeq 5 \tag{12}$$

where Eq. (7) has a minimum. On the other hand the $H \to \tau\nu$ branching fraction is large everywhere except the lower end of the allowed $\tan\beta$ space, i.e., $\tan\beta \simeq 0.5$. It is the product of these two branching fractions which controls the observable charged Higgs signal, since it has to be identified through its leptonic ($\tau\nu$) decay to avoid the large QCD background. Thus the potentially problematic regions are $\tan\beta \simeq 5$ and 0.5 where the $t \to bH$ and $H \to \tau\nu$ branching fractions are small respectively. Fortunately the small value of one is partly compensated by the large value of the other, so that for appropriate decay channels one expects the charged Higgs signal to be at least comparable to the W boson background throughout the allowed range of $\tan\beta$. It should be emphasized that this correlation between the two branching fractions is a

remarkable feature of Eq. (5) which does not hold for any of the alternative coupling schemes mentioned above. If both the quark Yukawa coupling terms are proportional to $\cot\beta$ then the $t \to bH$ branching fraction decreases monotonically and hence there is no observable signal beyond the $\tan\beta \sim 5$ region. And if the lepton Yukawa coupling term is proportional to $\cot\beta$ then $B_{H\to\tau\nu} < 1/4$ and hence no observable signal in the $\tan\beta \sim 5$ region. Thus it is only for the charged Higgs-fermion coupling scheme of eq. (5) that one expects an unambiguous signal up to $m_H = 100$ GeV.

The basic process of interest is $t\bar{t}$ production through gluon-gluon and quark-antiquark fusion followed by their decay into charged Higgs or W boson channels, i.e.,

$$\begin{aligned} gg(q\bar{q}) \to & t\bar{t} \to \bar{b}H^-(W^-) \\ & \to bH^+(W^+) \end{aligned} \tag{13}$$

To avoid excessive QCD background at least one of the two charged bosons is required to decay into the τ channel

$$H(W) \to \tau\nu_\tau \tag{14}$$

Finally the τ is to be observed in its hadronic or muonic decay

$$\tau \dashrightarrow \nu_\tau q\bar{q}' \ (64\%), \quad \nu_\tau\nu_\mu\mu \ (18\%) \tag{15}$$

as a narrow jet (τ-jet) or soft muon, accompanied by a large missing p_T. Universality predicts the WW background to any of the resulting final states unambiguously in terms of the hard dilepton channel (which has negligible cont. from H)

$$t\bar{t} \to b\bar{b}W^+W^- \to b\bar{b}\ell^+\ell^-\nu_\ell\nu_\ell \ (\ell = e, \mu) \tag{16}$$

A sizeable excess over this prediction would provide a viable signal for charged Higgs production. Figures 2 and 3 show the expected signal and background for two of the most promising channels - i.e., single and double τ-jet channels corresponding to τ decay of one of the charged bosons or both[5,6]. The scales on the right show the expected number of events for an integrated luminosity of 100 pb^{-1}. The single τ-jet channel provides a viable charged Higgs signature over most of the $\tan\beta$ space, except for a gap around $\tan\beta \sim 5$ (Fig. 2). The double τ-jet channel effectively closes this gap (Fig. 3). This channel has also the advantage of being free from the W + QCD jets background. The only problematic region for this channel is near the lower boundary, i.e., $\tan\beta \sim 0.5$. However, we see that the signal is considerably enhanced in this region by the inclusion of QCD correction[6], so that one has a signal/background ratio $\gtrsim 1$ throughout the allowed $\tan\beta$ space.

QCD Correction[11]: The dominant QCD correction to the charged Higgs couplings comes from the $H \to c\bar{s}$ decay width. The UV divergence cancels between the virtual gluon exchange contribution to this decay vertex and the corresponding counterterm; and the IR divergence cancels when one adds the real gluon emission terms from the decay quarks. The resulting first-order QCD contribution to the decay width reduces to a simple form for $m_H \gg m_{c,s}$; i.e.,

$$\Gamma_{H\to c\bar{s}} = \frac{3g^2 m_H}{32\pi m_W^2}[m_c^2 \cot^2\beta(1+\Delta_c) + m_s^2 \tan^2\beta(1+\Delta_s)] \tag{17}$$

where

$$\Delta q = \frac{2\alpha_s}{\pi}\,(3/2 - \ln m_H^2/m_q^2) \tag{18}$$

Thus the QCD correction term reduces the decay width. The width would of course become negative for very large m_H, signalling the necessity of higher order contributions. The leading log terms can be summed using the standard renormalization group technique[12] giving

$$\Gamma_{H\to c\bar{s}} = \frac{3g^2 m_H}{32\pi m_W^2}[\tilde{m}_c^2(m_H)\cot^2\beta + \tilde{m}_s^2(m_H)\tan^2\beta] \tag{19}$$

$$\tilde{m}_q(m_H) = m_q\,(\frac{\ln(2m_q/\Lambda)}{\ln(m_H/\Lambda)})^{\frac{12}{33-2N_f}}; \tag{20}$$

i.e., the leading log QCD correction is simply taken into account by substituting the running masses for the decay quarks, evaluated at the Higgs mass scale[11]. The effect is to reduce the $H \to c\bar{s}$ decay width, resulting in a significant increase of the branching fraction for $H \to \tau\nu$ at $\tan\beta \leq 1$ (Fig. 1). The corresponding increase in the charged Higgs signal is particularly significant for the double τ-jet channel (Fig. 3), which is seen to go up by as much as a factor of three in this region. There is a small decrease of the signal at very large $\tan\beta$ coming from the analogous QCD correction to the $t \to bH$ width; but this is rather marginal.

Summary: The decay of a top quark of mass $\simeq$ 150 GeV can probe charged Higgs mass up to $\simeq$ 100 GeV at the Tevatron collider energy. In the coupling scheme suggested by minimal SUSY and E_6 models one expects an observable signal throughout the allowed range of the coupling parameter $\tan\beta$. Departure from the universality prediction offers the best signature for charged Higgs production. The most promising channel is the two τ-jet channel. QCD correction enhances the signal significantly for $\tan\beta \leq 1$.

REFERENCES

[1] J. Ellis and G. Fogli, *Phys.Lett.* **B232** (1989) 139;
P. Langacker, *Phys.Rev.Lett.* **63** (1989) 1920.

[2] Sourendu Gupta and D.P. Roy, *Z.Phys.* **C39** (1988) 417;
H. Baer, V. Barger and R.J.N. Phillips, *Phys.Rev.* **D39** (1989) 3310.

[3] V. Barger and R.J.N. Phillips, *Phys.Rev.* **D41** (1990) 884;
A.C. Bawa, C.S. Kim and A.D. Martin, *Z.Phys.* **C47** (1990) 75;
R.M. Barnett et al., Proc. 1990 Summer Study on HEP, Snowmass.

[4] J.F. Gunion, H.E. Haber, G.L. Kane and S. Dawson, The Higgs Hunter's Guide, Addison Wesley (1990).

[5] R.M. Godbole and D.P. Roy, *Phys.Rev.* **D** (in press).

[6] M. Drees and D.P. Roy, CERN-TH.6080/91 (1991).

[7] S. Glashow and S. Weinberg, *Phys.Rev.* **D15** (1977) 1958;
E.A. Paschos, *ibid.* **D15** (1977) 1966;
K. Kang and J.E. Kim, *Phys.Lett.* **64B** (1976) 93.

[8] J.L. Hewett and T.L. Rizzo, *Physics Reports* **183** (1989) 193.

[9] ALEPH Collaboration, *Phys.Lett.* **B241** (1990) 623.

[10] V. Barger, J.L. Hewett and R.J.N. Phillips, *Phys.Rev.* **D41** (1990) 3421;
A.J. Buras et al., *Nucl.Phys.* **B337** (1990) 284;
J.F. Gunion and B. Grzadkiwski, *Phys.Lett.* **B243** (1990) 301.

[11] A. Mendez and A. Pomarol, *Phys.Lett.* **B252** (1990) 461;
C.S. Li and R.J. Oakes, *Phys.Rev.* **D43** (1991) 855.

[12] E. Braaten and J.P. Léveillé, *Phys.Rev.* D22 (1980) 715.

Fig. 1
Branching fractions for $t \to bH$ and $H \to \tau\nu$ decays for $m_H = 60 - 100$ GeV. Effect of QCD corrections is shown in parentheses.

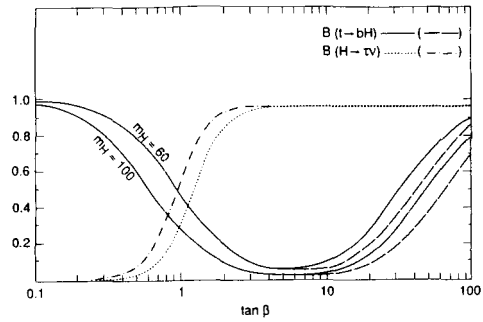

Fig. 2
Charged Higgs signal vs. WW background in the single τ-jet channel corresponding to τ-decay of one of the two charged bosons followed by its hadronic decay. Effect of QCD corrections is shown in parentheses.

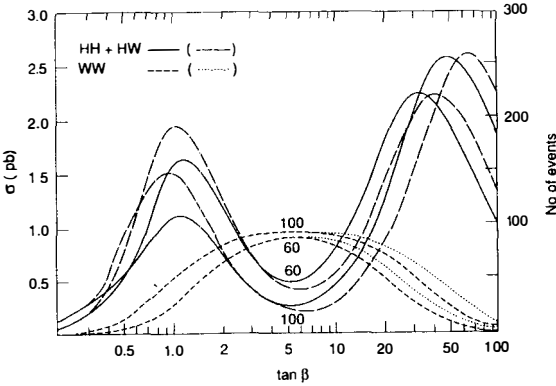

Fig. 3
Charged Higgs signal vs. WW background for the double τ-jet channel corresponding to τ-decay of both the charged bosons. The effect of QCD correction is shown in parentheses.

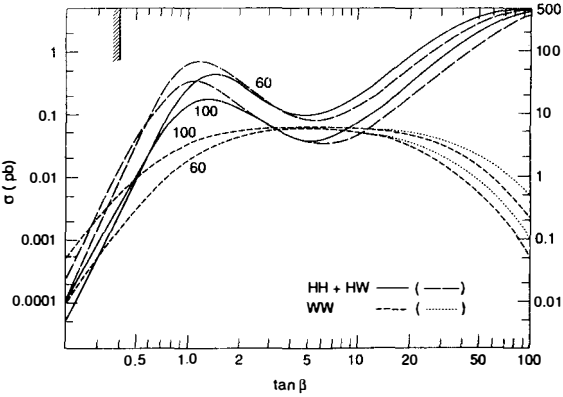

BOUNDS FROM LEP, CDF/UA2 AND ATOMIC PARITY EXPERIMENTS ON A MODEL OF A STRONGLY INTERACTING ELECTROWEAK SECTOR

Roberto Casalbuoni
Dipartimento di Fisica dell'Universita' and Sezione I.N.F.N.
I-50125 Firenze, Italy

ABSTRACT

We calculate the self-energies of the intermediate vector bosons from an effective lagrangian describing possible strongly interacting vector and axial-vector bosons, deduced on the basis of electromagnetic gauge invariance and $SU(2)$ custodial symmetry. Comparison with the standard low-energy parametrization of such self-energies suggests an isospin conserving contribution, called S according to the usual notation, which in principle could also take a negative value, within the permitted range of the model parameters. Technifermion loops in technicolor theories give positive S. Atomic parity experiments indicate a negative central value for S but are affected by large errors and one has to wait for future more accurate determinations. The case of pure vector resonances with direct fermionic couplings is briefly discussed.

This contribution deals with the vector boson self-energy corrections coming from a strongly interacting electroweak symmetry breaking sector. The characteristic feature of such a scenario is here assumed to be the occurrence of resonances with masses in the TeV range. Their origin may be traced back to the same, unspecified, strongly interacting sector which is responsible for the electroweak symmetry breaking. In such a situation no light quanta are present in the low-energy spectrum besides those of the SM. Moreover no new currents become relevant at the present energies other than the SM's ones. We can therefore think of parametrizing the deviations from the SM relations just in term of the gauge vector boson self-energy corrections.

In particular we will consider the case of vector and axial-vector resonances, which, through mixing, affect in principle the self-energies of the ordinary gauge vector bosons. Furthermore we will focus on isospin conserving effects, working in the framework of a model where isospin violating effects are forbidden from the beginning, because of an $SU(2)$ "custodial" symmetry.

The physical picture we have in mind is not bound to any particular explicit dynamical realization of the underlying strongly interacting sector, but one can think, as an example, to technicolor models. In this case the vector and axial-vector resonances would correspond to the techni-rho and techni-A_1 states and our procedure of evaluating the vector boson self-energies would correspond in saturating the dispersion integrals with the lower spin 1 resonances.

Our calculation will assume a model [1] for vector and axial-vector resonances of a possible strong electroweak sector, which we shall shortly review from the standpoint of electromagnetic gauge invariance and custodial symmetry. The dominant vacuum polarization effect from the new vector and axial-vector bosons is found in the isospin conserving parameter S of Peskin and Takeuchi [2], since the assumed custodial symmetry leads to negligible isospin breaking effects. It is interesting that, within the allowed range of the model parameters, S may also take negative values. In technicolor theories the loops of technifermions give positive S, for any number of technicolors and technidoublets. Present experiments on atomic parity violation give a negative central value for S which is however affected by large errors. Negative values for S could also be simulated by some Z' model. It is too early to draw conclusions on this subject and one has to wait for the forthcoming more precise atomic experiments and analysis. Our results only indicate that in principle a strongly interacting electroweak sector, such as described for instance by our effective lagrangian, could also allow for negative S.

The assumptions we do in order to obtain a lagrangian describing vector and axial-vector bound states are [3]:

i) invariance under $U(1)_{em}$,

ii) invariance under a global $SU(2)_c$ (custodial), necessary to guarantee that the parameter ρ, defined in terms of the ratio of the neutral to charged currents, is equal to 1 at tree level,

iii) resonances are described as massive Yang-Mills particles.

Let us start considering only vector resonances. Then, it follows from the previous hypothesis, and from the further assumption that the vector resonances ($V-$particles) form an isospin triplet under $SU(2)_c$, that the necessary parameters are: the mass of the V, m_V, and the gauge coupling g''. The coupling of V to fermions arises here because the V is mixed to ordinary vector bosons. For instance, in the charged sector, the mixing angle is given by $-g/g''$. More generally a direct coupling of V to fermions is allowed, and it is described by a further parameter b. The resulting model has been called BESS (Breaking Electroweak Symmetry Strongly). We will now restrict to $b = 0$ (minimal case) and we will comment about the more general case at the end. The minimal case can be described [4] by using a general approach discussed recently in ref. [5]. This approach describes effects of new physics due to heavy particles with no direct coupling to fermions. Therefore, all their effects regarding LEP physics are concentrated in modifications of the self-energies of the ordinary vector bosons. The main idea is to parametrize the self-energies through an expansion in q^2/Λ^2, where Λ is the scale of new physics. The relevant parameters turn out to be three, and they can be related to physical observables as the ratio m_W/m_Z (measured at CDF/UA2 [6]), the leptonic width, and the forward-backward asymmetry in leptons. The expansion of the self-energies is according to the following formula:

$$\Pi_{ij}^{\mu\nu}(q^2) = -ig^{\mu\nu}\left(A^{ij} + q^2 F^{ij}\right) + q^\mu q^\nu \; terms \tag{1}$$

where the indices i,j run over W, Z and photon fields. The combinations of the parameters A^{ij} and F^{ij} related to the observables are

$$\begin{aligned} \epsilon_1 &= \frac{A_{ZZ}}{M_Z^2} - \frac{A_{WW}}{M_W^2} \\ \epsilon_2 &= F_{WW} - F_{33} \\ \epsilon_3 &= \frac{\cos\theta}{\sin\theta} F_{30} \end{aligned} \tag{2}$$

and ϵ_3 is related to the parameter S of ref. [2] by $\epsilon_3 = \alpha S/(4\sin^2\theta)$. The recent experimental data from LEP [7] and CDF/UA2 [6] give: $m_W/m_Z = 0.7746 \pm 0.0065$, $g_A^2 = 0.2495 \pm 0.0012$, and $g_V^2 = 0.0013 \pm 0.00040$. One then gets [8]: $\epsilon_1 = -0.002 \pm 0.005$, $\epsilon_2 = -0.010 \pm 0.011$, $\epsilon_3 = -0.0004 \pm 0.0076$. For the BESS model we find (at the first order in q^2/M_V^2): $\epsilon_1 = \epsilon_2 = 0$, $\epsilon_3 = (g/g'')^2$.

The BESS model can be generalized to include a triplet of axial-vector resonances [1]. Assuming the same gauge coupling g'' for the axial-vector and vector resonances, one has to introduce two more parameters: the mass m_A of the axial-vector resonances, and the ratio of the mixing of the axial-vector with W and Z, to the mixing of the vector particle. The result is: $\epsilon_1 = \epsilon_2 = 0$ and $\epsilon_3 = (1-z^2)(g/g'')^2$. That is the axial-vector resonances contribute with an opposite sign with respect to the vector particles. This is easily understood by noticing that ϵ_3 can be expressed in terms of the combination $(\Pi_{VV} - \Pi_{AA})$ of the correlators of the vector and of the axial-vector currents. The parameter z is completely free, if however one would like to consider what would happen by scaling from QCD, then one would obtain $z = 1/2$.

Our result should be compared to the one usually quoted for technicolor theories [2,9]. In that case a positive S is found from the one-loop technifermion contributions: $S \sim 0.1 N_T N_D$, where N_T and N_D are the number of technicolors and technidoublets considered. Our analysis shows that the possibility of having a negative S is not a priori excluded in theories of electroweak symmetry breaking whose spectra contain spin 1 bound states, provided the parameters of the corresponding low energy effective lagrangian are such that the axial-vector contribution overcomes the vector one.

We also notice that the contribution to S we have found is of the same order of magnitude as the one in technicolor theories at one loop, at least in the range of parameters where a comparison between our phenomenological lagrangian and technicolor models is meaningful. By evaluating the $\rho\pi\pi$ coupling from hadron data, assuming the validity of the Kawarabayashi-Suzuki-Fayyazuddin-Riazuddin relation, we find:

$$g'' \sim 11.7\sqrt{\frac{3}{N_T}} \tag{3}$$

where the factor $\sqrt{3/N_T}$ comes from the usual large-N scaling argument. For $N_T = 3$ one finds $S \sim 0.4(1 - z^2)$ to be compared with $S \sim 0.3$ obtained in the corresponding one-loop technicolor with 3 technicolors and 1 technidoublet, and we see that the calculations agree quite well in the QCD scaled case, where $z = 1/2$.

Experiments on atomic parity violation and on asymmetries in polarized e-nucleus could provide accurate determinations of S. The analysis by Marciano and Rosner [10] leads to a theoretical estimate for the weak charge of the stable cesium isotope:

$$Q^W({}^{133}_{55}Cs) = -73.20 - 0.8S \pm 0.13 \tag{4}$$

This expression includes electroweak radiative corrections at one loop with their uncertainties from the hadronic contributions [11], hopefully to be reduced from a better knowledge of e^+e^- annihilation into hadrons. The experimental value is $-71.04 \pm 1.58 \pm 0.88$ [12]. Both the experimental (± 1.58) error and the atomic theory uncertainty (± 0.88) may eventually be reduced, particularly the experimental error. From comparison between the preceding present numbers Marciano and Rosner give $S = -2.7 \pm 2.0 \pm 1.1 \pm 0.16$, (where the uncertainties are, in the order, experimental, from atomic theory, from hadronic loop) and they express the hope of a future total uncertainty of ± 0.2. It must be said that a negative value for S from the fit of the theoretical Q^W for cesium to its experimental determination could be simulated by other effects, already at tree-level, such as some particular extra Z' boson, which, as indicated by Marciano and Rosner, would contribute with a positive sign into Q^W corresponding to a negative S.

In the case $b \neq 0$, one can perform a direct analysis by using the full LEP data including the hadronic and the total width [7]: $\Gamma_h = 1740 \pm 9\ MeV$, $\Gamma_Z = 2485 \pm 9\ MeV$. The 90% C.L. allowed region in the plane $(b, g/g'')$ accounting for all the data: m_W/m_Z, Γ_l, Γ_h, Γ_Z and A_{FB}, is given in Fig. 1 for $m_V = 1500\ GeV$, $m_{top} = 150\ GeV$ and $\alpha_s(m_Z) = 0.12$.

The region is practically independent on m_V and it gets shifted to the left by increasing m_{top} and/or α_s.

REFERENCES

[1] R. Casalbuoni, S. De Curtis, D. Dominici, F. Feruglio and R. Gatto Int. Journ. of Mod. Phys. **A 4** (1989) 1065.

[2] M.E. Peskin and T. Takeuchi, Phys. Rev. Lett. **65** (1990) 964.

[3] G. Altarelli, R. Casalbuoni, D. Dominici, F. Feruglio and R. Gatto, Nucl. Physics **B342** (1990) 15; the original formulation of the model is given in: R. Casalbuoni, S. De Curtis, D. Dominici and R. Gatto, Phys. Letters **155B** (1985) 95, and Nucl. Physics **B282** (1987) 235.

[4] R. Casalbuoni, S. De Curtis, D. Dominici, F. Feruglio and R. Gatto, Phys. Letters **258B** (1991) 161.

[5] G. Altarelli and R. Barbieri, Phys. Letters **253B** (1991) 161.

[6] See for instance: D. Froidevaux, Proceedings of the Neutrino Conference, Geneva (1990).

[7] The data on the widths were presented by G.J. Bobbins at the XXVI rencontres de Moriond, Les Arcs, France, March 10-17 1991. The data on g_V^2 and on g_A^2 were reported by P. Rutoff at the same meeting.

[8] The relations among the ϵ_i and the experimental quantities are given in ref. [5].

[9] For a complete list of references, see ref. [4].

[10] W. Marciano and J.L. Rosner, Phys. Rev. Lett. **65** (1990) 2963.

[11] G. Degrassi, A. Sirlin and W. Marciano, Pys. Rev. **D 39** (1989) 287.

[12] M.C. Noecker, B.P. Masterson and C.E. Wieman, Phys. Rev. Lett. **61** (1988) 310; S.A. Blundell, W.R. Johnson and J. Sapirstein, Notre Dame University preprint (1990), to appear in Phys. Rev. Lett.; V. Dzuba, V. Flambaum, P. Silvestrov and O. Sushkov, Phys. Lett. **A 141** (1989) 147.

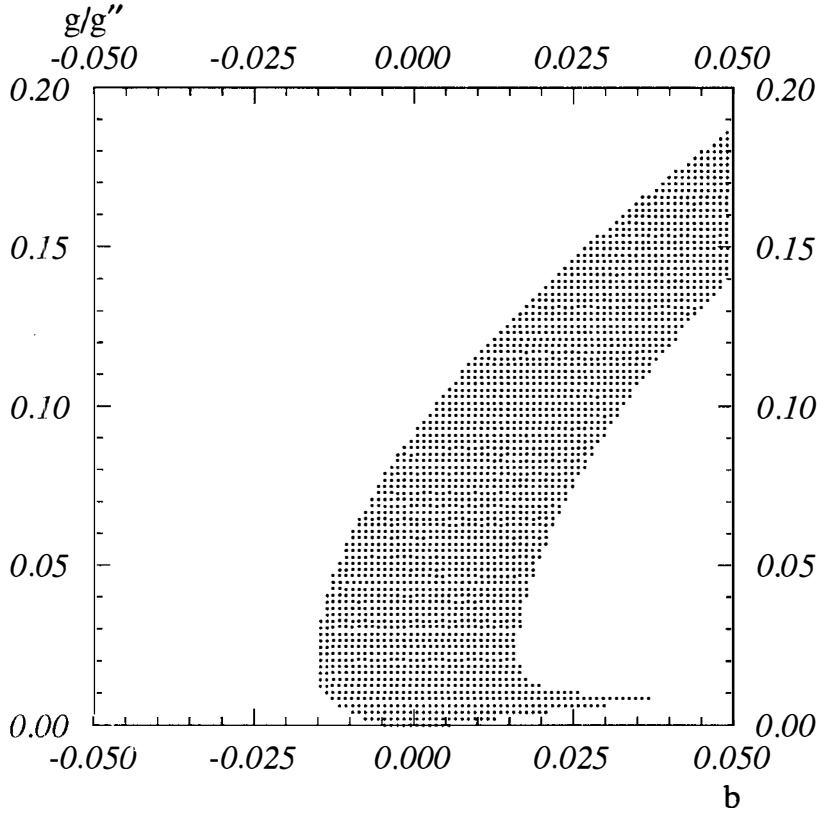

Fig. 1

WZ PRODUCTION FROM THE BESS MODEL AT THE LHC AND SSC COLLIDERS

Stefania De Curtis
Istituto Nazionale di Fisica Nucleare
Sezione di Firenze
I-50125 Firenze, Italy

ABSTRACT

We study WZ pair production at future hadron colliders in the presence of a strong interacting electroweak symmetry breaking sector. The calculations are carried out within the BESS model with parameters limited from present experiments. The fusion production mechanism via longitudinal WZ scattering is compared with the $q\bar{q}$ annihilation mechanism going through vector resonances. Detailed studies of background and statistical significance of signal versus background are made both at LHC and SSC. The new conclusion of our work is the generally dominant role, particularly at LHC, of production through $q\bar{q}$ annihilation. The increase of gauge boson pairs, as expected in the BESS model, together with its distinguished features in the p_T and invariant mass distributions, suggests an important role of LHC and SSC in the exploration of a possible strong electroweak symmetry breaking sector.

1. INTRODUCTION

One of the most exciting opportunity which is offered by the next generation of hadronic colliders is to find the mechanism responsible for the symmetry breaking of the electroweak (EW) interaction. The last years have seen the accumulation of a large amount of data confirming more and more the standard model (SM). Despite of this enormous progress, some sectors of the SM still remain unproved and, in particular, no direct evidence of the Higgs sector has been seen. With the LHC [1] (or SSC [2]) machines hopefully it will be possible either to find the Higgs particle with a mass below 1 TeV or some manifestation of a strongly interacting system, to which the longitudinal W/Z's belong, in the TeV energy regime [3]. Here we will assume that the mechanism responsible for the EW symmetry breaking is based on a strongly interacting sector. We have tried to single out the major feature of such a scenario by formulating a scheme which, reproducing them, remains at low energy as close as possible to the SM picture. Such a scheme is the so called BESS model (BESS standing for Breaking Electroweak Symmetry Strongly) [4]. The model has no Higgs particle. In addition to W and Z it contains a triplet of new massive vector bosons V which are assumed to be the main consequence of having a strong interacting sector (one can naively think to the analogy with the pion system - possessing the same global symmetry of the scalar sector in the SM - and the corresponding ρ vector mesons). In the BESS model the EW symmetry breaking is described in a non-linear way. A local "hidden" $SU(2)$ symmetry is implicit in the description and the bosons V are indeed the associated gauge bosons. It is explicitly assumed that they constitute effective dynamical degrees of freedom. The bosons V mix with the standard gauge bosons and due to this mixing they are unavoidably coupled to the known fermions. In Sect. 2 we briefly recall the main properties of the V bosons in the BESS model. Among the various features of the model, the relevant one for the present computation is the following: the scattering of the longitudinal W/Z's is dominated by the exchange of the V's which are strongly coupled to the external states. At hadron colliders possible signals of the BESS model will be visible in the gauge boson pair production (see Sect. 3). The most promising channel is $pp \to W^{\pm}Z + X \to l^{\pm}l^{+}l^{-} + X$ and there are two mechanisms which compete: $q\bar{q}$ annihilation and WZ fusion. The results are discussed in Sect. 4.

2. THE BESS MODEL

The vector resonances of the BESS model are bound states of a strongly interacting sector. In this sense they are similar to ordinary ρ vector mesons, or to the techni-ρ particle of technicolor theories [5]. Due to their composite nature, the V particles are then expected to mix to the photon and to the W and Z vector bosons. From this, a non trivial behaviour under the electromagnetic gauge group $U(1)_{em}$ is expected [6]. Using this fact and the requirement that the electroweak ρ-parameter be equal to 1 at tree level, one can easily construct the most general mixing term of the V-particles with the ordinary vector bosons. By diagonalizing the mass matrices in the charged and in the neutral sector one gets the expressions for the mixing angles and for the mass eigenstates [4,7]. For instance, in the

charged sector, by calling g'' the V gauge coupling and g the standard $SU(2)_L$ one, we find that for $g'' \gg g$ (the limit $g'' \to \infty$ corresponds to decoupled V particles) the mixing angle φ between $W^{\pm}$ and $V^{\pm}$ is of the order of g/g'' and the W mass gets a correction of the order of $(g/g'')^2$. One also finds that, at the zeroth order in the weak couplings, the V mesons are degenerate in mass and $M_V^2 = v^2 \alpha g''^2/4$ where v and α are free parameters.

As far as the interactions with fermions are concerned, one must specify the current $\vec{J}$ to which the new triplet of states $\vec{V}$ couples. If we assume $\vec{J} = \vec{J}_L$ (see ref. [4] for a more general discussion), the $U(1)_{em}$ gauge invariance fixes the form of the interaction lagrangian. The complete list of couplings to fermions can be found in refs. [4,7]. Here we will only be concerned with the couplings to the charged currents. For example, the coupling of $V^{\pm}$ to $J_L^{\pm}$ is given by $h_V = (g \sin\varphi + (g''/2) b \cos\varphi)/(1+b)$. The parameter b specifies a possible direct coupling of the fermions to the new gauge vector bosons. However, it must be stressed that also when $b = 0$ a coupling of the physical V-particles to fermions is present due to their mixing with the physical Weinberg-Salam vector bosons.

The parameter space of the model is given by (g, g', v, M_V, g'', b) with g' the $U(1)_Y$ gauge coupling. We trade off (g, g', v) for (α_{em}, G_F, M_Z) and therefore we remain with (M_V, g'', b). In turn, the parameter v can be rewritten in terms of M_W, and the expressions of (g, g', M_W) in terms of (α_{em}, G_F, M_Z) can be found in ref. [7]. In order to get the physical region for the parameters (M_V, g'', b) we have considered the envelope of the 90% C.L. curves obtained from the observables related to the Z-line shape measured at LEP1, and from the ratio M_W/M_Z measured at CDF and UA2. For example the allowed region in the plane $(b, g/g'')$ for $M_V = 1500\ GeV$ is given in ref. [8].

3. GAUGE BOSON PAIR PRODUCTION IN THE BESS MODEL

At hadron colliders, as far as detection of a signal from a strongly interacting symmetry breaking sector is concerned, vector boson pair production is particularly relevant. In the BESS model there are two main mechanisms which compete for the production of a pair of ordinary gauge vector bosons at a pp collider: the WW (WZ, ZZ) fusion and the $q\bar{q}$ annihilation [9]. The first one is the rescattering of a pair of ordinary gauge vector bosons, each being initially emitted from a quark or antiquark leg. In the so-called effective-W approximation the initial W/Z's are assumed to be real and the cross section for producing a W/Z pair is obtained by a double convolution of the cross section for the rescattering (or fusion) process with the luminosities of the initial W/Z's inside the quarks and the structure functions of the quarks inside the proton [10]. The relevance of this mechanism is then related to the strength of the fusion process. In the standard model such a fusion process is expected to be weak. The potentially large amplitudes, those among the longitudinally polarized W/Z's, are in fact asymptotically constant (for large energy), once the whole set of lowest order diagrams is taken into account. However such a constant depends on the Higgs mass M_H and for a sufficiently large value of M_H the asymptotic value of the amplitude violates the perturbative unitarity requirement. The speculations on a possible strongly interacting regime for the SM [3,4] are based on this observation. In BESS the

rescattering process is naturally strong. In fact the scattering of two longitudinally polarized W/Z's proceeds via the exchange of a V vector boson with large couplings (of order $\alpha g''$) at each vertex. If some W/Z's is taken to be transverse, the corresponding amplitude is strongly depressed and will be neglected in our analysis. We have computed the scattering amplitudes among longitudinal W/Z's in the BESS model, by making use of the equivalence theorem [11]. Such amplitudes approach the ones among the corresponding goldstone bosons as the value of the energy increases, the difference being of order (M/E) $(M = M_W$ or $M_Z)$. The full expressions for the corresponding amplitudes can be found in ref. [9].

Another mechanism to produce W/Z pairs is the quark-antiquark annihilation into a V vector boson, which in turn decays into a pair of ordinary gauge vector bosons. In fact, at least in the range of masses for V we are interested in (few TeVs), the decay of V's is dominated by the WW, WZ channels, due to the large coupling, (of order $\alpha g''$), for $V^0 W_L^+ W_L^-$ and $V^\pm W_L^\mp Z_L$ (L stands for the longitudinal components). We have evaluated the $q\bar{q}$ contribution in the context of the parton model along the lines described in ref. [7], and the relevant expressions are given in ref. [9]. We stress that this process is always operating in BESS independently of the existence of a direct coupling of V to fermions. In fact, the mixing of V with W, Z and γ always induces a coupling between the mass eigenstates V and the fermions, even if the original, unmixed, states were not coupled to matter. On this basis we expect (and we shall verify quantitatively) that, even in the case $b = 0$, the $q\bar{q}$ mechanism remains efficient in producing a W/Z pair.

4. DISCUSSION OF THE RESULTS

In hadronic collisions the $pp \to W^\pm Z + X$ reaction appears to be the most promising one in the framework of the BESS model. In the ZZ does not proceed via an s-channel contribution in BESS and the W^+W^- mode is expected to suffer from a very severe $t\bar{t}$ background (if $m_{top} > M_W$). Final leptonic configurations from $t\bar{t}$ production might also simulate configurations from $W^\pm Z$, but the Z mass reconstruction should protect the signal from such a background [12]. The WZ pair is expected to be revealed more easily in the pure leptonic mode. Our results will be given in the Table 1 in terms of numbers of produced $W^\pm Z$ pairs. For both bosons decaying leptonically one has to multiply by the branching factor $B(Z \to \ell^+\ell^-) \cdot B(W^\pm \to \ell^\pm \bar{\nu}_\ell) \approx 1.5\%$, for $(\ell = e, \mu)$. The assumed energy parameters for LHC and SSC are 16 TeV and 40 TeV respectively. The luminosities we have assumed are 10^{34} cm^{-2} sec^{-1} for LHC, and 10^{33} cm^{-2} sec^{-1} for SSC, and all the numbers refer to one effective year $= 10^7$ sec of running of the colliders. Use has been made of a Montecarlo simulation to study the details of the p_T (the transverse momentum of the Z) and of the M_{WZ} (the invariant mass of the WZ-pair) distributions. In our calculation we have used the DFLM structure functions [13], for $\Lambda_{QCD} = 260$ MeV. We have also run the computer programs by using the EHLQ1 structure functions [14] obtaining very similar results (actually the DFLM structure functions give a number of events which is about 6-8% lower than for EHLQ1). The value of Q^2 inside the structure functions for the fusion process is taken to be equal to the square of the invariant mass of the produced gauge boson

pair. The K-factor coming from soft gluon resummation is not known for all the processes considered here, and we have decided not to introduce it. As a consequence the number of events we have evaluated is probably underestimated by about 20-30%. A cut on the rapidity of the final W and Z, $|y_{W,Z}| \leq 2.5$, was applied to all cases.

The relevant backgrounds included in this calculation are: the standard model production of $W^{\pm}Z$ through quark-antiquark annihilation [15], $\gamma W^{\pm}$ fusion [16], and $W_T^{\pm}Z_T$ fusion. Their relative contributions with respect to the total one, for $M_{WZ} > 0.5\ TeV$ and $p_T > 100\ GeV$, are the following: 66%, 17 %, 17 % at LHC and 45%, 24%, 31% at SSC.

In order to optimize the statistical significance of the signal we have applied a lower cut in M_{WZ}, approximately corresponding to the beginning of the resonance at the left of the peak. An upper cut has been fixed $M_{WZ} = 3\ TeV$, where in all the practical cases considered here, the resonance tail is already extinguished. Finally a cut in p_T has been obtained from the requirement of maximizing $S/(S+B)^{1/2}$, S being the signal and B the background. The results are summarized in Table 1 for the process $W^+Z + W^-Z$ (the W^-Z channel is roughly one half of the W^+Z one) at LHC and at SSC. We have considered an extensive choice of the BESS parameters which are well inside the region allowed from LEP1, and CDF/UA2 data [8]. The range of M_V values we have explored runs from 1 TeV up to 2.5 TeV. The expression for the width of the V particle (in the limit $M_V \gg M_W, M_Z$ and ignoring the fermionic decays which turn out to be completely negligible) is $\Gamma_V = (G_F^2/24\pi)(M_V^5/g''^2)$. Notice that the case $M_V = 2\ TeV$, $\Gamma_V = 353\ GeV$ corresponds almost exactly to a techni-ρ obtained by scaling from QCD [5]. For smaller g'' the resonance becomes broader. In the third and fourth columns of the Table 1 we have reported the optimal lower cuts performed in the various cases.

(M_V, g'', b)		$(p_T)_c$	$(M_{WZ})_c$	Fusion	$q\bar{q}$	Signal	Backgr.	Total
(1000,13,0)	LHC	360	850	858	10089	10947	4786	15733
Γ_V=11	SSC	300	800	1280	3969	5249	3963	9212
(1500,13,0)	LHC	480	1250	498	1929	2427	1121	3548
Γ_V=84	SSC	420	1250	895	1030	1925	1063	2988
(2000,13,.02)	LHC	540	1400	339	3863	4202	608	4810
Γ_V=353	SSC	480	1600	671	2814	3485	462	3947
(2000,13,0)	LHC	600	1600	241	443	684	310	994
Γ_V=353	SSC	480	1600	671	339	1010	462	1472
(2000,13,-.01)	LHC	540	1400	339	4186	4525	608	5133
Γ_V=353	SSC	480	1400	772	3119	3891	636	4527
(2500,20,0)	LHC	600	1400	212	57	269	430	699
Γ_V=455	SSC	540	1500	486	54	540	428	968
(2500,20,-.01)	LHC	600	1800	141	1807	1498	211	2159
Γ_V=455	SSC	600	1800	360	1721	2081	211	2292

Table 1 - *Events per year in* $pp \to (W^+Z + W^-Z) + X$ *at LHC and SSC from the BESS model. Masses, widths and cuts are expressed in GeV.*

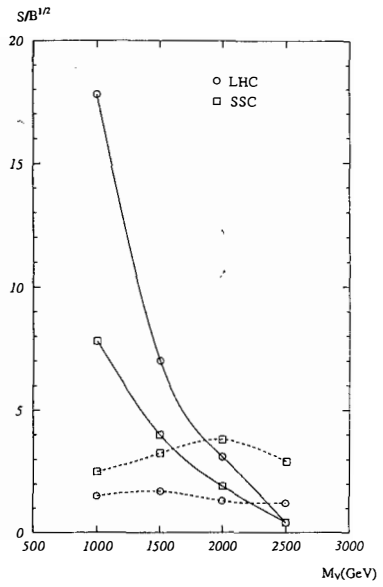

Fig. 1 - *Statistical significance of the signal in leptonic events as a function of M_V for $b = 0$. The two contributions are separated: fusion (dashed lines) and $q\bar{q}$ annihilation (solid lines).*

For a better understanding of the results, we have separately exhibited in Table 1 the fusion and $q\bar{q}$ annihilation contributions to the signal. We have also given the number of events from the background and the total number of events. Notice that the $b = 0$ case corresponds, in practice, to the most pessimistic situation, since in general allowing for a direct coupling ($b \neq 0$) a much larger signal from production via $q\bar{q}$ annihilation is predicted. Direct couplings of techni-ρ to fermions emerge in extended technicolor theories (for calculations at SSC energies see ref. [17]). From the Table 1 we see that the fusion signal increases going from LHC to SSC, whereas the signal from $q\bar{q}$ decreases (of course the decreasing in the luminosity by a factor 10 has to be considered). In particular, for $b = 0$, at LHC the $q\bar{q}$ annihilation dominates for low M_V up to $M_V = 2\ TeV$, whereas at SSC the two mechanisms are already comparable at $M_V = 1.5\ TeV$ (see Fig. 1).

However for $b \neq 0$ the situation changes and, increasing $|b|$, the $q\bar{q}$ annihilation will overcome again the fusion contribution. We see that, if we require more than 10 leptonic events/year and a good statistical significance (for example $S/\sqrt{B} > 3$), the discovery limit for $b = 0$ at SSC is $M_V \leq 2.5\ TeV$, while at LHC $M_V = 2\ TeV$ is the limiting value for discovery in the luminosity configuration considered. In fact it can be shown that in order to have more than 10 leptonic events/year for $M_V = 2.5\ TeV$ and $b = 0$ one have to run LHC at a luminosity of about $3.5 \times 10^{34}\ cm^{-2}\ sec^{-1}$ at least. About this point notice that in the present computation of the background, we have not distinguished in the polarizations of the final W and Z. Since the signal is almost totally given by $W_L Z_L$-pairs, one would get a better statistical significance of the signal (and perhaps push forward the discovery limit) by considering the background contribution only in the longitudinal channel [18]. This work is now in progress.

We have also made an extensive study of the $(p_T)_Z$ and M_{WZ} distributions. Here we give examples in Figs. 2, 3 of the two distributions both at LHC and SSC. The figures show that, even after multiplying by the branching factor corresponding to selecting only leptonic decays of W and Z, one is left with a statistically significant signal having quite well distinguished features both in M_{WZ} and $(p_T)_Z$ distributions. The vertical lines in the graphs indicate where the lower cuts in M_{WZ} and p_T have been put for the illustrated cases (see corresponding entries in Table 1). Also the lower, intermediate and higher histograms

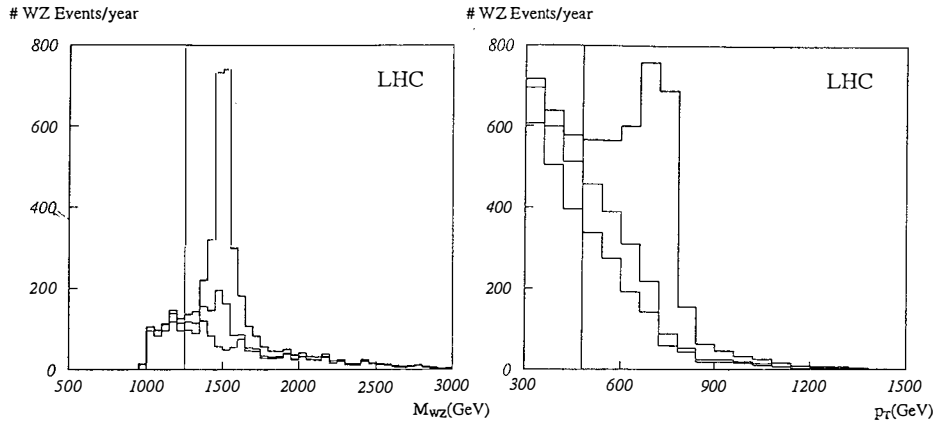

Fig. 2 - *Invariant mass and* $(p_T)_Z$ *distribution of the* $W^+Z + W^-Z$ *pairs produced per year at LHC for* $M_V = 1500\ GeV$, $g'' = 13$ *and* $b = 0$.

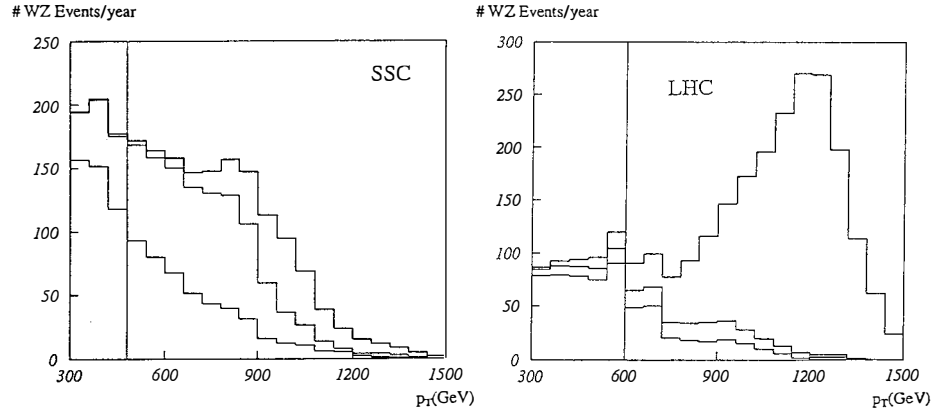

Fig. 3 - $(p_T)_Z$ *distributions of the* W^+Z+W^-Z *pairs produced per year for* $M_V = 2500\ GeV$, $g'' = 20$ *at SSC for* $b = 0$ *(left-hand side) and at LHC for* $b = -0.01$ *(right-hand side).*

in the figures refer to the background, background plus fusion signal and background plus fusion signal plus $q\bar{q}$ annihilation signal, respectively. In Fig. 2 we have both the M_{WZ} and the p_T distributions for a V resonance with $M_V = 1.5\ TeV$ and $\Gamma_V = 84\ GeV$ at LHC. In Fig. 3 (left-hand side) is well visible how the fusion contribution to the signal makes a resonance of 2.5 TeV detectable at SSC. The large increase of the $q\bar{q}$-annihilation contribution to the signal obtainable even with a small value of b is clear in Fig. 3 (right-hand side). The figures shown are only some examples and we emphasize that the statistical significance of the signal versus the background is very good practically in all the cases we have considered in this note. The new conclusion of our work is the generally dominant

role, particularly at LHC, of production through $q\bar{q}$ annihilation, as compared to the extensively studied boson pair fusion mechanism. The increase of gauge boson pairs, resulting from the $q\bar{q}$ mechanism, as expected in the BESS model, together with its distinguished features in the p_T and invariant mass distributions, suggests an important role of LHC and SSC in the exploration of a possible strong electroweak symmetry breaking sector.

REFERENCES

[1] C. Rubbia, seminar given at CERN on November 2, 1989; "Large Hadron Collider in the LEP Tunnel", ed. G. Brianti et al., CERN 84/10.

[2] "Superconducting Super Collider Conceptual Design", Central Design Group, SSC Report SR-2020, March 1986.

[3] M. Veltman, Acta Phys. Polon. **B8** (1977) 475; B.W. Lee, C. Quigg and H.B. Thacker, Phys. Rev. **D 16** (1977) 1519; see also the review by M.S. Chanowitz, Ann. Rev. Nucl. Part. Sc. **38** (1988) 363.

[4] R. Casalbuoni, S. De Curtis, D. Dominici and R. Gatto, Phys. Lett. **B155** (1985) 95; Nucl. Phys. **B282** (1987) 235.

[5] S. Weinberg, Phys. Rev. **D 13** (1976) 974; **D 20** (1979) 1277; L. Susskind, Phys. Rev. **D 20** (1979) 2619; for extended technicolor, see: S. Dimopoulos and L. Susskind, Nucl. Phys. **B155** (1979) 237. See also the review by E. Fahri and L. Susskind, Phys. Rep. **74** (1981) 277.

[6] G. Altarelli, R. Casalbuoni, D. Dominici, F. Feruglio and R. Gatto, Nucl. Phys. **B342** (1990) 15.

[7] R. Casalbuoni, P. Chiappetta, D. Dominici, F. Feruglio and R. Gatto, Nucl. Phys. **B310** (1988) 181.

[8] see the contribution of R. Casalbuoni in this volume.

[9] R. Casalbuoni, P. Chiappetta, S. De Curtis, F. Feruglio, R. Gatto, B. Mele and J. Terron, Phys. Lett. **249B** (1990) 130; Proceedings of Large Hadron Collider Workshop, Aachen, 4-9 October 1990, CERN Report 90-10; ECFA 90/133, vol. 2, pag. 786.

[10] S. Dawson, Nucl. Phys. **B249** (1985) 42. G.L. Kane, W.W. Repko and W.B. Rolnick, Phys. Lett. **148B** (1985) 367; M.S. Chanowitz and M.K. Gaillard, Phys. Lett. **142B** (1984) 85.

[11] J.M. Cornwall, D.N. Levin and G. Tiktopoulos, Phys. Rev. **D 10** (1974) 1145. C.G. Vayonakis, Lett. N. Cimento **17** (1976) 17; M.S. Chanowitz and M.K. Gaillard, Nucl. Phys. **B261** (1985) 379; G.J. Gounaris, R. Kögerler and H. Neufeld, Phys. Rev. **D 34** (1986) 3257.

[12] I. Josa, F. Pauss and T. Rodrigo, Proceedings of Large Hadron Collider Workshop, Aachen, 4-9 October 1990, CERN Report 90-10; ECFA 90/133, vol. 2, pag. 796.

[13] M. Diemoz, F. Ferroni, E. Longo and G. Martinelli, Z. Phys **C39** (1988) 21.

[14] E. Eichten, I. Hinchliffe, K. Lane and C. Quigg, Rev. Mod. Phys. **56** (1984).

[15] R.W. Brown, D. Sahdev and K.O. Mikaelian, Phys. Rev. **D 20** (1979) 1164; K.O. Mikaelian, M.A. Samuel and D. Sahdev, Phys. Rev. Lett. **43** (1979) 746.

[16] B. Mele, Proceedings of the Workshop on Physics at Future Accelerators, La Thuile and Geneva, ed. J.H. Mulvay, CERN report 87-07, vol. 2, p. 13, Geneva (1987)

[17] R.S. Chivukula, Proc. of the 12^{th} Johns Hopkins Workshop, Baltimore June 1988, eds. G. Domokos and S. Kövesi-Domokos, World Scientific, Singapore (1988).

[18] D. Denegri, private communication.

STRONGLY INTERACTING HIGGS SECTOR

Keiji IGI

Department of Physics

University of Tokyo

Hongo, Bunkyo-ku

Tokyo 113, Japan

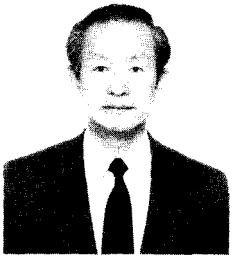

ABSTRACT

We construct unitary partial-wave amplitudes for longitudinal WW scattering from general requirements of scalar dominace and low-energy theorem of broken chiral symmetry. The amplitude is uniquely determined by specifying the mass of the scalar particle. For small masses, the amplitude reduces to the lowest-order standard model result. For larger masses, the enhancement becomes broader and deviation from the standard model becomes more pronounced. For large masses above 1 TeV, the amplitude shows saturation behaviour above the mass. Our result can serve as a basis of phenomenological studies of WW scattering at hadron colliders such as LHC/SSC, e^+e^- linear colliders above TeV energies.

My talk is mainly based on ref. 1) which has been done in collaboration with Ken-ichi Hikasa. As is well known, the origin of electroweak symmetry breaking is one of the most pressing puzzles in particle physics. In the standard model, the breaking of $SU(2)\times U(1)$ gauge symmetry is caused by an elementary Higgs field. Although it is the simplest of all, there is no experimental indication if it is a correct one or not. Any particle process observed to date is attributable to gauge interactions, and the sole raison d'etre of the Higgs sector comes from the fact that the W and Z bosons are not massless.

As a key process to study the $SU(2)\times U(1)$ symmetry breaking, the study of $W_L W_L$ scattering in the laboratory would become important due to the equivalence theorem[2-4]. (Hereafter W denotes both $W^{\pm}$ and Z^0 bosons.) In the minimal standard model, the self-coupling of Higgs bosons is proportional to the Higgs mass squared. If the Higgs is heavy, perturbation expansion breaks down. For a Higgs mass above 1 TeV, the lowest-order amplitude for WW scattering is known to violate partial-wave unitarity.[5,3] If an elementary Higgs boson does not exist, W_L's should interact strongly with themselves at high energies, since the theory without a scalar gives a bad high-energy behaviour[2]. Absence of a light Higgs thus inevitably leads to a new strong interaction for which the perturbative method is not applicable. The observed ratio of the $W^{\pm}$ and Z^0 boson masses constrains the symmetry-breaking sector considerably. The relation $\rho \equiv m_W^2/m_Z^2\cos^2\theta_W \simeq 1$ is satisfied to high accuracy. This strongly indicates that the breaking sector has a large $SU(2)_L\times SU(2)_R$ global symmetry, as in the minimal standard model, and so implies that

the sector has a diagonal "isospin" symmetry even after the symmetry breaking, which we assume to be the case.

$W_L W_L$ scattering amplitude : Let us construct scattering amplitudes for $W_L W_L$ scattering satisfying unitarity based on general requirements only, without relying on perturbative methods. Let us assume that the scattering amplitude is dominated by exchanges of a single particle with I=J=0, and impose the requirements of low-energy theorem[4] of the broken chiral symmetry. We are then led to a unique amplitude for a given scalar mass. For small scalar masses, our result reproduces the lowest-order amplitude of the standard model. The deviation from the standard model result is more pronounced for larger masses, and we find saturating behaviour of the amplitude for very large scalar masses.

Let us concentrate on the partial-wave amplitude a_0 for the channel I=J=0. Since we are mainly interested in the case in which strong interaction appears, it is a good approximation to neglect the gauge couplings altogether, which also implies massless W's. The W_L's form an isotriplet (W_L^+, W_L^-, Z_L^0), and the scalar is an isosinglet. For convenience we call the scalar particle a Higgs boson. Higgs exchange in the crossed t- and u-channel produces attractive force in the I=0 channel (and repulsive force in I=2). The contribution of Higgs exchange to a_0 is found by partial-wave projection $a_0^L(s)=(Gm_H^4/s)\log(1+s/m_H^2)$, where G is proportional to the W_L-W_L-Higgs coupling squared, normalized as giving the Higgs decay width $\Gamma_H=(3/2)Gm_H^3$. In the standard model, G is given in the lowest order by $G=A\equiv G_F/8\sqrt{2}\pi$. This tree-level relation may not hold for a strongly interacting Higgs boson, however.

The N/D method : Let us employ the N/D formalism[6] to assure that the amplitude satisfies unitarity. We can write the partial-wave amplitude as $a_0(s)=N(s)/D(s)$, where the left-hand ($s<-m_H^2$) discontinuity is contained in N(s), and only D(s) has the right-hand ($s>0$) cut. So, we have $\mathrm{Im}\, N(s)=D(s)\,\mathrm{Im}\, a_0(s)$ ($s<-m_H^2$) and $\mathrm{Im}\, D(s)=N(s)\,\mathrm{Im}\,(1/a_0(s))=-N(s)R(s)$ ($s>0$), where $R(s)=\sigma_{tot}^{J=0}(s)/\sigma_{el}^{J=0}(s)$.

Since the W'_Ls are equivalent to Goldstone bosons, their interaction at low energies is prescribed by the low-energy theorem of broken chiral symmetry such as $a_0(s)\simeq As+o(s^2)$. This low-energy behaviour is realized by requiring $N(0)=A$, $D(s)=1/s$ +finite (s 0).

Let us write once-subtracted dispersion relations for N and D.

$$N(s)=N(s_0)+\frac{1}{\pi}(s-s_0)\int_{-\infty}^{-m_H^2}\frac{ds'}{(s'-s_0)(s'-s)}\,\mathrm{Im}\, N(s') \qquad (1)$$

$$D(s)=D(s_0)+\frac{1}{s}-\frac{1}{s_0}+\frac{1}{\pi}(s-s_0)\int_0^{\infty}\frac{ds'}{(s'-s_0)(s'-s)}\,\mathrm{Im}D(s'). \qquad (2)$$

Here, s_0 is an arbitrary subtraction point which is to be taken in the range $-m_H^2<s_0<0$. Inserting (2) into (1), we can obtain the Fredholm-type integral equation for N(s) as

$$N(s)=N(s_0)+D(s_0)[a_0^L(s)-a_0^L(s_0)]+(\frac{1}{s}-\frac{1}{s_0})[a_0^L(s)-a_0^L(0)]$$
$$+\frac{1}{\pi}(s-s_0)\int_0^{\infty}\frac{ds'}{(s'-s_0)(s'-s)}[a_0^L(s')-a_0^L(s_0)]R(s')N(s'). \qquad (3)$$

Once N(s) is determined, D(s) can be calculated from (2) together with $\mathrm{Im}\, D(s)= -N(s)R(s)$. The inelasticity parameter R(s) has to be fixed to solve the integral equation for N. We assumed $R(s)=1$.

Then we can obtain the amplitude $a_0(s)$ as $N(s)/D(s)$. We

can define the s-channel mass m_H as the energy at which the phase shift passes through $\pi/2$, i.e., the real part of D vanishes : $ReD(s=m_H^2)=0$, and Γ_H from $\Gamma_H=-N(m_H^2)/m_H ReD'(m_H^2)$, where the prime denotes the derivative with respect to s. Consistency of the formalism is only attained if the mass and width in the s-channel agrees with those in the crossed channel. This gives us two conditions besides another condition $N(0)=A$ from the low-energy theorem. On the other hand, we have four parameters; m_H, Γ_H, $N(s_0)$ and $D(s_0)$. Therefore, we have one free parameter (e.g., m_H), which determines the whole I=J=0 amplitude.

We plot the resulting Higgs width as a function of its mass in Fig. 1. Our result agrees with the standard tree-level formula for small m_H, but increases faster for large masses. We also show the scattering amplitude squared for representative masses in Fig. 2. A sharp resonance curve is clearly seen for small Higgs masses which in fact agrees with the lowest-order standard model result. For larger masses, the enhancement becomes broader. For $m_H \gtrsim 1$ TeV, the amplitude shows saturation. In either case, a "bump" structure exists only for $m_H \lesssim 1$ Tev.

We have some comments :

1) If there is a strong resonance with a relatively low mass in other channels, e.g., in I=J=1 as expected[7] in QCD-type models such as technicolour, it couples with the I=J=0 wave through crossing and the amplitude would receive modification accordingly.

2) Our result can serve as a basis of phenomenological studies of WW scattering at hadron colliders such as LHC/SSC and e^+e^- linear colliders above TeV energies.

ACKNOWLEDGMENT

This work was supported in part by the Grant-in-Aid for Scientific Research (International Scientific Research Program) from the Ministry of Education, Science and Culture (No.02045009).

REFERENCES

1) K. Hikasa and K. Igi, KEK-TH-278, UT-576 (1991) Phys. Lett. B (to be published).
2) J. M. Cornwall, D. N. Levin, G. Tiktopoulos, Phys. Rev. D10, 1145 (1974) ; 11, 972(E) (1975).
3) B. W. Lee , C. Quigg, and H. B. Thacker, Phys. Rev. D16, 1519 (1977)
4) M. S. Chanowitz and M. K. Gaillard, Nucl. Phys. B261, 379 (1985)
5) D. A. Dicus and V. S. Mathur, Phys. Rev. D7, 3111 (1973).
6) G. F. Chew and S. Mandelstam, Phys. Rev. 119, 467 (1960).
7) A. Dobado, M. J. Herrero, and T. N. Truong, Phys. Lett. B235 129 (1990).

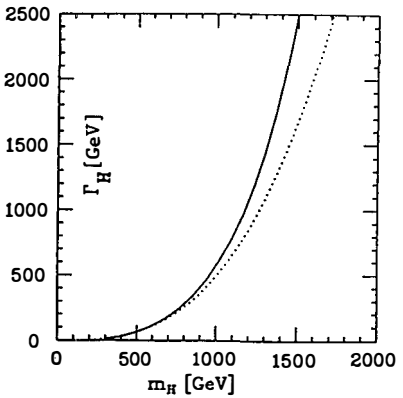

Fig.1 Mass-width relations for the Higgs boson. Dotted curve: The lowest order prediction of the standard model. Solid curve: our result.

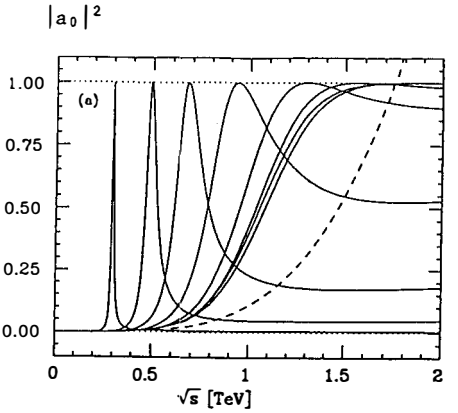

Fig. 2 The I=J=o $W_L W_L$ partial-wave amplitude for various Higss Masses. Dashed curve: extrapolated low-energy theorem prediction.

Observing the Higgs Boson and the ZZ lineshape

E. W. N. Glover*
Fermi National Accelerator Laboratory,
P. O. Box 500, Batavia, IL 60510, U.S.A.

Abstract

The discovery potential of the LHC and SSC for observing the Higgs boson in the 'gold plated' $pp \to ZZ \to \ell^+\ell^-\ell'^+\ell'^-$ mode is reviewed. The processes contributing to the ZZ lineshape are discussed and approximations to the Higgs boson signal compared with more precise calculations. Finally, the approximations to the Higgs boson signal available in parton shower Monte Carlos are summarized.

*SSC Fellow; Address after 1 September 1991, Physics Department, University of Durham, Durham DH1 3LE, England

1 Introduction

One of the major objectives of the LHC and SSC is to search for the standard model Higgs boson in the mass range,

$$2M_Z \leq m_H \leq \mathcal{O}(1\ TeV), \tag{1.1}$$

where the dominant decay modes are $H \rightarrow W^+W^-$ and $H \rightarrow ZZ$. The cleanest or 'gold plated' mode for discovery is $H \rightarrow ZZ \rightarrow \ell^+\ell^-\ell'^+\ell'^-$ where $\ell = e,\ \mu$ and all four charged leptons are detected. In this case, each unlike sign lepton pair reconstructs the parent Z while the Higgs boson would appear as a resonance in the ZZ invariant mass distribution.

Fig. 1 shows the expected event rates in this channel for $m_H = 600$, 800 and 1000 GeV assuming an integrated luminosity of 10^4 pb^{-1} at both the LHC and SSC which corresponds to one 'year' of operation at the nominal luminosity of 10^{33} cm^{-2}s^{-1} [1]. The solid line represents the continuum background while the 'data' points are the signal with statistical errors. In order to simulate the leptonic coverage of future hadron collider experiments, a rapidity cut is imposed on the Z bosons,

$$|y_Z| < 2.5, \tag{1.2}$$

while to enhance the signal relative to the background, the Z boson is required to have a transverse momentum,

$$p_{TZ} > m_{ZZ}/4. \tag{1.3}$$

Furthermore the top quark mass m_t is assumed to be 120 GeV and the lepton identification efficiency to be 100%. With these assumptions and integrated luminosity, Fig. 1 shows that the LHC may be able to discover a 600 GeV Higgs as a resonance in the four lepton mode. However, too few events are produced in the resonance region to make a 800 GeV Higgs visible at the LHC. At the SSC, the cross sections are somewhat larger due to the higher beam energy and a 800 GeV Higgs is visible with about the same significance as a 600 GeV Higgs at the LHC. On the other hand, if we allow a factor 10 increase in integrated luminosity, the LHC can make up for the smaller beam energy and extend its discovery range up to 800 GeV. Recent studies making somewhat different assumptions for m_t, lepton coverage and the lepton identification efficiency [3, 4] reach similar conclusions for the discovery potential of the two machines.

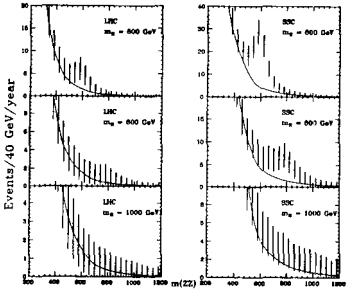

Fig. 1. Expected event rates for $pp \rightarrow ZZ \rightarrow \ell^+\ell^-\ell'^+\ell'^-$ as a function of m_{ZZ} at (a) the LHC and (b) the SSC. 'Data' points show the Higgs boson signal in 40 GeV bins for $m_H = 600$, 800 and 1000 TeV with statistical errors, while the continuous curve represents the background.

If $m_H > 800$ GeV, Fig. 1 shows that the signal is spread out over such a large range* that there is essentially no resonance structure, although there is an excess of events at large m_{ZZ}. In this case, by making a cut on the Z boson invariant mass $m_{ZZ} > m_{min}$, one can enhance the total number of signal events above m_{min} relative to the background [2, 1] which, for $m_H = 1$ TeV and 10^4 pb^{-1},

*It is worth noting that a 1 TeV Higgs has a width of about 500 GeV.

produces a 1.1 (4.4)σ deviation from the background with $m_{min} = 700$ GeV at the LHC (SSC) [1]. Such an analysis is extremely sensitive to our knowledge of the background, however we can clearly see that, *given the same integrated luminosity, the SSC is more sensitive to the presence of very heavy Higgs bosons or a strongly interacting electroweak sector than the LHC.*

2 The ZZ lineshape

The largest source of Z boson pairs is quark-antiquark annihilation [6],

$$q\bar{q} \rightarrow ZZ, \tag{2.1}$$

which contributes solely to the continuum background. Recently the next-to-leading QCD corrections to this process have been computed [7, 8], which show that the shape of the ZZ invariant mass distribution is significantly changed at large m_{ZZ} due to terms that grow as $\log^2(m_{ZZ}/M_Z)$. This indicates that higher order effects are important and that more theoretical work is needed to determine the $q\bar{q}$ contribution to the m_{ZZ} distribution at the 10% level.

There are two important mechanisms which contribute to the Higgs signal; the $\mathcal{O}(\alpha_s^2\alpha^2)$ 'gluon fusion' process [9, 11, 12],

$$gg \rightarrow H \rightarrow ZZ, \tag{2.2}$$

and the $\mathcal{O}(\alpha^4)$ 'vector boson fusion' process [10, 13, 14],

$$qq \rightarrow qqH \rightarrow ZZ. \tag{2.3}$$

In the gluon fusion process, the gluons couple to the Higgs boson via a top quark loop, so that this process is extremely dependent on m_t. In contrast, the vector boson fusion process depends only on the coupling of the Higgs with the W and Z and directly probes the electroweak symmetry breaking sector; the incoming quarks radiate vector bosons which then annihilate into a Higgs boson.

The contributions to the ZZ invariant mass distribution from these three processes is shown in Fig. 2 for $m_H = 800$ GeV at the SSC. The $q\bar{q}$ process is shown at leading order [6] and, apart from the $m_{ZZ} \sim 2M_Z$ threshold region, monotonically decreases with increasing m_{ZZ}. On the other hand, both the gluon fusion and vector boson fusion processes show a resonance structure around $m_{ZZ} \sim m_H$. On the low side of the resonance, the non-resonant gluon fusion graphs in which the Z bosons couple directly to the quark loop generate a significant cross section that falls sharply with increasing m_{ZZ}. It is also worth noting that, apart from the resonance region, the gluon fusion process becomes relatively less important at larger m_{ZZ} compared to the $q\bar{q}$ process. This is mainly due to the decrease in the gluon-gluon luminosity compared to that for $q\bar{q}$. In contrast, the vector boson fusion process is much flatter due to the exchange of massive vector bosons which generate logarithms of m_{ZZ}/M_Z and hence a harder m_{ZZ} spectrum.

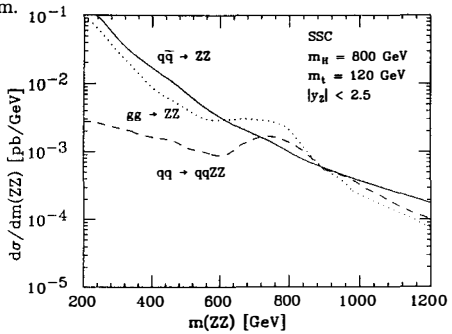

Fig. 2. The ZZ invariant mass distribution for $m_H = 800$ GeV at the SSC.

In the following, I will compare different matrix elements for the Higgs signal for the benchmark case $m_H = 800$ GeV with the following standard model parameters, $m_t = 120$ GeV, $M_Z = 91.1$ GeV, $\alpha = \alpha(M_Z) = 1/128$, $\sin^2\theta_W = 0.23$ and $M_W = M_Z \cos\theta_W = 80$ GeV. With these parameters, the width of an 800 GeV Higgs boson is $\Gamma_H = 258.8$ GeV. Furthermore, I will use the parton distributions of Duke and Owens (set 1) [5] evaluated at scale $Q^2 = \hat{s}/4$. Since all approximations are evaluated with the same input, our comparisons are independent of the choice of scales, *etc.*

3 The s-channel approximation

In the s-channel approximation [9, 10], only Higgs exchange graphs are included. The motivation for this is quite straightforward because in the resonance region $\sqrt{s} = m_{ZZ} \sim m_H$, the Higgs propagator has the form,

$$\frac{1}{s - m_H^2 + i m_H \Gamma_H} \sim \mathcal{O}\left(\frac{1}{\alpha}\right), \tag{3.1}$$

since $m_H\Gamma_H$ is $\mathcal{O}(\alpha)$ and the s-channel Higgs graphs are effectively lower order in the coupling. In this region it is therefore consistent at lowest order to include only Higgs exchange graphs in evaluating the cross section [9, 10]. This is completely analogous to including only the Z exchange graph at LEP energies. On the other hand, since the Higgs boson is relatively much wider than the Z, interference effects between the Higgs exchange and non-resonant graphs can be important even within the resonance region, particularly for the gluon fusion process where the gluon luminosity is sharply falling. This is shown in Fig. 3 for gluon fusion where the s-channel approximation is compared with the result obtained by including all tree level graphs [11, 12].

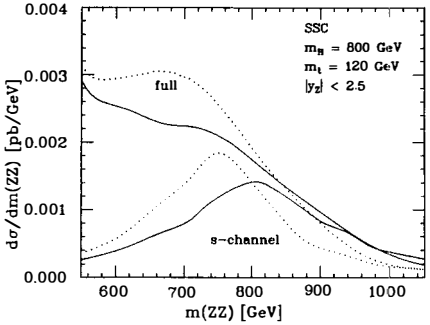

Fig. 3. The ZZ invariant mass distribution for $gg \to ZZ$ for $m_H = 800$ GeV at the SSC. The solid (dotted) lines show the full and s-channel approximation with a fixed (energy dependent) width.

It is important to remember that outside the resonance region at $m_{ZZ} >> m_H$, this approximation violates unitarity. Of course, here the Higgs graph is of the same order in coupling constant as all of the non-Higgs graphs [11, 12, 13, 14]. When all graphs are included unitarity is preserved outside the resonance region. *The s-channel approximation should only be used within the resonance region.*

4 The Higgs propagator

The bare Higgs propagator is given by, $1/(s - m_0^2)$, where m_0 is the bare Higgs mass. When $s - m_0^2 \sim \mathcal{O}(\alpha)$, a certain class of higher order corrections, the set of one-particle-irreducible (1PI) self energy graphs, may be resummed to give the effective propagator,

$$\frac{1}{s - m_H^2 + \mathcal{I}m\ \Pi(s)}, \tag{4.1}$$

where $\Pi(s)$ is the 1PI self energy, and,

$$\mathcal{I}m\ \Pi(s) \sim \alpha\frac{s^2}{M_Z^2} + \mathcal{O}(\alpha^2) \sim \alpha\frac{m_H^4}{M_Z^2} + \mathcal{O}(\alpha^2). \tag{4.2}$$

Note that $\mathcal{I}m\ \Pi(m_H^2) = m_H\Gamma_H$. At lowest order, it is therefore consistent to use either a fixed width (as in the previous section) or an energy dependent width. On the other hand, the energy dependent width is in principle more correct since the self energy is a function of s and not m_H. The difference between the two is illustrated in Fig. 3. The s-dependent width shifts the resonance to smaller m_{ZZ} and significantly modifies the shape. This is easily understood since the effective width beneath $m_{ZZ} = m_H$ is reduced thus increasing the cross section while the opposite occurs above the resonance [15]. *At lowest order all four curves are equivalent*, although they differ at next-to-leading order. Current theoretical thought [15] suggests that including all tree level diagrams with an energy dependent width is the best thing to do, however, to determine a fully consistent cross section at next-to-leading order requires a significant theoretical input before the supercolliders commence operation.

It is important to note that outside the resonance region, it is inconsistent to resum these self energy graphs and the Higgs propagator should therefore be $1/(s - m_H^2)$. Using an energy dependent width at $s >> m_H^2$ suppresses the Higgs exchange graphs so that unitarity is not violated in the s-channel approximation but is violated in the full calculation. In both cases, this is not a correct thing to do.

5 The effective W approximation

In the effective W approximation, gauge boson distribution functions $f^q_{\lambda,V}(x)$ describe the probability that on-shell vector boson V with polarisation λ is found carrying fraction x of the parent quarks momentum [10, 16]. The vector boson process is thus reduced to the $2 \to 2$ processes $WW \to ZZ$ and $ZZ \to ZZ$ convoluted with the gauge boson distribution functions while the quarks scatter at very small angles. As with ordinary parton distributions, these gauge boson distributions are evaluated at a scale Q^2 which is a scale associated with the hard process, typically m_{ZZ}^2 or p_{TZ}^2. Unfortunately, the distributions for transversly polarised gauge bosons depend strongly on the scale choice and lead to an unreliable prediction as shown in Fig. 4. This is not the case for longitudinally polarised gauge bosons which are essentially scale independent and which, after all, couple strongest to the Higgs boson. For comparison, Fig. 4 also shows the result obtained by including all of the $\mathcal{O}(100)$ tree level diagrams [13, 14]. We see that in the resonance region the effective W approximation works extremely well *provided that only longitudinal polarisations are included.*

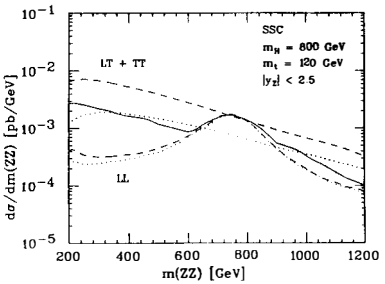

Fig. 4. The ZZ invariant mass distribution in the effective W approximation for $m_H = 800$ GeV at the SSC for $Q^2 = m_{ZZ}^2$ (dashed) and $Q^2 = m_{ZZ}^2/4$ (dotted) for longitudinal (LL) and transverse (LT+TT) polarisations. The exact $qq \to qqZZ$ calculation is shown solid.

6 The $m_H \to 0$ approximation

In this approximation, the full set of tree level diagrams is evaluated with m_H set to a small value which therefore satisfies unitarity everywhere [14]. In practice, the precise value of m_H does not matter provided $m_H << 2M_Z$. This is essentially equivalent to setting the partial waves involving the symmetry breaking sector to zero and represents the minimal contribution to the ZZ lineshape from both gluon fusion and vector boson fusion. Any strongly interacting Higgs sector or Higgs boson will increase the cross section above the $m_H \to 0$ limit. As illustrated by Fig. 5, this approximation shows that the ZZ background is increased by about 60% at the SSC relative to lowest order $q\bar{q} \to ZZ$ which is comparable to the effect of higher order QCD corrections. At the LHC this enhancement is about 30%. The background curve in Fig. 1 is thus obtained from the $q\bar{q} \to ZZ$ process added to the $m_H \to 0$ approximation for $gg \to ZZ$ and $qq \to qqZZ$.

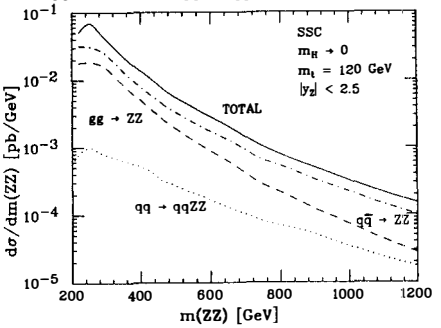

Fig. 5. The ZZ invariant mass distribution in the $m_H \to 0$ approximation at the SSC.

7 Shower Monte Carlos

By way of summary, Table 1 shows which approximations for ZZ production are available in PYTHIA [18], ISAJET [19] and HERWIG [20],

Table 1. ZZ production processes available in PYTHIA, ISAJET and HERWIG.

	PYTHIA	ISAJET	HERWIG
$q\bar{q} \to ZZ$	yes	yes	no
$Z \to f\bar{f}$	yes	yes	no
Γ_Z	yes	no	no
$gg \to ZZ$	no	no	no
$gg \to H \to ZZ$	yes	yes	yes
$Z \to f\bar{f}$	yes	yes	yes
Γ_Z	yes	no	yes
$m\Gamma$	$\Pi(s)$	$m_H\Gamma_H$	$m_H\Gamma_H$

$qq \to qqZZ$	no	no	no
$qq \to qqH \to qqZZ$	yes	no	yes
$Z \to f\bar{f}$	yes	-	yes
Γ_Z	yes	-	yes
$m\Gamma$	$\Pi(s)$	-	$m_H\Gamma_H$
$VV \to ZZ$	yes	yes	no
V polarisations	L only	L only	-
Z polarisations	L only	L + T	-
$Z \to f\bar{f}$	yes	yes	-
Γ_Z	yes	no	-
$m\Gamma$	$m_H\Gamma_H$	$m_H\Gamma_H$	-

References

[1] U. Baur and E. W. N. Glover, Fermilab preprint FERMILAB-PUB-90/154-T.

[2] M. S. Chanowitz and M. K. Gaillard, Nucl. Phys. **B261** (1985) 379.

[3] D. Froidevaux, Large Hadron Collider Workshop, CERN report CERN 90-10, Vol II (1990) 444.

[4] G. Trilling *et al.*, Letter of Intent by the SOLENOIDAL DETECTOR COLLABORATION, (1990).

[5] D. W. Duke and J. F. Owens, Phys. Rev. **D30** (1984) 49.

[6] R. W. Brown and K. O. Mikaelian, Phys. Rev. **D19** (1979) 922.

[7] B. Mele. P. Nason and G. Ridolfi, CERN preprint CERN-TH-5890 (1990).

[8] J. Ohnemus and J. F. Owens, Florida State preprint FSU-HEP-901212 (1990).

[9] H. Georgi, S. L. Glashow, M. E. Mahacek and D. V. Nanopoulos, Phys. Rev. Lett. **40** (1978) 692.

[10] R. N. Cahn and S. Dawson, Phys. Lett. **B136** (1984) 196, *ibid* **B138** (1984) 464(E).

[11] D. A. Dicus, C. Kao and W. W. Repko, Phys. Rev. **D36** (1987) 1570;
D. A. Dicus, Phys. Rev. **D38** (1988) 394.

[12] E. W. N. Glover and J. J. van der Bij, Nucl. Phys. **B321** (1989) 561.

[13] D. A. Dicus, S. L. Wilson and R. Vega, Phys. Lett. **B192** (1987) 231.

[14] U. Baur and E. W. N. Glover, Nucl. Phys. **B347** (1990) 12.

[15] S. S. D. Willenbrock and G. Valencia, Phys. Lett. **B247** (1990) 341.

[16] S. Dawson, Nucl. Phys. **B249** (1984) 42;
G. L. Kane, W. W. Repko and W. B. Rolnick, Phys. Lett. **B148** (1984) 367;
M. S. Chanowitz and M. K. Gaillard, Phys. Lett. **B142** (1984) 85.

[17] A. Abbasabadi and W. W. Repko, Phys. Rev. **D36** (1987) 289.

[18] H.-U. Bengtsson and T. Sjostrand, PYTHIA 5.4 (1990).

[19] F. Paige and S. Protopopescu, ISAJET 6.36 (1991).

[20] G. Marchesini, I. Knowles, M. Seymour and B. Webber, HERWIG 5.1 (1991).

QCD STRONG COUPLING CONSTANT

Measurement of α_s from the Structure of Particle Clusters Produced in Hadronic Z Decays

Dr. Richard D. St. Denis
CERN PPE Division – Geneva, Switzerland
for the ALEPH Collaboration

Abstract

Using 106000 hadronic events obtained with the ALEPH detector at LEP at energies close to the Z resonance peak, the strong coupling constant α_s is measured by an analysis of energy-energy correlations (EEC) and the global event shape variables Thrust, C-parameter and Oblateness. It is shown that the theoretical uncertainties can be significantly reduced if the final state particles are first combined in clusters using a minimum scaled invariant mass cut, y_{cut}, before these variables are computed. The combined result from all shape variables of pre-clustered events is $\alpha_s(M_Z^2) = 0.117 \pm 0.005$ for a renormalization scale $\mu = M_Z/2$. For μ values between M_Z and the b-quark mass, the result changes by $^{+0.006}_{-0.009}$.

1. Introduction

The determination of the strong coupling constant $\alpha_s(M_Z^2)$from the structure of hadronic events at LEP energies generally requires direct comparison of data with the structure of partonic final states as calculated in second order perturbative Quantum Chromo-Dynamics (QCD). This paper shows that the theoretical uncertainties associated with this comparison can be reduced by considering variables which are not computed for the single particle momenta of the final state (as done in our earlier work [1]) but for clusters of neighbouring particles in phase space. Naively, these clusters should more closely resemble the structure of a purely partonic final state as accessible in finite order perturbation theory.

2. Analysis

2.1 Event Selection and Data Correction

The ALEPH detector, which provides both tracking information and calorimetry over almost the full solid angle, is described in detail in reference [2]. The analysis is based on 106000 hadronic events at center-of-mass energies in the range 91.0 GeV $\leq E_{CM} \leq$ 91.5 GeV. Further details may be found in [3]. The experimental distributions are constructed using only charged particle information and are corrected for detector effects as described in [1,3,4].

2.2. Definition of Clusters

Before computing event shape variables the final state particles are combined in clusters, with every particle initially representing a cluster. For each pair (i,j) of clusters a scaled mass y_{ij} is defined according to the JADE metric [3,5]. If the pair with the smallest y_{ij} fulfills $y_{ij} < y_{cut}$, the corresponding clusters are combined according to the E_0 recombination scheme [6]. The E_0 scheme was preferred over alternative schemes [6] because it was found to have consistently the smallest sensitivity to fragmentation processes.

2.3. Second Order QCD Predictions

As the basic theoretical ingredient the second order QCD matrix elements as calculated by Ellis, Ross and Terrano (ERT) [7] are used. These can be integrated to predict the distribution for a given event shape variable, X, as described for example in reference [6],

$$\frac{1}{\sigma_0}\frac{\mathrm{d}\sigma}{\mathrm{d}X} = \frac{\alpha_s(\mu^2)}{2\pi}A(X) + \left(\frac{\alpha_s(\mu^2)}{2\pi}\right)^2\left[A(X)\cdot 2\pi b_0 \log\left(\frac{\mu^2}{s}\right) + B(X)\right] + \mathcal{O}\left(\alpha_s^3\right) \quad (1)$$

with $b_0 = (33 - 2n_f)/12\pi$. Here, $n_f(=5)$ denotes the number of active flavours and $\sqrt{s}$ is the center-of-mass energy. The functions A and B are specific to the particular event shape variable, contain the full information of the second order matrix elements, and, in the case of shape variables for pre-clustered events, they also depend on the value chosen for y_{cut}. The parameter μ denotes the renormalization scale used for the calculation. An example of the result is shown in Figure 1 for the functions $A(\cos\chi, y_{cut})$, $B(\cos\chi, y_{cut})$ for $\sin^2\chi \cdot \mathrm{EEC}(\cos\chi)$, where $\mathrm{EEC}(\chi)$ is the energy-energy correlation.

2.4. Choice of Renormalization Scale

Comparing equation (1) to the data one can now determine $\alpha_s(\mu^2)$ for any choice of the renormalization scale μ and then translate it into $\alpha_s(M_Z^2)$ using the two-loop

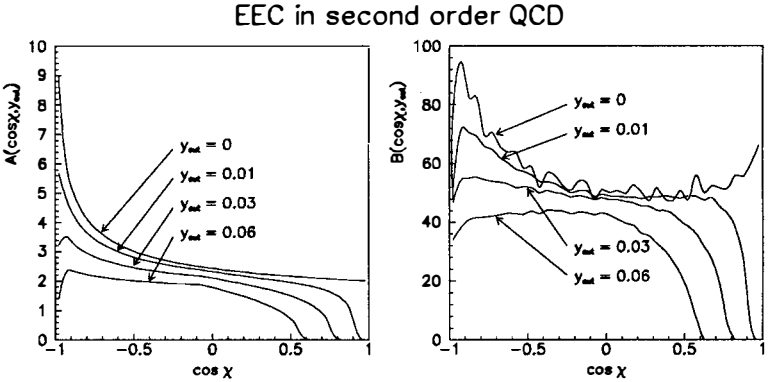

Figure 1: *Second order QCD prediction for the functions A, B of the EEC after pre-clustering(see text). The fluctuations are due to the finite statistics of the Monte Carlo integration.*

expression for the running coupling constant [6]. The choice of μ enters the result to third order, reflecting our ignorance of higher order corrections. Since α_s is relatively large this third order effect still has a significant impact on the numerical results and constitutes a source of theoretical uncertainty. Theoretical prescriptions to reduce the sensitivity to the scale by choosing appropriate and typically very small values for μ [8] cannot guarantee that third order terms become small. Therefore, we prefer to determine the value $\alpha_s(M_Z^2)$ using $\mu = M_Z$ and to give an explicit parameterization of the shifts induced if the scale is varied. The impact of higher order contributions is estimated by means of parton shower Monte Carlo models based on the leading-logarithm approximation. In addition the renormalization scale is allowed to vary between M_Z (which is taken to be 91.2 GeV) and the b-quark mass.

2.5. Correction for Fragmentation and Systematic Errors

The methods used to extract $\alpha_s(M_Z^2)$ from distributions of event shape variables and to estimate the theoretical uncertainties are described in detail in references [1] and [3]. The fit results for $\alpha_s(M_Z^2)$ are corrected for the effects of higher order perturbative effects and for the effects of hadronization (both together in the following being referred to as effects of *fragmentation*) using the Lund second order matrix element (ME) model (JETSET 7.2) [9]. The correction was performed using a transition probability matrix (from parton to hadronic states) or a simple ratio (in the case of the EEC).

In all cases the magnitude of the correction enters the theoretical error estimate. One should therefore try to find variables where the corrections are very small, i.e. typically less than 10%.

For the study of systematic errors inherent in the correction based on the ME model the transition from the parton level to the hadron level was studied in addition for the Lund ME model and for the Parton Shower model [10]. In the case of the Parton Shower model, two calculations were done, differing in the minimum virtuality of the partons. In one case, the virtuality was set so that the average number of partons was the same as in the ME model. In the second case, the average number of partons was four. The theoretical error is defined to be the maximum deviation of the corrected value of $\alpha_s(M_Z^2)$ from the results using any of these alternative response matrices.

In order to separate the effects of perturbative higher order effects from the non-perturbative final hadronization process, the transition of the final shower states into hadrons was also studied in the LUND and HERWIG [11] PS models which are both based on the leading-logarithm approximation but employ very different hadronization schemes.

3. Determination of $\alpha_s(M_Z^2)$ from Energy-Energy Correlation of Clusters

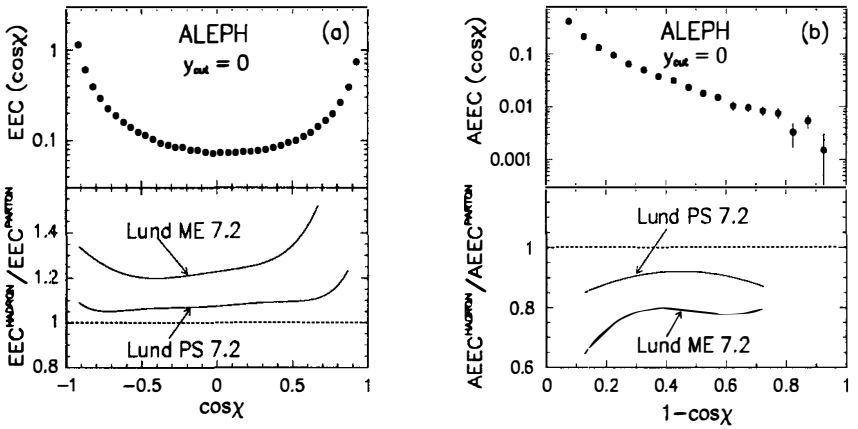

Figure 2: *Measured EEC (a) and AEEC (b) distributions together with the ratio of distributions on hadron and parton level, as derived from the Lund ME model and the Lund PS model.*

The experimental result for the EEC and AEEC distributions are shown in figure 2 together with the prediction of the hadron and parton level distributions from model calculations. In the Lund PS model these ratios deviate from 1 by at least $5 - 10\%$, indicating a moderate sensitivity of the EEC and AEEC distributions to hadronization effects. The ratios derived from the Lund ME model, however, deviate from 1 by more than 20%, suggesting that higher order perturbative corrections are very important even at LEP energies. Therefore one expects relatively large theoretical uncertainties for α_s if derived from these distributions.

The systematic distortions of the EEC distribution vanish to a large extent if one considers pre-clustered events (CEEC variable). This is shown in figure 3 where the measured CEEC distribution is displayed together with the ratio of hadron and parton level distributions from model calculations for two values of y_{cut}. The CEEC distribution changes in shape with varying y_{cut}. This is quantitatively predicted by the second order QCD calculation which is shown in figure 3 after correction using the Lund ME model.

Although the residual fragmentation effects for the CEEC are small they are slightly asymmetric in $\cos\chi$. The range $-0.5 < \cos\chi < 0$ has consistently small and constant distortions and is therefore chosen to fit $\alpha_s(M_Z^2)$. The change of the results when moving to a symmetric range $-0.25 < \cos\chi < 0.25$ has been included in the theoretical error. The results from fits of the second order QCD prediction to the data are presented in figure 4 as function of y_{cut} before correction for residual fragmentation effects (figure 4(a)), and after correction with theoretical uncertainties for a fixed scale $\mu = M_Z/2$

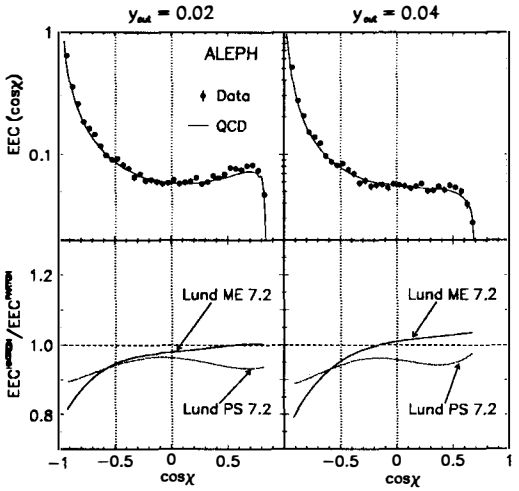

Figure 3: *Measured CEEC distribution together with the ratio of CEEC distributions on hadron and parton level from model calculations for two values of y_{cut}. Also shown are second order QCD predictions for $\alpha_s(M_Z^2) = 0.118$ and $\mu = M_Z/2$ after correction for fragmentation effects.*

included in the errors.

Finally $y_{cut} = 0.02$ was chosen. Comparison of the uncorrected value of α_s to the value after correction for hadronization and higher order effects and to the value after correction for hadronization alone [3] gives:

$$\alpha_s(M_Z^2)\,|_{\mathrm{CEEC}} = 0.118 \pm 0.002 \pm 0.001 \pm 0.005 \quad \text{for} \quad \mu = \frac{M_Z}{2} \ ,$$

the errors denoting the statistical error, the experimental systematic error, and the theoretical uncertainties defined in section 2.5. Varying μ between M_Z and the b-quark mass changes the result in addition by $^{+0.006}_{-0.010}$. The dependence of the uncorrected result on the choice of $f = \mu^2/M_Z^2$ was found to be $\alpha_s(M_Z^2, f) - \alpha_s(M_Z^2, f = 0.25) = 0.00371 \ln(4f) + 0.00034 \ln^2(4f)$ for $f \geq 0.002$.

The analysis was repeated using the covariant E recombination scheme [6] together with the JADE metric. In the E0 scheme, the Lund ME correction is 3% and in the E scheme it is 6%, but the corrected result for α_s agrees within 1%.

4. Influence of Clustering on Global Event Shape Variables

In this section the variables thrust, T, oblateness, O, and the C-parameter, as defined in reference [6], are reconsidered in the context of pre-clustered events.

The fits of $\alpha_s(M_Z^2)$ were performed in intervals contained in those chosen in reference [1]. In addition it was required that the ranges are well inside the kinematic boundaries imposed on the event shape distribution due to pre-clustering up to $y_{cut} = 0.06$. The results of the fits are displayed in figure 4(c,d).

The smallest value of y_{cut} at which all three variables start to give stable values for $\alpha_s(M_Z^2)$ is 0.03. The results are shown in table 1 and are not only consistent with

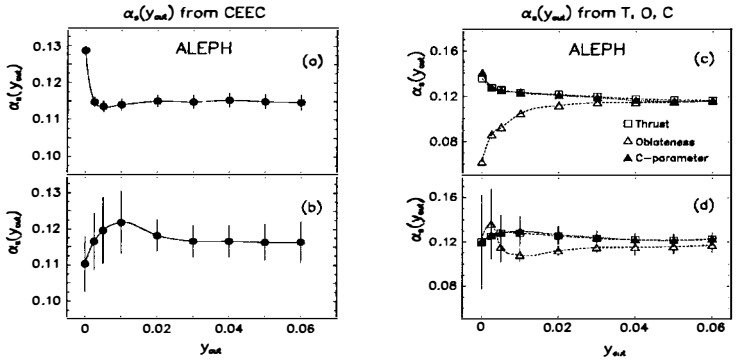

Figure 4: *Results for $\alpha_s(M_Z^2)$ as function of y_{cut} from QCD fits to event shape distributions before correction for fragmentation effects (a,c), and after correction with estimated theoretical uncertainties for a fixed scale $\mu = M_Z/2$ included in the errors (b,d).*

Distribution	$\alpha_s(M_Z^2)$, $f = 0.25$	c_1	c_2	f_{min}
CEEC	$0.118 \pm 0.002 \pm 0.005$	0.00371	0.00034	0.002
T	$0.123 \pm 0.004 \pm 0.006$	0.00449	0.00035	0.001
C	$0.124 \pm 0.004 \pm 0.006$	0.00427	0.00037	0.001
O	$0.115 \pm 0.004 \pm 0.005$	0.00375	0.00035	0.001

Table 1: Results for $\alpha_s(M_Z^2)$ with combined experimental errors and errors due to model corrections together with coefficients of a parameterization for the change $\alpha_s(f) - \alpha_s(f = 0.25) = c_1 \cdot \ln(4f) + c_2 \cdot \ln^2(4f)$. The last column gives a lower limit for the scale parameter f where the parameterization is still within the statistical error of the fitted value.

each other but also very close to earlier measurements using y_3 [1,12,13] and EEC or AEEC [14]. The fragmentation effects for all pre-clustered variables are small and the theoretical uncertainties are dominated by the scale dependences.

5. Combination of the Results

In order to derive a final result from the numbers in table 1, the correlations between the statistical and between the theoretical errors of the various measurements were determined [3]. The combined result for $\mu = M_Z/2$ is

$$\alpha_s(M_Z^2) = 0.117 \pm 0.005,$$

where the error contains both experimental and theoretical errors. The combined scale dependence is then $\alpha_s(M_Z^2, f) - \alpha_s(M_Z^2, f = 0.25) = 0.00356 \ln(4f) + 0.00035 \ln^2(4f)$ which leads to a variation of $^{+0.006}_{-0.009}$ for scales ranging from the b-quark mass up to M_Z.

6. Conclusions

The strong coupling constant has been measured from an analysis of the structure of pre-clustered events. Energy-energy correlation, Thrust, C-parameter and Oblateness all yield consistent values for $\alpha_s(M_Z^2)$ with moderate theoretical errors. The combined result of all four variables is $\alpha_s(M_Z^2) = 0.117 \pm 0.005$ for $\mu = M_Z/2$, where renormalization scales varying between the b-quark mass and M_Z lead to changes of $^{+0.006}_{-0.009}$. The

combined value is almost identical to that obtained from CEEC alone, indicating that the results from the different event-shape variables have strongly correlated theoretical uncertainties. The final value is also in good agreement with our earlier measurement from y_3, $\alpha_s(M_Z^2) = 0.121 \pm 0.002(stat.) \pm 0.003(syst.) \pm 0.007(theory)^{+0.007}_{-0.012}(scale)$ [1].

Acknowledgements

We would like to thank P. Nason for very useful discussions and his help with the theoretical predictions for pre-clustered events. We congratulate our colleagues of the LEP division for the excellent performance of the storage ring. Thanks are also due to engineers and technical personnel at all collaborating institutions for their support in constructing and maintaining ALEPH . Those of us from non-member states thank CERN for its hospitality.

References

[1] D. Decamp et al., ALEPH Collaboration, CERN-PPE/90-176.

[2] ALEPH – *a Detector for Electron-Positron Annihilation at LEP,* Nucl. Instr. Meth. **A294** (1990) 121.

[3] D. Decamp et al., ALEPH Collaboration, CERN-PPE/90-196.

[4] D. Decamp et al., ALEPH Collaboration, Phys. Lett. **B234** (1990) 209.

[5] W. Bartel et al., JADE Collaboration, Z. Phys. **C33** (1986) 23;
S. Bethke et al., JADE Collaboration, Phys. Lett. **B213** (1988) 235.

[6] Z. Kunszt, P. Nason, G. Marchesini and B.R. Webber, *QCD* , in *Proceedings of the Workshop on Z Physics at LEP,* eds. G. Altarelli, R. Kleiss and C. Verzegnassi, CERN Report 89-08.

[7] R.K. Ellis, D.A. Ross and A.E. Terrano, Nucl. Phys. **B178** (1981) 421.

[8] P.M. Stevenson, Phys.Rev. **D16** (1981) 2916;
S.J. Brodsky, G.P. Lepage and P.B. Mackenzie, Phys. Rev. **D28** (1983) 228;
G. Grunberg, Phys. Lett. **B95** (1980) 70.

[9] T. Sjöstrand and M. Bengtsson, Comp. Phys. Comm. **43** (1987) 367.

[10] M. Bengtsson and T. Sjöstrand, Phys. Lett. **185B** (1987) 435.

[11] G. Marchesini and B.Webber, Cavendish-HEP-88/7 (1988);
G. Marchesini and B. Webber, Nucl. Phys. **B310** (1988) 461;
I. Knowles, Nucl. Phys. **B310** (1988) 571.

[12] S. Komamiya et al., MarkII Collaboration, Phys. Rev. Lett. **64** (1990) 987.

[13] M.Z. Akrawy et al., OPAL Collaboration, Phys. Lett. **B235** (1990) 389;
M.Z. Akrawy et al., OPAL Collaboration, CERN-PPE/90-143;
P. Abreu et al., DELPHI Collaboration, Phys. Lett. **B247** (1990) 167;
B. Adeva et al., L3 Collaboration, Phys. Lett. **B248** (1990) 462.

[14] P. Abreu et al., DELPHI Collaboration, CERN-PPE/90-122;
M.Z. Akrawy et al., OPAL Collaboration, CERN-PPE/90-121;
B. Adeva et al., L3 Collaboration, L3 Preprint #023 (1990).

Recent Tests of QCD at OPAL

G. Azuelos

Université de Montréal / TRIUMF

representing the OPAL collaboration

Abstract

A review of selected recent tests of QCD using the OPAL data is presented. It includes analyses of three-jet and four-jet event distributions sensitive to the gluon spin and to the non-abelian nature of QCD, studies of recombination-scheme dependence of jet rates, and precision α_s measurements from multihadronic event distributions.

1 Introduction

Because of the large e^+e^- annihilation cross-section at the Z^0 resonance and the large hadronic branching ratio of Z^0 decays, LEP provides ideal opportunities for performing high-statistics measurements of multihadronic event distributions. Furthermore the good jet resolution obtainable at that energy, and the low fragmentation corrections allow fundamental tests of perturbative QCD and local parton-hadron duality. We present here selected recent QCD results from OPAL data.

2 Three-Jet Distributions

Although the vector nature of the gluon is now a well-accepted postulate of QCD theory, previous direct evidence is based on measurements at around 30 GeV of poor statistical significance [1] With the higher statistics, improved jet resolutions and reduced fragmentation effects at LEP energies, a much clearer discrimination between vector and scalar gluon theories is feasible.

Kinematically, a three-parton event at the Z^0 vertex is describable by two independent degrees of freedom. Defining $x_i = E_i/E_{cm}$ as the fractional energy of the i^{th} parton, the double differential cross-sections in first-order of α_s are very different in the scalar and vector gluon cases:

$$\frac{d^2\sigma^V(x_1,x_2)}{dx_1dx_2} \sim \frac{x_1^2+x_2^2}{(1-x_1)(1-x_2)} \quad (1)$$

$$\frac{d^2\sigma^S_{(v)}(x_1,x_2)}{dx_1dx_2} \sim \frac{[(1-x_1)+(1-x_2)]^2}{(1-x_1)(1-x_2)} \quad (2)$$

$$\frac{d^2\sigma^S_{(a)}(x_1,x_2)}{dx_1dx_2} \sim \frac{[(1-x_1)+(1-x_2)]^2}{(1-x_1)(1-x_2)} - 2(1+x_3) \quad (3)$$

The case of the scalar gluon ($\frac{d^2\sigma^S(x_1,x_2)}{dx_1dx_2}$) receives different contributions from vector and axial couplings in Z^0 decays [2]. The above expressions assume that x_1 and x_2 are associated with the quarks (x_2 being the quark which radiates), and x_3 with the radiated gluon. In practice, the x_i are ordered in decreasing value ($x_1 > x_2 > x_3$), and the symmetrized cross-sections are integrated over one of the degrees of freedom.

Two distributions are of particular interest: (i) the x_2 distribution: the vector-gluon cross section exhibits a pole for the limiting case $x_1 > x_2 \to 1$ whereas the scalar gluon cross section remains constant. The sensitivity to this variable can be understood since it is the second-most energetic parton which most often radiates the gluon and which is therefore most affected. (ii) the Ellis-Karliner distribution: the three-parton system is boosted to a frame of reference where the two least energetic ones are in their center of mass system, defining the angle θ_{EK}.

The above distributions have been histogrammed for the multihadrons collected by OPAL in 1990. They are corrected for detector effect, initial-state radiation and fragmentation using JETSET Monte Carlo events with parameters optimised to fit the observed event shapes and are therefore directly comparable to theoretical shapes derived at the parton level. Comparison to first-order parton shower Monte Carlo predictions and to analytical calculations are shown in

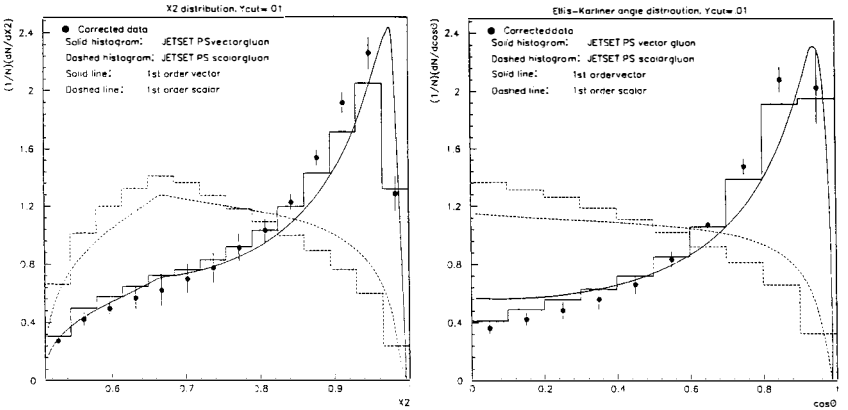

Figure 1: The x_2 and Ellis-Karliner distributions compared to predictions of a vector-gluon and a scalar gluon first- order and parton shower calculations.

fig. 1 leaving no doubt as to the vector nature of the gluon. This unambiguous result is obtained thanks to the possibility of using a small value of $y_{cut} = 0.01$, the jet-definition parameter of the JADE algorithm [3].

3 Four-Jet Distributions

In $O(\alpha_s^2)$ theory, four diagrams contribute to 4-parton final states: (i) gluon radiation from each of the initial quarks of the $Z^0 \to q\bar{q}$ decay, (ii) double gluon radiation from one of the quarks, (iii) $Z^0 \to q\bar{q}g$ followed by $g \to q\bar{q}$ and (iv) $Z^0 \to q\bar{q}g$ followed by $g \to g\bar{g}$. The last diagram is specific to a nonabelian theory, in which the mediating boson interacts with itself. The vector nature of the gluon leads to different angular distributions for the different cases.

Among the observables suggested for the confirmation of this property of the strong interaction are the distributions with respect to the Bengtson-Zerwas χ_{BZ} angle and the modified Nachtman-Reiter angle $cos(\theta^*_{NR})$, defined in fig 2a. From the OPAL data, four-jet events were selected using the y_{cut} values of 0.01 and 0.02, and these distributions reconstructed subject to the criteria that (i) for the observable χ_{BZ} the angles between the jet axes that define a plane are smaller than 160 degrees. (ii) in the case $cos(\theta^*_{NR})$, the energy-ratio between the second- and third- largest energy jets E_2/E_3 be larger than 2. This leaves 3880 4-jet events for the χ_{BZ} distribution and 2978 for the $cos(\theta^*_{NR})$ distribution, with $y_{cut} = 0.01$ Fig. 2b,2c show these distributions, after correction for detector and fragmentation effects, compared to predictions from Monte Carlo based on parton shower and $O(\alpha_s^2)$models of abelian and nonabelian (QED-like) theories. Both distributions are in agreement with the standard QCD theory, and are not compatible with the abelian theory.

Closer inspection reveals that the difference in the prediction of the two theories is due mainly to the difference of the predicted four-quark fraction of the events: 4.7% in QCD theory, 31.4% in a nonabelian theory. Both distributions appear to discriminate mainly between $q\bar{q}q\bar{q}$ states and the other states $q\bar{q}gg$. This feature can be used to give an upper limit on the presence of spin-1/2 gluons (gluinos). Based on the expected and observed mean values $< \chi_{BZ} >$ and

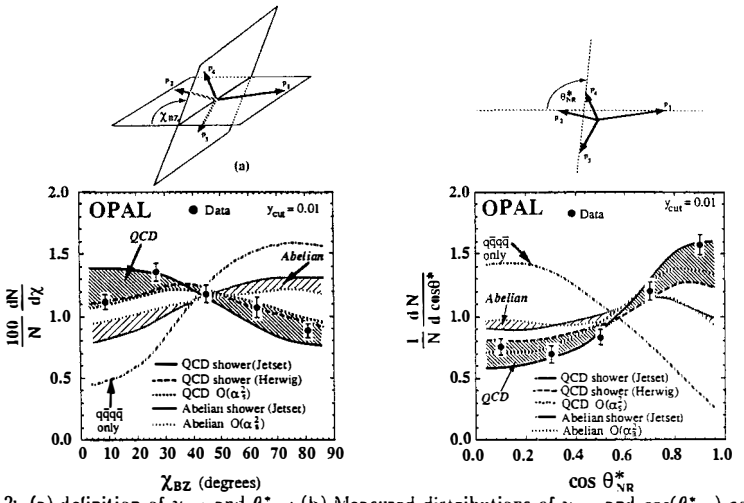

Figure 2: (a) definition of χ_{BZ} and θ^*_{NR}; (b) Measured distributions of χ_{BZ} and $cos(\theta^*_{NR})$ compared to abelian and nonabelian theory predictions.

$< cos(\theta^*_{NR}) >$, an excess of four-fermion final states arising from $q\bar{q}\tilde{g}\tilde{g}$ is ruled out with 89% confidence level. Further details can be found in [4].

4 Recombination Scheme Studies

The most commonly used jet definition is based on the JADE algorithm [3] which depends on a parameter y_{cut} : all pair combinations of particles are considered, and the one having the smallest invariant mass M_{ij} is clustered into one pseudoparticle if the relation $y_{ij} = M^2_{ij}/E^2_{cm} > y_{cut}$ is satisfied. The procedure is repeated until no pair satisfies the relation. However, ambiguities are introduced in the stage of combining two unresolvable pseudoparticles since $O(\alpha_s^2)$ QCD calculations are performed for massless partons.

Four recombination schemes have been studied. After selecting the jets which must be recombined, (i) the *E-scheme* conserves momentum and energy but leads to a non-zero mass value of the new jet, (ii) the *E0-scheme* conserves energy, but rescales the momentum so that the recombined jets have zero mass, (iii) the *p-scheme* conserves momentum and forces the recombined jet to have zero mass ($E_k = |\vec{p}_k|$); here the total energy of the event decreases after each recombination, and (iv) the *p0-scheme* is like the *p-scheme* except that in the calculation of y_{ij}, the visible energy E_{vis}, recalculated after each recombination is used in the denominator, rather than the c.m. energy E_{cm}.

Fig. 3 shows the recombination-scheme dependence of the jet rates and of the hadronisation correction, based on a sample of simulated events generated with the JETSET shower model. The E-scheme yiels larger multi-jet rates and leads to large differences in jet rates between showers at the parton stage and at the hadron stage. In general, it can be concluded that the *E0-scheme* is recommended for jet counting since it leads to close correspondence between the parton and hadron jets, and the *p0-scheme* offers good angular and energy resolution of reconstructed jets.

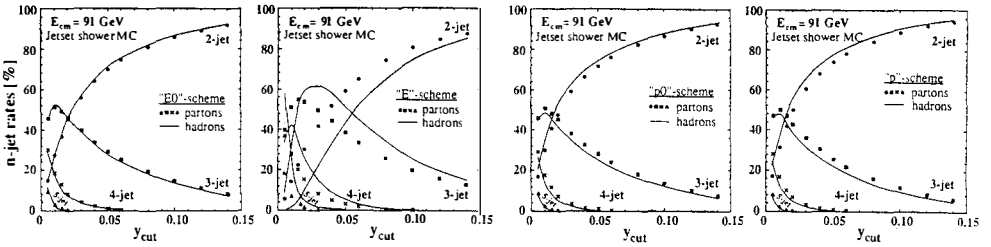

Figure 3: Relative production of n-jet events, determined from model calculations before and after the hadronisation process for the four recombination schemes, as a function of y_{cut}.

5 Measurements of α_s

Several α_s-sensitive observables have been studied, using the OPAL multihadron data. For each of them, simulated Monte Carlo data served to correct the distribution observed at the detector level to a presumed distribution immediately after the parton shower, but preceding hadronisation. It is this corrected distribution which can be directly compared to $O(\alpha_s^2)$calculations. In each case, the sources of the systematic error which have been generally considered are: (i) $\Delta\alpha_s$(exp) is estimated from the results of separate analyses, one which uses calorimeter information alone, one which uses charged track information alone, and one which uses the combined data. (ii) For each of the distributions, a bin-by-bin correction of the data to the parton-level distribution is applied using standard Monte Carlo techniques. $\Delta\alpha_s$(had) is obtained from a comparison of results corrected for hadronization using JETSET or Herwig Monte Carlo generators. (iii) $\Delta\alpha_s(Q_0)$ accounts for variations due to the value of parton virtualities to which the data are corrected. For large values of Q_0, the parton multiplicity is lower at the end of the shower, leading to a smaller influence of higher order QCD contributions. (iv) $\Delta\alpha_s(scale)$ due to the choice of the effective scale $f = \mu^2/E_{cm}^2$ at which α_s is calculated. In $O(\alpha_s^2)$ calculation, the 2-jet and 3-jet rates are sensitive to this scale, and hence an optimised value of f can be obtained from a fit. For each observable X, one can write in second-order,

$$\frac{1}{\sigma_0} X \frac{d\sigma}{dX} = \frac{\alpha_s(\mu)}{2\pi} A_X(X) + \left(\frac{\alpha_s(\mu)}{2\pi}\right)^2 \left[2\pi b_0 \log(\mu^2/s) A_X(X) + B_X(X)\right] \qquad (1)$$

where σ_0 is the leading order hadronic cross section, and b_0 is the coefficient of the lowest order evolution equation for α_s: $b_0 = (33 - 2n_f)/12\pi$. In the absence of a conventional definition of the scale, we define an error in α_s as half of the difference of the α_s values obtained at the scale $\mu^2 = E_{cm}^2$ and at the scale μ^2 = best-fit value.

5.1 Jet rates

The jet rates discussed in sect. 4 provide one direct method of measuring α_s since they are related to the parton multiplicity at the Z^0 decay vertex. In order to account correctly for the statistical uncertainties, it is the derivative of the 2-jet curve which is fitted to $O(\alpha_s^2)$ analytical calculations. In the present study, the calculations of Kunszt and Nason [5], based on the ERT

matrix elements [6] were used since they have been carried out for the $E-$, $E0-$, $p-$, and $p0-$ schemes. A complete report on the analysis has been published in [7].

The results of the fits for the different schemes are summarized in table 1 where various systematic errors are also evaluated.

Scheme	$\alpha_s(M_{Z^0})$	$\Delta\alpha_s$(exp.)	$\Delta\alpha_s$(had.)	$\Delta\alpha_s(Q_0)$	$\Delta\alpha_s$(scale)	$\Delta\alpha_s$(tot.)
$E0$	0.118	±0.003	±0.003	±0.003	±0.007	±0.007
E	0.126	±0.003	±0.003	±0.003	±0.013	±0.014
$p0$	0.118	±0.003	±0.003	±0.005	±0.004	±0.008
p	0.118	±0.003	±0.003	±0.006	±0.003	±0.008

Table 1: $\alpha_s(M_{Z^0})$ for different recombination schemes

5.2 EEC, AEEC, PTEC

The energy-energy correlations (EEC) are defined as the histogram of the angle between all combinations of pairs of tracks in hadronic events, weighted by their energies, suitably normalized, and averaged over all events:

$$EEC(\chi) = \frac{1}{\Delta\chi \cdot N} \int_{\chi-\frac{\Delta\chi}{2}}^{\chi+\frac{\Delta\chi}{2}} \sum_{events}^{N} \sum_{i\neq j} \frac{E_i E_j}{E_{vis}^2} \delta(\chi' - \chi_{ij}) d\chi' \tag{5}$$

where χ_{ij} is the angle between particles i and j and $\Delta\chi$ is the width of the histogram bin. The distribution is sensitive to α_s since the 2-jet contribution is peaked around 0^o and 180^o whereas 3-jet events will fill the central angular region. Calculations to $O(\alpha_s^2)$ have been performed by several groups [5,8] with good, but in some cases fair agreement.

The asymmetry of the EEC correlations, or $AEEC(\chi) = EEC(\pi - \chi) - EEC(\chi)$ is also sensitive to α_s since the 2-jet contribution cancels whereas in 3-jet events, because of energy-weighting, jets with large opening angles contribute more than those with small opening angles. In addition, it is found to be less sensitive to fragmentation corrections and to systematic effects which are likely to have a symmetric dependence on χ.

In analogy with EEC, the planar triple-energy correlation (PTEC) can also serve as a measure of α_s. Here, one looks for triplets of tracks instead of pairs and imposes a planarity condition: $\chi_1 + \chi_2 + \chi_3 > 2\pi - \delta$, where $\chi_{1,2,3}$ are the angles between the tracks and δ is a parameter,. In order to exclude further a region of phase space sensitive to 2-jet events, one also requires that each of the angles be greater than an angle β.

Tables 2,3 summarize the results from the three distributions. In each case, the integral over the appropriate angular region is used for the calculation of α_s. The error estimates are indications of the sensitivity of these distributions to the various effects. Included here are theoretical uncertainties arising from the different predictions of the $O(\alpha_s^2)$ calculations. For PTEC, sytematic errors are regrouped into one error. They include, for example, variations due to the choice of the parameter δ since, in the limit of exact coplanarity, a very small fraction of tracks contribute, whereas in $O(\alpha_s^2)$ calculations, 3-parton final states contribute fully. For larger values of δ multijet events have a major contribution because of the larger combinatorial

possibilities. For this reason, clustering of the tracks was done, with various values of y_{cut}, before the calculation of the correlations. AEEC was found to have a small sensitivity to scale. More detailed results from EEC and AEEC can be found in ref. [9]

Distribution	$\alpha_s(M_{Z^0})$	$\Delta\alpha_s$(exp.)	$\Delta\alpha_s$(had.)	$\Delta\alpha_s(Q_0)$	$\Delta\alpha_s$(th.)	$\Delta\alpha_s$(scale)	$\Delta\alpha_s$(tot.)
EEC	0.124	± 0.004	± 0.002	± 0.004	± 0.007	± 0.007	± 0.012
AEEC	0.117	± 0.007	± 0.001	± 0.003	$^{+0.006}_{-0.002}$	-	± 0.009

Table 2: $\alpha_s(M_{Z^0})$ for EEC and AEEC

$\alpha_s(M_{Z^0})$	$\Delta\alpha_s$(stat.)	$\Delta\alpha_s$(syst.)	$\Delta\alpha_s$(th.)	$\Delta\alpha_s$(scale)	$\Delta\alpha_s$(tot.)
0.108	± 0.002	$^{0.008}_{0.004}$	$^{0.004}_{0.005}$	± 0.001	$^{0.009}_{0.007}$

Table 3: *Preliminary* results on $\alpha_s(M_{Z^0})$ from PTEC

5.3 Other Event Shapes: C-planarity, Oblateness, Thrust

Results from other traditionally used infrared-safe quantities sensitive to α_s are presented in table 4.

Observable	$\alpha_s(M_{Z^0})$	$\Delta\alpha_s$(exp.)	$\Delta\alpha_s$(had.)	$\Delta\alpha_s(Q_0.)$	$\Delta\alpha_s$(scale)	$\Delta\alpha_s$(tot.)
C planarity	0.128	± 0.002	$+ 0.008$	± 0.001	± 0.016	$^{0.018}_{0.016}$
Oblateness	0.123	$^{0.002}_{0.004}$	$+ 0.001$	$+ 0.052$	± 0.00	$^{0.052}_{0.004}$
Thrust	0.130	± 0.002	$+0.001$	-0.006	± 0.018	$^{0.018}_{0.019}$

Table 4: Final results of $\alpha_s(M_{z^0})$ for different observables.

- *C-Planarity:* It is defined in terms of the eigenvalues λ_n of the momentum tensor θ_{ij}:

$$\theta_{ij} = \frac{\sum_a \frac{P_a^i P_a^j}{|P_a|}}{\sum_a |P_a|} \tag{6}$$

$$C = 3 \ (\lambda_1\lambda_2 + \lambda_2\lambda_3 + \lambda_3\lambda_1) \tag{7}$$

where P_a^i is the i^{th} component of the momentum of particle a. The value of C vanishes for two-parton states.

- *Thrust:*

$$T = max \left(\frac{\sum_i |\vec{p}_i \cdot \hat{n}_t|}{\sum_i |\vec{p}_i|} \right) \tag{8}$$

where the direction of the unit vector $\hat{n}_t$ is chosen to maximize the quantity in parentheses. The thrust has a value of unity for 2-parton final states, smeared by hadronisation, but varies between $\frac{2}{3} < T < 1$ for 3-parton states.

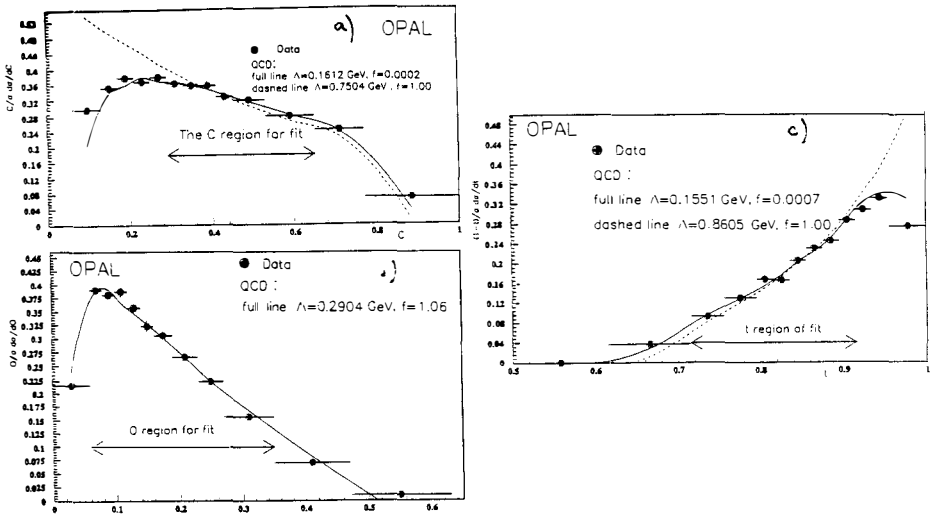

Figure 4: Measured distributions of (a) C-planarity, (b) Oblateness, and (c) Thrust, compared to $O(\alpha_s^2)$ QCD calculations

- *Oblateness:* Defining t_{major} in the same way as thrust above, but with the constraint $\hat{n}_{major} \cdot \hat{n}_t = 0$, and t_{minor} with $\hat{n}_{minor} = \hat{n}_t \times \hat{n}_{major}$, then

$$O = t_{major} - t_{minor} \tag{9}$$

These distributions are shown in fig. 4 along with the fit to theoretical calculations of Kunszt and Nason [5]. Table 4 is a summary of the α_s measurements from these observables.

6 Summary

A selected review of some fundamental QCD tests performed at OPAL was presented. Very clear direct evidence for the vector nature of the gluon was shown. Four-jet distributions were found to be consistent with the presence of a triple gluon vertex, characteristic of a nonabelian theory of QCD, but inconsistent with the predictions of a QED-like theory. Jet rates were found to be sensitive to the recombination scheme used in the jet finding algorithm. Finally, results from precision measurements of α_s from jet rates, energy correlations, C-planarity, oblateness and thrust were also shown. These results are summarized in fig. 5 where we have included a value of α_s obtained from a standard model fit of the measured Z^0 line shape and asymmetries. The "average" shown has been arbitrarily assigned an error equal to the smallest of the individual errors.

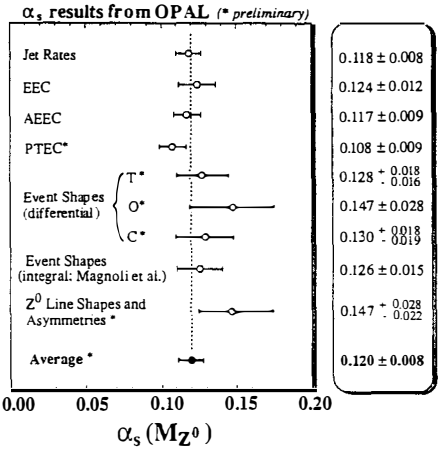

Figure 5: Summary of OPAL α_s measurements.

References

1. TASSO collaboration, R.Brandelik et al., Phys.Lett. 97B (1980) 453;
   CELLO collaboration, H.J.Behrend et al., Phys. Lett. 110B (1982) 329;
   PLUTO collaboration, Ch.Berger et al., Phys. Lett. 97B (1980) 459;
   Mark J collaboration, J.D.Burger et al., proceedings of the 21st International Conference on High Energy Physics, Journal de Physique 43, C3-C6;
   S. L. Wu, Physics Reports 107 (1984)

2. E. Laermann, K.H. Streng, and P.M. Zerwas, Z. Phys. C3 (1980) 289;
   P. Zerwas, private communication

3. JADE collaboration, S. Bethke et al., Phys. Lett. B213 (1988) 235

4. OPAL collaboration, M.Z. Akrawy et. al., Z. Phys. C49 (1991) 49

5. Z. Kunszt and P. Nason [conv.], in "*Z Physics at LEP I*", (eds. G. Altarelli, R. Kleiss, and C. Verzegnassi), CERN 89-08 (1989)

6. R.K. Ellis, D.A. Ross and A.E. Terrano, Nucl. Phys. B178 (1981) 421

7. OPAL collaboration, M.Z. Akrawy et. al., Z. Phys. C49 (1991) 375

8. A. Ali and F. Barreiro, Phys. Lett. 118B (1982) 155; Nucl. Phys. B236 (1984) 269;
   D.G. Richards, W.J. Stirling and S.D. Ellis, Phys. Lett. 119B (1982) 193; Nucl. Phys. B229 (1983) 317;// N. K. Falck and G. Kramer, Z. Phys. C42 (1989) 159

9. OPAL collaboration, M.Z. Akrawy et. al., Phys. Lett. B252 (1990) 159

L3 results on the strong coupling constant α_s

The L3 Collaboration

S.Banerjee
Tata Institute of Fundamental Research
Bombay 400005

Abstract

L3 has measured the strong coupling constant α_s from the Z^0 hadronic decays using several methods. All these results are consistent with each other. Asymmetry in Energy Energy correlation yields $\alpha_s = 0.115 \pm 0.009$ at $\sqrt{s} = M_Z$. The energy dependence of α_s is consistent with expectations from QCD. α_s has been found to be flavour independent within measured uncertainties, $\alpha_s^b/\alpha_s^{udsc} = 1.08 \pm 0.09$, and $\alpha_s^{up}/\alpha_s^{down} = 0.92 \pm 0.11$.

1 Introduction

Hard quarks or gluons produced in e^+e^- annihilations manifest themselves in the form of jets. One can distinguish four different phases in this process corresponding to different time scales.

- Production of the $q\bar{q}$ pair from Z^0 decays as described by the electroweak theory.
- Emissions of hard gluons and parton cascade as calculated in the framework of perturbative QCD [1], the theoretical model for strong interactions.
- Hadronization process, which cannnot be calculated in the perturbative approach and can be described only by fragmentation models [2].
- The decays of unstable hadrons as parametrized from the experimental data

The only free parameter in QCD is the coupling constant α_s. LEP provides an excellent possibility of measuring this parameter with small theoretical and experimental uncertainties. LEP provides a high centre of mass energy and hence better jet resolution, large hadronic cross section, high luminosity and small radiative correction at Z^0. These are supplemented by the large acceptance and small systematic error from the L3 experiment.

The L3 detector covers 99% of 4π [3]. The detector consists of a central tracking chamber, a high resolution electromagnetic calorimeter composed of bismuth germanium oxide crystals, a ring of scintillation counters, a uranium and brass hadron calorimeter with proportional wire chamber readout, and an accurate muon chamber system. These detectors are installed in a 12 m diameter magnet which provides a uniform field of 0.5 T along the beam direction. The primary trigger for hadronic events requires a total energy of about 15 GeV in the calorimeters.

The detector provides an excellent energy and angular resolution for hadronic jets. For hadronic events at $\sqrt{s}$ = 91 GeV, the energy resolution is 10% and jet angular resolution is 2.5°. The overall trigger efficiency for hadronic events is found to be better than 99.9%.

The selection of $e^+e^- \rightarrow$ hadrons events is based on the energy measured in the electromagnetic detector and in the hadron calorimeter. Events are accepted if

$$0.6 < \frac{E_{\rm vis}}{\sqrt{s}} < 1.4 \; ; \; \frac{|E_\parallel|}{E_{\rm vis}} < 0.40, \; \frac{E_\perp}{E_{\rm vis}} < 0.40 \; ; \; N_{cluster} > 12$$

where $E_{\rm vis}$ is the total energy observed in the detector, $E_\parallel$ is the energy imbalance along the beam direction, and $E_\perp$ is the transverse energy imbalance.

Monte Carlo events were generated by the parton shower program JETSET 7.2 [4] and passed through the L3 detector simulation program. Acceptance of hadronic events is estimated to be 97% and background due to final states e^+e^-, $\tau^+\tau^-$ and e^+e^-+hadrons is below 0.2%.

2 Determination of α_s from total cross sections

A model independent line shape analysis [5] is performed with total cross section data from 115K hadronic and 10K leptonic events using the ZFITTER [6] program package. Systematic errors due to event selection and on the luminosity measurement are properly taken into account. A simultaneous fit, assuming leptonic universality, yields for the ratio of the hadronic and the leptonic partial widths

$$R_{had} \equiv \frac{\Gamma_{had}}{\Gamma_l} = 20.84 \pm 0.29.$$

In the standard model framework, R_{had} can be expressed in terms of α_s

$$R_{had} = R^0_{had}[1 + \frac{\alpha_s}{\pi} + 1.4(\frac{\alpha_s}{\pi})^2]$$

where R^0_{had} depends weakly on the top and the Higgs mass values. Using the measured value of M_Z from this experiment ($M_Z = 91.181 \pm 0.022$GeV) and a wide range of variation in the top and the Higgs masses ($M_t = 150 \pm 50$GeV and $50\text{GeV} \leq M_H \leq 1000$GeV), one gets

$$R^0_{had} = 20.00 \pm 0.03.$$

This yields a value of the strong coupling constant

$$\alpha_s = 0.125 \pm 0.041.$$

In the above determination of α_s, some of the α_s sensitive quantities (like total width of Z^0, Γ_Z) are not used. This can be taken care of by performing a simultaneous fit to all the cross section and asymmetry data with a standard model program (also provided by ZFITTER) with four free parameters, M_Z, M_t, M_H and α_s. The resulting fit yields

$$\begin{aligned} \alpha_s &= 0.134 \pm 0.030 \pm 0.003\,, \\ M_t &= 165^{+70}_{-110} \pm 14\,\text{GeV}. \end{aligned}$$

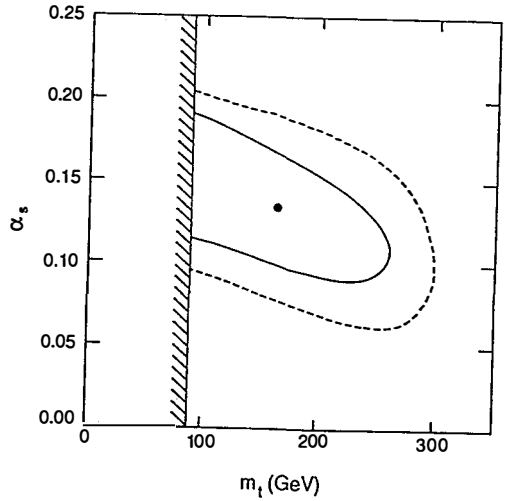

The central values of α_s, M_t correspond to a Higgs mass value of 300 GeV and the second error corresponds to the range 50 GeV $\leq M_H \leq$ 1000 GeV). The best fit values and the 68% and the 95% confidence level contours in the $\alpha_s - M_t$ plane are shown in figure 1.

Figure 1 Values of M_t and α_s obtained from the fit. Solid (dashed) contours represent the 68% (95%) confidence level limits.

3 Determination of α_s from jet multiplicity

We use a data sample at a centre of mass energy of 91.2 GeV from the early 1990 LEP running period to carry out a study on jet multiplicities [7]. The standard event selection yields 37,000 hadronic events.

Jets are reconstructed out of clusters in the calorimeters using the JADE version [8] of an invariant mass jet algorithm. The jet multiplicity thus obtained is shown in figure 2a as a function of the jet resolution parameter $y_{\rm cut}$. The jet rates have been corrected for detector effects (acceptance and resolution) using a migration matrix determined from JETSET 7.2 Monte Carlo. The detector effects change the 3-jet rate typically by $-(5..10)\%$. In addition, a small correction for initial and final state photon radiation is applied (using JETSET 7.2), which changes the 3-jet fraction by typically $+3\%$.

For a given parton recombination scheme, QCD (calculated to second order) predicts the rate of 2-, 3- and 4-jet events as a function of the parameter $\Lambda_{\overline{\rm MS}}$, the center of mass energy squared s, the scale μ^2 and the jet resolution $y_{\rm cut}$.

$$\begin{aligned} f_3 &= A_3(y_{\rm cut}) \cdot \alpha_s + B_3(y_{\rm cut}, \mu^2/s) \cdot \alpha_s^2 \\ f_4 &= B_4(y_{\rm cut}) \cdot \alpha_s^2 \\ f_2 &= 1 - f_3 - f_4 \,, \end{aligned}$$

For A_i and B_i we use the parametrizations for 'E_0' recombination scheme by Kunszt and Nason [9], which is equivalent to the 'JADE' jet algorithm. The effect of hadronization (using JETSET 7.2) is found to increase the 3-jet rate by (1-5)%, depending on $y_{\rm cut}$.

Choosing a value of $y_{\rm cut} = 0.08$ and $\mu^2/s = 0.08$, so that 4-jet rate is negligible ($< 1\%$) while the 3-jet rate is still large $(18.4 \pm 0.9)\%$, we estimate $\Lambda_{\overline{\rm MS}} = 190$ MeV corresponding to $\alpha_s = 0.115$ with 3% statistical error. QCD predictions for $\Lambda_{\overline{\rm MS}} = 190$ MeV and $\mu^2/s = 0.08$ are compared with the data in figure 2b.

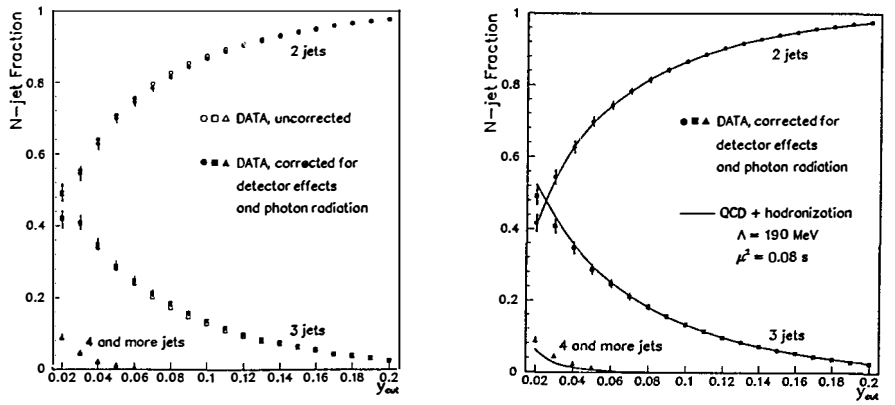

Figure 2 Measured jet fractions (a) before and after correction from detector effects, (b) after correction compared to the second order QCD.

The experimental systematic error is studied from (a) time dependence of the 3-jet rates; (b) 3-jet rates as a function of orientation of the thrust axis; (c) change in jet rates by varying detector response by 10% (energy scale and relative normalization). The overall error is estimated to be $\delta f_3/f_3 = 5\%$.

The theoretical uncertainty has several components : (a) effect of hadronization, studied by changing the fragmentation parameters giving rise to $\delta f_3/f_3 = 3\%$; (b) effect due to choice of recombination scheme, looked into by calculating α_s in several schemes, leading to an uncertainty of α_s at the level of 4%; (c) effect of the renormalization scale, studied by varying μ^2/s from 0.001 to 1.0.

This study yields

$$\begin{aligned} \Lambda_{\overline{\rm MS}} &= 190^{+60}_{-50}(exp)\,^{+170}_{-90}(theory)\,MeV \\ \alpha_s &= 0.115 \pm 0.005(exp)\,^{+0.012}_{-0.010}(theory) \end{aligned}$$

4 Determination of α_s from EEC and AEEC

The energy energy correlation (EEC) defined as a histogram of angles χ_{ij} between all particles (i,j) weighted with their energies (E_i, E_j)

$$EEC(\chi_{bin}) = \frac{1}{\Delta_{bin} \cdot N} \sum_{\text{events}}^{N} \sum_{i,j} \frac{E_i \cdot E_j}{E_{\text{vis}}^2}\, \delta_{bin}(\chi_{bin} - \chi_{ij})\,.$$

provides a way of measuring α_s without defining any a priori jet direction. In this definition $\delta_{bin}(\chi_{bin} - \chi_{ij})$ takes the value 1 or 0 depending if χ_{ij} is inside the bin (of size Δ_{bin}) around χ_{bin} or not.

Two-jet events populate angles χ close to 0° or 180°, whereas hard gluon radiation contributes to the region around 90°. So the height of the EEC distribution in the central region (between 30° and 150°) measures the rate of hard gluon emission and hence α_s. Hard gluon radiation contributes asymmetrically to the EEC distribution. The asymmetry defined as

$$AEEC(\chi) = EEC(180° - \chi) - EEC(\chi)$$

also measures α_s with small uncertainties.

We use 83000 hadronic events from the 1990 running period at $\sqrt{s} = 91.2$ GeV [10]. The observed EEC distribution can be described well with the JETSET 7.2 parton shower Monte Carlo with a complete simulation of the L3 detector. The same Monte Carlo is used on a bin-by-bin level to correct the observed distribution for (a) detector acceptance and resolution; (b) hadronization and decays; (c) initial state radiation. The correction factors due to (a) and (c) are small and reasonably flat over the entire angular region. The hadronization correction is also close to 1 over most of the angular region

investigated ($25° < \chi < 155°$). The corrected AEEC distribution is then calculated from the corrected EEC distribution.

QCD (calculated to second order) predicts the EEC and AEEC distributions as a function of the strong coupling constant α_s, the center of mass energy squared s, and the renormalization scale $f = \mu^2/s$:

$$\mathrm{EEC}(\chi) = F(\chi) \cdot \alpha_s \cdot [1 + (b_0 \cdot \ln f + R(\chi)) \cdot \alpha_s] ,$$

and similarly for AEEC.

The second order correction term R has been calculated by several groups using different methods for cancelling singularities and R varies by about ±25% for EEC and AEEC. Since this discrepency is not understood, we attribute this difference to the theoretical uncertainty in the evaluation of α_s.

We study the systematic effects by varying the detctor response by up to 10% yielding an error of 4%. We recalculate the hadronization correction by varying the fragmentation parameter over a wide range to study the uncertainty due to hadronization. The dependence due to renormalization scale parameter is looked into by evaluating the central value of α_s (or $\Lambda_{\overline{\mathrm{MS}}}$) at the position of minimal sensitivity (f_0) and then changing f from $\frac{1}{4}f_0$ to 1. Fitting a range of χ from 36° to 144°, we get

$$\begin{aligned} \Lambda_{\overline{\mathrm{MS}}} &= 270 \pm 60\,(exp)\,{}^{+190}_{-110}\,(theory)\,MeV \\ \alpha_s &= 0.115 \pm 0.004\,(exp)\,{}^{+0.011}_{-0.009}\,(theory) \end{aligned}$$

from the EEC distribution at $\mu^2/s = 0.1$ and

$$\begin{aligned} \Lambda_{\overline{\mathrm{MS}}} &= 190^{+50}_{-40}\,(exp)\,{}^{+100}_{-70}\,(theory)\,MeV \\ \alpha_s &= 0.115 \pm 0.004\,(exp) \pm 0.009\,(theory) \end{aligned}$$

from the AEEC distribution. The data are shown in figures 3a and 3b together with the results from the fit.

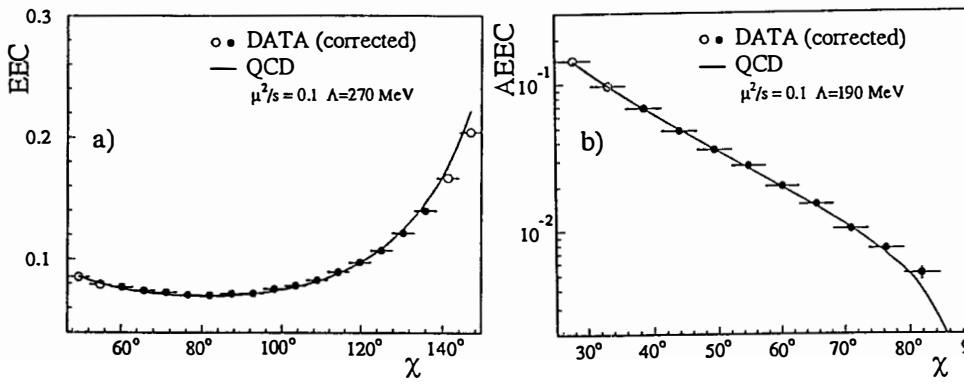

Figure 3 Comparison of corrected EEC (a) and AEEC (b) distributions with their statistical errors to the second order QCD.

The measured value of α_s (for $\mu^2/s = 1$) is shown in figure 4 together with similar measurements from other experiments at LEP and also at lower energies. Our measurements are consistent with other experiments and the energy dependence can be reproduced by QCD with $\Lambda_{\overline{MS}} = 220^{+110}_{-90}$ MeV.

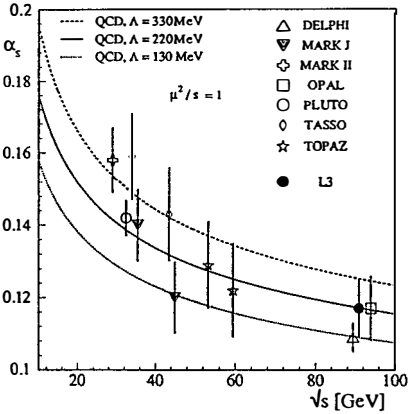

Figure 4 Energy dependence of α_s measured from AEEC in e^+e^- annihilation at different centre of mass energies in comparison with second order QCD.

5 Flavour Dependence of α_s

At LEP energies, hadronic events are primarily due to Z^0's decaying to $q\bar{q}$ pairs. On average 22% of the hadronic events are due to $b\bar{b}$ production. However, the proportion of $b\bar{b}$ content can be enhanced by tagging high momentum leptons in hadronic events. Using inclusive muons of momenta above 4 GeV and p_T with respect to the nearest jet above 1.5 GeV, the b quark content is enriched to 83% [11]. One gets 1300 such events out of a total sample of 110000 hadronic events.

Three jet rates are studied in both samples. After correcting for detector effects, hadronization and bottom mass, one gets for $y_{cut} = 0.05$,

$$f_3^{\mu}/f_3^{had} = 1.05 \pm 0.04\,(\text{stat}) \pm 0.05\,(\text{syst})$$

which can be translated to 3–jet rates for b quarks and u,d,s,c quarks :

$$f_3^b/f_3^{udsc} = 1.08 \pm 0.10$$

Using the second order calculation of $f_3 = 1.83\,\alpha_s + 1.9\,\alpha_s^2$ (for $\mu^2/s = 0.05$),

$$\alpha_s^b/\alpha_s^{udsc} = 1.08 \pm 0.09$$

This measurement is consistent with earlier measurements at PETRA energies with larger errors [12].

Flavour composition at LEP energies (quarks couple to Z^0) is different from that at lower energies (quarks couple to photon). The 'up' and 'down' type quarks have cross

sections proportional to $(v_q^2 + a_q^2)$ at LEP energies and proportional to Q_q^2 at $\sqrt{s} \approx 30$ GeV, resulting in

$$\alpha_s^Z = 0.34\,\alpha_s^{up} + 0.66\,\alpha_s^{down}$$

$$\alpha_s^\gamma = 0.73\,\alpha_s^{up} + 0.27\,\alpha_s^{down}$$

From measured 3 jet rates ($y_{cut} = 0.08$) at 29–35 GeV [8,13], one gets

$$\alpha_s^\gamma(M_Z^2) = 0.111 \pm 0.003(\text{stat})$$

which compared to L3 measurements of α_s^Z yields

$$\alpha_s^{up}/\alpha_s^{down} = 0.92 \pm 0.11$$

I would like to thank all my colleagues in L3 and in particular Dr.T.Hebbeker for many helpful discussions.

References

[1] M. Gell-Mann, Acta Physica Austriaca, Suppl. IX (1972) 733;
H. Fritzsch and M. Gell-Mann, Int. Conf. on High Energy Physics, Batavia (1972);
H. Fritzsch *et al.*, Phys. Lett. **47B** (1973) 365;
D.J. Gross and F. Wilczek, Phys. Rev. **8** (1973) 3633;
H.D. Politzer, Phys. Rev. Lett. **30** (1973) 1346.

[2] T. Sjöstrand *et al.*,"Z Physics at LEP 1", CERN Report CERN-89-08, Vol.III., p. 143

[3] L3 Collaboration, B. Adeva *et al.*, Nucl. Instr. and Meth. A 289 (1990) 35.

[4] T. Sjöstrand, Comput. Phys. Commun. **39** (1986) 347;
T. Sjöstrand and M. Bengtsson, Comput. Phys. Commun. **43** (1987) 367.

[5] L3 Collaboration, B. Adeva *et al.*, L3 preprint #28, March 1991 to be published in Z. Phys. **C**.

[6] D. Bardin *et al.*, Nucl. Phys. **B351** (1991) 1;
D. Bardin *et al.*, Z. Phys. **C44** (1989) 493;
D. Bardin *et al.*, Phys. Lett. **B255** (1991) 290;
M. Bilenky and A. Sazonov, JNIR Dubna preprint E2-89-792 (1989) unpublished.

[7] L3 Collaboration, B. Adeva *et al.*, Phys. Lett. **248B** (1990) 464.

[8] JADE Collaboration, W. Bartel *et al.*, Z. Phys. **C33** (1986) 23;
JADE Collaboration, S. Bethke *et al.*, Phys. Lett. **B213** (1988) 235.

[9] Z. Kunszt and P. Nason in "Z Physics at LEP 1", CERN Report CERN-89-08, Vol.I., p. 373.

[10] L3 Collaboration, B. Adeva *et al.*, Phys. Lett. **257B** (1991) 469.

[11] L3 Collaboration, B. Adeva *et al.*, L3 preprint #27, March 1991 to be published in Phys. Lett. **B**.

[12] W. Braunschweig *et al.*, Z. Phys. **C42** (1989) 17;
N. Magnussen *et al.*, Talk given at XX International Symposium on Multiparticle Dynamics, Gut Holmecke, Dortmund, (1990)

[13] S.Bethke *et al.*,, Z.Phys. **C43** (1989) 325.

QCD Results from DELPHI

Klaus Hamacher

Bergische Universität - Gesamthochschule Wuppertal, Germany

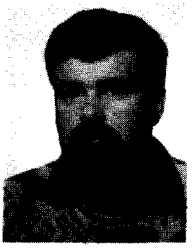

Abstract

The α_s measurements of DELPHI using the 3-jet rate and the asymmetry of the energy-energy correlation obtained in hadronic Z decays at LEP are presented and compared to results of other LEP experiments [1]. The angular distribution of 3-jet events with respect to the beam axis is observed to agree with the expectation of QCD, however is contradictory to the scalar gluon theory.

[1]The introductory remarks on data / monte carlo comparisons for multijet rates, event shapes, string effect and factorial moments are omitted here because of space limitations.

α_s-Measurements

The DELPHI collaboration published measurements of the strong coupling constant α_s based on the jet production rates [1] and on the asymmetry of the energy-energy correlation [2]. Here a reanalysis of these quantities using the 135k hadronic Z events taken in 1990 is presented.

In both analyses the following cuts are applied to the data: charge tracks are retained, if they are detected in the TPC and extrapolate back to the beam (or beam crossing point) within 4 cm in r (10 cm in z), their momentum p is in the range $400MeV \leq p \leq 50GeV$ and their polar angle θ is between 25° and 155°. In the analysis of the jetrates also the photons with $E \geq 400MeV$ which have been identified by the DELPHI electromagnetic calorimeters are included. The events are required to have more than 5 charged particles, a total charged energy exceeding 15 GeV and at least 3 GeV charged energy in each hemisphere. The polar angle of the sphericity axis has to be in the range $|\cos\Theta| \leq 0.75$.

The data are corrected for apparatus effects and QED initial state radiation using a detailed Monte Carlo simulation of the DELPHI detector.

Jetrates

The JADE jetfinder is used to determine the jet multiplicities. This algorithm is close to the so called E_0-scheme and the jetrates measured at hadron level reproduce best the jetrates at parton level. Fig. 1 compares the 2-, 3-, and 4-jet rate as measured by L3 [3] OPAL [4] and DELPHI. The agreement between the experiments is perfect. For the extraction of α_s the quantity D_2 is used:

$$D_2 = 1/\Delta y \cdot (R_2(y_{cut}) - R_2(y_{cut} - \Delta y))$$

The effects of hadronization on D_2 have been unfolded using different fragmentation models. Fig. 2 compares D_2 before and after this small correction. To extract α_s, D_2 is fitted to the QCD expressions given by Kunst and Nason [5]. This formulae describes D_2 well in the range $0.02 \leq y_{cut} \leq 0.33$, if Λ and the renormalisation scale factor $f = \mu^2/s$ are fitted (see fig. 2, here $f = 0.003 \pm .0007_{stat.}, \alpha_s(M_Z^2) = 0.11 \pm 0.011_{stat.}$). For further fits f is set to 0.25 and the D_2-range $0.1 \leq D_2 \leq 0.2$ is used. In this range all corrections are save and the 4-jet rate is negligible. The following results are obtained for different hadronization corrections:

Hadronization Correction	$\alpha_s(M_z^2)$	Λ_{MS} [MeV]	$\frac{\chi^2}{ndf}$
none	0.118	231 $\pm$36	1.8
LUND 7.2 PS $Q_0 = 1$	0.122	281 $\pm$40	0.9
LUND 7.2 PS $Q_0 = 13$	0.123	292 $\pm$45	0.9
LUND ME (E_0-scale)	0.123	290 $\pm$40	1.5
LUND 7.2 PS DELPHI tune	0.124	306 $\pm$50	1.3
HERWIG 4.3 OPAL tune	0.125	335 $\pm$52	0.9

Thus the systematic error due to the hadronization correction is about $\Delta\alpha_s^{hadr.} \approx 0.002$. The experimental systematic error is estimated to be of similar size. The scale uncertainty (varying f from 0.002 to 1) is $\Delta\alpha_s^{scale} \approx 0.01$.Finally:

$$\alpha_s(M_Z^2) = 0.123 \pm 0.002_{exp.} \pm 0.002_{hadr.} \pm 0.01_{scale}$$

This can be directly compared to the results from Opal: $\alpha_s(M_Z^2) = 0.118 \pm 0.008_{tot.}$ and ALEPH: $\alpha_s(M_Z^2) = 0.121 \pm 0.002_{stat.} \pm 0.003_{syst.} \pm 0.007_{theor.}$ Also the L3 result, obtained at a

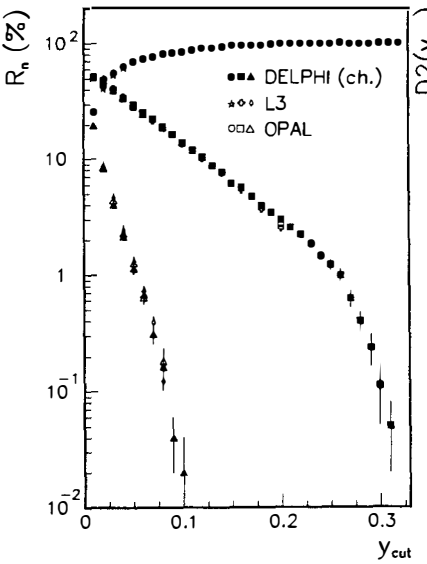

Figure 1: Comparison of Jetrates from DELPHI, L3 and Opal

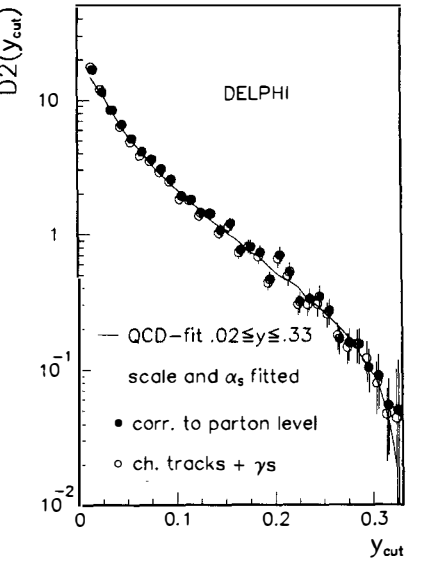

Figure 2: D_2 as a function of y_{cut} before and after unfolding the hadronization correction. Also shown is the QCD fit with Λ and f as free parameters.

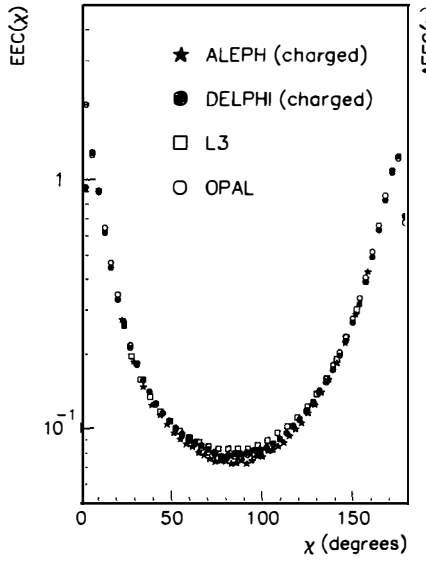

Figure 3: Comparison of the EEC from the 4 LEP experiments

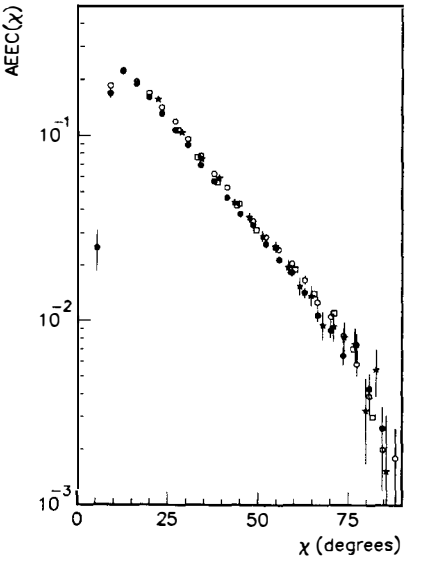

Figure 4: Comparison of the AEEC from the 4 LEP experiments

smaller scale is consistent with this result as should be expected from the excellent agreement between the different data sets.

Energy-Energy Correlation Asymmety AEEC

The asymmetry of the energy-energy correlation (EEC), defined as

$$AEEC(\chi) = EEC(180^\circ - \chi) - EEC(\chi)$$

is considered to be a 'good' observable to determine α_s. It is insensitive to fragmentation effects contributing symmetrically to the EEC:

$$EEC(\chi) = \frac{2}{N} \sum_{events}^{N} \sum_{i}^{N_{particles_s}-1} \sum_{j>i}^{N_{particles}} \frac{E_i E_j}{E_{vis}^2} \cdot \left(\frac{1}{\Delta\chi} \int_{\chi-\frac{\Delta\chi}{2}}^{\chi+\frac{\Delta\chi}{2}} \delta(\chi' - \chi_{ij}) d\chi' \right)$$

χ is the opening angle for which the correlation is studied. The EEC shows 2 peaks corresponding to the particles in one jet ($\chi < 30^\circ$) and in opposite jets ($\chi > 150^\circ$). Gluon radiation causes an asymmetry in the valley around 90°. The size of this asymmetry is proportional to α_s. α_s determined from the AEEC or related observables has been published by all 4 LEP experiments [6]. Figs. 3 and 4 compare the EEC and AEEC from these measurements. Contrary to the jetrates these results only agree within the quoted statistic and systematic errors. The total spread in the EEC and AEEC is 10 – 20%. Given the correlation between the EEC and its asymmetry no coherent trend is observed. Further experimental studies are needed.

Because the available second order calculations for the AEEC differ by ± 25% DELPHI has choosen to directly fit the LUND 7.2 ME monte carlo to the $\int AEEC(\chi)d\chi$ to determine α_s. This model contains the exact second order ERT matrix elements. Small scales are used in the model to correctly reproduce the 4-jet rate. The result for α_s is:

$$\alpha_s(M_Z^2) = 0.106 \pm 0.005_{exp.} \pm^{0.003}_{0.000\ scale}$$

The experimental error is mainly due to a 'walk' of α_s with the lower limit of the integral and the influence of different monte carlo parameter choices. This result can be compared to the result of OPAL: $\alpha_s = 0.117 \pm^{0.007}_{0.009 exp.} \pm^{0.006}_{0.002 theo.}$ and L3: $\alpha_s = 0.115 \pm 0.004_{exp.} \pm^{0.007}_{0.004 had_r} \pm^{0.003}_{0.005 theo.}$. The differences between the α_s values are dominantly due to the differences in the experimental distributions.

Orientation of 3-Jet Events

The measurement of the angular distribution of 3-jet events is a natural extension of the $(1 + \cos^2\theta)$ polar angle distribution of 2-jet events. This distribution is a paramater free [7] prediction of QCD and also allows to distinguish between vector and scalar gluon theories if the qqg-final state is mediated by Z exchange. The 3-jet angular distributions in the helicity frame is characterized by the angles θ and χ:

$$\frac{d^2\sigma}{d\cos\theta d\chi} \propto (1 + \cos^2\theta)\sigma_U + 2\sin^2\theta\sigma_L + 2\sin^2\theta\cos 2\chi\sigma_T - \sqrt{8}\sin^2\theta\cos\chi\sigma_I$$

θ is the polar angle of the thrust direction with respect to the beam. χ is the angle between the event plane and the plane defined by the beam and the thrust axis. $\sigma_{U(L)}$ is the cross section for transverse unpolarized (logitudinally polarized) Z's or γ's. $\sigma_{T(I)}$ is the transverse / longitudinal (+/-) interference term respectively. Integration over χ yields :

$$\frac{d\sigma}{d\cos\theta} \propto (1 + \alpha(T)\cos^2\theta) \qquad where \qquad \alpha(T) - \frac{1 - 2\sigma_L/\sigma_U}{1 + 2\sigma_L/\sigma_U}$$

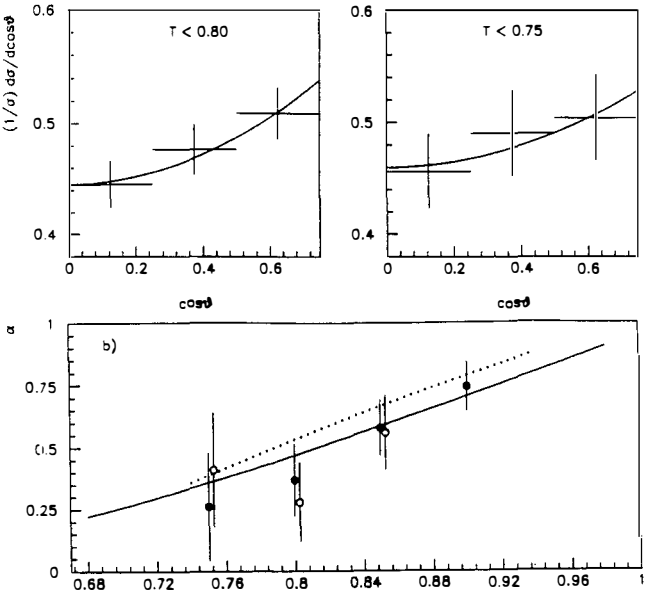

Figure 5: $cos(\theta)$-distributions for 3-jet events and α for different thrust cuts. Also shown is the QCD prediction and the LUND 7.3 PS model.

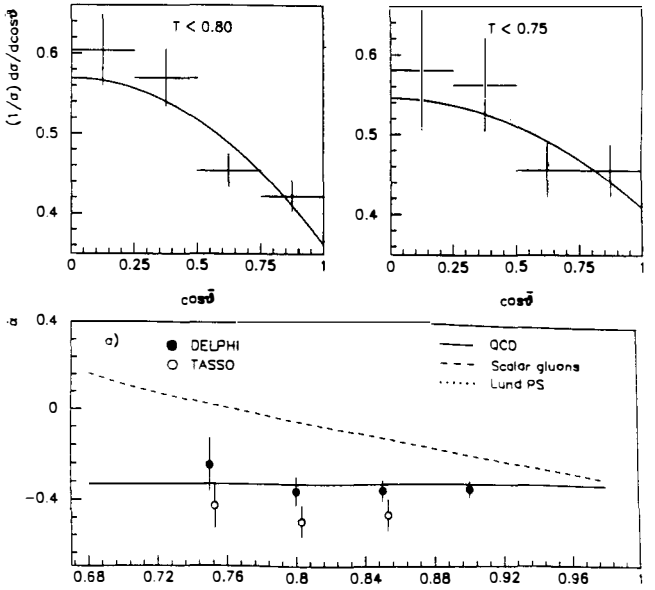

Figure 6: $cos(\bar{\theta})$-distributions for 3-jet events and $\bar{\alpha}$ for different thrust cuts. Also shown is the QCD prediction $\bar{\alpha} = 1/3$ and the prediction of a scalar gluon theory.

$\sigma_{L(U,T,I)}$ is predicted by QCD as a function of the thrust cut [8]. Similary the angular distribution can be determined as function of the polar angle $\bar{\theta}$ of the normal to the event plane.

$$\frac{d\sigma}{d\cos\theta} \propto (1 + \bar{\alpha}(T)\cos^2\bar{\theta}) \qquad with \qquad \bar{\alpha}(T) \propto -\frac{1}{3} \cdot \frac{\sigma_U + \sigma_L - 3(\sigma_L - 2\sigma_T)}{\sigma_U + \sigma_L - (\sigma_L - 2\sigma_T)/3}$$

QCD predicts $\sigma_L = 2\sigma_T$ [8] and therefore independent of the value of σ_U and σ_L : $\bar{\alpha} = -\frac{1}{3}$. Thus if $\sigma_U/\sigma_L \neq 0$ (i.e. $\alpha(T)$ extracted from the $\cos\theta$ distribution is smaller than 1) this prediction allows for a significant test of QCD.

The event selection and cuts are similar to those mentioned above. 3-jet events are identified using the LUCLUS algorithm [9]. Here the jet resolution parameter d_o was set to $6 \cdot E_{vis}/\sqrt{s}$GeV. 6308, 3934, 2018 and 756 3-jet events are obtained for thrust $\leq$ 0.9, 0.85, 0.8 and 0.75 respectively.

Beside the usual correction for limited acceptance, resolution etc. the measured angular distributions are also corrected for effects of initial state radiation and fragmentation. The correction factors obtained for the $\cos\theta$ ($\cos\bar{\theta}$) distribution change by less than 3% (1%) if fragmentation and radiation correction are omitted. The variation with the thrust cut is smaller than 10% (15%) for the $\cos\theta$ ($\cos\bar{\theta}$) distribution, respectively.

Fig. 5 shows the (appropriately folded) angular distribution as function of $\cos\theta$. It clearly deviates from the well known $(1 + \cos\theta)$ behaviour for small thrust. The fitted values of the anisotropy parameter α as well as the previous results from the TASSO experiment [10] (see fig. 5) coincide with the QCD prediction. $\bar{\alpha}$ obtained from fits to the $\cos\bar{\theta}$ distributions (see fig. 6) also agrees well with the QCD prediction $\bar{\alpha} = -\frac{1}{3}$ independend of the thrust cut. The TASSO points are somewhat lower. This may be due to the different selection of 3-jet events, the smaller energy available or the omitted fragmentation correction.

In fig. 6 $\bar{\alpha}$ is also compared to the prediction of a scalar gluon theory [7]. The Born term in such a theory includes vector and axial vector contributions. The VV part of the hadron tensor (i.e. γ exchange) leads to $\bar{\alpha} = -\frac{1}{3}$. At the Z pole, due to the presence of the AA contribution, the predicted value of $\bar{\alpha}$ is bigger especially for small thrust. Contrary to the previous TASSO data (dominated by γ exchange) the DELPHI data exclude scalar gluon theories.

References

[1] DELPHI Collab., Phys. Lett. B 247(90) 167
[2] DELPHI Collab., Phys. Lett. B 252(90) 149
[3] L3 Collab., Phys. Lett. B 248 (90) 464
[4] OPAL Collab., Z. Phys. C 49 (91) 375
[5] Kunst & Nason in Z-Physics at LEP 1, CERN 89-8
[6] ALEPH Collab., Phys. Lett. B 257 (91) 479; L3 Collab., Phys. Lett. B 257 (91) 469; OPAL Collab., Phys. Lett. B 252 (90) 159; for DELPHI see [2]
[7] J. Körner et al. Phys. Lett. B 188(87) 272; J. Körner & H.D. Schiller DESY 81-43
[8] G. Kramer et al. Phys. Lett. B 79 (78) 249, erratum B 80 (79) 433; E. Laermann et al. Z. Phys C 3 (80) 289; K. Koller et al. Z. Phys. C 6 (80) 131
[9] T. Sjöstrand, Comp. Phys. Comm. 27 (82) 243; T. Sjöstrand & M. Bengtson, Comp. Phys. Comm. 43 (87) 367
[10] TASSO Collab., Z. Phys. C 47 (90) 181

A DETERMINATION OF THE STRONG COUPLING CONSTANT α_s FROM W PRODUCTION AT THE CERN $p\bar{p}$ COLLIDER

The UA2 Collaboration
Bern-Cambridge-CERN-Dortmund-Heildeberg-Melbourne-
Milano-Orsay(LAL)-Pavia-Perugia-Pisa-Saclay(CEN)

presented by
Elisabetta Pennacchio
INFN-Sezione di Pavia, Italy
Dipartimento di Fisica Nucleare e Teorica

ABSTRACT

The large sample of $W \rightarrow e\nu$ events collected by the UA2 experiment at the CERN $p\bar{p}$ collider between 1988 and 1990 has been used to determine the strong coupling constant α_s. From a measurement of the ratio of the production rate of W events with one jet to that with no jets, a value for α_s has been extracted to second order in the $\overline{MS}$ scheme : $\alpha_s(M_W^2)=0.123 \pm 0.018$ (stat) $\pm$ 0.017 (syst.). This value is in good agreement with LEP results and provides an independent measurement of the strong coupling constant in a hadronic experiment.

Introduction

The production of W bosons in $p\bar{p}$ collisions is described to leading order in perturbation theory by the Drell-Yan mechanism. The strong interaction accounts for corrections which result in hadron jets produced in association with the W. The dependence of the rate of W+jets events on the strong coupling constant can be used to measure the value of α_s in hadronic collisions. More precisely, the value of α_s is determined from the one-jet to zero-jet ratio, by comparing its experimental value R_{exp} to the QCD predicted value, R_{MC}, obtained from a Monte Carlo simulation of W production.

1. Determination of the experimental ratio R_{EXP}.

The W data sample, collected with the upgraded UA2 experiment[1] in the data taking period between 1988 and 1990 at the CERN $p\bar{p}$ collider, corresponds to an integrated luminosity of 13 pb^{-1}. Details of the event samples and a brief description of the detector components relevant for electron identification can be found in Ref [2]. In the present analysis the same identification criteria as described in [2] are used to select electron candidates in the central calorimeter ($\eta < 1$) and the same kinematic selection is applied to define a clean sample of $W \rightarrow e\nu$ events:

$$p_T^e > 20GeV, \quad p_T^\nu > 20GeV$$
$$M_T^{e\nu} > 40GeV$$

where p_T^e is the transverse momentum of the electron candidate and p_T^ν is the missing transverse momentum attributed to the neutrino. $M_T^{e\nu}$ is the transverse mass of the electron neutrino system, defined as $M_T^{e\nu} = \sqrt{2p_T^e p_T^\nu(1 - cos\Delta\phi)}$, where $\Delta\phi$ is the azimuthal separation between the measured electron and neutrino directions. The 2964 events selected with these cuts are then investigated for jet activity. The jet energy is computed using a cone algorithm[3] in $\eta - \phi$ space, with $\Delta R_{cone} < 0.70$. Only jets with $E_T > E_{T0}$ (E_{T0}=20GeV) and $|\eta| < \eta_{cut}$ (η_{cut}=1.6) are retained. The cut values are chosen to reduce the systematic uncertainties in the jet energy measurement and to minimize the contribution of particles belonging to the underlying event[3]. With these cuts, 114 W+1 jet events are selected. After background subtraction (3.8%[3.1%] from $W \rightarrow \tau\nu$ and 0.4±0.1% [3.1±1.4%] from misidentified electrons for W + 0[1] jet events), the experimental ratio is found to be:

$$R_{exp} = \frac{\text{number of (W + one jet) events}}{\text{number of (W + zero jet) events}} = \frac{106.7 \pm 10.8}{2725.5 \pm 53.4} = 3.91 \pm 0.40\%$$

2. Calculation of K factors

The evaluation of R_{MC} is based on a Monte Carlo simulation of W events. This requires first to simulate the production of a W boson, incorporating in principle all QCD correction terms. In practice the EKS Monte Carlo[4] is used, which includes the matrix elements of all tree-level diagrams for W production, up to order α_s^3.

The infrared and collinear divergencies are regularized by appling cut-offs on the transverse momentum p_T of each outgoing parton and on the angular separation ω of each pair of outgoing partons:

$$p_t > p_t^{min}\,,\ \omega > \omega^{min} \tag{1}$$

The EKS simulation represents only a partial calculation of the total W production cross-section, because loop diagrams and tree level diagrams, which do not fulfil the conditions (1), are not taken into account. The size of these missing contributions is given by multiplicative corrections called K factors[3]. The total cross section to second order in α_s can be written as:

$$\sigma^{[2]} = \sigma_0 K_0 + \sigma_1 K_1 + \sigma_2 K_2 = K_{tot}^{[2]} \sigma_0$$

where σ_i are the tree level cross section for producing W+ i partons, K_i are the topological K factors to take into account higher order diagrams where the parton is soft or virtual, $\sigma_i K_i$ are the topological cross sections. A detailed description of the calculation of such factors using available second order calculation of W production can be found in reference [5].

3. Determination of the predicted ratio R_{MC}

In order to determine the QCD prediction for W + jet rates, the K factors are used in conjuction with the tree level Monte Carlo simulation of the W production. Three sets of Monte Carlo events were generated according to the tree level cross section σ_i (i=0,1,2) using the EKS program. They represent the production of a W boson with 0, 1, 2 partons. For the EKS event generation p_t^{min} is set at 12 GeV and ω_{min} at 20°; the value of the scale μ is equal to the mass of the W, and the structure functions HMRSB[6] are used. Partons are then fragmented according to the Field-Feynman prescription[7], adjusted to reproduce the energy flow distribution observed experimentally for jets in W events. The underlying event is simulated superimposing minimum bias events as measured in UA2. The calorimeter response is then simulated and the generated events are submitted to the same analysis chain as the real data. Due to the experimental jet definition (E_T^0 and η cuts) and to acceptance and resolution effects, the number of jets passing the identification criteria in a simulated W event is not necessarily equal to the number of produced partons. Each accepted cross-section (σ_i^{det}) is split into several components:

$$\sigma_i^{det} = (\sigma_{i0} + \sigma_{i1} + \sigma_{i2} + ...) \quad i = 0, 1, 2$$

where σ_{ij} represents the cross section for i partons generated and j jets reconstructed. The ratio R_{MC} is then given by:

$$R_{MC}(\alpha_s^{MC}) = \frac{\sigma_{01} K_0 + \sigma_{11} K_{11} + \sigma_{21}}{\sigma_{00} K_0 + \sigma_{10} K_{10} + \sigma_{20}}$$

where α_s^{MC} is the α_s value used in the Monte Carlo simulation. For the definitions of K_{11} and K_{10} see Ref [5]. The Monte Carlo predictions are found to be consistent

with the experimentally measured ratio (see figure 1), and the η dependence of the measured ratio is well described by the simulation. For the cuts $E_T^0 = 20\ GeV$ and η_{cut}=1.6, keeping Λ_{QCD} fixed at 0.19 GeV, R_{MC} is found to be 3.62% which is consistent with the experimentally measured value of R_{EXP} quoted in section 1.

4. Determination of α_s and systematic uncertainties

To extract the measurement of α_s the equation

$$R_{MC}(\alpha_s) = R_{EXP}$$

has to be solved, which implies that the α_s dependence of the Monte Carlo has to be known[5]. In order to take into account properly the dependence of the structure functions on α_s, three different parametrizations, corresponding to different Λ values, are used (HMRSB, $\Lambda^{(4)}_{\overline{MS}}$=0.100, 0.190, 0.300). The K factor calculation and the full Monte Carlo simulation are performed for all three structure function parametrizations, leading to predictions for R_{MC} at three different α_s values. The results are shown in figure 2. The experimentally measured value R_{exp} is indicated as a dashed line together with the band resulting from the statistical uncertainties; the dependence of R_{MC} on α_s is given by a linear fit. The measured value of α_s and its uncertainty are then given by the intercepts of the line with the horizontal lines representing the measured value R_{EXP} and its error. The systematic uncertainties are shown in table 1. The final result is:

$$\alpha_s(M_W^2) = 0.123 \pm 0.018(stat) \pm 0.017(syst)$$

Table 1 Summary of the systematic uncertainties

energy scale	$\pm$0.005
low energy response	$\pm$0.003
underlying event	$\pm$0.011
structure functions	$\pm$0.005
fragmentation	$\pm$0.010
theoretical uncertainties	$\pm$0.002
total systematic error	$\pm$0.017

Figure 1 R_{MC} and R_{EXP} as a function of the rapidity cuts for different jet cuts (sf HMRSB, $\alpha_s^{[MC]}$=0.1098)

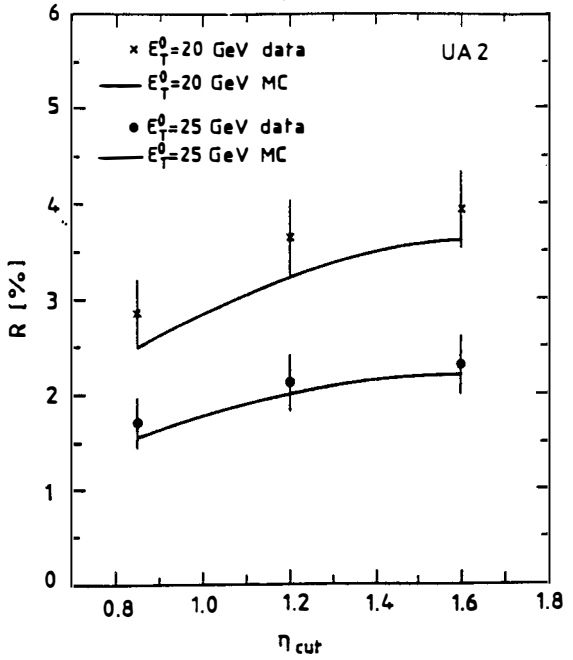

Figure 2 $R_{MC}(\alpha_s)$ compared to the experimental value R_{EXP}

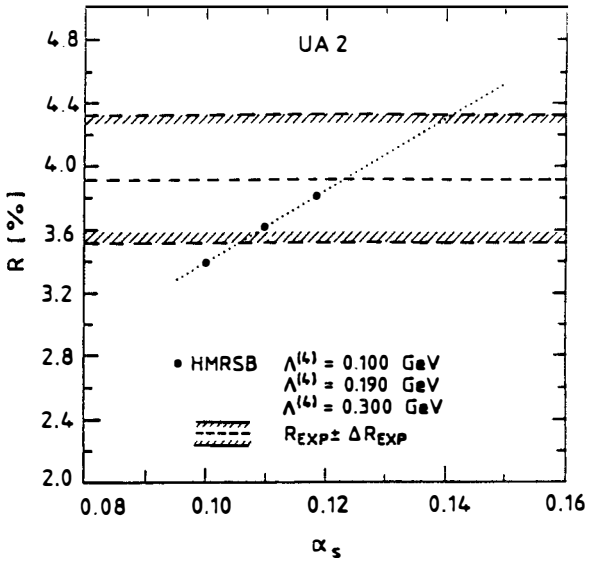

REFERENCES

[1] UA2 Collaboration, C.N. Booth, Proc. 6th Topical Workshop on Proton Antiproton Collider Physics, Aachen 1986

[2] UA2 Collaboration,J.Alitti et al.,Z.Phys.C47(1990)11;

[3] UA2 Collaboration,R.Ansari et al.,Phys.Lett.B215(1988)175

[4] S.D.Ellis,R.Kleiss,W.J.Stirling,Phys.Lett.B154(1985)435;
F.A.Berends,W.T.Giele,H.Kuijf,Nucl.Phys.B321(1989)39;
F.A.Berends,W.T.Giele,H.Kujf,R.Kleiss,W.J.Stirling,Phys.Lett.B224(1989)237

[5] UA2 Collaboration,J.Alitti at al.,CERN-PPE/91-62 Submitted to Phys.Lett.

[6] P.N.Harriman,A.D. Martin,R.G.Roberts,W.J.Stirling,Durham University DTP/90/04 (revised version April 1990);

[7] R.D.Field,R.P.Feynman,Nucl.Phys,B318(1978)1.

Comparison of Grand Unified Theories with electroweak and strong Coupling Constants measured at LEP

Hermann Fürstenau*
Institut für Experimentelle Kernphysik,
Universität Karlsruhe, D-7500 Karlsruhe

Abstract

Using the renormalization group equations one can evolve the electroweak and strong coupling constants, as measured at LEP, to higher energies in order to test the ideas of Grand Unified Theories, which predict that the three coupling constants become equal at a single unification point. With data from the DELPHI Collaboration we find that in the minimal *non-supersymmetric* Standard Model with one Higgs doublet a single unification point is excluded by more than 7 standard deviations. In contrast, the minimal *supersymmetric* Standard Model leads to good agreement with a single unification scale of $10^{16.0\pm0.3}$GeV. Such a large scale is compatible with the present lower limits on the proton lifetime. The best fit is obtained for a SUSY scale around 1000 GeV and limits are derived as function of the strong coupling constant. The unification point is sensitive to the number of Higgs doublets and only the minimal SUSY model with two Higgs doublets is compatible with GUT unification, if one takes the present limits on the proton lifetime into account.

*Bitnet: FURSTENA@CERNVM
Postal address: Inst. für Experimentelle Kernphysik
Universität Karlsruhe, Postfach 6980, D-7500 Karlsruhe 1

1 Definition of the coupling constants

In the SM based on the group $SU(3)_C \otimes SU(2)_L \otimes U(1)$ the usual definitions of the coupling constants are:

$$\alpha_1 = 5/3\, g'^2/(4\pi) = 5 \cdot \alpha/(3 \cdot \cos^2\theta_{\overline{MS}}), \quad (1)$$

$$\alpha_2 = g^2/(4\pi) = \alpha/\sin^2\theta_{\overline{MS}}, \quad (2)$$

$$\alpha_3 = g_s^2/(4\pi) \quad (3)$$

where g_s is the $SU(3)_C$ coupling constant. The factor $5/3$ in the definition of α_1 has been included for the proper normalization at the unification point[1]. The running coupling constant $\alpha_i(\mu)$ is completely determined by the particle content and their couplings inside the loop diagrams of the gauge bosons, as expressed by the renormalization group equations. In second order the renormalization group equations can be written as:

$$\mu\frac{\partial}{\partial\mu}\alpha_i(\mu) = \frac{2}{4\pi}\left(b_i + \frac{b_{ij}}{4\pi}\alpha_j(\mu) + \frac{b_{ik}}{4\pi}\alpha_k(\mu)\right)\cdot\alpha_i^2(\mu) + \frac{2\cdot b_{ii}}{(4\pi)^2}\alpha_i^3(\mu), \quad (4)$$

where μ is the energy at which the couplings are evaluated, $i,j,k = 1,2,3$ and $i \neq j \neq k$. The b_{ij}'s for the SM and for the SUSY model are given in Ref. [2]. The b_i's for the SM are[2]:

$$b_i = \begin{pmatrix} b_1 \\ b_2 \\ b_3 \end{pmatrix} = \begin{pmatrix} 0 \\ -22/3 \\ -11 \end{pmatrix} + N_{Fam}\begin{pmatrix} 4/3 \\ 4/3 \\ 4/3 \end{pmatrix} + N_{Higgs}\begin{pmatrix} 1/10 \\ 1/6 \\ 0 \end{pmatrix}, \quad (5)$$

while for the minimal SUSY they have been calculated to be[2]:

$$b_i = \begin{pmatrix} b_1 \\ b_2 \\ b_3 \end{pmatrix} = \begin{pmatrix} 0 \\ -6 \\ -9 \end{pmatrix} + N_{Fam}\begin{pmatrix} 2 \\ 2 \\ 2 \end{pmatrix} + N_{Higgs}\begin{pmatrix} 3/10 \\ 1/2 \\ 0 \end{pmatrix}, \quad (6)$$

where N_{Fam} is the number of families of matter fields and N_{Higgs} is the number of Higgs doublets. In the minimal SM and in the minimal SUSY model $N_{Fam} = 3$ and $N_{Higgs} = 1$ and 2, respectively. Note that in the supersymmetric model the dominating first order coefficients lead to a much weaker running of α_3 than predicted by the standard model, while the running of α_2 has the opposite sign and α_1 runs somewhat faster.

2 Measurement of the coupling constants

Using a recent calculation of $\triangle r$ including the QCD and M_{top}^4 corrections[10], one can obtain limits on the top mass from the average value of $\sin^2\theta_W = 1 - M_W^2/M_Z^2 = 0.2290 \pm 0.0035$, obtained in neutrino scattering[5,6,7] and $p\overline{p}$ collisions[8,9]. We find for $M_{Higgs} = 45(1000)$ GeV a value of $M_{top} = 116 \pm 38(144 \pm 37)$ GeV. The errors include the uncertainty from the Z^0 mass and the vacuum polarization[11]. With the limits on M_{top} one can calculate the electroweak mixing angle in the $\overline{MS}$ scheme to be[12]:

$$\sin^2\theta_{\overline{MS}} = 0.2336 \pm 0.0018. \quad (7)$$

To define the electroweak coupling constants at a scale M_Z we use for the fine structure constant the parametrization of Ref. [13] and one gets $\alpha(M_Z) = \frac{1}{128.8}$ With the value of $\sin^2\theta_{\overline{MS}}$ given above one obtains:

$$\alpha_1(M_Z) = 0.016887 \pm 0.000040, \quad (8)$$

$$\alpha_2(M_Z) = 0.03322 \pm 0.00025. \quad (9)$$

The present analysis uses the two values of α_s from Refs. [14], which are based on the measurements of the differential jet rates and of the asymmetry of the energy energy correlation. After symmetrizing the theoretical errors, we obtain for the weighted average and its estimated 68% C.L. error:

$$\alpha_3(M_Z) = \alpha_s(M_Z) = 0.108 \pm 0.005. \quad (10)$$

This value of α_s agrees with the recent α_s determination from deep inelastic lepton nucleon scattering and single γ production ($\alpha_s(M_Z) = 0.109^{+0.004}_{-0.005}$)[15].

3 Comparison with Grand Unified Theories

The coupling constants should evolve smoothly until they become identical at the unification scale. Here we make the simplifying assumption that at the unification point the couplings cross without changing slopes.

The evolutions of the three coupling constants with the new data are shown in Fig. 1b using the minimal SM with 3 families and 1 Higgs doublet. Compared to the results of 1987 (Fig. 1a), the errors, indicated by the width of the lines, are considerably smaller.

It is clear that a single unification point cannot be obtained within the present errors: the α_3 coupling constant misses the crossing point of the other two by more than 7 standard deviations. Only with $\alpha_s(M_Z)$=0.07 one can force $1/\alpha_3$ to pass through the crossing point of the other two or, alternatively, if one leaves $\alpha_s(M_Z)$ at 0.108, one has to lower $\sin^2\theta_{\overline{MS}}$ to 0.21 in order to get a single unification point. These values are in disagreement with the experimental values quoted in the previous section.

In SUSY GUT's [16] we fitted both the unification scale M_{GUT} and the SUSY breaking scale M_{SUSY} , which is defined as the transition point where the slopes of the extrapolation change. The mass of the lightest Higgs doublet was chosen to be equal to M_Z and the mass of the heavier doublet was taken to be equal to M_{SUSY}. These choices have practically no influence on our conclusions as long as the Higgs masses are less than a few times M_{SUSY}.

The second evolutions give the results shown in Fig. 2a. The values of M_{GUT} and M_{SUSY} are correlated. By taking this correlation into account, one finds:

$$M_{SUSY} = 10^{3.0\pm1.0}\text{GeV}, \quad (11)$$

$$M_{GUT} = 10^{16.0\pm0.3}\text{GeV}, \quad (12)$$

$$\alpha_{GUT}^{-1} = 25.7 \pm 1.7. \quad (13)$$

We have repeated the fits for different values of $\alpha_3(M_Z)$ and the results are shown in Figs. 2b and 2c. One observes that M_{SUSY} is a steep function of α_s: for $\alpha_s(M_Z)$ between 0.10 and 0.12, M_{SUSY} varies between 30 TeV and 10 GeV.

Until now the assumption was made that the slopes change from SM values to SUSY values exactly at M_{SUSY}. This abrupt change is unphysical, not only because the particles are virtual, but also because different SUSY particles are likely to have different masses. To model the actual behaviour we have smeared this change over 1 to 3 orders of magnitude symmetrically around M_{SUSY} by taking the average of the SM and SUSY slopes in this interval. This smearing lowers the fitted value of M_{SUSY} and has little influence on M_{GUT}, as shown by the dashed and dotted lines in Figs. 3a and 3b.

4 Summary

It was shown that the evolution of the coupling constants within the minimal Standard Model with one Higgs doublet does not lead to Grand Unification,

On the contrary, the minimal supersymmetric extension of the Standard Model leads to unification at a scale of $10^{16.0\pm0.3}$ GeV. The best fit to the allowed minimal SUSY model, shown in Fig. 2, is obtained for a SUSY scale around 1000 GeV or, more precisely, $M_{SUSY} = 10^{3.0\pm1.0}$ GeV, where the error originates mainly from the uncertainty in the strong coupling constant. If this minimal supersymmetric GUT describes nature, SUSY particles, which are expected to have masses of the order of M_{SUSY}, could be within reach of the present or next generation of accelerators.

Acknowledgments

We are greatly indebted to our colleagues of the DELPHI Collaboration for the results and many discussions. We thank Giuseppe Degrassi and Bernd Kniehl for providing us with their programs for calculating $\sin^2\theta_{\overline{MS}}$ and Δr, respectively, and Ignatios Antoniades, Giuseppe Cocconi, Vanna Cocconi, Jean-Pierre Derendinger, John Ellis, Pierre Fayet, Sergio Ferrara, Wolfgang Hollik, Hans Kühn, Dimitri Nanopoulos, Fridger Schrempp, Barbara Schrempp, Peter Renton, James Stirling, Wilbur Venus, Julius Wess and Fabio Zwirner for interesting discussions and helpful remarks.

References

[1] H. Georgi and S.L. Glashow, Phys. Rev. Lett. **32** (1974) 438;
H. Georgi, H.R. Quinn and S. Weinberg, Phys. Rev. Lett. **33** (1974) 451

[2] M.B. Einhorn and D.R.T. Jones, Nucl. Phys. **B196** (1982) 475 and references therein.

[3] P. Fayet, Phys. Lett. **B64** (1976) 159; ibid. **B69** (1977) 489
S. Dimopoulos and H. Georgi, Nucl. Phys. **B193** (1981) 150

[4] DELPHI Coll., Contribution to Aspen Conf, DELPHI 90-62 PHYS 80 (1991)

[5] CDHS Collab., H. Abramowicz et al., Phys. Rev. Lett. **57** (1986) 298 and
A. Blondel et al., Z. Phys. **C45** (1990) 361

[6] CHARM Collab., J.V. Allaby et al., Phys. Lett. **B177** (1986) 446 and Z. Phys. **C36** (1987) 611

[7] CHARM II Collab., D. Geiregat et al., CERN-PPE/91-15

[8] UA2 Collab., J. Alitti et al., Phys. Lett. **B241** (1990) 150

[9] CDF Collab., F. Abe et al., Phys. Rev. Lett. **65** (1990) 2243
F. Abe et al., FNAL-PUB-90/162E, to be publ. in Phys. Rev.

[10] B.A. Kniehl, private communication.
F. Halzen and B.A. Kniehl, (Wisconsin U., Madison) MAD-PH-588 (1990)

[11] H. Burkhard, F. Jegerlehner, G. Penso and C. Verzegnassi, Polarization at LEP **Vol. 1** CERN 88-06 (1988) 145

[12] G. Degrassi, private communication.
G. Degrassi, S. Fanchiotti and A. Sirlin, New York University preprint, May 1990.

[13] M. Consoli, F. Jegerlehner, W. Hollik, "Z Physiscs at LEP", CERN 89-08 Vol. 1 p. 55.

[14] DELPHI Collab., P. Abreu et al., Phys. Lett. **247B** (1990) 167
DELPHI Collab., P. Abreu et al., Phys. Lett. **252B** (1990) 149

[15] A.D. Martin, R.G. Roberts, W.J. Stirling, RAL-90-084 (1990)

[16] Yu.A. Gol'fand, E.P. Likhtman, JETP Lett. **13** (1971) 323
D.V. Volkov, V.P. Akulow,Phys. Lett. **46B** (1973) 109
J. Wess and B. Zumino, Phys. Lett. **49B** (1974) 52

Figure captions

Fig. 1. a) First order evolution of the three coupling constants in the minimal Standard model (world average values in 1987 from Ref. 1). The small figure is a blow up of the crossing area.

b) As above but using M_Z and $\alpha_s(M_Z)$ from DELPHI data. The three coupling constants disagree with a single unification point by more than 7 standard deviations.

Fig. 2. a) Second order evolution of the three coupling constants in the minimal SUSY model. M_{SUSY} has been fitted by requiring crossing of the couplings in a single point. The two lower plots show M_{SUSY} (b) and M_{GUT} (c) as function of $\alpha_3(M_Z)$. The uncertainties in M_{GUT} and M_{SUSY} from the errors in $\alpha_1(M_Z)$ and $\alpha_2(M_Z)$ are small. The full line assumes that all SUSY particles have the mass of the SUSY scale. The dashed, dotted and dashed-dotted lines indicate the results if the SUSY particle spectrum is smeared over the range indicated in the figure.

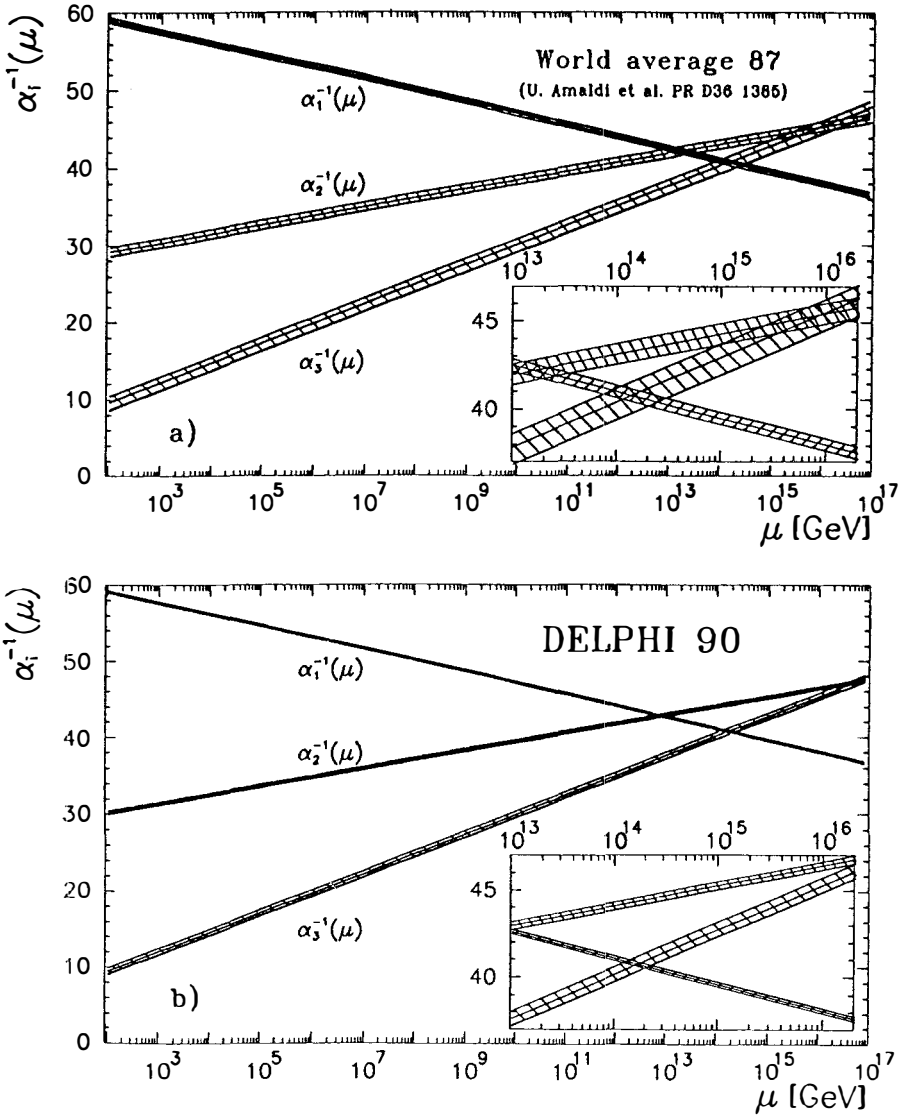
World average 87
(U. Amaldi et al. PR D36 1385)
$\alpha_1^{-1}(\mu)$
$\alpha_2^{-1}(\mu)$
$\alpha_3^{-1}(\mu)$
a)
$\alpha_i^{-1}(\mu)$
μ [GeV]
DELPHI 90
b)

Fig. 1

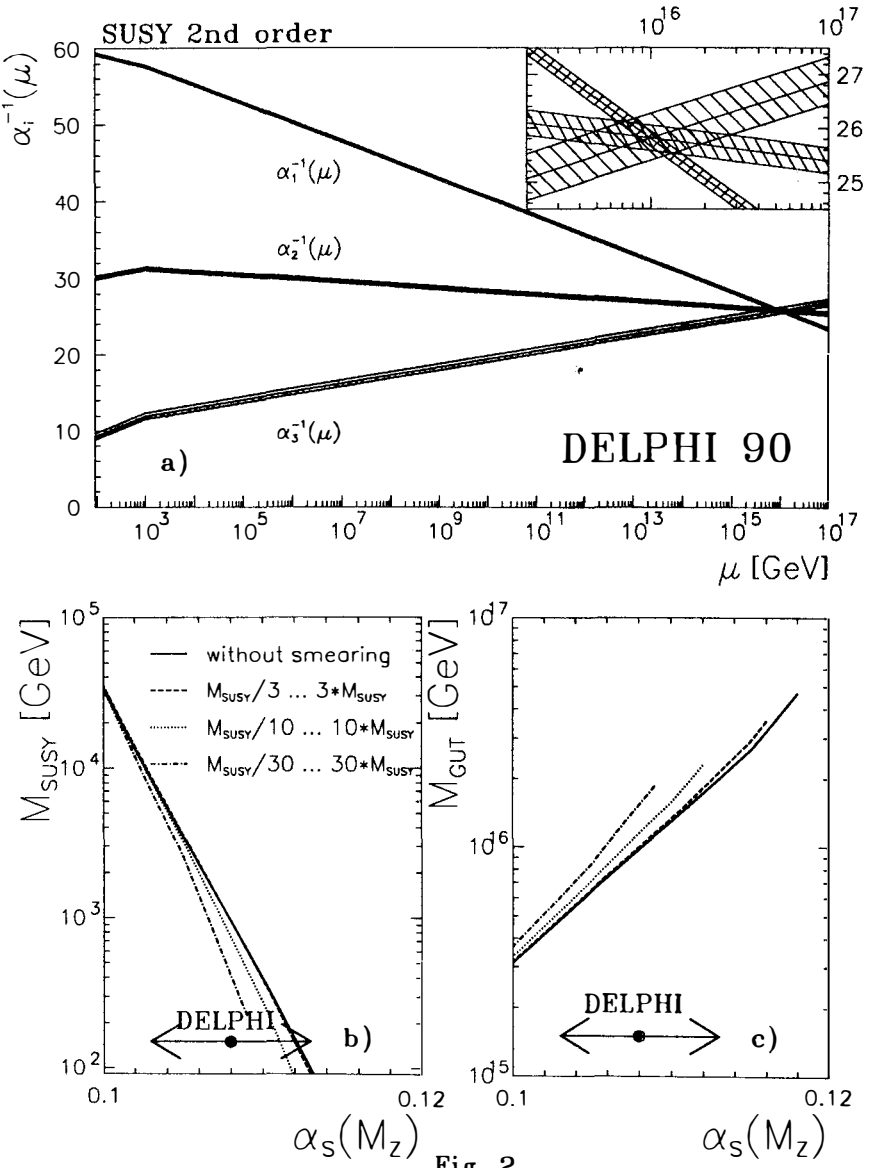
SUSY 2nd order
$\alpha_i^{-1}(\mu)$
$\alpha_1^{-1}(\mu)$
$\alpha_2^{-1}(\mu)$
$\alpha_3^{-1}(\mu)$
a)
DELPHI 90
μ [GeV]
without smearing
$M_{SUSY}/3 \ldots 3*M_{SUSY}$
$M_{SUSY}/10 \ldots 10*M_{SUSY}$
$M_{SUSY}/30 \ldots 30*M_{SUSY}$
M_{SUSY} [GeV]
DELPHI
b)
$\alpha_s(M_Z)$
M_{GUT} [GeV]
DELPHI
c)
$\alpha_s(M_Z)$

Fig. 2

STRUCTURE FUNCTIONS

PRELIMINARY MEASUREMENTS OF SHADOWING AT VERY LOW X_{BJ}

David E. Jaffe
University of Illinois at Chicago
Fermilab E665 collaboration

Abstract

The ratio of cross sections for deeply inelastic muon scattering on xenon and deuterium nuclei was measured at very low X_{Bj} ($.00002 < X_{Bj} < .25$) for $.01 < Q^2 < 60$ $(GeV/c)^2$. The data were taken at Fermilab experiment E665 with an average muon beam energy of 490 GeV incident on 1.1 meter long deuterium and xenon target vessels. Two largely independent analysis techniques gave statistically consistent results and show a smooth decrease in the ratio of the xenon-to-deuterium per-nucleon cross sections from $\sim$ 1 to $\sim$ 0.7 as X_{Bj} decreases from $\sim$ 0.1 to $\sim$ 0.002. In the X_{Bj} range 0.00002 to 0.002, the ratio remains roughly constant at $\sim$ 0.7.

Introduction: The term "shadowing" usually means that the per–nucleon cross section for some process on a nuclear target is smaller than the cross section for the same process on a free nucleon. Shadowing has been observed in collisions of real and virtual photons in several experiments[1-4] as shown in figure 1. The figure shows that the ratio of the deeply inelastic per–nucleon cross sections of heavy nuclei(calcium or xenon) to deuterium decreases from unity as X_{Bj} ($X_{Bj} = Q^2/2M\nu$ where Q^2 and ν are the four–momentum squared and energy transfered from the muon to the target and M is nucleon mass) decreases from .1 to .002[2,3]. In addition the lowest X_{Bj} point is consistent with an extrapolation of photoproduction data[1] to a xenon target although the trend of the Xe/D_2 data is a monotonic decrease with X_{Bj}. It is the aim of this paper to investigate the behavior of the ratio of the Xe/D_2 cross sections down to X_{Bj} of .00002.

Apparatus: The data were taken at Fermilab experiment 665 shown in figure 2[5]. Positive muons with an average momentum of 490 GeV/c impinged upon either a liquid deuterium or pressurized xenon gas target located in the first of two analysis magnets. See Table 1. Tracks are momentum–analyzed with a series of wire chambers and muons are identified with four stations of proportional chambers and hodoscopes located behind a three–meter thick steel absorber. Essential to the extraction of the cross section ratio at low X_{Bj} is the electromagnetic calorimeter located in front of the steel absorber. The calorimeter consisted of 20 lead–proportional tube layers(total thickness of 20 radiation lengths) with pad read–out giving a transverse position resolution of approximately 1 cm.

Table 1: Target properties and luminousities

TARGET	Pressurized Xenon gas	Liquid Deuterium
Density (g/cm^3)	0.08535	0.1630
Length (cm)	113	115
Radiation lengths	1.13	0.15
Luminousity($\times 10^{35} cm^{-2}$)	2.95	2.84

Analysis: In figure 3 the event distribution as a function of X_{Bj} for the two targets after kinematic cuts is shown. The kinematic cuts applied were $0.01 < Q^2 < 60(GeV/c)^2$, $\nu > 40$ GeV, $Y_{Bj} < 0.75$, $E_{BEAM} > 400$ GeV and $|\phi_{\mu'} - \pi| > 0.2$ where E_{BEAM} is the incident muon energy, $Y_{Bj} \equiv \nu/E_{BEAM}$, and $\phi_{\mu'}$ is the azimuthal angle of the scattered muon. The Q^2 and ν cuts limit the data to regions of reasonable resolution, the Y_{Bj} cut reduces contamination by radiative, quasi–elastic

and coherent scattering events, the E_{BEAM} cut removes low momentum beams accumulated due to a slight flaw in the trigger and the cut on the azimuthal angle of the scattered muon eliminates muons that interacted downstream of the target but were incorrectly reconstructed as having an interaction vertex in the target.

The large electromagnetic backgrounds present at low X_{Bj} are apparent in figure 3. The peak at $X_{Bj} = M_{electron}/M_{nucleon}$, clearly visible in the deuterium data, is due to elastic muon–electron(μe) scattering while the large broad peak in the xenon data results mainly from coherent muon–nucleus scattering (bremsstrahlung). To extract the DIS events from these large backgrounds, two largely independent and complementary cuts were employed — the "hadron requirement" and "electromagnetic" cuts.

To satisfy the hadron requirement, an event needed to have at least two positive tracks, not including the scattered muon, or at least two negative tracks fitted to the interaction vertex. This requirement, essentially a multiplicity cut, explicitly excludes elastic muon–electron scatters and photon conversions in the target and implicitly assumes that relatively high multiplicity events are due to DIS.

Two "electromagnetic" cuts were created and applied; each cut was designed to remove a specific component of the background: bremsstrahlung and μe scattering. The bremsstrahlung cut attempted to reject events where the beam, scattered muon and the hypothesized bremsstrahlung "photon" lie in the same plane where $\vec{P}_{\mu}$= beam muon momentum, $\vec{P}_{\mu'}$= scattered muon momentum and $\vec{P}_{\gamma}$= "photon" momentum. The direction from the μ-μ' interaction vertex to the highest energy glob in the calorimeter is used to form the "photon" momentum vector. The "bremsstrahlung planarity" is then defined as $\mathcal{P} \equiv \left| \frac{(\vec{P}_{\mu} \otimes \vec{P}_{\mu'}) \cdot \vec{P}_{\gamma}}{|\vec{P}_{\mu}||\vec{P}_{\mu'}||\vec{P}_{\gamma}|} \right|$.

Figure 4 shows the logarithm of the bremsstrahlung planarity versus E_{CAL}/ν, $E_{CAL} \equiv$ total energy in calorimeter, for the deuterium and xenon data sets and for two xenon data subsets identified as " μe " and " $\mu\gamma$ " data. Events having one incoming muon, one scattered muon and exactly one outgoing negatively–charged track comprise the " μe " sample. The " $\mu\gamma$ " sample contained events with one incoming and scattered muon and zero outgoing tracks. Each of these samples is dominated by the specified electromagnetic process but still contain a small fraction of DIS events. The region "excluded" by the bremsstrahlung cut, $\mathcal{P} < 1.0 \times 10^{-5}$ AND $E_{CAL}/\nu > 0.45$, as shown in the plots was determined from the distribution of events in the " $\mu\gamma$ " sample.

Similarly the muon–electron cut attempts to reject events with an energy glob in the calorimeter that is consistent with μe elastic scattering. Let $\vec{P}_e = \vec{P}_\mu - \vec{P}_{\mu'}$ = "scattered electron" momentum, D = distance in meters of closest glob to predicted electron impact at the calorimeter, and E = energy in GeV of the closest glob. The "excluded" curves shown in Figure 5 were determined empirically from the distribution of events in the "μe" sample and has the form $D > .003E\, e^{-E/105}$.

Figure 6 shows the resulting distribution of events vs X_{Bj} after the application of cuts for the xenon and deuterium data. Both the hadron requirement and the electromagnetic cuts reduce the number of events by at least an order of magnitude at low X_{Bj} . As X_{Bj} increases (decreasing ν), the number of events satisfying the hadron requirement decreases as expected from a multiplicity cut. The number of events passing the electromagnetic cuts is consistent with the events passing the hadron cuts at low X_{Bj} and makes a smooth transition to the events passing the kinematic cuts as X_{Bj} increases.

Since the xenon and deuterium data were taken during separate running periods, the ability to reconstruct tracks differs due to differences in chamber efficiencies. The relative reconstruction correction factor for X_{Bj} above .001 as calculated in a previous similar analysis[6] of 0.95 was applied to the Xe/D_2 ratio with an estimated systematic uncertainty of ± 0.03.

An estimate of the systematic uncertainty of the two analysis techniques was obtained by comparing the Xe/D_2 ratio versus X_{Bj} ,Q^2 and ν using monte carlo. The ratios are consistent with unity for the limited amount of monte carlo events available for analysis, and the spread in the points was used to obtain an overall estimate of the systematic uncertainty in the two techniques of $\pm 7.0\%$. In addition, an estimate of the additional uncertainty as a function of X_{Bj} ,Q^2 and ν was obtained by judicious variation of the analysis methods. Included in the comparison were 1) tightening of the bremsstrahlung cut, 2) a cut on the resolution in X_{Bj} , 3) the use of the kinematics from the μ-μ'–only vertex, and 4) cutting well within the endcaps of the target vessels.

The terms described above are added in quadrature to give the overall systematic uncertainty shown in the figures as a shaded band. In the figures, one adds or subtracts the shaded band from the points to obtain the maximum variation due to systematic uncertainty.

Results: The two analysis techniques are compared in Figure 7 which shows the Xe/D_2 per-nucleon cross section ratio as a function of X_{Bj} ,Q^2 and ν . Both techniques yield statistically consistent results in each variable. In figure 8 the results obtained in the previous analysis[6] are compared with the current results using the electromagnetic cuts. The two techniques yield consistent results in the region of overlap. Figure 9 compares the Xe/D_2 ratio measured in this experiment (electromagnetic analysis) with the results of EMC[2] for the Ca/D_2 ratio and the photoproduction results[1] . The A-dependence of shadowing measured in EMC — larger nuclei have increased shadowing — is consistent with the results shown here within the systematic uncertainty shown and the quoted $\approx$ .05 systematic uncertainty for EMC. For X_{Bj} below 0.002-0.003, the ratio remains constant within the statistical precision of the data, is consistent with the photoproduction point indicated by the arrow and indicates a saturation in shadowing at very low X_{Bj} .

References

1. D.O. Caldwell *et al.*, Phys. Rev. Lett. **42**, 553 (1979).
2. M. Arneodo *et al.*, Phys. Lett. **B333**, 1 (1990) and M. Arneodo *et al.*, Phys. Lett. **B211**, 493 (1988).
3. M.R. Adams *et al.*, E665 collaboration, in preparation.
4. D.M. Alde *et al.*, Phys. Rev. Lett. **64**, 2479 (1990).
5. M.R. Adams *et al.*, Nucl. Inst. and Meth., **A291**, 533(1990).
6. S.R. Magill, "Xe/D_2 cross section ratio from muon scattering at 490 GeV/c", Ph.D. dissertation, 1990, University of Illinois at Chicago(unpublished).

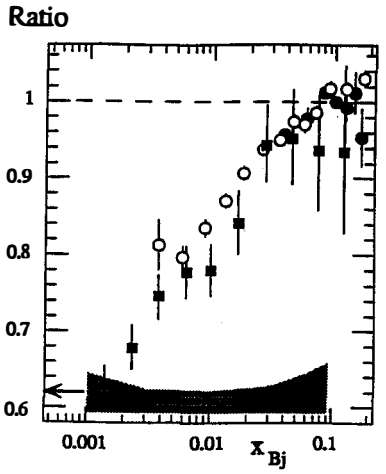

Figure 1. Shadowing measurements. Solid squares and shade band: previous E665 Xe/D_2 cross section ratio and systematic uncertainty[3]. Open circles: NMC Ca/D_2 ratio[2]. Shaded circles E772 dimuon experiment[4]. Arrow on vertical axis: 60 GeV photoproduction data[1] extrapolated to 150 GeV for a xenon target

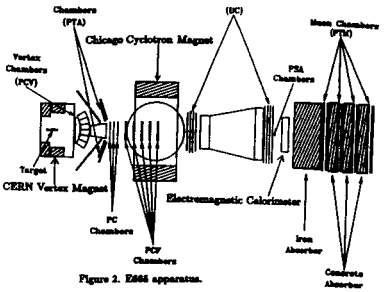

Figure 2. E665 apparatus.

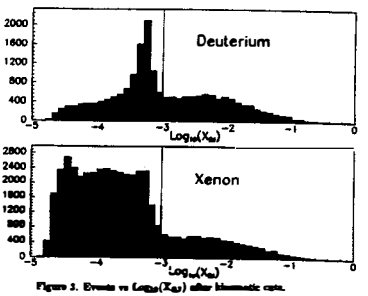

Figure 3. Events vs $Log_{10}(X_{Bj})$ after kinematic cuts.

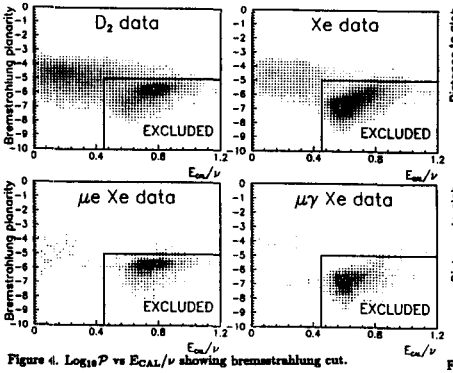

Figure 4. $\mathrm{Log_{10}}\mathcal{P}$ vs E_{CAL}/ν showing bremsstrahlung cut.

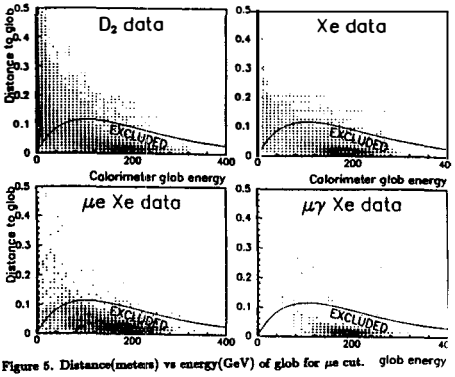

Figure 5. Distance(meters) vs energy(GeV) of glob for μe cut. glob energy

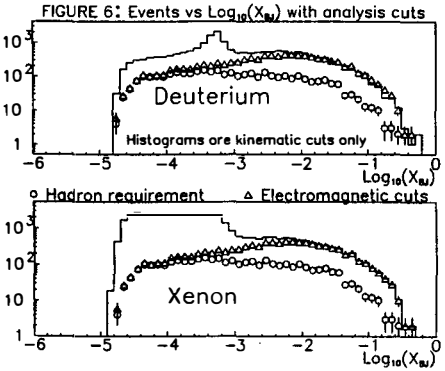

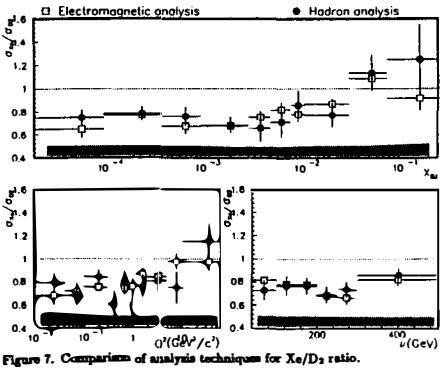

Figure 7. Comparisons of analysis techniques for Xe/D_2 ratio.

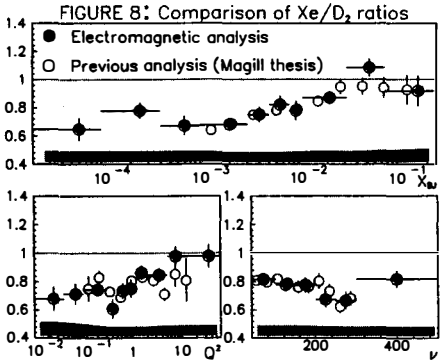

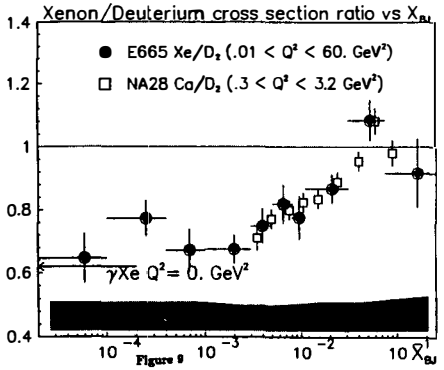

Figure 9

MUOPRODUCTION OF J/ψ- MESONS AND THE GLUON DISTRIBUTION IN THE NUCLEON

Ewa Rondio
New Muon Collaboration (NMC)
Warsaw University, Poland

Abstract

Results are presented on inelastic J/ψ-production from muon interactions with hydrogen, deuterium, carbon and tin. The data were collected by the experiment NA37 at the CERN SPS. The measured cross section ratio per nucleon for muon-induced J/ψ-production in deuterium and hydrogen was found to be $R(D_2/H_2) = 1.01 \pm 0.15$. The Colour Singlet model is shown to provide a good description of the observed differential cross section apart from a normalisation factor. The comparison between the observed cross section and the Colour Singlet model prediction allows the extraction of the gluon structure function G(x) of the nucleon. The momentum fraction x of the nucleon carried by the gluon is measured in the range of x=[0.02,0.3]. The normalised gluon distribution of free nucleons thus found can be parametrised as: $xG(x) = \frac{\eta+1}{2}(1-x)^{\eta}$, with $\eta = 5.1 \pm 0.9(stat.)$.

The cross section ratio per nucleon for carbon and tin was studied as a function of the energy fraction, z, taken by the J/ψ-meson and its squared transverse momentum, p_T^2.

Introduction

The production of J/ψ mesons in deep inelastic scattering (DIS) can be related to the gluon distribution in the nucleon. Data from muon interactions with hydrogen and deuterium were used extract the gluon distribution using the colour singlet model based on photon-gluon fusion, after it had been verified that this model describes the data.

The question how the gluon distribution is modified in nuclear matter was approached by comparing of J/ψ production in tin and carbon targets.

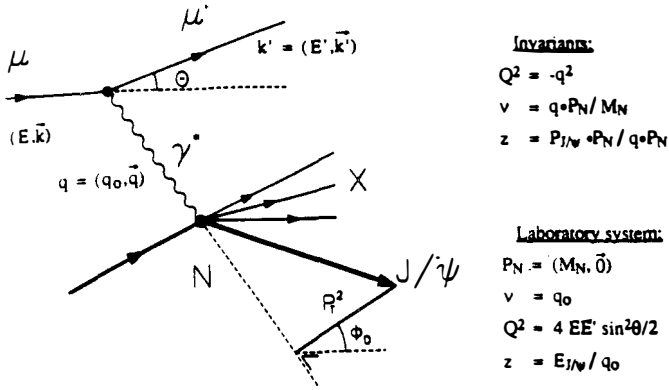

Figure 1: The kinematics of muon induced J/ψ production in one photon exchange approximation.

Experimental data

The experiment was performed in the M2 beam at the CERN-SPS with muons of 280 GeV incident energy using an upgraded version of the EMC forward spectrometer [1]. The kinematics of the μ-nucleon interaction producing a J/ψ meson (in the one-photon exchange approximation) is shown in fig.1. For hydrogen and deuterium the trigger accepting DIS events with scattering angles larger than 10 mrad was used whereas for carbon and tin a special multimuon trigger was applied. Special care was taken to observe muons at small scattering angles (in the beam region). Only J/ψ mesons decaying into a muon pair were detected. All events with at least three reconstructed tracks were considered. For such cases the invariant mass of oppositely charged muons was calculated and the scattered muon was selected from the remaining reconstructed tracks with the same charge as that of the incident muon.

J/ψ production on hydrogen and deuterium

The invariant mass distributions for inelastic interactions on hydrogen and deuterium are presented in fig.2 a) and b). Inelastic events were selected by requiring $z \leq 0.9$ and transverse momentum squared $p_T^2 \geq 0.1\ GeV^2/c^2$. The sum of a gaussian distribution and an exponentially falling background were fitted to the mass spectra. The fitted value of the J/ψ mass is $3.093 \pm 0.005\ GeV^2/c^2$, which is in good agreement with [2]. The width corresponds to the spectrometer momentum resolution of 1%. The background corrected number of J/ψ mesons was found to be 85 ± 10 and 194 ± 15 on hydrogen and deuterium respectively. This yields the ratio of the cross sections per nucleon for muoproduction of the J/ψ in deuterium and hydrogen to be R(D/H)=1.01 ± 0.15 where

the error is statistical only. The systematic error was estimated to be small due to the cancelation of acceptances and beam fluxes [1].

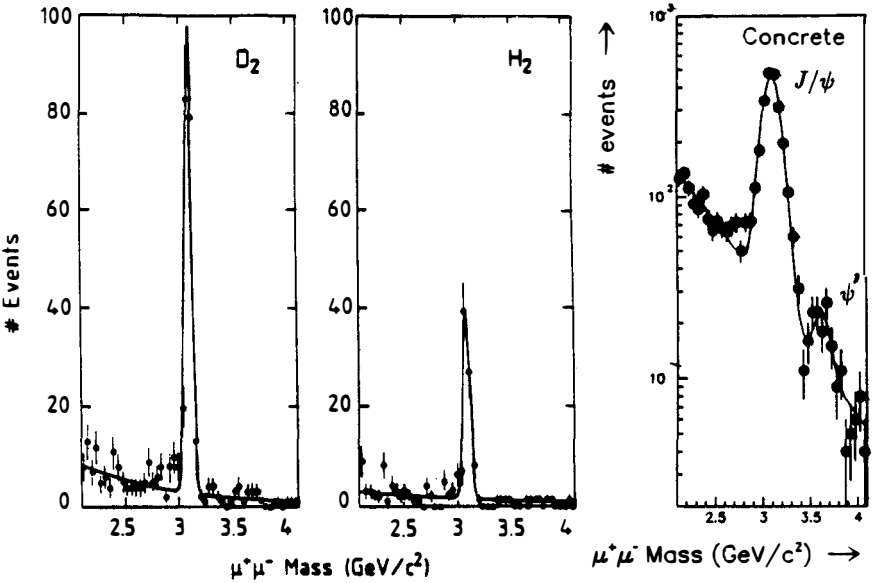

Figure 2: The invariant mass distribution of selected $\mu^+\mu^-$ pairs produced in deuterium(a), hydrogen(b) as well as pairs produced in the concrete absorber placed behind the carbon and tin target(c) where the high statistics allows the observation of the ψ' peak.

This result is consistent with equal J/ψ production rates for neutron and proton. In the subsequent analysis the hydrogen and deuterium data were therefore combined giving 279 inelastic J/ψ events in the invariant mass interval 2.9-3.3 GeV/c^2 and 41 background events.

To obtaine absolute cross sections from the experimental counting rates, the acceptance was calculated using a Monte Carlo simulation. The branching ratio of J/ψ into a muon pair was taken to be (6.9±0.9)% [2]. Radiative effects on the measured cross section were estimated to be 5% or less [3,4]. The background contribution to the inelastic J/ψ rate coming through ψ' production and subsequent decay into J/ψ was estimated using data from interactions in the concrete absorber placed behind the carbon and tin targets. The invariant mass distribution for this sample is shown in fig.2 c). The signal of ψ' is clearly visible and after the corrections for branching ratios one obtains $\sigma(\psi')/\sigma(J/\psi) = 0.24 \pm 0.05 \pm 0.08$. Using this ratio in a Monte Carlo simulation, the ψ' contribution to the inelastic J/ψ production is found not to exceed a few percent and was therefore neglected.

As possible mechanisms of J/ψ production the vector meson dominance with the Drell-Yan mechanism and photon-gluon fusion [5] were considered. The corresponding graphs are presented in fig.3. The model predictions were compared to experimental distributions. The two mechanisms give largely different predictions for the J/ψ rapidity distribution. In fig.4 the observed differential cross section is shown together with the

model expectations. The data which is peaking at high values of the rapidity, favour the CS model description. The normalisation factor applied in the CS model necessary to give a good description of the data was estimated to be 2.4. The comparison of the differential cross section as a function of z and p_T^2 extracted from the data with the predictions of the CS model (applying again the same normalisation factor) is shown in fig.5. For z values corresponding to inelastic J/ψ production ($z \leq 0.9$) the agreement is good. The model also gives a good description of the differential cross sections as a function of Q^2 and ν.

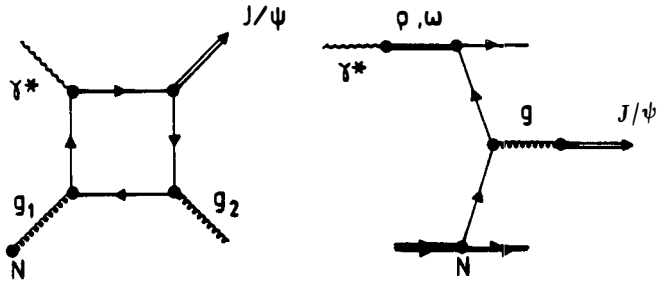

Figure 3: The diagrams for muon induced J/ψ production in the Colour Singlet model (CS) and Vector Meson Dominance description with the Drell-Yan mechanism (VMD-DY).

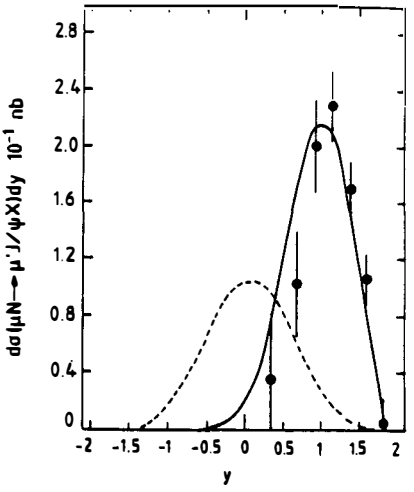

Figure 4: Cross section for J/ψ muoproduction as a function of rapidity and comparison with model predictions. The CS prediction (times 2.4) is represented by the solid curve; the dashed curve represents the VMD-DY expectation.

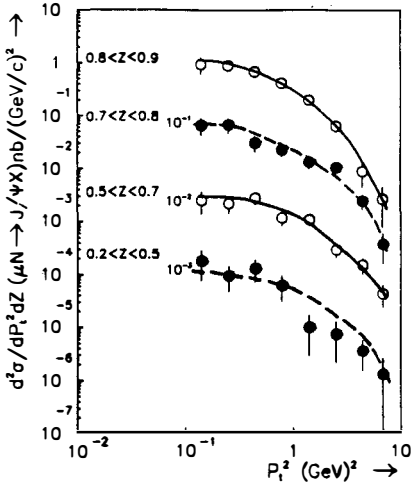

Figure 5: Cross section for J/ψ muoproduction as a function of z and p_T^2 and a comparison with the CS model prediction with a normalisation factor of 2.4 (the same as for the rapidity distribution).

Colour Singlet Model

In the CS model, the J/ψ is represented by a definite wave function of the $c\bar{c}$ system, describing a colour singlet state of spin and parity $J^P = 1^-$ and the mass of the J/ψ.

The calculation was performed according to ref [6] with a QCD radiative correction factor to the leptonic width $\Gamma_{J/\psi}$ of $1 - 16\alpha_s M^2_{J/\psi}/3\pi$ (ref[7]). The values of α_s and the charm quark mass were taken from [2]. The normalisation is not described correctly but the shape of rapidity distribution as well as the other differential cross-sections are in good agreement with the data in the region where the model is applicable (i.e. the inelastic domain).

Gluon distribution

Since the CS model provides a good description of the data it has been used to extract the gluon distribution of the nucleon. The function $:c \cdot \frac{\eta+1}{2} \cdot (1-x)^\eta$ was used in fitting the data, which yielded c=2.4±0.4 (i.e.the above introduced normalisation factor) and $\eta = 5.1 \pm 0.9$ The variable $x = \frac{\hat{s}_{\gamma^* g}}{s_{\gamma^* N}}$ in CS model can be express as $x = \frac{1}{s}[\frac{M^2_{J/\psi}}{z} + \frac{p_T^2}{z(1-z)}]$. The normalised (c=1) gluon distribution is presented in fig.6.

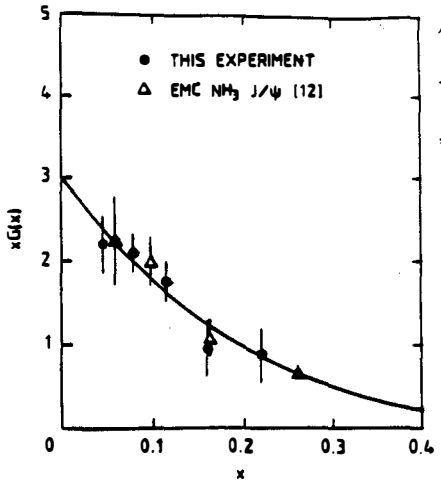

Figure 6: The normalised nucleon gluon distribution $x \cdot G(x)$ from hydrogen and deuterium data extracted with the CS model. Also shown are earlier results from an EMC measurement on amonia [3] .

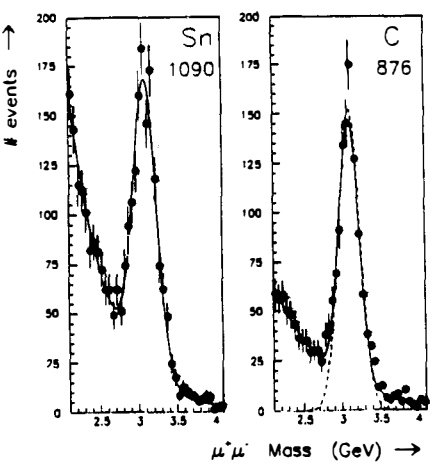

Figure 7: The invariant mass distribution of $\mu^+\mu^-$ pairs produced in tin and carbon.

J/ψ production on nuclear targets

A complementary setup of carbon and tin targets [8] was exposed to muons with an average energy 280 GeV. The J/ψ events were selected by a dedicated multimuon trigger. The results presented here are preliminary.

The invariant mass spectra of $\mu^+\mu^-$ pairs are shown in fig.7 for both materials. The widths of the peaks are larger than those fot the hydrogen and deuterium data due to higher multiple scattering in the targets and the absorber placed behind it. The number of J/ψś (in the mass interval 2.7-3.5 GeV/c^2 after background subtraction) is 1090±34 for tin and 876±30 for carbon.

Production of the J/ψ in nuclear target can take place through:

* a coherent process (elastic on the nucleus),

* a diffractive process (elastic on the nucleon),
* an inelastic process (inelastic on nucleon).

Coherent production on the nucleus is expected at z near unity and at low p_T^2. The corresponding cross section should be dependent on the size of the nucleus.

To study the first two processes, a sample of interactions with $z \geq 0.9$ was selected. Distributions of p_T^2 for this sample are shown in fig.8 a). One can clearly distinguish two slopes corresponding to coherent scattering at low p_T^2 and elastic scattering on the nucleon. The coherent signal for tin is larger than that for carbon. Smearing effects dominate the slope of this part of the distribution. At higher p_T^2, the distributions for both materials are described by the same exponential slope.

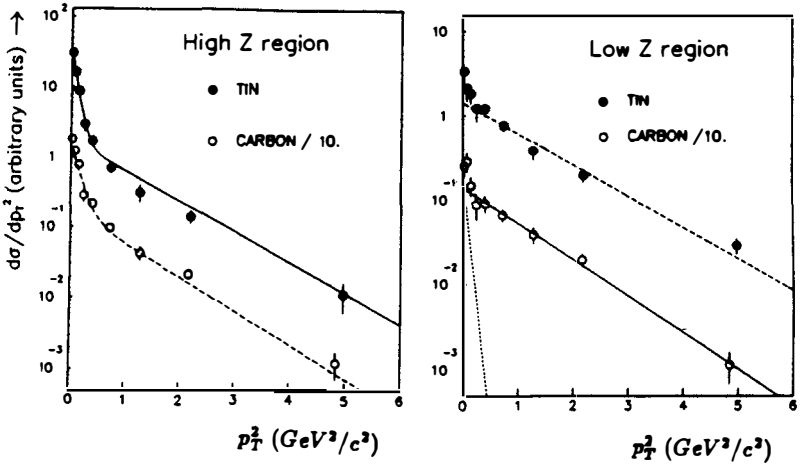

Figure 8: The p_T^2 distribution for J/ψ mesons for carbon and tin in two z intervals high z ($z \geq 0.9$)-the coherent and diffractive region and low z ($0.2 \leq z \leq 0.9$)-the inelastic region. The solid and dashed lines show the fitted exponential curves for tin and carbon respectively. Dotted line, for the low z region, represents estimated coherent contribution for carbon.

In fig.8 b) the p_T^2 distribution for the inelastic region ($z \leq 0.9$) is shown. The dotted line corresponds to the expected coherent contribution of ψ', and its subsequent decay, for carbon. A p_T^2 cut of $p_T^2 \geq 0.4\ GeV/c^2$ is applied to reduce this contribution.

The ratio of cross sections for J/ψ production in the inelastic sample was found to be $\frac{\sigma(J/\psi)_{Sn}}{\sigma(J/\psi)_C} = 1.20 \pm 0.13$

In the Colour Singlet model the cross section is proportional to the gluon momentum distribution, so that within this model the ratio of gluon distributions in tin and carbon is equal to this cross-section ratio.

Summary

The gluon distribution has been extracted from the J/ψ muo-production on hydrogen and deuterium with the Colour Singlet model. The accuracy of this result is comparable with that reached in the QCD analysis of scaling violations in F^2 structure functions [9]. The J/ψ production on the neutron and the proton was found to be the same. For carbon and tin the J/ψ production ratio is strongly dependent on z and p_T^2.

This fact might explain the discrepancy between previous results obtained by EMC [10] and at FNAL [11]. In the inelastic domain the ratio was found to be 1.20 ± 0.13.

References

[1] NMC,D.Allasia et al,Phys.Lett.B249(1990),366.

[2] Review of Particle Properties,Phys.Lett. B223(1990).

[3] N.Dyce, Ph.D.thesis, Lancaster University(1980).

[4] L.W.Mo and Y.S.Tsai,Rev.Mod.Phys.41(1969),205; Y.S.Tsai, SLAC-848(1971).

[5] NMC,D.Allasia et al,Phys.Lett.258B(1991),493.

[6] K.J.Abraham,Phys.Lett.240B(1990),224.

[7] R.Barbieri,R.Gatto and E.Remiddi, Phys.Lett.106B(1981),497.

[8] M.de Jong,Ph.D.thesis, Free University Amsterdam(1991)

[9] EMC,J.J.Aubert et al,Nucl.Phys. B272(1986),158 and BCDMS,A.C.Benvenuti et al, Phys.Lett. B223(1989),490.

[10] EMC,J.J.Aubert et al,Phys.Lett. 152B(1985),433.

[11] M.D.Sokoloff et al,Phys.Rev.Lett. 57(1986),3003.

Q^2 DEPENDENCE OF THE STRUCTURE FUNCTION RATIO F_2^n/F_2^p

Antje Brüll
University of Freiburg
New Muon Collaboration (NMC)

Abstract

The structure function ratio F_2^n/F_2^p is determined in measurements of deep inelastic muon scattering on hydrogen and deuterium. The results were obtained at incident energies of 90 and 280 GeV and cover the x_{bj} range down to 0.002 and a Q^2 range of 0.1 GeV^2 < Q^2 < 190 GeV^2. The observed Q^2 dependence of the ratio F_2^n/F_2^p is stronger than predicted by perturbative QCD, indicating a different higher twist contribution to the proton and neutron structure functions. Together with the deuterium structure function determined from a fit to published data, the ratio is used to derive the difference $F_2^p - F_2^n$. The value of the Gottfried Sum $\int(F2p - F2n)/x\,dx$ is significantly below the Quark Parton Model expectation of 1/3.

Introduction

The ratio of the proton to neutron structure function $F_2^n(x)/F_2^p(x)$ measures the ratio of parton distributions and in particular constrains the ratio of up to down quark distributions, important for reliable predictions of hard scattering cross sections at future colliders.

Perturbative QCD describes the scaling violations of the nucleon structure functions as a function of $\log(Q^2)$. Thus an accurate measurement of the Q^2 dependence of F_2^n/F_2^p allows the determination of possibly different nonperturbative contributions to the structure functions of neutron and proton.

The Experiment

The NMC results presented here were evaluated from a simultaneous measurement of deep inelastic scattering on hydrogen and deuterium at two incident muon energies of 90 and 280 GeV. The experiment was performed at the M2 muon beam line of the CERN SPS, using an upgraded version of the EMC spectrometer [1]. To optimise the measurement of cross section ratios, two complementary sets of targets, identical except for the sequence of the target materials, were alternately exposed to the beam. The frequent exchange (every $\sim$ 30 min) of the two target sets, leads to a cancellation of apparatus acceptance and flux normalisation. The cross section ratio then only depends on the measured number of events and the ratio of molar volumes κ:

$$\sigma(D)/\sigma(H) = \kappa \cdot \sqrt{\frac{N_{up}^D \cdot N_{dn}^D}{N_{up}^H \cdot N_{dn}^H}}$$

In this way important sources of systematic uncertainties are eliminated and the kinematic range could reliable be extended down to $x_{bj} = 0.002$. In the single photon exchange approximation, neglecting nuclear binding effects in deuterium and assuming the ratio of longitudinal to transverse virtual cross section to be the same in hydrogen and deuterium, the structure function ratio F_2^n/F_2^p is related to the nuclear cross section ratio by

$$F_2^n/F_2^p = \sigma(D)/\sigma(H) - 1$$

No corrections for Fermi motion were applied, they are negligible at $x < 0.6$.

Results on F_2^n/F_2^p

The x dependence of the structure function ratio F_2^n/F_2^p measured at 90 and 280 GeV incident muon momentum is shown in fig. 1. Due to the complementary target set-up the systematic errors, indicated by the bands at the bottom, are small over the whole measured range $0.002 < x_{bj} < 0.8$. At low x_{bj} they are dominated by the uncertainty in the radiative corrections, at high x_{bj} by the accuracy of the determination of incoming and scattered muon momenta.

At the lowest x_{bj} of 0.003 the ratio F_2^n/F_2^p is 0.990 ± 0.016, consistent with unity. Apparently in the kinematic region of this experiment, there is no evidence for a sizeable shadowing effect in deuterium. However, the data cannot exclude the 2-3 % effect of shadowing at $x = 0.003$ predicted in ref. [2].

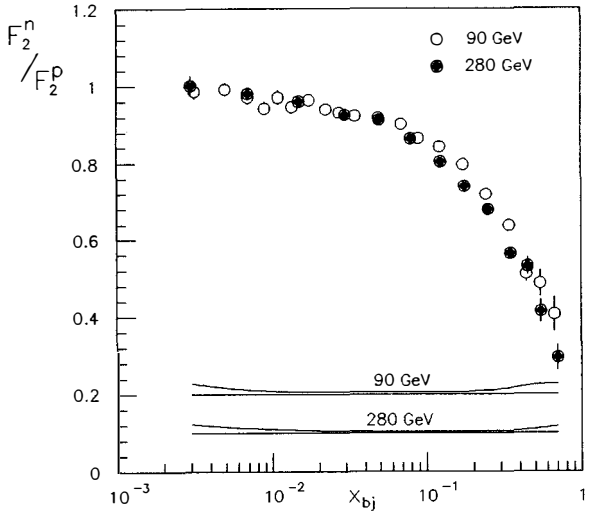

Figure 1: $F_2^n/F_2^p(x)$ for 90 and 280 GeV. The bands show the size of the systemtic errors

At a given x_{bj} the average Q^2 depends on the incident muon momentum. Thus the small differences seen in the x dependence of F_2^n/F_2^p obtained at 90 and 280 GeV indicate a Q^2 dependence of the ratio. This dependence is presented in more detail in fig. 2, where F_2^n/F_2^p is shown for fixed values of x_{bj} as a function of Q^2, seperately for 90 and 280 GeV. Since in the overlap region the data obtained at different energies are in agreement, they are combined.

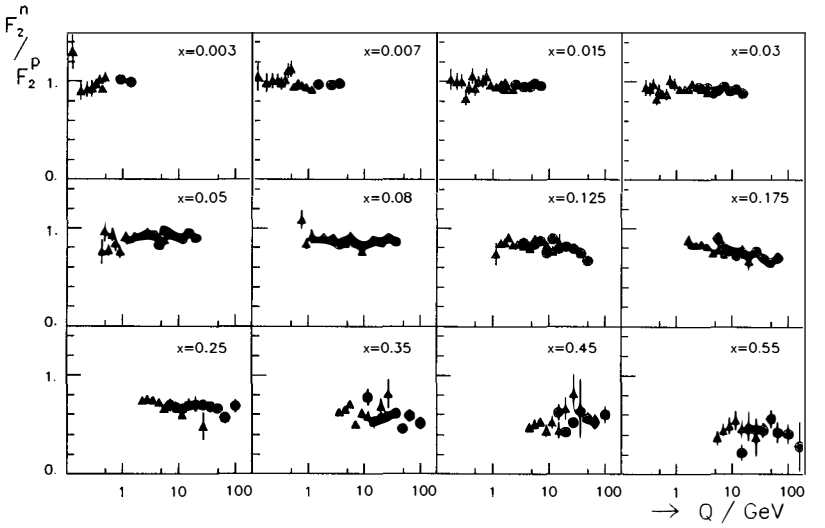

Figure 2: $F_2^n/F_2^p(x, Q^2)$ for 90 and 280 GeV

For each x_{bj} bin the ratio has been parametrised as a linear function of $\log(Q^2)$. The slopes obtained in this way are shown in fig. 3 as a function of x_{bj}. Also shown is a next-to-leading order QCD calculation including target mass corrections [3]. For x_{bj} between 0.1 and 0.4 the measured Q^2 dependence is significantly stronger than predicted by perturbative QCD, while at low values of x_{bj} no Q^2 dependence of the ratio F_2^n/F_2^p is observed.

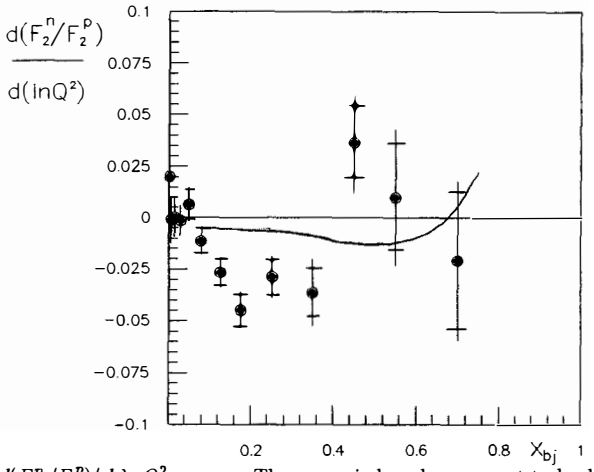

Figure 3: $d(F_2^n/F_2^p)/d\ln Q^2$ vs. x_{bj}. The curve is based on a next-to-leading order QCD calculation including target mass effects.

A comparison of the NMC result on F_2^n/F_2^p to data from SLAC and BCDMS [4] is given in fig. 4. Shown are the four x_{bj} bins, where our measured Q^2 dependence most significantly differs from the QCD prediction. Good agreement between the different data sets is observed. Moreover, the large Q^2 range of the NMC experiment determines the relativ normalisation of the other data sets, one of the main uncertainties in these measurements.

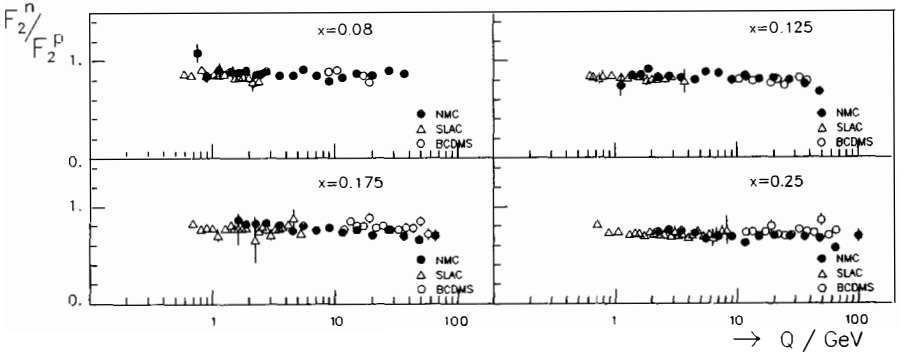

Figure 4: $F_2^n/F_2^p(x,Q^2)$ from NMC, SLAC and BCDMS

Higher Twist Contributions

The discrepancy between the measured Q^2 dependence of F_2^n/F_2^p and the next-to-leading order QCD calculation leads to the conclusion that for x_{bj} between 0.1 and 0.4 nonperturbative effects are different for neutron and proton. One interpretation might be a different higher twist contribution to the Q^2 evolution of F_2^n and F_2^p. Parametrising F_2 as

$$F_2 = F_2^{lt} \cdot (1 + C/Q^2)$$

where F_2^{lt} corresponds to the leading twist part as predicted by perturbative QCD and C/Q^2 describes the higher twist contribution (neglecting terms with twist greater 4), F_2^n/F_2^p becomes

$$F_2^n/F_2^p = (F_2^n/F_2^p)^{lt} \cdot (1 + (C^n - C^p)/Q^2)$$

The difference in higher twist contributions to the neutron and proton structure function can thus be determined from the measured ratio. The result, converted to $C^p - C^d$, is given in fig. 5 as a function of x_{bj}. At $0.1 < x_{bj} < 0.4$ significant differences between C^p and C^d are observed.

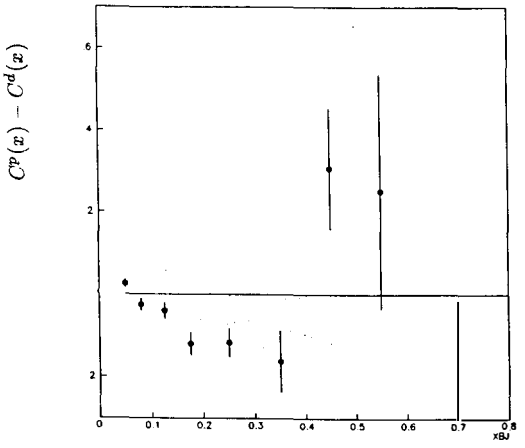

Figure 5: $C^p(x) - C^d(x)$ extracted from NMC data

The Gottfried Sum Rule

In the Quark Parton Model assuming isospin invariance between the proton and the neutron the Gottfried Sum can be written as

$$S_G = \int_0^1 (F_2^p - F_2^n)/x \, dx = 1/3 + 2/3 \int_0^1 dx \, (\bar{u} - \bar{d})$$

where $\bar{u}$ and $\bar{d}$ denote the sea quark distributions in the proton. As QCD corrections to the integral are small [5], for a flavour symmetric sea this yields $S_G = 1/3$. Using the precise NMC measurement of F_2^n/F_2^p together with the deuterium structure function obtained from a fit to published data, the Gottfried Sum can be evaluated [6], expressing $F_2^p - F_2^n$ as $2F_2^d(1 - F_2^n/F_2^p)/(1 + F_2^n/F_2^p)$.

The difference as determined at $Q^2 = 4$ GeV^2 and the resulting cumulative integral are shown in fig. 6. The value of the Gottfried Sum calculated in the measured range is

$$\int_{0.004}^{0.8} = 0.227 \pm 0.007 \pm 0.014$$

The contributions from the unmeasured regions are estimated by extrapolating $F_2^p - F_2^n$ to $x_{bj} = 0$ and $x_{bj} = 1$. The contribution from the high x region is negligible. Assuming at small x_{bj} a Regge like behaviour of $F_2^p - F_2^n$,

$$F_2^p - F_2^n \sim x^\alpha$$

the Gottfried Sum is determined [6]to be

$$S_G = 0.240 \pm 0.016$$

significantly below the simple Quark Parton Model result of 1/3.

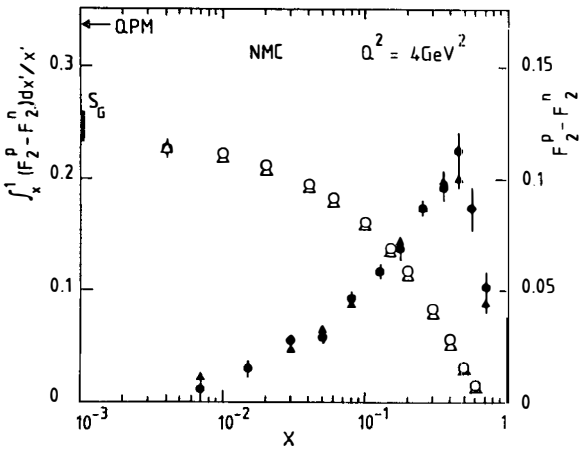

Figure 6: $F_2^p - F_2^n(x)$ (full sumbols and the scale to the right) and $\int_{x_{min}}^1 (F_2^p - F_2^n)\,dx/x$ (open symbols and the scale to the left) at $Q^2 = 4$ GeV^2. The circles and triangles represent two different extrapolations to $Q^2 = 4$ GeV^2.

References

[1] O. C. Allkofer et al. (EMC), Nucl. Instr. & Meth. **179** (1981), 445

[2] B. Badelek + J. Kwiecinski, Warsaw Univ. preprint IFD 3/91, (1991), submitted to Nucl. Phys. B

[3] M. Virchaux, Saclay report DPhPE 90-20, (1990)

[4] L. W. Whitlow, Ph. D. Thesis, Stanford University, 1990, SLAC-Report-357, 1990.

[5] D. A. Ross and C. T. Sachrajda, Nucl. Phys. **B149**, (1979), 497

[6] P. Amaudruz et al. (NMC), CERN report CERN-PPE/91-05, 1991

PARTON DISTRIBUTIONS AT SMALL x.

J. Kwieciński,
Department of Theoretical Physics, H. Niewodniczański Institute of Nuclear Physics, ul. Radzikowskiego 152, 31-342 Krakow, Poland,
A.D. Martin, W.J. Stirling
Department of Physics, University of Durham, Durham DH1 3LE, UK,
and
R.G. Roberts,
Rutherford Appleton Laboratory, Chilton, Didcot, OX11 OQX, UK.
(Presented by J. Kwieciński)

Abstract.

We perform a next-to-leading order QCD analysis of the recent data for deep inelastic lepton-nucleon scattering and related processes, in which we pay particular attention to the forms of the parton distributions at very small x. We discuss, and we incorporate in the analysis the theoretical QCD results leading to the singular $x^{-1/2}$ type behaviour of the gluon and sea quark distributions, as well as the modifications due to shadowing effects. We find the QCD shadowing corrections are significant for $x \leq 10^{-3}$ even though the parton distributions are below their saturation limit. We give predictions for the structure functions F_2 and F_L accessible at HERA, and for W and Z production up to LHC and SSC energies. We discuss the possibility at these colliders probing the parton distributions in the very small x region.

I. INTRODUCTION

The small x limit of parton distributions is of considerable importance both theoretically and phenomenologically. We shall be primarily concerned with deep inelastic lepton-proton scattering for which $x = Q^2/(2M\nu)$ where M is the proton mass, $Q^2 = -q^2$, $\nu = pq/M$, with q being the 4 - momentum transfer between the incoming and outgoing lepton and p being the proton 4 - momentum. We are particularly interested in the small x region, $2M\nu >> Q^2$, in which Q^2 is also kept large (i.e. at least a couple of GeV^2 or so), so that the QCD improved parton model is applicable. This region of very small x and large Q^2 will soon be probed by experiments at HERA.

It is expected in perturbative QCD that the gluon and sea quark distributions (multiplied by x) should grow in the limit $x \Rightarrow 0$ [1]. The purpose of this talk is to present results of the phenomenological QCD analysis of the deep inelastic lepton scattering and of related processes incorporating theoretical QCD expectations on small x behaviour of parton distributions. We give predictions for the structure functions F_2 and F_L in the region of **very small** values of x ($x \geq 10^{-4}$ or so) which will be soon accessible in HERA as well as the predictions for W and Z production up to the SSC and LHC energies. This talk is based on the analysis presented in [2] where all the details can be found.

II. THEORETICAL QCD EXPECTATIONS FOR THE SMALL X LIMIT OF PARTON DISTRIBUTIONS.

It is conventional to determine the form of the parton distributions as functions of x and Q^2 using the Altarelli-Parisi evolution equations, which take into account the leading powers (and usually the next-to-leading) powers of $\ln Q^2$. Starting distributions are assumed at some scale Q_0 of the order of a few **GeV** and the Altarelli-Parisi evolution equations are then employed to determine the distributions at higher values of Q^2. In the small x region the dominant role is played by the gluons. Also the sea quark distributions in this region are predominantly driven by the gluons. Starting from the non-singular input distribution $xg(x,Q_0^2)$ it is possible to solve the Altarelli-Parisi equations analytically at very small x and large Q^2 to give

$$xg(x,Q^2) \propto \exp\{2[\xi(Q^2)\ln(1/x)]^{1/2}\} \qquad (1)$$

with

$$\xi(Q^2) = \int_{Q_0^2}^{Q^2} \frac{dq^2}{q^2} \frac{C_A \alpha_s(q^2)}{\pi} \tag{2}$$

where $C_A = N_c = 3$, the number of colours and $\alpha_s(q^2)$ is the running QCD coupling. The expression (1) corresponds to the so-called double logarithmic approximation as it comes from the sum of the leading powers of $\ln(Q^2)$ and $\ln(1/x)$. In axial gauges it is generated by ladder diagrams with strongly ordered transverse and longitudinal momenta of the exchanged gluons [3]. The double logarithmic approximation is still incomplete since it neglects the terms containing the leading powers of $\ln(1/x)$ which are not accompanied by the leading powers of $\ln(Q^2)$. The sum of the leading powers of $\ln(1/x)$ is generated by the Lipatov equation [4] which corresponds again to ladder-like diagrams with reggeised gluon exchange. Important point here is that the transverse momenta of the exchanged gluons are not longer ordered. The Lipatov equation generates the "bare QCD Pomeron" with large intercept $\alpha_P^B \cong 1.5$ [4-6]. This singularity should controll the small x limit of gluon distributions i.e.:

$$xg(x,Q^2) \propto x^{1-\alpha_P^B} \cong x^{-1/2} \tag{3}$$

with similar behaviour for sea quarks.

We see from (1) and (3) that $xg(x,Q^2)$ grows rapidly with increasing $\ln(1/x)$ at fixed Q^2. But this increase, as x decreases, cannot go on indefinitely. If the density of gluons becomes too large they can no longer be treated as free partons. Their interaction leads to shadowing effects which modify the evolution equations in the following way [2,7]:

$$Q^2 \frac{\partial xg(x,Q^2)}{\partial Q^2} = P_{gg} \otimes g + P_{gq} \otimes q - \frac{81\alpha_s^2(Q^2)}{16R^2Q^2}\,\theta(x_0-x)\int_x^{x_0} \frac{dx'}{x'}\,[x'g(x',Q^2)]^2 \tag{4}$$

$$Q^2 \frac{\partial xq_s(x,Q^2)}{\partial Q^2} = P_{qg} \otimes g + P_{qq} \otimes q_s - \frac{27\alpha_s^2(Q^2)}{160R^2Q^2}\,[xg(x,Q^2)]^2$$

$$+ \frac{\alpha_s(Q^2)}{\pi Q^2}\,\theta(x_0-x)\int_x^{x_0} \frac{dx'}{x'}\,\frac{x}{x'}\,\gamma(x/x')x'G_H(x',Q^2) \tag{5}$$

where $\gamma(y)=-2y+15y^2-30y^2+18y^4$ and G_H satisfies

$$Q^2\frac{\partial xG_H(x,Q^2)}{\partial Q^2} = -\frac{81\alpha_s^2(Q^2)}{16R^2}\,\theta(x_0-x)\int_x^{x_0}\frac{dx'}{x'}\,[x'g(x',Q^2)]^2 \tag{6}$$

The additional non-linear shadowing terms arise from diagrams shown in figs. 1 and 2. We introduce these terms only for small x i.e. for $x \leq x_0 = 10^{-2}$. The radius parameter R in the non-linear terms in eqs. (4) - (6) arises from the integration over the 4-momentum flowing along the gluon ladders in figs. 1 and 2. Specifically R comes from the integration over its transverse components

$$1/R^2 \propto \int dk_\perp^2\,[F(-k_\perp^2)]^2 \tag{7}$$

and its value depends on exactly how the gluon ladders couple to the proton. If, as is generally assumed, the ladders couple to different partons then the form factor F is characterised by the proton radius, that is $R \cong 5GeV^{-1}$. It has however been argued [7 ,8] that we should include the possibility that the ladders couple to the same constituent of the proton and then it is appropriate to take R to be the radius of a valence quark, that is $R \cong 2GeV^{-1}$. The shadowing effects tame the indefinite increase of the parton distributions leading instead to the parton saturation for suffiently small values of x and/or Q^2. The saturation limit $xg^{sat}(x,Q^2)$

$$xg^{sat}(x,Q^2) \propto Q^2R^2/\alpha_s(Q^2) \tag{8}$$

exhibits the linear scaling violation. Before this limit is reached one should take into account the higher order shadowing terms in the evolution equations. They modify the saturation limit by a factor which is a slowly varying function of x and Q^2 [9].

III. PHENOMENOLOGICAL IMPLEMENTATION OF QCD EXPECTATIONS AND PREDICTIONS FOR HERA, SSC AND LHC EXPERIMENTS.

In order to implement phenomenologically the singular $x^{-1/2}$ type behaviour and screening effects within the QCD evolution formalism we proceed in the following way [2]:

(i) We incorporate the singular behaviour and screening effects in the

parametrisation of the input distributions at the reference scale $Q_0^2 = 4GeV^2$. (We label the "singular" parametrisations as the B_- set of partons while the "non-singular" parametrisations are labelled as B_0).

(ii) We use the QCD evolution equations with the non-linear terms describing parton screening (eqs. 4-6);

(iii) In the region of "large" x ($x \geq 10^{-2}$ or so) we constrain phenomenologically the parton distributions by the available data on deep inelastic lepton-proton scattering and on related processes. As the result of this procedure we are able to produce the parton distributions which are constrained as tightly as possible by present data and which are consistent with the correct theoretical behaviour as $x \Rightarrow 0$. We are also able to examine what aspects of this behaviour can be probed in the future - in particular at HERA. In fig. 3 we show the predictions for the structure function F_2^{ep} for the different sets of partons down to $x = 10^{-4}$ at the representative value $Q^2 = 20\ GeV^2$. The curves correspond to the B_- and B_0 predictions , with strong ($R = 2GeV^{-1}$) and weak ($R = 5GeV^{-1}$) shadowing included for B_-. We can regard fig. 4 as giving a reasonable representation of the spread of the predictions for F_2^{ep} at HERA. In fig.4 we show our predictions for the longitudinal structure function F_L for the same four sets for partons. It may be noticed that F_L is more sensitive to the forms of the input distributions and to the strength of shadowing than the structure function F_2. In fig. 5 we show our predictions for W an Z production in the SSC and LHC energy range.

IV. CONCLUSIONS

To summarise the following points should be emphasised:

(1) Very interesting physics that will be revealed at HERA will be new phenomena at very small x.

(2) For the first time we attempt to incorporate the theoretical QCD expectations (i.e. the singular small x behaviour of parton distributions and parton screening) into the standard QCD pohenomenology of quark and gluon distributions consistent with data in the x - region already probed by experiment.

(3) We find that screening corrections are important yet parton distributions are , in the relevant region of x ($x \geq 10^{-4}$) still significantly smaller than their saturation limit.

(4) Different theoretical scenarios lead to different predictions and the final answer will be given by experiment.

ACKNOWLEDGMENTS.

I thank Jean Tran Thanh Van for his kind invitation to the Moriond meeting and for the traditional warm hospitality.

REFERENCES.

[1] L..V. Gribov, E.M. Levin and M.G. Ryskin, Phys. Rep. 100 (1982) 1.

[2] J. Kwieciński, A.D. Martin, R.G. Roberts and W.J. Stirling, Phys. Rev. D42 (1990) 3645.

[3] Yu.L. Dokshitzer, D.I. Dyakonov and S.I. Troyan, Phys. Rep. 58C (1980) 269.

[4] Ya. Ya. Balitzkij and L.N. Lipatov, Sov. J. Nucl. Phys. 28 (1978) 822; L.N. Lipatov in "Perturbative QCD" (World Scientific) ed. A.. Mueller (1989) p. 411.

[5] L.N. Lipatov, Sov. Phys. JETP 63 (1986) 904; J.C. Collins and J. Kwiecinski, Nucl. Phys. B316 (1989) 307.

[6] J. Kwiecinski, A.D. Martin and P.J. Sutton, Durham Univ. preprint DTP/91/10.

[7] A.H. Mueller and J. Qiu, Nucl. Phys. B268 (1986) 427.

[8] E.M. Levin and M.G. Ryskin, Phys. Rep. 189 (1990) 267.

[9] A.H. Mueller, Nucl. Phys. B335 (1990) 119.

[10] UA2 collaboration: J. Alitti et al., Z.Phys. C47 (1990) 11.

[11] CDF collaboration: presented by P. Derwent at the XXV Rencontre de Moriond, March (1990).

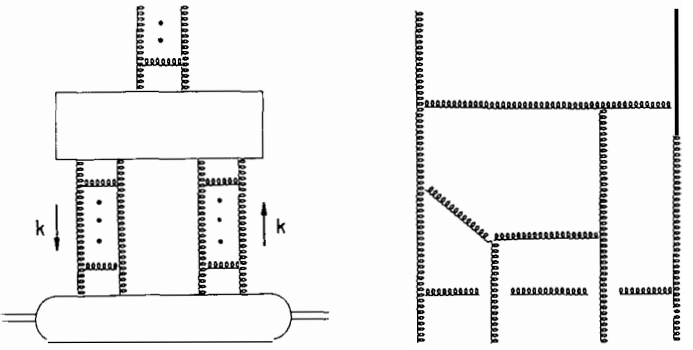

(a) (b)

Fig. 1 (a) Diagrammatic representation of the quadratic shadowing term in the evolution equation (4). The box represents all possible perturbative QCD diagrams which couple 4 gluons to two gluons; an example of one such contribution is shown in (b).

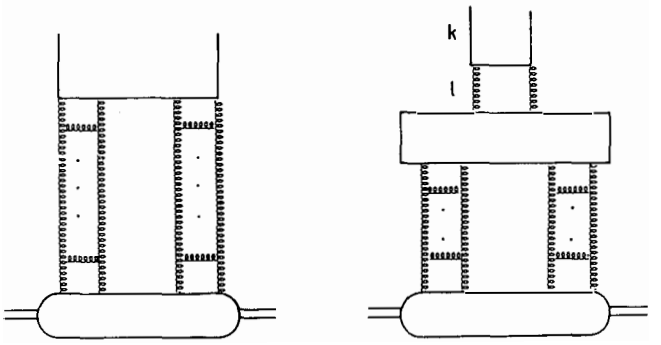

(a) (b)

Fig. 2 Diagrams giving rise to shadowing corrections to the evolution equations ,(5) and (6), for the sea quark distributions.

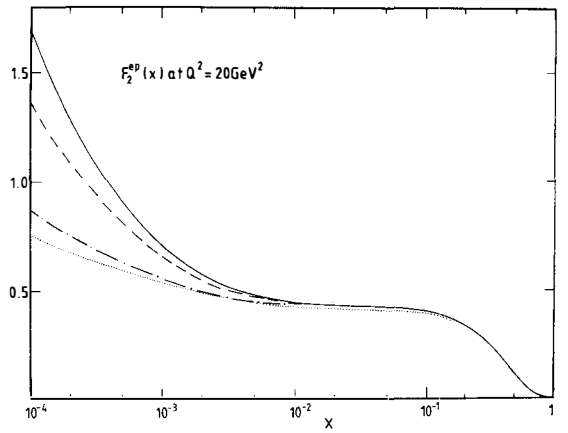

Fig.3 The structure function F_2^{ep} as a function of x at Q^2 = 20 GeV^2. The solid, dashed and dot-dashed lines show the predictions for the B_- set of partons with no shadowing, shadowing with R = 5 GeV^{-1} and R = 2 GeV^{-1} respectively. The dotted line corresponds to the B_0 set.

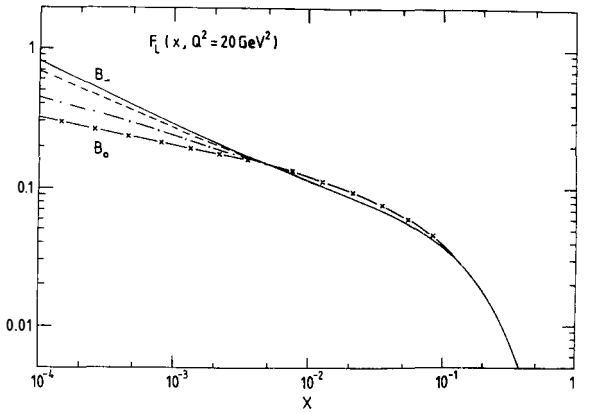

Fig.4 The longitudinal structure function F_L^{ep} as a function of x at Q^2 = 20 GeV^2. The solid, dashed and dot-dashed lines show the predictions for the B_- set of partons with no shadowing, shadowing with R = 5 GeV^{-1} and R = 2 GeV^{-1} respectively. The line with crosses corresponds to the B_0 set.

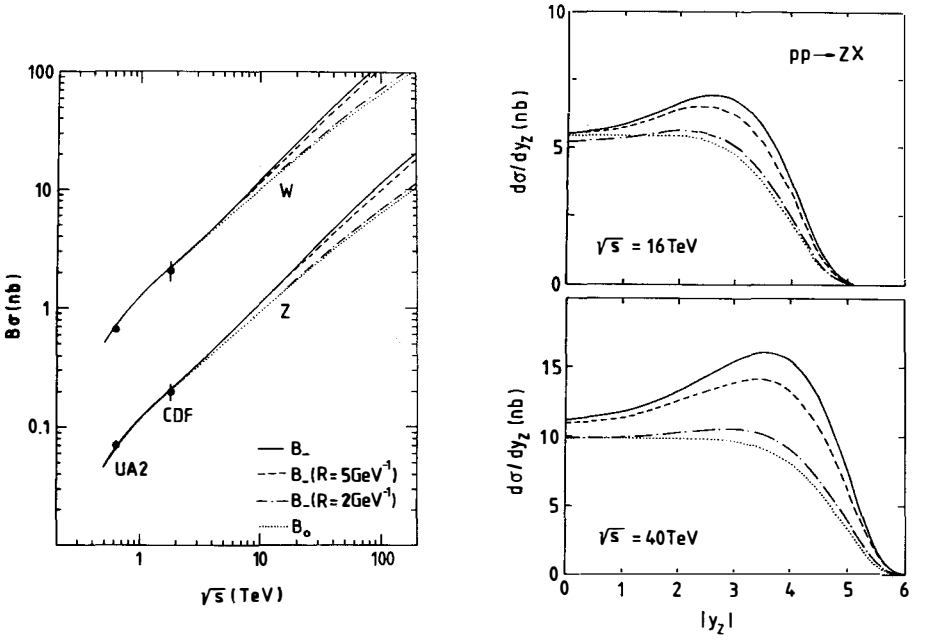

(a) (b)

Fig.5 (a) The W and Z cross sections as a function of the $p\bar{p}$ collider energy, as calculated using B_- (continuous curves) and B_0 (dotted curves) sets of partons. The dashed and dot-dashed curves correspond to the B_- predictions with shadowing corrections with R = 5 and 2 GeV^{-1} respectively. The data points correspond to the measurements of the UA2 [10] and CDF [11] collaboration. At LHC and SSC energies $\sigma_{W,Z}(pp) = \sigma_{W,Z}(p\bar{p})$ to within less than 1%. (b) The rapidity distribution of Z bosons produced in in pp collisions at $\sqrt{s}$ = 16 TeV and $\sqrt{s}$ = 40 TeV respectively. The correspondence between different curves and the sets of partons is the same as in (a).

HADRON-NUCLEUS AND NUCLEUS-NUCLEUS COLLISIONS

Strange and multistrange baryon production in sulphur-tungsten interactions at 200 GeV/c per nucleon

The WA85 Collaboration

S. Abatzis[1], F. Antinori[5], R.P. Barnes[4], M. Benayoun[6], W. Beusch[5], I.J. Bloodworth[4], A. Bravar[7], J.N. Carney[4], B. de la Cruz[5a], D. Di Bari[2], J.P. Dufey[5], D. Evans[4], R. Fini[2], B.R. French[5], B. Ghidini[2], M. Girone[2], H. Helstrup[3], A.K. Holme[3], A. Jacholkowski[5], J. Kahane[6], J.B. Kinson[4], A. Kirk[5], K. Knudson[5], J.C. Lassalle[5], V. Lenti[2], Ph. Leruste[6], L. Lima Frances[6], R.A. Loconsole[2], A. Malamant[6], V. Manzari[2], F. Navach[2], J.L. Narjoux[6], A. Palano[2], A. Penzo[7], E. Quercigh[5], L. Rossi[5b], K. Šafařik[6], M. Sené[6], R. Sené[6], M. Tamazouzt[6], M.T. Trainor[5c], G. Vassiliadis[1], O. Villalobos Baillie[4], A. Volte[6] and M.F. Votruba[4]

1 Athens University, Athens, Greece.
2 Università di Bari and Sezione INFN, Bari, Italy.
3 Universitetet i Bergen, Bergen, Norway.
4 University of Birmingham, Birmingham, U.K.
5 CERN, European Organization for Nuclear Research, Geneva, Switzerland.
6 Collège de France, Paris, France.
7 INFN, Trieste, Italy.

Presented by David Evans
University of Birmingham
Birmingham, U.K.

Abstract

Multi-strange baryon and anti-baryon production is expected to be a useful probe in the search for Quark-Gluon Plasma formation. We present the transverse mass distributions of negative particles, Λs and Ξ^-s produced in sulphur-tungsten interactions at 200 GeV per nucleon and give the fully corrected ratios $\overline{\Lambda}/\Lambda$, Ξ^-/Λ and $\overline{\Xi^-}/\overline{\Lambda}$. We compare our results with published results of $\overline{\Xi^-}/\overline{\Lambda}$ for p p and p $\overline{\text{p}}$ interactions and note that our ratio $\overline{\Xi^-}/\overline{\Lambda}$ appears large in comparison to that from normal hadronic interactions.

[a] On leave from CIEMAT, Madrid, Spain.
[b] Now at INFN, Genoa, Italy.
[c] Now at Oxford University, Oxford, U.K.

Hyperon production is expected to be a useful probe for the dynamics of hadronic matter under the extreme conditions realised in central heavy ion collisions [1]. If a Quark-Gluon Plasma (QGP) is produced during the collisions the hyperon and, in particular, antihyperon yields are expected to be enhanced with respect to normal hadronic interactions and give rise to an anomalously large $\overline{\Xi^-}/\overline{\Lambda}$ ratio [2]. WA85 is the only experiment which has obtained results on the production of cascades in heavy ion interactions. In this paper the m_T distributions for negative particles (mostly pions), Λs and Ξ^-s produced in S W interactions at 200 GeV/c per nucleon are presented. The $\overline{\Lambda}/\Lambda$, Ξ^-/Λ and $\overline{\Xi^-}/\overline{\Lambda}$ ratios, corrected for contamination from Ξ decays are also given.

The WA85 experiment [3] was performed using the CERN Omega Spectrometer with a 200 GeV/c per nucleon beam of ^{32}S ions incident on a tungsten target. The aim is to study strangeness production at $p_T \geq 1$ GeV/c and central rapidity. The Omega multiwire proportional chambers were modified to select only high p_T tracks so that several tracks are recorded out of the several hundred produced in a central collision, making reconstruction of both strange and multi-strange baryons possible in this kinematic region. Figure 1 shows a fully reconstructed event with a cascade candidate where it can be seen that the number of background hits is not excessive. The apparatus and trigger, which select central collisions, have been discussed in a previous publication [4].

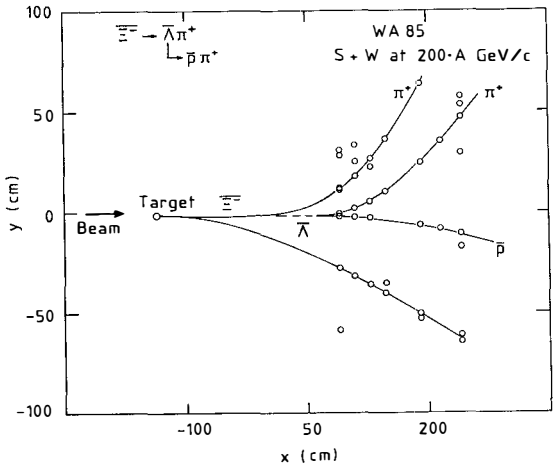

Figure 1: Example of a fully reconstructed event with a cascade candidate

The method of reconstructing $\Lambda^{\dagger}$ [4] and Ξ^- [5] decays has already been explained in previous publications. From the full statistics of our 1987 S W data (10 million triggers) we have 13,307 Λ and 3,407 $\overline{\Lambda}$ candidates and 108 Ξ^- and 44 $\overline{\Xi^-}$ andidates. The phase space window used for Λs and $\overline{\Lambda}$s is $2.3 < y_{lab} < 3.0$ and $0.9 < p_T < 2.8$ GeV/c; for Ξ^-s and $\overline{\Xi^-}$s it is $2.3 < y_{lab} < 3.0$ and $1.1 < p_T < 3.3$GeV/c.

Our Λ and $\overline{\Lambda}$ candidates include K^0_S contamination which is around 7% for Λs and 27% for $\overline{\Lambda}$s. For this study we select only unambiguous decays ($\cos\theta^* < -0.5$)‡ leaving us with 5,856 Λs and 1,138 $\overline{\Lambda}$s. These are then corrected for geometrical acceptance, decays outside the fiducial region, unseen decay modes and reconstruction efficiencies, giving the ratios $\overline{\Xi^-}/\Xi^- = 0.39 \pm 0.07$ and $\overline{\Lambda}/\Lambda = 0.19 \pm 0.01$.

Particles from a thermal source, in a narrow rapidity window, are expected to have a transverse mass distribution given by [6],

$$\frac{1}{m_T}\frac{dN}{dm_T} \sim e^{-\beta m_T} \tag{1}$$

where β is the inverse temperature of the source and m_T the transverse mass ($m_T = \sqrt{p_T^2 + m^2}$). For our study of m_T distributions we choose the rapidity interval $2.4 < y_{lab} < 2.6$ where both Λ and Ξ^- acceptances are good.

The Λ sample need to be corrected for contamination from Ξ^- and Ξ^0 decays because the decay region is far from the target for our experiment [4,5]. This contamination is estimated by Monte-Carlo to be about 8% from Ξ^- decays and about 14% from Ξ^0 decays giving a total contamination $C_\Lambda = 22 \pm 4$ % in our Λ sample.

Figure 2 shows $\frac{1}{m_T}\frac{dN}{dm_T}$ versus m_T for fully corrected negative particles (mostly pions), Λs (corrected for contamination from Ξ decays) and Ξ^-s . Their inverse slopes ($1/\beta$) are given in table 1. These inverse slopes also have a systematic error estimated by simulation to be about $\pm$ 13 MeV.

We note from figure 2 that all the slopes are similar and that the number of Λs at a given m_T is greater than the number of negative particles. From figure 2 we can also deduce the ratio Ξ^-/Λ at a given m_T ; at $m_T = 2$ GeV the ratio $\Xi^-/\Lambda = 0.20 \pm 0.04$.

Although our statistics for $\overline{\Xi^-}$s in this narrow y_{lab} window are too small to plot their m_T distribution we can estimate the $\overline{\Xi^-}/\overline{\Lambda}$ ratio. Using the contamination of Λs from Ξ decays

†We use the notation Λ for $\Lambda + \Sigma^0$.

‡where θ^* is defined as the angle between the flight of the V^0 and the positive decay particle in the V^0 rest frame.

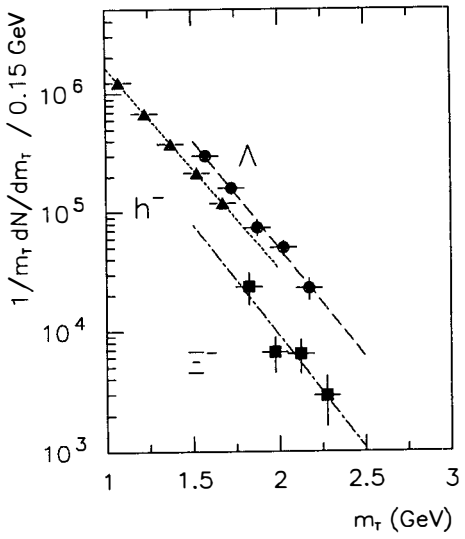

Figure 2: $\frac{1}{m_T}\frac{dN}{dm_T}$ vs m_T for negative particles (h^-), mostly π^-s, Λs and Ξ^-s

(C_Λ) and our measured ratios $\overline{\Lambda}/\Lambda$ and $\overline{\Xi^-}/\Xi^-$ (R_Λ and R_Ξ respectively), the contamination of $\overline{\Lambda}$s from $\overline{\Xi}$ decays will be

$$C_{\overline{\Lambda}} = \frac{R_\Xi}{R_\Lambda} \times C_\Lambda = \frac{0.39}{0.19} \times 22\% = 45 \pm 12\ \%$$

The true $\overline{\Lambda}/\Lambda$ ratio, $R_{\Lambda\ (true)}$ will therefore be

$$R_{\Lambda\ (true)} = R_\Lambda \times \left(\frac{1 - C_{\overline{\Lambda}}}{1 - C_\Lambda}\right) = 0.13 \pm 0.03$$

Table 1: Inverse slopes ($1/\beta$) for different particles from figure 2.

Particle	inverse slope (MeV)	statistical error
negative	256	± 3
Λ	238	± 9
Ξ^-	233	± 54

and the ratio $\overline{\Xi^-}/\overline{\Lambda}$ is

$$\frac{\overline{\Xi^-}}{\overline{\Lambda}} = \frac{R_\Xi}{R_\Lambda \text{ (true)}} \times \frac{\Xi^-}{\Lambda} = 0.6 \pm 0.2$$

The ratios Ξ^-/Λ and $\overline{\Xi^-}/\overline{\Lambda}$ have been measured in p p [8] and $\bar{p}$ p [9] interactions. These results are for Ξ^- and Λ production in the same (or similar) p_T range, so in order to compare our results directly we must consider our ratios for a given p_T (not m_T). If we consider our ratios for a p_T of 1.66 GeV/c (corresponding to an m_T of 2 GeV for Λs) we may then compare our results directly to those for other interactions. Table 2 shows our results together with those from p p collisions at 63 GeV [8] and $\bar{p}$ p collisions at 900 GeV [9].

Table 2: The ratios Ξ^-/Λ and $\overline{\Xi^-}/\overline{\Lambda}$ in the region $2.4 < y_{lab} < 2.6$ and $p_T = 1.66$ GeV/c for central S W interactions. Also given are p p data at 63 GeV [8] and $\bar{p}$ p data at 900 GeV [9].

Exp.	int.	$\sqrt{s}$ (GeV)	p_T (GeV/c)	Ξ^-/Λ	$\overline{\Xi^-}/\overline{\Lambda}$
WA85	S W	19	1.66	0.11 ± 0.02	0.33 ± 0.11
AFS	p p	63	1-2		0.06 ± 0.02
UA5	$\bar{p}$ p	900	> 1	$0.07\ ^{+0.08}_{-0.04}$	

Contamination from Ξ decays in these experiments is negligible because of the short decay distances of their hyperons.

As can be seen from table 2, our ratio Ξ^-/Λ is compatible with that from $\bar{p}$ p interactions. However, the ratio $\overline{\Xi^-}/\overline{\Lambda}$ is 5.5 times greater than that quoted by the AFS collaboration; this corresponds to a two standard deviation effect with the current statistics.

In conclusion, we show that the m_T distributions of negative particles (mostly pions), Λs and Ξ^-s are well described by the function $\frac{1}{m_T}\frac{dN}{dm_T} \sim e^{-\beta m_T}$ and yield a value of $1/\beta$ consistent with 250 MeV as given in table 1.

In table 3 we summarise the ratios obtained in this paper and our previous publications [5]. We note that our ratios are high in comparison to normal hadronic interactions; however, such high ratios have been predicted in sudden hadronisation QGP models [2].

Table 3: Summary of ratios from WA85

Ratio	m_T = 2 GeV	p_T = 1.66 GeV/c
$\overline{\Lambda}/\Lambda$	0.13 ± 0.03	0.13 ± 0.03
$\overline{\Xi^-}/\Xi^-$	0.39 ± 0.07	0.39 ± 0.07
Ξ^-/Λ	0.20 ± 0.04	0.11 ± 0.02
$\overline{\Xi^-}/\overline{\Lambda}$	0.60 ± 0.20	0.33 ± 0.11

References

[1] J. Rafelski and B. Müller, Phys. Rev. Lett. 48 (1982) 1066; 56 (1986) 2334 (E).
P. Koch, B. Müller, and J. Rafelski, Phys. Rep. 142 (1986) 167.
J. Ellis and U. Heinz, Phys. Lett. B 233 (1989) 223.

[2] J. Rafelski, AZPH-TH/91-11 (1991), submitted to Phys. Lett. B.

[3] WA85 Proposal, A. Apostolakis et al., CERN/SPSC 84-76, SPSC/P206 (1984)
and CERN/SPSC 87-18, SPSC/P206 Add.1 (1987).

[4] The WA85 Collaboration, S. Abatzis et al., Phys. Lett. B 244 (1990) 130.

[5] The WA85 Collaboration, S. Abatzis et al., Quark Matter 90, presented by D. Evans.
The WA85 Collaboration, S. Abatzis et al., to be published in Phys. Lett. B.

[6] J. Rafelski, GSI-90-37 July 1990.

[7] The WA85 Collaboration, S. Abatzis et al., Quark Matter 90, presented by J. L. Narjoux.

[8] AFS Coll., T. Åkesson et al., Nucl. Phys. B246 (1984) 1-11.

[9] UA5 Coll., R. E. Ansorge et al., CERN-EP/89-41.

PRODUCTION OF CHARGED KAONS IN CENTRAL S+S COLLISIONS AT 200 GEV/NUCLEON

M. Kowalski
Max-Planck-Institut für Physik, München, Germany
and Institute of Nuclear Physics, Cracow, Poland
NA35 Collaboration

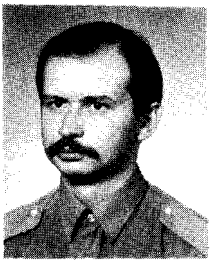

Abstract:
Production of charged kaons in central S+S interactions at 200 GeV/nucleon has been studied in the NA35 Streamer Chamber experiment. The mean multiplicities were obtained. Results are compared with data from elementary collisions and with model predictions.

One of the first predicted signatures of the deconfined phase of strongly interacting matter was an enhancement of the s and $\bar{s}$ quark concentration in a quark gluon plasma[1]. Therefore it is of great interest to study the production of strange particles in collisions of nuclei at relativistic energies. Here we present preliminary results on the production of charged kaons in central (2 % of σ_{tot}) S+S collisions at 200 GeV/nucleon obtained by the NA35 collaboration. The detailed experimental setup was already shown elsewhere[2]. The data presented here come from the 2 m streamer chamber placed in the magnetic field of 1.5 T. The trigger selected events in which the remaining energy in the projectile fragmentation domain, $\theta_{lab} < 0.3°$, was less than 1.4 TeV.

The events were scanned for 2-body decays with one charged and one neutral secondary (kink topology) and 3-body decays into charged secondaries (τ topology). These decays were measured and run through a kinematical fit. The contamination of the kaon sample by 2-body decays of charged hyperons and by the decays of kaons into 1 charged and 2 neutral secondaries was found to be negligible (< 0.5 %). The contamination coming from decays and elastic scatterings of pions was found to be equal to 6 % and 11 % for positive and negative kaons respectively, and the appropriate corrections were applied to the data. Due to scanning losses of 2-body decays with small decay angle, a cut of $\theta_{decay} > 2°$ had to be applied and was taken into account by corresponding corrections. Our data do not cover the full phase space due to systematical losses in scanning in the region with a large track density around the beam. The final bias free sample consists of 347 K^+ and 171 K^- within $0.6 < y < 2.4$ and $p_T < 1.1$ GeV/c. We remark that charged kaons cover the low p_T domain, not available for K°_s studies in our experiment[3].

Fig. 1 shows the comparison of the transverse mass distributions for neutral and charged kaons. Because of the isospin symmetry one expects that $K^+ + K^- \simeq 2 \cdot K^\circ_s$, if the corresponding rapidity distributions are not very different. This expectation is very well confirmed by our data, which proves the consistency of our analysis. Fig. 2 and 3 show the transverse mass distributions for K^+ and K^- respectively compared with predictions of the FRITIOF[4] and the VENUS[5] model. The spectra show an exponential behaviour and the corresponding values of slopes are presented in Table 1. One can conclude that VENUS describes our data relatively well, however the experimental distribution for K^- seems to be flatter (with a significant error margin). The FRITIOF model disagrees with the data. The symmetry of the colliding system al-

lows us to calculate K^+ and K^- multiplicities in full 4 π phase space. In Table 2 we present the results and compare them with models and with data from nucleon-nucleon collisions[6]. One can see an increase of the K^+/π^+ ratio as compared to N+N collisions, while there is no such increase for K^-/π^-.

The charged kaon multiplicity ($\langle K^+\rangle + \langle K^-\rangle$) agrees, as expected, with the K° multiplicity [3]. The K/π ratios as well as the mean multiplicities are better reproduced by VENUS than by FRITIOF.

Summarizing, we present new data on strangeness production in central S+S collisions at 200 GeV/nucleon. The increase of the K^+ multiplicity together with the corresponding increase of the Λ yield[3] suggests the associated production mechanism as the dominant source of the strangeness enhancement. The VENUS model seems to reproduce our data better than FRITIOF.

Table 1
Slopes of the transverse mass distributions within rapidity range 0.6 - 2.4

	K^+	K^-
Data	- 4.7 ± 0.4	- 4.0 ± 0.9
VENUS	- 5.2 ± 0.1	- 5.5 ± 0.1
FRITIOF	- 6.8 ± 0.1	- 6.2 ± 0.1

Table 2
Results on multiplicities of K^+ and K^-

	$\langle K^+\rangle$	$\langle K^-\rangle$	$\frac{\langle K^+\rangle}{\langle \pi^+\rangle}$	$\frac{\langle K^-\rangle}{\langle \pi^-\rangle}$	$\frac{\langle K^+\rangle}{\langle K^-\rangle}$
Data	11.8 ± 0.8	6.6 ± 0.8	13 ± 1 %	7 ± 1 %	1.8 ± 0.2
VENUS	10.57	7.48	11.7 %	8.3 %	1.41
FRITIOF	9.35	7.02	10.2 %	7.7 %	1.33
N+N	0.24 ± 0.06	0.17 ± 0.05	8 ± 1 %	6 ± 1 %	1.42

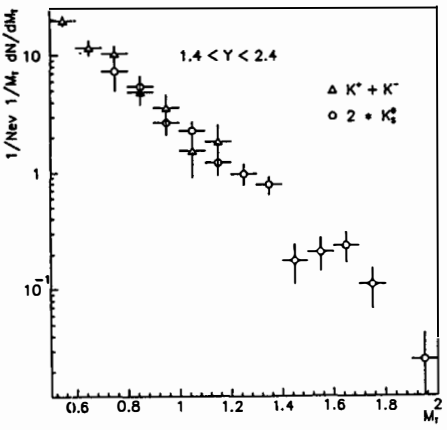

Fig. 1 Transverse mass distribution for neutral and sum of charged kaons in the common rapidity domain

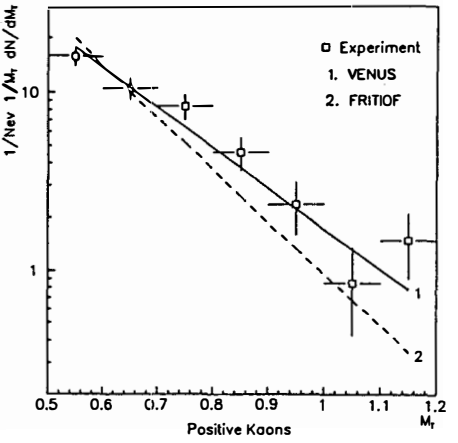

Fig. 2 Transverse mass distribution for positive kaons

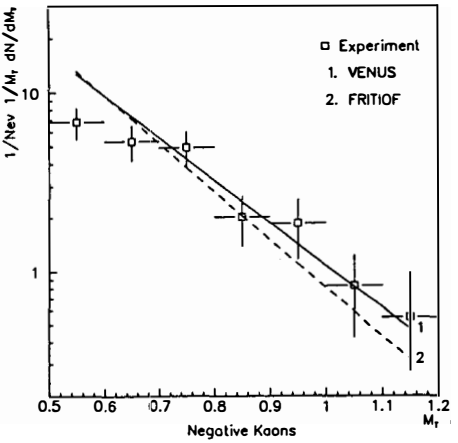

Fig. 3 Transverse mass distribution for negative kaons

REFERENCES

1. P. Koch, B. Müller, J. Rafelski; Phys. Rep. **142** (1986) 321
2. A. Bamberger et al.; Phys. Lett. **B184** (1987) 271
3. J. Bartke et al.; Z. Phys. **C48** (1990) 191
4. K. Werner; Phys. Rev. Lett. **62** (1989) 2460 (version 3.07)
5. B. Anderson et al.; Nucl. Phys. **B281** (1987) 289 (version 1.6)
6. M. Gaździcki, O. Hansen, BNL-43601 (1989)

STRANGENESS ENHANCEMENT IN RELATIVISTIC NUCLEAR COLLISIONS†

Frédérique Grassi
Instituto de Física-Departamento de Física Matemática, Universidade de São Paulo
C.P.20516, 01498 São Paulo- SP, Brazil
and
Henning Heiselberg
Department of Physics, University of Illinois at Urbana-Champaign
1110 W. Green St., Urbana, IL 61801, U.S.A.

ABSTRACT

Enhanced strangeness production in nuclear collisions has been proposed as a possible signature of quark-gluon plasma formation: in particular, the ϕ production might increase. We find however that the observed enhancement of the $\phi/(\rho_o + \omega)$ ratio observed in relativistic heavy ion collisions at CERN, might be due to the smaller size of the ϕ absorption cross section and that the enhancement of the ϕ to continuum ratio could be an artifact of the p_t cutoff applied to the data.

†Presented by F.Grassi

1. Why strangeness enhancement ?

Since the topic of strangeness enhancement is perhaps not very familiar to everyone, I will start with a very short discussion of the theoretical and experimental situations.

Enhanced strangeness production has been proposed as a possible signature of quark-gluon plasma (QGP) formation. To understand this [1, 2], let us first consider the production of strange hadrons in proton-proton collisions. As protons contain no s quarks, strange particles are produced in association with an antistrange-particle. For example

$$pp \longrightarrow p\Lambda K^+ \quad (1)$$

$$pp \longrightarrow pp\Lambda\bar{\Lambda} \quad (2)$$

$$pp \longrightarrow ppp\bar{\Lambda}K^- \quad (3)$$

The threshold energy for the first reaction is $M_\Lambda - M_p + M_K \sim 0.7$ GeV in the p-p center-of-mass system. In the same way, the threshold energy for the second reaction is 2.2GeV and for the third 2.5 GeV. In contrast, in QGP (with partially restored chiral symmetry), the threshold for strangeness creation is $2m_s \sim$ 300-400 MeV. Therefore, it is expected that strangeness is easier to create in QGP than in pp collisions.

In fact, strangeness is also higher in a thermally and chemically equilibrated hadronic gas than in pp collisions. However the approach to chemical equilibrium in that case is slow and it is thought that not enough time is available for strangeness to build up. Therefore, strangeness enhancement remains a possible signature of QGP formation.

2. Experimental results

Results on strange particle production have been obtained by various collaborations at the A.G.S. in Brookhaven and the S.P.S. at Cern. Table 1 contains a summary of these experiments and their results (see e.g. [3] and [4] for more details).

Table 1: Summary of results on strangeness production in heavy ion collisions.

Place	Collab.	Nuclei	Results on strangeness prod.	Exp. and theor. ref.
BNL E=14.5 GeV A	E802	Si+Au	-$K^+/\pi^+ > K^+/\pi^+_{pp}$ $K^-/\pi^- > K^-/\pi^-_{pp}$ -K/π increses with $p_\perp$	E:[5] T: [6, 7, 8, 9, 10, 11]
	(E810)			
CERN E=200 GeV A	NA34	S+W	- no excess of K/π low $p_\perp$ data central events not selected	ET:[3]
	NA35	O+Au	- K^0_s/h^-,Λ/h^-,Λ equal to pAu	E:[12]
		S+S	- K^0_s/h^-,Λ/h^-,$\Lambda \sim 2\times$ pS - K^+, K^- not enhanced?	T:[13] E:[14]
	(NA36)			
	NA38	O+U,S+U	- no excess of K/π - $\phi/cont.$ increases with E_t	E:[15] E:[16] T:[17, 18]
	WA85	S+W	- $\Lambda/mult.$, $\Lambda/mult.$ cst with mult. - $\bar{\Lambda}/\Lambda$ equal to pW but $\bar{\Xi}^-/\Xi^- >$.	E:[19], [20]

As can be seen the experimental situation is not very clear with some collaborations obtaining an enhancement and others none. There is a clear need for more experimental data and more theoretical reflection to unify these findings.

3. ϕ-enhancement of NA38

In this section, I present a possible explaination of the ϕ enhancement seen by NA38. This collaboration studies [16] the ϕ and $\rho_0+\omega$ production in relativistic heavy ion collisions. They detect dimuons coming from 1) resonance decays, e.g., $\phi \rightarrow \mu^+\mu^-$, 2) continuum processes, e.g., $q\bar{q} \rightarrow \mu^+\mu^-$ (Drell-Yan) (continuum is designated thereafter by c) and 3) background, e.g. $\pi^\pm\pi^\pm \rightarrow \mu^\pm\mu^\pm$. To reduce the background, which is very important at low invariant mass, cutoffs are introduced: only muon pairs with $p_t > p_t^{cut}$ GeV and $p_z > p_z^{cut}$ GeV are kept. Two different sets of cutoffs were used: p_t^{cut}=1.3 GeV and p_z^{cut}=26 GeV or p_t^{cut}=1.1 GeV and p_z^{cut}=19 GeV. The background muon pairs are then eliminated from the signal (resonances and continuum) by doing:

$$N_{signal}(\mu^+\mu^-) = N(\mu^+\mu^-) - 2\sqrt{N(\mu^+\mu^+)N(\mu^-\mu^-)}. \quad (4)$$

It is found that the ratios $\phi/(\rho_0+\omega)$ and ϕ/c increase with the transverse energy, E_t, respectively by a factor ~ 2 and $1.5-2.5$ while $(\rho_0+\omega)/c$ remains approximatively constant (see fig. 1a-c). Given that higher E_t's are expected to correspond to more central collisions and higher particle densities, these observations could signal the appearance of a quark-gluon phase.

As of today there exist however two non-plasma explainations of these results. Koch et al. [17] suppose that $(\rho_0+\omega)/c$ is flat with E_t because these particles are in chemical equilibrium in the hot hadronic gas. With some additional approximations, they are able to reproduce the shape of $\phi/(\rho_0+\omega)$ as a function of E_t, which means that production of ϕ's in secondary collisions in the hot hadronic gas overcomes their absorption. In contrast, the approach developped by H.Heiselberg and myself [18] starts from the remark that high p_t massive particles must be hard to create in secondary collisions in the hot hadronic gas but can be absorbed. The increase of $\phi/(\rho_0+\omega)$ then follows from the fact that the absorption cross section of the ϕ is smaller than that of the ρ_0 or ω.

We are also able to reproduce the ϕ/c and $(\rho_0+\omega)/c$) data (not done in [17]). The increase of ϕ/c comes from the following fact. A cutoff in transverse momentum is applied to the data, i.e. only vector mesons with momentum greater that p_t^{cut} are recorded. On the other side, it is known that for light particles, the transverse momentum distribution flattens as E_t increases (this is the so-called Cronin effect. See for exemple in this conference proceedings, the NA38 data about $\pi + K$ [21]) so they are more and more particles above the cutoff as E_t increases. [1] This causes an artificial increase in the yields. For the ϕ, absorption is small and may be overcome by this increase; for the $\rho_0+\omega$, absorption is higher and may be balanced by the increase. In [18], we developed a more detailed model to reproduce the experimental data. Here I will just show in order of magnitude that the two mecanisms identified above (absorption and increase due to cutoff) are efficient enough to reproduce the experimental data.

The vector mesons V (where V=$\phi, \rho_0+\omega$) are embedded in a gas of average particle density $\bar{\rho}$ from an initial time t_0 to a final (average) time t_f. Neglecting the production of V mesons

[1] The slope of the continuum stays approximatey constant with increasing E_t (see for exemple NA38 data in this proceedings [22]) and no cutoff is applied to the continuum. For particles created in hard processes such as the J/Ψ, there is also an increase of $\langle p_t \rangle$ with E_t but it is not experimentally clear that it also corresponds to a flattening of the transverse momentum distribution [22]. It cannot be excluded that this is also the case for high transverse mass vector mesons.

and expansion, the rate of change of the density of V's is

$$\frac{d\rho_V}{dt} \sim \sigma_{abs}^V \times \bar{\rho} \times \rho_V \tag{5}$$

so

$$\frac{N_\phi(t_f)}{N_{\rho_0+\omega}(t_f)} \sim \frac{N_\phi(t_0)}{N_{\rho_0+\omega}(t_0)} \exp[\bar{\rho}(\sigma_{abs}^{\rho_0,\omega} - \sigma_{abs}^\phi)(t_f - t_0)] \tag{6}$$

Inserting the assumptions $\bar{\rho} \simeq \rho_{nucl.matt.} = 0.17$ fm^{-3} and $t_f - t_0 \simeq R/c_s \simeq 5$ fm (if c_s, the sound speed, is $\sim c/\sqrt{3}$ and R is the oxygen radius), one sees that the ϕ production compared to that of $\rho_0 + \omega$ is enhanced by a factor 3-8, when going from peripheral collisions where no absorption is expected ($N_\phi(t_f)/N_{\rho_0+\omega}(t_f) \sim N_\phi(t_0)/N_{\rho_0+\omega}(t_0)$) to central ones, provided that the initial production ratio $N_\phi(t_0)/N_{\rho_0+\omega}(t_0)$ does not change with centrality or E_t. This increase is consistent with the NA38 data described above.

To calculate the effect of the cutoff, we parametrize the p_t-distribution as $dN/dp_t^2 \propto \exp(-\beta m_t)$, where m_t is the transverse mass of the particle with mass m. The slope parameter β decreases with increasing A in pA collisions or E_t in A-B collisions. Since the cutoff was applied to the p-U data but not to the continuum, we obtain (neglecting absorption)

$$\frac{N_V}{N_c} = \frac{N_V^{pU}}{N_c^{pU}} \exp[(\beta^{pU} - \beta(E_t))(m_t^{cut} - m)] \tag{7}$$

From NA38 J/Ψ data, one gets $\Delta\beta \sim 1.50 \pm 0.25$ GeV^{-1}. From their $K + \pi$ data, one gets $\Delta\beta \sim 0.33$ GeV^{-1}. Therefore we expect the V/c ratio to be enhanced by a factor $\sim$ 1.2-3.6 when going from peripheral to central collisions. This enhancement may be enough to explain the NA38 data for ϕ/c, for which absorption is small. The observed $(\rho_0 + \omega)/c$ ratio however is almost constant. This is understandable since absorption in that case is important, so should be included in eq. (7) and, as alredy mentioned, may balance the enhancement due to the p_t cutoff.

In summary, though other effects might be at work, absorption in nuclear matter (which decreases N_V with E_t) plus Cronin effect (which increases N_V with E_t above some p_t cutoff) may explain the NA38 data. (No strangeness enhancement is needed and indeed we expect the creation of high p_t massive mesons at midrapidity in secondary collisions to be rare.) One possible way to know whether there is a Cronin effect in the momentum distribution of the observed vector mesons would be to plot ϕ/c in a high E_t bin divided by the same quantity in a low E_t bin (at some value of the cutoff) as a function of the cutoff. If absorption is small, this ratio should increase. This is currently being investigated [23]. If indeed there is a cutoff effect in the data, it should be removed before one can really talk of strangeness enhancement. This may be tricky to do so a more promising line of work would be to extract data without p_t cutoff. This is also currently under investigation [23].

This work was supported in part by N.S.F. grant PHY 84-15064 in the U.S.A. and F.A.P.E.S.P. in Brazil.

REFERENCES

[1] B.Müller. "The Physics of Quark-Gluon Plasma", Springer-Verlag (1985).
[2] P.Koch, B.Müller, and J.Rafelski. Phys.Rep. 142 (1986) 1.
[3] R.A.Salmeron. Lecture at the Winter School on Quark-Gluon Plasma, Puri, Orissa, India, 5-16 December 1989.
[4] H.C.Eggers and J.Rafelski. Preprint AZPH-TH/90-28.
[5] T.Abbott and others (E802). Z.Phys.C 38 (1988) 135; Nucl. Phys. A 498 (1989) 67c; Phys. Rev. Lett. **64** (1990) 847.
[6] J.Cleymans, H.Satz, E.Suhonen, and D.W. von Oertzen. Phys. Lett. B242 (1990) 111.
[7] P.Lévai, B.Lukács, and J.Zimányi. Preprint KFKI-1989-47/A, Budapest.
[8] U.Heinz, P.Koch, E.Schnedermann, and H.Weigert. Preprint TPR-90-31, to appear in: "Phase Structure of Strongly Interacting Matter", Springer-Verlag, Lecture Notes in Physics.
[9] H.W. Barz, B.L. Friman, J.Knoll, and H.Schulz. Nucl. Phys. A498 (1989) 161c; To appear in Nucl. Phys. A.
[10] C.M. Ko and L.Xia. Nucl. Phys.Lett. A498 (1989) 561c.
[11] R.Matiello, H.Sorge, H.Stöcker, and W.Greiner. Phys. Rev. Lett. 63 (1989) 1459.
[12] A.Bamberger etal. (NA35) Z.Phys.C 43 (1989) 25; Nucl.Phys.A498 (1989) 375c; preprint IKF90-2; contribution in the Proceedings of the International Quark Matter Conference, Menton 90.
[13] F.Grassi and Y.Hama. Work in progress.
[14] M.Kowalski (NA35). Proceedings of the Rencontres de Moriond, Les Arcs, France (1991).
[15] M.C.Abreu etal. (NA38) Z.Phys.C 38 (1988) 129; Nucl.Phys.A498 (1989) 249c.
[16] M.C.Abreu etal. (NA38). To appear in the Proceedings of the International Europhysics Conference on High Energy Physics, Madrid 89; to appear in the Proceedings of the XXVth "Rencontres de Morond", Les Arcs 90; to appear in the Proceedings of the International Quark Matter Conference, Menton 90; A.Baldisseri Ph.D. Thesis, May 90.
[17] P.Koch, U.Heinz, and J.Pišút. Phys.Lett. B243 (1990) 149; Z.Phys.C 47 (1990) 477.
[18] F.Grassi and H.Heiselberg. Submitted to Phys.Lett.B.
[19] S.Abatzis etal. (WA85). Phys. Lett.B244 (1990) 130.
[20] D.Evans (WA85). Proceedings of the Rencontres de Moriond, Les Arcs, France (1991).
[21] L.Peralta (NA38). Proceedings of the Rencontres de Moriond, Les Arcs, France (1991).
[22] O.Drapier (NA38). Proceedings of the Rencontres de Moriond, Les Arcs, France (1991).
[23] C.Gershel and D.Jouan (NA38). Private communication.

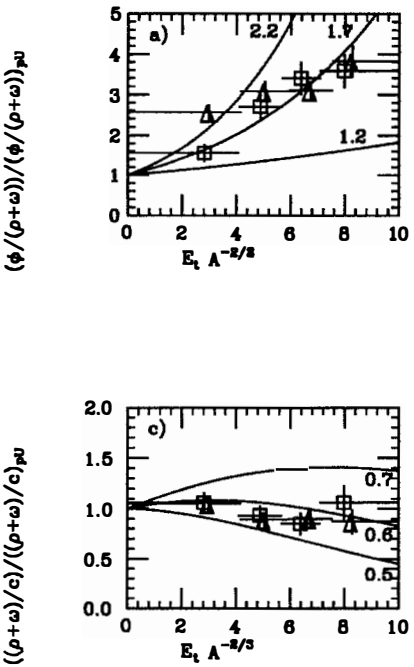

Fig. 1a–c: NA38 data for O+U (squa es) and S+U (triangles) Theoretical fits from [18].

MESON PRODUCTION IN p+U, O+U AND S+U INTERACTIONS AT 200 GeV/NUCLEON

NA38 Collaboration

M.C. Abreu[5], M. Alimi[6], C. Baglin[1], A. Baldisseri[1], A. Baldit[3], M. Bedjidian[6], P. Bordalo[5], A. Bussière[1], P. Busson[4], R. Cases[9], J. Castor[3], T. Chambon[3], C. Charlot[4], B. Chaurand[4], D. Contardo[6], E. Descroix[6], A. Devaux[3], O. Drapier[6], J. Fargeix[3], X. Felgeyrolles[3], R. Ferreira[5], P. Force[3], L. Fredj[3], J.M. Gago[5], C. Gershel[7], P. Gorodetzky[8], B. Grosdidier[8], J.Y. Grossiord[6], A. Guichard[6], J.P. Guillaud[1], R. Haroutunian[6], D. Jouan[7], L. Kluberg[4], R. Kossakowski[1], G. Landaud[3], P. Liaud[1], C. Lourenço[5], S. Papillon[7], L. Peralta[5], J.R. Pizzi[6], C. Racca[8], S. Ramos[5], A. Romana[4], R.A. Salmeron[4], P. Sonderegger[2], F. Staley[1], S. Silva[5], X. Tarrago[7], J. Varela[5], F. Vazeille[3]

(1)-Annecy, (2)-CERN, (3)-Clermont-Ferrand, (4)-Ecole Polytechnique, (5)-Lisbon, (6)-Lyon, (7)-Orsay, (8)-Strasbourg, (9)-Valencia

Presented by Luis Peralta

LIP - Av. Elias Garcia 14 - 1, P-1000 Lisboa, Portugal

Abstract

Meson production in proton, oxygen and sulphur interactions with uranium targets at 200 GeV/nucleon is studied, using like-sign decay muons. We measure the inclusive positive and negative meson cross sections $d\sigma/dP_T^2$ and study their evolution with the projectile mass assuming a $A_{proj}^{\alpha(P_T)}$ dependence. Unlike negative mesons, the $\alpha(P_T)$ parameter shows no P_T dependence for positive mesons in the range 0.4 to 3.0 GeV/c. Cross sections fitted to an exponential, give an inverse slope P_{T0} of the order of 210 MeV/c. As a function of the neutral transverse energy, P_{T0} values show a sligth rise followed by a plateau. The difference between positive and negative kaons is studied as a function of transverse energy, in O+U and S+U collisions.

An important fraction of the NA38 data arises from uncorrelated π and K decays which generate both opposite-sign and like-sign muon pairs. This like-sign muon pair sample can be unambiguously traced back to π and K decays. A strong correlation in P_T exists between the parent meson and its decay muon [1]. Therefore, it is possible to extract meson distributions from the measured muon ones. Morever, like-sign muon pairs are almost background free, as the contribution from correlated decays is found to be less than 1% .

The muon pairs are measured in the NA10 spectrometer [2], optimized to detect low mass dimuons. An electromagnetic calorimeter [3] provides a measurement of the transverse neutral energy E_T released in the interaction ($1.9 < \eta_{lab} < 4.1$). A more complete description of the experimental setup can be found elsewhere [4,5].

As only decay muons are measured, the meson production cross section must be computed in two steps: in first place a muon yield is extracted and afterwards the meson cross section is calculated using a Monte Carlo simulation based on the Fritiof Lund generator [6]. In this way, we study inclusive meson production in proton, oxygen and sulphur interactions and compare them to previous pN results.

Table 1: P_{T0} values (in MeV/c) from a fit in the range $0.7 \leq P_T \leq 1.4$ GeV/c

Charge	$p+U$	$O+U$	$S+U$
+	209± 3	213±2	211±2
−	199± 3	203±2	211±2

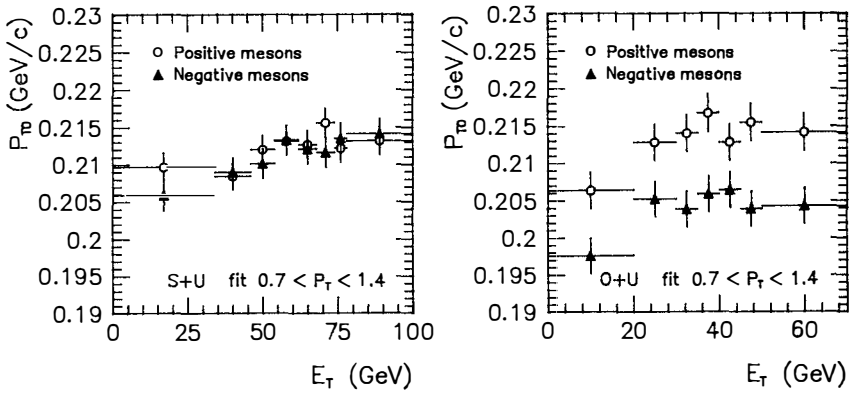

Figure 1: Inverse slope P_{T0} as a function of E_T for positive and negative mesons in S+U and O+U collisions

A fit to the differential cross section using the parametrization

$$\frac{d\sigma}{dP_T^2} \propto exp\left(-\frac{P_T}{P_{T0}}\right)$$

is performed in the range 0.7 to 1.4 GeV/c. P_{T0} values range from 199 to 213 MeV/c (see table 1) and are close to some QCD predictions on the lattice for the transition temperature between hadron and plasma phases [7,8]. A small rise in P_{T0} with the projectile mass is also measured. Positive particle P_{T0} values are systematically above the negative particle ones. This could be attributed to kaons having a higher P_{T0} as compared to pions, as well as the fact that $K^+/\pi^+ > K^-/\pi^-$ [9].

The same analysis can be performed in different E_T regions. Figure 1 shows the behaviour of P_{T0} as a function of the transverse energy E_T, for S+U and O+U systems, and for both charges. A slight increase with E_T, followed by a plateau is seen. The same picture has already been reported by other heavy ion experiments [10,11].

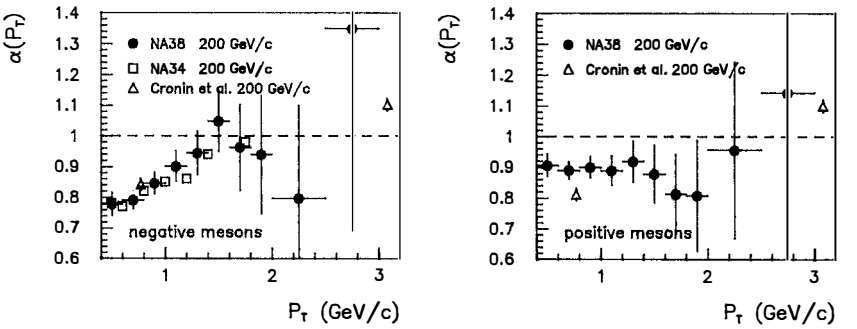

Figure 2: The $\alpha(P_T)$ parameter for negative and positive mesons, measured in S+U and O+U interactions

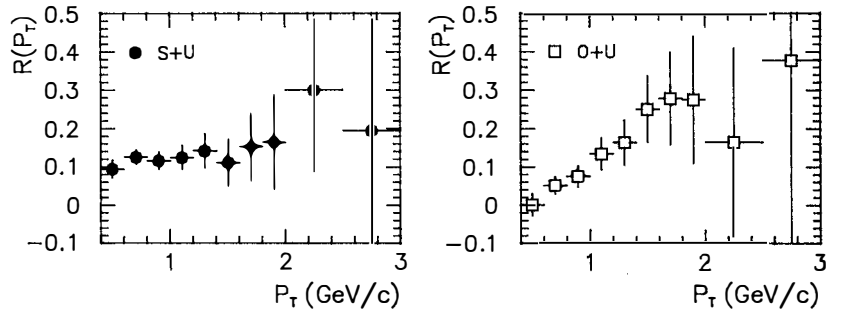

Figure 3: The ratio $R(P_T)$ for S+U and O+U collisions

We study the evolution of the differential production cross section with the projectile mass A assuming a power law dependence $\left(d\sigma/dP_T^2\right)_{AB} \propto A^{\alpha(P_T)}$. The variation of α as a function of P_T taking into consideration only the ion data (O+U and S+U interactions) is shown in fig. 2. For negative mesons $\alpha(P_T)$ increases with P_T (Cronin effect [12]). The measured values are compatible with the ones obtained by other experiments [11,12]. For positive mesons $\alpha(P_T)$ shows no P_T dependence in the measured range.

Information on K production can be extracted from the normalized difference between positive and negative meson cross sections $(\sigma^+ - \sigma^-)/\sigma^-$. Assuming that, for O+U and S+U interactions, π^+ and π^- production rates are equal in the central rapidity region, we have:

$$R = \frac{\sigma^+ - \sigma^-}{\sigma^-} \equiv \frac{(\pi^+ + K^+) - (\pi^- + K^-)}{(\pi^- + K^-)} \approx \frac{K^+ - K^-}{\pi^- + K^-} \ .$$

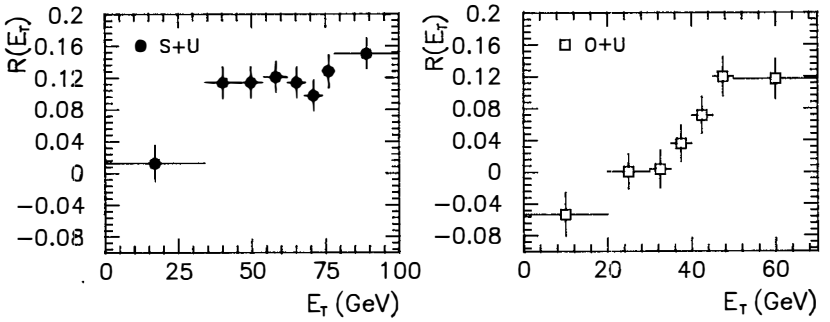

Figure 4: The ratio $R(E_T)$ for S+U and O+U collisions

The ratio R as a function of P_T is showed in fig. 3 for S+U and O+U collisions. A rise with P_T is observed for both systems. This shows an increase in the K^+/π production in comparison to K^-/π production with P_T. The ratio R can also be computed as a function of E_T for $P_T \geq 0.4$ GeV/c. For both S+U and O+U collisions (fig. 4) a clear increase of R with E_T is observed.

References

[1] P. Sonderegger et al., Z. Phys. C38 (1988) 129
[2] L. Anderson et al., Nucl. Instr. Meth. 223 (1984) 26
[3] A. Devaux, Nucl. Phys. A498 (1989) 509c
[4] C. Baglin et al., Phys. Lett. 220B (1989) 471
[5] J.Y. Grossiord et al., Nucl. Phys. A498 (1989) 249c
[6] B. Nilsson-Almqvist, E. Stenlund, Comp. Phys. Commun. 43 (1987) 387;
B. Andersson, G. Gustafson and B. Nilsson-Almqvist, Nucl.Phys. B281 (1987) 289
[7] T. Çelik, J. Engels, H. Satz, Nucl. Phys. B 256 (1985) 670
[8] J. Cleymans, R. V. Gavai and E. Suhonen, Phys. Rep. 130 (1986) 217
[9] P. Vincent et al., Nucl. Phys. A498 (1989) 67c
[10] R. Albrecht et al., Phys. Lett. 201B (1988) 390
[11] T. Åkesson et al., Z. Phys. C46 (1990) 361
[12] J.W. Cronin et al., Phys. Rev. D11 (1975) 3105;
D. Antreasyan et al., Phys. Rev. D19 (1979)764

TRANSVERSE MOMENTUM OF DIMUONS PRODUCED IN p-Cu, p-U, ^{16}O-Cu, ^{16}O-U and ^{32}S-U COLLISIONS AT 200 GeV PER NUCLEON

NA38 Collaboration

M.C. Abreu[4], M. Alimi[9], C. Baglin[1], A. Baldisseri[1], A. Baldit[2], M. Bedjidian[9], P. Bordalo[4], A. Bussière[1], P. Busson[6], R. Cases[8], J. Castor[2], T. Chambon[2], C. Charlot[6], B. Chaurand[6], D. Contardo[9], E. Descroix[9], A. Devaux[2], O. Drapier[9], J. Fargeix[2], X. Felgeyrolles[2], R. Ferreira[4], P. Force[2], L. Fredj[2], J.M. Gago[4], C. Gerschel[5], P. Gorodetzky[7], B. Grosdidier[7], J.Y. Grossiord[9], A. Guichard[9], J.P. Guillaud[1], R. Haroutunian[9], D. Jouan[5], L. Kluberg[6], R. Kossakowski[1], G. Landaud[2], P. Liaud[1], C. Lourenço[4], S. Papillon[5], L. Peralta[4], J.R. Pizzi[9], C. Racca[7], S. Ramos[4], A. Romana[6], R.A. Salmeron[6], P. Sonderegger[3], F. Staley[1], S. Silva[4], X. Tarrago[5], J. Varela[4], F. Vazeille[2]

(1)-Annecy, (2)-Clermont-Ferrand, (3)-CERN, (4)-Lisbon, (5)-Orsay, (6)-Ecole Polytechnique, (7)-Strasbourg, (8)-Valencia, (9)-Lyon

Presented by Olivier Drapier
Institut de Physique Nucléaire de Lyon, IN2P3-CNRS et Université Claude Bernard
43 Bd du 11 Novembre 1918 - F-69622 Villeurbanne Cedex, France

Abstract : The NA38 experiment measured the muon pair production in interactions of p and ^{16}O with Cu and U and in ^{32}S-U collisions at 200 GeV per nucleon incident energy. The transverse momentum distribution of the J/ψ and of muon pairs in the mass continuum ($1.7 < M_{\mu\mu} < 2.7$ GeV/c^2) has been studied, taking into account the acceptance and smearing effects of the apparatus. For the J/ψ, the average values of the transverse momentum $<P_T>$ and $<P_T{}^2>$ show a clear increase with the energy density reached in ^{16}O and ^{32}S induced reactions, which is not observed for muon pairs in the mass continuum. Such a behaviour is in agreement with quark-gluon plasma models. However, models based on parton multiple scattering in the initial state are also able to reproduce the data.

The NA38 collaboration measured the dimuon production in p-Cu, p-U, ^{16}O-Cu, ^{16}O-U and ^{32}S-U reactions at 200 GeV per nucleon, in correlation with the neutral transverse energy E_T^0 produced in the interaction, which reflects the centrality of the collision. It has been observed[1] that the J/ψ yield relative to the dimuons in the mass continuum decreases with increasing E_T^0. In addition[2], this effect was found to be enhanced at low transverse momentum P_T. Such a behaviour is in agreement with the predictions of quark-gluon plasma (QGP) models[3] in which the colour screening effect prevents the binding of the $c - \bar{c}$ pair, depending on its transverse momentum[4]. It is therefore important to study the P_T dependence of J/ψ production as a function of E_T^0.

Measurements were performed at the CERN SPS, using the highest available intensity (up to 10^7 ions/s). The spectrometer detected muon pairs in the lab rapidity range $2.8 < y < 4.1$, in correlation with E_T^0, the neutral transverse energy deduced from the energy flow measured by an electromagnetic calorimeter in the pseudorapidity range $1.7 < \eta_{lab} < 4.1$. More details on the experimental set-up and event selection criteria can be found elsewhere[1,2].

Only dimuons with invariant mass $M_{\mu\mu} \geq 1.7$ GeV/c^2 are considered here. In this mass region, the signal in the opposite sign (OS) dimuon spectra originates mainly from J/ψ and ψ' meson decays, semi-leptonic decays of $D\bar{D}$ pairs, and from the Drell-Yan mechanism. For each kinematical variable, the number N_{Bk}^{+-} of background pairs coming from pion and kaon decays is estimated from the like sign (LS) pair spectra, using the formula :

$$N_{Bk}^{+-} = 2\sqrt{N^{++}N^{--}}$$

where N^{++} (N^{--}) is the number of $\mu^+\mu^+$ ($\mu^-\mu^-$) pairs in the corresponding distribution. In the following, J/ψ's are defined as events with mass between 2.7 and 3.5 GeV/c^2, and continuum dimuons as events outside this mass interval.

In order to study the transverse momentum distributions of J/ψ's and continuum dimuons, the acceptance and smearing effects of the apparatus are taken into account. This treatment is performed by the means of transfert matrices obtained from the simulation of the NA38 detector[2]. The P_T distributions of the OS muon pairs are parametrized according to :

$$P_T \; e^{-\left(\frac{P_T}{P_{T0}}\right)^{\beta}}$$

A fit through the acceptance and smearing matrices, taking into account the background contribution in the OS spectra, leads to the parameters P_{T0} and β of this phenomenological P_T distribution for J/ψ's and for muon pairs in the mass continuum. The average values $<P_T>$ and $<P_T{}^2>$ deduced from the resulting distributions are gathered in table 1 for proton and ion induced reactions. As one can see from these results, for the J/ψ, the values obtained for proton induced reactions are not compatible with those corresponding to ion-uranium collisions.

In order to investigate this effect as a function of the centrality, the same procedure is applied for different E_T^0 intervals. For proton-copper and proton-uranium collisions, no analysis as a function of E_T^0 is performed, as E_T^0 and impact parameter are in this case loosely correlated. For each E_T^0 bin, the energy density reached in the collisions is

estimated using the Bjorken formula :

$$\varepsilon = \frac{3 < E_T^0 >}{\Delta\eta \ \tau_0 \ \bar{S}}$$

where $< E_T^0 >$ is the mean neutral transverse energy measured in the pseudorapidity range $\Delta\eta$, and $\bar{S}$ is the mean overlap area of the colliding nuclei at the time τ_0=1fm/c.

	Continuum		J/ψ	
all E_T^0	$< P_T >$	$< P_T^2 >$	$< P_T >$	$< P_T^2 >$
p-Cu	0.83 ± 0.03	0.94 ± 0.05	1.04 ± 0.02	1.41 ± 0.04
p-U	0.84 ± 0.03	0.96 ± 0.06	1.06 ± 0.02	1.49 ± 0.05
^{16}O-Cu	0.84 ± 0.03	0.94 ± 0.06	1.08 ± 0.01	1.52 ± 0.04
^{16}O-U	0.85 ± 0.02	0.98 ± 0.05	1.12 ± 0.01	1.64 ± 0.03
^{32}S-U	0.87 ± 0.02	1.06 ± 0.05	1.14 ± 0.01	1.69 ± 0.03

Table 1 : *Values of $<P_T>$ and $<P_T{}^2>$ obtained after correction for acceptance and smearing, for J/ψ's and for muon pairs in the mass continuum.*

The values of $<P_T>$ and $<P_T{}^2>$ as a function of ε are plotted in figure 1 for the J/ψ, and in figure 2 for continuum events. As shown in figure 1, for the J/ψ, $<P_T>$ and $<P_T{}^2>$ display a clear increase with ε. Such a behaviour is not seen in the case of continuum dimuons, for which the values of $<P_T>$ and $<P_T{}^2>$ obtained in ion-nucleus collisions are, within statsitics, compatible with those measured in p-Cu and p-U reactions.

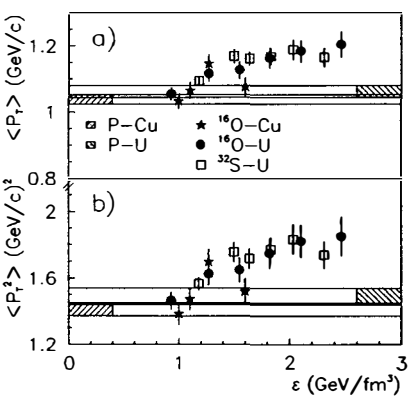

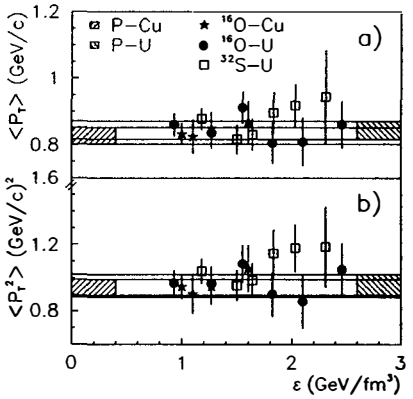

Figures 1 and 2 : *Values of $<P_T>$ (a) and $<P_T{}^2>$ (b) as a function of the energy density ε, for the J/ψ (1) and for events in the mass continuum (2).*

To study the transverse momentum dependence of the J/ψ suppression, the ratio $R(P_T)$ of the transverse momentum distributions corresponding to the two extreme E_T^0 bins is calculated. Each distribution is normalized to the number of continuum events in the J/ψ mass range, in the corresponding E_T^0 interval :

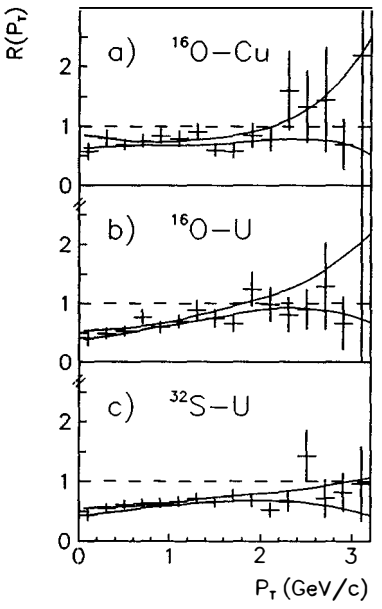

$$R(P_T) = \frac{\left(\frac{1}{N_C}\frac{dN^{\psi}}{dP_T}\right)_{High E_T^0}}{\left(\frac{1}{N_C}\frac{dN^{\psi}}{dP_T}\right)_{Low E_T^0}}$$

This ratio is shown in figure 3 as a function of P_T. One can see that R increases with P_T, indicating that the J/ψ suppression is enhanced for low transverse momentum values. Such an increase is expected from quark-gluon plasma models, which predict, in addition, a saturation of R with P_T. However, other interpretations[5], based on parton multiple scattering in the initial state, and J/ψ absorption in a dense hadron gas, are also able to account for the data. In these models, the multiple scattering in the entrance channel allows the incident partons to acquire transverse momentum, leading, for the J/ψ, to a value of $<P_T{}^2>$ which increases with the centrality of the collision. In this frame, $R(P_T)$ should not saturate with P_T. Unfortunately, the available statistics do not permit to distinguish between both models.

Figure 3 : *$R(P_T)$ for ^{16}O-Cu, ^{16}O-U and ^{32}S-U collisions, deduced from the fitted P_T distributions (solid lines), and calculated directly from the data (error bars).*

Another analytical form of the J/ψ P_T distribution, using the transverse mass parametrization :

$$P_T\, e^{-\frac{\sqrt{P_T^2+M_\psi^2}}{T}}$$

leads to the values of the parameter T, presented in figure 4. The ε dependence of this parameter, usually considered as a temperature in thermal models, has been fitted according to $T = a\,\varepsilon^{1/b}$. With T expressed in GeV, the results of the fit (represented by the solid line in figure 4) are :
$a = 0.212 \pm 0.002$ and $b = 3.9 \pm 0.4$

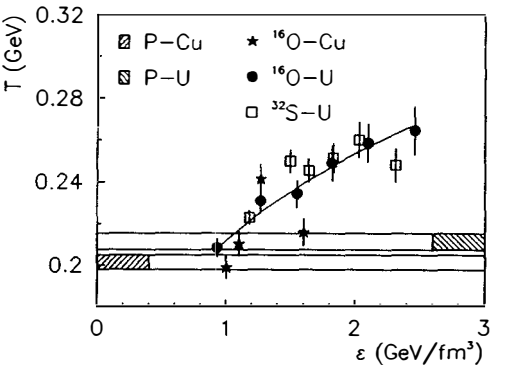

Figure 4 : *Values of the parameter T, as a function of the energy density ε*

REFERENCES

[1] - NA38 Collab., C. Baglin et al., Phys. Lett. B 255 (1991) 459.
[2] - NA38 Collab., C. Baglin et al., Phys. Lett. B 251 (1990) 465.
NA38 Collab., C. Baglin et al., Phys. Lett. B, to be published.
[3] - T. Matsui and H. Satz, Phys. Lett. B 178 (1986) 416.
[4] - J.P. Blaizot and J.Y. Ollitrault, Phys. Rev. D 39 (1989) 232.
[5] - J. Hüfner, Y. Kurihara and H.J. Pirner, Phys. Lett. B 215 (1988) 218.

CLASSICAL AND QUANTUM SIGNATURES OF QUARK-GLUON PLASMA FORMATION IN RELATIVISTIC HEAVY ION COLLISIONS

R. L. Thews
Department of Physics
University of Arizona
Tucson, AZ 85721 USA

ABSTRACT

We note that the production mechanism of centrally-produced J/ψ particles in heavy ion collisions localizes the initial quark-antiquark pair within a spacetime region much smaller than the size of the observed bound state. The time evolution of the state then requires spreading wave packets with substantial relativistic components. Calculations of survival probability due to initial color force screening in a quark-gluon plasma are compared with that obtained when assuming classical motion of the quarks. Crucial differences are found in the characteristic dependence on transverse momentum, which will have significant impact on interpretation of future data.

Substantial attention has been focused lately on explanations for the observed suppression of J/ψ production in heavy ion collisions in events which are accompanied by large transverse energy.[1] Some years ago, Matsui and Satz[2] first predicted such a suppression would be a signature of the creation of a plasma phase of quarks and gluons. The argument was that the confining force between the quark-antiquark pair would be screened in the region where a plasma existed, and that during the plasma phase some of the pairs would separate by a distance greater than the range of the confining force. These pairs would not be able to form a bound state after the screening disappeared, and they would preferentially recombine with the more abundant light up and down quarks, thus producing the suppression. The observed suppression also revealed a dependence on the transverse momentum of the J/ψ's. The suppression was not complete, with the largest suppression at low transverse momentum, and decreasing with larger transverse momentum up to a critical value beyond which there was no suppression. Several analyses[3] of this dependence noted the reasons for this behavior in the plasma scenario. One effect is that quark-antiquark pairs with large transverse momentum could propagate outside the plasma region before their separation became large enough to prohibit recombination. Another effect is the finite lifetime of the plasma, which must be greater than the (Lorentz-dilated) separation time in the laboratory system. Both of these effects produce a critical value of transverse momentum, beyond which the quark-antiquark pairs form the normal bound states without suppression. To see how these effects work, it is useful to consider the one-dimensional case. Suppose that a fraction ϵ of the quark-antiquark pairs are uniformly produced in a spatial region of size d where the plasma formation has screened their attractive force. Each pair has total (center of mass) momentum p and total mass M. In the rest system of the pair, let t_s be the time for them to separate a distance equal to the range of the non-screened force which would produce the bound states. I note that in initial treatments of this problem, this time was called the "formation time" for the bound state. This identification is correct only if the quark-antiquark pair were separating in the normal QCD relative potential, where this concept is useful in describing the absorption cross section dependence on time due to the expanding total size of the bound system. One would expect that the separation rate would be increased in the plasma phase where the binding force is screened. Hence we allow the separation time to be a free parameter in data fitting. The separation time acquires a momentum dependence in the laboratory system, since it is Lorentz dilated by the factor $\gamma = \frac{E}{M}$ where $E = (p^2 + M^2)^{1/2}$ is the transverse energy (we work in the boosted laboratory system where the longitudinal momentum of the pair is zero). The two other time parameters in the problem are the plasma lifetime t_p and the time for the center of mass of the

pair to reach the plasma boundary $t_b = xE/p$, where x is the distance of the production point from the boundary. The quark-antiquark pair can then form a bound state even in the presence of a plasma phase if

$$\gamma t_s > \min\{t_p,\ t_b\} \tag{1}$$

This produces a critical value of transverse momentum p_c beyond which no suppression will occur.

$$p_c = \min\left\{ M\left(\left(\frac{t_p}{t_s}\right)^2 - 1\right)^{1/2},\ \frac{Mx}{t_s} \right\} . \tag{2}$$

The momentum-dependent suppression factor is then $f = \theta(p - p_c)$, which must be averaged over the production position $\bar{f} = \frac{1}{d}\int_0^d f(x)dx$ to give finally the total suppression factor,

$$S(p) = 1 - \epsilon + \epsilon\bar{f} . \tag{3}$$

The effect of the geometric factor ϵ just gives the suppression at zero transverse momentum, and is of order 0.5. The average over spatial production point produces a linear rise in S with slope $\frac{\epsilon t_s}{Md}$. For $d < (t_p^2 - t_s^2)^{1/2}$ the total suppression factor reaches unity at the critical value $\frac{Md}{t_s}$, and the plasma lifetime effect does not enter. For $d > (t_p^2 - t_s^2)^{1/2}$, however, the critical value of p_c is reduced to $M((\frac{t_p}{t_s})^2 - 1)^{1/2}$ such that the total suppression factor suddenly jumps to unity from the linearly increasing curve.

It is clear that the simple connection between model parameters and experimental results depends on the classical picture of time evolution for the quark-antiquark pair during the plasma phase. In particular, the step-function dependence for suppression clearly needs a well-defined particle trajectory crossing a plasma boundary to define a time with which to compare the plasma life time and separation time scales. It was pointed out some time ago[4] that the quantum nature of this process would produce substantial deviations from this simple picture. The necessity of a quantum description of time evolution is obvious, since the space-time region of the production process in the hard collision is limited by the scale of the quark or bound state masses to a region of order 1/m, i.e. $\lesssim$ 0.1 fm. This not only requires momentum uncertainties at least as large as the quark mass which clearly require the consideration of spreading wave packets, but also involves large momentum components in the relativistic region so that the wave packet width is essentially limited by causality.[5] For a definite model, we use one-dimensional wave packets spreading freely during an initial time interval to simulate the plasma phase. The initial state is a product of two wave packets, each with average momenta p_1 and p_2;

$$\psi(r_1,\ r_2,\ t = 0) = \varphi_{p_1}(r_1)\varphi_{p_2}(r_2) . \tag{4}$$

The free time evolution is obtained by expanding in the usual energy-momentum eigenstates.

$$\varphi_p(r,t) = \frac{1}{\sqrt{2\pi}} \int dk\ e^{ikr}\ b_p(k)\ e^{-iE_k t} \tag{5}$$

This product two-particle wave function is then expanded in terms of relative (r) bound state and center of mass (R) eigenstates.

$$\psi(r_1, r_2, t) = \sum_m \int dp\ a_{pm}(t)\ \Gamma_p(R)\ \chi_m(r) \tag{6}$$

The inversion is most easily obtained by using the corresponding relative $k = \frac{1}{2}(k_1 - k_2)$.

$$a_{pm}(t) = \frac{1}{\sqrt{2\pi}} \int dk\ b_{p_1}\ (k + \frac{1}{2}p)\ b_{p_2}\ (-k + \frac{1}{2}p)\ f_m(k)\ e^{-i(E_{k_1} + E_{k_2})t} \tag{7}$$

where $f_m(k) = \int dr\ \chi_m^*(r)\ e^{ikr}$ is used for the bound state eigenfunctions.

The suppression factor for a given bound state is then

$$S_Q(t) = \left| \frac{a_p(t)}{a_p(0)} \right|^2 . \tag{8}$$

It is revealing to assume gaussian initial wave packets, and also to approximate the bound state eigenfunctions with a gaussian, such that the integrals may be done analytically in the nonrelativistic approximation. We take $\varphi_i(x_i) = Ae^{ip_i x_i} e^{-\frac{x_i^2}{4\sigma^2}}$ for the initial quark and antiquark wave packets, where in one dimension $\langle x_i^2 \rangle = \sigma^2$. The ground state wave function is assumed to be a similar form, $\chi_0(r) = \bar{A} e^{-\frac{r^2}{4\sigma_B^2}}$ with σ_B parameterizing the size of the bound state. If one uses the nonrelativistic energy-momentum relation for the time evolution, the suppression factor is easily calculated in closed form:

$$S_Q^{NR}(t) = \eta e^{\frac{2\sigma^4 (p_1 - p_2)^2 (\eta^2 - 1)}{2\sigma^2 + \sigma_B^2}} , \tag{9}$$

where

$$\eta \equiv \left(1 + \frac{t^2}{4\mu^2 (2\sigma^2 + \sigma_B^2)} \right)^{-\frac{1}{2}} ,$$

and μ is the bound state reduced mass.

It can be shown for typical hadronic time scale and sizes, that the factors which depend on p_1 and p_2 become important only for $|p_1 - p_2| \gtrsim 10$ GeV, and in this region the probabilities for forming the bound state are negligible. Thus in all further treatments we take $p_1 = p_2 = 0$. We see that due to the assumed gaussian form of the packets and eigenfunctions, this suppression factor is independent of the total bound state momentum. This form has been used[6] to extract an effective quantum mechanical separation time, defined

to be the time at which the suppression factor is reduced to 0.5, $t_s = 2\sqrt{3}\mu(2\sigma^2 + \sigma_B^2)$. Although the time evolution assumed free space expansion, it is tempting to insert this separation time into the classical formula for momentum dependence to see a possible quantum effect. It has been noted[6] that quantum effects tend to increase the critical transverse momentum parameter to values larger than can fit the experimental data. However, there is an additional momentum dependence if the correct relativistic energy-momentum relation is used in (7) to evaluation the suppression factor. This effect cannot be expressed in closed form, but the results are shown in Figure 1 for various total momenta. It is seen that for higher momentum the suppression factor decreases less rapidly, effectively increasing the analog of a classical separation time. Of course, part of this effect is just the relativistic time dilation, since we are using the laboratory system (assumed to be the plasma rest system) in which to evaluate the probability amplitudes. There is a real increase in effective separation time left over however, even after factoring out the dilation effect. This is shown in Figure 2, in contrast to the constant value in the non-relativistic approximation. The overall effect on the momentum dependence is shown in Figure 3. Here the nonrelativistic approximation is shown in the lower curve for each assumed bound state size (the initial wave packet sizes are taken equal to the inverse quark mass, and the geometric factor $\epsilon = 0.5$). The upper curve for each case shows the effect of using the relativistic time evolution, and as anticipated the tendency is for the critical momentum values to decrease. It should be noted that the correct procedure for extracting the time scales of the suppression factor is still not on solid ground. In principle, one should account for the Lorentz contraction of the bound state size for high transverse momentum states, or also for similar effects on initial wave packets if one works exclusively in the rest frame of the bound state. A simple rescaling of these sizes by the appropriate gamma factors unfortunately does not lead to consistent results, so that further study is necessary to resolve the matter.

It is clear that since we used $p_1 = p_2 = 0$ for the initial wave packets, there is no classical-like effect of particle separation to cause the suppression of bound state formation. The entire cause of the decrease in probability to retain the bound state is due to the spreading and phase incoherence of the time-evolved wave packets. Rather than merely extracting an effective classical separation time, it makes sense to use the complete time-dependent suppression factor for a fixed plasma lifetime and production position, and then average over the production point in the plasma phase to get the overall transverse momentum dependence. For fixed production point distance from the plasma boundary,

$$f = \begin{cases} S_Q(t_p) & t_p < t_b \\ S_Q(t_b) & t_p > t_b \end{cases} . \qquad (10a)$$

The effective position-averaged suppression factor for pairs produced in the plasma region can be evaluated in closed form for the nonrelativistic approximation, and yields

$$\bar{f}_{NR} = \begin{cases} \left(1 - \frac{pt_p}{ED}\right)\left(1 + \frac{t_p^2}{a^2}\right)^{-1/2} + \frac{pa}{Ed} \ln\left[\frac{t_p}{a} + \left(1 + \frac{t_p^2}{a^2}\right)^{1/2}\right] & \frac{pt_p}{Ed} < 1 \\ \frac{pa}{Ed} \ln\left[\frac{Ed}{pa} + \left(1 + \left(\frac{Ed}{pa}\right)^2\right)^{1/2}\right] & \frac{pt_p}{Ed} > 1 \end{cases} \tag{10b}$$

where $a \equiv 2\mu(2\sigma^2 + \sigma_B^2) = t_s/\sqrt{3}$ is the previously-defined analog of the classical separation time.

The momentum dependence is shown in the curve labeled "quantum, non-rel" of Figure 4. We have used parameters t_p=1.05 fm, d = 0.5 fm, σ_B=0.5 fm, and σ=.075 fm. The curve is very flat, indicating that in this approximation the critical p_c values are very large. The corresponding relativistic calculation is shown in the curve labeled "quantum, rel." It is seen that the suppression rises much faster, as expected from the behavior of the time evolution curves in Figure 1. For comparison, the classical curves are shown also in Figure 4 for the same parameter set, with a separation time t_s= 0.7 fm. This is the set of parameters which fits the experimental curves from NA38, and the effect of using an effective quantum separation time in the classical formulas is seen to flatten the curve. The slope of these curves is very dependent upon choice of quantum/classical, and relativistic/nonrelativistic calculations. Clearly the parameters either input or extracted from data will be quite different in each case, and no definitive statement can yet be made concerning the quantitative transverse momentum slope of the suppression as a signature of plasma phase formation.

REFERENCES

1) NA38 Collaboration: Abreu et al., Z Phys. C38, 117 (1988).
2) T. Matsui and H. Satz, Phys. Lett. 178B, 416 (1986).
3) F. Karsch and R. Petronzio, Z. Phys. C37, 627 (1988); Phys. Lett. 212B, 255 (1988); J. P. Blaizot and J. Y. Ollitrault, Phys. Lett. 199B, 499 (1987); Phys. Rev. D39, 232 (1989).
4) J. Cleymans and R. L. Thews, University of Arizona preprint AZPH-TH 89/7, December 1988 (unpublished); Z. Phys. C45, 391 (1990).
5) R. L. Thews, University of Arizona preprint AZPH-TH/90-37, to be published in Nucl. Phys. A (1991).
6) V. Cerny, I. Horvath, R. Lietava, and J. Pisut, Z. Phys. C46, 481 (1990).

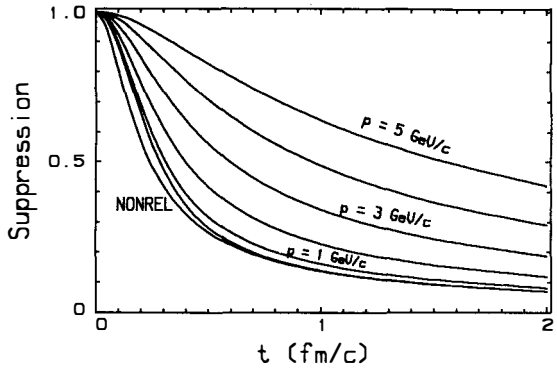

Figure 1. Time dependence of quantum bound state survival probability

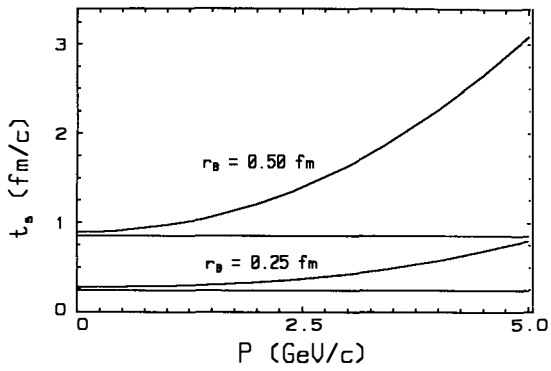

Figure 2. Effective formation time from quantum model

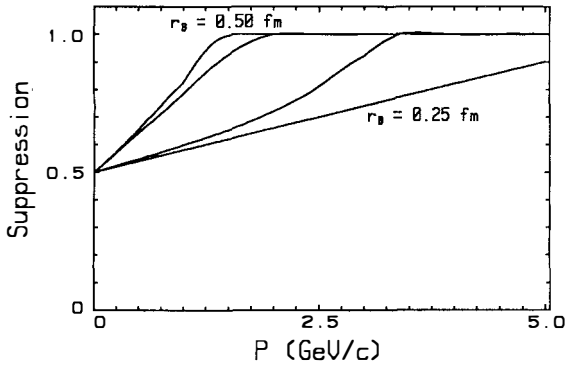

Figure 3. Suppression factors from finite plasma boundary

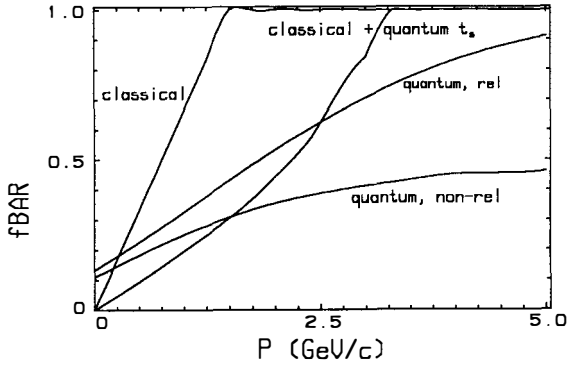

Figure 4. Comparison of classical/quantum, relativistic/nonrelativistic suppression

NUCLEAR EFFECTS FOR HEAVY-QUARKS AND LEPTON-PAIR PRODUCTION

K.G. Boreskov
Institute for Theoretical and Experimental Physics, Moscow 117259, U.S.S.R.

A.B. Kaidalov
Université Paris-Sud, Laboratoire de Physique Théorique et Hautes Energies*, 91405 Orsay Cedex, France and Institute for Theoretical and Experimental Physics, Moscow 117 259, U.S.S.R.

Production of particles containing heavy quarks and the Dreil-Yan process on nuclei are investigated in the framework of the parton model and reggeon calculus. It is shown that A-dependence of these reactions can be understood in this approach which gives a good description of the light-quark states production on nuclei. An existence of a new large-energy scale for production of heavy states is emphasized. Predictions for future experiments are given.

---

* Laboratoire associé au Centre National de la Recherche Scientifique

Investigation of nuclear effects for production of heavy (c, b, ...)-quarks and the Drell-Yan process is important in order to obtain a consistent space-time picture of strong interactions at high energies. This problem is also essential for heavy ions interactions to clarify an origin of J/ψ-suppression. The data on A-dependence of inclusive cross sections of both heavy states and those made of light (u, d, s)-quarks can serve for critical tests of theoretical models.

Here we will use the approach, based on the parton picture of hadronic interactions at high energies and the reggeon calculus, first introduced for interactions with nuclei by Gribov[1]. This approach is very general and should be valid for any field theory, uncluding QCD.

Production of hadrons, made of light quarks in hadron-hadron (hh), hA and AA-collisions is rather well understood and quantitatively described in some particular realizations of this approach like the Dual parton model[2] or Quark-gluon strings model[3].

Usually A-dependence of inclusive cross section for production of a hadron "a" in hA-collisions $\frac{d\sigma^a_{hA}}{dx}$ is parametrized in the form $\frac{d\sigma^a_{hA}}{dx} \sim A^{\alpha_a(x)}$ and experiments show that for "ordinary" hadrons (π, K, N, Λ, ...) $\alpha_a(x)$ is changing from the values $\alpha_a(x) \simeq 1$ for $x \to 0$ to $\alpha_a(x) = 0.4 \div 0.5$ as $x \to 1$. This is in agreement to the prediction of the reggeon approach, which leads asymptotically as $s \to \infty$ for small x to A^1-dependence (for the Glauber-type nonenhanced diagrams), while the decrease of $\alpha_a(x)$ as $x \to 1$ is connected to the energy-momentum conservation effects (see for example recent reviews[4,5]).

For heavy-quarks production and the Drell-Yan process a situation is less clear. Experimental data[6,7] show that :

a) for the Drell-Yan process $\alpha(x) \approx 1$ at present energies.

b) For J/ψ and ψ'-production $\alpha(x) < 1$ and decreases with x from values $\alpha \approx 0.9 \div 0.95$ at small x to $\alpha \approx 0.7 \div 0.8$ as $x \to 1$. Analogous behaviour is observed for production of states with open charm. Even for such a heavy state as Υ there are some nuclear effects, leading to $\alpha(x) < 1$[7].

These experimental facts are difficult to explain in theoretical models[8]* . In the parton model, which we will use in the following a fast moving hadron is considered as a system of partons (quarks and gluons) and soft partons of a projectile interact with a target. For hadron-nucleus collisions the shadowing effects are due to interactions of partons of a projectile with different nucleons of nuclei (Fig. 1).

Note that successive rescatterings of the initial hadron on nucleons of a nucleus decrease with energy[1,5] at energies $E > E_0 = m_N \cdot \mu \cdot R_A$, where $R_A = R_0 A^{1/3}$ is a radius of a nucleus and μ is a characteristic hadronic scale $\sim$ 1 GeV. Though a space-time picture of interaction is completely different from the Glauber one, the generalized Glauber-type formula for elastic hA-scattering

---

* There is one model[9] which takes into account intrinsic charm component of the initial hadron and is able to describe experimental data. However we emphasize in this paper that this mechanism does not lead to nuclear shadowing for J/ψ at energies $E_L \lesssim 100$ GeV and thus contradicts to the data[6].

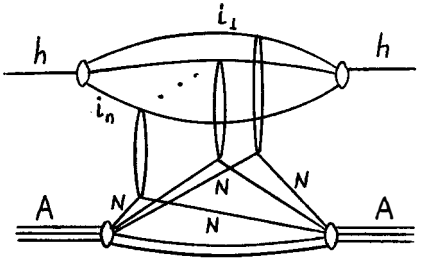

Fig. 1

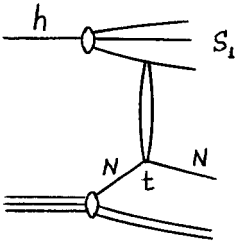

Fig. 2

amplitude is valid[1] in the high energy region. The nonplanar (Mandelstam type) diagrams start to dominate in the energy region $E \gtrsim E_0$, where the diffractive production on nucleons with small momentum transfer $t \sim 1/R_A^2$ (Fig. 2) becomes possible. This corresponds to a condition

$$t_{min} = -\frac{m_N^2\left(S_1 - m_h^2\right)^2}{S^2} = -\frac{\left(S_1 - m_h^2\right)^2}{4E_0^2} \approx \frac{3}{R_A^2} \quad . \tag{1}$$

For processes, involving "ordinary" hadrons (light quarks and gluons) $E_0 \sim 10$ GeV.

In the energy region $E > E_0$ the AGK-cutting rules[10] give a possibility to calculate different inelastic process if contributions of rescatterings to the elastic amplitude are known. Each of iN-elastic amplitudes (Pomerons) in Fig. 1 can be either "cut" and gives a multiparticle final state or "uncut" (absorption) - Fig. 3. This leads to the cancellation of contributions of all rescattering

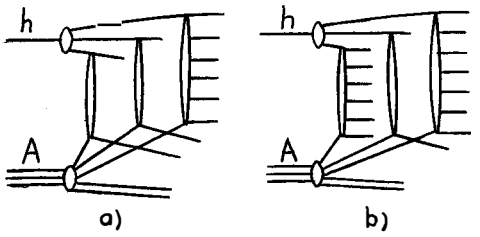

Fig. 3

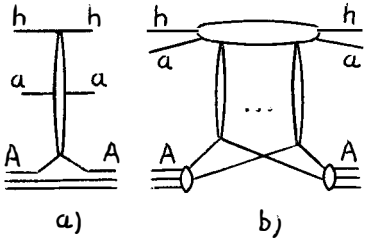

Fig. 4

diagrams to inclusive cross section[10] and $\frac{d\sigma_{hA}^a}{dx} = A\,\frac{d\sigma_{hN}^a}{dx}$, i.e. $\alpha = 1$ (the corresponding diagram for inclusive cross section is shown in Fig. 4a)). This theorem is valid, however, only for particles,

which are due to cuttings of Pomerons in the Fig. 1. There is also a contribution to inclusive cross section from partons, which are in the upper blob of the Fig. 1 (Fig. 4b)). These contributions are especially important in the fragmentation region of a projectile and are necessary to account for energy-momentum conservation effects[11,12]. They include the interaction of partons, which are in the same partonic configuration as $Q\bar{Q}$ (or $\mathcal{L}\bar{\mathcal{L}}$), and the $Q\bar{Q}$-interaction. The first one leads to a behaviour $\frac{d\sigma^a_{hA}}{dx} \sim A^{2/3}$ (as $A \to \infty$) and it exists for both $Q\bar{Q}$-production* and the Drell-Yan process. For hadrons "a", which are $q\bar{q}$-states these diagrams lead for $\frac{d\sigma^a_{hA}}{dx}$ as $x \to 1$ to the behaviour of the type

$$\frac{d\sigma^a_{hA}}{dx} \sim \int d^2b\, e^{-C\sigma_{Q\bar{Q}} \cdot n_A(b)} \left(1 - e^{-\sigma n_A(b)}\right) \qquad (2)$$

where $n_A(b)$ is a standard nuclear profile function in the impact parameter space, $\sigma_{Q\bar{Q}}$ is the inelastic cross-section of $(Q\bar{Q})$-interaction with a nucleon, σ is the effective cross section for interaction of other partons and C is a constant ~ 1. For light hadrons $\sigma_{Q\bar{Q}} \approx 20$ μb and $\alpha(x) \to \frac{1}{3}$ as $A \to \infty$ (only edge of a nucleus is important). For realistic values of A calculations[2-5] show that $\alpha(x) \approx 0.4 \div 0.5$ as $x \to 1$. For $c\bar{c}$-systems $\alpha(x) \approx 0.7 \div 0.8$ and for $b\bar{b}$-systems $\alpha(x) \approx 0.9 \div 0.95$ as $x \to 1$.

In the region of small x the contributions of the "nonenhanced"-type diagrams (fast partons with $x_i \sim 1$ in the blob) give asymptotically $\alpha(x) = 1$, but in this region it is also necessary to take into account possible contributions of "enhanced" diagrams (Fig. 5) with interactions between Pomerons. As a result an inclusive cross section can be represented by a sum of terms proportional to A^1 and A^γ (with $\gamma = \frac{2}{3}$ as $A \to \infty$). It is known, however, that the triple-Pomeron coupling is rather small[13], so the deviations from A^1-behaviour should not be very large. This effect can be considered either as due to rescatterings of soft partons of the initial partonic fluctuation, or as a shadowing of soft partons from different nucleons of the target. Note, that they should also be present for the Drell-Yan process, while the absorption-like effects,

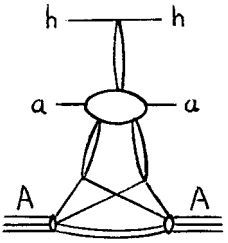

Fig. 5

* Nuclear shadowing due to the "intrinsic charm" component, proposed in ref. 9) corresponds to this mechanism.

discussed above do not exist in this case. So we predict that asymptotically there should be deviations from the A^1-behaviour even in the case of the Drell-Yan process.

All these results are valid only at very high energies $E >> E_0$, where the partonic fluctuations with heavy $Q\bar{Q}$-pair or $\ell^+\ell^-$ with large mass M satisfy to the condition (1). It follows from the kinematics of the process that in this case $S_1 \approx x_- S = M^2/x_+$, where $x_\pm = \frac{1}{2}(\sqrt{x^2 + \frac{4M^2}{S}} \pm x)$ and thus

$$E_0 = \frac{M^2}{2x_+} \frac{R_A}{\sqrt{3}} \quad . \tag{3}$$

At lower energies AGK-rules are modified. This modification has been studied in our recent paper[14]. It was shown that at $E << E_0$, where the diagram of Fig. 1 is close to zero, its different cuttings have some definite values, which differ from those of AGK. For example for double rescatterings the diffractive cutting (Fig. 2) is zero (instead of 1 for $E >> E_0$), the absorption (cutting of one Pomeron - Fig. 3a) 6a)) is reduced (- 2 instead of - 4) and the inelastic interaction with two nucleons - Fig. 3b), 6b) is not modified (+ 2). So the total contribution to the elastic hA-amplitude is zero due to cancellation of last two terms (instead of - 1 for $E >> E_0$). It is easy to see that as a result the rescattering of soft partons of the initial configuration does not lead to the shadowing in the region $E << E_0$. Thus for the Drell-Yan process there should be no deviations from the A^1-behaviour for $E < E_0$ (they are proportional to $e^{\frac{1}{3} R_A^2 t_{min}}$). This result also imply that soft partons of the "intrinsic charm" component[9] cannot produce shadowing effects for energies $E < E_0$. On the other hand for the $Q\bar{Q}$-states, which have strong interaction with nucleons of the target the diagrams of Fig. 6a) and 6b) do not cancel in inclusive cross section, because of the energy-momentum conservation effects (the x-distributions of the $Q\bar{Q}$-state are different for diagrams of Figs. 6a) and 6b)) and the fact that a projection of the $Q\bar{Q}$ on a given hadronic state (ψ, ψ', χ, Υ, ...) are in general different for diagrams 6a) and 6b). These absorption-like effects are present even for energies $E < E_0$. The energy-momentum conservation effect is especially important as $x \to 1$. This in our opinion explains a

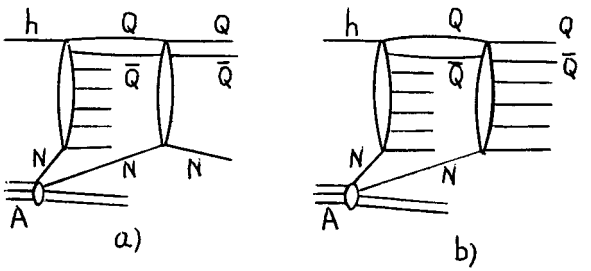

Fig. 6

qualitative difference in A-dependence between the Drell-Yan process and J/ψ or ϒ-production and the decrease of $\alpha_{\psi}(x)$ as $x \to 1$.

Now we summarize our results and give qualitative predictions for future experiments.

Table 1

Values of E_0 (in GeV) for J/ψ, Drell-Yan (M = 5 GeV) and ϒ for different values of x

	x = 0	x = 0.2	x = 1
J/ψ	10^3	280	70
DY (M = 5 GeV)	$2.5 \cdot 10^3$	700	170
ϒ	10^4	$2.5 \cdot 10^3$	650

There should be an increase of nuclear effects (decrease of α(x)) for energies $E > E_0$. Values of E_0 for some particular cases are given in the Table I ($A \sim 100$). It follows from this table that :

a) for J/ψ there should be some decrease of α(x) in the region x = (0.2 ÷ 0.4) in the energy region 200 ÷ 800 GeV. While for $x \approx 0$ it should start at higher energies. At $x \gtrsim 0.5$ α(x) has a very weak energy dependence already for $E \gtrsim 200$ GeV. This agrees with the recent data on J/ψ-production at 800 GeV[7].

b) Deviations from A^1 ($\alpha < 1$) for the Drell-Yan process with $M \approx 5$ GeV should appear for $x_F \gtrsim 0.5$ at energies $E \gtrsim 400$ GeV. The first indication for this effect has been observed at 800 GeV[7]. Let us note that for $\frac{M^2}{x_+ s} > \frac{1}{m_N R_A}$ the shadowing is absent for any energy (this condition corresponds to $x_B > \frac{1}{m R_A}$) for quarks (antiquarks of nuclei).

c) Increase of nuclear effects for $b\bar{b}$-states (like ϒ) occurs in the energy range $E \gtrsim 10^3 \div 10^4$ GeV and can be studied at future accelerators (UNK, RHIC, LHC).

Our results for production of heavy quarks imply that in general A-dependent effects cannot be totally attributed to the A-dependence of structure functions of gluons or quarks in nuclei and correspond to a violation of the factorization theorem.

References

1. V. N. Gribov, ZhETF 56 (1969) 892 ; 57 (1969) 1306.
2. A. Capella et al., Zeit. für Phys. C3 (1980) 329.
   A. Capella and J. Tran Thanh Van, Phys. Lett. 114B (1982) 450.
   A. Capella and J. Tran Thanh Van, Zeit. für Phys. C10 (1981) 249.
3. A.B. Kaidalov, Phys. Lett. 116B (1982) 459.
   A.B. Kaidalov and K.A. Ter-Martyrosyan, Phys. Lett. 117B (1982) 247.
   A.B. Kaidalov, K.A. Ter-Martirosyan and Yu. M. Shabelski, Yad. Fiz. 43 (1986) 1282.

4. A. Capella, Nucl. Phys. A525 (1991) 133.
5. A.B. Kaidalov, Nucl. Phys. A525 (1991) 39.
6. J.G. Branson et al., Phys. Rev. Lett. 38 (1977) 1334.
Yu. M. Antipov et al., Phys. Lett. 76B (1978) 235.
M.J. Corden et al., Phys. Lett. 110B (1982) 415.
J. Badier et al., Zeit. für Phys. C20 (1983) 101.
S. Katzanevas et al., Phys. Rev. Lett. 60 (1988) 2121.
7. D.M. Alde et al., Phys. Rev. Lett. 66 (1991) 133.
C.S. Mishra et al., Proc. of the XXVth Rencontre de Moriond, High Energy Hadronic Interactions, p. 255, Editions Frontiers (1990).
8. S.J. Brodsky and A.H. Mueller, Phys. Lett. 206B (1988) 685.
S. Gavin, M. Gyulassy and A. Jackson, Phys. Lett. B207 (1988) 257.
J.P. Blaizot and J.Y. Ollitrault, Phys. Lett. B217 (1989) 386.
S. Gavin and R. Vogt, Nucl. Phys. B345 (1990) 104.
9. S.J. Brodsky and P. Hoyer, Phys. Rev. Lett. 63 (1989) 1566.
S.J. Brodsky, P. Hoyer and R. Vogt, Preprint UCRL-JC-106453 (1991).
10. V. Abramovsky, Y.N. Gribov and O.V. Kancheli, Yad. Fiz. 18 (1973) 595.
11. A. Capella, A. Kaidalov, Nucl. Phys. B111 (1976) 477.
12. M.A. Braun, Yad. Fiz. 47 (1988) 262 ; 52 (1990) 257.
13. A.B. Kaidalov, Phys. Reports 50 (1979) 157.
14. K.G. Boreskov, A.B. Kaidalov, S.M. Kiselev, N. Ya. Smorodinskaya, preprint ITEP 90-75.

A parton model for hA interactions at high energies

M.A.Braun
Department of particle physics, Physical faculty,
University of Santiago de Compostela, 15706 Santiago de Compostela, Spain

Abstract

A parton model for hA interactions at high energies is developed based on the assumption that parton amplitudes do not depend on virtualities provided only nonplanar diagrams are retained in the elastic amplitude. It is shown that although the AGK rules are exactly fulfilled in the model the interference between the direct and spectator mechanisms of particle production restores the conservation of energy. Conditions are studied under which Glauber-like formulas result for the amplitude and crosss-sections. The difference is analyzed between the predictions of the proposed model and current models of hA interactions based on the probabilistic interpretation of the Glauber theory.

1.Introduction There exist two versions of the parton model for hA interactions in the current literature. The original idea of [1] developed in [2] starts from a parton wave function of the incoming hadron, which gets slightly deformed in the process of interaction in its low-energy component part. The spectrum of produced states then essentially coincides with the rest part of the wave function, that is, the spectator part. Less ambitious constituent parton models (e.g. [3-5]) assume that partons which form the incoming hadron independently interact with nucleons of the target by interchanging some extended objects (e.g. coloured strings) with the spectrum of produced particles determined by their decay. However both type of parton models leave open some crucial questions. First, they do not produce in a convincing manner a Glauber-like form of the elastic amplitude (and the total cross-section), which agrees well with experimental facts. Rather the Glauber probabilities are postulated for n-fold hN interactions inside nuclei [5]. Second, they have problems with energy-momentum conservation.

It is the aim of the present paper to propose a slightly more general parton model for hA interactions, which clarifies upon these points [6,7]. The model is quite in the spirit of the original version of [2] with the only difference that elementary amplitudes are separated from the wave function not by their short range in rapidity but rather by the topology of the corresponding Feynman diagrams. This enables us to establish exat energy momentum conservation in the model. On the other hand, as a price, elementary amplitudes now become extended in rapidity and their spectrum overlaps with that of spectators. The model is thus an interpolation between the two extreme cases: that of the wave-function model of [2], where all the spectrum comes from spectators, and of constituent parton models with the spectrum due to interactions. Under some rather general assumptions the model leads to the Glauber formula for the hA elastic amplitude and the total cross-section. The inclusive cross- sections consist of two parts in our model. One, coming from spectators, behaves like $A^{2/3}$ for heavy nuclei. The direct part coming from interactions exactly satifies the AGK rules [8] and is proportional to A. A simple case with only one type of partons is discussed here. Generalizations to more realistic situations as well as corresponding numerical results are postponed for future publications.

2.The hA amplitude. As in [1,2] the starting point is that in the hA scattering long before the interaction the fast incoming hadron decays into weakly virtual partons each of which subsequently once interacts with one of the nucleons from the target nucleus and finally joins with the others to form the outgoing hadron (Fig. 1). By definition B_n is two particle irreducible with respect to each pair of lines p_i, p'_i. Separating the n-fold nuclear form factor from the hA amplitude in the standard manner we get for the hA elastic amplitude at fixed impact parameter

$$\mathcal{A} = \sum_{1}^{A} C_A^n T^n(b) W_n \tag{1}$$

where T is the usual nuclear profile function and W_n the high-energy part, which is an integral of a product of B_n and n forward parton-nucleon amplitudes a over parton momenta p_i and transferred longitudinal momenta q_{iz}.

The amplitudes a depend on their energies and in general on parton virtualities. Our basic asumption is that the dependence of a's on parton virtualities may be neglected. It is implied that first one has to drop all planar diagrams taking the asymptotical value for the

amplitude when $p_h \to \infty$ and only aftewards in the nonplanar contribution, which survives in that asymptotical limit, one considers partonic amplitudes as not depending upon virtualities.

We compare W_n with the n-fold form-factor F_n of the incoming hadron (Fig. 2) integrated over all q_{i-} and with $q_{i+} = q_{i\perp} = 0$. Instead of parton amplitudes a it contains parton form-factors f. We assume that the latter do not depend on virtualities either. Then F_n goes over to W_n if the form-factor f as a function of the light-cone variable p_+ coincides with $a(p_+)$. In a quantum field theory such a form-factor can be generated by a composite operator $j(x) = \phi^{(+)}(x)a_0(-i\partial_-)\phi^{(-)}(x)$ where $\pm$ components of the unrenormalized field ϕ are defined according to the frequency sign with respect to x_+ . The "bare" amplitude a_0 has to be 2-particle irreducible in the t-channel. In terms of j we find

$$\delta^3(p_h - p'_h)iW_n = m\sqrt{2} < p_h|(i\hat{a}(x_+))^n|p'_h > \tag{2}$$

where up to a normalization factor $\hat{a}(x_+)$ is a "charge" associated with the "current" j:

$$\hat{a}(x_+) = (m\sqrt{2})^{-1} \int dx_- d^2x_\perp j(x) \tag{3}$$

and $< p_h|$ ($|p'_h >$) is the final (inicial) hadron state.

To calculate (2) we introduce a complete set of bare N-parton states and the corresponding wave-function $\Psi(k_i)$. Then we find

$$iW_n = \int \prod_1^n (d\alpha_i i a_0(\alpha_i))\rho_n(\alpha_i) \tag{4}$$

Here $\alpha_i = k_{i+}/p_{h+}$. The quantity

$$\rho_n(\alpha_i) = \sum_{N \geq n} N!/(N-n)! \int \prod_1^n \frac{d^2k_{i\perp}}{2\alpha_i} \prod_{n+1}^N \frac{d^3k_i}{2k_{i+}} 2p_{h+}\delta^3(p_h - \sum k_i)|\Psi_N(k_i)|^2 \tag{5}$$

is the probability for n bare partons to have their "+" components of momenta $k_{i+} = \alpha_i p_{h+}$. From (5) it follows that ρ_n obey the energy conservation sum rule:

$$\int \alpha d\alpha \rho_{n+1}(\alpha, \alpha_i) = (1 - \sum_1^n \alpha_i)\, \rho_n(\alpha_i) \tag{6}$$

Another sum rule can be deduced for a separate term ρ_{nN} in the sum over N in (5):

$$\int d\alpha \rho_{n+1,N}(\alpha, \alpha_i) = (N-n)\, \rho_{nN}(\alpha_i) \tag{7}$$

The probabilities ρ are evidently real. Therefore in our model the AGK cutting rules will be exactly fulfilled in spite of the dependence of the amplitudes $a_0(s)$ on energy (see [9]).

3.Inclusive cross-sections. Various contributions to the inclusive cross-sections can be obtained by cutting diagrams for the forward elastic scattering amplitude and fixing the registered particle in one of these cuts. It divides into a direct part coming from observing the particle in the cut parton-nucleon amplitude a_0 and a spectator part with the particle in the cut ρ or lines of active partons. According to the AGK cutting rules in the direct part all contributions with additional parton interactions cancel and we are left with the impulse approximation proportional to A:

$$J_A^{(1)}(\alpha) = A \int d\beta \rho_1(\beta) j_0(\beta, \alpha) \tag{8}$$

Here $j_0(\alpha_1, \alpha)$ is a bare inclusive cross-section to observe a particle with the longitudinal momentum αp_{h+} produced by a hadron with the longitudinal momentum $\alpha_1 p_{h+}$ incident on a nucleon at rest.

For the spectator contribution we have to consider the same structure as (2) with an additional particle in the initial and final hadronic states $|p_h, k>$ where k refers to the observed particle. As one can see from Fig. 3 only the disconnected part of the corresponding partonic wave function $\Phi_N(k_i)$ contributes to the absorptive part of interest. So we represent Φ_N as a sum over $i = 1, ...N$ of disconnected parts with $k_i = k$. We then split Φ_N in two terms containig summation over i in the limits from 1 to n and from n+1 to N respectively. Then the product of terms with $i \geq n+1$ gives rise to the absorptive part corresponding to the observation of spectators:

$$D_n^{(1)}(\alpha) = -2\,\mathrm{Re} \int \prod_1^n (d\alpha_i i a_0(\alpha_i)) \rho_{n+1}(\alpha, \alpha_i) \tag{9}$$

The mixed product of terms with $i \leq n$ and $i \geq n+1$ describes the observation of active partons:

$$D_n^{(2)}(\alpha) = -2\,\mathrm{Re} n i a_0(\alpha) \int \prod_1^{n-1} (d\alpha_i i a_0(\alpha_i)) \rho_n(\alpha, \alpha_i) \tag{10}$$

The last contribution with $i \leq n$ in both inicial and final states corresponds to a planar diagram contribution and we neglect it. As a consequence of (6) the sum D_n of (9) and (10) satisfies the sum rule

$$\int \alpha d\alpha D_n(\alpha) = 2\mathrm{Im} W_n \tag{11}$$

For the cross-sections it implies that particles described by the spectator contribution carry all the energy available.

The contribution $D_n^{(2)}$ does not exist for $n = 1$ as in that case there is no interaction in one of the parts of the cut amplitude. This leads to a correction term which results in an additional contribution to the cross-section proportional to A. In (8) $J_1^{(1)}$ has to be replaced by ,

$$J_1(\alpha) = \int d\alpha_1 \rho_1(\alpha_1) j_0(\alpha_1, \alpha) - \rho_1(\alpha) \sigma_0(\alpha) \tag{12}$$

where $\sigma_0 = 2\,\mathrm{Im} a_0$ is a cross-section for parton- nucleon interaction. The elementary inclusive cross-section j_0 has to satisfy the energy conservation sum rule: $\int \alpha d\alpha j_0(\alpha_1, \alpha) = \alpha_1 \sigma_0(\alpha_1)$ With this sum rule we find from (12)

$$\int \alpha d\alpha J_1(\alpha) = 0 \tag{13}$$

Together with (11) this demonstrates the conservation of energy in our inclusive cross-sections.

4.Glauber cross-sections. Two conditions are needed to secure that the hA amplitude (1) coincide with the Glauber one. First one has to assume that the elementary amplitude a_0 does not depend on energy, that is on α. As we shall see this does not imply that the resulting hadron-nucleon cross-section is independent of energy. With constant a_0 using (7) we obtain

$$iW_n = (ia_0)^n \rho_n^{(0)} \tag{14}$$

where numbers $\rho_n^{(0)}$ are defined according to $\rho_n^{(0)} = \sum_{N \geq n} N!/(N-n)! \rho_{0N}$ The probabilities ρ_{0N} give the distribution in the number of partons in the projectile. If we impose a second

condition, namely, that ρ_{0N} are Poissonian, then the sum over N gives $\rho_n^{(0)} = \lambda^n$ where λ is the mean number of partons. Together with (14) it leads to the Glauber formula for the hA amplitude with the hN amplitude given by λa_0. The hN cross-section will depend on energy if λ depends on it.

The spectator part of the inclusive cross-section also simplifies for constant a_0. For the corresponding absorptive part we get

$$D_n(\alpha) = -\mathrm{Re}(ia_0)^n \rho_n^{(1)}(\alpha) \tag{15}$$

where the distribution $\rho_n^{(1)}$ is defined as $\rho_n^{(0)}$ with $\rho_{1N}(\alpha)$ instead of ρ_{0N}. If we assume the Poissonian form for the latter then we get sum rules

$$\int d\alpha \rho_n^{(1)}(\alpha) = \lambda^n(\lambda + n); \quad \int \alpha d\alpha \, \rho_n^{(1)}(\alpha) = \lambda^n \tag{16}$$

With a parametrization

$$\rho_n^{(1)}(\alpha) = c_n \lambda^n \alpha^\beta (1-\alpha)^{\gamma_n} \tag{17}$$

the conditions (16) require: $\gamma_n = (n + \lambda - 1)\beta - 1, c_n^{-1} = \mathrm{B}(\beta + 1, \gamma_n + 1)$. Assuming (17) one can perform the summation over all n for the spectator part of the inclusive cross section. For heavy nucleus $A >> 1$ one obtains the cross-section

$$I_A(\alpha) = \alpha^\beta (1-\alpha)^{\gamma_0} \sigma_A^{tot} / \mathrm{B}(\beta + 1, \gamma_0 + 1) \tag{18}$$

which means that the spectator part is proportional to $A^{2/3}$.

Thus we come to the conclusion that at least in this simplified case and choice of $\rho_n^{(1)}$ the total inclusive cross-section contains two contributions: the direct one, proportional to A, and the spectator one, proportional to $A^{2/3}$.

References

1. O.V.Kancheli, Pis'ma JETP **18** (1973) 46
2. J.Koplic and A.H.Mueller, Phys. Rev. **D12** (1975) 3638
3. A.Capella and A.Kaidalov, Nucl. Phys. **B111** (1976) 477
4. A.Capella and A.Krzywicky, Phys. Lett **67B** (1977) 84
5. A.Capella, J.A.Casado, C.Pajares, A.V.Ramallo and J.Tran Thanh Van, Phys. Rev. **D35** (1987) 2921
6. M.A.Braun, Yad. Fiz. **47** (1988) 262
7. M.A.Braun, Yad. Fiz. **52** (1990) 257
8. V.A.Abramovsky, V.N.Gribov and O.V.Kancheli, Yad. Fiz. **18** (1973) 595
9. M.A.Braun, Yad. Fiz. **48** (1988) 409

Figures

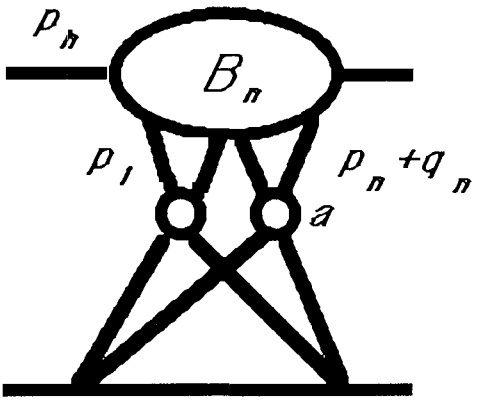

Fig. 1
The hA elastic scattering amplitude

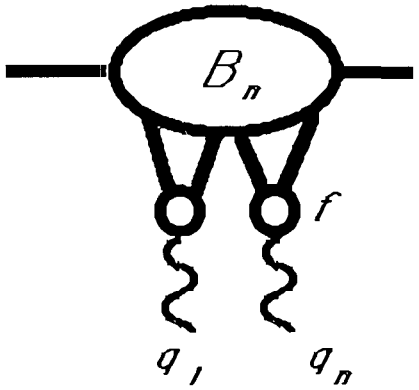

Fig. 2
The n-fold form-factor of the projectile

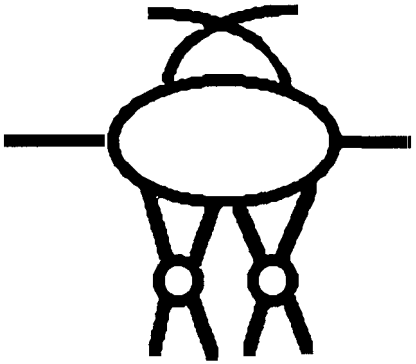

Fig. 3

The diagram for the spectator mechanism of particle production. Only the disconnected part of the wave function contributes

SOFT PHYSICS AND FRAGMENTATION

INTERMITTENCY, A SHORT EXPERIMENTAL REVIEW

B. Buschbeck
Institut für Hochenergiephysik
der Österreichischen Akademie der Wissenschaften
A-1050 Vienna, Austria

Abstract

The search for intermittency is a search for selfsimilarity in the dynamics of multiparticle production, the search for a new scaling law. Recent data from the 2-dimensional analysis give good evidence for its existence in the higher dimensional phase space not only in e^+e^- reactions but also in μp and hadron-hadron reactions and - with unexpected strength - also in heavy ion reactions.

What can we learn from intermittency study? This is often asked and I hope to answer this question in the course of this short review. Since the number of contributions has been strongly rising in the past few years ($\gtrsim$ 50 publications in 1990) it is not possible to cover all the fascinating aspects of this new topic. Therefore I want to restrict mainly to the experimental work and refer for further consultations to three recent very informative reviews [1-3] and references therein.

1 Motivation

The search for intermittency is a search for self-similarity in the dynamics of particle production. It is the search for a new scaling law in multiparticle correlations (or equivalently: fluctuations) [1, 3, 4]. The idea has been brought up already in 1979 when the picture of "fraying" jets was emphasized by R.P. Feynman [5], A. Giovannini [6] and G. Veneziano [7]. Veneziano recognizes: "The resulting picture of a jet is formally similar to that of certain mathematical objects, known as fractals, which look more and more irregular and complex as we look at them with a better and better resolution."

Let me illustrate the idea with fig.1 which represents jet-cascading and is taken from ref.[7]. We cannot directly observe the evolution of the jet, but can measure the correlations of the resulting hadrons in the final state phase space. We hope that we can get information about the Q^2-evolution by measuring particle correlations in dependence of the resolution in the phase space e.g. in dependence of the scale in rapidity δy. It can be expected (if the hadronisation phase does not destroy it) that self-similarity at the evolution stage would produce self-similar fluctuations in the phase space.

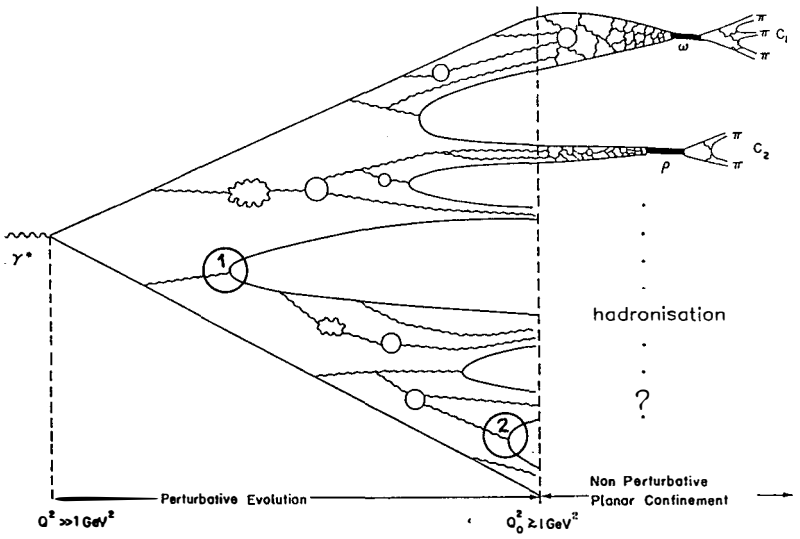

Fig.1: Jet evolution, the selfsimilarity in the parton cascade is due to the fact that the mechanism of evolution is the same at each step (e.g. compare (1) with (2)).

Fig.1 is the picture of a very energetic jet ($\gtrsim$ 100 GeV). Of course this picture cannot be applied to soft hadronic interactions. But early considerations do also exist about this case [8]. Several years later strong particle fluctuations in rapidity (spikes) have been observed in heavy ion reactions and hadron-hadron reactions [9, 10, 11]. Starting at this time from analogy

arguments to the hydrodynamics of turbulent flows, A. Bialas and R. Peschanski [12] conjectured that these strong and unexpected fluctuations in very small rapidity domains could be due to self-similar dynamics in multiparticle production. With a model (α-model) they illustrated the mechanism (multiplication of the fluctuations which occure at each step of the evolution) which can create strong local fluctuatons. They called this phenomenon "intermittency" and argued that in the case of the very energetic JACEE event it could be due to the formation of the Quark Gluon Plasma (QGP). These and other exciting ideas about the physical reasons for such a behaviour [13] - the hope to find new physics and the possibility to quantify the fluctuation study motivated strongly the experimentalists to restart an intense and elaborate study of particle correlations.

2 Definitions

The proposed method in ref.[12] to measure particle density fluctuations quantitatively, consists of the measurement of the factorial moments $\langle F^i \rangle$ of the order i as a function of the resolution δy

$$\langle F^i \rangle = \frac{1}{M} \sum_{m=1}^{M} \frac{\langle n_m(n_m-1)\dots(n_m-i+1)\rangle}{\langle n_m \rangle^i} \tag{1}$$

They are obtained by dividing an original rapidity interval Δy successively into more and more (M) subintervals. The number n_m is the (charged) particle multiplicity in a distinct event in bin m ($m = 1 \dots M$) of the size $\delta y = \Delta Y/M$. The averages under the sum are taken over all events in the sample. Intermittency is defined by a power law dependence

$$\langle F^i \rangle \propto (1/\delta y)^{f_i}\,,\ f_i > 0 \tag{2}$$

$$\log \langle F^i \rangle = a_i + f_i . \log(1/\delta y) \tag{3}$$

and the powers f_i are called intermittency indices which characterize the strength of the effect. In the case of statistical fluctuations only the $\langle F^i \rangle$ are independent from δy (i.e. $f_i = 0.$).

Eq.(2) is a scaling law, because the quantity R depends only on the ratio L/l:

$$R = \langle F^i(l) \rangle \,/\, \langle F^i(L) \rangle = (L/l)^{f_i} \tag{4}$$

In the strict sense intermittency can be said to occur only if the power law (2) holds for $\delta y \to 0$. Experimentally, one can test this behaviour only in a limited δy region, because of a) physical reasons (occurence of a cutoff parameter, e.g. end of the parton cascade), and b) practical reasons (limited detector resolution, limited event statistics).

The $\langle F^i \rangle$ are integrals over the correlation functions C_i [14]. Intermittency (only in the strict sense!) would show up as a singularity in $C_2(y_1 = y_2)$.

3 A short review of experimental data

Within a short time various experiments gave results from the 1-dimensional intermittency study in the variables rapidity (y), pseudorapidity (η) and azimuthal angle (ϕ). Data exist now for e^+e^- [15-20], μp [21], νA [22], hh [23, 24], hA [25, 26] and AA [25, 27-30] collisions. Some examples are shown in fig.2.

In fig.3 (taken from refs.[1,2]) a comparison is shown of the parameters $d_i = f_i/(i-1)$, the anomalous dimensions [31, 32] for different reactions. The f_i values have been obtained from linear fits applied to the $\log\langle F^i \rangle$ vs $\log\,(1/\delta y)$ plots in the resolution region $1 \gtrsim \delta y(\delta\eta) \gtrsim 0.1$ where good linearity has been observed in all reactions considered. We observe [1] that a) the

d_i increase with the order i, b) the d_i become smaller with increasing complexity of the reaction type, and c) for AA reactions, they are only weakly dependent on i.

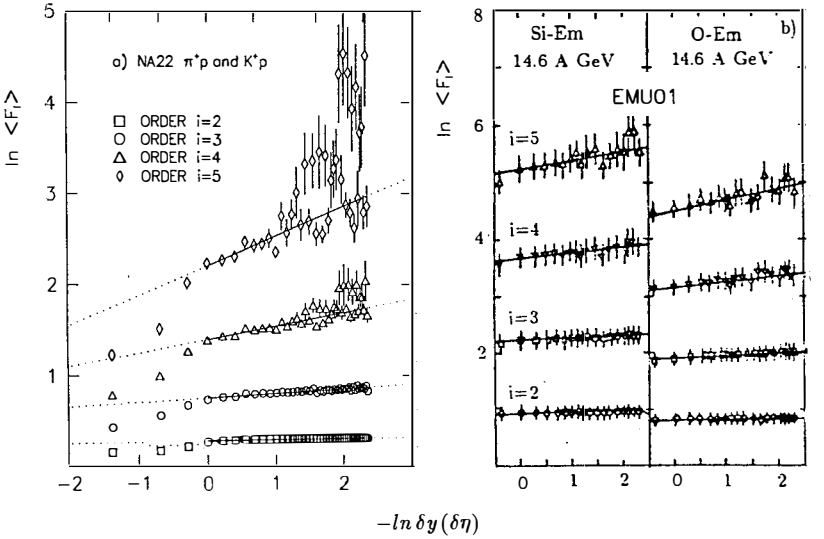

Fig.2: Two examples for the linearily rising $ln \left\langle F^i \right\rangle$ for small δy (refs.[23, 27]).

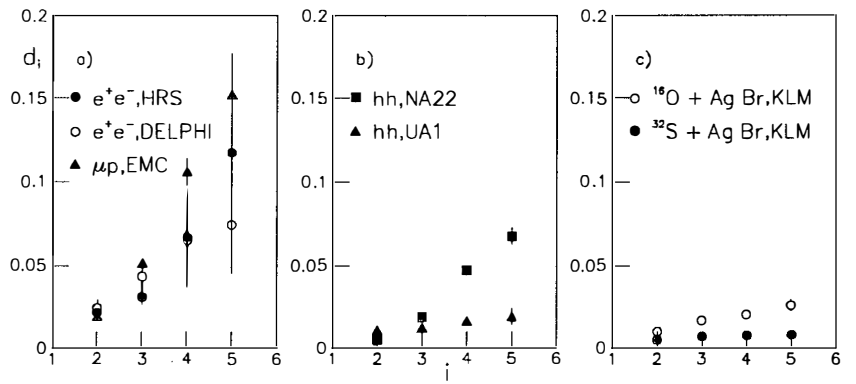

Fig.3: Anomalous dimensions d_i as a function of the order i.

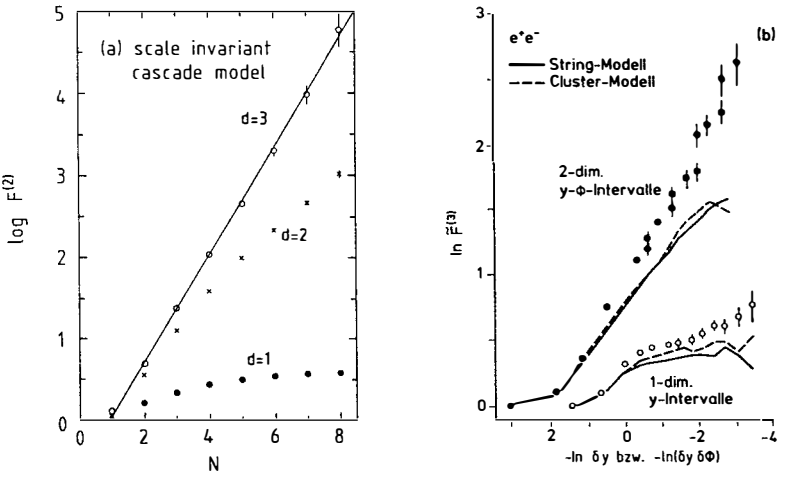

Fig.4: The effect of projections on lower dimensional phase space: a) Monte Carlo simulation according to a simple scale invariant cascade model [4], b) experimental verification with e^+e^- reactions from TASSO [17, 33].

Enlivening discussions have been going on in the last year, if the observed linearity of log $\langle F^i \rangle$ vs log $(1/\delta y)$ in a restricted region of δy is really enough to claim that one has observed intermittency in the data [14]. Sometimes a bending is observed for $\delta y < 0.1$ which cannot be attributed to limited detector resolution [27], moreover there is normally a bending at $\delta y = 1$ (fig.2a). However, the evolution of quarks and gluons naturally proceeds in the 4-dimensional energy-momentum space and it was W. Ochs and J. Wosiek [13b] who repeatedly demanded an analysis in more than one dimension. W. Ochs [34] and in the same year also A. Bialas and J. Seixas [35] explained how projections from higher dimensional intermittency can destroy the linearity and diminish the f_i values dramatically. This is shown in fig.4a and confirmed by e^+e^- data (fig. 4b). Presently there exist data for different reaction types as shown in fig.5. A good linearity is observed over the whole range of investigations already in 2-dimensional plots. In particular no bending at $(\delta y \,.\, \delta\phi) = 1$ is visible.

4 Can the observations be explained with known mechanisms?

As already mentioned, it was the hope to find something new that motivated intermittency work to a large extent. However, before claiming new physics it is necessary to discuss carefully what can be predicted by - or explained with - already known mechanisms.

The effects of standard short-range correlations on the behaviour of $\langle F^i \rangle$ has been discussed by the Orsay [37] and Arizona [38] groups. A recent review with a very interesting and competent discussion has been given by K. Fialkowski [39]. Some remarks can be made: (i) The behaviour of $\langle F^2 \rangle$ at small δy is governed by the shape of the correlation function C_2 at $|y_1 - y_2| \to 0$ where no predictions exist from the Muller Regge Theory (except that C_2 should be finite). (ii) Similarly there do not exist predictions for higher order[1] correlations, contributing to $\langle F^i \rangle$ for $i \geq 3$.

[1]The linked pair ansatz, proposed by the Arizona group is highly non-trivial and may be compatible with a cascading mechanism [40].

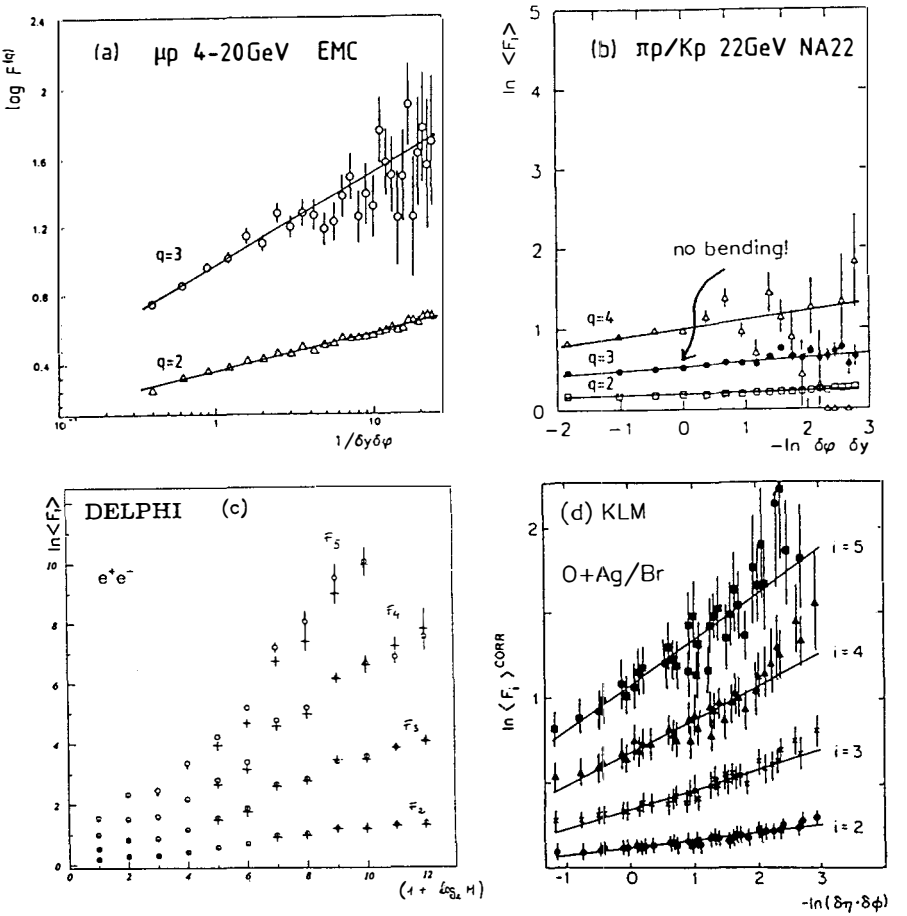

Fig.5: Analysis in 2-dimensional $y(\eta)$ and azimuthal angle $\phi(\varphi)$ space with different reactions [19, 21, 23, 25]. In fig.5c the data (0) are compared with predictions of the LUND shower model (+) [36].

Another approach to answer the question, is to investigate the influence of distinct known effects like resonance production and hard parton scattering with jet production in hadronic interactions, the Bose Einstein effect and - in the case of e^+e^- reactions - the effect of QCD cascading as shown in fig.1. This can best be done with Monte Carlo Models. The result of the various Monte Carlo studies are illustrated with few examples in figs.4b, 5c, 6, 7. In contrast to earlier studies (fig.4b) more recent investigations of e^+e^- reactions of DELPHI (fig.5c) CELLO and OPAL show agreement with versions of the LUND shower Monte Carlo. From the initial considerations (fig.1) we expect self-similarity in these Monte Carlos based on parton cascading, however, in ref.[2] is demonstrated that the relative contributions from the hard parton cascade and the soft phase depend strongly on the assumptions about the cutoff parameter for the perturbative part.

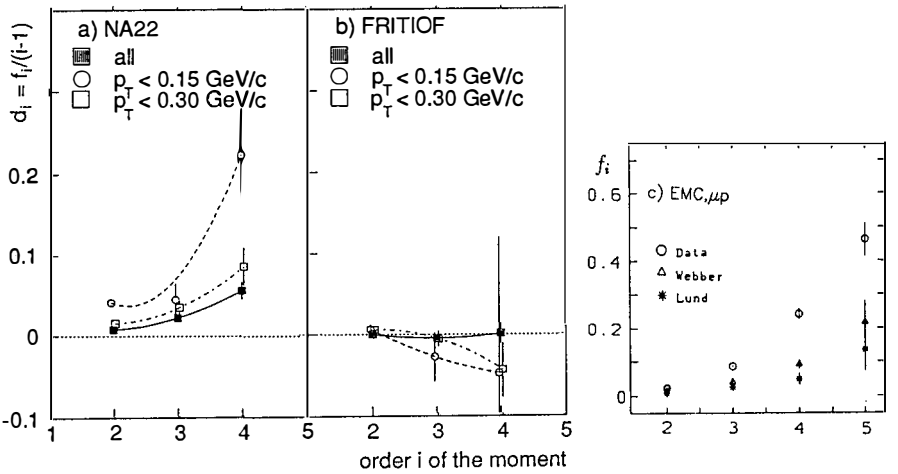

Fig.6: Comparison of the slope parameters in terms of d_i or f_i with Monte Carlo models: a) b) is a comparison of hadronic reactions at $\sqrt{s} = 22$ GeV [41] and c) of μp reactions [21].

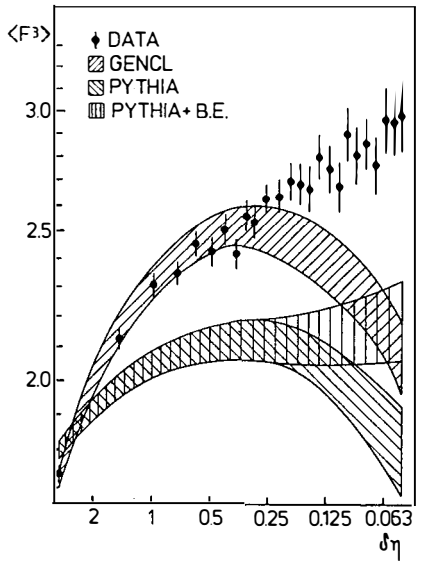

Fig.7: Comparison of the $\langle F^3 \rangle$ values for a low multiplicity sample of collider events from UA1 with different Monte Carlos [24].

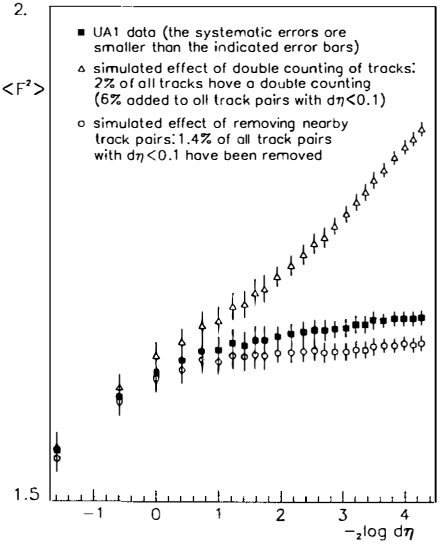

Fig.8: A demonstration of the danger of introducing systematical erros in bins with low average multiplicities.

Moreover, when searching for intermittency from parton cascading, one has to go to sufficiently high energy of the jets, otherwise more trivial effects could play the dominant role [42]. All other reactions (figs.6,7) disagree with the Monte Carlo predictions[2].

At the end of this section I want to warn about the danger of introducing biases into the data [2]. As demonstrated in fig.8, double counting of tracks or the loss of nearby pairs could cause large systematic errors in bins with small average multiplicity, i.e. in very small rapidity bins or even in moderate bins in the higher dimensional analysis.

5 The puzzle of heavy ion reactions

Fig.9 is a comparison of intermittency parameters f_3 of hh reactions with heavy ion reactions in dependence of the multiplicity density $dn/d\eta$ as proposed by A. Bialas [1, 31, 43].The strong dependence of f_i on $dn/d\eta$ observed in the UA1 data has been explained by the simple assumption that events with high multiplicity represent emissions of particles by several independent sources whereas only one (or few) sources contribute to low multiplicity events [32]. The chains of the Dual Parton Model may be good candidates for such sources [44].

One can argue [31, 37, 45] that such a superposition leads to the simple and approximate relations

$$f_i(N) = f_i(1)/N\,,\; f_i(dn/d\eta) \propto (dn/d\eta)^{-1} \tag{5}$$

where N is the number of sources which are assumed to be proportional to $dn/d\eta$.

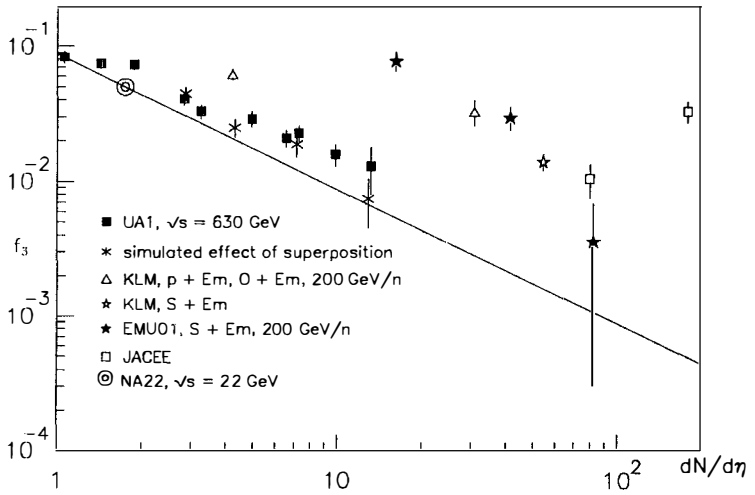

Fig.9: Bialas plot: a comparison of intermittency parameters of hh reactions with heavy ion reactions.

The UA1 data follow quite reasonable such a law. The straight line represents eqn.(5). If heavy ion reactions were superpositions of NA22 events (which have comparable energy/nucleon), the corresponding f_i values would lie all on the line. However, the observed f_3 values are about 10 times higher and indicate the existence of collective[3] effects. A similar effect is shown for f_2

[2]However, the influence of the Bose Einstein effect needs to be studied in more details. It could play a dominant role in very small phase space bins [46].

[3]The weak dependence of d_i on the order i (fig.3c) in heavy ion reactions could be another indication for new effects [47].

[1, 43]. But again, before claiming new effects we have to be sure that the enhanced f_i values cannot be explained[4] by more conventional effects. A. Capella et al. [48] obtained some rough estimates for f_2 values from Bose-Einstein correlations in heavy ion reactions. They are comparable with the observed ones. However, their arguments are incompatible with the decrease of f_i values with increased centrality of the ion reactions which have been observed by EMUO1 [49] and is also visible in fig.9.

6 What can we learn from intermittency study ?

Intermittency study is a new type of correlation study. It consists of the investigation of the dependence of the factorial moments (or even better: the factorial cumulants [40]) on the resolution (scale) in the phase space. Though we lose information by integrating over correlation functions, we gain on the other side another piece of information by the increased statistical accuracy. This enables us to study correlations in much smaller phase space bins than before and investigate the dependence on the scale over a wider range. It enables us also to extend our studies to higher phase space dimensions and to higher orders. Intermittency study should not replace ordinary correlation study[5] but supplement it.

The search for intermittency is a search for a power law dependence of the $\langle F^i \rangle$ on the scale. The experimental data from various reactions in a 2-dimensional analysis show good evidence for its existence. If further confirmations can be obtained in the future this will signalize self-similarity in the dynamics of multiparticle production - the existence of a new scaling law. This possibility has stimulated many new and exiting theoretical considerations (examples are found in refs.[1, 3, 4, 13]). In particular, the multiparticle systems could be investigated in analogy to other complex statistical systems which exhibit self-similarity or (multi) fractality [3, 50].

I want to restrict here to the experimental achievements which I have shown briefly in this short review:

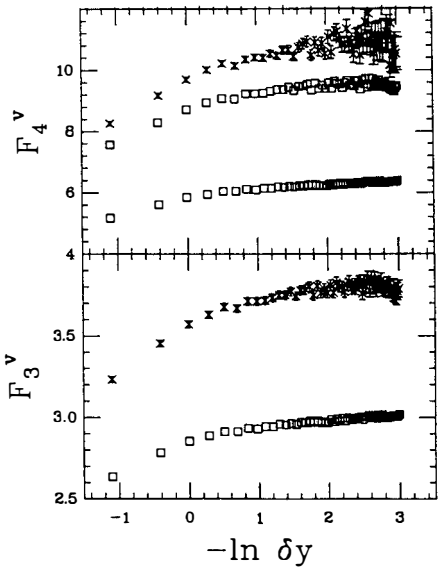

a) we have gained new data on correlations in very small phase space regions down to $\delta y \approx 0.1$, sometimes even to $\delta y \approx 0.01$,

b) we have gained new data on higher order correlations. As an example let me mention the beautiful cumulant decomposition of collider data from the UA1 experiment by the Arizona group [40]. It is shown in fig.10 and demonstrates that genuine higher order correlations do exist in the data down to the smallest bin ($\delta\eta = 0.05$) which has been investigated and at least up to the 4-th order,

Fig.10: shows the decomposition of UA1 factorial moments into components deriving from particle correlations of lower order. The crosses show the data. In each case, the lowest squares exhibit the contribution of the two-particle correlation function. The next higher squares show the effect of including the (experimentally determined) three particle correlations [40].

[4]The HELIOS collaboration shows the danger that measurements in emulsions include the bias of γ-conversions [30].

[5]Another extention - to study the factorial correlators - has been proposed in ref.[51], new results are given in ref.[52].

c) we have gained very recently new data on correlations in the 2-dimensional[6] phase space.

Can we learn something about new physics?

a) With the exception of e^+e^- reactions, in all other reaction types the observed rise of the $\langle F^i \rangle$ cannot be reproduced by Monte Carlo Models up to now. Further investigations are necessary to answer the question if we need new physics or if some known effects are not sufficiently treated in the Monte Carlo Models. The Bose Einstein correlations may play an important role [54].
b) Of special interest is the question, if the observed behaviour of heavy ion reactions as discussed in section 5 is due to some known effect (again the Bose Einstein effect is a candidate) or signalizes new physics (maybe the formation of the QGP, or droplets [55] of it?)

Acknowledgements

I want to thank A. Bialas, A. Capella, P. Carruthers, G. Cohen-Tannoudji, H. Dibon, I. Dremin, W. Kittel, P. Lipa, M. Markytan, N. Neumeister, W. Ochs, R. Peschanski, D. Seibert and J. Seixas for helpful discussions.
With gratitude I remember our teacher and friend Léon Van Hove.

References

[1] *A. Bialas*, "Intermittency 90", CERN-TH 5791/90 (to be published in Nucl. Phys. A (Proc. Suppl.).

[2] *W. Kittel*, "Intermittency, a review of experimental results", Nijmegen Pre HEN-335/90.

[3] *R. Peschanski*, "Intermittency in Particle Collisions", CERN-TH 5891/90, subm. to Int. J. Mod. Phys. A.

[4] *W. Ochs*, "Scaling and scale breaking phenomena in multiparticle production", MPI-PAE 78/90; "Selfsimilar cascade structure in multiparticle production processes", MPI-PAE/PTh 73/90.

[5] *R.P. Feynman*, Proc. of the 3rd Workshop on Current Problems in High Energy Particle Theory, Florence, 1979, eds. R. Casalbuoni et al., Johns Hopkins University Press, Baltimore.

[6] *A. Giovannini*, Proc. of the 10th Intern. Symposium on Multiparticle Dynamics, Goa (India), Sept. 25-29, 1979, eds. S.N. Ganguli, P.K. Malhotra and A. Subramanian.

[7] *G. Veneziano*, Proc. of the 3rd Workshop on Current Problems in High Energy Particle Theory, Florence, 1979, eds. R. Casalbuoni et al., Johns Hopkins University Press, Baltimore.

[8] *P. Carruthers and Minh Duong-Van*, "Evidence for a commen fractal dimension in turbulence, galaxy distributions and hadronic multiparticle production", Los Alamos preprint LA-UR-83-2419.

[9] *T.H. Burnett et al. (JACEE)*, Phys. Rev. Lett. 50 (1983) 2062.

[10] *M. Adamus et al. (NA22)*, Phys. Lett. B185 (1987) 200.

[11] *P. Carlson (UA5)*, 4th Topical Workshop on $p\bar{p}$ Collider Physics, Bern, March 1983 and *G.J. Alner et al. (UA5)*, Phys. Rep. 154 (1987) 247.

[12] *A. Bialas and R. Peschanski*, Nucl. Phys. B273 (1986) 703 and B308 (1988) 857.

[13] a) *I. Dremin*, JETP Lett. 30 (1980) 140, Mod. Phys. Lett. A13 (1988) 1333 and contribution to this conference;
b) *W. Ochs and J. Wosiek*, Phys. Lett. B214 (1988) 617, B232 (1989) 271;
c) *A. Bialas and R. Peschanski*, Phys. Lett. B207 (1988) 59;
Ph. Brax and R. Peschanski, Phys. Lett. B253 (1991) 225.
d) *P. Dahlqvist, B. Andersson and G. Gustafson*, Nucl. Phys. B328 (1989) 76.
e) *L. Van Hove*, Annals of Physics 192 (1989) 66.
f) *C.B. Chiu and R. Hwa*, Phys. Lett. B236 (1990) 466.
g) *M. Biyajima et al.*, Phys. Lett. B237 (1990) 563;
h) *J. Dias de Deus and J. Seixas*, Phys. Lett. B246 (1990) 506.

[6] Preliminary data exist in three dimensions [53].

[14] See for instance contributions of *K. Fialkowski, I. Sarcevic and E.A. De Wolf* to the Santa Fe Workshop on "Intermittency in High Energy Collisions", eds. F. Cooper, R.C. Hwa and I. Sarcevic, World Scientific, Singapore, 1990.

[15] *B. Buschbeck, P. Lipa and R. Peschanski*, Phys. Lett. B215 (1988) 788.

[16] *S. Abachi et al. (HRS)*, "Study of Intermittency in e^+e^- Annihilations at 29 GeV, preprint ANK-HEP-CP-90/50.

[17] *W. Braunschweig et al. (TASSO)*, Phys. Lett. B231 (1989) 548.

[18] *H.-J. Behrend et al. (CELLO)*, Intermittency in Multihadronic e^+e^- Annihilations at 35 GeV, paper submitted to the XXV Int. Conf. on High Energy Physics, Singapore, 1990.

[19] *P. Abreu et al. (DELPHI)*, Phys. Lett. B247 (1990) 137;
A. DeAngelis, Mod. Phys. Lett. A5 (1990) 2395.

[20] *M.Z. Akrawy et al. (OPAL)*, CERN-PPE/91-37.

[21] *I. Derado, G. Jancso, N. Schmitz and P. Stopa (EMC)*, Z. Phys. C47 (1990) 23 and Santa Fe Workshop (ref.[14]).

[22] *L. Verluyten et al. (WA59 and E180)*, "Study of Factorial Moments in Neutrino Neon and Deuteron Charged Current Interactions", paper submitted to the XXV Int. Conf. on High Energy Physics, Singapore, 1990.

[23] *I.V. Ajinenko et al. (NA22)*, Phys. Lett. B222 (1989) 306 and B235 (1990) 373;
W. Kittel (NA22), "Low p_t Intermittency in π^+p and K^+p Collisions at 250 GeV/c", Proc. Santa Fe Workshop on Intermittency in High Energy Collisions.

[24] *C. Albajar et al. (UA1)*, Nucl. Phys. B345 (1990) 1.
preliminary data on 2-dim. analysis are given by *H. Dibon and M. Markytan*, XX Int. Symp. on Multiparticle Dynamics, Gut Holmecke, Germany, 1990, and at the Singapore Conference 1990 and in the Thesis of P. Lipa, Univ. of Vienna, 1990.

[25] *R. Holynski et al. (KLM)*, Phys. Rev. Lett. 62 (1989) 733 and Phys. Rev. C40 (1989) R2449.

[26] *NA22 Collaboration*, "Factorial Moments and Correlations in Meson-Nucleus Interactions at 250 GeV/c", paper submitted to the XXVth Int. Conf. on High Energy Physics, Singapore, 1990.

[27] *M.I. Adamovich et al. (EMU-01)*, Phys. Rev. Lett. 65 (1990) 412;
M.I. Adamovich et al. (EMU-01), "Energy, Target, Projectile and Multiplicity Dependence of Intermittency Behaviour in High Energy $O(Si, S)$ Induced Interactions", Wuhan preprint HZPP-90-8 (1990).

[28] *K. Sengupta, P.L. Jain, G. Singh and S.N. Kim (EMU-08)*, Phys. Lett. B236 (1990) 219.

[29] *I. Derado (NA35)*, "Investigations of Intermittency in Reaction $^{32}S + ^{32}S$ at 200 GeV per Nucleon", Festschrift Léon Van Hove, eds. A. Giovannini and W. Kittel (World Scientific 1990).

[30] *T. Åkesson et al. (HELIOS)*, "A Search for Multiplicity Fluctuations in High Energy Nucleus-Nucleus Collisions", preprint CERN-PPE/90/120.

[31] *A. Bialas*, Festschrift Léon Van Hove, eds. A. Giovannini and W. Kittel, World Scientific, 1989.

[32] *P. Lipa and B. Buschbeck*, Phys. Lett. B223 (1989) 465;
P. Lipa, Thesis, Univ. of Vienna (1990).

[33] *W. Ochs*, Physikalische Blätter 46 (1990) 123.

[34] *W. Ochs*, contribution to the Santa Fe Workshop, see ref.[14]; MPI-PAE/PTh 26/90; MPI-PAE/PTh 35/90.

[35] *A. Bialas and J. Seixas*, Phys. Lett. B250 (1990) 161.

[36] *T. Sjöstrand*, Comp. Phys. Comm. 27 (1982) 243, ibid. 28 (1983) 229.
T. Sjöstrand and M. Bengtsson, Comp. Phys. Comm. 43 (1987) 367.

[37] *A. Capella, K. Fialkowski and A. Krzywicki*, Phys. Lett. B230 (1989) 271; Festschrift L. Van Hove, eds. A. Giovannini and W. Kittel, World Scientific, 1989, p.413.

[38] *P. Carruthers and I. Sarcevic*, Phys. Rev. Lett. 63 (1989) 1562;
I. Sarcevic, Santa Fe Workshop, see ref.[14].
H.C. Eggers, Thesis, Univ. of Arizona (1991).

[39] *K. Fialkowski*, Santa Fe Workshop, see ref.[14].

[40] *P. Carruthers, H.C. Eggers and I. Sarcevic*, Phys. Lett. B254 (1991) 258.

[41] *N.M. Agababyan et al. (NA22)*, Nijmegen HEN 338/1991.

[42] *O. Podobrin*, this conference.

[43] *B. Buschbeck*, Santa Fe Workshop, see ref.[14].

[44] *G. Cohen-Tannoudji, A. El Hassouni, J. Kalinowski, O. Napoly, R. Peschanski*, Phys. Rev. D21 (1980) 2689;
F.W. Bopp, A. Capella, J. Ranft and J. Tran Thanh Van, "Multiparticle Correlations in a Two Component Dual Parton Model", Orsay preprint 1990, to be subm. to Z. Phys. C.

[45] *D. Seibert*, Phys. Lett. B240 (1990) 215.

[46] *N. Neumeister*, private communication.

[47] *A. Bialas and R. Hwa*, Phys. Lett. B253 (1991) 436.

[48] *A. Capella, A. Krzywicki and E.M. Levin*, LPTHE Orsay 91/3.

[49] *M.I. Adamovich et al. (EMU-01)*, Cosmic and Subatomic Physics Report LUIP 9011 (University of Lund).

[50] see the theoretical contributions to the Santa Fe Workshop (ref.[14]); in the case of the multifractal analysis proposed by *C. Chiu and R.C. Hwa* also first experimental results were presented by *M. Markytan, H. Dibon and K. Sugano.*

[51] *A. Bialas and R. Peschanski*, Nucl. Phys. B308 (1988) 857;
R. Peschanski and J. Seixas, CERN-TH-5903/90, DF/IST-3-90.

[52] *W. Kittel*, this conference and HEN-332-90.

[53] *A. De Angelis and N. Demaria*, DELPHI 90-45 PHYS72 (1990).
H.J. Behrend et al., DESY-90-114.

[54] *M. Gyulassy*, Festschrift Léon Van Hove, ref.[31].

[55] *D. Seibert, J. Seixas*, private communication.

Intermittency and Bose-Einstein Correlations in e^+e^- Annihilation

O. Podobrin, DESY, Notkestraße 85, W-2000 Hamburg 52, Germany
representing the CELLO collaboration

ABSTRACT

Intermittency studies in one, two and three dimensions are presented, based on e^+e^- annihilation data taken by CELLO at the PETRA storage ring at 35 GeV centre of mass energy. The results are compared to predictions from different Monte Carlo models and are discussed in context with measurements from other experiments at PETRA and LEP. A variety of hadronization models, although based on very different approximations to QCD, all provide a consistent description of factorial moments in all dimensions. We conclude that the resolution dependence of factorial moments is due to a superposition of many effects, and that the structure of soft gluon radiation is obscured by resonance decays and therefore remains unresolved.

Bose-Einstein correlations are analyzed using two methods to obtain a reference density. The data are compared to the predictions from the approach taken in Jetset and are further used to determine the relevant Monte Carlo parameters.

INTRODUCTION

In this talk the notion of intermittency in e^+e^- annihilation is discussed on the basis of CELLO data, with attention to results from other e^+e^- experiments. Following this, results on Bose-Einstein correlations are presented.

The basic aim of intermittency studies [1] is to analyze particle production in variable regions of phase space by means of factorial moments $\langle F_i \rangle$:

$$\langle F_i \rangle = \frac{M^i}{\langle N \rangle^i} \cdot \left\langle \frac{1}{M} \cdot \sum_{m=1}^{M} n_m(n_m-1)\cdots(n_m-i+1) \right\rangle \qquad (1)$$

This formula defines an observable which is sensitive to density fluctuations inside *single* events and in addition is insensitive to Poissonian noise.

In e^+e^- annihilation the first direct measurement of factorial moments of rapidity (y) distributions and rapidity and azimuth (y, ϕ) correlations was performed by TASSO [2], showing qualitative agreement between data and Monte Carlo, although the quantitative description was rather poor. However, no attempt was made to tune the relevant Monte Carlo parameters. The first three-dimensional phase space analysis was done by CELLO [3], using the decomposition $dLIPS \propto dp_x/\sqrt[3]{E} \cdot dp_y/\sqrt[3]{E} \cdot dp_z/\sqrt[3]{E}$. In this analysis factorial moments were expressed in terms of fractal dimensions, making the underlying physics more transparent. Owing to the excellent Monte Carlo description, provided by Jetset 7.2 PS, the contributions to the resolution dependence of factorial moments of individual processes in the fragmentation of quarks and gluons could be isolated. At LEP, analyses in one and two dimensions are available from DELPHI [4] and OPAL [5]. Factorial moments from both experiments are well described by standard Monte Carlo programs. Here we present a comprehensive intermittency analysis in one, two and three dimensions, some aspects of which have already been presented elsewhere [6,7].

INTERMITTENCY IN ONE, TWO AND THREE DIMENSIONS

The dependence of factorial moments on the resolution scale is studied by dividing D_0-dimensional projections of phase space simultaneously in each dimension into halves. After

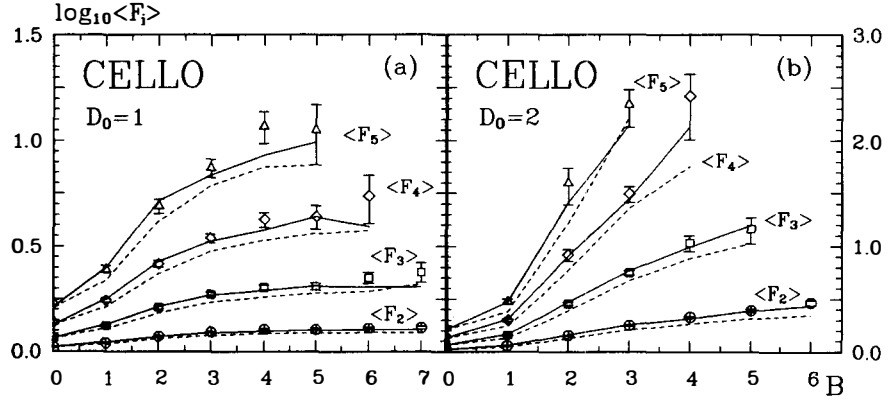

Figure 1: $F_2 - F_5$ from analyses in y (a) and y, ϕ (b) projections. The rapidity has been restricted to the interval $-2 \leq y \leq +2$. The data are shown with statistical errors, the dashed lines correspond to results from Jetset 7.2 PS after detector simulation, the solid lines include Bose-Einstein correlations. The detector resolution limit is between $B = 5 - 6$.

B bisections a total of $M = 2^{D_0 \cdot B}$ symmetric bins is obtained. In Fig. 1a the results from a one-dimensional y analysis are seen to be in perfect agreement with the Jetset 7.2 PS Monte Carlo [9]. It is also evident that the inclusion of Bose-Einstein correlations, as treated in Jetset, results in larger moments, consistent with the data. This increase reflects the effective reduction of phase space for identical pions. Apparently the moments in the one-dimensional analysis saturate after a strong initial rise.

Such an effect is expected for a multi-dimensional system being projected on to a one-dimensional axis [10]. In the two-dimensional y, ϕ analysis (Fig. 1b), the bending effect, although still visible, is much less severe, indicating that the underlying process is probably three-dimensional. This is as expected, of course. As before, excellent agreement between data and Monte Carlo is observed, with the Bose-Einstein effect accounting partly for the observed effect. In Fig. 2 a comparison between predictions from Jetset 7.2 [9], Ariadne 3.1 [11] and Herwig 5.0[1] [12] is presented. Striking agreement is observed amongst the different approaches. This is in fact astounding since these models differ in the treatment of the perturbative QCD phase (parton shower, dipole radiation or matrix element) and moreover use different hadronization schemes (cluster or strings).

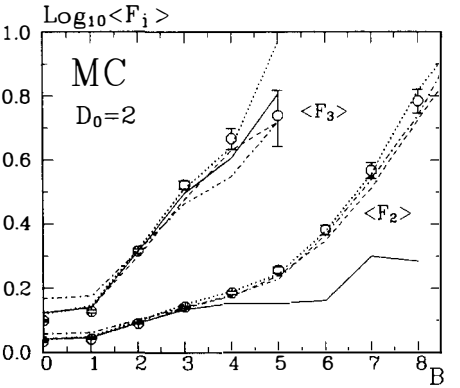

Figure 2: Monte Carlo studies of F_2 and F_3 in y, ϕ. The points with error bars correspond to Jetset 7.2 PS (parton shower+string), the dotted curve is Jetset 7.2 ME (Matrix element+string). The results from Ariadne 3.1 (dipole radiation+string) are shown as the dashed curve and the Herwig 5.0 model (parton shower+cluster) gives the dash-dotted curves. The solid line is Jetset 7.2 PS without π^0 Dalitz decays.

From this we conclude that the sensitivity of factorial moments to details of the soft hadronization process is rather poor. In particular resonance decays obscure the fine structure of F_2, explicitly shown in Fig. 2 for the π^0 Dalitz decay. It is to note that besides the common interpretation of intermittent behaviour as a consequence of random cascading, an equally good explanation is provided by the matrix element approach.

It has been argued that there is a discrepancy between TASSO and CELLO data, the former being only qualitatively reproduced by the Monte Carlo, whilst the latter is perfectly described. However, this effect is to a large extend due to the different Monte Carlo programs and parameters used. This is apparent in Fig. 3, where factorial moments obtained

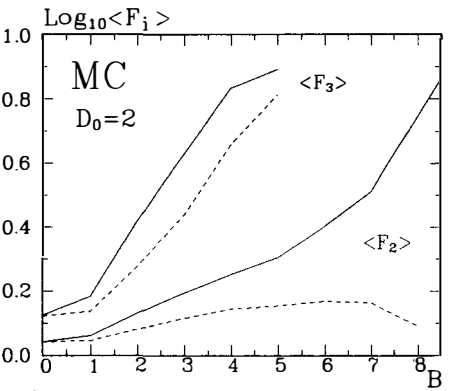

Figure 3: Comparison of F_2 and F_3 in y, ϕ from Jetset 6.3 PS as used by TASSO [15] (dashed curves) and Jetset 7.2 PS, including Bose-Einstein correlations, as used by CELLO (solid lines).

[1] Herwig has been modified to invoke Jetset for particle decays.

from the TASSO version of Jetset 6.3 PS [15] are compared to the corresponding results from the default Jetset 7.2 PS, as used in our studies.

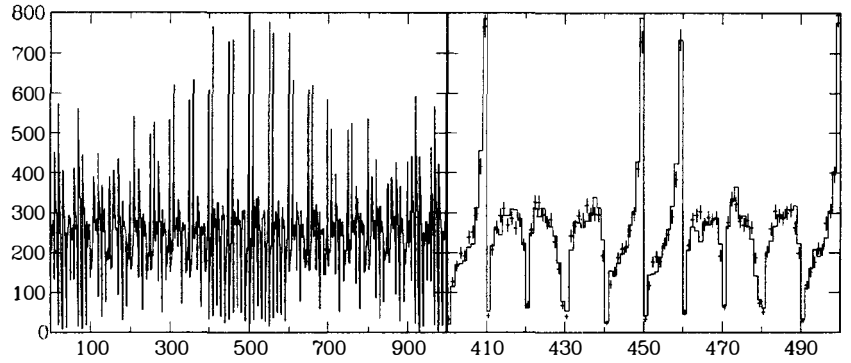

Figure 4: Particle density after the transformation [16], for ten bins in each dimension. The resulting 1000 boxes are labeled $100 * I(\vec{y}) + 10 * I(\vec{\phi}) + I(\vec{p_\perp^2}) : I = 0, ..., 9$. The right plot shows a detail, where the data (crosses) are compared to the Jetset 7.2 PS simulation (histogram).

Besides the three-dimensional analysis presented in [3] we have applied the procedures advocated by Ochs [16] and Bialas and Gazdzicki [17]; for details the reader is referred to a forthcoming publication [8]. The basic aim of both procedures is to unfold fluctuations induced by non constant inclusive distributions. This is of special importance in a three-dimensional analysis, involving strongly varying distributions such as $p_\perp^2$. In [17] this is achieved by dividing the phase space in a way that on average every phase space box contains the same number of particles. The method proposed by Ochs treats the three variables (e.g. $y, \phi, p_\perp^2$) independently. In the ideal case of uncorrelated variables the particle distribution in the transformed space would be flat, i.e. every box would contain the same number of particles. This condition is apparently not fulfilled (Fig. 4), since a clearly non constant

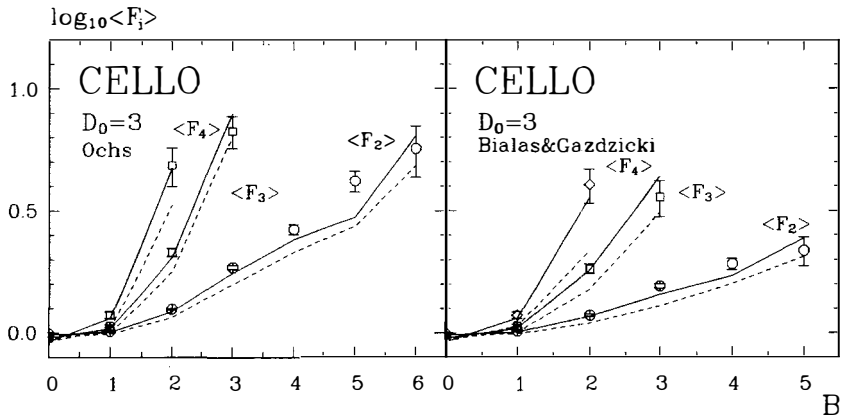

Figure 5: $F_2 - F_4$ from three-dimensional analyses according to the procedures proposed in [16] and [17]. The Jetset 7.2 PS simulations are superimposed as the solid (including Bose-Einstein correlations) and dashed lines.

particle density is observed after the transformation. The high quality of the Monte Carlo simulation is demonstrated in Fig. 4, where it is seen to reproduce the phase space population extremely well. In Fig. 5 the results from both procedures are displayed together with the corresponding Monte Carlo curves. As for the one- and two-dimensional analyses, good agreement is observed between data and Monte Carlo. It is also seen that the method [16] results in larger moments compared to the method [17]. This is due to the fact that in the former procedure the inclusive distribution is not constant (Fig. 4).

It should be noted that even after the transformation [17], fluctuations remain due to the mixture of different event topologies; e.g. 2-jet and 3-jet events, or light and heavy quark events. Since the correction procedure is based on the average of all events, fluctuations are eventually induced in the subgroups, complicating the interpretation of the data. This is clearly a disadvantage compared to the method used in [3].

To illustrate the influence of different physical processes on the factorial moments we have performed some studies with Jetset. In addition, the analysis of 2-jet events gives information about the contribution from hard gluon radiation. In Fig. 6 the resulting moments are presented; compared to the total event sample in Fig. 5, a much slower rise is observed.

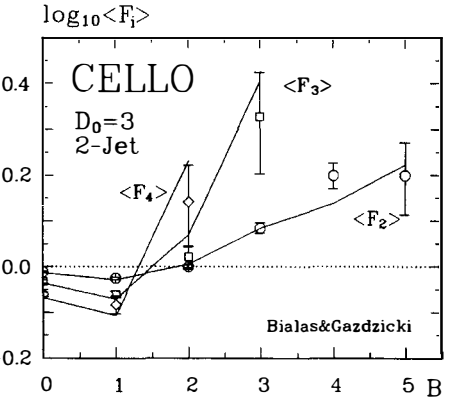

Figure 6: $F_2 - F_4$ from a three-dimensional analysis of 2-jet events according to [17]. The Jetset 7.2 PS simulation including Bose-Einstein correlations is represented by the solid lines.

This indicates that hard gluon radiation is an important source of fluctuations at PETRA energies and probably the dominant source at LEP energies [4,5]. The dominant contribution of hard gluon radiation, in contrast to the *noise* from soft gluons, to the fluctuations observed in hadronization processes is also discussed in [13]. At coarse resolution the 2-jet data show negative slopes, which can be interpreted as anti-correlations [14]. Such an effect is expected as a consequence of local $p_\perp$ conservation, which reduces the probability to find particles with the same y and ϕ coordinates. This is made clearer in Fig. 7, where strong anti-correlations are observed for primary particles produced in $q\bar{q}$ events without gluon radiation. The decay products of these primary particles show only a residual effect, since the momentum transfer involved in the decays (cf. Fig. 9) is of the same order

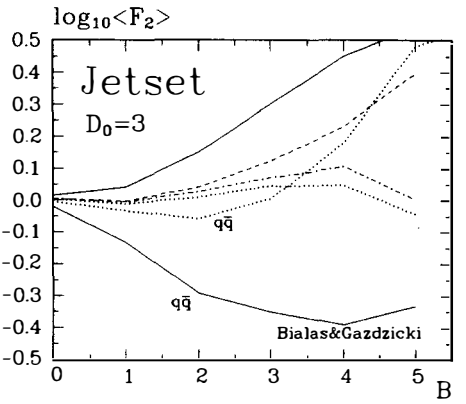

Figure 7: F_2 from various Jetset 7.2 scenarios: **Curves labeled $q\bar{q}$:** Solid line: primary particles from $q\bar{q}$ events: Dotted line: ditto, after decays. **Unlabeled curves:** Dashed line: default PS simulation: Solid line: ditto, including initial state radiation: Dash-dotted line: default PS, neglecting e^+e^- pairs from π^0 Dalitz decays: Dotted line: ditto, in addition $\pi^+\pi^-$ pairs from $\eta \to \pi^+\pi^-\pi^0$ and $\eta' \to \pi^+\pi^-\eta$ decays are neglected.

of magnitude as the $p_\perp$ in the fragmentation process. The factorial moments are strongly influenced by both hard photon and hard gluon radiation. This becomes very clear in Fig. 7 where a simple $q\bar{q}$ model is compared to the standard Jetset 7.2 parton shower with and without initial state photon radiation. This situation is different on the Z^0 resonance, where initial state radiation is suppressed. Particle decays are of prime importance for understanding the intermittency behaviour in $\epsilon^+\epsilon^-$ interactions, as is demonstrated by the π^0 Dalitz decay and the decays $\eta \rightarrow \pi^+\pi^-\pi^0$ and $\eta' \rightarrow \pi^+\pi^-\eta$, which are responsible for the main part of the effect observed at intermediate and high resolution.

BOSE-EINSTEIN CORRELATIONS

In the previous discussion of intermittency, the relevance of particle correlations has been pointed out. In this context the analysis of Bose-Einstein correlations can provide further information on the underlying physics. Bose-Einstein correlations appear as an enhancement

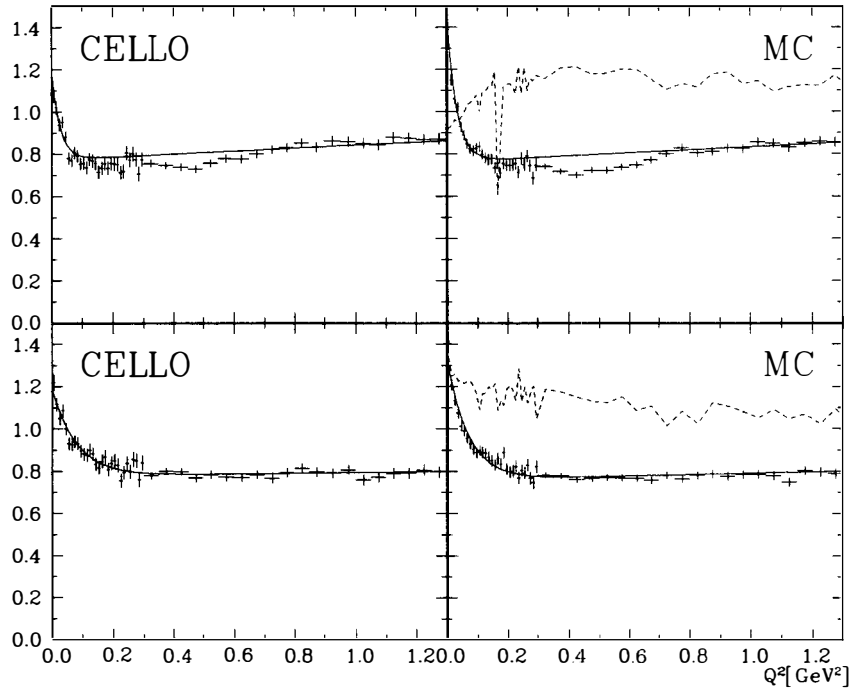

Figure 8: Ratio of Q^2 distributions, the solid line shows the fit result and the dashed curve shows the Monte Carlo correction function. Upper plots: reference density from $\pi^+\pi^-$ pairs. Lower plots: reference density from $\pi^+\pi^-$ pairs after *jet mixing*.

in the Q^2 distribution of like sign pion pairs over a suitably chosen reference density. Here we have applied two procedures to obtain the reference density: The conventional way is to take $\pi^+\pi^-$ combinations from the same event. This method is fairly simple, but suffers from strong contributions of resonance decays and kinematical reflections in the interesting Q^2 range (Fig. 9). The corresponding ratios of Q^2 distributions are displayed in Fig. 8. Correlations due to resonance decays and kinematical reflections can be circumvented by

reflecting all positive particles at a plane perpendicular to the sphericity axis *(jet mixing)* [7]. By means of this procedure, correlations due to unlike sign pion pairs are destroyed, whilst Bose-Einstein correlations are retained and moreover the event topology is preserved.

In Fig. 8 the resulting Q^2 distributions are shown. Compared to the previous case, a much smoother behaviour is observed. Also the correction function, i.e. passing from Monte Carlo generator to the detector level, is well behaved. To determine the correlation strength and the associated radius of the pion source, the following function has been fitted to the Q^2 distributions: $F(Q^2) = a \cdot (1 + b \cdot Q^2) \cdot (1 + c \cdot \exp[-d \cdot Q^2])$, where a is the correlation strength and d is related to the radius by $r = 0.193/\sqrt{d}$. The resulting values are listed in Table 1. It is worthwhile noting that the radius generated by Jetset is recovered when using *jet mixing* to compute the reference density, while the simple method results in an approximately 50% larger radius.

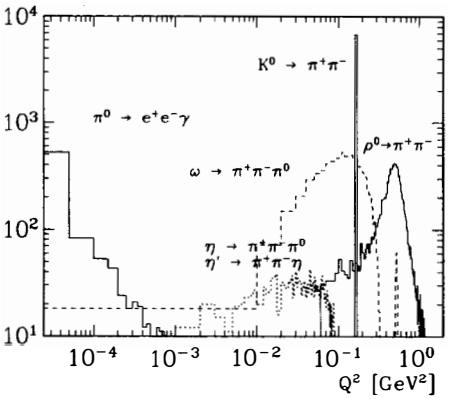

Figure 9: Q^2 distribution from resonance decays and kinematical reflections.

Reference density	Strength	Radius[fm]
$\pi^+\pi^-$	0.52 ± 0.06	1.2 ± 0.1
$\pi^+\pi^-$ from mixed jets	0.53 ± 0.04	0.69 ± 0.06
Jetset 7.2	$PARJ(92)$	$PARJ(93)$
	$2.6 \pm 0.2 \pm 0.2$	$0.25 \pm 0.02 \pm 0.02$

Table 1: Bose-Einstein results and parameters for Jetset 7.2.

CONCLUSIONS

In summary we have presented intermittency analyses in one, two and three dimensions. In general the data appear to be consistently described by conventional Monte Carlo models. This holds for the PETRA data (TASSO, CELLO) as well as for the LEP data (DELPHI, OPAL) and can be regarded as a great success for these models, since they have never been tuned with respect to factorial moments. The equally good description of factorial moments provided by various QCD inspired Monte Carlo models indicates a lack of sensitivity for details of the soft gluon phase. In particular, hard gluon and hard photon radiation appear to be the dominant source of fluctuations observed in e^+e^- annihilation. Besides this, strong effects due to resonance decays are found, making it impossible to resolve the fine correlation structure.

Bose-Einstein correlations are found to give a contribution to the observed resolution dependence of factorial moments. Their parameters have been measured using the conventional method and a new method, avoiding contributions from resonance decays, has been proposed.

REFERENCES

[1] A. Bialas and R. Peschanski: Nucl. Phys. B 273 (1986) 703

[2] TASSO Coll. W. Braunschweig et al.: Phys. Lett. B 231 (1989) 548

[3] CELLO Coll. H.-J. Behrend et al.: Phys. Lett. B 256 (1991) 97

[4] DELPHI Coll. P. Abreu et al.: Phys. Lett. B 247 (1990) 137

[5] OPAL Coll. M.Z. Akrawy et al.: CERN Preprint CERN-PPE/91-37
N. Geddes: These proceedings

[6] M. Feindt: Talk given at the XXV. Int. Conf. on High Energy Physics (Singapore, 1990), to appear

[7] O. Podobrin: Talk given at the XX. Int. Symp. on Multiparticle Dynamics (Gut Holmecke, 1990). to appear

[8] CELLO Coll. H.-J. Behrend et al.: *Intermittency and particle correlations in multihadronic e^+e^- annihilation*, to appear

[9] B. Andersson, G. Gustafson, G. Ingelman and T. Sjöstrand: Phys. Rep. 97 (1983) 31
T. Sjöstrand and M. Bengtsson: Comp. Phys. Commun. 43 (1987) 367

[10] W. Ochs: Phys. Lett. B 247 (1990) 101

[11] G. Gustafson and U. Pettersson: Nucl. Phys. B 306 (1988) 746
L. Lönnblad: Lund Preprint LU TP 89-10 (1989)

[12] G. Marchesini and B.R. Webber: Nucl. Phys. B 310 (1988) 461

[13] B. Andersson, G. Gustafson, A. Nilsson and C. Sjögren: Z. Phys. C – Particles and Fields 49 (1991) 79

[14] T. Sjöstrand: Lund Preprint LU TP 88-20 (1988)

[15] E. Lohrmann (TASSO Coll.): private communication
TASSO Coll. W. Braunschweig et al.: Z. Phys. C – Particles and Fields 41 (1988) 359

[16] W. Ochs: MPI Preprint MPI-PAE/PTh 63/90 (1990)

[17] A. Bialas and M. Gazdzicki: Phys. Lett. B 252 (1990) 483

CORRELATION STUDIES FOR HIGH ENERGY COLLISIONS

David Seibert
Department of Physics, University of Jyväskylä
P.O. Box 35, SF–40351 Jyväskylä, Finland

ABSTRACT

I discuss the phenomenology of correlation data in high energy collisions. In particular, I show that all moments of a correlation function are determined by the second moment in the limit of weak correlations, and that the prediction of independent superposition is that correlation functions vary as $1/(dN/dy)$, where dN/dy is the single-particle density. All current data from leptonic and hadronic scattering follow the same independent superposition prediction reasonably well. Nuclear collision data also follow the independent superposition prediction; however, the observed correlations are an order of magnitude larger in the nuclear collisions than for leptons and hadrons, and cannot be explained without the assumption of new physics. I end by discussing correlation analysis using the split-bin correlation functions, in order to determine the new physics behind these anomalously strong nuclear correlations.

1. Why?

The best reason to study correlations is the fact that rapidity correlations in nuclear collisions are 10–30 times stronger than predicted by the independent superposition of $\bar{p}p$ or e^+e^- collisions[1–4]. This is all old news; right now, I would just like to remind the reader that the correlations observed in nuclear collisions are so strong that new physics is required to explain them.

I originally suggested that these large correlations are due to the formation of quark-gluon plasma droplets, that subsequently decay into 10 charged pions[5] (15 total pions, assuming isospin symmetry). However, they can be explained equally well by the less radical assumption that superheavy resonances are formed, and that these resonances decay into 15 pions. Unfortunately, as there is no model that predicts any difference in behavior between quark-gluon plasma droplets and superheavy resonances, there is no test to distinguish between these explanations. The size of the structures needed to reproduce the data indicates that the nuclear correlations almost certainly arise from some new many-body effects.

I will now describe the phenomenology of these correlation functions, using as an example the scaled factorial moments[1,6] (SFMs),

$$F_i(\delta y;\Delta Y) = \frac{< \rho^{(i)} >_{\delta y}}{< \rho^{(i)} >_{\Delta Y}} \ , \tag{1}$$

where $\rho^{(i)}$ is the i-particle rapidity density and δy (ΔY) is a small (large) rapidity interval. I suppose that I have some model or experiment that gives me the total number of particles, N, the number of correlated pairs, N_c, and the distribution of rapidity separations for any given correlated pair, $p_c(|y_1 - y_2|)$. The pair correlation I refer to here is the *effective* pair correlation, due to whatever 2-body, 3-body, or higher-order interactions are present in the system; this effective correlation almost always dominates in the small-fluctuation limit[7].

Once I have these, I can calculate F_i perturbatively:

$$F_i = 1 + \frac{i(i-1)}{2}\left(\frac{N_c}{N(dN/dy)}\right)[g(\delta y) - g(\Delta Y)] + \mathcal{O}\left(\frac{N_c^{3/2}}{N^3}\right) \ , \tag{2}$$

where

$$g(z) = \frac{1}{z^2}\int_0^z dx\,(z-x)\,p_c(x) \ . \tag{3}$$

A prescription for calculating three-body and higher-order terms is given in Ref. 8; I usually drop everything past the lowest non-trivial order, as higher-order terms give small contributions whenever the lowest-order term is small, as is the usual case in the data with the exception of the highest energy hadronic collisions. It is obvious from the last equation that all of the moments are related:

$$\frac{2\,[F_i(\delta y;\Delta Y) - 1]}{i(i-1)} = F_2(\delta y;\Delta Y) - 1 \ . \tag{4}$$

All existing data follow this moment scaling relation very well[1,3,7].

So far, I have assumed almost nothing about the physics behind these correlations. I want to compare correlation functions in events with different multiplicities, so I have to make some assumptions. The simplest assumption is that the physics is unchanged, so that the superposition of two events with multiplicities N_1 and N_2 produces an event with multiplicity $N_1 + N_2$; this is sometimes referred to as the "independent superposition" assumption. Independent superposition is equivalent to saying that $N_c \propto N$, as pairs from different events are clearly uncorrelated, and that p_c does not change. I thus take

$$N_c = kN \ , \tag{5}$$

where k is some unknown proportionality constant, and find that

$$(dN/dy)\,[F_2(\delta y;\, \Delta Y) - 1] = k\,[g(\delta y) - g(\Delta Y)] \ . \tag{6}$$

Thus, if I have only the trivial multiplicity dependence of independent superposition, the quantity $(dN/dy)(F_2 - 1)$ is the same for all event samples *independent* of the multiplicity density. This product therefore provides a multiplicity-independent measure of the correlation strength.

The preceding discussion of rapidity correlations can be summarized as follows. To first approximation, F_i depends only on F_2, and the shape of $F_2 - 1$ depends only on p_c. The proper multiplicity-independent correlation function is $(dN/dy)(F_2 - 1)$, and when I compare this correlation function I find that the correlations in nuclear collisions are an order of magnitude larger than the correlations in hadronic or leptonic collisions.

This trivial multiplicity dependence is of crucial importance in correlation analyses. Working without these, many groups have found that correlation strength decreases with increasing multiplicity, and thus the conventional wisdom of intermittency studies has been that "correlations decrease with increasing complexity [multiplicity]." It is clear from the data of references 3 and 4, which are compared to the trivial $1/(dN/dy)$ scaling from independent superposition, that correlations actually *increase* with increasing multiplicity. This is not very surprising, as it is obvious that increasing multiplicity allows the formation of more complex structures and thus more correlation.

I would like to emphasize the normalization that I use for SFMs, that is a generalization of the so-called exclusive definition[6]. This form has two distinct advantages over the so-called inclusive definition of the SFMs. First, for a system with a flat, uncorrelated rapidity distribution, $F_i = 1$ for all values of i and all bin sizes, independent of the multiplicity distribution, for this normalization of F_i. Thus, I always know what the signal is for an uncorrelated system; this is not true for the inclusive normalization.

Second, using this normalization, I have shown above that the strength of the correlations can be measured as a function of δy and ΔY, independent of the multiplicity distribution. Thus, the *magnitude* of the correlation function, and not just the slope (as often argued), is physically significant. Again, this is not the case for the inclusive normalization. As a result of these two advantages, I continue to use the exclusive normalization in the next section, where I discuss the best means for studying correlations.

2. How? (with Sergei Voloshin)

Our goal was to produce a more flexible set of correlation functions, in order to extract the maximum information from high-energy events. SFMs are very useful, but they do have two difficulties that we wanted to avoid. First, there is a lot of duplication – the moment scaling law indicates that almost all of the available information is in the second moment. Second, we wanted to be able to construct transverse energy correlation functions, and other correlation functions of *continuous* variables, just as easily as we could study multiplicity correlations using SFMs.

We call this new family the split-bin correlation functions, or SBCFs. They are well described in references 9 and 10, so I will just describe their important features. We concentrate on second-order SBCFs[9] such as S_2, to avoid duplication of information. The second-order SBCFs are basically the ratios of two-particle densities in large and small rapidity bins, similar to the second factorial moment F_2. Unlike SFMs, however, SBCFs are off-diagonal, so they are insensitive to short-range instrumental correlations that make measurement of SFMs difficult for small bin sizes.

S_2 only covers half of the phase space that F_2 does for each bin size, so it suffers from statistical errors that are apparently a factor of 2 larger. However, if we start with a fixed rapidity window, and successively cut our bins in half for each measurement, we find that S_2 uses all of the available two-particle phase space, and that no region of phase space is used twice, while F_2 reuses some regions of phase space many times. Thus, the S_2 data are *independent*, unlike the F_2 data, and the real statistical error for S_2 is the same as for F_2.

The independence of the SBCF data greatly facilitates the data analysis. It has been suggested that the correlations in the SFM data can be treated through the use of sophisticated covariance matrix techniques, that work perfectly if the fit goes exactly through all points, but the fit is never exact for real data. If the fit misses some data points, and correlations between points are strong, the covariance matrix technique can amplify systematic effects that are present in the data, producing best-fit curves that are *systematically* arbitrarily far above or below the data[11].

I have explained why the SBCFs are superior to the SFMs for making equivalent measurements; now, I will show how their flexibility allows for additional measurements that give added information on the correlations. One useful quantity is the transverse energy correlation function, $S_2^{\mathcal{E}}$, that is obtained by substituting the transverse energy density for the multiplicity density in the definition of S_2. Comparisons of S_2 and $S_2^{\mathcal{E}}$ give almost theory-independent information on the transverse energies of the correlated particles:

- if $S_2 < S_2^{\mathcal{E}}$, the transverse energies of the correlated particles are larger than average;
- if $S_2 \approx S_2^{\mathcal{E}}$, the transverse energies of the correlated particles are average;
- if $S_2 > S_2^{\mathcal{E}}$, the transverse energies of the correlated particles are smaller than average.

This information, that is not available from SFM data, can distinguish between correlations due to jets (high E_T), resonances (average E_T), and Bose-Einstein correlations (low E_T).

We can also construct S_2^ϕ, to look for structures like jets that are correlated in rapidity but anti-correlated in azimuthal angle ϕ, by splitting our bins into two equal-ϕ subbins rather than two equal-y subbins. In this case, we again obtain almost theory-independent information about the correlated particles:

- if $S_2 < S_2^\phi$, the correlated particles emerge back-to-back in ϕ;
- if $S_2 > S_2^\phi$, the correlated particles emerge together in ϕ.

This information separates correlations due to heavy resonances, that have a small transverse velocity compared with the velocities of their decay products, from correlations due to light resonances with relatively large transverse velocities. This test has a significant advantage over the E_T tests – for small bin sizes δy, the corrections for the shape of the single-particle distribution are the same for S_2 and S_2^ϕ. As a result, this comparison test is insensitive to effects that change the shape of the single-particle distribution, such as spatially varying efficiencies.

Thus, SBCFs have three clear advantages over SFMs for correlation studies. First, they provide better and cleaner data than SFMs, with no loss in statistics. Second, SBCFs (unlike SFMs) include E_T correlation functions, which can provide valuable information about correlations through almost theory-free comparison tests. Third, SBCFs increased flexibility can provide more stringent tests for models of multi-particle production, using comparisons of correlation functions that have almost the same dependence on the single-particle distribution, such as S_2 and S_2^ϕ.

I have performed an SBCF analysis of O+Ag(Br) and S+Ag(Br) collisions at 200 GeV/nucleon[12] using data provided by the KLM collaboration. S_2 is the same for these two event samples, provided that corrections are made for the shape of the single-particle distribution and for varying multiplicity density. The equality of these data indicates that the correlations are the same for the two samples. S_2^ϕ is also the same for the two samples, but smaller than S_2, so the correlations are probably due to sources with relatively large transverse velocities.

The values of S_2 seen in [O,S]+Ag(Br) collisions are a factor of 8 larger than the values of F_2 from leptonic or hadronic collisions [after construction of the equivalent multiplicity-independent correlation function (6)]. The statistical errors are large, as the nuclear event sample is small; however, the nuclear data is almost five standard deviations higher than the hadronic data, so these anomalously strong correlations are more than a four-sigma effect. As a result, it would be invaluable to have clean SBCF analyses for large samples of both nuclear and light-particle collision data, in order to determine, through direct comparison, how similar the physics behind these different types of collisions really is.

3. Summary.

My results can be summarized with two statements:

- Correlations in nuclear collisions are huge, and should be explored further.
- Split-bin correlation functions (SBCFs) provide the best means for studying correlations in high energy events.

I also have two questions for anyone who is reading this:

- What other SBCFs are useful to theorists?
- What other SBCFs can be measured?

I end with a response to the talks of D. Amati and C. Quigg, both of which I enjoyed very much: I believe that correlations are crucial to the future of ultra-relativistic heavy ion collisions, and that this field has a rich future ahead in the study of high energy many-body effects that are seen in the complicated physical environment created only in high energy nuclear collisions.

References.

1. D. Seibert, Phys. Rev. D **41** (1990) 3381.
2. A. Capella, K. Fialkowski and A. Krzywicki, Phys. Lett. B **230** (1989) 149.
3. B. Buschbeck, these proceedings.
4. EMU01 Collaboration, M. Adamovich *et al.*, Lund University preprint LUIP 9011 (December 1990), submitted to Phys. Lett. B.
5. D. Seibert, Phys. Rev. Lett. **63** (1989) 136.
6. A. Bialas and R. Peschanski, Nucl. Phys. **B273** (1986) 703.
7. D. Seibert, Phys. Lett. B **254** (1991) 253.
8. P. Carruthers, H. Eggers and I. Sarcevic, Phys. Lett. B **254** (1991) 258.
9. S. Voloshin and D. Seibert, Phys. Lett. B **249** (1990) 321.
10. D. Seibert and S. Voloshin, Phys. Rev. D **43** (1991) 119.
11. D. Seibert, University of Minnesota preprint UMSI 90/152 (July 1990), to be published in Phys. Lett. B.
12. D. Seibert, University of Minnesota preprint UMSI 90/230 (November 1990), submitted to Phys. Rev. C.

SELECTED TOPICS ON (ULTRA-)SOFT EFFECTS

W. Kittel
University of Nijmegen
The Netherlands

ABSTRACT

Factorial correlators are studied in 250 GeV/c π^+p and K^+p collisions as a function of the distance in rapidity. The correlators are found to increase with decreasing correlation distance, independently of the rapidity resolution. The increase approximately follows a power law, but the power is considerably larger than expected from a log-normal approximation in the simple α model of intermittency. Also the FRITIOF results are independent of the resolution, but slopes and p_T behaviour cannot be reproduced by this model.

Inclusive production of direct soft photons is studied in K^+p and π^+p interactions at 250 GeV/c. Total cross sections, Feynman-x and transverse momentum distributions of direct γ's are presented. The measured cross sections are several times larger than expected from QED inner bremsstrahlung, indicating the presence of an anomalous soft photon source. The model of Lichard and Van Hove, based on a "cold quark-gluon plasma" picture, agrees with the data.

In hadron-hadron collisions, the K/π ratio increases with increasing energy, increasing multiplicity n, increasing transverse momentum p_t, but not with increasing transverse mass m_t. The strange quark suppression factor λ_s, furthermore, is larger in the central than in the fragmentation regions.

1 Factorial Correlators

Intermittency[1] has now been studied in e^+e^-, μp, νA, hadron-hadron, hadron-nucleus and nucleus-nucleus collisions, and has beautifully been reviewed at this Rencontre by B. Buschbeck[2]. The study has been performed in terms of a power law dependence of the scaled factorial moments

$$\langle F_i \rangle = \frac{1}{M} \sum_m \frac{\langle n_m(n_m-1)\ldots(n_m-i+1)\rangle}{\langle n_m \rangle^i} \quad , \tag{1}$$

where M is the number of phase-space bins of size $\delta = \Delta/M$ into which an original region Δ is subdivided, n_m is the multiplicity in bin m ($m = 1, .., M$). The averages under the sum are over the events in the sample.

While in the early stage of the analysis the interest mainly arose from the difficulties of currently used models to reproduce the effect, recent e^+e^- results are reproduced by a number of models and a number of alternative attempts exist to explain the residual effect in the other types of collisions. These range from conventional short range correlations and Bose-Einstein interference, via pencil jets and extended parton cascades, to a possible signal for quark-gluon-plasma. Different data support different interpretations, so that more discriminative information is needed experimentally.

While the moments defined in (1) measure local density fluctuations in phase space, additional information is contained in the correlation between these fluctuations within a given event. This correlation can be extracted by means of the factorial correlators[1]

$$\langle F_{ij}^{mm'} \rangle = \frac{\langle n_m(n_m-1)\ldots(n_m-i+1)\; n_{m'}(n_{m'}-1)\ldots(n_{m'}-j+1)\rangle}{\langle n_m \ldots (n_m-i+1)\rangle \langle n_{m'}\ldots(n_{m'}-j+1)\rangle} \quad , \tag{2}$$

where n_m is the multiplicity in bin m and $n_{m'}$ that in bin m'. The correlators are calculated at given δ for each combination mm' and then averaged over all combinations with given D, as shown below.

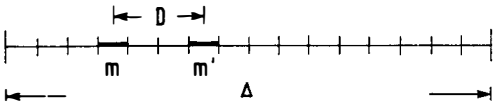

According to a simple intermittency model (α-model)[1], the $\langle F_{ij} \rangle$ should depend only on D and not on δ, and the dependence should be according to the power law

$$\langle F_{ij} \rangle \propto (\Delta/D)^{f_{ij}} \quad . \tag{3}$$

For the power f_{ij} (slope in a log-log plot) the following relation has been derived:

$$f_{ij} = f_{i+j} - f_i - f_j = ij f_2 \quad , \tag{4}$$

where the first equal sign is due to the α model, the second to the log-normal approximation.

Preliminary results for pseudo-rapidity resolution $\delta\eta \geq 0.4$ have been reported by the HELIOS Collaboration[3], where, however, the multiplicities had to be estimated from the transverse energy. New results come from the NA22 experiment[4] for the resolution $\delta y \geq 0.1$. The $\ln\langle F_{ij} \rangle$ are shown as a function of $-\ln D$ in Fig.1a-d, for four values of δy, respectively.

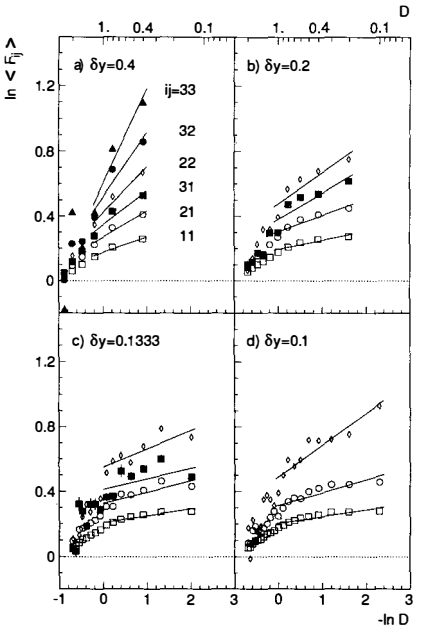

Fig. 1

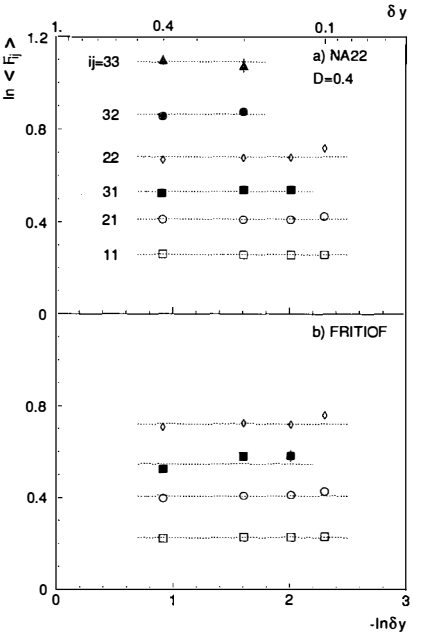

Fig. 2

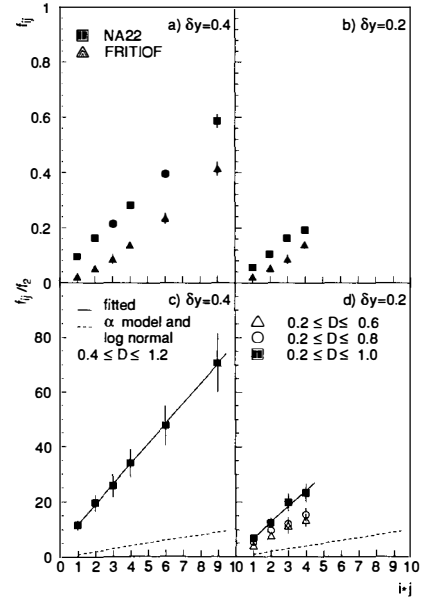

Fig. 3

Fig.1 $\ln\langle F_{ij}\rangle$ as a function of $-\ln D$ for four values of δy, as indicated.

Fig.2 Dependence of $\ln\langle F_{ij}\rangle$ on the bin size δy for a correlation distance $D = 0.4$,
a) for NA22 data, b) for a sample of 60 000 FRITIOF Monte Carlo events. The dashed lines correspond to horizontal line fits through the points.

Fig.3 a) b) The increase of the slopes f_{ij} with increasing order ij compared to the expectation from FRITIOF, for two values of δy, respectively; c) d) the increase of f_{ij}/f_2 with increasing order ij, compared to that expected from the α model (dashed line), for two values of δy, respectively.

In all cases an increase of $\ln\langle F_{ij}\rangle$ is observed with increasing $-\ln D$.

In Fig.2a) the $\ln\langle F_{ij}\rangle$ at fixed D=0.4 are compared for the four different values of δy. As expected from the α model, the $\langle F_{ij}\rangle$ indeed are independent of δy. However, this property is not unique to the α-model. Fig.2b shows that the δy independence is also reproduced by the FRITIOF model[5] and is probably common to any model with short-range order.

For $\langle F_{11}\rangle$, the δy independence can be extracted from the integral over the two-particle density, with two integration domains of size δy separated by D. Using exponential short range order[6], this gives

$$\langle F_{11}\rangle - 1 \quad \propto \quad \frac{1}{a^2} e^{-D/L} \cdot (e^a - 1)(1 - e^{-a}) \tag{5}$$

where L is a correlation length and $a = \delta y/L$. According to (5), $\langle F_{11}\rangle$ becomes independent of δy for $a < 1$. Since $e^{-D/L} \to 1$ with $D \to 0$, this form also leads to the deviations from (3) observed as a bending in Fig.1.

Because of the bending, fitted slopes f_{ij} only can be used as an indication for the increase over a certain range. For two values of δy they are compared to FRITIOF predictions in Fig.3a) and 3b), respectively. As already observed for single moments, the FRITIOF increase is too slow also for the correlators $\langle F_{ij}\rangle$. This shortcoming is related[6] to the failure of the model to reproduce the two-particle rapidity correlations in the same[7] and other data[8]. Future improvements of the model should account for these results simultaneously.

According to (4), the ratio f_{ij}/f_2 is expected to grow with increasing orders i and j like their product ij. In Figs.3c) and 3d) this is tested for δy=0.4 and δy=0.2, respectively. In both cases, the experimental results lie far above the dashed line corresponding to the expected $f_{ij}/f_2 = ij$. Since the dependence of $\ln\langle F_{ij}\rangle$ on $-\ln D$ is not strictly linear, the comparison depends on the range of δy and D used to determine f_2 and f_{ij}. In Fig.3d), therefore, a number of fits are compared. Slopes are reduced when reducing the upper limit in D, but do not reach the α-model prediction (dashed line).

A convincing explanation for the violation of expectations (3) and (4) is given by Peschanski and Seixas[9], also reported here. Agreement can be restored from a 3 dimensional intermittency ansatz. Furthermore, a projection independent scaling relation can be derived and shown to hold for the NA22 data. The multi-dimensional ansatz closes the circle with recent conjectures of W. Ochs[10] and Białas and Seixas[11] discussed here by Buschbeck[2].

2 Anomalous Sources of Soft Electromagnetic Radiation

Over the past decade experiments have found persisting evidence for anomalous sources of electromagnetic radiation in hadron-hadron collisions. Electron production at low p_T is more abundant than expected from known origins, including hadronic bremsstrahlung and charmed particle decays. A dilepton (e^+e^- and $\mu^+\mu^-$) continuum of masses well below 600 MeV/c^2 is measured, up to two orders of magnitude larger than estimated from the Drell-Yan process. The ratio of prompt e^+ to π production in the rapidity region $|y| < 1$ and $p_T < 0.4$ GeV/c rises approximately linearly with n_{ch}, the charged particle multiplicity of events, indicating that the production rate is proportional to n_{ch}^2. A possible explanation is "soft annihilation" where lepton pairs are created through annihilation of quarks and antiquarks

produced during the collision. Alternative explanations are based on thermodynamic models (see ref.12 for a list of references on this topic).

Sea-quark annihilation into virtual photons, observed as lepton pairs, implies that soft real photons must also be produced in the same collision. The first evidence for a direct soft photon signal comes from a $\pi^+ p$ experiment at 10.5 GeV/c beam momentum[13]. There, the signal was found to be compatible with hadronic inner bremsstrahlung. However, an excess of direct soft photons, four times larger than expected from this last process, has been measured in $K^+ p$ collisions at 70 GeV/c [14].

More recent results of AFS[15] exclude a strong increase of the γ signal beyond that observed in[14]. Preliminary data from the HELIOS Collaboration[16] show a prompt-γ signal in the central rapidity region for $p_T < 30$ MeV/c in p Be and p Al collisions at 450 GeV/c. The signal may, however, be compatible with that expected from known sources. A clear excess of direct soft photons is seen by the EMC Collaboration in μp interactions at 200 GeV/c[17]. The anomalous effect is, therefore, not restricted to hadron collisions. This indicates that a phase transition from hadronic to quark matter is unlikely to be the origin.

The mechanism behind these soft phenomena is at present far from understood[18]. In the limit of very small p_T, the wavelength of the photons is large compared to the hadronic interaction region. Processes confined within this region with a typical size and lifetime of 1 fermi should not contribute. This was verified by B. Andersson et al.[19] using the space-time structure of the Lund string fragmentation model. Much larger scales, of the order of several to tens of fermi, seem to be involved.

Recently, three models have been proposed to explain the soft photon puzzle by non-standard mechanisms. The model by Barshay[20] is based on a "pion condensate", that by Shuryak[21] on a "pion liquid" picture. Lichard and Van Hove[22] suggest that this and other "ultrasoft" effects may find a common explanation in the formation of dense "globs" of cold partonic matter at the end of a QCD cascade, soft photons being produced via gluon Compton scattering and quark-antiquark annihilation in lowest order QED and QCD.

New results on prompt soft photon emission are reported for $M^+ p \to \gamma + X$ ($M^+ = K^+$ or π^+) at 250 GeV/c [23]. The distribution in Feynman-x of direct soft γ's (Fig.4) is determined using, on the one hand, FRITIOF for non-π^0 decays, and the properties of the $\pi^0 \to \gamma\gamma$ decay kinematics for the dominant π^0 contribution, on the other hand. The spectrum at 250 GeV/c is similar in shape to that measured in 70 GeV/c $K^+ p$ collisions[14], also shown in Fig.4a. The QED hadronic inner bremsstrahlung contribution to direct soft photons (full line) lies systematically below the data, although its shape is quite similar. The dashed histograms in Fig.4 are predictions by Lichard and Van Hove[22] derived in the "cold-quark gluon plasma" (CQGP) model. The agreement with the NA22 data is quite remarkable.

To extract the prompt photon cross section as a function of transverse momentum, FRITIOF is used for background simulation. The model reproduces well the $d\sigma/dp_T$ distribution, except at very small p_T. The remaining signal is plotted in Fig.5. The dashed histograms show the CQGP-model predictions. They agree well with the data. In contrast, the inner bremsstrahlung cross section (full line) is several times smaller than the measured direct photon signal.

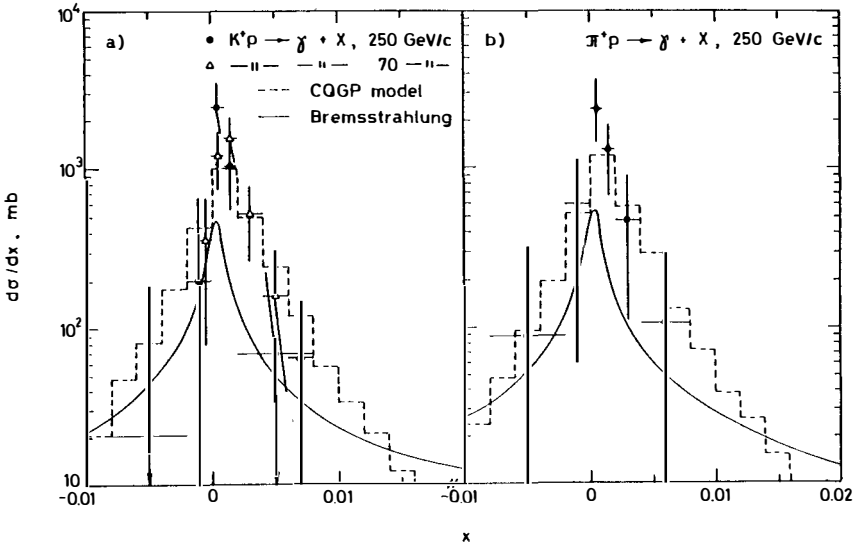

Fig.4 The $d\sigma/dx$ spectrum of γ's after subtraction of all hadron decays[23]. The curves show the hadronic bremsstrahlung contribution and the CQGP model prediction.

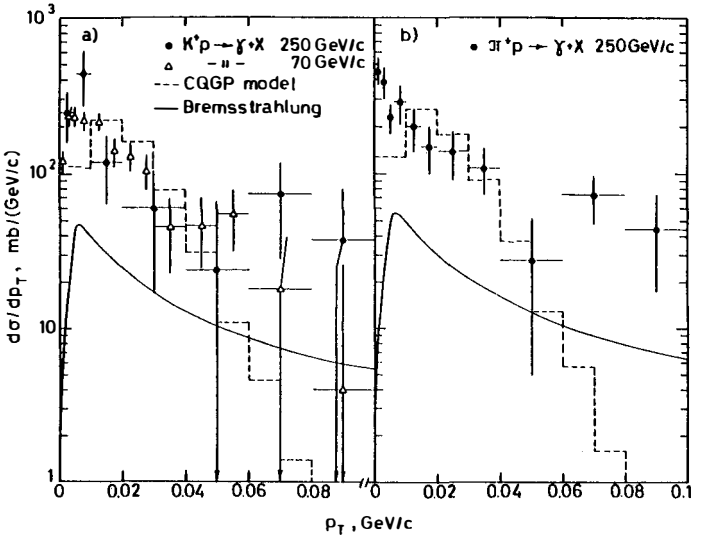

Fig.5 The $d\sigma/dp_T$ spectrum of γ's remaining after subtraction of all hadron decays[23]. The curves show the hadronic bremsstrahlung contribution and the CQGP model prediction.

3 Strangeness Production

Strange particles have many advantages for the study of particle production. They are in general more directly produced than pions, or at least carry more of the energy of the primarily produced meson. Strange particles can be used as a tag to allow the study of $q\bar{q}$ correlations on a much smaller combinatorial background than possible in $\pi\pi$ correlations. Strangeness can be used as a label to follow the fate of an incident valence quark through the collision to the final state particle. Λ^0 allows to study polarization in particle production. Finally, strange quark suppression $\lambda_s = s\bar{s}/\frac{1}{2}(u\bar{u} + d\bar{d})$ can give us information on the energy density, e.g. in the flux tube from the string tension κ in $\exp(-\pi m_q^2/\kappa)$.

In general, λ_s is assumed constant. Recent results, however, show that this is far from reality.

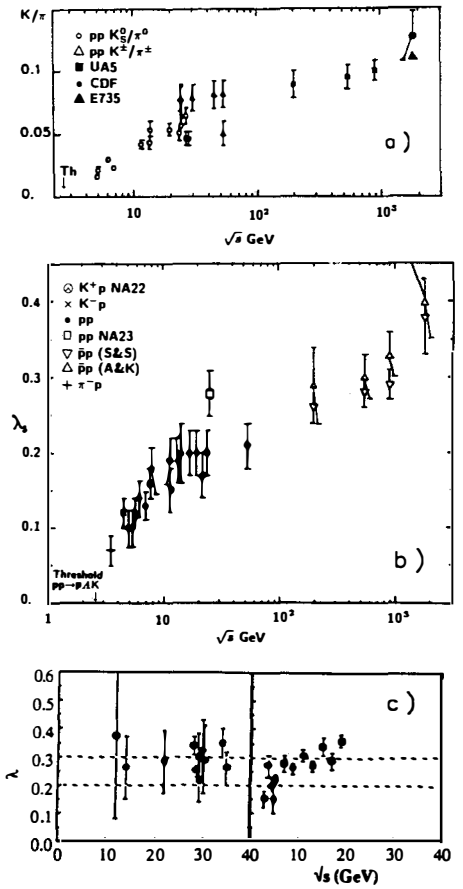

Fig.6 a) Energy dependence of the K/π ratio in $pp^{\pm}$ collisions[24,25,26], b) of the strangeness suppression λ_s in hp collisions[27], c) in e^+e^- and lh collisions[28].

3.1 *The energy dependence* between threshold and 1.8 TeV of the K/π ratio for minimum bias pp and $p\bar{p}$ events[24,25,26] is given in Fig.6a). Fig.6b) shows the strangeness suppression factor λ_s [27]. Both K/π and λ_s continue to rise through the CERN Collider and Tevatron energies. While λ_s first seemed to saturate at $\lambda_s = 0.2$ at ISR energies, it is now already above $\lambda_s = 0.35$ at 1.8 TeV.

It is interesting to note that similar values are reached in e^+e^- collisions already at much lower energies (Fig.6c [28]).

3.2 The *density (multiplicity) dependence* of the K/π and $\bar{p}/\pi^-$ ratio[26] is given in Fig.7a up to $n_{ch} = 120$ ($n_{ch}/d\eta \approx 20$). Over this multiplicity range, the K/π ratio grows by a much as 40%, On the other hand, the $\bar{p}/\pi^-$ ratio in Fig.7b) remains constant.

3.3 The p_t *and* m_t *dependence* of K/π and $\bar{p}/\pi^-$ ratios have recently been studied by UA2[29] and E735[26]. As can be seen from Fig.8a), both ratios increase as a function of p_t.

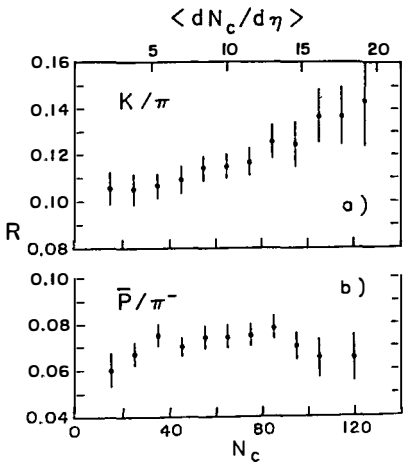

Fig.7 Ratios of a) K/π and b) $\bar{p}/\pi^-$ as a function of charge multiplicity N_c [26].

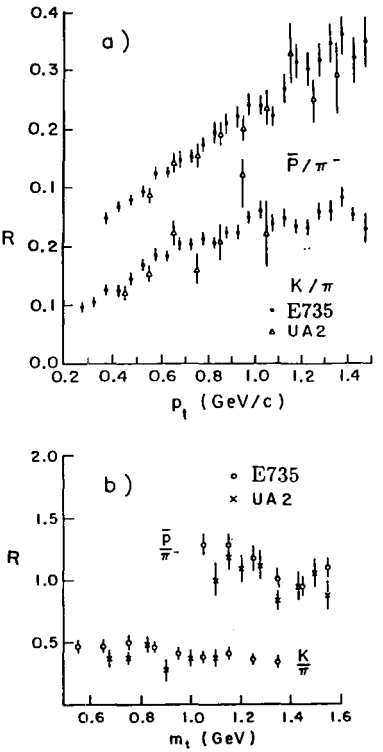

Fig.8 Ratios of K/π and $\bar{p}/\pi$ as a functions of a) p_t and b) m_t [28,29].

On the other hand, there is even an indication for a small decrease in m_t (Fig.8b).

3.4 The *Feynman x dependence* of strangeness suppression is less clear, but evidence exists also for that. K^* and ϕ have approximately the same mass and are produced more directly than K and π. In a K^+ beam, the $\bar{s}$ quark carries on the average more momentum than the u quark[30] and Monte Carlo Models show that K^* production from the u quark is strongly suppressed in the fragmentation region. After removing diffraction-dissociation and $K^*(1420)$ production, forward K^* therefore contains theoriginal $\bar{s}$ quark and a u-quark from the sea. A forward ϕ contains the original $\bar{s}$ quark and an $\bar{s}$-quark from the sea. Because of the similar mass and the direct production of these resonances, their production ratio can be used as a direct measure of λ_s.

In Fig.9a[31] the x dependence of K^{*0} and ϕ production is compared for K^+p experiments between 32 and 250 GeV/c. The ratios for the integrated forward region ($x \geq 0.2$) of $0.16 \pm 0.01 \pm 0.01$, $0.15 \pm 0.01 \pm 0.01$ and $0.17 \pm 0.01 \pm 0.01$ at 32, 70 and 250 GeV/c, respectively, are included in Fig.6b. The ratio of the ϕ and K^{*0} distribution at the three energies and the corresponding ratio from K^-p collisions at 110 GeV/c [32] are given in Fig.9b. Errors are large, but there is an indication for a decrease of this ratio (and therefore of λ_s) with increasing x. Confirming evidence comes from Λ [33] and K^0 [34] production in the same experiment, where $\lambda_s \geq 0.3$ appears necessary in the central, but $\lambda_s \leq 0.2$ in the proton fragmentation region.

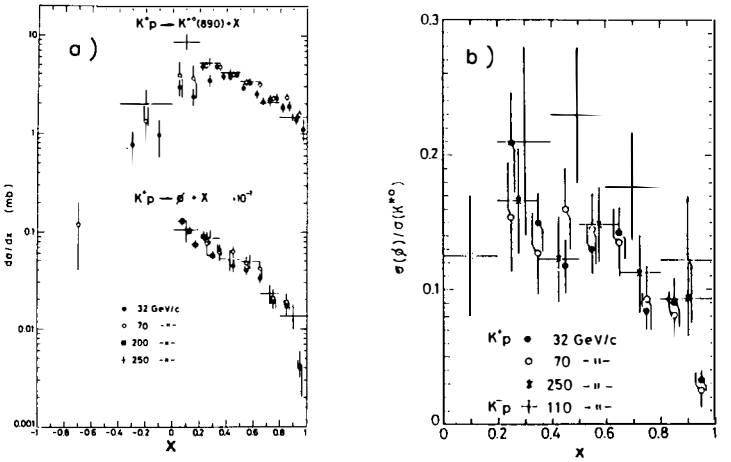

Fig.9 a) $d\sigma/dx$ of K^{*0} and ϕ in K^+p collisions[31], b) ratio of ϕ and K^{*0} distributions in K^+p and K^-p collisions [31,32].

An x dependence of s quark production is indeed expected in the quark-gluon string model of Kaĭdalov [35], from improved low Q^2 fragmentation functions. There, the ratios of fragmentation functions, however, lead to an *increase* of the K^+/π^+ ratio with increasing $|x|$, for directly produced K^+ and π^+. A full Monte Carlo now exists[36] and should be tested on the available data on energy, transverse momentum and Feynman x dependence of the K/π ratio and Λ production.

4 Conclusions

The correlators $\langle F_{ij} \rangle$ increase with decreasing correlation length D, but only approximately follow a power law for $D \lesssim 1$. For fixed D the values of $\langle F_{ij} \rangle$ are independent of the resolution δy, a feature expected from the α model, but also reproduced by FRITIOF and probably common to any model with short range order. The powers f_{ij} increase linearly with the product ij of the orders, but are considerably larger than expected from FRITIOF and from the simple α model. Agreement with the α model is restored with a 3 dimensional intermittency ansatz.

Besides earlier evidence for soft e^+e^- pair production, good evidence now exists for an "anomalous" direct soft signal with a cross section several times larger than that expected from inner hadronic QED bremsstrahlung. The data on direct photon emission at 70 and 250 GeV/c agree with the predictions of Lichard and Van Hove based on the existence of "globs" of cold quark-parton matter.

The K/π ratio, and with it the strangeness suppression factor λ_s, increases with increasing $\sqrt{s}$ up to Tevatron energies, where a value $\lambda_s \approx 0.35$ is reached. While the $\bar{p}/\pi$ is largely independent of the multiplcity n, the K/π ratio increases with increasing n. Both K/π and $\bar{p}/\pi$ increase with increasing transverse momentum p_t, but slightly decrease with

increasing transverse mass m_t. A number of results at $\sqrt{s}$=22 GeV (p_{lab} = 250 GeV/c) point in the direction of a Feynman-x dependence of strangeness suppression, with $\lambda_s \gtrsim 0.3$ in the central and $\lambda_s \lesssim 0.2$ in the fragmentation regions.

REFERENCES

1. A. Białas and R. Peschanski, Nucl. Phys. B273 (1986) 703 and B308, (1988) 857.
2. B. Buschbeck, "Review of Intermittency", these proceedings.
3. HELIOS Collaboration, "Results from Helios", paper submitted to the EPS Conf.on High Energy Physics, Madrid 1989.
4. V.V. Aivazyan et al. (NA22), "Factorial Correlators from π^+p and K^+p Collisions at 250 GeV/c", Nijmegen preprint HEN-332/90, to be publ. in Phys. Lett. B.
5. B. Andersson, G. Gustafson and B. Nilsson-Almqvist, Nucl. Phys. B281 (1987) 289.
6. E. De Wolf, Acta Phys.Pol. B21 (1990) 611.
7. L. Smirnova, "Rapidity Correlations in π^+p, K^+p and pp Interactions at 250 Gev/c", these proceedings and V.V. Aivazyan et al. (NA22), Nijmegen preprint HEN-330/90, to be publ. Z. Phys. C.
8. J. Bailly et al. (NA23), Z. Phys. C40 (1988) 13.
9. J. Seixas, these proceedings and R. Peschanski and J. Seixas, CERN-TH-5903/90.
10. W. Ochs, Phys. Lett. B247 (1990) 101 and "Multidimensional Intermittency Analysis", MPI-PAE/PTh 63/90.
11. A. Białas and J. Seixas, "Strong Intermittency in Momentum Space", CERN-TH 5757/90.
12. W. Kittel, Festschrift Léon Van Hove (Singapore 1989) p.323
13. A.T. Goshaw et al., Phys. Rev.Lett. 15 (1979) 1065
14. P.V. Chliapnikov et al., Phys. Lett. B141 (1984) 276
15. T.Åkesson et al.(AFS), Phys. Rev. D36 (1987) 2615
16. J. Schukraft (HELIOS), private communation
17. J.J .Aubert et al.(EMC), Phys. Lett. B2128 (1989) 248
18. V. Balek, N. Pišútová, J. Pišút, Acta Phys.Pol. B21 (1990) 149
19. B. Andersson et al., "Soft Photons in the Lund Model", Lund preprint LUTP 88-1, 1988
20. S. Barshay, Phys. Lett. B227 (1989) 279
21. E.V. Shuryak, "Pion Modification on Hot Hadronic Matter and Ultrasoft Phenomena in High Energy Collisions", CERN-TH-5386/89 (1989) and Phys.Lett. B231 (1989) 175
21. P. Lichard, L. Van Hove, Phys. Lett. B245 (1990) 485
22. F.B otterweck et al.(NA22), "Direct Soft Photon Production in K^+p and π^+p Interactions at 250 GeV/c", Brussels preprint to be publ. in Z. Phys. C.
23. R.E. Ansorge et al. (UA5), Phys. Lett. B199 (1987) 311; Z. Phys. C41 (1988) 179.
24. F. Abe et al. (CDF), Phys. Rev. D40 (1989) 3791.
25. N.N. Biswas et al. (E735), Phys. Rev. Lett. 64 (1990) 991 and "Production of TOF-Identified Pions, Kaons and Antiprotons in Antiproton-Proton Collisions at $\sqrt{s}$=1.8 TeV", Notre Dame Preprint UND-HEP-05-10-90
26. A. Wróblewski, "Soft Hadronic Physics", Rapporteur's Review, Proc. XXVth Int. Conf. on High Energy Physics, Singapore 1990, to be published.
27. W. Hofmann, Nucl. Phys. A479 (1988) 337c.
28. M. Banner et al. (UA2), Phys. Lett. 122B, 322 (1983) and Z. Phys. C27 (1985) 329.
29. J. Badier et al., Phys. Lett. B93 (1980) 354.
30. M. Adamus et al.(NA22), Phys. Lett. B198 (1987) 427;
    N.M.A gababyan et al. (NA22), Z. Phys. C41 (1989) 539.
31. S. Banerjee et al., Z. Phys. C31 (1986) 401.
32. I.V. Ajinenko et al. (NA22), Z. Phys. C44 (1989) 573.
33. I.V. Ajinenko et al. (NA22), Z. Phys. C46 (1990) 525.
34. A.B. Kaĭdalov, Sov. J. Nucl. Phys. 45 (1987) 902.
35. N.S. Amelin et al., Sov. J. Nucl. Phys. 51 (1990) 211 and 840.

SCALING RELATIONS: A WAY OUT OF AMBIGUITY?

J. Seixas*
CERN–Geneva

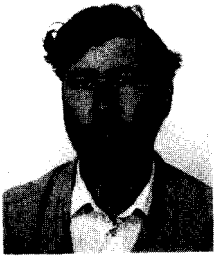

ABSTRACT

Higher dimensional intermittency has posed again the problem of distinguishing intermittent from non-intermittent behaviour. In this talk I will show that it is possible to eliminate this ambiguity by looking simultaneously at the behaviour of factorial moments and correlators.

* Permanent address: Departamento de Física, IST, Lisbon, Portugal.

It is by now a known fact that projection can reduce or even kill any signs of intermittency in any system presenting them[1,2]. If, on one hand, this is desirable in high energy interactions since the data shows precisely this reduction[3], it also re-establishes the problem of distinguishing intermittent from non-intermittent behaviour: it is clear that there is not much sense in trying to fit power laws where you know they should not be in principle.

Therefore, finding relations which are dimension-independent becomes a potentially interesting goal. Here I will show how at least one such type of relation can be found.

To do so I will make use of factorial correlators introduced already some time ago by Białas and Peschanski[4]. They are defined as

$$F_{p,q}(D,\delta) = \frac{k_m(k_m-1)\dots(k_m-p+1)k_n(k_n-1)\dots(k_n-q+1)}{\langle k_m\rangle^p\langle k_n\rangle^q} \tag{1}$$

where the bins m and n are considered as fixed, with bin size δ and separation distance D in the considered variable, say rapidity or rapidity-azimuth. The averaging $\langle\dots\rangle$ is taken over events.

For intermittent-like fluctuations one has the behaviour[1,2]

$$\begin{aligned} \langle F_p\rangle &\propto \delta^{\varphi_p} \\ \langle C_{p,q}\rangle \equiv \frac{\langle F_{p,q}\rangle}{\langle F_p\rangle\langle F_q\rangle} &\propto D^{\varphi_{p,q}} \ , \end{aligned} \tag{2}$$

where φ_p and $\varphi_{p,q} = \varphi_{p+q} - \varphi_p - \varphi_q$ are fixed (intermittency) indices characterizing the scaling behaviour of the moments and correlators. Note the important prediction[4] that the observables $\langle C_{p,q}\rangle$ are expected not to depend on the individual bin-size δ, at least for δ smaller than some limiting value δ_0.

Let me first point out a trivial remark, *viz.* that projection effects should affect factorial correlators as much as they affect factorial moments. For simplicity I will concentrate on F_2 and $F_{1,1}$. They both depend on the two-particle correlation function $\rho_2(y1,y2)$,

$$\begin{aligned} F_2 &= \frac{\int_0^\delta dy_1 \int_0^\delta dy_2 \rho_2(y_1,y_2)}{\left(\int_0^\delta \rho_1(y_1)dy_1\right)^2} \\ F_{1,1} &= \frac{\int_0^\delta dy_1 \int_D^{\delta+D} dy_2 \rho_2(y_1,y_2)}{\left(\int_0^\delta \rho_1(y_1)dy_1\right)\left(\int_D^{\delta+D} \rho_1(y_2)dy_2\right)} \end{aligned} \tag{3}$$

So, as can be seen, both F_2 and $F_{1,1}$ depend on the same functions – thus showing that they should both be sensitive to projection effects.

The *magnitude* of this projection effect can, however, be different for the two quantities. This is the case, for instance, in the model of singular two-particle distribution function in momentum space[2],

$$\rho_2(y_1,y_2) = C_1 \frac{e^{-(m_{\perp_1}+m_{\perp_2})/\beta}}{|p_1-p_2|^\alpha} \tag{4}$$

$F_{1,1}$ and F_2 show different aspects of this singularity. The reason is the following: when calculating F_2 we are looking for pairs of particles falling in the *same* bin δ and, therefore, we can hit the singularity anywhere in that interval. Thus, F_2 measures directly the presence of the singularity. In F_2 , however, we look for pairs of particles each falling in a *different* bin (the bins being separated by a distance D). So, except for neighbouring bins (in which case *both* particles must fall on the same point), when calculating F_2 one never hits the singularity: one only feels the form of the singularity.

In Fig. 1 one compares the result of ansatz (4) with NA22 data on factorial moments and correlators[5]. As can be seen, the agreement is exceedingly good for F_2 in the whole range of bin sizes and for $F_{1,1}$ in the range $D < 1$. For larger distances the agreement with the data for $F_{1,1}$ is qualitatively good and probably the discrepancy is due to incorrectness of the details of the assumed single particle distribution function[6].

Since $F_{1,1}$ and F_2 stem from the same correlation functions one might ask whether there is some relation between them. Let us assume – as is implied by the data – that $F_{1,1}$ is bin-size independent. In that case one can replace in the calculation of $F_{1,1}$ two bins of size δ separated by a distance D by two neighbouring bins of size $2D$. Using the trivial relation[6]

$$k_m k_n = \frac{1}{2}(k_m + k_n)(k_m + k_n - 1) - \frac{1}{2}k_m(k_m - 1) - \frac{1}{2}k_n(k_n - 1) \quad ,$$

one gets

$$\begin{aligned} F_{1,1}(\delta, D) &= \frac{\langle k_m k_n \rangle}{\langle k_m \rangle \langle k_n \rangle} = \frac{1}{2}\frac{\langle (k_m + k_n)^2 \rangle}{\langle k_m \rangle \langle k_n \rangle} - \frac{1}{2}\frac{\langle k_m^2 \rangle}{\langle k_m \rangle \langle k_n \rangle} - \frac{1}{2}\frac{\langle k_n^2 \rangle}{\langle k_m \rangle \langle k_n \rangle} \\ &= \frac{1}{2}\frac{\langle (k_m + k_n)^2 \rangle}{\langle k_m + k_n \rangle^2}\frac{\langle k_m + k_n{}^2 \rangle}{\langle k_m \rangle \langle k_n \rangle} - \frac{1}{2}\frac{\langle k_m^2 \rangle}{\langle k_m \rangle^2}\frac{\langle k_m \rangle}{\langle k_n \rangle} - \frac{1}{2}\frac{\langle k_n^2 \rangle}{\langle k_n \rangle^2}\frac{\langle k_n \rangle}{\langle k_m \rangle} \end{aligned} \tag{5}$$

If we have translational invariance, Eq. (4) reverts to the simple form

$$F_{1,1}(\delta, D) = 2F_2(2D) - F_2(D) \tag{6}$$

which is independent of the dimensions at which the real process exists.

In Fig. 2 one sees that the scaling relation (6) is quite well satisfied by the NA22 data. Once more for $D > 1$ the agreement is just qualitative, most probably due to the assumption that translational invariance is valid in such a wide range.

So, in conclusion, even just looking at one-dimensional variables one can have some insight on the physics by looking at the combined behaviour of factorial moments and correlators. The approach presented here allows perhaps for less ambiguity in distinguishing intermittent from non-intermittent behaviour in the near future.

ACKNOWLEDGEMENTS

I would like to thank W. Kittel and specially F. Botterweck and M. Charlet for providing me and Robi Peschanski with the NA22 data on factorial moments and correlators. Thanks are also due to R. Peschanski, J. Alberty, B. Buschbeck and J. Dias de Deus for illuminating discussions and remarks.

REFERENCES

1- W. Ochs, *Phys. Lett.* **B247** (1990) 101 and preprint MPI-PAE/PTh 63/90; see also W. Ochs, proc. of the Santa Fe Workshop on Intermittency in High Energy Collisions, World Scientific, 1991.
2- A. Białas and J. Seixas, *Phys. Lett.* **B250** (1989) 161.
3- For a review see *e.g.* J. Seixas, proceedings of the ECFA Large Hadron Collider Workshop, Aachen 4-9 October 1990.
4- A. Białas and R. Peschanski, *Nucl. Phys.* **B273** (1986) 703; A. Białas and R. Peschanski, *Nucl. Phys.* **B308** (1988) 857.
5- V.V. Aivazyan *et al.* (NA22 Coll.), Nijmegen preprint HEN-332/90.
6- R. Peschanski and J. Seixas, "Scaling Relations Between Fluctuations and Correlations in Multiparticle Production", CERN preprint CERN-TH-5903/90.

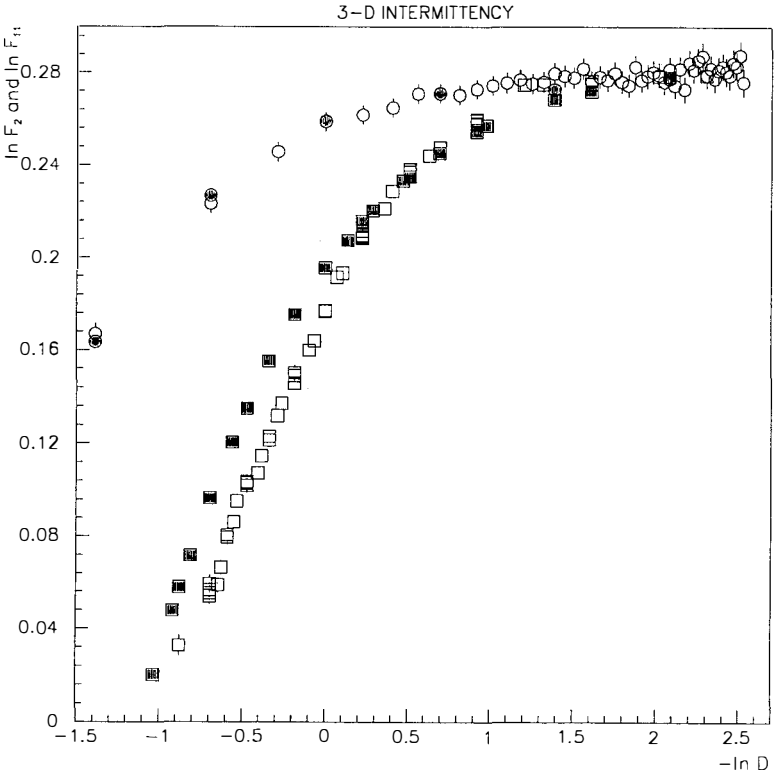

FIG. 1

Comparison between NA22 experimental results for factorial moment F_2 (open circles) and correlator $F_{1,1}$ (open squares) and simulation based on ansatz (4) (black circles and squares). The parameters used for the simulation are the same as in Ref. [2].

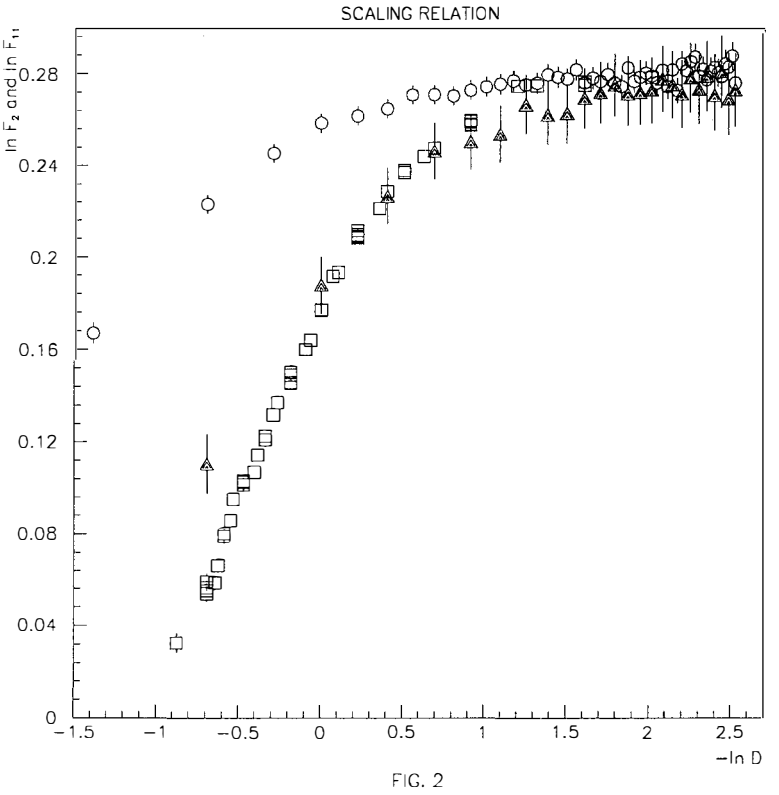

FIG. 2

Comparison between NA22 experimental results for factorial moment F_2 and correlator $F_{1,1}$ (open circles and squares, respectively) and relation (6) (black triangles).

FLUCTUATION THEORY OF PHASE TRANSITIONS IN MULTIPARTICLE DYNAMICS

I.M.Dremin

P.N.Lebedev Physical Institute, Moscow

M.T.Nazirov

Institute of High Energy Physics, Alma–Ata

Abstract. Field–theory approach is advocated where factorial moments substitute for Green functions. Their asymptotics at small rapidity intervals reveal the scaling behavior typical for critical phenomena.

1. Order parameter and field–theory variables. Large fluctuations of the number of particles in small phase–space bins have been observed in multiparticle production experiments and interpreted according to ideas of fractality and intermittency. In our opinion, however, their implications extend far beyond this since the general scaling behavior can reveal properties of phase transition and, even more, the classical nature of fields involved in soft hadron processes when the correlation length becomes infinitely large and the absolute value of the amplitude as well as the phase of the field are both **defined** at

a given point. Some speculations, based on a cascade model, concerning interrelation of large fluctuations and phase transition phenomena have been forwarded [1-4].

In analogy with fluctuation theory of second kind phase transitions in condensed matter physics [5], we propose here to describe fluctuation phenomena in multiparticle dynamics using the field–theoretical approach.

To start with, one should propose a local variable which plays a role of an order parameter. As such, one can use the fluctuation parameter introduced in [6]:

$$\varepsilon(y) = \frac{\rho_e(y)}{\rho(y)} - 1, \tag{1}$$

which shows deviation of the one–particle distribution in a given event $\rho_e(y)$ at the rapidity y from its inclusive hadronic partner $\rho(y)$ averaged over all events. Thus its average value in the hadron phase is equal to zero:

$$<\varepsilon>_h = 0. \tag{2}$$

This is an end–point for experimentalists but theorists using the notion of partons could imagine its average at the parton level which contains the ratio of parton to hadron inclusive spectra. According to the local parton–hadron duality they differ by the numerical factor only so that

$$<\varepsilon>_p \neq 0. \tag{3}$$

Thus, the variable $\varepsilon(y)$ can be treated as an order parameter related to the transition from parton to hadron states.

Moreover, one can treat $\varepsilon(y)$ as a local scalar field [7] to apply further all the machinery of field theory. Namely, one writes the probability of a given configuration ε as

$$W(\varepsilon) = Z^{-1}\exp[-F(\varepsilon)] \tag{4}$$

with $F(\varepsilon)$ interpreted as a free energy and the normalization factor

$$Z = \int D\varepsilon \exp[-F(\varepsilon)] \tag{5}$$

treated as a partition function.

Adding to $F(\varepsilon)$ the additional term $J(y)\varepsilon(y)$ with the external current $J(y)$ one gets correlators:

$$<\varepsilon_1 \ldots \varepsilon_q> = \frac{\delta^n \ln Z(J)}{\delta J(y_1)\ldots\delta J(y_q)}\Big|_{J=0} \tag{6}$$

According to (1) they are directly related to q–particle correlation functions ρ measured in experiment. For example,

$$<\varepsilon_1\varepsilon_2> = \frac{\rho(y_1,y_2)}{\rho(y_1)\rho(y_2)} - 1 \tag{7}$$

where

$$\rho(y) = \frac{dn}{dy}, \quad \rho(y_1,y_2) = \frac{d^2n}{dy_1dy_2}, \text{ etc.} \tag{8}$$

Therefore, the factorial moments are

$$F_q(\delta y)=(\delta y)^{1-q}\int_0^{\delta y} d\eta_1 \ldots \int_0^{\delta y} d\eta_{q-1} r_q(\eta_1,\ldots,\eta_{q-1}), \ (\eta_i=y_{i+1}-y_i)$$

(9)

with

$$r_q = \rho(y_1,\ldots,y_q)/\rho(y_1)\ldots\rho(y_q). \tag{10}$$

From the above formulae one can easily guess how factorial moments (9) are related to multiparticle Green functions (6).

Our main concern here is to show that the power–like behavior of factorial moments at small δy is determined by the scaling form of the Green functions well known to appear at the phase transition point for strong coupling in field theories.

One word of caution should be added here. For the sake of simplicity, we work with one–dimensional fluctuation $\varepsilon(y)$ while in general one should treat it in a three–dimensional phase space. It is unimportant for general conclusions about scaling behavior but can change results concerning the actual values of factorial indices and the position of the phase transition point. Having this in mind we proceed, first, to the phenomenological approach and then to general renormalization group treatment.

2. Phenomenology and perturbation theory [7]. If the fluctuations and their gradients are small enough, the function $F(\varepsilon)$ in (4) may be represented by a Taylor series:

$$F(\varepsilon) = F_0 + \int dy \left[\frac{b}{2}\left[\frac{d\varepsilon}{dy}\right]^2 + \frac{a}{2}\varepsilon^2 + c\varepsilon^3 + d\varepsilon^4 + \ldots\right] \tag{11}$$

which is a starting point for usual phenomenological approach well known due to

Ginzburg–Landau equation. In the free field case c=d=...=0 one gets

$$Z_f(J) = \exp\left\{-\frac{1}{2}\int dy_1 \int dy_2\, J(y_1) G_f(y_1-y_2) J(y_2)\right\} \tag{12}$$

$$G_f(y_1-y_2) = <\varepsilon_1\varepsilon_2>_f = \gamma \exp(-|y_1-y_2|/\xi), \tag{13}$$

$$\gamma = \pi\xi/b, \qquad \xi = (b/a)^{1/2}$$

so that

$$F_2(\delta y) = 1 + \gamma\xi(1-\exp(-\delta y/\xi))/\delta y \sim (\delta y)^{-\varphi(2)} \tag{14}$$

$$\text{if } a = a(\delta y)^{2\varphi(2)} \text{ at } \delta y \to 0 \tag{15}$$

To get an intermittency for higher moments one should treat $c \neq 0$, $d \neq 0$ etc. and ascribe the corresponding δy–dependence to these coefficients. This is a common deficiency of phenomenology where coefficients depend on external parameter (the temperature in usual phase transitions). Besides it, the above treatment shows that the perturbative approach is not a good starting point to describe intermittency so that it has been treated above for pedagogical purposes only. Therefore, we proceed to more rigorous field–theoretical treatment, where scaling behavior is due to power–like propagators and does not require any assumptions about coefficients.

3. Field–theory approach. We have learned that for small δy the free–field Green function (13) diverges ($\gamma \to \infty$, $\xi \to \infty$) if intermittent behavior is inserted in (14), (15). It implies that interaction drastically changes the free propagator and vertex functions, just as it happens usually in strong coupling theories with phase transition [8-11]. It has been shown by using renormalization group method, Feynman graph technique and unitarity condition that one gets power–like behavior of many–particle vertices at the phase transition. For theories of massless scalar fields with a fixed point (where Gell–Mann–Low function has a zero at some value of coupling constant) the non–perturbative propagator in a Fourier–conjugate space t behaves like

$$D(t) \sim |t|^{-(2-\eta)} \qquad \text{for } |t| \to \infty \tag{16}$$

where η is an anomalous field dimension.

In general, one can write

$$D(t)\sim|t|^{-\alpha};\ \Gamma_q(t_1,\ldots,t_q)\sim|t_1|^{-\gamma}\Gamma_q\left(1,\frac{t_2}{|t_1|},\ldots,\frac{t_q}{|t_1|}\right);\ |t|\to\infty \tag{17}$$

with $\alpha<1$ and

$$<\varepsilon(t_1)\ldots\varepsilon(t_q)> = \delta(\sum_1^q t_i)D(t_1)\ldots D(t_q)\Gamma_q(t_1,\ldots,t_q) \tag{18}$$

or in y–space

$$<\varepsilon(y_1)\ldots\varepsilon(y_q)> \sim |y_q-y_1|^{\gamma+2\alpha-1}\,|y_q-y_2|^{-1+\alpha}\ldots|y_q-y_{q-1}|^{-1+\alpha} \tag{19}$$

so that factorial moments behave as power–like functions

$$F_q(\delta y \to 0) \sim (\delta y)^{-\varphi(q)} \tag{20}$$

with

$$\varphi(q) = q(1-\alpha) - \gamma - 1 > 0 \tag{21}$$

Similarities and differences to the usual description of phase transitions will be discussed elsewhere but the reader can guess it from above formulae.

Two experimental consequences are easily seen from the above analysis. First, the factorial indices $\varphi(q)$ appear to be equidistant so that

$$\varphi(q+1) - \varphi(q) = \text{const} \tag{22}$$

i.e. it does not depend on q.

Second, two particle correlation function at small $|y_1-y_2|$ declines from the exponential form and, in general, should be better fitted by the function

$$r(y_1,y_2) \sim \frac{1}{|y_1-y_2|^{\alpha}}\exp[-|y_1-y_2|/\xi] \tag{23}$$

We hope to publish more detailed analysis anywhere including the graph technique and unitarity condition treatments which provide the same result. We are indebted to participants of high energy physics seminar at Theory Department of P.N.Lebedev Physics Institute for valuable discussions.

References

1. For the review see: I.M.Dremin, Sov. Phys. Uspekhi 33 (8), 647 (1990).
2. R.Peschanski, Nucl. Phys. B327, 144 (1989).
3. Ph.Brax, R.Peschanski, preprint SPhT/89.203, 1989.
4. A.Bialas, P.Szczerba, K.Zalewski, Z. Phys. C 46, 163 (1990).
5. A.Z.Patashinsky, V.L.Pokrovsky. Fluctuation theory of phase transitions, Moscow, Nauka, 1982.
6. I.M.Dremin, preprint CERN TH 4693/87, Geneva, 1987; see also[1].
7. M.T.Nazirov, Mod. Phys. Lett. A (1991) (to be published).
8. V.N.Gribov, A.A.Migdal, ZhETF 55(10), 1498 (1968).
9. A.M.Polyakov, ZhETF 55(9), 1026 (1968).
10. A.A.Migdal, ZhETF 55(11), 1964 (1968).
11. K.G.Wilson, J. Kogut Phys. Rep. 12C, 75 (1974).

HIGHER ORDER BOSE-EINSTEIN CORRELATIONS AT $\sqrt{s} = 630$ AND 900 GeV

N. Neumeister
(UA1-MINIMUM BIAS-Collaboration)
Institut für Hochenergiephysik
der Österreichischen Akademie der Wissenschaften
A-1050 Vienna, Austria

Abstract

Higher order Bose-Einstein correlations, up to 5^{th} order, are presented using UA1 data at $\sqrt{s} = 630$ and 900 GeV. The results are compared with theoretical calculations to investigate the primary assumptions for the parametrization of the correlation functions.

1 Introduction

Hanbury-Brown and Twiss [1] were the first who applied the Bose-Einstein correlations (BEC) to measure the size of distant stars. The method was first applied to particle physics by Goldhaber et al. [2] in 1959. Since then the size of the interaction region has been measured by numerous experiments in high energy collisions between many different types of particles [3-6].

The aim of this contribution is to present higher order BEC up to the 5^{th} order using data from $p\bar{p}$ collisions at center of mass energies of 630 and 900 GeV. The data for this analysis were collected in 1985 by the UA1 experiment at the SPS proton-antiproton collider.

2 Higher Order Correlations

To study BEC one compares the distribution of like-charged pion pairs with a distribution of reference sample pairs, which should be free of BEC. The ratio usually has been parametrized with a Gaussian function of the four momentum difference squared:

$$N^{(2)}/N^{BG} = 1 + \lambda e^{-r^2 Q_{2\pi}^2} \qquad \text{with} \qquad Q_{2\pi}^2 = -(q_1 - q_2)^2 \,. \tag{1}$$

The two parameters λ and r are to be determined by fitting the data. In the limit of a completely chaotic source and identical momenta the ratio is expected to produce: $N^{(2)}/N^{BG}(Q_{2\pi} \to 0) = 2$. The parameter λ expresses the degree of chaoticity of the source. For a fully coherent source λ is zero. One can interpret the parameter r as the extension of the pion producing region.

The analysis of BEC for more than two particles follows the procedure for pairs. The three particle correlation function depends on the three variables q_{12}, q_{13} and q_{23}. If one uses the pair parametrization (1), and

$$Q_{3\pi}^2 = q_{12}^2 + q_{13}^2 + q_{23}^2 \,, \tag{2}$$

the three particle function can be parametrized in analogy to the pair analysis:

$$N^{(3)}/N^{BG} = 1 + \lambda_3 e^{-r_3^2 Q_{3\pi}^2} \,. \tag{3}$$

The calculation for 4^{th} and 5^{th} order is straightforward but using this technique it becomes too complicated.

However, in [7] a new set of formulas to describe the higher order correlation functions is given. These formulas were originated using methods from quantum optics assuming the coherent part of the source to be pointlike and the chaotic one to be of a Gaussian form.

In the symmetric configuration for n particles when

$$q_{12}^2 = q_{13}^2 = q_{23}^2 = \ldots = q_{(n-1)n}^2 \qquad \text{with} \qquad q_{ij}^2 = -(p_i - p_j)^2 \tag{4}$$

there are $\frac{n\cdot(n-1)}{2}$ terms of q_{ij}^2 in $Q_{n\pi}^2$:

$$Q_{n\pi}^2 = q_{12}^2 + \ldots + q_{(n-1)n}^2 \tag{5}$$

Now the formulas for second to fifth order are [7]:

$$N^{(2)}/N^{BG} = 1 + 2\lambda(1-\lambda)e^{-r^2Q_{2\pi}^2} + \lambda^2 e^{-2r^2Q_{2\pi}^2} \tag{6}$$

$$N^{(3)}/N^{BG} = 1 + 6\lambda(1-\lambda)e^{-\frac{1}{3}r^2Q_{3\pi}^2} + 3\lambda^2(3-2\lambda)e^{-\frac{2}{3}r^2Q_{3\pi}^2} + 2\lambda^3 e^{-r^2Q_{3\pi}^2} \tag{7}$$

$$\begin{aligned} N^{(4)}/N^{BG} = 1 &+ 12\lambda(1-\lambda)e^{-\frac{1}{6}r^2Q_{4\pi}^2} + 6\lambda^2(7-8\lambda+2\lambda^2)e^{-\frac{1}{3}r^2Q_{4\pi}^2} \\ &+ 4\lambda^3(11-9\lambda)e^{-\frac{1}{2}r^2Q_{4\pi}^2} + 9\lambda^4 e^{-\frac{2}{3}r^2Q_{4\pi}^2} \end{aligned} \tag{8}$$

$$\begin{aligned} N^{(5)}/N^{BG} = 1 &+ 20\lambda(1-\lambda)e^{-\frac{1}{10}r^2Q_{5\pi}^2} + 10\lambda^2(13-18\lambda+6\lambda^2)e^{-\frac{1}{5}r^2Q_{5\pi}^2} \\ &+ 20\lambda^3(16-21\lambda+6\lambda^2)e^{-\frac{3}{10}r^2Q_{5\pi}^2} \\ &+ 5\lambda^4(53-44\lambda)e^{-\frac{2}{5}r^2Q_{5\pi}^2} + 44\lambda^5 e^{-\frac{1}{2}r^2Q_{5\pi}^2} \end{aligned} \tag{9}$$

In (6) to (9) there are only two parameters r and λ. In [7] it has been pointed out, that these parameters should be constant in all orders. Higher order BEC are a powerful tool to check the assumptions for two-particle correlations and to clarify further corrections (Coulomb interactions, final state interactions etc.).

3 Data

The data for this analysis were obtained during two periods of data taking, one at a fixed center of mass energy of $\sqrt{s} = 630$ GeV and the other at $\sqrt{s} = 900$ GeV. All data were taken using a 'minimum bias' trigger, requiring at least one charged particle in the pseudorapidity range of $1.5 < |\eta| < 5.6$ in each of the downstream arms of the detector. The first data-set with $\sqrt{s} = 630$ GeV includes about 147.000 events and the second with $\sqrt{s} = 900$ GeV about 66.000 events. All information used for this analysis was obtained from reconstructed trajectories measured by the UA1 Central Detector in a region of pseudorapidity of $|\eta| \leq 3$. The azimuthal regions with $|\Phi| \leq 15°$ and $|\Phi| \geq 165°$ were excluded because of the high uncertainty of momentum measurement in those regions. Only those tracks with projected length, in the plane normal to the magnetic field, larger than 40 cm and a $p_T \geq 0.15 GeV/c$ are considered for this analysis. Also a good fit to the vertex and a good track quality are required for all tracks. We assumed that all particles retained from these conditions are charged pions.

We have observed that a substantial number of low momentum tracks (about 2%) are misidentified by the pattern recognition as two tracks. This happens mainly when the particles are crossing the walls of the different parts of the central detector. Our results are very sensitive on these misidentifications, because two partly overlapping tracks produce a very low Q^2. Our algorithm removes only 98% of all split tracks, so we require each track-pair to have an invariant momentum-difference-squared $Q^2 = -(p_1 - p_2)^2 \geq 0.0001 (GeV/c)^2$.

Because we want to compare the results of higher orders (up to 5) of the BEC, it is nessecary that each event consists of at least 5 like-charged tracks.

4 Analysis

In order to analyse our data to obtain the radius and the coherence parameter of the pion source we had to divide the Q^2-distribution of tracks from the same event by the Q^2-distribution of a reference sample. We used the method of eventmixing: for the n^{th} order reference sample distribution we took n like-charged tracks, each of a different event, and calculated q_{ij}^2, the four momentum difference squared, of each pair of these tracks. We normalized our ratios in the region of $0.4 \leq Q^2 \leq 1.0\,(GeV/c)^2$.

For our fits we applied the normalizing correction for the reference sample distribution as outlined in [8]. So we divided all our functions used for fitting by the term $(1 + \delta Q^2)$.

For the correlated distributions of charged particles one has to correct for Coulomb-interaction with the inverse Gamow-factor [4].

This method is only possible for a two particle correlation, but in [4] an approximation for three particles is given: $W_3 = G_{12}^{-1} \cdot G_{13}^{-1} \cdot G_{23}^{-1}$.

Exact calculations for the Coulomb interaction for more than three particles do not yet exist, so we generalized this approximation for n^{th} order in a straightforward extension:

$$W_n = \prod_{i<j}^{n} G_{ij}^{-1} \,. \tag{10}$$

The systematic error due to our way of selecting the real data is estimated by variation of our data selection parameters to be about 5%.

We fitted our data samples with the following functions:

(i) (6) to (9) divided by the normalizing factor $(1 + \delta Q^2)$

(ii) (6) to (9) divided by the normalizing factor $(1+\delta Q^2)$, but the Gaussian form for the two particle correlation function is replaced in all orders by an exponential shape: $e^{-ar^2Q^2} \rightarrow e^{-arQ}$.

5 Results and Discussion

We studied BEC from second to fifth order. Our results for second and third order are in agreement with [3,4]. The normalized data were fitted with (i) and (ii) of section 4. We found, that all functions with an exponential assumption for the shape of the chaotic source reproduce the data better than functions with a Gaussian assumption (see Figure 1). Fitting our data with the functions (6) to (9) we found moreover, that with this set of functions it is not possible to describe all orders of the BEC with the same parameters as claimed in [7]. The radius r rises with the order, but the coherence parameter λ is almost constant. Because it is only useful to interpret the parameters of functions which are really able to descibe the data, we modified the functions given in [10] using an exponential expression to describe the chaotic source. The differences between these two sets of functions are shown in figure 1 and it is clear that the exponential fit describes the data much better. Again the coherence parameter is nearly constant and the radius r is rising (Fig. 2). We introduced a purely phenomenological factor $\sqrt{\frac{2}{n(n-1)}}$ so that the modified radius $R = r \cdot \sqrt{\frac{2}{n(n-1)}}$

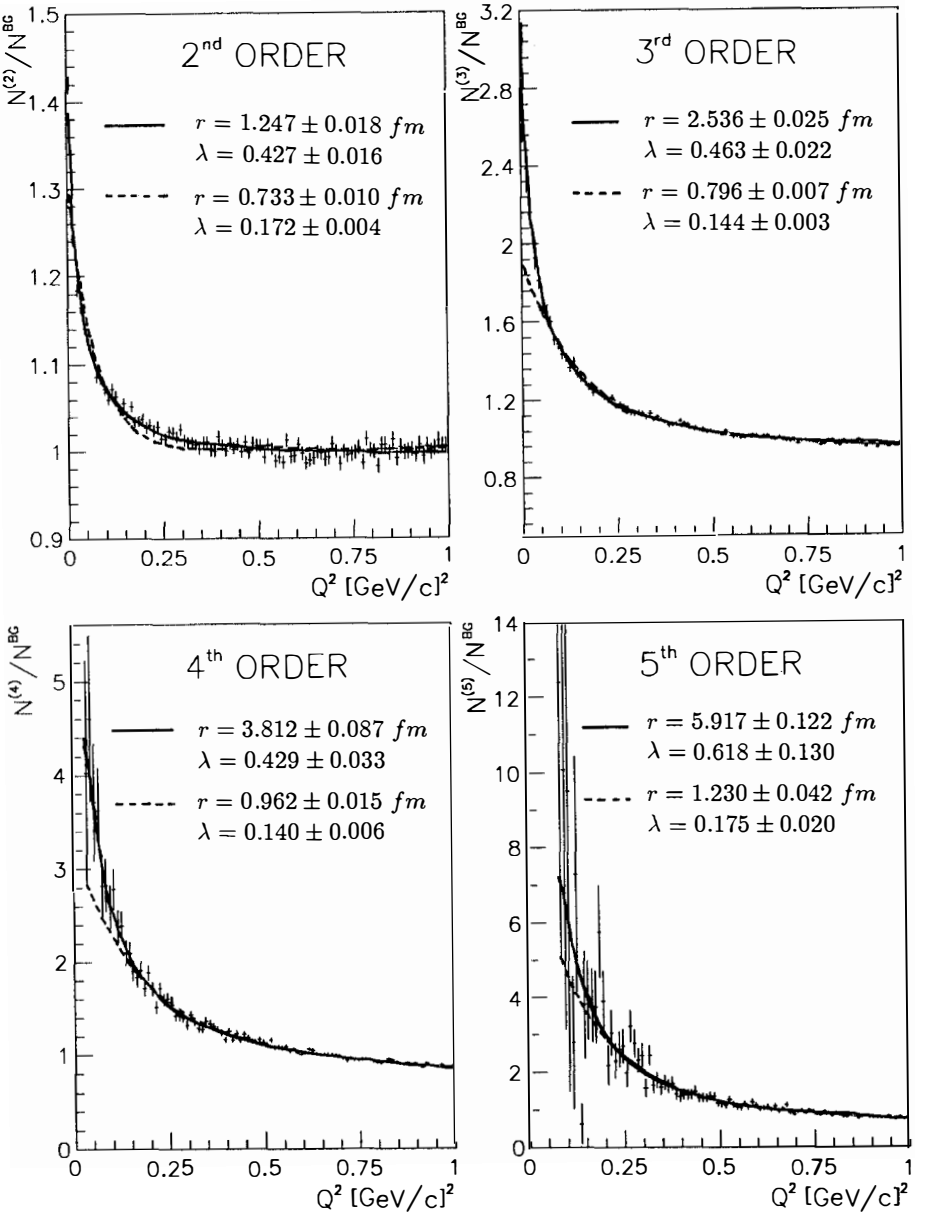

Fig. 1: Bose-Einstein ratio from second to fifth order for 630 GeV. The dashed line represents the fit with (6) to (9) and the solid line represents the fit with (ii) of section 2. All data are corrected for Coulomb interactions.

(compare: $Q^2_{n\pi}$ is the sum of $\frac{n(n-1)}{2}$ q^2_{ij}), is only slightly increasing with the order (almost constant).

Though we worked with just two energies, the parameters seem to be independent of the energy.

References

[1] R. Hanbury-Brown, R.Q. Twiss, Philos. Mag. 45(1954)663.

[2] G. Goldhaber *et al.*, Phys. Rev. 120(1960)300.

[3] C. Albajar *et al. (UA1 Collab.)*, Phys. Lett. B226(1989)410.

[4] I. Juricic *et al.*, Phys. Rev. D39(1989)39.

[5] P. Avery *et al. (CLEO Collab.)*, Phys. Rev. D32(1985)2294.

[6] T.J. Humanic *(NA35 Collab.)*, in *Quark Matter '87*, Proceedings of International School, Munster, 1987, Z.Phys. C38(1988)1.

[7] M. Biyajima, A. Bartl *et al.*, Progress Theor. Phys. 84,930(1990).

[8] J.L. Bailly *et al. (NA23, EHS-RCBC Collab.)*, Z. Phys. C43(1989)341.

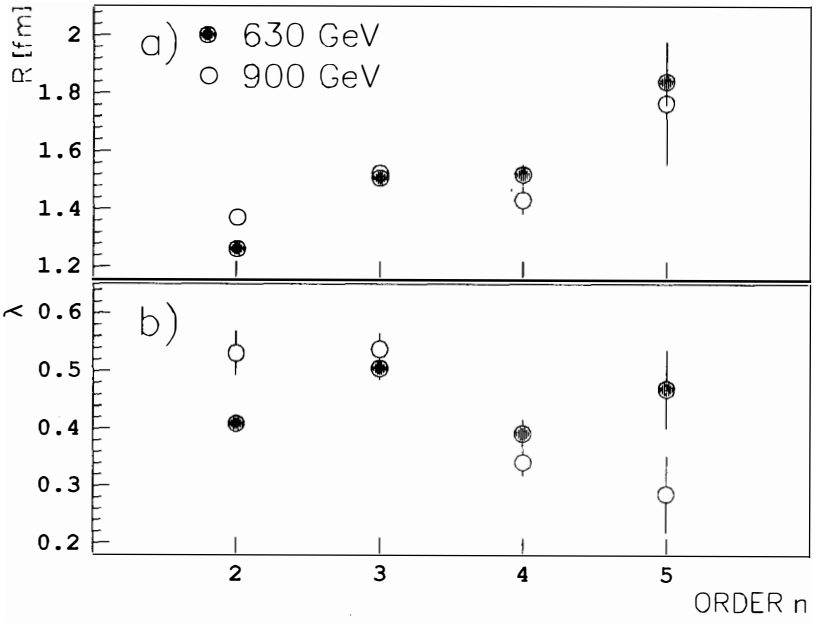

Fig. 2: Comparison of the modified radii $R = r \cdot \sqrt{\frac{2}{n(n-1)}}$ and of the coherence parameters λ, obtained by fitting the functions (ii) of section 2 to the data samples, for second to fifth order. The data samples are fully corrected.

Charged Particle Multiplicity Distributions in Restricted Rapidity Intervals in Z^0 Hadronic Decays

Vladimir UVAROV
Institute for High Energy Physics, Protvino (Moscow Region), USSR

Abstract

The multiplicity distributions of charged particles in restricted rapidity intervals in Z^0 hadronic decays measured by the DELPHI detector are presented. The data reveal a shoulder structure, best visible for intervals of intermediate size, i.e. for rapidity limits around ± 1.5. The whole set of distributions including the shoulder structure is reproduced by the Lund Parton Shower model. The structure is found to be due to important contributions from 3- and 4-jet events with a hard gluon jet. A different model, based on the concept of independently produced groups of particles, "clans", fluctuating both in number per event and particle content per clan, has also been used to analyse the present data. The results show that for each interval of rapidity the average number of clans per event is approximately the same as at lower energies.

In recent papers[1],[2] an analysis of the multiplicity distributions of charged particles produced in Z^0 hadronic decays in the DELPHI detector was performed. The present report is based on the results of paper[2] in which the properties of the charged particle multiplicity distributions in restricted intervals of rapidity have been studied.

The study was based on 94439 hadronic events with $n_{ch} \geq 5$ obtained in 1989-1990 with the DELPHI detector[3] at the LEP e^+e^- collider at energies near the Z^0-resonance. The charged particles were detected by the Time Projection Chamber (TPC). For event selection, the following cuts were applied: tracks were kept only if they extrapolated back to the nominal crossing point within $\Delta r < 5$ cm and $\Delta z < 10$ cm, if their momentum was greater 0.1 GeV/c, if the measured track length was above 50 cm and if the polar angle θ was between 25° and 155°. Events were kept only if the total energy of charged particles (assumed to have pion mass) in each of the two hemispheres with respect to the beam axis exceeded 3 GeV, if total energy of charged particles in both hemispheres exceeded 15 GeV, if there were at least 5 charged particles with momenta above 0.2 GeV/c and if the polar angle of the sphericity axis was in the range $40° < \theta < 140°$. The resulting data sample comprised 63434 events. The possible contaminations from events due to beam-gas scattering, $\gamma\gamma$ interactions and $\tau^+\tau^-$ events, were reduced to a negligible level by the imposed cuts. The correction procedure and the treatment of systematic uncertainties are described in details in refs. [1],[2].

The multiplicity distributions $P(n)$ are presented in Fig. 1a and, in the *KNO*-form ($\psi(z) = \langle n \rangle P(n)$ *versus* $z = n/\langle n \rangle$), in Fig. 1b for different rapidity intervals $|y| < y_{cut}$ (rapidity was calculated with respect to the thrust axis assuming pion mass for all particles). For clarity, each successive distribution in Figs. 1a and 1b is lowered by a factor of ten. From Fig. 1a it is seen that the multiplicity distribution becomes more narrow as the rapidity interval is reduced. On the contrary, the distribution in *KNO*-form (Fig. 1b) widens under the same imposed cuts in rapidity.

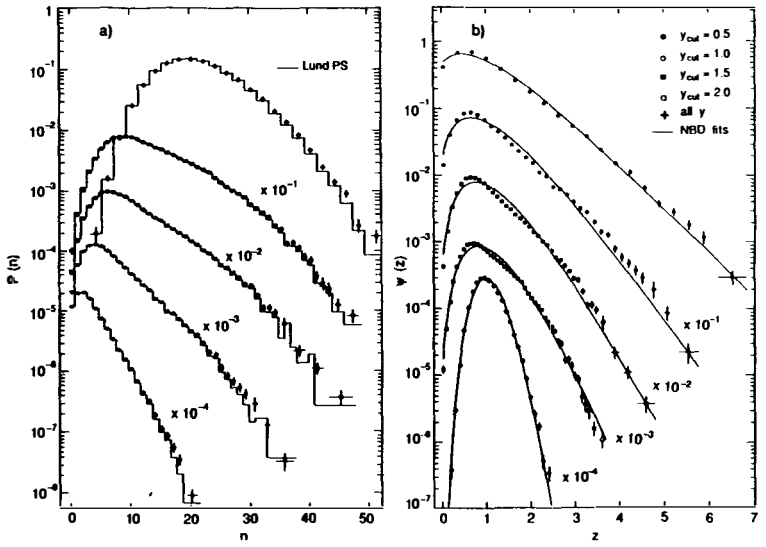

Fig.1 Corrected charged particle multiplicity distributions in central rapidity intervals *a)* $P(n)$ and *b)* $\psi(z) = \langle n \rangle P(n)$ *versus* $z = n/\langle n \rangle$. Each successive distribution is lowered by a factor of ten. The histograms show the Lund PS model predictions. Solid curves connect points of the *NBD* with parameters obtained from the data.

The predictions of the Lund Parton Shower (PS) model (Monte Carlo program JETSET version 6.3)[4] are plotted together with the corrected data in Fig. 1a. However, the judgment of the amount of agreement or disagreement has been made between the transformed predictions for frequencies of track-multiplicities and the raw, uncorrected data. The χ^2-values (χ^2/NDF = 55/20, 67/32, 81/42, 68/46 and 81/43 for $|y| <$ 0.5, 1.0, 1.5, 2.0 and full phase space, respectively) indicate rather poor agreement between the Lund PS predictions and the data. However, the origin of all the observed disagreements is found to be due to systematic differences in the high multiplicity tails of the various distributions, such that the frequencies of events in the model predictions fall below the data with some few percent. Thus it seems unavoidable to conclude that the Lund PS model slightly underestimates the frequencies of high multiplicity events.

An interesting feature of the data is a shoulder in the multiplicity distributions, best seen for intervals of rapidity $|y| < 1.5$ and $|y| < 2.0$. This shoulder structure is present already in the raw, uncorrected data and thus is not an artifact created by the correction procedure. The Lund PS model predicts this shoulder structure rather well. In an attempt to understand this structure the data were resolved into multi-jet hadronic final states, using the jet finding algorithm originally introduced by the JADE collaboration[5]. The choice of the lower limit for the scaled invariant mass $Y_{ij} = 2E_iE_j(1-\cos\theta_{ij})/E^2_{vis}$ has arbitrarily and conventionally been set at $Y_{min} = 0.04$.

With this jet definition and as an illustration, the multiplicity distribution for the rapidity interval $|y| < 2.0$ has been resolved into components of 2-, 3- and 4-jet events as shown in Fig. 2a. The figure contains also the Lund PS model predictions obtained by using the same JADE jet finding algorithm and demonstrates rather good agreement between model and data, apart from a slight systematic underestimation of the high multiplicity tails and of the number of 4-jet events. The main features seen from Fig. 2a are that the multiplicity distribution is dominated by contributions from 2-jet events at low multiplicities with a peak at $n \approx 10$, has a shoulder at $n \approx 20-25$ due to 3-jet event contributions and has a tail dominated by 3- and 4-jet events.

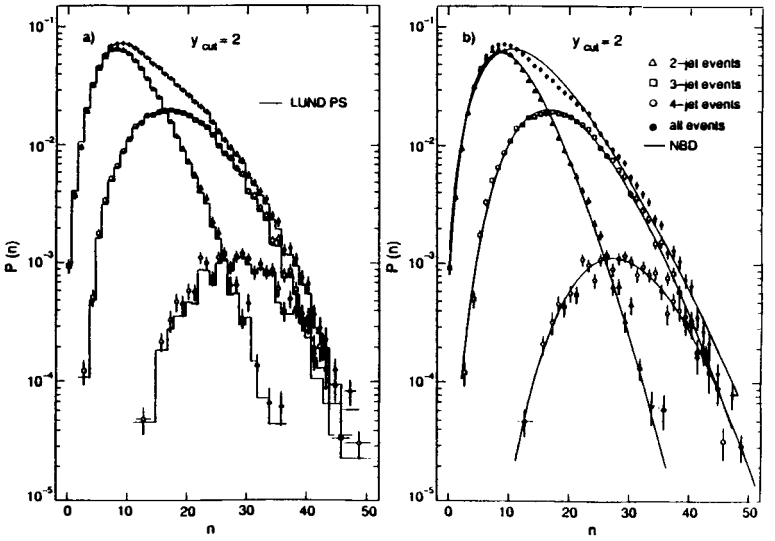

Fig.2 Multiplicity distributions $P(n)$ of charged particles for the rapidity range $|y| < 2$ for all events and for events with 2-, 3- and 4-jets in comparison *a)* with the Lund PS model predictions and *b)* with the results of the fits to *NBD's*.

The dominance of the multi-jet events at large multiplicities explains why the structure in multiplicity distributions is best seen in the central rapidity windows with $|y| < 1.5, 2.0$. Indeed, the multi-jet events are more "spherical" with respect to the thrust axis and therefore imposed cuts on rapidity reduce the multiplicities of multi-jet events much less than those of 2-jet events, thereby enhancing the difference between their respective average multiplicities.

The UA5 collaboration has observed that the negative binomial distribution (*NBD*), which was successfully fitted to the charged multiplicity distributions in full phase space and in limited parts of it for various interactions fails to give a good fit to data at the center-of-mass energy of 900 GeV [6] in full phase space and for large rapidity intervals due to a shoulder structure. The fit of the *NBD* to the DELPHI data in restricted rapidity intervals (Fig. 1b) is found to be of rather poor quality (χ^2/NDF = 75/18, 342/30, 478/40, 280/44 and 205/41 for $|y| <$ 0.5, 1.0, 1.5, 2.0 and full phase space, respectively) due to the shoulder structure of the experimental distributions. The maximum amplitudes of the deviations between the *NBD* model predictions and the data amount to about 10 to 15 %. However, the fit of the *NBD* to the multiplicity distributions of 2-, 3- and 4-jet events in rapidity interval $|y| < 2.0$ (Fig. 2b) is found to be of rather good quality (χ^2/NDF= 70/32, 79/40 and 33/28 for 2-, 3- and 4-jet events, respectively) then for all events in the same rapidity interval.

As the gross shapes of the experimental distributions including the tails at high multiplicities are reasonably well reproduced by the *NBD*'s and since several earlier investigations have been done along these lines, the data were also analysed in terms of the "clan" cascading picture, introduced by Ekspong, Giovannini and Van Hove[7]. The term "clan" refers to a group of particles with common and independently produced ancestor, the number of which per event therefore fluctuates according to a Poisson distribution with an average $\overline{N}$. The number of particles per clan also fluctuates (on the average according to a logarithmic distribution) with an average $\overline{n}_c$. These two quantities can be derived from the parameters of the *NBD* ($<n>$ and k) according to the following formulae: $\overline{N} = k \cdot ln(1 + <n>/k)$ and $\overline{n}_c = <n>/\overline{N}$

The dependence of the average number of clans, $\overline{N}$, on the size of the rapidity interval for the DELPHI data is compared with the Lund PS model prediction and with the lower energy TASSO data[8] in Fig. 3a. The dependence of the average number of particles per clan, $\overline{n}_c$, on the size of the rapidity interval for the same data is presented in Fig. 3b. The average number of clans is approximately energy independent in fixed rapidity intervals. On the other hand the average number of charged particles per clan, $\overline{n}_c$, shows strong energy dependence. Thus the data show that a scaling, which fails to hold in particle density[9], holds in clan density. It implies that the multiplicity increase with energy is due not to an increased clan density, but to the average clan getting larger in particles and, of course, also due to a wider rapidity range at higher energies. This agrees with conclusions about the "clan picture" made by Giovannini and Van Hove[10] in their "Monte Carlo experiment" based on the Lund PS model and with the similar results obtained for hadronic collisions[11].

In conclusion, the most important results of the study of the multiplicity distributions in restricted intervals of rapidity measured in the DELPHI experiment can be summarized as follows:

- The multiplicity distributions in intermediate sized rapidity intervals show a shoulder structure, less evident in full phase space. This structure is explained by the incoherent superposition of 2-jet events with mostly low multiplicities and 3- and 4-jet events yielding much larger multiplicities.

- The Lund Parton Shower model describes practically all of the studied features of the multiplicity distributions, including the shoulder structure. The model slightly underestimates the frequency of events in the high multiplicity tails of the distributions, where multi-jet contributions are dominant.

• The negative binomial distributions (*NBD*) fail to describe the shoulder structure of the multiplicity distributions and thus fail to give good fits to data. However, the gross shapes, including the high multiplicity tails, are represented by the *NBD*'s. The *NBD*'s describe also the multiplicity distributions of 2-, 3- and 4-jet events. When analysed in terms of independently produced groups of particles, "clans", the average number of clans per event at 91 GeV c.m. energy is found to be approximately the same as at lower energies for each rapidity interval where information exists, i.e. the clan density with respect to rapidity is approximately energy independent. The multiplicity increase with energy is in this picture due to the average clan containing more particles and also due to the wider rapidity range at higher energies.

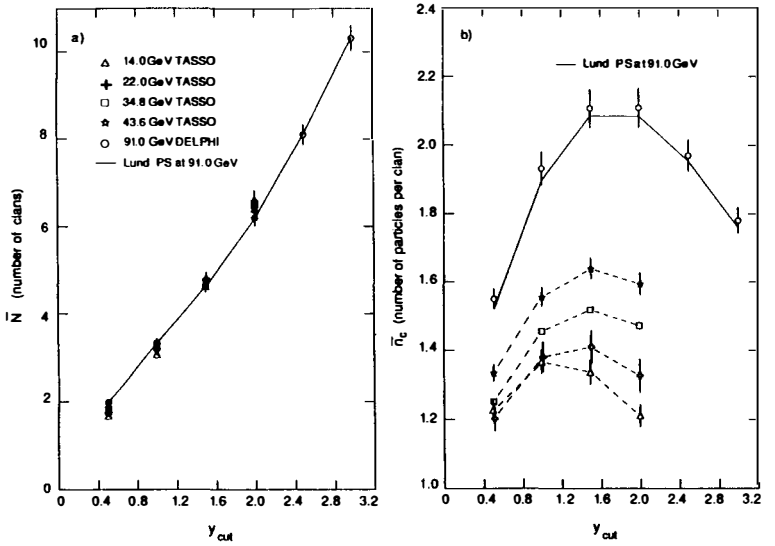

Fig.3 a) Average number of clans, $\bar{N}$, and *b)* average number of charged particles per clan, $\bar{n}_c$, as a function of the limit of the rapidity interval. Straight lines connect points predicted by the Lund PS model at the center-of-mass energy of 91 GeV. The TASSO data are from ref. [7].

References

1. *DELPHI Collaboration, P.Abreu et al.,* CERN-PPE/90-173 (submitted to Z.Phys.C).

2. *DELPHI Collaboration, P.Abreu et al., Charged Particle Multiplicity Distributions in Restricted Rapidity Intervals in Z^0 Hadronic Decays,* (to be submitted to Z.Phys.C).

3. *DELPHI Collaboration, P.Aarnio et al.,* CERN-PPE/90-128 (to appear in NIM).

4. *M.Bengtsson and T.Sjöstrand,* Phys.Lett. B185(1987)435; *T.Sjöstrand,* Comp.Phys.Comm. 27(1982)243; ibid. 28(1983)229; *T.Sjöstrand and M.Bengtsson,* Comp.Phys.Comm. 43(1987)367.

5. *JADE Collaboration, W.Bartel et al.,* Z.Phys. C33(1986)23; *S.Bethke et al.,* Phys.Lett. 213B(1988)235.

6. *UA5 Collaboration, R.E.Ansorge et al.,* Z.Phys. C43(1989)357.

7. *G.Ekspong,* Proc. XVI Intern. Symp. on Multiparticle Dynamics (Kiryat Anavim, 1985), ed. J.Grunhaus (Editions Frontieres, World Scientific, Singapore, 1985), p.309; *A.Giovannini and L.Van Hove,* Proc. XVII Intern. Symp. on Multiparticle Dynamics (Seewinkel, 1986), eds. M.Markytan et al. (World Scientific, Singapore, 1987), p.561; Z.Phys. C30(1986)391; *L.Van Hove,* Physica A147(1987)19.

8. *TASSO Collaboration, W.Braunschweig et al.,* Z.Phys. C45(1989)193.

9. *ALEPH Collaboration, D.Decamp et al.,* Phys.Lett. 234B(1990)209; *DELPHI Collaboration, P.Abreu et al.,* CERN-PPE/90-118 and paper presented to the XXV Int. Conf. on High Energy Physics, Singapore, 1990.

10. *L.Van Hove and A.Giovannini,* Acta Phys.Polonica B19(1988)917.

11. *NA22 Collaboration, M.Adamus et al.,* Z.Phys. C37(1988)215; Phys.Lett. B205(1988)401.

MESON AND BARYON CORRELATION STUDIES USING THE PEP-TPC/2γ FACILITY

Michael T. Ronan
Lawrence Berkeley Laboratory
University of California, Berkeley
California 94720, USA

Representing the TPC/Two-Gamma Collaboration

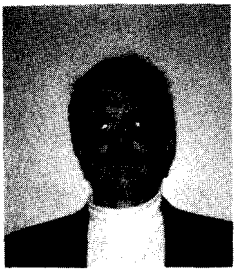

ABSTRACT

Results on vector meson, and strange and charmed-baryon production are presented for data taken during the period 1982-1986 using the TPC/2γ detector at PEP. Vector mesons (ρ^0, K^* and ϕ) with 0, 1 and 2 strange quarks are used to obtain redundant measures of strange-quark suppression and of the vector to pseudoscalar ratio in hadronization. Measurements of the production rates of Λ, Ξ^-, Ω and Ξ^{*0} hyperons and for the Λ_C and of rapidity correlations between $\Lambda\overline{\Lambda}$ pairs provide sensitive tests of baryon production in fragmentation models. In addition, two- and three-particle correlations between like sign pions provide further evidence for the Bose-Einstein effect in e^+e^- interactions including the relativistic motion of particle sources.

1. Introduction

Measurements of vector meson production provide an important probe of the hadronization process, for these particles are not as diluted as are the pseudoscalars by the decays of higher-mass states. I will report on unpublished measurements[1-2] of total multiplicities for ρ^0, K^{*0}, $K^{*\pm}$ and ϕ vector meson production. Combining these measurements with values for π and K production, we obtain redundant measures of strange-quark suppression and of the vector to pseudoscalar production ratio in hadronization.

Next, I will present a study[3] of Bose-Einstein interference effects, enhancements observed for pairs of particles produced in the hadronization process at small four-momentum difference, $q = (q_0, \mathbf{q}) = p_1 - p_2$. Measurements by several groups[4-6] indicate that Bose-Einstein correlations are well described by a function that depends only on $Q \equiv \sqrt{-q^2}$. To test if the enhancement disappears for pairs that are highly boosted, we measure the correlation function as a function of both Q and the energy difference in the laboratory frame, $q_0 = E_1 - E_2$.

Due to the high mass of strange and charmed baryons, their inclusive production rates give direct tests of various hadronization models, while their flavor correlations probe the detailed color confinement mechanism in the baryon formation process. Lastly, I will report on new preliminary results for Λ, Ξ^-, and Ω production and first observation of Ξ^{*0} and Λ_C production at $\sqrt{s} = 29$ GeV, and then compare our measurement of $\Lambda\overline{\Lambda}$ correlations with predictions of the Lund[7] and UCLA[8] models.

2. Inclusive Vector Meson Production

Data were recorded during 1982-1983 and 1984-1986 at PEP using the TPC/2γ Detector Facility with low-field (4 kG) and with high-field (13.2 kG) magnets. The detector and trigger systems as well as the hadronic event selection criteria are described in detail elsewhere[9]. Utilizing the unique particle identification capabilities of the TPC, pions and kaons are selected to form the mass spectra shown in Fig. 1 for $\pi^\pm$ pairs, charged pions plus charged and neutral kaons, and $K^\pm$ pairs. The observed signal to background varies from the ρ^0, at a level which is comparable to other experiments, to the ϕ, which is seen with superb separation. Extrapolating our measured differential cross sections to threshold, we determine the following multiplicites per event: for the ρ^0, $N(\rho^0) = 0.77 \pm 0.08 \pm 0.15$; for charged and neutral K^*, $N(K^{*\pm}) = 0.54 \pm 0.08 \pm 0.06$ and $N(K^{*0}) = 0.58 \pm 0.05 \pm 0.11$; and for the ϕ, $N(\phi) = 0.079 \pm 0.008 \pm 0.010$.

Subtracting the expected contribution to vector meson production from decays of charmed and bottom mesons, we perform a global Lund model fit to the number of primary ρ^0,K^*,ϕ and to world-average values for the total number of $\pi^\pm$ and $K^\pm$, varying the Lund Symmetric Fragmentation Function parameter a, the strange quark suppression factor, $\frac{s}{u}$, and the fraction of vector mesons, $\frac{V}{(V+PS)}$, while setting the $\frac{V}{(V+PS)}$ ratio for strange mesons equal to that for the light non-strange mesons. We obtain a good fit, with $\chi^2 = 0.7$ for two degrees of freedom, with $a = 1.10 \pm 0.29$, $\frac{s}{u} = 0.30 \pm 0.03$ and $\frac{V}{(V+PS)} = 0.45 \pm 0.11$. Each value is consistent with previous measurements, and the determination of strange quark suppression is obtained with errors comparable to the previous world average errors[8].

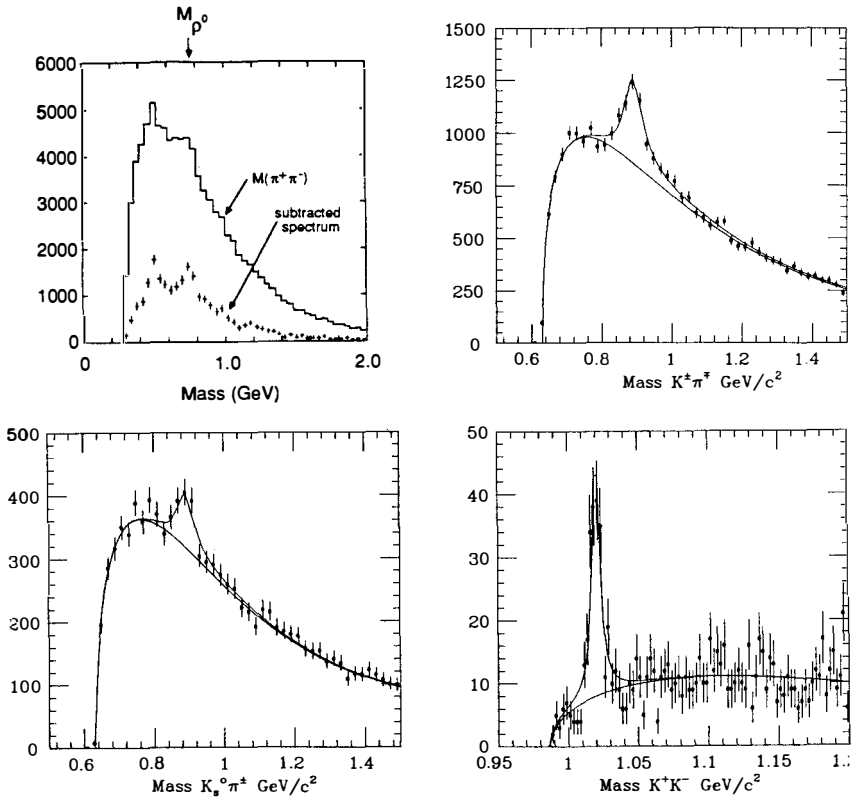

Figure 1: Mass spectra for $\rho^0 \to \pi^+\pi^-$, $K^{*0} \to K^\pm\pi^\mp$, $K^{*\pm} \to K^0_s\pi^\pm$, and $\phi \to K^+K^-$.

3. Bose-Einstein Correlations

We measure two-pion Bose-Einstein correlations using a correlation function defined as:

$$R(Q) = P(Q)/P_0(Q), \tag{1}$$

where $P(Q)$ is the probability distribution of like-sign pion pairs and $P_0(Q)$ is a similar reference distribution in which the correlations are absent. We choose two methods to determine appropriate reference distributions: One method uses unlike-signed pairs, which have the same correlations due to jet structure and energy conservation as like-sign pairs; the other uses event mixing by which tracks from two different events are combined to form a pair with the kinematic variables being determined from the momenta of the particles relative to the event axis in each event. Corrections for expected correlations, such as due to resonance production, and for detector acceptance effects are described in Ref.[3].

Here, we present the correlation function, $R(Q)$, using the unlike-sign and mixed-event reference distributions normalized with the correlation function obtained from Monte Carlo

simulations. To determine how well Bose-Einstein correlations can be described as depending only on Q, we form $R(Q)$ in bands of q_0 for each method as shown in Fig. 2. The correlation function is fit to the following function with 4 parameters,

$$R(Q) = A(1 + BQ)(1 + \alpha \exp[-(rQ)^2]), \tag{2}$$

where α is interpreted as the amount of enhancement at $Q = 0$, r as the effective size of the source of pions, and A,B describe a linear background term and an overall normalization. Fixing the background parameters, A and B, at values obtained in a separate fit to the data averaged over q_0, we plot our results for the remaining parameters as a function of q_0 in Fig. 3. We observe that a significant Bose-Einstein enhancement is obtained when Q is small even when the energy difference, q_0, is substantial. Thus providing evidence that the Bose-Einstein correlations are best described by models that account for the relativistic motion of the particle sources.

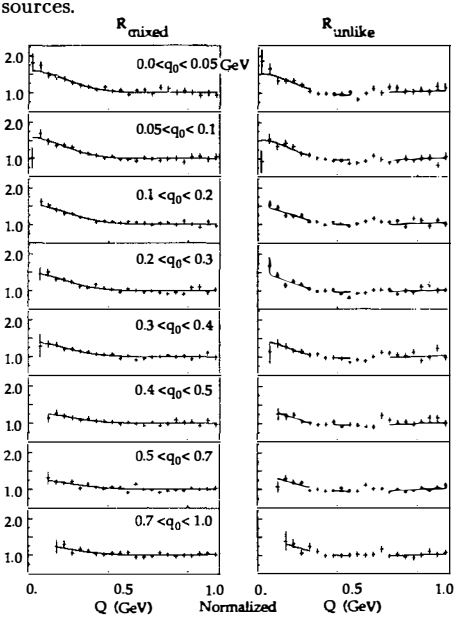

Figure 2: Correlation function vs Q with fit in bands of q_0.

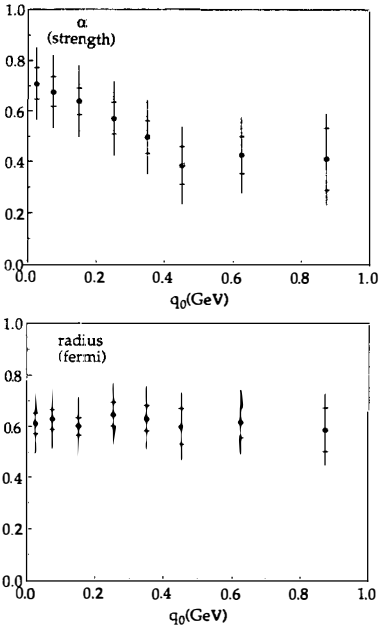

Figure 3: Weighted average of parameters from fits vs q_0 for different methods.

Three-pion correlations are observed using a simple generalization of the method used for two pions. The correlation function for triplets of identical particles is given by:

$$\begin{aligned} R_3(p_1, p_2, p_3) &= 1 + |\tilde{\rho}(q_{12})|^2 + |\tilde{\rho}(q_{23})|^2 + |\tilde{\rho}(q_{31})|^2 \\ &\quad + 2Re[\tilde{\rho}(q_{12})\tilde{\rho}(q_{23})\tilde{\rho}(q_{31})], \end{aligned} \tag{3}$$

where $\tilde{\rho}$ is the fourier transform of the source density and $q_{ij} := p_i - p_j$. The first three enhancement terms are just the correlations that must occur between pairs of pions in the triplet. The

last term is unique to triplets, and becomes small if any one particle in the triplet has a large momentum difference from the others.

In the three-pion analysis, only the event mixing technique is used to construct a reference sample, with the distribution obtained by mixing a pair of tracks from one event with a track from another event being used to measure the correlation between pairs of pions within a triplet. Subtracting the correlations due to the three pairs within the like-signed triplet distribution from one event, we form a triplet distribution that should only exhibit the "pure" triplet enhancement plus an uncorrelated background, and define the "pure" three-pion correlation function as,

$$R_3^{pure}(Q_3^2) = \frac{P^{pure}(Q_3^2)}{P^{+++}(Q_3^2)}. \tag{4}$$

where $P^{pure}(Q_3^2)$, $P^{+++}(Q_3^2)$ are the probability distribution of like-sign triplets and the triplet reference distribution, respectively, and $Q_3^2 = q_{12}^2 + q_{23}^2 + q_{31}^2$, as used by other groups[6], is a generalization of the two-particle variable Q^2.

The pure-triplet correlation function obtained in this way is shown in Fig. 4 for different normalizations: a) unnormalized, b) using a Monte Carlo correlation function, and c) normalized at large Q_3^2. Fitting the data in Fig. 4c to the form of Eq. 2, we obtain the following results: $\alpha_3 = 0.55 \pm 0.10 \pm 0.10$ and $r_3 = 0.77 \pm .09 \pm 0.10$ fermi, where the primary systematic uncertainty is in the correction for the effect that two-particle correlations have on the pure-three-pion correlations. The values for α_3 and r_3 are in agreement with the corresponding two-pion correlation parameters ($\alpha_2 = 0.62 \pm 0.03 \pm 0.13$, and $r_2 = 0.66 \pm 0.03 \pm 0.11$ fermi). Thus providing additional confidence that these correlations are really the result of Bose-Einstein interference.

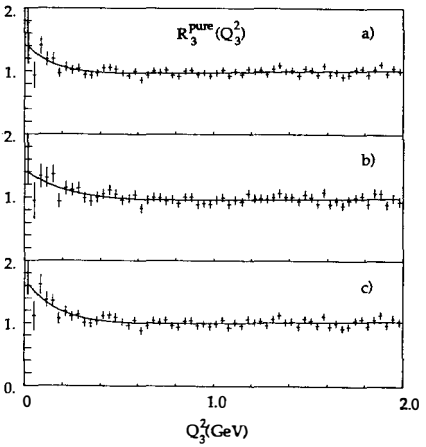

Figure 4: Pure 3 pion correlation function for different normalizations.

4. Inclusive Strange and Charmed Baryon Production

Our study of baryon production is based on approximately 26,000 hadronic events from our 1984-86 high-field sample. Our measurements of hyperon (Λ,Ξ^-,Ω,Ξ^{*0}) production, displayed in Figure 5, provide the first observation of the Ξ^{*0} in the higher energy fragmentation regime. We determine the following multiplicites per event: $N(\Lambda) = 0.211 \pm 0.009 \pm 0.014$, $N(\Xi^-) = 0.020 \pm 0.004 \pm 0.003$, $N(\Omega) = 0.0037 \pm 0.0018 \pm 0.0014$, and $N(\Xi^{*0}) = 0.0097 \pm 0.0039 \pm 0.0043$. Compared to the strange baryons, the Λ_C is a fairly difficult particle to search for. Applying dE/dx cuts which minimize the misidentification of pions as kaons or protons and restricting our search for Λ_C to $x_P > 0.5$, we obtain the signal for Λ_C production shown in Fig. 6. Using

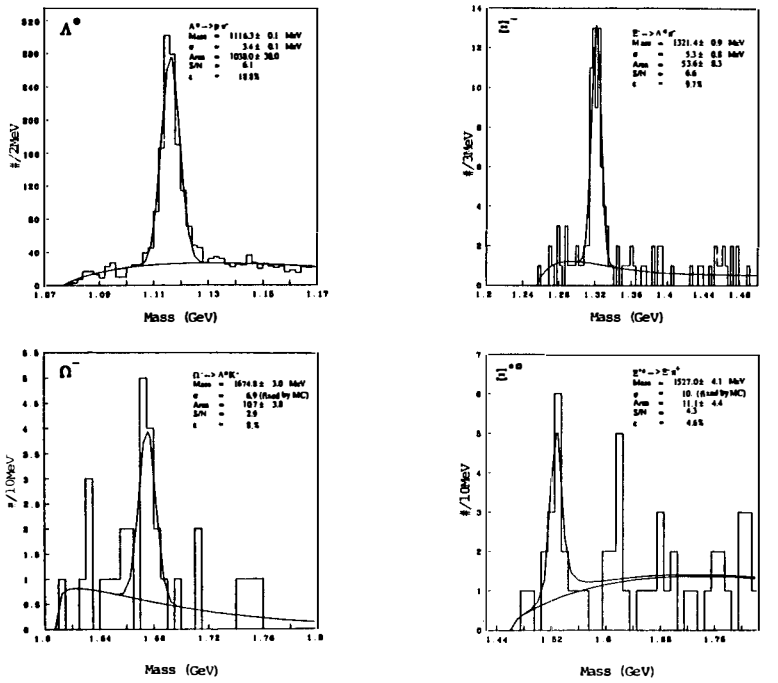

Figure 5: Mass spectra for $\Lambda^0 \to \pi^- p$, $\Xi^- \to \pi^- \Lambda^0$, $\Omega^- \to K^- \Lambda^0$, and $\Xi^{0*} \to \pi^+ \Xi^-$.

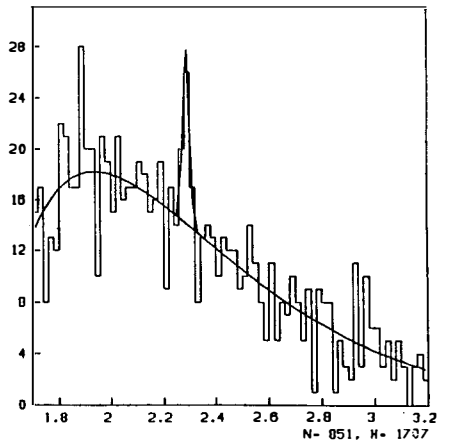

Figure 6: Reconstructed mass for $\Lambda_C \to pK^-\pi^+$.

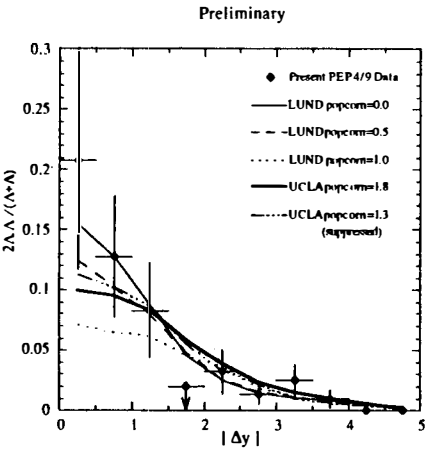

Figure 7: Rapidity separation between Λ and $\overline{\Lambda}$ compared with various predictions of the Lund[7] and UCLA[8] models.

the PDG value for the pKπ braching ratio, B.R. = 2.6±0.9%, we obtain the multiplicity for Λ_C production to be N(Λ_C) = 0.22±0.11, somewhat larger than predicted by hadronization models.

Measuring baryon correlations, we find (with a signal-to-noise ratio of 16:1) 55.4 ± 8.0 $\Lambda\overline{\Lambda}$ pairs, corresponding to 0.053 ± 0.007(stat.) ± 0.011(sys.) $\Lambda\overline{\Lambda}$ pairs per hadronic event after acceptance corrections. Models of baryon formation in the fragmentation process, such as "di-quark" and "popcorn" models, predict different baryon-antibaryon correlations. In Figure 7 we obtain a measure of the $\Lambda\overline{\Lambda}$ correlation length by plotting the distribution of $\Lambda\overline{\Lambda}$ as a function of the absolute value of the rapidity difference (| Δy|) between the Λ and $\overline{\Lambda}$. Predictions of the Lund model with popcorn fractions of 0, 0.5 and 1 (in solid, dashed and dotted lines, respectively), and the UCLA model with and without popcorn suppression (in dot-dashed and dark solid lines) are also shown. At this point, our preliminary data appears to disfavor the Lund model with 100% "popcorn" baryon production.

5. Conclusions

In terms of the final stage of hadronization, our measurements of vector meson production yield new results for: $\frac{s}{u}$ = 0.30 ± 0.03 and $\frac{V}{(V+PS)}$ = (45 ± 11)%. Our new precise measurements of strange and charmed baryon production are presently being compared to detailed Lund and UCLA model predictions.

As part of our systematic studies of correlations in the fragmentation process: We probe the space-time structure using Bose-Einstein interference effects and obtain consistent measurements of source size ~0.7f and strength ~0.6, in two- and three-pion correlations. The observation that these enhancements persist in two-pion correlations at large q_0 (~ 1 GeV) suggests a boosted source. Our measurements of strange baryon correlations provide sensitivity to physics in the fragmentation process at relatively high virtuality, Q ~ 3 GeV, and establish a test bed for models of baryon production in e^+e^- annihilation.

I would like to acknowledge my collegues on the TPC/2γ collaboration. I appreciated the warm, friendly atmosphere of "Moriond", especially during the time of world conflict, and thank the organizers for an enjoyable conference.

References

[1] T. K. Edberg, PhD thesis, University of California, Berkeley, 1988. LBL-25652.

[2] D. A. Crane, PhD thesis, Johns Hopkins University, 1988. JHU-HEP-88-1002.

[3] R. E. Avery, PhD thesis, University of California, Berkeley, 1989. LBL-26593.

[4] P. Avery et al. (CLEO Collaboration), Phys. Rev., **D32**, 2294 (1985).

[5] H. Aihara et al. (TPC/2γ Collaboration), Phys. Rev., **D31**, 996 (1985).

[6] M. Altoff et al. (TASSO Collaboration), Z. Phys., **C30**, 355 (1986).

[7] B. Andersson et al., Phys. Rep., **97**, 33 (1983).

[8] C.D. Buchanan and S.-B. Chun, UCLA-HEP-90-003 and references therein.

[9] H. Aihara et al., LBL-23737, Lawrence Berkeley Laboratory, 1988.

Inclusive Particle Spectra Measurements with the L3 Detector at LEP

Mourad Dhina
Institut für Hochenergiephysik
ETH-Zürich
CH-8093 Zürich, Switzerland

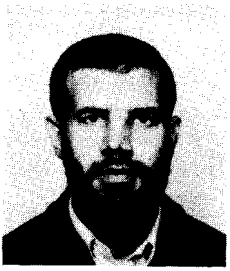

Abstract

I report on measurements of particle spectra using data from the L3 detector at LEP at $\sqrt{s} \sim M_Z$. Results from lower energy experiments are also considered, in order to study the center of mass energy dependence of the spectra. It is shown that the Modified Leading Logarithmic Approximation (MLLA) combined with the concept of Local Parton–Hadron Duality (LPHD) successfully describes the data over the whole center of mass energy range.

1 Introduction

Due to its quantum mechanical nature, QCD imposes on gluons to be emitted in an angular ordered region of phase space. This is a direct consequence of destructive interference in soft gluon emissions. A natural testing laboratory for this phenomenon is the study of the so-called small-x region, where $x = p/E_{beam}$.

The Modified Leading Logarithmic Approximation (MLLA) expression for the spectrum of small-x ($\zeta = ln(1/x) \gg 1$) relativistic particles can be written as [1]:

$$\frac{1}{\sigma}\frac{d\sigma}{d\zeta} = \frac{4N_c}{b}K(Y)\Gamma(B)\int_{\alpha_0-i\frac{\pi}{2}}^{\alpha_0+i\frac{\pi}{2}}\frac{d\tau}{\pi}e^{-B\alpha}\left[\frac{cosh\,\alpha + \left(\frac{2\zeta}{Y}-1\right)sinh\,\alpha}{\frac{4N_c}{b}Y\frac{\alpha}{sinh\,\alpha}}\right]^{B/2} I_B\left(\sqrt{D(\alpha,\zeta,Y)}\right) \tag{1}$$

where $a = 11N_c/3 + 2n_f/3/N_C^2$, $b = 11N_c/3 - 2n_f/3$, $B = a/b$, $Y = ln(\frac{\sqrt{s}}{2\Lambda_{eff}})$, $\alpha = \alpha_0 + i\tau$, and

$$D(\alpha,\zeta,Y) = \frac{16N_C}{b}Y\frac{\alpha}{\sinh\,\alpha}\left[\cosh\,\alpha + \left(\frac{2\zeta}{Y}-1\right)\sinh\,\alpha\right]$$

$N_c = 3$ is the number of colors and n_f the number of flavors. The following considerations should be taken into account for formula (1) :

- The factor $K(Y)$ embodies all fragmentation effects which are then reduced to an overall normalization factor, as suggested by the concept of Local Parton Hadron Duality (LPHD) [1].
- The number of quark flavors n_f has been set to 3 since only light quark flavors dominate quark production in the gluon cascade.
- Equation (1) is integrated numerically to fit the data. The integration variable α_0 is chosen as: $\tanh\,\alpha_0 = 1 - 2\zeta$.
- $K(Y)$ and Λ_{eff} are the only free parameters. They are extracted from a fit to the data. The scale parameter Λ_{eff} is not direcly connected to $\Lambda_{\overline{MS}}$.

In this report, I will first describe the measurement of particle production with the L3 detector. Finally, predictions from the MLLA+LPHD approach and Monte Carlo models are confronted to data from L3 and from lower energy experiments [7].

2 Particle Production Measurements

The successful operation of LEP in the year 1990 has enabled the L3 detector [8] to collect a total luminosity of 5.5 pb^{-1} in the energy range $88.2 \leq \sqrt{s} \leq 94.2$ GeV around the Z^0 peak. This represents approximately 115,000 hadronic events.

Charged tracks were reconstructed in the Time Expansion Chamber (vertex detector). Figure 1 shows the measured charged particle multiplicity. The distribution has been corrected for detector acceptance, resolution, reconstruction efficiency and photon radiation. The measured average multiplicity is $< n_{ch} >= 20.7 \pm 0.7$, where the error is dominated by

systematic uncertainties. This value agrees well with the predictions from the two Monte Carlo Carlo generators, JETSET [4] and HERWIG [5], respectively, $< n_{ch} >= 20.5$ and $< n_{ch} >= 20.8$. The parameters used in the generators are those obtained from a fit to the L3 data [6]. Figure 2 shows the energy evolution of the measured average charged particle multiplicity, from L3 and others experiments, compared to the prediction of QCD (MLLA) [3], it i.e.,

$$ln < n_{ch} > = a/\sqrt{\alpha_s(Q^2)} + b ln \alpha_s(Q^2) + \mathcal{O}(1)$$

where a and b are functions of the number of flavors. It is important to note that, due to gluon destructive interference, the factor a is reduced by a factor of $1/\sqrt{2}$.

Neutral particles were measured using photon pairs as reconstructed in the electromagnetic calorimeter. The excellent resolution of the BGO detector enables a clean extraction of π^0 and η signals from $\gamma\gamma$ invariant mass spectra, see figures 3 and 4.

3 Particle spectra

Figure 5 (a) and (b) show the x_p distributions for π^0 and charged particles respectively, compared to the predictions of JETSET 7.2 and HERWIG 4.2. The distributions are normalized to the total hadronic cross section. Whereas the x_p plot is obtained by a direct measurement of momenta for the charged tracks, it is obtained for π^0's by determining the particle yield, for each x_p intervall, from the $\gamma\gamma$ invariant mass spectra. The covered x_p regions are $0.002 < x_p < 0.1$ for charged particles and $0.0075 < x_p < 0.065$ for π^0's. The bin widths have been adjusted such that the migration between bins due to resolution was below $\sim 5\%$ for charged particles and $\sim 15\%$ for neutral pions.

One can also study the momentum distributions in terms of the ζ_p variable, figure 6. The two plots, (a) for π^0's and (b) for charged particles, show data from the L3 detector and from the lower energy experiments [7], compared to predictions of equation (1), which has been fitted to the L3 data in a range of $\sim \pm 1$ around the position ζ_p^* of the maximum. The only free parameters are Λ_{eff} and $K(Y)$. The obtained results are:

$$\begin{aligned} \Lambda_{eff} &= 220 \pm 3 \pm 20\, MeV, \quad K(Y) = 1.20 \pm 0.04 \quad \textit{for charged particles} \\ \Lambda_{eff} &= 115 \pm 32 \pm 20\, MeV, \quad K(Y) = 0.52 \pm 0.05 \quad \textit{for } \pi^0 \end{aligned} \tag{2}$$

The maxima ζ_p^* are then calculated from (1) using the above parameters. At the Z^0 peak, we obtain:

$$\begin{aligned} \zeta_p^* &= 3.71 \pm 0.01 \pm 0.05 \quad \textit{for charged particle} \\ \zeta_p^* &= 4.11 \pm 0.15 \pm 0.10 \quad \textit{for } \pi^0 \end{aligned} \tag{3}$$

In each case, the first error is the uncertainty corresponding to the combined statistical and systematic errors of the data points used in the fit. The second error is systematic and is estimated from a variation of the fit range. In figure 6, the MLLA predictions for lower center of mass energies are obtained from a fit to the corresponding data using the same value of Λ_{eff} as determined from the fit to the L3 data, with only $K(Y)$ as free parameter. One observes that:

- the position of the maximum ζ_p^* is shifted to higher values for increasing center of mass energy.

- the height of the maximum rises with increasing $\sqrt{s}$, reflecting the increase in multiplicity.
- the MLLA prediction, equation (1), provides a good description of the data around the peak position. The small deviations which start to appear for low x_p (ie. high ζ_p) are a natural manifestation of non-relativistic effects.
- since the charged particles are in fact a mixture of particles heavier than the π^0, Λ_{eff} for charged particles is expected to be higher than for π^0, as confirmed by the above results, equations (2) and (3). In the context of MLLA, this phenomenon can be simulated by cutting the development of the partonic shower by a cuttoff parameter $Q_0 = m_h$ (with the same Λ_{eff}), where m_h is the mass of the hadrons considered. It is therefore important to study the ζ_p for various identified hadron species.

The MLLA prediction for the evolution of the peak maximum ζ_p^* with $\sqrt{s}$ can be determined numerically from formula (1), once a value for Λ_{eff} has been fixed. It successfully describes the data, as can be seen from figures 7. In those figures, the Λ_{eff} used are the weighted mean values of the Λ_{eff} obtained for all π^0 and charged particle data. These are:

$$\begin{aligned} \Lambda_{eff} &= 160 \pm 15\ MeV, \qquad for\ \pi^0 \\ \Lambda_{eff} &= 240 \pm 15\ MeV, \qquad for\ charged\ particles \end{aligned} \tag{4}$$

The errors include uncertainties related to the choice of the fit range. An MLLA approximation for this peak evolution can be parametrized as:

$$\zeta_p^* = \frac{1}{2} ln\left(\frac{\sqrt{s}}{2\Lambda_{eff}}\right) + c_2\sqrt{ln\left(\frac{\sqrt{s}}{\Lambda_{eff}}\right)} + \mathcal{O}(1) \tag{5}$$

where $c_2 = B\sqrt{b/16/N_c}$ and B, b are defined in equation (1). This prediction, which depends on Λ_{eff} only and not on the normalization factor $K(Y)$, also provides a good description of the data.

4 Conclusions

Measurements of inclusive particle spectra at the Z^0 peak, and from lower energy experiments, strongly support the predictions of QCD calculations performed in the framework of MLLA. The concept of LPHD has further relegated the non-perturbative fragmentation effects to an overall, $\sqrt{s}$ dependent, normalization factor. From this study, one can make the following conclusions:

- The charged particle multiplicity is rising with $\sqrt{s}$, whereby establishing that subleading QCD corrections are important and cannot be accounted for by fragmentation effects only. Fixed order (2^{nd}) QCD fails to predict the multiplicity distribution at large center of mass energies, whereas parton shower (LLA) calculations do reproduce it. The energy evolution of the average charged particle multiplicity shows that coherence effects are important.

- the existence of a peak, ζ_p^*, in the ζ_p distribution is one of the manifestations of color coherence.
- the ζ_p distributions exhibit a shift of the maximum to higher values and a rise in the overall normalization, with increasing $\sqrt{s}$. This evolution is adequately described by the MLLA + LPHD approach.
- in order to study in more detail the evolution of the parton cascade in MLLA, there is a need to investigate the ζ_p distribution for different identified hadron species. Already, some interesting conclusions have been reached by the measurement of π^0's with the L3 detector at the Z^0 peak.

5 Acknowledgements

I would like to thank my colleagues from the L3 experiment for useful discussions, as well as the Moriond conference organizers for providing an adequate environment.

References

[1] Y.L. Dokshitzer and S.I. Troyan, Leningrad Preprint LNPI-922 (1984).
Y.I. Azimov *et al.*, Z. Phys. **C27** (1985) 65.
Y.I. Azimov *et al.*, Z. Phys. **C31** (1986) 213.
V.A. Khoze, Y.L. Dokshitzer and S.I. Troyan, Lund Preprint LU-TP 90-12.

[2] A.H. Mueller, Phys. Lett. **B104** (1981) 161.
A. Bassetto *et al.*, Nucl. Phys. **B207** (1982) 189.
B.I. Ermolaev and V.S. Fadin, JETP Lett. **33** (1981) 285.
Y.L. Dokshitzer, V.S. Fadin and V.A. Khoze, Phys. Lett. **B115** (1982) 242.

[3] Z. Kunszt *et al* "Z Physics at LEP 1", eds. G. Altarelli *et al.*, CERN Report CERN-89-08, Vol. 1 (1989) 373.

[4] T. Sjöstrand and M. Bengtsson, Comput. Phys. Commun. **43** (1987) 367;
T. Sjöstrand, "Z Physics at LEP 1", eds. G. Altarelli *et al.*, CERN Report CERN-89-08, Vol. 3 (1989) 143.

[5] G. Marchesini and B. Webber, Nucl. Phys. **B310** (1988) 461.

[6] L3 Collaboration, B. Adeva *et al.*, Phys. Lett. **B257** (1991) 469.

[7] Crystall Ball Collaboration, C. Bieler *et al.*, Z. Phys. **C49** (1991) 225.
Jade Collaboration, W. Bartel *et al.*, Z. Phys. **C20** (1983) 187.
Jade Collaboration, W. Bartel *et al.*, Z. Phys. **C28** (1985) 343.
Jade Collaboration, W. Bartel *et al.*, Z. Phys. **C46** (1990) 1.
Tasso Collaboration, W. Braunschweig *et al.*, Z. Phys. **C33** (1986) 13.
Tasso Collaboration, W. Braunschweig *et al.*, Z. Phys. **C42** (1989) 189.
Tasso Collaboration, W. Braunschweig *et al.*, Z. Phys. **C47** (1990) 187.

[8] L3 Collaboration, B. Adeva *et al.*, Nucl. Instr. and Meth. **A289** (1990) 35.

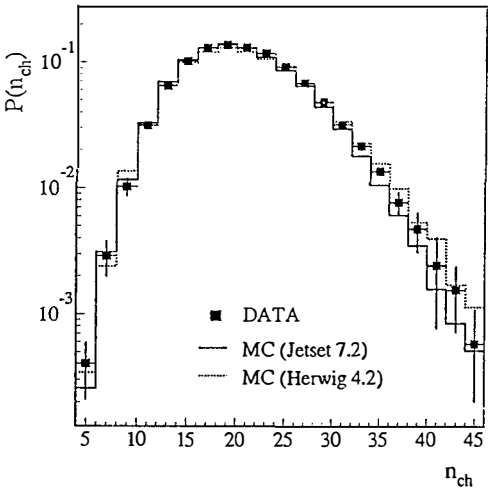

Fig. 1 Measured Charged Particle Multiplicity compared to predictions from the monte carlo programs JETSET and HERWIG. The vertical error bars include statistical and systematic uncertainties.

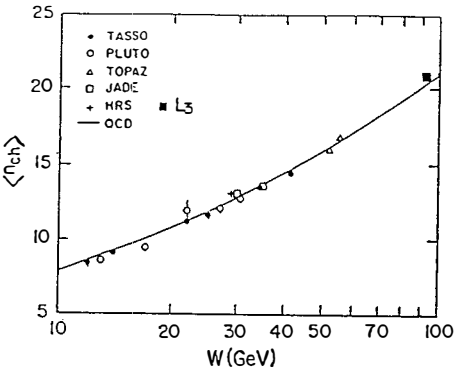

Fig. 2 Evolution of the measured average Charged Particle Multiplicity compared to the MLLA QCD prediction.

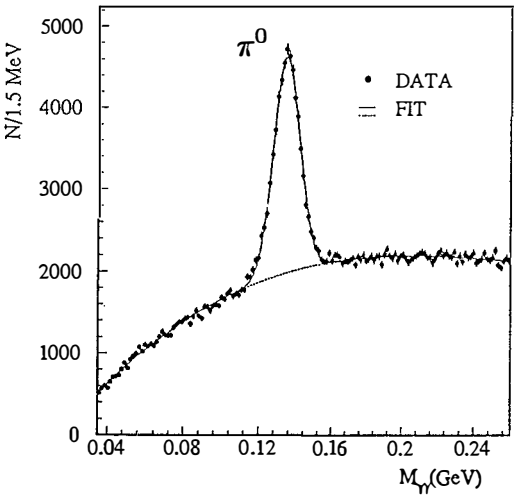

Fig. 3 π^0 signal from invariant mass distribution of photon pairs. The solid line is the sum of a gaussian and third order polynomial fit to the data. The dashed line indicates the background.

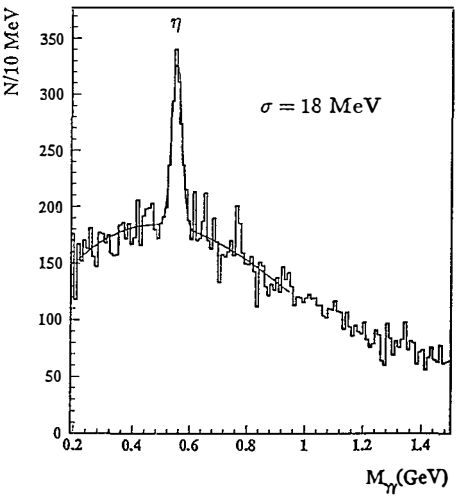

Fig. 4 η signal from invariant mass distribution of photon pairs. The solid line is the sum of a gaussian and third order polynomial fit to the data. The dashed line indicates the background.

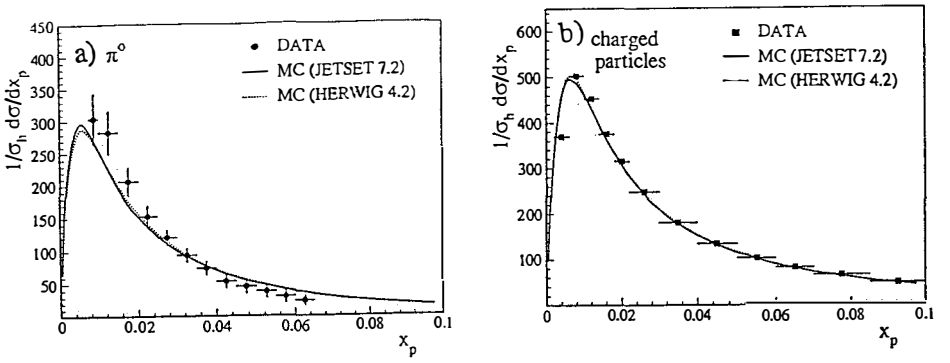

Fig. 5 x_p spectra for (a) neutral pions and (b) charged particles compared to shower monte carlo predictions. The plots are normalized to the total hadronic cross section. The vertical bars show the combiined statistical and systematic errors.

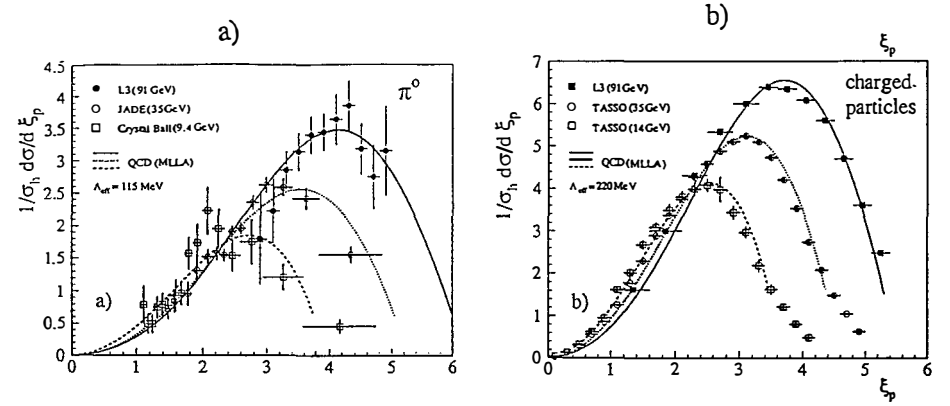

Fig. 6 ζ_p spectra for (a) neutral pions and (b) charged particles compared to QCD MLLA predictions. The data for lower energies are from the Crystal Ball, JADE and TASSO collaborations. The value of Λ_{eff} is the one obtained from a fit to the L3 data.

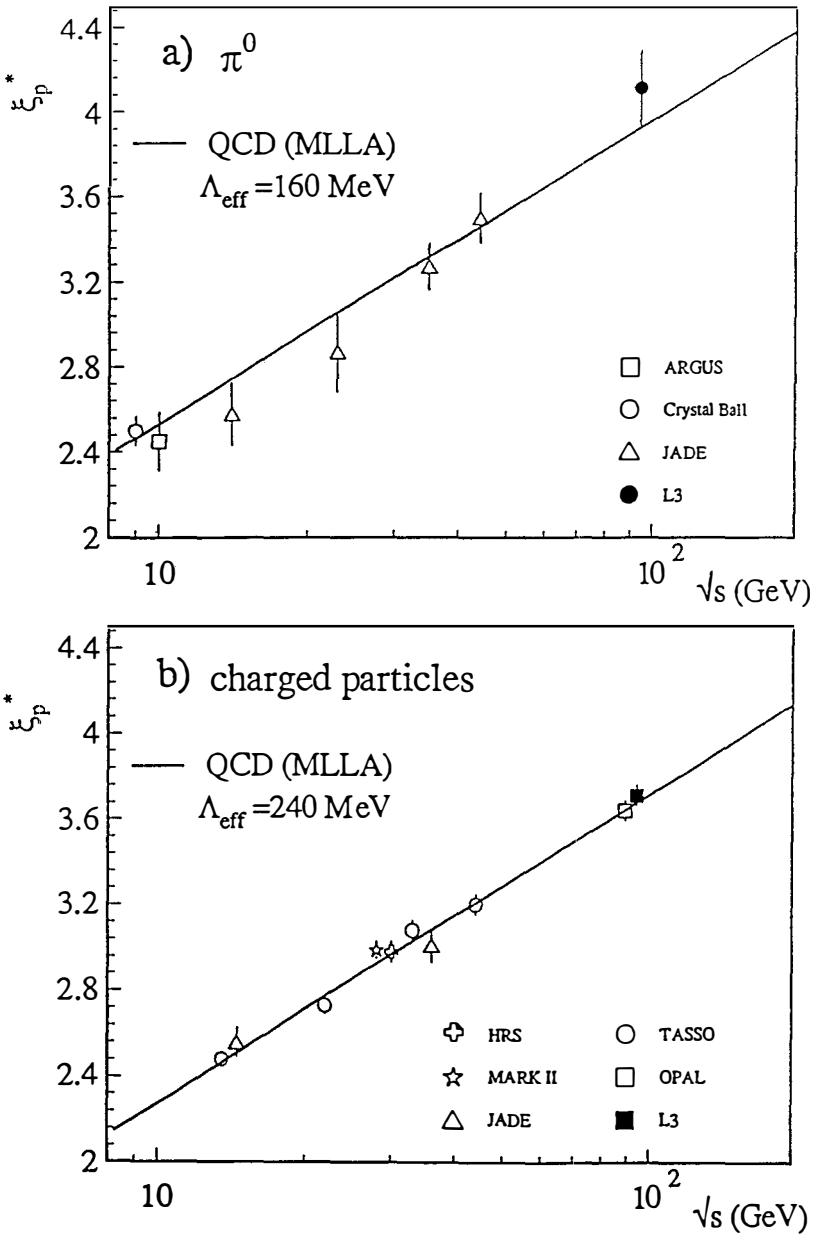

Fig. 7 Evolution of the position of the maximum of the ζ_p distributions for (a) neutral pions and (b) charged particles. The line is the prediction of MLLA with Λ_{eff} as fitted from the L3 data. The errors shown include systematic and statistical effects.

$Z^0 \rightarrow$ HADRONS
NEW RESULTS FROM **OPAL**

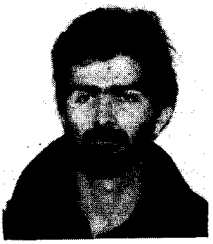

Neil Geddes
Rutherford Appleton Laboratory
Chilton
Oxon.
England

representing
The OPAL Collaboration

Abstract

Results of recent studies of intermittency and quark and gluon jet fragmentation in hadronic decays of the Z^0 are presented. A factorial moment analysis of rapidity distributions shows that intermittency in the hadronic decays of the Z^0 is well reproduced by QCD based fragmentation models. Lepton tagging in 3-jet events has been used to distinguish between quark and gluon jets. This technique has been used to provide a model independent observation of the so called string effect. Also, evidence for differences in the fragmentation of quarks and gluons is presented.

1 The Data Sample

The OPAL detector has been described in detail elsewhere[1]. The main features of the detector are a large volume central tracking chamber, an electromagnetic calorimeter, a hadron calorimeter and muon detection chambers. The detector has a high efficiency for detection of Z^0 multihadronic decays [2], and for isolation of high momentum muons and electrons within these events[3][4].

The analyses presented in this paper are based on 140,000 multihadronic events recorded during the 1990 LEP run. To reduce non-hadronic backgrounds events were selected for analysis if they contained at least 5 charged tracks associated with the interaction vertex, and were well contained within the detector (assessed via restrictions on visible energy balance and event axis orientation)[4][5].

2 Intermittency

Intermittency refers to the existence anomalous fluctuations in phase space distributions of hadronic events, in particular the existence of "self-similar" fluctuations, which may hint at a fractal structure in hadronic final states[6]. Assessing the statistical significance of rare or anomalous fluctuations is a difficult problem, however, a quantitative measure is provided by the method of *factorial moments* as proposed by Bialas and Peschanski[7]. This technique is normally applied to the experimental rapidity distribution as follows. The central rapidity plateau Y is divided into M bins of size $\delta y = Y/M$. If the number of particles in the m^{th} bin is n_m then the factorial moment of order j is given by:

$$F_j(M) = \frac{1}{\langle \bar{n}_m \rangle^j} \langle \frac{1}{M} \sum_{m=1}^{M} n_m(n_m - 1)...(n_m - j + 1) \rangle$$

$$\bar{n}_m = \frac{1}{M} \sum_{m=1}^{M} n_m$$

where the angle bracket indicates an average over all events. With this definition it is trivial to extend the calculation to other distributions such as the two dimensional rapidity vs azimuth (azimuthal angle around the reference axis) distribution. In this case the distribution is split into $\sqrt{M}$ rapidity $\times$ $\sqrt{M}$ azimuthal bins and the moments calculated according to the definition given above.

Factorial moments of order 2 to 5 have been determined from the OPAL multihadronic Z^0 decay sample. The analysis is restricted to charged particles in the range $-2 < y < 2$ (y is defined with respect to the sphericity axis and all particles are assumed to be pions). The excellent momentum resolution and two particle separation provided by the OPAL detector allow us to measure the factorial moments with rapidity bin size down to 0.01 units. The measured moments for both the rapidity and rapidity versus azimuthal angle are shown in Fig. 1 compared with the predictions of the HERWIG[8] and JETSET[9] (using both parton shower and ERT[10] matrix element formalism) Monte Carlo programs. There is good agreement between all three models and the data[5]. Detailed investigations of the source of the observed signals in the Monte carlo programs reveals that the major source is the jet structure of the events and the presence of 3 and 4 jet events.

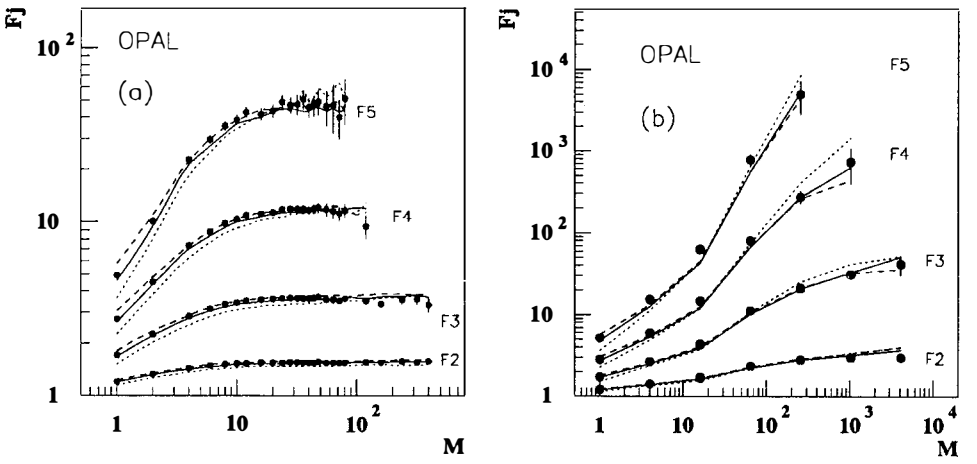

Figure 1: The corrected 2^{nd} to 5^{th} factorial moments , F_j (solid circles) versus number of bins, M for the rapidity (a) and rapidity vs azimuth (b) distributions compared with the predictions of the JETSET v7.2 parton shower (solid line), HERWIG v4.3, (dashed line) and JETSET/ERT matrix element (dotted line) Monte Carlo programs.

3 Tagging Quark and Gluon Jets.

The semi-leptonic decays of charm and bottom quarks can be used to separate quark and gluon jets in 3-jet events[4]. The principle known sources of high momentum leptons in hadronic electron-positron annihilation events are the weak decays of charm and bottom quarks. Furthermore these heavy quarks are produced almost exclusively at the electroweak vertex rather than during the subsequent fragmentation stage. Thus gluons jets will only rarely contain high momentum leptons and the observation of the latter may thus be used to tag quark (or anti-quark, no distinction is made here) jets.

To select a sample of 3-jet events the "JADE" jet finding algorithm was applied to the multihadronic event sample (the "P-scheme" recombination method was used with a resolution parameter $y_{cut} = 0.03$). All events where exactly 3 jets are reconstructed are retained. The following quality cuts are applied to ensure well reconstructed jets:

- The sum of the angles between the jets must be greater than 358°.
- Each jet must contain at least 3 charged tracks and have a measured energy of at least 5GeV.
- The measured jet energies must be consistent with those calculated from the relative jet angles.

Semi-leptonic decays are further selected by requiring that either;

- Two of the jets contain a high momentum muon ($p > 3$GeV) or electron ($p > 2$GeV). These jets are then "tagged" as the quark/anti-quark jets and the third jet is assumed to be the gluon jet.

or

- One jet, which must not be the highest energy jet (assumed to be the non-radiating quark/anti-quark), contains a high momentum muon or electron. The highest energy jet and the jet containing the lepton are then tagged as the quark/anti-quark jets.

These two samples are combined to provide a set of 3 jet events where the source of each jet (quark or gluon) is known with high probability. Monte Carlo estimates using the JET-SET program give the probabilities that the jets are correctly labelled as; 96%, 88% and 84% respectively for the highest and lowest energy quark jets and the gluon jets.

To permit direct comparisons of the quark and gluon jets and the regions between them, a set of "symmetric" events is selected where the angles between the highest and lowest energy quark jets and between the highest energy quark jet and the gluon jet are both $150° \pm 10°$. This gives a sample of events where the lowest energy quark and gluon jets have essentially equal energies and event environments. This final sample contains 188 events.

4 String Effect

The so called string effect refers to an asymmetry in the particle populations for regions between quark and antiquark and between (anti)quark and gluon jets in 3-jet events[4]. This effect arises naturally in models which explicitly contain "strings", such as the Lund model[9], where the particles produced along the string are naturally boosted towards the gluon. The effect may also arise, however, as a result of interference terms in soft gluon radiation or as a result of dynamical differences between quark and gluon jet fragmentation. Here "string effect" is used to indicate the experimental observation of an asymmetry with no interpretation implied.

The "particle flow", $(1/N)dn/d\psi$, is shown in figure 2 for the symmetric tagged 3-jet sample described above. Here ψ is the angle in the event plane between a particle and the highest energy quark jet, N is the total number of events and dn is the number of particles in a bin of width $d\psi$. The event plane is defined by the two eigenvectors of the sphericity tensor associated with the two largest eigenvalues. The points in figure 2 show the particle flow starting at the higher energy quark axis then proceeding through the lower energy quark jet ($\phi \simeq 150°$) to the gluon jet ($\phi \simeq 210°$) and back to the higher energy quark jet. The histogram shows the particle flow for the same data, again starting at the higher energy quark axis, but proceeding in theoppositee sense: first through the gluon jet ($\phi \simeq 150°$) then through the lower energy quark jet. ($\phi \simeq 210°$). Thus the points for $0° < \psi < 180°$ are the same as the histogram curve for $360° < \psi < 180°$ and vice versa. The data are all shown for the detector level, no corrections have been applied.

A significantly larger population of particles is present in the region between the gluon and higher energy quark jets than in the region between the two quark jets, as is expected for the string effect. The effect of biases due to the event selection criteria have been evaluated and are not found to account for the observed asymmetry. Consistent results are also obtained for other

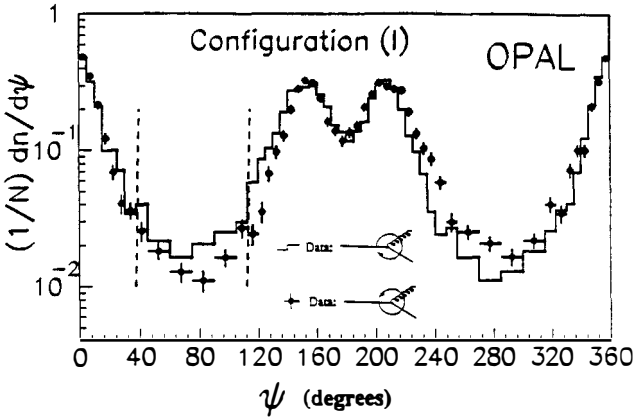

Figure 2: The particle flow distribution, $(1/N)dn/d\psi$. No corrections have been applied to the data. The points with errors show the flow from high energy quark jet to the low energy quark jet then to the gluon jet; the histogram shows the measured particle flow for the same events, again starting at the highest energy quark jet but then proceeding in the opposite sense

samples of 3-jet events[4], eg. selected with quark–antiquark and quark–gluon jet separations of 130° rather than 150°. independent, event samples

5 Quark and Gluon Fragmentation

Using the symmetric quark–gluon jet events selected above, it is possible to compare directly the properties of gluon jets and quark jets of similar energies embedded in similar environments. the event plane excluded from the string effect studies. Figure 3 shows the ratio of the particle flow for gluon jets to that for the quark jets in the region around the jet axis. Although the multiplicity of the quark and gluon jets is similar in the central region around the jet axis, the gluon jets clearly have more particles in the wings than the quark jets. Also shown in Figure 3 is the differential energy spectrum for particles in the cores of quark and gluon jets, defined as the region $135° < \psi < 165°$. The quark jet spectrum clearly is clearly harder, implying that particles in the cores of quark jets tend to be more energetic than those in gluon jets.

6 Summary

Intermittency in Z^0 hadronic final states is well reproduced by QCD based Monte Carlo programs. The major source of observed signals appears to be the jet structure of the events.

A definite asymmetry exists between the particle populations of the regions between quark and antiquark and between (anti)quark and gluon jets in 3-jet events. Also, in the jet regions themselves, gluon jets are observed to be softer and wider than quark jets.

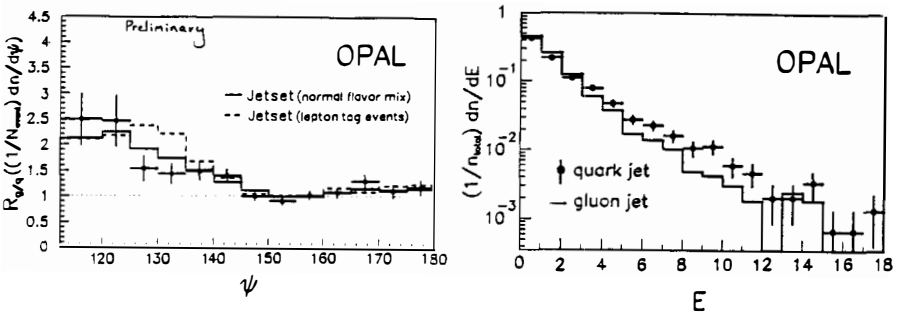

Figure 3: (a). The ratio of $(1/N_{evt})dn/d\psi$ in for gluon jets to that for quark jets in the region around the jet peak. (b). The inclusive energy spectrum $(1/n_{total})dn/dE$ of particles in the jet core regions ($135° < \psi < 165°$).

References

[1] K. Ahmet *et al.* (OPAL), CERN-PPE/90-114
(submitted to Nucl. Instr. and Meth.)

[2] M. Arignon *et al.* (OPAL), CERN-PPE/91-32
(submitted to Nucl. Instr. and Meth.)

[3] M. Akrawy *et al* (OPAL), CERN-PPE/91-48
(submitted to Phys. Lett. B)

[4] M. Akrawy *et al.* (OPAL), CERN-PPE/91-31
(to be published in Phys. Lett. B)

[5] M. Akrawy *et al.* (OPAL), CERN-PPE/91-37
(to be published in Phys. Lett. B)

[6] For recent reviews see, for example,
L. van Hove, Mod. Phys. Lett. A4 (1989) 1867.
B. Buschbeck and P. Lipa, Mod. Phys. Lett. A4 (1989) 1871.
R.Peschanski, CERN-TH5891/90, To be published in J. Mod. Phys.

[7] A. Bialas and R. Peschanski, Nucl. Phys. B273 (1986) 703.
A. Bialas and R. Peschanski, Phys. Lett. B207 (1988) 59.
A. Bialas and R. Peschanski, Nucl. Phys. B308 (1988) 857.

[8] G. Marchesini and B. Webber, Nucl. Phys. B310 (1988) 461.
G. Marchesini and B. Webber, Cavendish-HEP-88/7.

[9] T. Sjöstrand, Comp. Phys. Comm. 39 (1986) 347.
M. Bengtsson and T. Sjöstrand, Comp. Phys. Comm. 43 (1987) 367.
M. Bengtsson and T. Sjöstrand, Nucl. Phys. B289 (1987) 810.

[10] R. K. Ellis, D. A. Ross, A. E. Terrano, Nucl. Phys. B178 (1981) 421.

HADRONIZATION OF QCD

D.Ebert[1]

Joint Institute for Nuclear Research,

Head Post Office, P.O. Box 79,

Moscow, 101000, U.S.S.R.

Abstract

This talk is meant to give an introduction into the main ideas of hadronization of QCD without almost any formalism. As it turns out, QCD bound states, constituent quark masses and spontaneous chiral symmetry breaking may now be understood within a coherent framework.

[1]On leave of absence from Fachbereich Physik, Humboldt-Universität, Berlin

Introduction

Quantum chromodynamics (QCD), the nonabelian gauge theory of coloured quarks and gluons with gauge group $SU(3_c)$, is well known to be a successful theory in the description of high-energy interactions of hadrons. The QCD Lagrangian with three light quarks $q^i \equiv \begin{pmatrix} u^i \\ d^i \\ s^i \end{pmatrix}$ (i=1,2,3 - colour index) is defined by

$$\mathcal{L}_{QCD}(q, G_\mu) = -\frac{1}{4}\sum_{a=1}^{8} G^a_{\mu\nu} G^{a\mu\nu} + \bar{q}(i\gamma^\mu \partial_\mu - \hat{m}_0)q - g_s \sum_{a=1}^{8} \bar{q}\gamma^\mu \frac{\lambda^a}{2} q G^a_\mu. \quad (1)$$

Here G^a_μ is the gluon field, $G^a_{\mu\nu}$ is the gluon field strength tensor

$$G^a_{\mu\nu} = \partial_\mu G^a_\nu - \partial_\nu G^a_\mu - g_s f_{abc} G^b_\mu G^c_\nu, \quad (2)$$

with g_s the colour coupling constant ($\alpha_s = g_s^2/4\pi$), and $\hat{m}_0$ is the matrix of current quark masses. Notice the remarkable fact that QCD is asymptotically free, i.e. in the short distance ($r \ll 1\ fm$), large momentum transfer region ($Q \gg 1\ GeV$) the running coupling between quarks, $g_s(Q) = 4\pi(b \ln Q^2/\Lambda^2)^{-1/2}$, becomes weak. As a consequence, perturbation theory can be employed in close conceptual analogy to quantum electrodynamics (QED), the abelian gauge theory of electrons and photons with gauge group $U(1)$ (compare Table 1). On the other hand, at low energies the running coupling between quarks becomes strong and thus perturbation theory does not work. It is conjectured that this property of QCD would explain why quarks and gluons are not observed but bound inside colour-singlet $\bar{q}q$ meson or qqq nucleon states. Thus, the calculation of low energy hadron observables from QCD always involves the dynamics of bound states which are intrinsically nonperturbative and thus very complicated.

Among the most important aspects of low-energy hadron physics is the concept of chiral symmetry $SU(3)_L \times SU(3)_R$ and its spontaneous breakdown signalled by nonvanishing quark and gluon condensates $< \bar{q}q >$, $< G^a_{\mu\nu} G^a_{\mu\nu} >$. This mechanism is believed to be responsible for the transition of current quarks into constituent quarks as well as for the emergence of the $SU(3)$-

Table 1: Conceptual similarities between QED and QCD.

QED	QCD
electron field: $e(x)$	quark field: $q^{\alpha i}(x)$
	($i-$ colour, $\alpha-$ flavour)
local charge conservation: $U(1)$	local colour conservation: $SU(3_c)$
Lagrangian: $\mathcal{L}_{QED}(e, A_\mu)$	Lagrangian: $\mathcal{L}_{QCD}(q, G^a_\mu)$
photon A_μ	gluons $G^a_\mu (a = 1, \ldots 8)$
$\Downarrow$	$\Downarrow$
atoms	hadrons
molecules	nucleus

nonet of pseudoscalar mesons as Goldstone bosons. Thus, if QCD is the correct theory for the low-energy dynamics of the light hadrons, it must follow the scenario that the $SU(3)_L \times SU(3)_R$ chiral symmetry is broken down to the $SU(3)_V$ symmetry spontaneously. It has been a challenge for the theorists to construct an effective low-energy theory of hadrons that realizes these symmetry properties and reflects the underlying composite structure of the $q\bar{q}$-states (Table 2).

Hadronization and Effective Chiral Lagrangians (ECL)

To describe low-energy strong interaction processes and properties of hadrons it is necessary to use nonperturbative calculational schemes. The most popular ones among them are:

- the method of QCD sum rules [1],
- QCD lattice calculations [2],
- the functional integral approach to effective chiral Lagrangians [3], [4].

This talk is devoted to the ECL-method. There has recently been significant progress in the development of this approach in which one derives the low-energy effective Lagrangian for hadrons either directly from QCD [5] or from some simpler QCD-motivated Nambu-Jona-Lasinio quark models [6]

Table 2: Characteristics of perturbative and nonperturbative QCD.

Perturbative QCD ($\alpha_s \ll 1, Q \gg 1GeV$)	Nonperturbative QCD ($\alpha_s \sim 1$, $Q \lesssim 1GeV$)
Hard (deep inelastic) processes	Soft processes
Simple ground state (vacuum $\|0>$)	Complex ground state (vacuum $\|\tilde{0}>$)
Asymptotic freedom & conceptual similarity with QED	Spontaneous breakdown of chiral symmetry ($<\bar{q}q>\neq 0$, $<G^a_{\mu\nu}G^a_{\mu\nu}>\neq 0$)
	Confinement ?
Microscopic fields: quarks & gluons	Composite fields: hadrons (pion as Goldstone boson)

by using functional integration techniques. That is, in the generating functional of quark Green's functions of QCD one performs a change of variables from quark and gluon fields to the observable hadron fields. In this way, QCD bound states, constituent quark masses and spontaneous chiral symmetry breaking may be understood within a coherent framework. Let us discuss this in some more detail by starting with the generating QCD functional. The idea of hadronization is then summarized by the following relation

$$\int DqD\bar{q}DG_\mu \exp i \int d^4x[\mathcal{L}_{QCD}(q, G_\mu) + sources]$$
$$\approx \int D\sigma D\pi D\rho Da_1 DNDN \exp i \int d^4x[\mathcal{L}_{eff}(\sigma, \pi, \rho, a_1, N) + sources] \quad (3)$$

or

$$\mathcal{L}_{QCD}(q, G_\mu) \Longrightarrow \mathcal{L}_{eff}(\sigma, \pi, \rho, a_1, N). \quad (4)$$

Here σ, π, ρ, a_1 denote the four $SU(3)$-nonets of mesons with J^P=$0^+, 0^-, 1^-$ and 1^+, and N is the nucleon field. The proof of the above equivalence is a highly nontrivial task. For practical reasons, it requires to consider the limit of large numbers of colours N_c and to use an expansion in field derivatives

which is valid for low energies. Note that the masses and coupling constants of the composite mesons in $\mathcal{L}_{eff}$ are then expressed in terms of QCD parameters only: quark (gluon) condensates, current quark masses and numbers of colours.

For illustrations, let us quote the nonlinear meson Lagrangian including higher-order derivative terms. In the following we restrict ourselves to the sector of pseudoscalar mesons and consider the case of exact $SU(3)$ flavour symmetry ($\hat{m}_0 = m_0$ 1). The effective chiral meson Lagrangian $L_{eff}(\bar{\pi})$ is conveniently represented in terms of the chiral field U and $\mathcal{L}_\mu = (\partial_\mu U)U^+$,

$$U = \exp i\frac{2\bar{\pi}}{F}, \quad \bar{\pi} = \frac{1}{2}\sum_{a=0}^{8}\pi_a\frac{\lambda_F^a}{2}, \tag{5}$$

where π_a is the $SU(3)$-nonet of 0^--fields and $F = 93.3\,MeV$ is the pion decay constant. We have [6]

$$L_{eff}(\bar{\pi}) = L^{(2)}(\bar{\pi}) + L^{(4)}(\bar{\pi}) + L_{WZ}(\bar{\pi}) + L_{SB}(\bar{\pi}). \tag{6}$$

Here

$$L^{(2)}(\bar{\pi}) = \frac{F^2}{4}tr\partial_\mu U\partial^\mu U^+ \equiv -\frac{F^2}{4}trL_\mu L^\mu \tag{7a}$$

is the standard kinetic part of the chiral meson Lagrangian containing only second-order derivatives. The Lagrangian

$$L^{(4)}(\bar{\pi}) = \frac{N_c}{32\pi^2}tr\left\{\frac{1}{12}[L_\mu, L_\nu][L^\mu, L^\nu] - \frac{1}{3}(\partial_\mu L^\mu)^2 + \frac{1}{6}(L_\mu L^\mu)^2\right\} \tag{7b}$$

contains new interactions of fourth order in derivatives. In particular, the first term in the curly bracket is recognized as the well-known Skyrme Lagrangian, but now with a fixed coupling constant $e^2 = 12\pi^2/N_c$. Moreover,

$$\int d^4x L_{WZ}(\bar{\pi}) = \frac{iN_c}{240\pi^2}\int_B d^5x\epsilon^{\mu\nu k\lambda\rho}tr(L_\mu L_\nu L_k L_\lambda L_\rho)$$

$$= \frac{-2N_c}{15\pi^2F^5}\int d^4x\epsilon^{\mu\nu k\lambda}tr(\bar{\pi}\partial_\mu\bar{\pi}\partial_\nu\bar{\pi}\partial_k\bar{\pi}\partial_\lambda\bar{\pi}) + O(\bar{\pi}^7) \tag{7c}$$

is the famous anomalous Wess-Zumino term. Finally, $L_{SB}(\bar{\pi})$ is a term describing explicit breaking of chiral symmetry,

$$L_{SB}(\bar{\pi}) = \frac{F^2}{4}m_\pi^2 tr(U + U^+ - 2) \approx -\frac{m_\pi^2}{2}\pi_a^2 + O(\bar{\pi}^4). \tag{7d}$$

Note that in the limit $m_0 \to 0$

$$m_\pi^2 = -\frac{2m_0 < \bar{q}q >}{F^2} \longrightarrow 0, \tag{8}$$

i.e. the pion becomes a massless Goldstone boson. For the complete Lagrangian with $0^+, 0^-, 1^-$ and 1^+ mesons the reader is referred to [3]where a variety of other results as well as of phenomenological applications can be found. Let us quote among them the following ones: i) Weinberg relation $m_{a_1} = \sqrt{2} m_\rho$, ii) KSFR relation $m_\rho^2 = 2 g_{\rho\pi\pi} F^2$, iii) vector-axialvector dominance of electro-weak currents, iv) Goldberger-Treiman relation and v) predictions for CP-violation asymmetries in $K \to 3\pi$ decays. In conclusion, we mention the recent interesting approaches towards the baryon as a diquark-quark bound state [7].

References

[1] M.A.Shifman, A.I.Vainshtein, V.I.Zakharov, Nucl. Phys. B147(1979)385.

[2] See e.g. G.Martinelli, Nucl. Phys. B(Proc. Suppl.) 10A(1989)146.

[3] D.Ebert, H.Reinhardt, V.N.Pervushin, Sov. J. Part. Nucl. 10(1979)444; D.Ebert, A.N.Ivanov, M.K.Volkov, Fortschr. Phys. 37(1989)487; A.A.Bel'kov, D.Ebert, V.N.Pervushin, Sov. J. Part. Nucl. 22(1991)5 and references therein.

[4] H.Kleinert, in: Understanding the Fundamental Constituents of Matter (Erice Lectures 1978), ed. A.Zichichi (Plenum, New York, 1981).

[5] J.Praschifka, R.T.Cahill, C.D.Roberts, International Journal of Modern Physics A, vol. 4, No.18 (1989)4929.

[6] D.Ebert, H.Reinhardt, Nucl. Phys. B271(1986)188; Phys. Lett. B173(1986)453.

[7] R.T.Cahill, C.D.Roberts, J.Praschifka, Aust. J. Phys. 42(1989)129.

Transverse Jets in Diffractive Excitation

G. Gustafson

Dept. of Theoretical Physics
Lund University
Sölvegatan 14 a
S-223 62 LUND
Sweden

Abstract

The particle production from a diffractively excited proton is similar to that in DIS. A model is proposed in which transverse jets are obtained from gluon bremsstrahlung in a way similar to the emission in DIS. Good agreement is obtained with data from the UA8 collaboration. The model can be tested in an experiment with a larger acceptance than that of the UA8 detector.

1. Introduction

It is well known that in diffractive excitation in hadron–hadron collisions the excited hadron fragments essentially along the beam direction, with limited transverse momenta relative to this axis.

It seems as if the momentum transfer pulls out a quark (or an antiquark) from the initial hadron, stretching a colour field between this quark and the hadron remnant. If the excited hadron is a pion, the result is similar to a $q\bar{q}$ system in e^+e^- annihilation, and for an excited proton the system looks like a DIS event. This picture is further supported by the quantum number flow observed in fully reconstructed diffractive events of the reaction $pp \to (\Lambda\phi K^+)p$ at the ISR [1]: the Λ particle is found to go forward in the direction of the initial proton, while the K^+ goes backwards and the ϕ stays in the centre. The similarity between diffractive excitation and DIS has been stressed by Donnachie and Landshoff [2].

Although the dominant feature is a longitudinal structure with limited transverse momenta, the UA8 collaboration at the SPS collider has observed transverse jets with $E_\perp$ up to 12 GeV in the diffractive reaction $p\bar{p} \to pX$ [3]. These jets have properties similar to the transverse jets in hadronic collisions, e^+e^- annihilation, or DIS. It is, however, not possible to tell from the data whether these jets are more like quark or gluon jets.

The presence of such transverse jets was proposed by Ingelman and Schlein [4], based on a hard scattering model. In this model the pomeron is assumed to have a partonic substructure, and the jets are produced in hard parton–parton scatterings in the same way as in hadronic collisions.

Transverse jets would also be expected from the analogy with DIS. When colour charges are separated in DIS or e^+e^- annihilation, gluon bremsstrahlung is emitted. In the `Fritiof` model for hadronic scattering [5] it is assumed that also in hadronic collisions colour charge separation is a source of gluon emission. In ref. [6] we propose, that also in diffractive excitation the separation of colour charges leads to gluon bremsstrahlung, which can be seen as transverse jets.

In QCD, colour charge separation causes gluon radiation in the same way as an electric dipole radiates photons. In e^+e^- annihilation this dipole spectrum is the coherent sum of contributions from emission from the quark and the antiquark, while in DIS it can be described as the coherent sum of initial and final state radiation from the struck quark. There is a difference between these two processes: gluon radiation in DIS is similar to e^+e^- annihilation in the direction of the struck quark (i. e. in the current fragmentation region), but in the fragmentation region of the target proton, the gluon radiation is suppressed. This is related to the fact that the proton remnant does not correspond to a pointlike colour charge. Conventionally, this suppression is expressed in terms of the proton structure function, which tells us that it is unlikely that the struck (pointlike) quark initially carried a very large fraction of the proton momentum.

In reference [7], an alternative description of the suppressed radiation in the target fragmentation region was proposed. It was assumed that the original hadron can be treated as a string-like object (a vortex line in a colour superconducting vacuum) which implies that the energy distribution has an essentially one-dimensional structure. In ref [6] these ideas were used to describe the expected gluon radiation in diffractive excitation. As will be seen below, in this case the number of transverse jets is smaller than in DIS. This can be understood if the momentum transfer in diffractive collisions is a soft process which does not kick out a pointlike quark. We will see that if we assume that the pulled out quark corresponds to an extended object of the same character as the target fragmentation system, this model is able to give a good description of the jets observed by the UA8 collaboration.

2. Gluon Emission in Deep Inelastic Scattering

When a quark and an antiquark move apart in an e^+e^- annihilation event, gluons are emitted according to the well-known dipole formula

$$d\sigma = \frac{3\alpha_s}{4\pi^2}\frac{dk_\perp^2}{k_\perp^2}\,dy\,d\phi \tag{1}$$

The kinematically allowed region is given approximately by

$$|y| \lesssim \frac{1}{2}\ln\frac{s}{k_\perp^2} \tag{2}$$

which corresponds to a triangular region in the $y - \ln k_\perp^2$ plane.

In DIS, too, a colour 3 and a colour $\bar{3}$ move apart and emit gluons in a similar way. There is a difference, however, in that the proton remnant (the $\bar{3}$ if we assume the photon hit a quark) is an extended object and not localized to a point in space-time. The emission of radiation with wavelengths much shorter than this extension should then be damped in a way similar to the damping from an emitting antenna. An antenna cannot coherently emit radiation with a wavelength shorter than the antenna size. For such waves, only a fraction of the antenna with the extension of about one wavelength can emit coherently, and consequently only the energy available in that fraction can be used for emission.

In reference [7] it was assumed that the original hadron can be treated as an extended string, like a vortex line in a superconducting vacuum. This would give an essentially one-dimensional structure. In a Lorentz frame where the gluon is emitted at a right angle to the string, the wavelength of the gluon is is proportional to $1/k_\perp$. If the (transverse) extension of the hadron string is given by $1/\mu$ (with μ of the order of a hadron mass), then only a piece with the fraction

$$a(k_\perp) = \frac{\mu}{k_\perp} \tag{3}$$

of the hadronic energy-momentum can radiate coherently. Thus only this fraction of the energy is available for the emission. If W is the mass of the final hadronic state, and if y is the rapidity of the gluon in the hadronic CMS, we obtain the following kinematical limits for gluon emission:

$$-\ln\frac{W\mu}{k_\perp^2} \lesssim y \lesssim \ln\frac{W}{k_\perp} \tag{4}$$

(assuming $y < 0$ in the direction of the hadron remnant). Comparing this with the constraint in equation (2) valid for e^+e^- annihilation, we see that this result implies that the shaded region in figure 1a should be suppressed.

In ref. [7] it was found that available data from leptoproduction can be well reproduced by this simple model with the parameter μ given by $\mu \approx 1$ GeV. Before comparing with data, the full partonic cascade was included, in which the colour triplet and antitriplet can radiate further and the gluons split repeatedly into more gluons or quark-antiquark pairs. This was described using the dipole formulation of the QCD cascade [8] as implemented in the `Ariadne` MC simulation program [9]. Good agreement is obtained in comparisons with data from EMC. As an example figure 2 shows the distribution of $< p_\perp^2 >$ as a function of x_F. We also note that when extrapolating to HERA energies, this model differs noticeably from other predictions.

3. Gluon Emission in Diffractive Excitation

As mentioned in the introduction, a diffractively excited system looks very similar to a DIS event. In both cases a quark is separated from the target remnant. DIS is a hard process, and

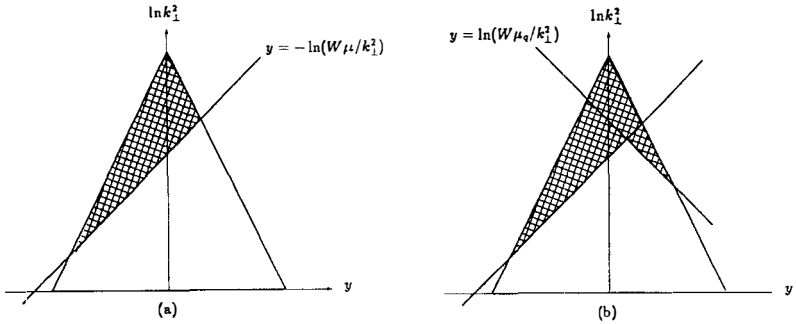

Fig. 1: The allowed phase space region in DIS (a) and diffractive excitation (b). Gluon emission is suppressed in the shaded areas.

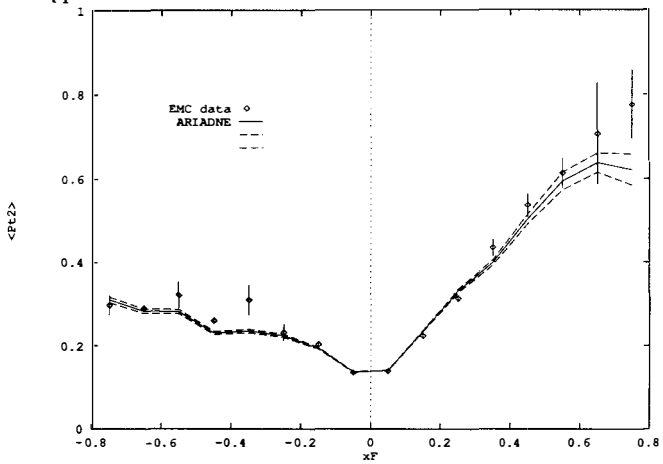

Fig. 2: Distribution of $\langle p_\perp^2 \rangle$ as a function of x_F in μp scattering. The data are from EMC [10] and the curves are from the `Ariadne MC 3.0` [9].

in our treatment, described in section 2, the kicked-out quark is treated as pointlike. Diffractive scattering, on the other hand, is a soft process, and the pulled-out quark is not expected to be pointlike. In the picture of section 2, it ought to be accompanied by a piece of the stringlike colour field.

We will here assume that the gluon emission in the quark fragmentation end of a diffractively excited proton is soft in the same way as the emission in the target fragmentation end. We imagine, however, that the transverse extension of the quark system may be smaller than for the target remnant diquark system. Thus we assume that the energy density in the quark end is described by a parameter μ_q, which is the analogue of μ in equation (3). The allowed region for gluon emission is then given by

$$-\ln\frac{W\mu}{k_\perp^2} \lesssim y \lesssim \ln\frac{W\mu_q}{k_\perp^2} \tag{5}$$

As before, y is the rapidity in the CMS of the excited proton and positive y values are in the direction of the single quark. Naturally, y must also satisfy the condition from energy-

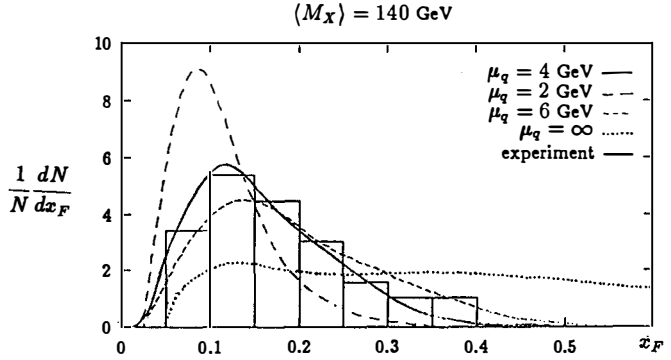

Fig. 3: Jet x_F distribution for the events with M_x in the range 125-155 GeV. The histogram shows the results of UA8 [3], and the curves are model results for different values of μ_q, as indicated. The value $\mu_q = \infty$ would correspond to gluon emission like in DIS events.

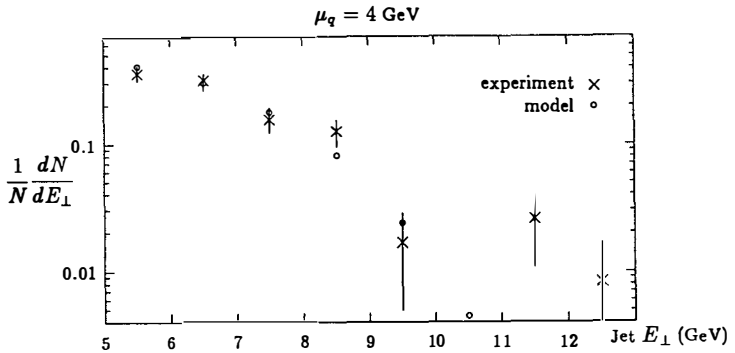

Fig. 4: Jet $E_\perp$ distribution for $\mu_q = 4$ GeV. The results correspond to the full M_X range, $105 < M_X < 190$ GeV, of the UA8 experiment [3].

momentum conservation in eq. (2). The allowed region is indicated in figure 1b. We note that the situation in DIS corresponds to the limiting case where μ_q is very large.

We want to compare the model with the data from the UA8 experiment at the CERN SPS collider [3]. In this experiment a quasielastic forward proton is measured using a Roman Pot spectrometer, while the diffractively excited $\bar{p}$ is measured in the UA2 detector. The acceptance of this calorimeter is $40° < \theta < 140°$ (corresponding to the pseudorapidity range $-1 < \eta < 1$) in the total $p\bar{p}$ CMS. This means that only part of the excited system is observed, viz. a region connected to the pulled-out quark.

In our MC simulations we used the `Ariadne MC 3.0` program [9] for the gluon emission together with the Lund string fragmentation. As we had no possibility to take the exact properties of the UA 2 detector into account, we assumed a calorimeter with perfect acceptance and energy resolution within the range $-1 < \eta < 1$.

Figure 3 shows the distribution of jet x_F (defined as $2p_{\parallel}/M_x$ in the CMS of the excited system) for jets from events satisfying the trigger condition, and figure 4 shows the transverse energy distribution of these jets. With $\mu_q = 4$ GeV the experimental data are well represented

by the model. After the presentation of this talk I have been informed, however, that the acceptance corrections to the UA8 data are larger than previously expected. Thus a better description is obtained with a larger value of μ_q, around 6 GeV [11].

We note that a pointlike quark as in DIS, corresponding to $\mu_q = \infty$, would give far too many jets with large $E_\perp$ and large x_F. On the other hand, we find that we must take $\mu_q > \mu$, and thus the spatial extension of the quark is smaller than that of the hadron remnant.

In our model the jet production is very asymmetric in the rest frame of the excited hadron. This is a consequence of the difference between μ and μ_q, which determine the radiation in the direction of the target remnant and the pulled-out quark, respectively. It can be tested in an experiment where also the negative x_F–region is observed. The UA8 collaboration is presently analysing data from an experiment with larger acceptance. We look forward to a comparison between our model and these data, for which, however, a detailed treatment of the detector acceptance is needed.

4. Conclusions

Diffractively excited protons fragment in a way similar to DIS events. It seems as if the momentum transfer pulls out a quark from the initial proton, stretching a colour field between this quark and the proton remnant. In analogy with DIS, we expect gluon bremsstrahlung as a result of this colour charge separation. The emitted gluons ought to show up as transverse jets, and such transverse jets have been observed by the UA8 collaboration.

In ref. [7] a model for gluon radiation in DIS was proposed, in which the energy in the target remnant is assumed to have a spatial distribution as in a string or a vortex line. An extended antenna does not coherently emit radiation with wavelengths shorter than the antenna size. In the same way hard gluon emission is in this model suppressed in the target fragmentation region. Good agreement with data from EMC has been obtained. The model gives noticeable effects at HERA.

The ideas of ref [7] are generalized in ref [6] to describe gluon emission in diffractive excitation. Good agreement is obtained with data from the UA8 coll. The model can be tested in an experiment with a larger acceptance region than that of the UA8 detector.

References

[1] A. M. Smith et al., R608 Collaboration, *Phys. Lett.* **163B** (1985) 267

[2] A. Donnachie and P. V. Landshoff, *Phys. Lett.* **185B** (1987) 403

[3] R. Bonino et al., UA8 collaboration, *Phys. Lett.* **211B** (1988) 239

[4] G. Ingelman and P. Schlein, *Phys. Lett.* **152B** (1985) 256

[5] B. Andersson, G. Gustafson, B. Nilsson-Almqvist, *Nucl. Phys.* **B281** (1987) 289

[6] G. Gustafson, M. Olsson, *Transverse jets in high mass diffractive excitation* **L** und preprint LU TP 91-1

[7] B. Andersson, G. Gustafson, L. Lönnblad and U. Pettersson, *Z. Phys.* **C43** (1989) 625

[8] G. Gustafson, *Phys. Lett.* **175B** (1986) 453
G. Gustafson and U. Pettersson, *Nucl. Phys.* **B306** (1988) 746

[9] L. Lönnblad, Ariadne 3 – A Monte Carlo for QCD cascades in the colour dipole formulation, Lund University preprint LU–TP 89–10 (1989)

[10] EMC Coll. M. Arneodo et al., *Z. Phys.* **C36** (1987) 527

[11] A. Brandt, private communication

NEW PHYSICS IN HADRONIC DIFFRACTION

Kyungsik KANG
Department of Physics, Brown University,
Providence, RI 02912, U.S.A.
and
Alan R. WHITE
High Energy Physics Division
Argonne National Laboratory
Argonne, IL 60439, U.S.A.
(presented by Kyungsik Kang)

ABSTRACT

We suggest that a short-lived axion-like η_6 of mass 30 GeV, with two photons as a major decay mode, should be produced diffractively at hadron colliders. This causes a genuine physical threshold around $\sqrt{s} = 500\,GeV$, which enables us to explain all high energy elastic scattering data, diffractive cosmic-ray exotics and hadronic photon events. New physics involving the new particle η_6 as well as other observable effects are also discussed.

1 - Introduction

The idea of dynamical symmetry breaking of the electroweak gauge symmetry is to effectively provide the role of the Higgs sector by a dynamical bound-state of some fundamental fermions. In the usual technicolor models[1], dynamical bound-states are formed by some fundamental techniquarks that have an extra-strong technicolor interaction. Another possibility[2] is to form dynamical condensates of some hyper-quarks belonging to a higher-color representation of the ordinary color group SU(3). The latter scheme is not only simpler but also attractive because the ordinary QCD is also responsible for the electroweak symmetry breaking. The color–exotic hyper-quarks can have a dramatic effect on the β-function in the renormalization equation and chiral symmetry breaking can occur at around 1 TeV scale. Because of asymptotic freedom in QCD, the simplest extension [3] beyond the six flavors of the ordinary color–triplet quarks is to assume a doublet of color–sextet quarks. In other words, the color sextet quarks play the role of technicolor fermions and the electroweak scale is a QCD scale of dynamical condensation which generates masses for the $W^{\pm}$ and Z^0 and also for the color–triplet quarks and leptons. We then expect a host of electroweak-strong unification effects not too far above the condensation scale. A flavor doublet of color–sextet quarks $Q_6 = (U, D)$ would produce new "hadrons" containing sextet quarks such as new pseudoscalar mesons, vector mesons, baryons and their antiparticles. In addition, because of a new component in the color anomalies due to the sextet current, there will be a new axion η_6, a Goldstone bason associated with the U(1) axial current which is made of an appropriate combination of color–triplet and sextet currents. The conservation of this axial current is violated by the instanton generated interactions, making η_6 to be massive. It is expected that the effective interactions responsible for the mass of η_6 will acquire a large anomalous dimensions (such is the case for the heavy top condensations[4]) in the strong-coupling large momentum region where sextet-quark condensates are formed so that η_6 mass may be as large as $30 GeV$, which is much larger than the ordinary axion mass anticipated from the naive dimensional estimate. Nevertheless this axion-like η_6 will be the lightest new particle due to the sextet-quark sector that will produce new physical effects beyond that which the standard model can anticipate.

We believe that [5] we may have already seen several "exotic" experimental phe-

nomena which may all be related to the existence of a new quark sector. They are: (1) the large real part of the forward $p\bar{p}$ amplitude observed by UA4[6]; (2) new diffractive physics[7] seen in cosmic ray air showers above $\sqrt{s} = 500\,GeV$, and (3) the excess muons[8]. It can easily be shown from a derivative dispersion relation[9] that such a large real part of the forward amplitude as observed by UA4 is incompatible with a slowly varying and low total cross-sections as reported[6] by E710. If both results are right it seems that [5] a genuine physical threshold must occur just below the UA4 energy. Exotic cosmic ray events, in particular "mini-Centauros" and "Geminions", exhibit a similar threshold[7] at $\sqrt{s} = 400 \sim 500\,GeV$ and can consistently be interpreted as different decays of the same diffractively produced and short-lived particle with a mass around $30\,GeV$. The excess muon events[8] observed in high energy cosmic point source showers suggest a new hadronic interaction for the photon which both absorbs the electromagnetic e^+e^- pair production process and produces hadrons diffractively. The three phenomena are consistent with the existence of a threshold for a diffractively produced particle of a mass around $30\,GeV$ with partial cross sections $2 \sim 3\,mb$ for 2γ decay mode (Geminion events) and $1 \sim 2\,mb$ for hadronic decay modes (mini- Centauro events). It will be interesting to see if CDF can detect the 2γ mode of this new $30\,GeV$ state (their present em calorimeter covers down to 2^o to the beam[11]).

2 - Sextet Quark Model

The idea to replace the spontaneous symmetry breaking via elementary Higgs scalars by a dynamical condensation mechanism of techni-fermions has been around for some time. At some strong enough value of the effective coupling, certain bound state condensates of the new fermions are formed to give rise to chiral symmetry breaking whereby producing Goldstone bosons which play the effective role of Higgs scalars. In order to give the right mass of $W^{\pm}$ in this picture, the Goldstone boson coupling F, i.e., the technipion decay constant, to the gauge current should be about 2,600 times larger than the pion decay constant $f_\pi \simeq 132\,MeV$, the chiral breaking parameter of the ordinary hadron physics. To achieve this, one can either suppose a new extra-strong interaction based on an unbroken (larger) technicolor group along with additional technifermions[1] belonging to its fundamental representation or new exotic quarks belonging to a higher dimensional representation[2] of the ordinary SU(3)

color group. In the latter case, because of their large quadratic Casimir invariant, the exotic quarks have a dramatic effect on the β function and chiral-symmetry breakdown in exotic sectors may occur at around the 1 TeV scale.

An attractive possibility for the second type of dynamical symmetry breaking scheme is the minimal color-condensate model[3] which contains the gauge and fermion sectors of the standard model and a flavor doublet Q_6 = (U,D) with conventional electric charges and transforming as **6** under SU(3) color. With the usual three doublets of ordinary quarks with color **3**, the requirement of asymptotic freedom of the SU(3) color group allows just one such doublet. As the QCD running coupling $\alpha_s(\mu_6)$ grows a $\bar{Q}_6 Q_6$ condensate forms at a scale $\Lambda_6 = | < \bar{Q}_6 Q_6 > |^{\frac{1}{3}} \sim 250\, GeV$ signaling the spontaneous breaking of chiral U(2) $\times$ U(2) symmetry down to SU(2)$\times$ U(1) in the sextet quark sector and producing a triplet of Goldstone pions, $\pi_6^{\pm}$ and π_6^0, and a singlet eta-like meson. The triplet of Goldstone pions is then responsible for $W^{\pm}$ and Z^o masses a la the Higgs mechanism. There will be new QCD baryons and vector mesons that are made of sextet quarks. (In the simplest model there are two new lepton doublets with conventional electric charges to cancel the electroweak gauge anomaly but further higher-color quarks appearing at an even larger energy scale may play this role[12]). The physical axion η_6 is associated with the axial U(1) chiral symmetry with the axial current made of an appropriate anomaly free combination of the axial U(1) currents of color triplet and sextet quarks.

As noted above, the composite operators involving sextet quarks are expected to acquire large anomalous dimensions which should make the sextet quark interaction very strong in the large momentum range and also give a major effect to the large mass of η_6. Recently Fukazawa et al[13] estimated the sextet quark mass to be about $350\, GeV$, which is rather insensitive to the choice of the t-quark mass in the range $77 - 160\, GeV$, by studying the nontrivial solution of the ladder Schwinger-Dyson equation for the sextet quark propagator. The sextet quarks of such mass should be visible in the 6-jet final states at LHC[14]. But the new effects associated with η_6 should soon be tested by the projected new experiment at CERN[15] and at Fermilab Tevatron collider[11].

3 - New Physics in Hadronic Diffraction

We suggest that[5] several "exotic" experimental phenomena mentioned above may all be related to the existence of the sextet quark sector and in particular to the diffractive production of the new axion-like particle η_6.

The UA4 Real Part - In an asymptotic regime a derivative dispersion relation[9] implies that the real part of the elastic scattering amplitude is directly given by the derivative of the total cross-section (if there is no Odderson[16]). Therefore a SLOWLY VARYING total cross-section and a LARGE real part are INCOMPATIBLE. In particular the "large" UA4 value[6] of 0.24 ± 0.04 for $\rho = \mathrm{ReA/ImA}$ and the "low" E710 results[10] of $\sigma_{tot} = 72.1 \pm 3.3$ mb for the total cross-section, can not be fit by any smooth asymptotic model (for example a minijet model) which also fits the lower energy data. IF both results are right, the only possible explanation seems to be A GENUINE PHYSICAL THRESHOLD just below the UA4 energy. To see this we can write a simple threshold model[5,17] for Im A, e.g.,

$$ImA/s = 37 + 80\sqrt{s} + 6.5\ln\left[\sqrt{s}/25\right] + 9\left[1 - 520^2/s\right]^{1/2}\theta\left[s - 520^2\right] \qquad (1)$$

which when the real part is constructed from a dispersion relation, fits the data as shown in Fig. 1.

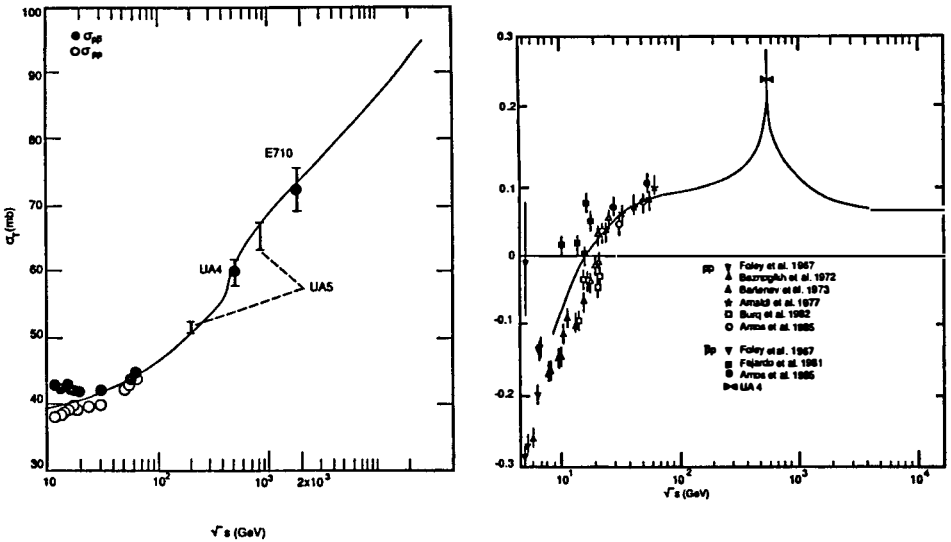

Fig. 1: σ_{tot} and ρ from Eq. (1).

While the effect of the threshold in this simple model is surely too dramatic, it does illustrate how the data could be compatible. A more important issue is what the "New Physics" represented by the threshold could possibly be. Could it perhaps be related to "exotic" Cosmic Ray events? The existence of a threshold for such events was a major part of the argument[18] for raising the SPS collider energy to $\sqrt{s} = 900\,GeV$ in 1982.

Diffractive Air-Shower "Exotics" - The lowest energy exotics fall into two classes[7].

Mini-Centauros - which can be characterized as 1) diffractive, 2) hadron-rich, 3) average multiplicity ~ 15, 4) fireball mass $\sim 30GeV$ 5) cross-section $\sim 2-4\%$ of inelastics, 6) threshold - $\sqrt{s} \sim 400 - 500\,GeV$ and

Geminions - which can be characterized as 1) diffractive, 2) JUST two widely separated cores, 3) fireball mass $\sim 30\,GeV$, 4) cross-section $\sim 5-10\%$ of inelastics, 5) threshold - $\sqrt{s} \sim 400 - 500\,GeV$.

Our proposal[5] is that diffractive production of a new state of mass O(30) GeV is the new threshold represented by our simple model of Eq. (1) and we identify Geminions and Mini-Centauros as different decay modes of this new state. We note that the cross-sections are of the right magnitude and the threshold the right energy for this identification. The kinematics also fits well with a diffractive threshold i.e. $M^2/s < 0.01 \Rightarrow M/0.1 > 300GeV$

Hadronic Photons - An accumulating number of observations[8] of Cosmic point sources (Cygnus X-3, Hercules X-1, Crab Nebula ...)indicate that photon showers above some threshold energy in the range 10-100 TeV contain at least as many muons as a hadron shower. Since this is more than an order of magnitude greater than expected from a normal photon shower, a new "hadronic" photon interaction is suggested. This phenomenon, and all the "hadron- rich" air-shower phenomena[7] (including Centauros, mini-Centauros etc.), can be explained[19] if the photon develops a new diffractive interaction which both absorbs the electromagnetic e^+e^- pair production process and diffractively produces hadrons. In addition the Geminion events described above can be directly interpreted as TWO-PHOTON decays of a SHORT-LIVED state.

Our conclusion from study of the above three phenomena is that they are all

consistent with the existence of a threshold for diffractive production of a new state with mass 20-40 GeV and the cross-sections (of the order of magnitude), 2 - photon decay mode (Geminions) $\sim$ 2-3 mb and hadronic decay mode (mini-Centauros) $\sim$ 1-2 mb.

4 - Concluding Remarks

We suggest[5] identifying the axion η_6 as a candidate for the new particle of $30\,GeV$ mass associated with the diffractive threshold mentioned above. Because of the instanton interactions coupled with very strong sextet quark QCD interactions in the dynamical momentum range of $100\,GeV - 100TeV$ the η_6 can acquire a mass as high as $30\,GeV$, much larger than the naive estimate of an ordinary axion. As a light Goldstone boson, i.e., $30\,GeV << \Lambda_6$, the η_6 automatically has a major two-photon decay via the anomaly giving a lifetime $\tau(\eta_6 \to 2\gamma) \sim (100keV/m_{\eta_6})^3 \sim 3 \times 10^{-17}$ sec which is very close to the π^o lifetime and is nicely consistent with the fireball interpretation of Geminion events. Also the approximate equality for the cross-sections of mini-Centauros and Geminions interpreted as hadronic and electromagnetic decay modes of the η_6 respectively, combined with the appropriate axial current divergence equation gives $\alpha_{e.m.} \sim (m_{\eta_6}/F_{\eta_6})^2$ so that $m_{\eta_6} \simeq 25\,GeV$ for $F_{\eta_6} = \Lambda_6$ providing a nice consistency.

We note that an appropriately increased diffractive cross- section due to the diffractive production of η_6 would explain the apparent low collider results for diffraction. The measured single diffractive cross-sections at the collider energies are lower than that anticipated from a straightforward extrapolation of the ISR value, while the threshold term in Eq. (1) contributes 2mb at UA4 energy and about 8 mb at the Tevatron energy. As we mentioned above, CDF may be able[11] to look for the 2γ decay mode in their current diffractive data. Their electromagnetic calorimeter covers down to 2^o and this may be just enough to see a $30\,GeV$ state.

The cross-section for perturbative QCD production of Q_6 is, apart from color factors, the same as that of color–triplet quarks with the same mass M_{Q6}. The consistent mass M_{Q6} for sextet quarks appears [13] to be around $300\,GeV$ - $400\,GeV$ for the t-quark mass range of $77 - 160\,GeV$. The hard cross-section is therefore less than 1 pb at CDF making the η_6 undetectable in such processes in hadron colliders.

It could be seen[20] at LEP in the future as a rare radiative Z^o decay when LEP accumulates enough Z^o's, as the branching ration $\Gamma(Z^o \to \eta_6\gamma)/\Gamma(Z^o \to \mu^+\mu^-)$ is about 10^{-5}. However we expect that diffractive production of sextet flavors and of the η_6 in particular will be large. This can be thought of as due to instanton interactions contributing to the small t component of high-energy hadron collisions.

A strongly interacting Q_6 sector has an absorption effect for e^+e^- pair production via the interference[19] between the diffractive excitation of a photon into a $Q_6\bar{Q}_6$ state (and the Z^o in particular) that decays into e^+e^-, and the electromagnetic production of e^+e^- pairs. The production of hadrons and 2γ via the η_6, together with direct production of the Z^o, will drastically modify the properties of high-energy photon-initiated air showers and the development of electromagnetic clusters within hadron initiated showers. This could be an explanation of the muon-rich photon showers and the wide range of anomalous shower development seen in high energy cosmic ray events.

Since Eq. (1) gives σ_{tot} that increases slower than the conventional $(\ln s)^2$ - fit and the threshold term disappears rapidly with energy, the large value of ρ must be very localized with respect to energy. Projected new measurements of ρ at CERN[15] and of total cross-sections at Fermilab covering a number of energies should soon determine the existence of a new hadronic diffractive threshold that we suggest to associate with diffractive production of η_6.

This work is supported in part by the U. S. Department of Energy, Contract DE-AC02-76ER03130 and Contract W-31-109-Eng-38.

References and Footnotes

1. S. Weinberg, Phys. Rev. **D13**, 974 (1976); **D19**, 1277 (1979); L. Susskind, Phys. Rev. **D20**, 2619 (1979).

2. W. J. Marciano, Phys. Rev. **D21**, 2425 (1980).

3. E. Braaten, A. R. White and C. R. Willcox, J. Mod. Phys. **A 1**, 693 (1986). See also K. Konishi and R. Tripiccione, Phys. Lett. **121B**, 403 (1983) with different charge assignments of the sextet quarks.

4. V. A. Miransky and K. Yamawaki, Mod. Phys. Lett. **A4**, 129 (1989).

5. K. Kang and A. R. White, Phys. Rev. **D42**, 835 (1990).

6. UA4 Coll., D. Bernard et al., Phys. Lett. **198B**, 583 (1987).

7. Chacaltaya and Pamir Collaboration contribution to VI Int. Sym. on Very High Energy Cosmic Ray Interactions, Tarbes, France, 8-17 July 1990, ICRR-Report - 216-90-9.

8. G. Yodh, Nucl. Phys. **B** (Proc. Suppl.) **12**, 277 (1990) and presentation at the 25th Int. Conf. High Energy Phys., Singapore (1990).

9. S. Hadjitheodoridis and K. Kang, Proc. 2nd Int. Conf. Elastic and Diffractive Scattering, Rockefeller University, New York, 1987; K. Kang and B.Nicolescu, Phys. Rev. **D11**, 2641 (1975) in which earlier references can be found.

10. N. A. Amos et al., Phys Lett. **B243**, 158 (1990).

11. N. Giokaris (Private communication).

12. K. Kang and A. R. White, J. Mod. Phys. **A2**, 409 (1987).

13. K. Fukuzawa et al., Prog. Theory Phys. **85**, 111 (1991); T. Muta, in Proc. 25th Int. Conf. H. E. Phys., Singapore (1990).

14. R. S. Chivukula, M. Golden and E. H. Simmons, Phys. Lett. **B207**, 453 (1991).

15. Genoa-Palaiseau-Roma-Valencia Collaboration, CERN/DG/RB 90-156.

16. L. Lukaszuk and B. Nicolescu, Nuovo Cim. Lett. **8**, 405 (1973); K. Kang and B. Nicolescu (Ref. 9).

17. K. Kang and A. R. White, Proc. 4th Asia Poc. Phys. Conf. Yonsei University, Seoul, Korea (1990); Proc. 20th Int's Symp. Multipart. Dyn. Gut Holmeche, Germany (1990).

18. J. Rushbrooke, 21st Int'l Conf. High Energy Phys., J. Phys. (Paris) Collog. **43**, C3 (1982).

19. F. Halzen, P. Hoyer and N. Yamdagni, Phys. Lett. **B190**, 211 (1987).

20. T. Hatsuda and M. Unezawa, Seattle preprint INT 3-90 (1990).

POMERON-ODDERON DEGENERACY AND HIGH ENERGY (ANTI)PROTON-PROTON CROSS SECTIONS IN THE REGGE-EIKONAL APPROACH

V.A.Petrov and A.P.Samokhin
Institute for High Energy Physics,142 284 Protvino,Moscow Region,USSR

Abstract
This talk is devoted to the influence of confinement on high-energy hadronic scattering.

1. ON THE ANALITICITY PROPERTIES OF THE GREEN FUNCTIONS OF CONFINED FIELDS.

As it is well known the physical content of any quantum field theory is written in the infinite set of its Green functions(GF).In particular,the physical spectrum is represented by singularities of GF in the momentum space, and S-matrix is a set of multifold residues of external (one particle) poles.If one insists that physical spectrum of QCD consists of observed hadrons only then it seems reasonable to assume that only singularities of full nonperturbative GF are poles and cuts defined by masses of observed hadrons.When this property is implied on amputated GF then it is clear that all colour nonsinglet channels are free of any singularities at finite distances in corresponding complex plane.It is worth to note that in general this does not forbid simple poles (but not cuts) for quark and gluon propagators.It is not main goal of this talk to discuss in details confinement criterium formulated above.We only mention that analoguous ideas were developed in the past 1)(though in a somewhat restricted sense).We also should like to stress that GF with such properties are likely to have perturbative RG asymptotics at the most in some directions only of momentum complex plane(s).

2.REGGE TRAJECTORIES IN QCD.

As it was said above GF display physical spectrum in colour singlet channels.E.g. in $q\bar{q}$-channel of the 4-fermion GF there are poles at masses of mesons,consisting of these q and $\bar{q}$.It is natural to expect that in this way GF not only yield the very masses of mesons but also "organize" them into experimentally observed recurrences ,i.e. Regge trajectories.An important feature of the 4-quark GF is that only two from three two particle channels may have colour singlet contributions.From this we readily conclude that Regge trajectories so generated are "signature blind",i.e. they are exchange degenerate.Similarly we can analyse gluon GF with a conclusion that "glueballs" also populate Regge trajectories without skipping any value of angular momentum.In this respect the leading trajectory(we assume its existence)which is associated with "glue rich"states is not an exclusion. This means that "Pomeron"(C-even) and "Odderon"(C-odd) 2) trajectories are in fact "parts" of a single leading trajectory.However "noblesse oblige" and the lack of signature leads to important consequences.For example it is impossible for the leading trajectory to intercept the J-axis at J=1 3) without loosing its leadership,i.e. the management of the rise of total cross-sections at high energies.So its

intercept lies higher than 1. Perturbative analysis[4] leads to the same conclusion about the Pomeron intercept. There are however some problems with asymptotic properties of perturbative trajectories[5].

3. REGGE-EIKONAL.

What are the scattering functions which possess the leading Regge poles in crossed channel analitically continued partial wave? Unitarity hints that it is definitely not the full hadron scattering amplitude. To this end it is valuable to recall Hove construction of Regge behaving functions as a formal series in one particle t-channel exchanges with infinitely rising spins[6] what can be related to the realisation of the "quasipotential" by Logunov and Tavkhelidze[7]. This leads to the conclusion that it is the function $V(s,t)=\Sigma(2l+1)\,\delta_l(s)P_l(\cos\theta)$ (where δ_l is the s-channel partial scattering phase) which accumulates Regge poles in its t-channel partial wave. For further estimates we use the impact parameter representation

$$T(s,t)=4i\pi s\int dbb J_0(b\sqrt{-t})[1-\exp(-\Omega(s,b))] \qquad (1)$$

$$i\Omega(s,b)=2\delta_{l=pb}(s)=(8\pi s)^{-1}\int dt J_0(b\sqrt{-t})V(s,t) \qquad (2)$$

In concrete case of $\bar{p}p$ and pp reactions we get asymptotically ($s\gg t$)

$$V_{\bar{p}p}(s,t)=[i\lambda(t)-(\lambda(t)+\eta(t)\cos\pi\alpha(t))/\sin\pi\alpha(t)]s^{\alpha(t)} \qquad (3)$$

$$V_{pp}(s,t)=[i\eta(t)-(\eta(t)+\lambda(t)\cos\pi\alpha(t))/\sin\pi\alpha(t)]s^{\alpha(t)} \qquad (4)$$

where $\lambda+\eta(\lambda-\eta)$ are the analytical continuations of the ppJ vertex from even(odd) J at $J=\alpha(t)$. $T(s,t)$ with $V(s,t)$ from Eq.(3) or (4) obeys to known "AKM-theorem"[8], i.e. at infinitely high energy and $\tau=-t_0(\log s)^2$ fixed the ratio $T(s,t)/T(s,0)$ tends to some limiting function $f(\tau)$ which is an entire function of the order less or equal to 1/2. In our case $f(\tau)=J_1(2\sqrt{4\Delta\alpha'(0)t_0\tau})/\sqrt{\tau}$ where t_0 is the nearest t-channel singularity

and $\Delta=\alpha(0)-1$. Upper bound from Ref.8) leads to not very restrictive bound $4\Delta\alpha'(0)t_0<1$.

4.CONSEQUENCES.

First of all we notice that for linear trajectory lowest excitations have masses $O(2GeV)(2^{++})$ and $O(3GeV)(3^{--})$ if we take $\Delta=O(0.1),\alpha'(0)=0.2-0.3$.

Possible decay is $(3^{--})\to(2^{++})+\omega$. As to the asymptotic behaviour one gets

$$\delta\sigma_{tot}(\bar{p}p-pp)\to 8\pi^2\alpha'(0)\operatorname{arctg}\varepsilon.$$

where $\varepsilon=(\lambda-\eta)/(\lambda+\eta)$. This was obtained first in Ref.9). Less expected result is 10)

$$\delta\sigma_{el}(\bar{p}p-pp)=-\delta\sigma_{inel}(\bar{p}p-pp)=-4\pi\alpha'(0)\log[(1-\varepsilon)/(1+\varepsilon)]\ \log s+\ldots$$

To this we add the behaviour of $d\sigma/dt$ in the "Orear region"

$$d\sigma/dt=\text{const}[\log s/|t|]\exp(-\text{const}\sqrt{|t|})$$

What concerns other processes we only claim that all $\delta\sigma(\pi p)$ disappear at high s, while $\delta\sigma(Kp)\to$const. Total cross-sections of $\pi p\to\rho p,\gamma p\to(\pi,\eta,\eta')p$, $K_L p\to K_S p$ tend to some limiting constant values.

These and other consequences will be considered in more details elsewhere.

REFERENCES.

1.G.Preparata,Phys.Rev.D7(1973)2973.

2.L.Lukaszuk and B.Nicolescu,N.Cim.Lett.8(1973)405.
P.Gauron,E.Leader and B.Nicolescu,Phys.Lett.B238(1990)406.

3.V.A.Petrov,Yad.Fiz.46(1987)202.

4.L.N.Lipatov,Sov.Phys.JETP63(1986)904.

5.V.A.Petrov and A.P.Samokhin,Phys.Lett.B237(1990)500

6.L.Van Hove,Phys.Lett.B24(1967)183

7.A.A.Logunov and A.N.Tavkhelidze,N.Cim.29(1963)380.

8.G.Auberson,T.Kinoshita and A.Martin,Phys.Rev.D12(1971)3185.

9.J.Finkelstein,H.M.Fried,K.Kang and C.-I.Tan,Phys.Lett.B232(1989)257.

10.V.A.Petrov and A.P.Samokhin,in Proc.XXV Renc.de Moriond:High Energy Hadronic Int.Ed.J.Tran Thanh Van(Editions Frontieres,1990)

TWO PHOTON PHYSICS

A REVIEW OF TWO PHOTON PHYSICS

Michael Feindt
C.E.R.N., 1211 Geneva 23, Switzerland
BITNET: FEINDT @ CERNVM

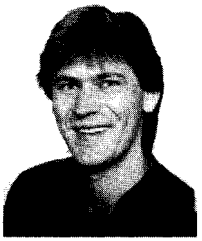

ABSTRACT

A qualitative review is given of the results obtained in $\gamma\gamma$ scattering experiments performed at the storage rings DORIS, PEP and PETRA, with special attention to recent results. Apart from the merits already earned still open questions are emphasized which should be addressed at the next generation of $\gamma\gamma$ experiments, already existing detectors at CESR, TRISTAN and LEP.

1 Introduction

You might think that it is not very easy to begin this session about Two Photon Physics after yesterday night's talk "Fundamental Concepts in Physics" [1] and the following partly philosophical discussion. However, being slightly modest and pragmatic, this turns out to be no problem: There are qualitatively new results which influence our picture of an important – if also not so popular – front of the Standard Model: that of low energy strong interactions, the transition region from asymptotic freedom to confinement and – through a study of the properties of the bound states (mesons) – the confinement region itself. In the absence of a rigorous calculus in this domain experimental results are currently compared mainly to phenomenological models like vector meson dominance or non-relativistic quark models, not regarded as "fundamental". However, the measurements themselves retrieve "fundamentality" as providing constraints to be met by (and perhaps guidelines for the construction or solution of) the ultimate theory.

In the Eighties Two-Photon Physics has developped to an industry: Experiments performed at DESY (ARGUS, CELLO, Crystal Ball, JADE, PLUTO and TASSO (alphabetical order)) and SLAC (MARK II, TPC/$\gamma\gamma$) dominated the scene, complemented by some publications from MARK J, DELCO, ASP and experiments at Novosibirsk. Recently, the TRISTAN experiments AMY, TOPAZ and – at this conference for the first time [2] – VENUS also provided their first results. A large potential is still to be exploited using CLEO II at CESR. At LEP, two photon physics will eventually also play a role different from just being "background" – at latest when it will run at energies far beyond the Z^0 peak, when one will be happy to have some events to analyze...

A series of dedicated workshops document experimental and theoretical progress, see e.g. the latest proceedings from 1986 [3] and 1988 [4]. In addition, there are a number of general review articles [5-9]. Since the appearance of these reviews significant progress has been made in some areas. In this short article I will try to summarize ***qualitatively*** what has been learnt from the experiments performed in the 80ies and provide references to more quantitative reviews and recent original literature. New insights have mainly been gained in the area of meson spectroscopy and jet production.

2 Kinematics

The basic Feynman graph for the two photon reaction at e^+e^- storage rings is shown in Fig.1. High energetic electrons and positrons each radiate off spacelike-virtual Bremsstrahlung photons (mainly low energetic and at small angles), which subsequently interact to form a final state X. The majority of events has too small lepton scattering angles to be detected ("tagged") in the forward calorimeters just around the beam pipe. The virtual photons of these "antitagged" events are restricted to small masses $Q^2 = -q^2$ and can be considered as "quasi-real" with the important consequence of being transversely polarised. The independently continuous energy spectra of the two photons lead to a continuum of invariant masses as well as boosts of the final state X along the beam axis. The Feynman graph can be split into two pieces, the purely QED and thus exactly calculable electron-photon vertices and the interesting $\gamma\gamma \rightarrow X$ vertex. A formalism exists which connects the measurable $e^+e^- \rightarrow e^+e^-X$ cross section to the interesting

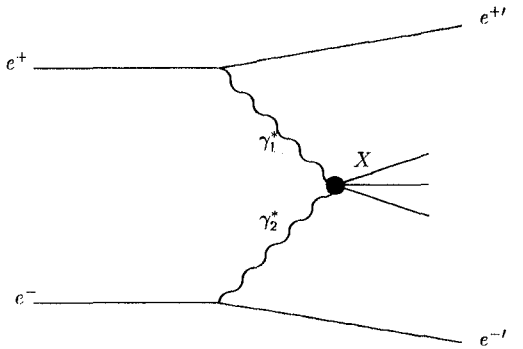

Figure 1: Feynman graph for a two-photon process in an e^+e^- reaction

$\gamma\gamma \rightarrow X$ cross section. The complicated kinematics leads to typically very low experimental acceptances which have to be calculated by detailed Monte Carlo simulations. Formed by two photons, the C parity of the final state X is positive. Due to the transversality of quasi real photons only the helicity states 0 and ± 2 can be produced, furthermore the Landau-Yang theorem [10] forbids the system X to have spin 1. In the single or double tag mode, however, with one or both of the photons being substantially off-shell, also helicity states ± 1 and spin 1 mesons can be formed. The kinematics has been extensively reviewed in the classical paper by Budnev et al. [11].

3 What can be / has been measured?

- **QED tests** of order α^4 and α^5 have been performed and show excellent agreement.
- The **total hadronic cross section** has been measured as a function of $W_{\gamma\gamma}$ and Q^2; it is roughly constant in energy with a possible rise towards low $W_{\gamma\gamma}$ and exhibits a VDM- or GVDM-like fall-off with Q^2, which becomes flatter at about $5\,GeV^2$ due to the onset of pointlike coupling [12, 13, 14].
- The **photon structure function** $F_2^\gamma(x, Q^2)$, which can be derived from the hadronic cross section and interpreted as the momentum distribution of quarks inside the photon (see below).
- High $p_\perp$ **jet and inclusive hadron production** show hadronic behaviour at low $p_\perp$, and pointlike coupling at high p_T and high Q^2 (see below).
- High t **exclusive meson and baryon pair production** are measured with still low statistical significance. A QCD inspired model works reasonably well for mesons, but calculations for baryons grossly underestimate the data.
- There exist an enormous amount of data on many **exclusive final states** (multipions, vector meson pairs), mainly by the ARGUS experiment, and some models to describe

them. None of the models is completely successful. The most striking feature is the enormous sub-threshold cross section for the quasi-elastic reaction $\gamma\gamma \rightarrow \rho^0\rho^0$ and the comparativley low cross section for charged ρ pairs, which needs an explanation in terms of isospin 0 / isospin 2 - interference. Some authors interprete this as evidence for 4-quark states (see below, reviews [15] and recent results [16, 17, 18])

- **Single resonance formation** with positive charge conjugation is a large field and provides important contributions to modern meson spectroscopy (see below).

4 Basic Concepts of the Photon

The photon can essentially be regarded as a two component object. From low Q^2 electroproduciton, photoproduction and electromagnetic form factors we know that photons behave like vector mesons. This is phenomenologically parameterized in various forms of the vector meson dominance model (VDM). In this picture $\gamma\gamma$ collisions look like soft hadron interactions. The bulk of $\gamma\gamma \rightarrow$ *hadrons* events can be well described by such models. Typical features are small transverse momentum of produced particles an thus jets with respect to the $\gamma\gamma$ axis, showing an exponential fall-off. As a function of the photons' virtualities Q^2 the cross sections fall like a pole form, with typical pole masses in the order of m_ρ or slightly larger.

However, since the discovery of scaling in deep ineleastic ep scattering and from high energy e^+e^- annihilation we know that photons couple to pointlike charged fermions (quarks) inside hadrons, as described in the Quark Parton Model QPM. Whenever a large momentum transfer is involved in a $\gamma\gamma$ scattering event, i.e. if either at least one of the photons' Q^2 is large ($>\approx 5\,GeV^2$), or high $p_\perp$ jets or particles are produced, the relatively flat dependence of the QPM cross sections with respect to these variables let the QPM prediction dominate the VDM prediction clearly, which also is proven experimentally.

Below it will be argued that perhaps there is a so-called *third component* in high $p_\perp$ interactions involving quasi-real photons, in which virtual quark "constituents" inside the photon undergo a hard scattering with the target, the momentum distribution of which can be described by a "photon structure function" F_2^γ.

5 The Photon Structure Function

In analogy to the measurement of the proton structure function in deep inelastic ep scattering, one can interprete a certain kinematical region of two photon reactions (single tagged events, one electron scattered to a large angle, the corresponding photon having large and measurable Q^2) as *deep inelastic* $e\gamma$ *scattering*, and extract from the measurable cross section $\sigma_{\gamma\gamma}(W_{\gamma\gamma}, Q^2)$ a structure function $F_2^\gamma(x, Q^2)$, where $x = Q^2/(Q^2 + W^2)$. Like Feynman's interpretation of the proton structure function, F_2^γ can be regarded as a (weighted) momentum distribution of pointlike charged constituents (quarks and antiquarks) inside the target photon, and x is the fractional momentum carried by the struck quark in an infinite momentum frame.

Experiments on F_2^γ are not easy, because in all existing detectors an acceptance hole around the beam pipe leads to a considerable smearing between true and visible x, which has to be

accounted for by applying a distinguished unfolding procedure [19]. Nevertheless, a number of experiments have reported results.

Typical features of the photon structure function are the following: In contrast to hadronic structure functions it peaks at high x. The integral $\int F_2(x)dx$ exhibits a logarithmic rise with Q^2 (i.e. scale breaking). This is true already for the $\gamma\gamma \rightarrow q\bar{q}$ Born term without gluonic corrections.

Early experiments extracted a value for $\Lambda_{\overline{MS}}$ from their measurement of F_2^γ, which inside errors agree with values obtained from other methods [6, 20]. However, there is an ongoing theoretical discussion [21, 22, 23] whether or not it really is the QCD scale parameter what one measures, or perhaps some phenomenological scale where non-perturbative effects (usually parameterized by vector meson dominance) sets in. QCD delivers a next-to-leading log asymptotic prediction, which is not free from technical difficulties (regularization procedure needed to cancel poles in the pointlike component against poles in the non-calculable "hadronic" or "VDM" part). Furthermore, mass effects are neglected, and (due to the log approximation) only transverse polarization is taken into account. The QCD scale essentially comes into the game by renormalization of an infinite series of (soft gluon emission) ladder diagrams, which does not diverge if a finite quark mass were used. The main result is that at $Q^2 \rightarrow \infty$ the QCD prediction does not differ much from the simple QPM Born term result (i.e. without gluon emission), which can be understood intuitively by means of asymptotic freedom. In the formula of the Q^2 variation the fermion mass in the QPM result is replaced by Λ in the QCD expression.

It should be noted that published experiments still are not in the real "asymptotic" region, and to reduce interpretational difficulties it is of great interest to perform analyses at highest possible Q^2, a task for TRISTAN (first results by AMY see [24], by VENUS see [2]) and LEP experiments.

It is interesting to note that due to the way Λ enters into the expression for F_2^γ and expressing Λ in terms of the strong coupling constant α_S, the photon structure function is sometimes regarded to be of order $\alpha \cdot \alpha_S^{-1}$. This leads to the fact that the "third component" contribution of photon interactions, although corresponding to higher order Feynman diagrams, is considered to be of order 0 in α_S and thus as important as the Born term in the hard scattering expansion. An important consequence appears e.g. at HERA, where in some kinematic regions the two jet rate due to this third component is very large [25].

6 Jet Production

One area where this concept of the third component can be tested experimentally is high $p_\perp$ jet production in two-photon reactions. Some evidence for such an effect has been provided by PLUTO and CELLO [12], who observe an excess of events in the transition $p_\perp$ region between the hadronic (VDM) and pointlike (QPM) regime; these events are generally more spherical than those from the VDM and QPM processes, resembling the characteristics of multi-jet events (however, there is no positive evidence yet for multi-jet structure). Very recently (in fact after the workshop), AMY [26] at TRISTAN has observed a similar effect and claims that it can well be described by a newly developped Monte Carlo model for the "third component" including QCD evolution equations and thus implicitely also needing a gluon component in the photon.

While this is very promising and might show the usefulness of the photon structure function concept, I personally would like to see real evidence for the photon "target jets" in addition to two high $p_\perp$ jets in single events by employing cluster algorithms or similar techniques. This, of course, is difficult because these target jets are just going along the beam pipe, and usually only tails of these jets are visible in the detectors.

7 Meson spectroscopy

Two photon formation of C- even meson resonances is an important tool for the analysis of their quark composition, their radiative widhts being proportional to the 4^{th} power of the constituents' charges. As such it plays an important role in the low energy frontier of QCD, the search and unambiguous classification of non- quark model particles (see e.g. [27]). A wealth of experimental data (see e.g. the reviews [28]) is existing on the two- photon widths of the pseudoscalar (0^{-+}, $L = 0, S = 0\, q\bar{q}$) and tensor mesons (2^{++}, $L = 1, S = 1\, q\bar{q}$), in good agreement with quark model expectations. Octet- singlet mixing angles derived from these measurements agree with those determined from other methods (mass formulae, radiative and flavour tagging (VP-, VT-) J/ψ decays). In the following sections I summarize what is currently known about the accessible nonets.

7.1 Pseudoscalar mesons, $J^{PC} = 0^{-+}$

All the ground state pseudoscalar mesons have been observed, the π^0, η and η'. The latter is the most-studied object in two-photon physics, and more than 17 numbers on the radiative width have been reported by a large number of experiments and a variety of decay modes studied; for a recent review see [32]. Crystal Ball has observed all pseudoscalars simultaneously in the reaction $\gamma\gamma \to \gamma\gamma$, but the accuracy of this measurement still cannot compete with that of the π^0 lifetime measurement. The following features have been derived from the two-photon experiments:

1. the octet-singlet mixing angle is $\approx -20°$;
2. nonet symmetry is nearly satisfied, the η_1 does not behave differently from the η_8;
3. no additional glueball component is needed in the η' wave function;
4. the η_c is now unambiguously seen in CLEO [33] and ARGUS [34], with the expected rate ($\Gamma_{\gamma\gamma}$ somewhat lower than 10 keV);
5. no other pseudoscalar states are seen, especially no radial excitation candidate [35]. The low upper limits are hardly understandable in the non-relativistic quark model, but may find their explanation in subtle dynamical effects (chiral symmetry) [36].
6. Also no glueball candidates have been observed, in particular there exists an hard upper limit on the radiative width of the $\iota/\eta(1460)$ of 0.75 $keV/B(K\bar{K}\pi)$, which translates to a stickiness ratio of 128 : 1 compared to the η [44]. This qualitatively supports a glueball interpretation, but is in no way a sufficient argument.

7.2 Tensor (2^{++}) and Scalar (0^{++}) Mesons

An exhaustive, quantitative review about the two-photon coupling of tensor and scalar mesons has just recently been issued [17]. The most spectacular recent result in this sector is the extensive analysis of the reaction $\gamma\gamma \to \pi^+\pi^-$ by the CELLO Collaboration [37, 38], which found a clear evidence for a broad scalar just below and under the f_2 signal. For 10 years the standard interpretation of the "continuum" on the left side of the f_2 peak was to stem from the non-resonant $\gamma\gamma \to \pi^+\pi^-$ Born term (pointlike box diagram). This has now been proven to be wrong by the measurement of the differential cross section: At masses above about 0.7 GeV the pions do not appear pointlike any more; form factor effects reduce the Born term calculation strongly. This is also true for the K^+K^- Born term directly from threshold on, which massively overestimates the cross section as recently measured by ARGUS [39, 17]. This result confirms the first claims for such a scalar by a reanalysis of Mark II and Crystal Ball results by Morgan and Pennington [40]. New Crystal Ball results presented here also agree with this conclusion [41]. Qualitative results for the tensor mesons are:

- f_2 and f_2' are ideally mixed, the latter consisting of merely $s\bar{s}$;
- nonet symmetry is satisfied;
- Delicate interference phenomena in the reaction $\gamma\gamma \to K\bar{K}$ confirm this picture: As expected in the quark model, destructive interference between the f_2 and a_2 is observed in the reaction $\gamma\gamma \to K_S^0 K_S^0$, and constructive interference in the charged kaon final state [42].
- helicity 0 is dynamically suppressed with respect to helicity 2, as expected in the non-relativistic quark model and relativistic extensions [43];
- apart from f_2, a_2 and f_2' no other tensor meson states are seen in $\gamma\gamma$ reactions: no $AX(1530)$ as seen in $p\bar{p}$ annihilations, no $\Theta/f_2(1720)$, no radial excitation candidate.

The following features are known for the scalars:

- A broad isoscalar $f_0(\approx 1400)$ is there as expected with $\Gamma_{\gamma\gamma} \approx 3 - 8\,keV$ [37, 41];
- $S^*/f_0(980)$ and $\delta/a_0(980)$ have a small $\gamma\gamma$ widths well below $1\,keV$ [44], making their interpretation as the scalar $q\bar{q}$ ground state mesons improbable and supporting an interpretation as $4q$ states or $K\bar{K}$ molecules [45];
- No other scalars are seen, in particular no $G/f_0(1590)$.

7.3 Pseudotensor mesons; $J^{PC} = 2^{-+}$

The 2^{-+} nonet is not well known experimentally: apart from the strange members, only the charged substates of the isovector $\pi_2(1680)$ (the old A_3) have been seen, and the isoscalar states are completely unknown [20]. In the quark model these mesons are spin singlet states ($S = 0$) with two units of orbital angular momentum. In potential model calculations their $\gamma\gamma$ couplings are sensitive to the second derivative of the $q\bar{q}$ wave function at the origin. The discovery of the

neutral π_2 in quasi real two photon scattering into 3 pion final states by Crystal Ball and CELLO [46] and the surprisingly large radiative width in the order of 1-1.5 keV have triggered interest into the search for the isoscalar partner(s), of which the mainly non-strange should have a radiative width around 3 keV from SU(3) expectations. Given the dominant (S-wave) $\pi_2 \to f_2\pi$ branching fraction, a large decay mode of the hypothetical η_2 could be $a_2\pi$, which decays into $\eta\pi\pi$ as well as 4π. The latter "suffers" from a huge (and still not unambigously understood) positive parity cross section, making the former the better candidate for an η_2 search. Indeed, two experiments have found positive evidence: CELLO [47] in the $\eta\pi^+\pi^-$ channel and Crystal Ball [48] in the decay mode $\eta\pi^0\pi^0$. Both mass spectra show a resonance like behaviour, with the parameters $m = 1850 \pm 50 MeV$, $\Gamma \approx 360\, MeV$, and $(2J+1)\cdot\Gamma_{\gamma\gamma}\cdot B(\eta\pi\pi) = 15 \pm 5\, keV$ (CELLO, preliminary) and $M(X) = 1.876 \pm 0.035 \pm 0.045 GeV$, $\Gamma_{tot}(X) = 0.229 \pm 0.090 \pm 0.033 GeV$, and $(2J+1)\cdot\Gamma_{\gamma\gamma}(X)\cdot BR(\eta\pi\pi) = 4.5 \pm 1.0 \pm 1.5\ keV$ (Crystal Ball). A likelihood test of the decay kinematic distributions cannot be fully conclusive, given the small statistics available. However, both experiments report consistency with $2^{-+}a_2\pi$, as expected for the isoscalar partner of the π_2. Positive parities are not favoured, but $0^{-+}f_0\eta$ also gives a quite good description. The possibility of more than one state contributing cannot be ruled out at all, and acceptances are quite different for different interpretations, such that the parameters given above have to be taken with care. A recent quark model calculation by Cahn et al. [49] predicts very small values for $\Gamma_{\gamma\gamma}$ in the order of 0.001 – 0.01 keV for pseudotensor $q\bar{q}$ states. If this turns out to be true, one needs other interpretations for the signals usually assigned to π_2 and η_2. In the flux tube model, hybrid states with correct quantum numbers and decay characteristics are predicted in this mass range [50]. It will be interesting to observe how the situation develops.

7.4 Spin 1 Mesons

Two spin 1 states are seen in $\gamma\gamma$ experiments, with only low statistics, but consistently in 5 experiments reporting. Their spin 1 nature is identified by the presence in the single tag mode and the simultaneous absence in the no tag mode, a behaviour expected due to the Landau-Yang theorem. In the last years no more information has become available, such that the discussions in [44, 51] still are completely up to date. The numerical results are not really radiative widths (which are zero), but some limits taking into account the known Q^2 behaviour at $Q^2 = 0$ proportional to the squared coupling constant (see e.g.[44]); a fact which earns a note in the Particle Data Group listings [20]. The $f_1(1285)$ is seen in the final state $\eta\pi\pi$ and the $f_1(1420)$ in $K^0_S K^\pm\pi^\mp$, and an upper limit on the $f_1(1530)$ is available. The parity of the $f_1(1420)$ is not yet unambiguously settled, but its exotic nature is evident: As a 1^{++} it would be extra in the nonet (and too light for a radial excitation), and a 1^{-+} cannot be built by two spin **1/2** quarks. In the latter case a dynamic suppression of the coupling to the LT as compared to the TT polarisation state is necessary to describe the data [44]. The non-observation of the $f_1(1530)$ is not yet critical, because of its expected large $s\bar{s}$ component and the low sensitivity reached up to now. Also, there up to now is no measurement of the isovector a_1, which would be very comforting to have before drawing too strong conclusions.

8 Form factor measurements

In Quantum Electro- Dynamics (QED) one can compute electromagnetic transition amplitudes from first principles. Possible deviations from the expected behaviour are parameterized in terms of *vertex form factors*, scalar functions of Lorentz scalar quantities (e.g. invariant masses). Form factors are expected to be constant for pointlike particles, deviations may be created by finite size effects or strong final state interactions. Hadrons clearly are extended and composite objects, such that severe deviations from constancy are expected, as is well known for the nucleon electric and magnetic form factors and the (charged) pion form factor. The latter, describing the $\gamma^*\pi^+\pi^-$ vertex, is known to be dominated by the ρ resonance in the timelike region (for positive photon "mass squares" $q^2 > 0$), and is well approximated by the ρ pole tail also in the spacelike region ($q^2 < 0; Q^2 := -q^2 > 0$). This has lead to the hypothesis of Vector Meson Dominance (VMD), suggesting that photons interact with hadrons largely via intermediate virtual vector meson states. A pole form (from the vector meson propagator) is a natural parameterization of the Q^2 dependence: $F(Q^2) \propto 1/(1 + Q^2/\Lambda^2)$, where Λ can be identified with the vector meson mass (in the timelike region also the imaginary part $(-im\Gamma)$ due to its finite life time has to be taken into account). In the spacelike region, cross sections are smaller than the QED prediction; the slope b of the form factor at $Q^2 = 0$ can be interpreted as the effective mean charge radius of the pion: $r = \sqrt{6 \cdot b}$.

C parity conservation forbids the existence of an analogous vertex for neutral pions. The electromagnetic structure of the neutral pion can however be accessed in the coupling to *two* photons. This is described by the amplitude $T_{\mu\nu} = i \cdot \varepsilon_{\mu\nu\alpha\beta} \cdot q_1^\alpha q_2^\beta \cdot F(Q_1^2, Q_2^2)$ in terms of a single *transition form factor* $F(Q_1^2, Q_2^2)$. Here we are interested in the case $Q_2^2 = 0$, i.e. the Q^2 dependence of the transition of a π^0 to a real photon initiated by a virtual photon of mass Q^2. There is a third ansatz to describe meson-photon transition form factors: the model of Brodsky and Lepage [52], which is an interpolation between the aysmptotic QCD prediction at $Q^2 \to \infty$ and the PCAC prediction at $Q^2 \to 0$. Formally it has a pole form like the VDM, and the pole mass is related to the pseudoscalar decay constants by $\Lambda = 2\pi\sqrt{2}f_p$.

Experimentally, this form factor can be accessed by two methods: in the timelike region (for $-Q^2 = q^2 = (2m_e)^2 - m_{\pi^0}^2$) using conversion decay experiments ("Dalitz" decays $\pi^0 \to e^+e^-\gamma$) (see the review by Landsberg [53]), and in the spacelike region by single tag two photon experiments. Here one measures the π^0 formation rate as a function of Q^2 in the process $e^+e^- \to e^+e^{-\prime}\gamma\gamma^*(Q^2) \to e^+e^{-\prime}\pi^0$ at an e^+e^- storage ring, where the incoming electron is scattered to a large, observable angle ("tag") allowing the reconstruction of the photon's virtuality Q^2, whereas the positron emits a quasi real photon and remains unobserved in the beam pipe (or vice versa). Analogous measurements are possible for the other neutral pseudoscalar mesons, the η and η'. Both of these are already known to follow roughly a ρ pole, from measurements in the spacelike and timelike region (for a bibliography see [54]). New data exists from TPC/$\gamma\gamma$ [55] and CELLO [54]. The π^0 form factor is hitherto more or less unknown: Conversion decay experiments performed during 30 years [20] could not even decide on the sign of the form factor slope at $Q^2 = 0$. From a theoretical point of view, many different ansatzes (VDM, quark model, current algebra, QCD interpolation) clearly need a positive slope (with respect to q^2, i.e. negative w.r.t. Q^2), and a verification of the latest negative slope measurement [56] would be desasterous [57]. The results of the new comprehensive analysis of the π^0, η and η' form factors in the spacelike region by the CELLO experiment [54, 32, 47] are very well described by

pole forms. With the help of the much larger Q^2 lever arm in this experiment, the confusing situation in the π^0 case is clearly resolved and in good agreement with theoretical expectations. Pole masses (effective interaction radii) [pseudoscalar meson decay constants] are measured to be 748 ± 30 MeV (0.65 ± 0.03 fm) [84 ± 3 MeV] for the π^0, 839 ± 63 MeV (0.58 ± 0.04 fm) [94 ± 7 MeV] for the η, and 794 ± 44 MeV (0.61 ± 0.03 fm) [89 ± 5 MeV] for the η'. Thus for all pseudoscalar mesons and all models the measurement gives meaningful results in the expected range. We have to consider finite size effects, vector meson dominance and the QCD interpolation formula all as dual descriptions of the low Q^2 behaviour, there is no way of distinguishing between these ansatzes. An extension to higher Q^2 as well as to double tag measurements would be very interesting.

Not much is known about the form factors of other meson nonets. In general, these are much more complicated because the number of independent form factors (related to independent helicity amplitudes) is larger than one.

9 Exclusive final states – vector meson pairs

One of the most striking effects found in two photon reactions is the large cross section for $\gamma\gamma \to \rho^0\rho^0$ below threshold (for reviews about $\gamma\gamma \to VV'$ see e.g. [15]). The much lower $\rho^+\rho^-$ cross section rules out a single resonance interpretation; both isospin 0 as well as 2 amplitudes and their interference must be present. This is of special importance since such a feature can naturally be explained by 4 quark states [58, 59] which have been predicted in this mass region in the MIT bag model [60]. In the ansatz of Achasov et al.[58] only spin 2 resonances are needed, whereas Li and Liu describe the data by spin 2 and spin 0 states. For further theoretical details see [61] and references therein.

Experimental spin parity analyses of the $\rho\rho$ enhancement are controversial, it may be 0^+ and/or 2^+ [15]. Whereas a recent ARGUS analysis [62, 16] claims the dominance of the 2^+, helicity 2 amplitude, the preliminary result of CELLO [17] requires next to the 2^+ also a 0^+ contribution in the same order of magnitude, in agreement with former analyses. Note that both, 0^+ and 2^+ can couple to two 1^- (photons, $\rho's$) states in S-wave. A recent, not yet published ARGUS partial wave decomposition of the $\rho^+\rho^-$ cross section [63] shows the same qualitative features as the CELLO result: Both (2, 2) and (0, 0) components are needed, with a hint of a structure ($f_2(1270)$?) at low masses. A recent spin parity analysis of the reaction $\gamma\gamma \to \omega\rho$ by CELLO [18] also did not confirm a dominance of the (2, 2) wave. This final state is best described by a mixture of many different amplitudes.

Evidence has been presented for an anomalously large cross section for charm quarks (inclusive D^* mesons, $D^0\bar{D}^0$ pairs) by TASSO [64], but not confirmed by CELLO [14] and TPC/$\gamma\gamma$ [65].

10 Summary and Conclusions

In summary, even long after the shutdown of DORIS and PETRA we still obtain interesting results. An explanation for the relativly long time delay is the fact that two-photon analyses are complicated and need a very detailed understanding of the detector, reconstruction and simulation software. One fact experienced at CELLO was that just due to this heavy needs

many bugs have been located and corrected and many improvements installed - which finally are interesting for every member of the collaboration - also for those who are interested in "high energy physics". Two photon experiments have provided many results in the last ten years, answered many questions, but also provided new questions. In almost all the different areas, higher statistics is urgently needed. It is comforting to see that TRISTAN now contributes, and other existing apparatus should be used more extensively to continue this line of research - ARGUS at DORIS II, CLEO II at CESR and eventually LEP experiments. If you want, this type of experiment is somehow more interesting than most of the analyses performed up to now at LEP: there are no Standard Model predictions which prove to be so reliable, and the chance to observe something unexpected or something we simply don't know is not so small.

11 Acknowledgements

I like to thank the organizers of this workshop for their excellent work creating such a pleasant and creative atmosphere. Especially I want to mention Prof. L. Montanet for his interest in this line of research and the organization of a whole two-photon session at this Moriond workshop.

The material presented in this talk is a short summary of the experience I gained at the II. Institut für Experimentalphysik of the University of Hamburg at DESY, where I worked the last 8 years in the PLUTO and CELLO Collaborations and contributed significantly to many of the results presented here. I want to take this opportunity to thank all those who made this time very comfortable and constructive: my colleagues from FCE, in particular J. Ahme, V. Blobel, P. Bussey, H. Fenner, J. Harjes, S. Lumsdon, J.H. Peters and O. Podobrin for the excellent and fruitful collaboration; and Prof. H. Spitzer and the Bundesministerium für Forschung und Technologie for financial support (FKZ05 4 HH 23 P).

REFERENCES

[1] D. Amati, these proceedings
[2] M. Chiba, these proceedings
[3] Procs. VIIth Int. Workshop on $\gamma\gamma$ Collisions, Paris 1986, Ed. A. Courau and P. Kessler, World Scientific
[4] Procs. VIIIth Int. Workshop on $\gamma\gamma$ Collisions, Shoresh (Israel) 1988, Ed. U.Karshon, World Scientific
[5] H. Kolanoski, Springer Tracts in Modern Physics, 105:187, 1984
[6] H.Kolanoski, P.Zerwas, in *High Energy Electron and Positron Physics*, editors A. Ali and P. Söding, p.695
[7] J. Olsson, Procs. 1987 Int. Symp. on Lepton and Photon Interactions at High Energy, Hamburg 1987, Ed. W. Bartel and R. Rückl, Nucl. Phys B (Proc.Suppl.) 3 1988, p. 613
[8] Ch. Berger, W. Wagner, Phys. Rep. 146 (1987) 1
[9] R.N. Cahn, Procs. 1989 Int. Symp. on Lepton and Photon Interactions at High Energy, Stanford, CA, 1989
[10] L.Landau, Dokl.Akad.Nauk.SSSR 60(1948)207;
C.N.Yang, Phys.Rev. 77(1950)242
[11] V.M.Budnev, I.F.Ginzburg, G.V.Meledin, V.G.Serbo, Phys.Rep. 15C(1975)181
[12] P. Bussey, these proceedings

[13] TPC/$\gamma\gamma$ Coll., H. Aihara et al., Phys. Rev. D 41 (1990) 2667
[14] CELLO Coll., H.J. Behrend et al., DESY-91-006, subm. to Z. Phys. C
[15] A. Nilsson, in [4], p. 261,
U. Maor, in [4], p. 282
A. Levy, Procs. XXIV. Int. Conf. on High Energy Physics, p. 655, Munich 1988, Eds. R. Kotthaus and J.H. Kühn, Berlin: Springer 1988
P.M. Patel, in [29], p.477
M.T. Ronan, in [29], p.494
G. Tsipolitis, in [30], p. 139
N.N. Achasov, G.N. Shestakov, in [30], p. 195
[16] B. Boštjančič, these proceedings, in[31]
[17] M. Feindt, J. Harjes, DESY 90-146, to be published in
[18] CELLO Coll., H.J.Behrend et al., Phys. Lett. B257 (1991) 505 [31]
[19] V. Blobel, *Unfolding in High Energy Physics*, Procs. 1984 CERN School of Computing, Aiguablava, Spain
[20] Particle Data Group, Phys. Lett. 2399 (1990) 1
[21] J. Field, F. Kapusta, L. Poggioli, Phys. Lett. 181B (1986) 362; Z. Phys. C36 (1987) 121; J. Field, in [4], p. 349
[22] J.H.DaLuz Viera., J.K. Storrow, Manchester Preprint MC TH 90/25
[23] T. Walsh, Contribution to the 25. Int. 25. Int. Conf. on High Energy Physics, Singapore 1990
[24] AMY Coll., T. Sasaki et al., Phys. Lett. B252 (1990) 491
[25] M. Drees, R.M. Godbole, Phys. Rev. Lett. 61 (1988) 682; Phys. Rev. D39 (1989) 169; Nucl. Phys. B339 (1990) 355
[26] AMY Coll., R. Tanaka et al., *Evidence for Hard Scattering of Hadronic Constituents of Photons in Photon-Photon Collisions at TRISTAN*, KEK-Preprint May 1991, subm. to Phys. Rev. Lett.
[27] T.H. Burnett and S.R. Sharpe, *Non-Quark-Model Mesons*, DOE-40423-04, to be published in Ann. Rev. Nucl. Part. Sci.
M.S. Chanowitz, LBL-29347, to be published in Procs. PANIC XII, MIT 1990
[28] M. Poppe, Int. J. Mod. Phys. 1 (1986) 545; G. Gidal (in[29]); articles in [4]
[29] Procs. BNL Workshop on Glueballs, Hybrids and Exotic Hadrons, Upton, New York 1988, AIP Conference Proceedings No. 185
[30] Procs. III. Int. Conference on Hadron Spectroscopy, Ajaccio (France) 1989, éditions Frontières
[31] Procs. Rheinfels '90 Workshop on the Hadron Mass Spectrum, St.Goar (Germany) 1990, in press
[32] J.H. Peters, Ph.D. thesis, DESY-FCE-90-01
[33] CLEO Coll., T. Jensen et al., DOE/ER/01545-429, 1989
[34] B. Bostancic, these proceedings
[35] J. Bienlein, in [29], p.486
[36] A. Lundin, H. Snellman, Phys. Lett B202 (1988) 251
[37] J. Harjes, Ph.D. thesis, DESY-FCE-91-01
[38] CELLO Coll., H.J. Behrend et al., to be published

[39] ARGUS Coll., H. Albrecht et al., Z. Phys. C 48 (1990) 183
[40] D. Morgan, M.R. Pennington, Z. Phys. C 48 (1990) 623
[41] K.H. Karch, DESY-91-022, these proceedings
[42] see [17], M. Feindt, in [4]
[43] Z.P. Li, F.E. Close, T. Barnes, Phys. Rev. D43 (1991) 2161
[44] M. Feindt, in [29], p. 501
[45] N. Isgur, J. Weinstein, Phys. Rev. D41 (1990) 2236
[46] CELLO Coll., H.J. Behrend et al., Z. Phys. C 46 (1990) 583;
Crystal Ball Coll., D. Antreasyan et al., Z. Phys. C 48 (1990) 561
[47] M. Feindt, DESY 90-128, to appear in Procs. 25. Int. Conf. on High Energy Physics, Singapore 1990; CELLO Coll., contributed paper #533 to that conference
[48] Crystal Ball Coll., K.H. Karch et al., Phys.Lett. B 249 (1990) 353; K.H. Karch, DESY-90-117, and [41]
[49] J.D. Anderson, M.H. Austern, R.N. Cahn, Phys. Rev. D 43 (1991) 2094
[50] S. Godfrey, in [29], p. 373
[51] D.A. Caldwell, in [29], p.465
[52] S.J. Brodsky, G.P. Lepage, Phys. Rev. D24 (1981) 1808
[53] L.G.Landsberg, Phys.Rep. 128 (1985) 301
[54] CELLO Coll., H.J. Behrend et al., Z. Phys. C 49 (1991) 401
[55] TPC/$\gamma\gamma$ Coll., Phys. Rev. Lett. 64 (1990) 172
[56] H. Fonvieille et al., Phys. Lett. B233 (1989) 65
[57] L. Bergström, Stockholm Preprint USITP-90-04
[58] N.N.Achasov, S.A.Devyanin, G.N.Shestakov, Phys.Lett. 108B (1982) 134; Z.Phys. C16 (1982) 55; Z.Phys. C27 (1985) 99
[59] B.A.Li, K.F.Liu, Phys. Lett. 118B (1982) 435 and Erratum Phys. Lett. 124B (1983) 550; Phys. Rev. Lett. 51 (1983) 1510; Phys. Rev. D30 (1984) 613; Phys. Rev. Lett. 58 (1987) 2288
[60] R.L. Jaffe, Phys. Rev. D 15 (1977) 267, Phys. Rev. D 15 (1977) 281
[61] N.N. Achasov, in [31]
[62] ARGUS Coll., H. Albrecht et al., DESY 89-179
[63] G. Tsipolitis, Ph.D. thesis, DESY- F15-90-01 (1990)
[64] TASSO Coll., Z. Phys. C47 (1990) 499
[65] TPC/$\gamma\gamma$ Coll., M. Alston-Garnjost et al., Phys.Lett. B252 (1990) 499

Recent Crystal Ball Results On Resonance Formation in Photon-Photon Collisions

Karl-Heinz Karch
Deutsches Elektronen-Synchrotron DESY
D-2000 Hamburg 52, Germany

Representing the Crystal Ball Collaboration

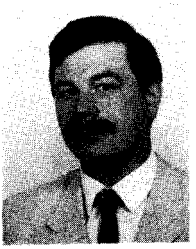

Abstract

The Crystal Ball detector has been used to analyse the formation of resonances in photon-photon collisions. The $\pi_2(1670)$ resonance has been observed in the $3\pi^\circ$ final state, as well as the $\eta'(958)$ and $X(1900)$ resonances in the $\eta\pi^\circ\pi^\circ$ final state. The $X(1900)$ decay distributions are consistent with the assumption that it is the $J^{PC} = 2^{-+}$ η_2 meson. Preliminary analyses of the 8, 10 and 12γ final states are presented. The tensor meson $f_2(1270)$ is the most prominent structure in the energy dependence of the total cross section $\sigma(\gamma\gamma \to \pi^\circ\pi^\circ)$, but close investigation of the differential cross section indicates the presence of a sizeable S wave contribution. This observation is consistent with a broad scalar meson $f_0(1250)$, degenerate in mass with the f_2. Indications for the $f_0(975)$ mesons have been found, too.

Introduction

The Crystal Ball detector[1] is a nonmagnetic segmented NaI(Tl) calorimeter with spherical geometry. It has good energy resolution ($\sigma_E/E = 2.7\%/\sqrt[4]{E/GeV}$) and good angular resolution ($\sigma_\Theta = 3^\circ$ to 1°) for electromagnetically showering particles, combined with a solid angle coverage of 93 % of 4 π. Four layers of cylindrical proportional tubes were placed inside the calorimeter to detect charged particles. While operating at the DORIS-II e^+e^- collider between 1982 and 1986, an integrated luminosity of 255 pb^{-1} was collected at an average beam energy of 5 GeV. Due to rather low trigger thresholds ($E_{thres} \approx 1\%$ to $10\% \times \sqrt{s}$) and an excellent photon detection efficiency, this experiment is well suited for the study of all-photon final states which are produced in photon-photon ($\gamma\gamma$) collisions. The scattered leptons have not been detected (no-tag analysis), thus the transverse momentum distribution of the detected events peaks at very small values.

Formation of 2^{-+} Resonances in $\gamma\gamma \to \pi^\circ\pi^\circ\pi^\circ$ and $\gamma\gamma \to \eta\pi^\circ\pi^\circ$

The two-photon formation of the $\pi_2(1670)$ meson has been observed in the three-pion final state[1,2]. The Crystal Ball collaboration has found clear evidence for the decay chain $\pi_2 \to f_2(1270)\pi^\circ \to \pi^\circ\pi^\circ\pi^\circ$. The data are well described by $J^{PC} = 2^{-+}$, and the two-photon partial width has been measured to be[1]:

$$\Gamma_{\gamma\gamma}(\pi_2) = (1.41 \pm 0.23 \pm 0.28)\ \text{keV}, \tag{1}$$

where the first error is statistical and the second systematic.

Recent analyses of the $\eta\pi\pi$ final state in $\gamma\gamma$ collisions by the Crystal Ball[3] and the CELLO collaborations[4] have found an enhancement of events at $M(\eta\pi\pi) \approx 1900\ \text{MeV}/c^2$. Under the assumption that these events come from one resonance $X(1900)$, the Crystal Ball collaboration has analysed the decay angular distributions and the mass distributions of the $\eta\pi^\circ$ and $\pi^\circ\pi^\circ$ subsystems, and has compared them to various models. Spin-parity 2^- is favoured by the data, with the decay isobars $a_2(1320)\pi^\circ$ and $a_0(980)\pi^\circ$ in the following ratio:

$$BR\left(X \to \left\{ \begin{array}{l} a_2\pi^\circ \\ a_0\pi^\circ \end{array} \right\} \to \eta\pi^\circ\pi^\circ\right) = \left\{ \begin{array}{l} (70 \pm 20)\% \\ (30 \pm 20)\% \end{array} \right. \tag{2}$$

We assume that X is an $I = 0, J^{PC} = 2^{-+}$ resonance, but this assignment can not be proven unambigiously because of the small number of events. The resonance sits on top of a smoothly falling background. Its parameters have been determined to be:

$$\begin{array}{rcl} M(X) & = & (1876 \pm 35 \pm 50)\ \text{MeV}/c^2 \\ \Gamma_{tot}(X) & = & (228 \pm 90 \pm 34)\ \text{MeV}/c^2 \\ \Gamma_{\gamma\gamma}(X)\, BR(X \to \eta\pi^\circ\pi^\circ) & = & (0.9 \pm 0.2 \pm 0.3)\ \text{keV}. \end{array} \tag{3}$$

A possible explanation for the state $X(1900)$ is that it is the η_2, an isoscalar partner of the π_2. Predictions have been obtained with quark model calculations[5] for the mass, total width and decay modes of the η_2 which are in agreement with our data. However, the two-photon width may be a problem: Recent $q\bar{q}$–potential model calculations[6] have found values which are in agreement with data for the 2^{++} mesons, but are two to three orders of magnitude too small for the π_2. If these calculations are correct, new explanations for the π_2 and $X(1900)$ have to be found.

Analysis of $\gamma\gamma \to 8,\ 10,\ 12\gamma's$

In an attempt to understand the background in the 6γ final state of the $\eta\pi^\circ\pi^\circ$ analysis, the Crystal Ball data have been searched for 8, 10 and 12 γ final states, which are created in $\gamma\gamma$ collisions. The well established reactions $\gamma\gamma \to \eta\pi^\circ$ and $\gamma\gamma \to \eta\pi^\circ\pi^\circ$, as well as the yet unobserved reaction $\gamma\gamma \to \eta\eta$, might contribute in those cases, where the η decays to $3\pi^\circ$. If two, four or six photons escape detection, these events are background sources for the 6γ final state. A large part of the events between 1100 MeV/c^2 and 1500 MeV/c^2 in the $\eta\pi^\circ\pi^\circ$ analysis can be explained by these processes.

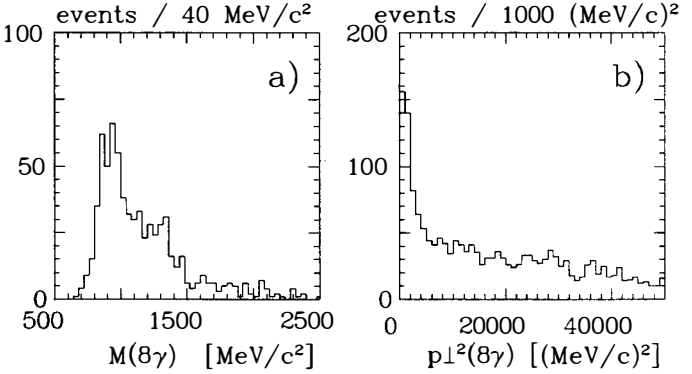

Figure 1: Invariant mass spectrum (a), with $p_t < 100$ MeV/c, and p_t^2 spectrum (b) for events with 8 photons.

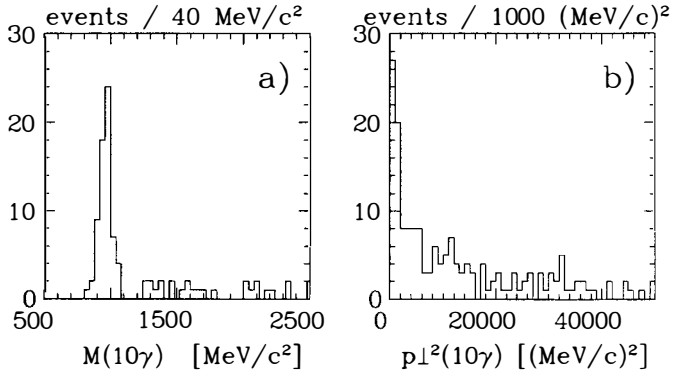

Figure 2: Invariant mass spectrum (a), with $p_t < 100$ MeV/c, and p_t^2 spectrum (b) for events with 10 photons.

The mass spectrum of events with 8 and 10 photons, which are well contained in the detector, and which have $p_t < 100$ MeV/c, are presented in Figs. 1a) and 2a), respectively. Because of the large combinatorial background, no attempt has been made to identify η's or π°'s. The corresponding p_t^2 spectra, without the cut on p_t, are displayed in Figs. 1b) and 2b). In both cases, an enhancement towards $p_t^2 = 0$ is evident, as expected for $\gamma\gamma$ formation.

In the 8γ sample, a rather large background is present, but indications for the $a_0(980)$

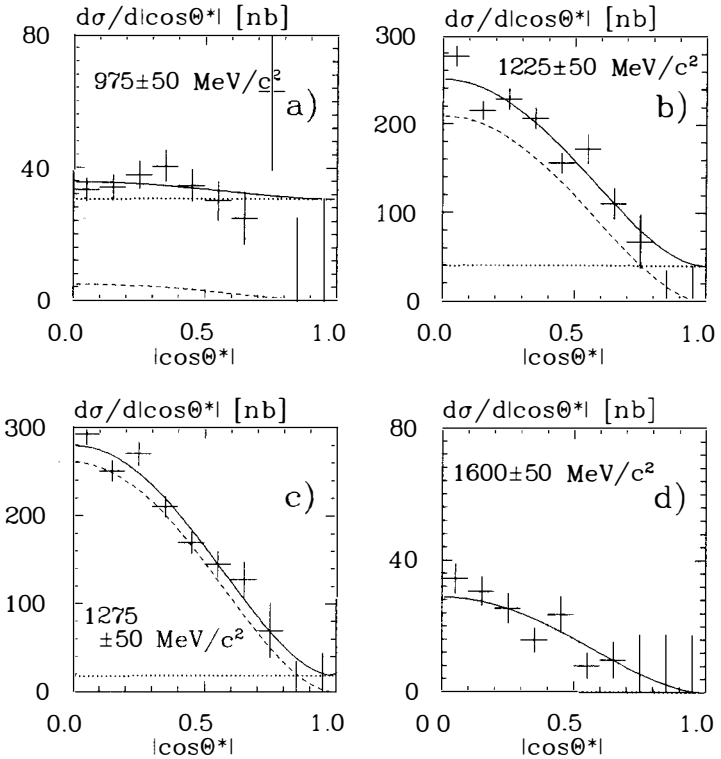

Figure 3: Differential cross section for four different mass intervals. The intervals are indicated in the figures. Crosses are data, the dashed curve is the D_2-wave contribution, the dotted curve the $S-$wave contribution and the full curve is the sum. The fit interval is $|\cos\Theta^*| < 0.7$.

($f_0(975), f_0(1250)$), and one Breit-Wigner for the $f_2(1270)$ to drive the D_2 wave. Typical fit results are displayed as curves in Fig. 4. These fits give the following resonance parameters:

$$\begin{array}{rcl} \Gamma_{\gamma\gamma}(f_0(975)) & = & (0.25 \pm 0.10)\ \text{keV} \\ \Gamma_{tot}(f_0(1250)) & = & (250 \pm 90)\ \text{MeV} \\ \Gamma_{\gamma\gamma}(f_0(1250))BR(f_0(1250) \to \pi^\circ\pi^\circ) & = & (1.2 \pm 0.3)\ \text{keV} \\ \Gamma_{\gamma\gamma}(f_2(1270)) & = & (3.1 \pm 0.2)\ \text{keV} \end{array} \quad \text{(preliminary)}. \qquad (5)$$

The systematic errors have not yet been determined.

The numbers in (5) are in agreement with our previously published results and upper limits. The possible broad scalar resonance $f_0(1250)$ with large $\Gamma_{\gamma\gamma}$ is in nice agreement with the combined (re-)analysis of CELLO and MARK-II data by Feindt and Harjes[10], as well as with the rather elaborate analysis of Crystal Ball and MARK-II data by Morgan

and $a_2(1320)$ mesons are visible in the mass spectrum. The 10γ sample is dominated by a peak of some 50 events at the $\eta'(958)$ mass. Monte Carlo studies give a detection efficiency of 0.3%. The number of events can be converted into a value for the two-photon partial width of the η'

$$\Gamma_{\gamma\gamma}(\eta') = (5.5 \pm 1.0 \pm 0.7) \text{ keV} \quad \text{(preliminary)}, \tag{4}$$

which is of about the same magnitude as found in previous measurements. Some 20% background may still be present (see Fig.3b). No evidence has been found for the $\gamma\gamma$ formation of 12γ final states.

Analysis of $\gamma\gamma \to \pi^\circ\pi^\circ$

The reaction $\gamma\gamma \to \pi^\circ\pi^\circ$ can be analysed more easily than the reaction $\gamma\gamma \to \pi^+\pi^-$, as no huge QED ($\gamma\gamma \to e^+e^-, \mu^+\mu^-$) background has to be subtracted. Furthermore, there is no Born term contribution to the $\pi^\circ\pi^\circ$ final state, thus it is easier to extract resonance parameters. We have analysed this reaction using the full data sample of the Crystal Ball experiment. Compared to the previously published analysis[7], we have gained a factor of 2.5 in luminosity, but due to higher trigger thresholds, the analysis can reconstruct $\pi^\circ\pi^\circ$ events only for $M(\pi^\circ\pi^\circ) > 800$ MeV/c^2. The selection efficiency was raised by a factor of 2.5 by including events in which the decay photons of a π° merge into one energy deposition. The π°'s can be reconstructed up to $E_\pi \approx 1.5$ GeV, and discriminated from single photon showers, by analysing the lateral distribution of the energy in the calorimeter; the second moment of the energy distribution is proportional to the squared mass of the decaying system. Thus, we have selected events with $p_t < 125$ MeV/c and two, three or four neutral energy depositions. Events with four energy depositions have been accepted, if two pairs of energy depositions (photons) were found, whose invariant mass $m_{\gamma\gamma}$ were compatible with the π° mass. Events with three energy depositions were required to have one $m_{\gamma\gamma}$ combination, which was compatible with m_{π°, and one high eneregtic ($E > 500$ MeV) deposition, which had the shape of an overlapping shower. Finally, the events with two high energetic depositions were required to be compatible with two overlapping showers.

We have found some 7100 $\pi^\circ\pi^\circ$ events. The background has been measured to be about 150 events. The majority of the events is clustered between 1100 and 1400 MeV/c^2, i.e. in the region of the well known $f_2(1270)$ resonance. In Fig. 3 we present the differential cross section $d\sigma(\gamma\gamma \to \pi^\circ\pi^\circ)/d|\cos\Theta^*|$ for various mass intervals. Θ^* is the polar angle between the beam axis and one π°, measured in the $\gamma\gamma$ rest frame. The measured total cross section $\sigma(\gamma\gamma \to \pi^\circ\pi^\circ)$, for $|\cos\Theta^*| < 0.7$, is displayed in Fig. 4.

There is an unresolvable ambiguity in the angular analysis of $\gamma\gamma \to \pi^\circ\pi^\circ$: without polarized beams the cross section exhibits no Φ dependence and thus any helicity-2 component can be expressed as a coherent sum of helicity-0 amplitudes[8]. However, Li, Close and Barnes[9] have shown that the spin-2, helicity-0 amplitude should be suppressed in $\gamma\gamma$ reactions. Thus we have fitted the differential cross section in each mass bin by a sum of spin-0 (S wave) and spin-2, helicity-2 (D_2 wave) intensities for $|\cos\Theta^*| < 0.7$. A large $S-$wave contribution is found in the bin centered at 975 MeV/c^2, which can be attributed to the $f_0(975)$. Dominance of the D_2 wave is found everywhere between 1000 and 1800 MeV/c^2, but a sizeable S wave is present up to 1350 MeV/c^2. This observation is consistent with a broad scalar resonance $f_0(1250)$.

To extract the maximum information from the data, we have employed a 2-dimensional fit to $d^2\sigma/dM_{\pi\pi}d|\cos\Theta^*|$. Two Breit-Wigner functions were used to drive the S wave

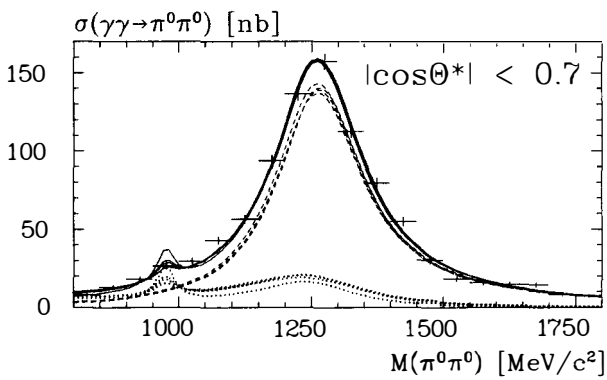

Figure 4: Total cross section $\sigma(\gamma\gamma \to \pi^\circ\pi^\circ)$ for $|\cos\Theta^*| < 0.7$. Crosses are data, dashed curves are the D_2-wave contributions, dotted curves the $S-$wave contributions and the full curve is the sum. The various curves have been obtained by shifting the mass bins by 12.5 MeV/c^2.

and Pennington[11]. Probably Chanowitz' conjecture[12] that the "true" scalar mesons are degenerate in mass with the corresponding tensors is correct.

References

1) D. Antreasyan et al. (Crystal Ball Coll.): Z. Phys. C48(1990)561.

2) H.J. Behrend et al. (CELLO Coll.): Z. Phys. C46(1990)583.

3) K. Karch et al. (Crystal Ball Coll.): Phys. Lett. B249(1990)353.

4) H.J. Behrend et al. (CELLO Coll.): Contributed paper no. 533 to the XXV Int. Conf. on High Energy Physics, Singapore, Aug. 2–8, 1990.

5) S. Godfrey and N. Isgur: Phys. Rev. D34(1986)899; R. Kokoski and N. Isgur: Phys. Rev. D35(1987)907.

6) J.D. Andersson, M.H. Austern and R.N. Cahn: preprint LBL-29059, May 1990.

7) H. Marsiske et al. (Crystal Ball Coll.): Phys. Rev. D41(1990)3324.

8) T. Oest et al. (JADE Coll.): Z. Phys. C47(1990)343.

9) Z.P. Li, F.E. Close and T. Barnes: preprint RAL-90-061 (1990).

10) M. Feindt and J. Harjes: preprint DESY 90-146 (1990), to appear in: Procs. Rheinfels Workshop on Hadron Mass Spectrum, St. Goar, Sept. 3–6, 1990.

11) D. Morgan and M.R. Pennington: Z. Phys. C48(1990)632.

12) M.S. Chanowitz in: Procs. VIII Int. Workshop on Photon-Photon Collisions, Shoresh, April 24–28, 1988, (World Scientific, Singapore 1988), p. 205.

MULTIHADRONIC FINAL STATES IN TWO-PHOTON INTERACTIONS IN CELLO.

P. J. Bussey
Department of Physics and Astronomy, University of Glasgow.

Abstract

The cross section and Q^2-dependence of the reaction $\gamma\gamma \rightarrow$ multihadrons have been measured using the CELLO detector at DESY, for visible final-state masses between 4 and 9 GeV. The data are well fitted by an incoherent sum of Generalised Vector Meson Dominance and Quark Parton Model terms, but at low Q^2 require the addition of a third component, in agreement with previous results from PLUTO. With and without this term, the GVDM cross section at $Q^2=0$ is found to be 200 ± 20 and 250 ± 25 nb, respectively.

Introduction.

This talk describes a study by the CELLO collaboration of multihadron production in photon-photon interactions. Fuller details can be found in 1). Previous experiments[2-4] have established the existence of at least two distinct subprocesses in the reaction

$$\gamma\gamma \rightarrow hadrons$$

at effective mass (W) values above a few GeV. For events whose tracks have low average momentum p_t transverse to the beam line, the reaction appears to be dominated by non-perturbative processes. At large values of Q^2 or p_t, however, a point-like component becomes increasingly important which is well described by the Quark Parton Model, where the two virtual photons couple to $q\bar{q}$ pairs. We therefore start by adopting the model

$$\sigma(\gamma\gamma \rightarrow X) = \sigma_0(W)F(Q_1^2)F(Q_2^2) + \sigma_{QPM}.$$

As the Q^2 of the virtual photons increases, the form factors $F(Q^2)$ become increasingly important. It is natural to attempt to represent these by some form of the vector meson dominance model. The Generalised Vector Meson Dominance Model (GVDM) was found by PLUTO[2,3] to be the most successful, although the TPC/2γ collaboration[4] favoured other forms. The "untagged" cross section σ_0 is found to be consistent with being constant for W greater than a few GeV. However, an additional third component to the cross section at low Q^2 and medium p_t was found to be required by PLUTO[3]. It should be noted that double tagged events are rare, and are not included in the present analysis. At most one virtual photon is normally found with a substantial non-zero value of Q^2.

2. Apparatus and data treatment.

The data used were taken in 1986 with the CELLO detector at PETRA, DESY, with an integrated luminosity of 86 pb^{-1}. The energy of each beam was 17.5 GeV. Full details of CELLO have been given elsewhere[5]. The central tracker gave a usable track measurement for $|\cos\theta| \leq 0.95$. Electromagnetic showers were measured in lead liquid argon calorimeters lying outside the thin superconducting solenoid, extending to $|\cos\theta| = 0.87$. Endcap calorimeters measured tagging electrons between 150 and 360 mrad to the beam, while forward tagging devices measured tagging electrons in a region which for the present analysis was defined as 55–80 mrad to the beam.

After some quality cuts on the tracks, events with a minimum of 4 charged tracks were selected for analysis, with the visible mass W_{vis} of charged plus neutral tracks exceeding

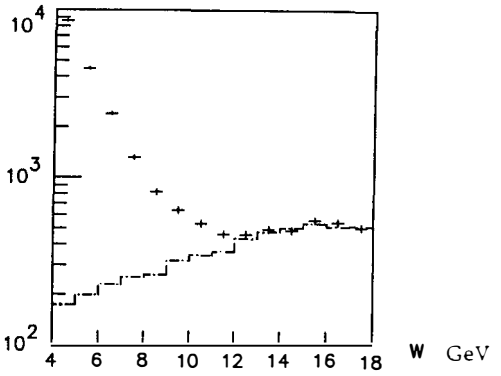

Figure 1: Numbers of accepted events per GeV with given visible mass W_{vis}, compared with the calculated annihilation background.

4 GeV. (Tags were excluded from the calculation of W_{vis}.) Cuts were also imposed to demand approximate charge and momentum balance on the event, whose origin was required to be within ± 4 cm of the interaction point.

Backgrounds to the process $\gamma\gamma \rightarrow$ multihadrons arise from a variety of sources. The largest of these was from e^+e^- annihilation, where events with initial-state radiation or much missing energy can resemble photon-photon events, and high-energy, low angle π^0s can simulate tags. The process was simulated using a standard generator with initial-state radiation and Lund 6.3 fragmentation; the events were passed through a detector simulation and the same selection cuts as the data. The resulting W_{vis} distribution is shown in fig. 1. It can be seen that without any further renormalisation, the annihilation background accounts well for the total observed data above $W_{vis} = 12$ GeV. The background varies from 5% of the total events at $W_{vis} = 4$ GeV to approximately 50% at 9 GeV. It was subtracted from the various histograms on a bin-by-bin basis; the error bars in all plots take the background subtraction into account. Other backgrounds come mainly from beam-gas and beam-pipe collisions. These were evaluated and subtracted in a standard way.

Table 1: Final numbers of events. The numbers of data events include the background.

Tagging region	Q^2 range $(\mathrm{GeV/c})^2$	$< Q^2 >$	Data	Background
Untagged	0.–0.3	0.1	15610	1859
Forward	0.6–1.8	1.0	371	30
Endcap	4–28	12.7	302	54

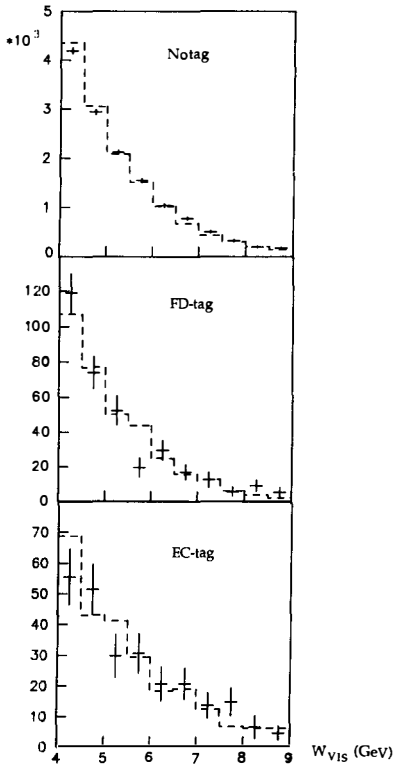

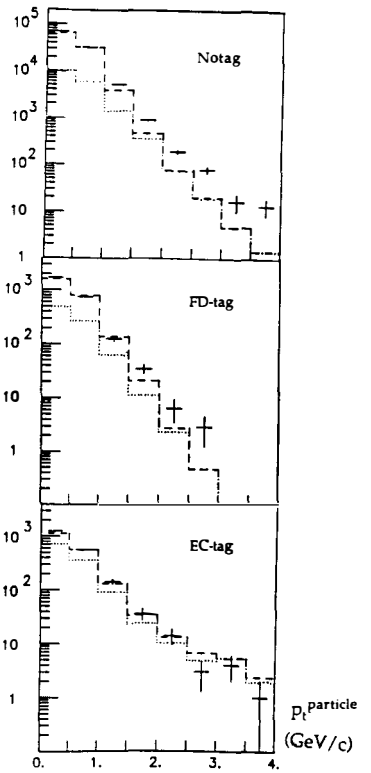

Figure 2: Distributions of W_{vis} for the three Q^2 ranges compared with GVDM+QPM.

Figure 3: Inclusive particle p_t distributions for the three Q^2 ranges (events / 0.5 GeV/c), compared with GVDM+QPM (dashed) and QPM alone (dotted).

The final numbers of events with (i) no tag (ii) forward tag (iii) endcap tag are shown in Table 1. The events were subjected to a thrust analysis in the centre of mass frame of the observed tracks. From this, the tracks in each event were divided into two "jets", whose transverse momentum p_t^{jet} relative to the photon-photon direction was calculated.

3. Results.

Some kinematic features of the events are shown in figs. 2–4, compared with the predictions of theory. The hadronic component to the cross section was simulated by generating parton-parton pairs in the $\gamma\gamma$ centre of mass frame and allowing them to fragment with a fragmentation width σ=450 MeV/c. GVDM form factors were included; the events were subsequently reweighted when other form factors were required. These

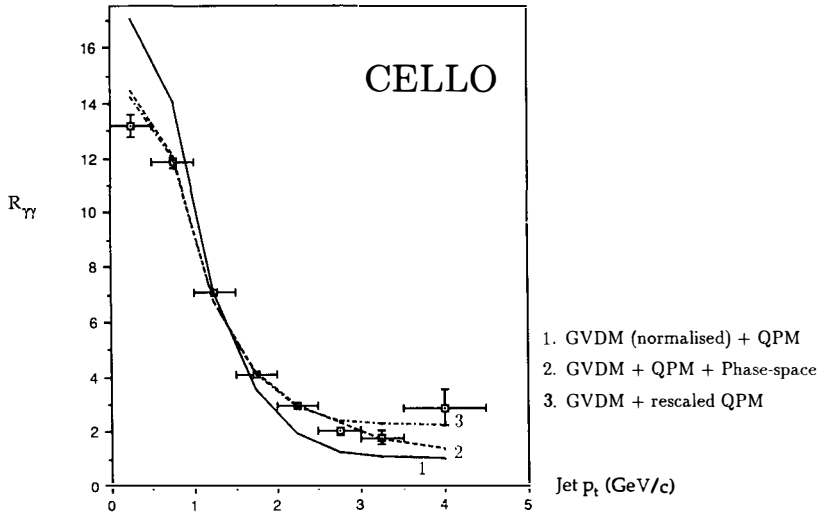

Figure 4: p_t^{jet} distribution for the untagged data. Plotted is the ratio $R_{\gamma\gamma}$ between the observed cross section and that of QPM alone.

and the generated QPM events were then passed through a detector simulation and event cuts, and plotted in the normal way. Although the fragmentation width is broader than normal, the data are well fitted by it at small p_t and seem to require some such value, as found by PLUTO. We find, however, that at higher transverse momenta the data do not fit the model GVDM+QPM, even if the normalisation of the GVDM is allowed to vary. The p_t^{jet} distributions in particular display an excess above 1.5 GeV/c in the untagged data which is much less evident or absent in the tagged data (fig. 5). The distribution of the jet angle (thrust axis) shows this effect equally clearly. Apart from this, the model GVDM+QPM gives a good general description of the data.

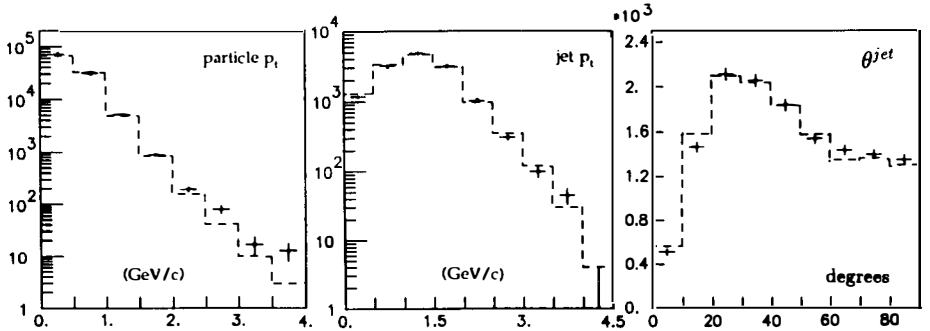

Figure 5: Kinematic features of the untagged data after inclusion of a third component (a higher QPM cross section in this case).

Table 2: Cross sections σ_0 in nb required to fit the measured data at varying Q^2 using the models quoted. No third component is included in the fit of the untagged data; errors are statistical only.

Process	Untagged	Forward tag	Endcap tag
GVDM	252±2	229±16	225±26
VMD	264±2	341±24	633±73
ρ-pole	271±2	498±35	2982±343

We have been unable to model fully the third component. It is possible to fit all distributions except thrust by either (a) scaling up the QPM component (fig. 6) or (b) including a phase space term weighted as $1/W$. However the observed thrust lies in between these two models. It can be accurately modelled if 3- and 4-jet processes are generated according to the recipe of PLUTO[3]; however these models do not give an adequate description of the other features of the data. We conclude that some multi-jet model is likely to be needed to fit the data, but that a suitable model has not yet been identified.

The Q^2 behaviour of the hadronic term was now investigated. Table 2 shows the value of σ_0 which is required to fit the hadronic cross section in the various Q^2 regions using (i) GVDM (ii) VMD (i.e. GVDM without the continuum term) and (iii) a simple ρ pole. Of these models, only GVDM gives consistent results — i. e. σ_0 constant with Q^2. 10% systematic errors should be taken on these numbers; the conclusion is unchanged even if the systematic errors are treated as random between the different Q^2 regions. To minimise model-dependency, we quote an untagged hadronic cross section of 250±25 nb obtained from the untagged GVDM data. This includes the "third component", estimated at 20% of the hadronic cross section at $Q^2 = 0$. Our results agree well with PLUTO, but show disagreement with TPC/2γ, who find that GVDM+QPM fails to fit their data as a function of Q^2 and quote a somewhat higher σ_0 value based on a VMD+QPM fit.

References.

1) S. J. Lumsdon, Ph. D. Thesis, Glasgow University, Dec. 1990; DESY preprint 91–006.
2) PLUTO Collaboration, Ch. Berger et al., Z. Phys. **26C** (1984) 191;
Z. Phys. **26C** (1984) 353; Phys. Lett. **149B** (1984) 421
3) PLUTO Collaboration, Ch. Berger et al., Z. Phys. **33C** (1987) 351
4) TPC/2γ Collaboration, H. Aihara et al., Phys. Rev. **41D** (1990) 2667
5) H. J. Behrend et al., Physica Scripta **23** (1981) 610

RECENT RESULTS ON TWO PHOTON PROCESSES FROM THE VENUS EXPERIMENT

Masami Chiba
Department of Physics, Tokyo Metropolitan University
Minami Ohsawa 1-1, Hachioji-shi, Tokyo, 192-03, Japan
The VENUS Collaboration

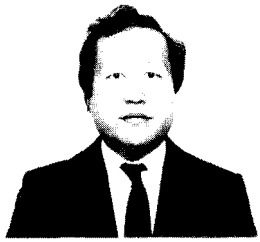

ABSTRACT

Recent results (preliminary) on two photon processes from the VENUS experiment at the TRISTAN are reported. Two photon coupling widths of $f_2(1270)$ and $\chi_{c2}(3555)$ have been measured as $\Gamma_{\gamma\gamma}(f_2)=2.3\pm0.1$keV and $\Gamma_{\gamma\gamma}(\chi_{c2})<4.2$keV at 95% C.L., respectively. We present the photon structure function F_2 with respect to the Q^2 between 32 and 150$(GeV/c)^2$ with the average of 58$(GeV/c)^2$.

1.Introduction

Two photon processes in e^+e^- collider yield unique opportunity to measure characteristics of particles. Two photon coupling strengths of mesons give important informations for the quarks and the quark wave function in the potential.[1] In the no tagging condition of scattered e^+ or e^-, we have measured the two-photon widths of $f_2(1270)$ and $\chi_{c2}(3555)$. Deep inelastic scattering of e^+ or e^- on nearly real photon has been also measured at large Q^2. We report their preliminary results. The reactions were detected by the VENUS detector[2),3),4),5)] in the TRISTAN e^+e^- storage ring, KEK at the c.m. energy 54-64GeV with the average of 58GeV.

2. Two photon coupling widths of $f_2(1270)$

Two-photon coupling width of $f_2(1270)$ was measured by detecting a $\gamma\gamma\to f_2(1270)\to\pi^+\pi^-$ process. The integrated luminosity was $50pb^{-1}$. The invariant mass distribution of the two-prong events was got in the assumption that the detected particles were pions. In order to get the cross section of $\gamma\gamma\to\pi^+\pi^-$, we subtract the QED processes $\gamma\gamma\to\pi^+\pi^-$ and $\gamma\gamma\to\mu^+\mu^-$ (F.A.Berends et al.[6)]). The QED processes were dominant in $M_{\pi^+\pi^-}>2GeV/c^2$. The result is shown in Fig.1(a). The detector acceptance is determined by a Monte-Carlo simulation using an event generator based on J.A.M.Vermasseren.[7)]

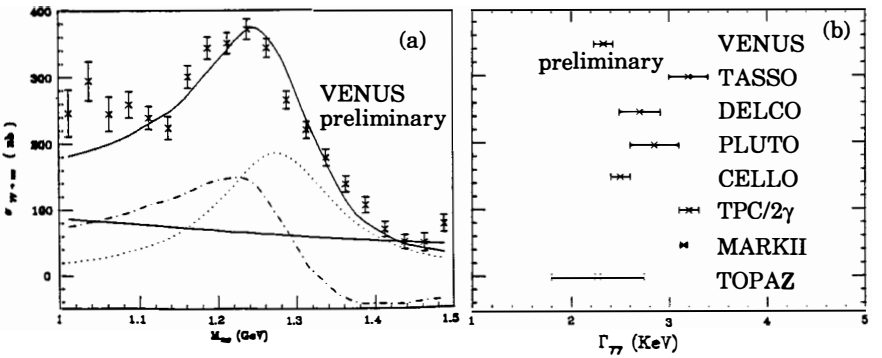

Fig.1 (a)$d\sigma(\gamma\gamma\to\pi^+\pi^-)/dM_{\pi^+\pi^-}$. The data are fitted by a Born approximation (solid curve), a Breit-Wigner (dotted curve), the interference (dotted-dash curve) and the sum of them (solid curve). (b)$\Gamma_{\gamma\gamma}(f_2(1270))$ compared with previous measurements.

In the fitting of the shape we express the cross section as:

$$\sigma=B+\Gamma_{\gamma\gamma}R+\sqrt{B\Gamma_{\gamma\gamma}}\cos(\phi-\phi_0), \qquad (1)$$

where $\Gamma_{\gamma\gamma}$ and ϕ are fitting parameters as the two photon-coupling strength of $f_2(1270)$ and a mixing angle between the Born term B and the Breit-Wigner resonance R, respectively. ϕ_0 is a phase[7] depending on $M_{\pi^+\pi^-}$. R is expressed as:

$$R=8\pi(2J+1)\Gamma/((W_{\gamma\gamma}-M^2)^2+\Gamma^2M^2) \qquad (2)$$

We assume that the mass of f_2 resonance is M=1274MeV and the total width Γ=185MeV.[8] The fitting results were $\Gamma_{\gamma\gamma}$=2.3±0.1keV and ϕ=2.61±0.06rad. θ^* distribution of the pions for $\gamma\gamma\to\pi^+\pi^-$ in the $f_2(1270)$ region of $M_{\pi^+\pi^-}$=1.20-1.35GeV/c^2 was derived. θ^* is the polar angle of one of the decaying particles with respect to the $\gamma\gamma$ direction in the $\gamma\gamma$ center of mass system. The data was consistent with a $|Y_2^2(\cos\theta^*)|^2\propto\sin^4\theta^*$ behaviour as expected if helicity 2 dominates. The $\Gamma_{\gamma\gamma}(f_2(1270))$ is compared with other measurements[9] in Fig.1(b).

3. Search for χ_{c2} production

We have searched for a channel of $\gamma\gamma\to\chi_{c2}(3555)\to\gamma J/\Psi(3097)$, $\gamma J/\Psi(3097)\to l^+l^-$, where l is e or μ. The details will be consulted on elsewhere.[10] The total branching ratio is (0.93± 0.14)%[8] for each lepton flavour. However, so far, no measurements to obtain the two-photon coupling of the $\chi_{c2}(3555)$ has been reported by using this channel.

The data corresponding to the integrated luminosity of 62pb^{-1} at the c.m. were used for the present analysis. After suitable selections, 70 events remained. We show the distributions for the invariant mass difference $M_{+-\gamma}-M_{+-}$ in Fig.2(a) for the selected events, where $M_{+-\gamma}$ is the invariant mass for the system of the three particles and M_{+-} the one for the two charged particles. We selected events whose mass difference was between $M_{\chi c2}-M_{J/\Psi}$-0.15 and $M_{\chi c2}-M_{J/\Psi}$+0.15GeV/c^2. Fig.2(b) shows the M_{+-} distribution for the survived events. No prominent peak is observed near $M_{+-}=M_{J/\Psi}$. We made the cut $M_{+-}-M_{J/\Psi}<0.10$GeV/c^2. One event has been remained, and this is a candidate for the χ_{c2}. The background of 1.3±0.3 events were estimated by a Monte-Calro simulation.

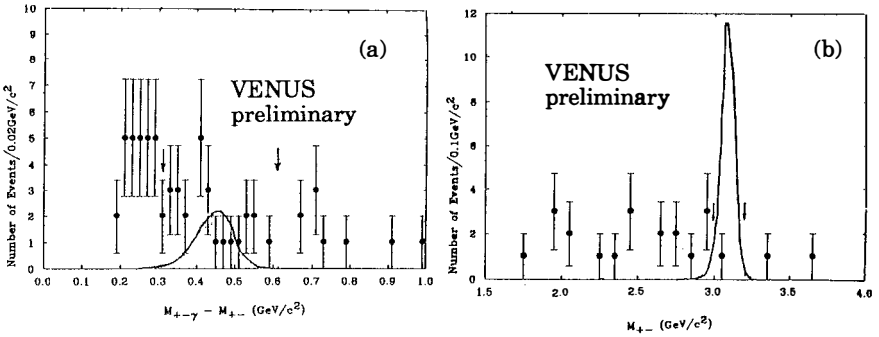

Fig.2 The distribution for the invariant mass difference (a)$M_{+-\gamma}$-M_{+-} and (b)the invariant mass M_{+-}. The curves are the estimation from the χ_{c2} Monte-Carlo calculation, where $\Gamma_{\gamma\gamma}$ is set to be 10keV. Arrows show the cut criteria.

We have made a Monte-Carlo calculation for estimating the yield for the χ_{c2} events. In that, the decay angular distributions for the χ_{c2} and the J/Ψ are assumed to be derived from a pure helicity-2 state in the production of χ_{c2}[11] and a pure E1 transition for $\chi_{c2}\rightarrow\gamma J/\Psi$.[12),13)] The yield of 1.20/(keV)x$\Gamma_{\gamma\gamma}$ events is estimated to be obtained. The curves in Fig.2(a) and (b) are the estimation for the χ_{c2} by the calculation set to $\Gamma_{\gamma\gamma}$=10keV.

We have obtained the upperlimit for $\Gamma_{\gamma\gamma}(\chi_{c2}(3555))$ of 4.2 keV at 95% C.L. by taking into account 1.0 events of background and the systematic error of totally 18%. The present result is consistent with the past measurements which give finite $\Gamma_{\gamma\gamma}(\chi_{c2}(3555))$ values from $\chi_{c2}\rightarrow\gamma\gamma$: 2.9+1.3-1.0±1.7keV(ISR)[14)]; 2.8±2.0keV (Crystal Ball)[15)] and the ones which give more stringent <1.0keV (95% C.L., CLEO)[16)] and the similar <4.2keV(95% C.L., TPC/2γ)[17)] limits from the two-photon process, in which the purely hadronic decay channels as $\chi_{c2}\rightarrow\pi^+\pi^-\pi^+\pi^-$, $k^+k^-\pi^+\pi^-$ so on have been used. The theoretical predictions[1),18),19)] are within range 0.5-2.0keV, which are consistent with the present result.

4. The photon structure function F_2

We measured the Q^2 dependence of the two-photon total hadronic cross section for the case that the Q^2 of one of the photon is high and the Q^2 of the other

kept small. In this case the cross section is usually expressed in terms of the structure functions of the photon. The scattering of a highly virtual photon on a quasi-real photon target can be thought as a deep-inelastic e^+e^- scattering.[20] The point like structure of the photon becomes visible at large Q^2. On the other hand at low Q^2 the target photon interact like hadrons (vector meson dominance, VMD picture).

The cross section of deep inelastic scattering into hadrons is expressed:

$$\frac{d\sigma}{dxdy} \approx \frac{16\pi\alpha^2 EE_\gamma}{Q^4}[(1-y)F_2(x,Q^2)], \qquad (3)$$

where the Lorentz invariant variables are used: $Q^2=-q_1^2=4EE'\sin^2(\theta/2)$, $p^2=-q_2^2\approx 0$, $x=Q^2/(2q_1q_2)=Q^2/(Q^2+W_{\gamma\gamma}^2)$, $y=q_1q_2/(p_1q_2)=1-(E'/E)\cos^2(\theta/2)$. The data corresponding to the integrated luminosity of $59pb^{-1}$ were used for the present analysis. After an event selection, 433 events were remained with $20<Q^2<270(GeV/c)^2$. The events were corrected by background estimated by a Monte-Carlo simulation. After subtracting a total of 44±3 background events, 389±3 events remained.

In the Monte-Carlo event simulation, event generator based on QPM(udsc) ($e^+e\rightarrow e^+e^-qq$ by F.A.Berends et al.)[6] and VMD were used. The produced quarks were fragmented into hadrons using LUND63 string fragmentation model.[21] Distribution of Q^2, energy and angle of the tagged electrons, W_{vis} and x_{vis} were well reproduced. In order to compare the data with a theoretical prediction, x_{vis} was changed to x using an unfolding techniques.[22]

We define a phenomenological parameter p_t as the transverse momentum of the virtual quark against the target photon. p_{t0} is the boundary of the photon behaving as hadrons ($p_t<p_{t0}$) and as point like ($p_t>p_{t0}$). We fix Λ at 0.2GeV[8] because of low sensitivity against F_2^{QCD}.

The data are fitted by analytic formula as: $F_2^{VDM}(x)=0.2\alpha(1-x)$, $F_2^{QPM_{(c)}}(x,Q^2)$ by V.M.Budnev et al.[23], and $F_2^{QCD_{(uds)}}(x,Q^2,t_{cut},\Lambda)$ by K.Kapusta.[24] The x distribution of F_2 compared with theoretical calculations are shown in Fig.3(a). The

p_{t0} is fitted to be 0.02±0.27. In order to compare the results of F_2 with previous data the contribution from the heavy flavour (c) is subtracted fom the data. The results at the $<Q^2>$ of 32, 52, 87 and 150(GeV/c^2)^2 are compared with other data[25] as shown in Fig.3(b).

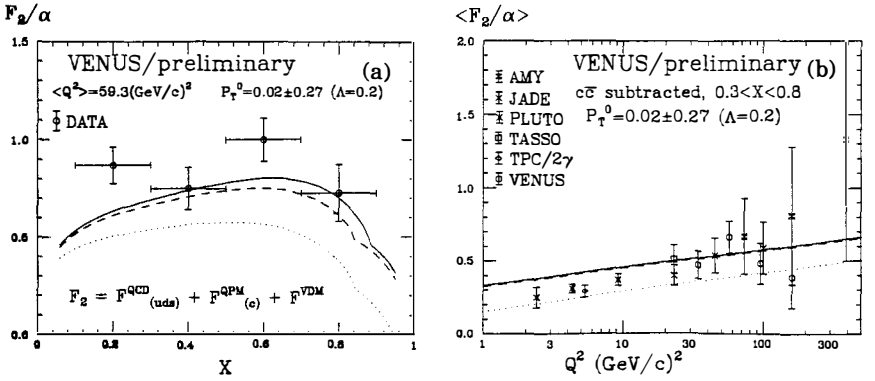

Fig.3 (a)F_2/α versus x for $<Q^2>=58(GeV/c)^2$. The curves are $F_2=F_2^{VDM}(x)+F_2^{QPM}{}_{(c)}(x,Q^2)+F_2^{QCD}{}_{(uds)}(x,Q^2,p_{t0},\Lambda=0.2GeV)$ with $p_{t0}=0.02\pm0.27$ GeV/c (fitted solid curve), 1.0GeV/c (dotted) and 0.1GeV/c (dashed). (b)The Q^2 dependence of $F_2(x,Q^2)$ of the structure function averaged over the intermediate x region between 0.3 and 0.8, compared with results from previous measurements. The curves are the predictions of $F_2^{VDM}+F_2^{QCD}{}_{(uds)}(\Lambda=0.2GeV)$. The QCD predictions are calculated for $p_{t0}=0.02\pm0.27GeV/c$ (solid curve), 1.0GeV/c (dotted) and 0.1GeV/c (dashed).

5. Conclusion

We have presented the preliminary results on two-photon precesses from the VENUS detector at TRISTAN. The two-photon coupling width of $f_2(1270)$ and $\chi_{c2}(3555)$ have been measured to be $\Gamma_{\gamma\gamma}=2.3\pm0.1$keV and $\Gamma_{\gamma\gamma}<4.2$keV at 95% C.L.. The photon structure function F_2 were measured at the Q^2 of 32-150(GeV/c^2)^2. They are consistent with $F_2=F_2^{VDM}(x)+F_2^{QPM}{}_{(c)}(x,Q^2)+F_2^{QCD}{}_{(uds)}(x,Q^2,t_{cut},\Lambda)$ model.

We gratefully acknowledge the outstanding efforts of the TRISTAN accelerator group and the support groups. The author deeply appreciates to the Yamada-Science-Promotion Fund for supporting him to attend the XXVIth RECONTRES DE MORIOND (HIGH ENERGY HADRONIC INTERACTIONS) held at Les Arcs, Savoie, France from March 17 to 23, 1991.

References

1)T.Appelquist, R.M.Barnett and K.Lane, Ann.Rev.Nucl.Sci.**28**,387(1978).
2)R.Arai et al., Nucl.Instr. and Meth.**A217**,181(1983).
3)Y.Hemmi et al.,Jpn.J.Appl.Phys.**26**,982(1987).
4)Y.Hemmi et al.,Nucl.Instr. and Meth.**A281**,462(1989).
5)T.Sumiyoshi et al.,Nucl.Instr. and Meth.**A271**,432(1988).
6)F.A.Berends et al.,Nucl.Phys.**B253**,441(1985);
Comput.Phys.Comm.**40**,285(1986); Comput.Phys.Comm.**40**,309(1986).
7)J.A.M.Vermaseren,Nucl.Phys.**B229**,347(1983).
8)Particle Data Group,Phys.Lett.**B239**,1(1990).
9)R.Brandelik et al.(TASSO),Z.Phys.**C10**,117(1981).
A.Courau et al.(DELCO),Phys.Lett.**147B**,227(1984).
Ch.Berger et al.(PLUTO),ZPhys.**C26**,199(1984).
H.J.Berend et al.(CELLO),Z.Phys.C**23**,223(1984).
H.Aihara et al.(TPC/2γ),Phys.Rev.Lett.**57**,404(1984).
I.Adachi et al.(TOPAZ),Phys.Lett.234,**185**(1990).
J.Boyer et al.(MARK II), phys.Rev.**D42**,1350(1990).
10)S.Uehara et al.(VENUS) will be submitted to elsewhere.
11)M.Poppe,Intern.J.Mod.Phys.**A1**,545(1986).
12)L.S.Brown and R.N.Cahn,Phys.Rev.**D13**,1195(1976).
13)M.Oreglia et al.,Phys.Rev.**D25**,2259(1982).
14)Baglin et al.(R704),Phys.Lett.**B187**,191(1987).
15)R.A.Lee,SLAC-Report-282(1985).
16)W.Y.Chen et al.(CLEO),Phys.Lett.**B243**,169(1990).
17)H.Aihara et al.(TPC/2γ),Phys.Rev.Lett.**60**,2355(1988).
18)L.J.Reinders,H.Rubinstein and S.Yazaki,Phys.Rep.**127**,1(1985).
19)W.Kwong and P.B.Mackenzie,Phys.Rev.**D37**,3210(1988).
R.Berbieri et al.,Nucl.Phys.**B154**,535(1979).
20)S.J.Brodsky,T.Kinoshita and H.Terazawa,Phys.Rev.Lett.**27**,280(1971);
T.F.Walsh,Phys.Lett.**35B**,121(1971).
21)T.Sjostrand,Comput.Phys.Commun.**39**,347(1986).
22)A.Backer,VI'th International Workshop on $\gamma\gamma$ collision,205(1986);
W.Bartel et al.(JADE),Z.Phys.**C24**,231(1984).
23)V.M.Budnev et al.,Phys.Rep.**C15**,181(1975).
24)K.Kapusta,Z.Phys.**C42**,225(1989).
25)Ch.Berger et al.(PLUTO),Phys.Lett.**B107**,168(1981);Phys.Lett.**B142**,111(1984);
Nucl.Phys.**B281**,365(1987).
H.J.Berend et al.(CELLO),Phys.Lett.**B126**,391(1983).
A.Aihara et al.(TPC/2γ),Phys.Rev.Lett.**58**,97(1987);Z.Phys.**C34**,1(1987).
M.Althoff et al.(TASSO),Z.Phys.**C31**,527(1986).
W.Bartel et al.(JADE),Z.Phys.**C24**,231(1984).
T.Sasaki et al.(AMY),Phys.Lett.**B252**,491(1990).

SPECTROSCOPY

FOUR-QUARK STATES AND $\Lambda\bar{\Lambda}$ PRODUCTION[1]

Winston Roberts
Lyman Laboratory of Physics
Harvard University
Cambridge, Massachusetts 02138, USA

We discuss the use of four-quark states as intermediates in the description of the process $p\bar{p} \to \Lambda\bar{\Lambda}$. In its present form, the model describes some of the observed features well, but fails to describe others.

[1]Work supported by the Natural Sciences and Engineering Research Council of Canada, and by the National Science Foundation under Grant #8714654.

1 Motivation

Among the many exotic hadrons allowed to exist by QCD, the four-quark states ($q^2\bar{q}^2$) have commanded a reasonable amount of attention. These states first came into being theoretically by way of duality arguments [1]. It was suggested that such states should be present in processes like $B_1\bar{B}_2 \to B_3\bar{B}_4$, shown in figure 1a. Subsequently, the properties of these proposed states were studied in various models: their masses, couplings to baryon-antibaryon systems (figure 1b) and meson-meson systems (figure 1c) were all estimated [2].

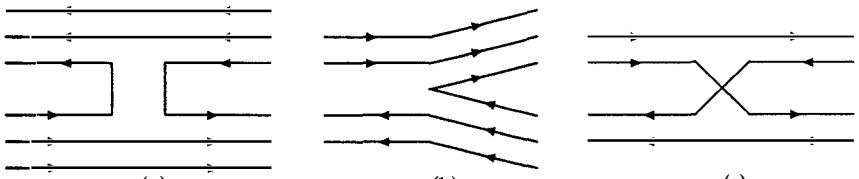

Figure 1: (a) $B_1\bar{B}_2 \to B_3\bar{B}_4$ via 4-quark state; (b) 4-quark state $\to B\bar{B}$; (c) 4-quark state $\to MM$.

In this note, we describe a model in which these states appear as intermediate states in the process $p\bar{p} \to \Lambda\bar{\Lambda}$. In section 2 of this article we briefly describe the model we propose, and the results we obtain are presented in section 3. We use section 4 to comment on a few aspects of our results, and to present our conclusions. A more thorough description of everything discussed herein is available in ref. [3].

2 The Model

The couplings of these states to baryon antibaryon pairs are obtained in the $^3P_0$ model [4], illustrated in figure 1b. For the meson meson contribution to the total decay widths of these states, we simply make the ansatz that these widths should be large enough to wipe out resonant effects, but not so large as to make these states useless for our purposes. Without fitting, we choose a meson meson width of 1 GeV for all states.

We calculate the differential cross section $\frac{\partial\sigma}{\partial\Omega}$, the polarization of the Λ P_i^Λ, and the spin correlation functions of the final state baryons C_{ij}, in terms of the spin matrix $\mathcal{M}$, where

$$\mathcal{M} = \begin{pmatrix} M_{++++} & M_{+++-} & M_{++-+} & M_{++--} \\ M_{+-++} & M_{+-+-} & M_{+--+} & M_{+---} \\ M_{-+++} & M_{-++-} & M_{-+-+} & M_{-+--} \\ M_{--++} & M_{--+-} & M_{---+} & M_{----} \end{pmatrix}, \tag{1}$$

The density matrix ρ is

$$\rho = \mathcal{M}\mathcal{M}^{\dagger}, \tag{2}$$

and the quantities of interest are given by

$$\begin{aligned} \frac{\partial\sigma}{\partial\Omega} &= \frac{2\pi^2 I(\theta)}{k^2} = \frac{2\pi^2 Tr(\mathcal{M}\mathcal{M}^{\dagger})}{k^2}, \\ P_i^{\Lambda} &= \frac{Tr(\mathcal{M}\sigma_i^{\Lambda}\mathcal{M}^{\dagger})}{I(\theta)}, \\ C_{ij} &= \frac{Tr(\mathcal{M}\sigma_i^{\Lambda}\sigma_j^{\bar{\Lambda}}\mathcal{M}^{\dagger})}{I(\theta)}. \end{aligned} \tag{3}$$

The σ^{Λ} are the Pauli spin matrices appropriate to the Λ and k is the momentum of $\bar{p}$.

To calculate the helicity amplitudes, we assume that Breit-Wigner forms are suitable for describing the scattering processes. For a single intermediate diquonium D of total angular momentum J, the scattering amplitude is

$$\tilde{M}_{J\ell\ell SS'}(E,k,k') = \frac{m_D A_{D\to p\bar{p}}(E,k,\ell,S) A_{D\to\Lambda\bar{\Lambda}}(E,k',\ell',S')}{E^2 - m_D^2 - i m_D \Gamma_D(E)}. \tag{4}$$

E is the total center of momentum energy, k, k' is the momentum in the initial or final state state, respectively, and m_D is the mass of the intermediate diquonium state. Details of the construction of the helicity amplitudes are given in ref. [3].

We take ISI and FSI into account by adopting the simple form used by Sopkovich [5]. We write a modified reduced matrix element $\tilde{T}^J_{\mu\nu}$, as

$$\tilde{T}^J_{\mu\nu} = \sqrt{S_i^J} T^J_{\mu\nu} \sqrt{S_f^J}, \tag{5}$$

where S_i^J and S_f^J parametrize the ISI and FSI interactions, respectively, with

$$S^J = \exp\left[\frac{-E\sqrt{\pi}V_0}{\mu k}\exp\left(\frac{-J(J+1)\mu^2}{k^2}\right)\right]. \tag{6}$$

E is the total center of mass energy, and k is the magnitude of the center of mass 3-momentum of the states involved. V_0 and μ are parameters that are determined by fitting the theoretical cross section to the experimentally measured value.

3 Results

Our results for the total and differential cross sections are shown in figures 2a and 2b, respectively. In the case of the latter, we find that the theoretical distributions do not reproduce all the features of the experimental distributions, although the general trends appear to be adequately described. All data are from ref. [6].

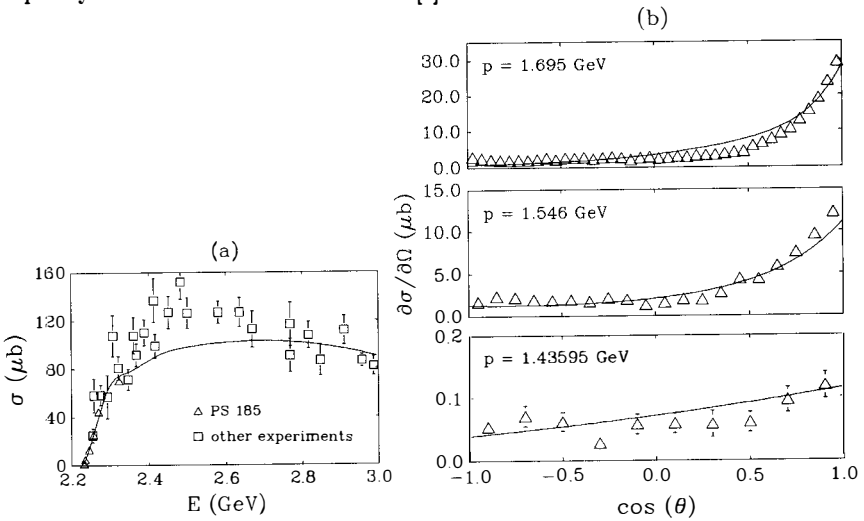

Figure 2: (a) Total cross section for $p\bar{p} \to \Lambda\bar{\Lambda}$; (b) Differential cross section for $p\bar{p} \to \Lambda\bar{\Lambda}$ at three different beam momenta.

Our predictions for some of the measurable spin variables are shown in figure 3. The singlet fraction (S) is exactly zero, and is predicted to have this value at all energies and angles. This prediction is understood by noting that the spectator diquark and antidiquark must each have both isospin 0 and spin 0. Thus, the spin of the $\Lambda\bar{\Lambda}$ pair must be the spin of the created pair of quarks which, in the $^3P_0$ model is 1. The singlet fraction is therefore identically zero. The experimental data are consistent with this. Note that the singlet fraction must be a positive number between 0 and 1, so that measurement of negative singlet fractions must be considered consistent with zero.

The model describes the polarization fairly well, though the predicted forward distribution differs from the measured one. C_{yy} and C_{zz} are also fairly well described by the model. However, C_{xx} and C_{zz} are not as well described. This, coupled with the failure of the model to describe

4 Conclusions

This model makes two predictions that will be easily tested at LEAR or SuperLEAR, or at similar colliders. The first is that the singlet fraction in the $\Lambda\bar{\Lambda}$ channel will be identically zero at all energies and angles. This prediction also holds true for production of $\Lambda_c\bar{\Lambda}_c$, $\Lambda_b\bar{\Lambda}_b$, etc. The second prediction is that in all processes of the type $B_1\bar{B}_2 \to B_3\bar{B}_4$, the contribution of high partial waves near the reaction threshold will be significant.

We conclude by noting that four-quark states may be useful in explaining some of the features observed in hyperon-pair production. We expect that similar features in other baryon-pair production processes will also be explainable in terms of four-quark states.

References

[1] J. L. Rosner, Phys Rev. Lett. 21 (1968) 950; Phys. Rep. 11C (1974) 189.

[2] See, for example, R. L. Jaffe, Phys. Rev. D15 (1977) 267, 281; Phys. Rev D17 (1978) 1444; W. Roberts, B. Silvestre-Brac and C. Gignoux, Phys. Rev. D41 (1990) 182; Phys. Rev. D41 (1990) 2258.

[3] W. Roberts, Harvard Preprint HUTP-90/A020, to appear in Z. Phys. C.

[4] See, for example, W. Roberts and B. Silvestre-Brac, Harvard Preprint HUTP-90/A031, submitted to Z. Phys. A.

[5] N. J. Sopkovich, Nuovo Cimento 26 (1962) 186.

[6] P. D. Barnes *et al.*, CERN preprint CERN PPE 90-169, submitted to Nucl. Phys. A, 1990; V. Flaminio, W. G. Moorehead, D. R. O. Morrison and N. Rivoire, *Compilation of Cross Sections III: p and $\bar{p}$ Induced Reactions*, CERN-HERA, 1984.

the forward distribution in the polarization, means that modifications are needed for this model to be more successful.

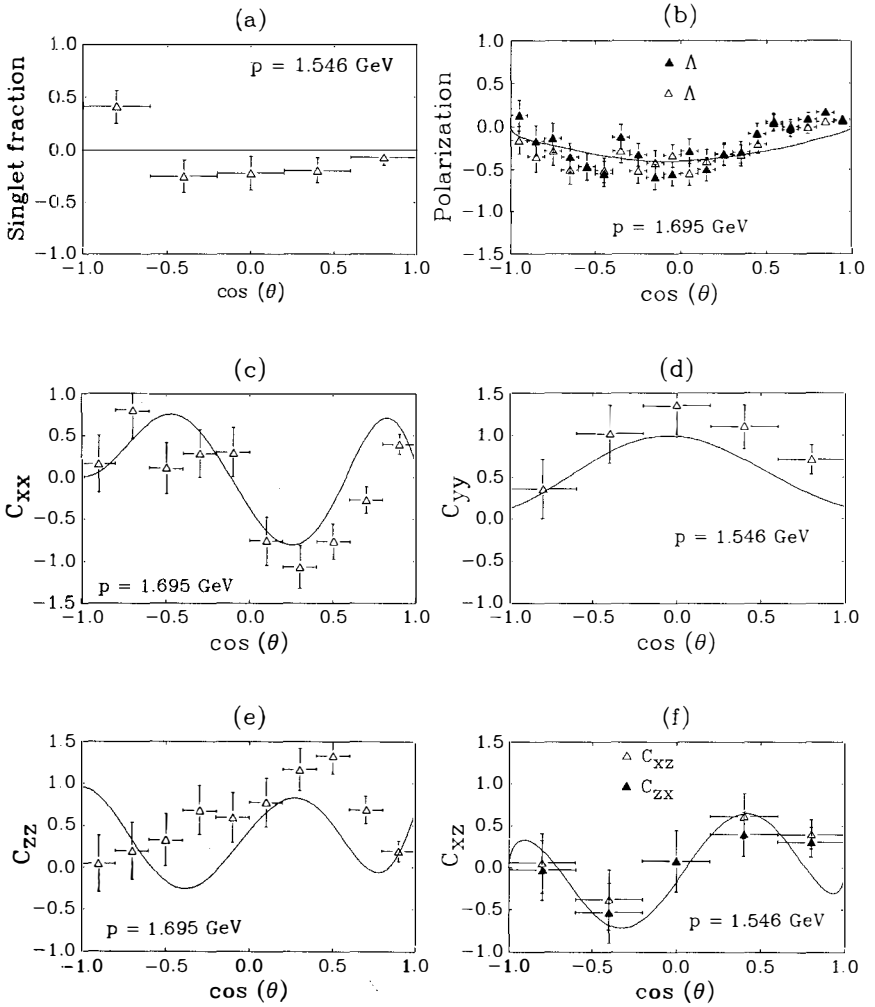

Figure 3: (a) Spin singlet fraction; (b) Polarization; (c) C_{xx}; (d) C_{yy}; (e) C_{zz}; (f) C_{xz}; of the $\Lambda\bar{\Lambda}$ pairs in $p\bar{p} \to \Lambda\bar{\Lambda}$.

HYPERON RADIATIVE DECAYS, THE α PARAMETER OF $\Sigma^+ \to p\gamma$ FIRST RESULTS FROM FERMILAB E761

Maurice Foucher
Yale University
Current Address: E761 MS219, Fermilab, Batavia IL 60510, U.S.A.

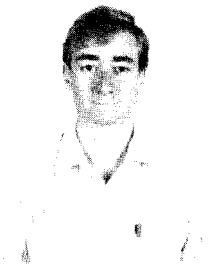

Abstract

A high statistics study of the hyperon radiative decay, $\Sigma^+ \to p\gamma$, has been performed in the Proton Center charged hyperon beam at Fermilab. A preliminary result for the α parameter for $\Sigma^+ \to p\gamma$ is presented. We find the α parameter to be -0.69 ± (0.11 statistical) ± (0.11 ± 0.11 systematic).

A high statistics study of one of the hyperon radiative decays, $\Sigma^+ \to p\gamma$, has been performed by the Fermilab E761 collaboration[1]. We report here a preliminary result for the α asymmetry parameter for $\Sigma^+ \to p\gamma$.

Hyperon radiative decays represent a class of baryon decays which require both weak and electromagnetic contributions. These decays test the interplay of electroweak and strong interactions as applied to the underlying quark structure of baryons. Hyperon radiative decays have been analyzed theoretically using single quark transitions, internal W exchange, penguin diagrams, long distance effects, and QCD sum rules.[2] Some of the diagrams that contribute to these decays are shown in Figure 1.

What is the α parameter in hyperon radiative decays? In the rest frame of a polarized Σ^+, the angular distribution of the decay proton with respect to the Σ^+ polarization direction is given by:

$$\frac{dN}{d\Omega} = \frac{A(\theta) N_0}{4\pi} [1 + \alpha P_\Sigma \cos\theta] \qquad (1)$$

where α is the asymmetry parameter we are measuring, $A(\theta)$ is the acceptance, P_Σ is the polarization of the Σ^+, N_0 is the total number of events, Ω is the solid angle, and θ is the angle between the proton momentum and the Σ^+ polarization direction.

Hyperon radiative decay experiments are difficult to perform. The branching ratio[3] of $\Sigma^+ \to p\gamma$ is 1.25×10^{-3}. The branching ratio[3] for $\Sigma^+ \to p\pi^\circ$ is 0.5157. Therefore the primary background occurs at a rate $\approx$400 times the signal. This provides a challenge to the trigger and the analysis. The α parameter[3] for $\Sigma^+ \to p\gamma$ is $-0.83 \pm .12$ based on 3 experiments[4] with a total of 297 events. The α parameter[3] for $\Sigma^+ \to p\pi^\circ$ is $-0.980 \pm .016$. Since the background has a large asymmetry it is important that the experimenters understand and control this background.

A schematic view of the experiment is shown in Figure 2. It consists of 3 spectrometers, one for each of the particles in the decay, $\Sigma^+ \to p\gamma$, a hyperon , a baryon , and a photon spectrometer. The hyperon spectrometer measures the Σ^+ momentum to 0.7% (σ). It is made up of 3 stations of silicon strip detectors (SSD)

and 1 magnet. The baryon spectrometer measures the proton momentum to 0.2%(σ). It is made up of 4 stations of proportional wire chambers (PWC) and 3 magnets. The angular resolution of both the hyperon and baryon spectrometers is ≈10μrad(σ). The photon spectrometer measures the photon position and energy. We measure the photon position by converting the photon in two steel plates, each 2.54 cm thick. The high energy charged component of the produced shower follows closely the original photon direction. We use transition radiation detectors (TRD) to detect this high energy component. The threshold of the TRD is about 2.5 GeV. Wire chambers are used to supplement the TRD.

An 800 GeV/c proton beam impinges onto the Cu target at a finite targetting angle of ±4 mrad horizontal, producing a 375 GeV/c polarized hyperon beam. The polarization is along the direction given by the cross product of the incident proton momentum and the outgoing Σ^+ momentum. We can reverse the targetting angle and thus reverse the polarization direction. This gives us 2 sets of data, spin up and spin down and allows us to cancel biases in the apparatus by averaging over them. The center of mass angular distribution of the proton is given by (1). We take the ratio of the difference over the sum of the spin up and spin down data. This yields

$$\alpha P_\Sigma \cos\theta \equiv A\cos\theta \qquad (2)$$

where A is defined as the asymmetry. We average over cosθ to determine A. From the measured asymmetries for both decay modes $\Sigma^+ \to p\pi^0$ and $\Sigma^+ \to p\gamma$ we find for α_γ

$$\alpha_\gamma = \frac{A_\gamma}{A_0}\,\alpha_0 \qquad (3)$$

where α_0 is -0.980 ± 0.016. We measure A_γ and A_0 from our data sample we collected in the 1990 Fermilab fixed target run. Shown in Figure 3 is the missing mass squared distribution from our full data sample assuming the decay $\Sigma^+ \to p + X$. After making reasonable track fitting and kinematic cuts, we find a value for A_0 = -0.1135 ± 0.0003 (statistical) ± 0.0120 (systematic). Our preliminary systematic error is taken from the scatter in the run to run measurements and probably can be decreased significantly.

From Figure 3 it is clear that the dominant background is $\Sigma^+ \to p\pi^o$. How do we separate $\Sigma^+ \to p\gamma$ from $\Sigma^+ \to p\pi^o$? Assuming the decay $\Sigma^+ \to p + X$ we project the missing neutral direction onto the photon spectrometer. We form a TRD χ^2 of the miss distance from the projected neutral track to the closest wire to the track. $\Sigma^+ \to p\gamma$ should have a low TRD χ^2. $\Sigma^+ \to p\pi^o$ should have a larger TRD χ^2 because of the finite opening angle of the photons from the π^o decay. We also require that there be a large amount of local energy in the photon calorimeter around the projected neutral track. Shown in Figure 4 is the missing mass squared distribution for TRD $\chi^2 < 100$ and TRD $\chi^2 > 200$ normalized in the mass squared region 0.0072 to 0.0100 GeV^2/c^4. The mass squared distribution with TRD $\chi^2 > 200$ is a good model to our background. A clear peak is seen at the mass squared of the photon.

We construct 4 regions;

signal	$-0.0040 < m^2_x < 0.0040$ GeV^2/c^4	TRD $\chi^2 < 100$,
background	$-0.0040 < m^2_x < 0.0040$ GeV^2/c^4	TRD $\chi^2 > 200$,
normalization	$0.0072 < m^2_x < 0.0100$ GeV^2/c^4	TRD $\chi^2 < 100$,
normalization	$0.0072 < m^2_x < 0.0100$ GeV^2/c^4	TRD $\chi^2 > 200$.

We define the signal fraction, f, to be the number of $\Sigma^+ \to p\gamma$ events in the signal region over the total number of events in the signal region. We find $f = 0.6767 \pm .0024$. The asymmetry in the signal region is made up of 2 terms, the asymmetry of $\Sigma^+ \to p\gamma$ times f and the asymmetry of the background times (1-f). If we invert this we get this expression for the asymmetry of $\Sigma^+ \to p\gamma$,

$$A_\gamma = \frac{A_s - (1-f)A_b}{f} \qquad (4)$$

where A_s is the asymmetry in the signal region and A_b is the asymmetry in the background region. We find $A_s = -0.087 \pm .008$ and $A_b = -0.103 \pm .007$. Thus we find $A_\gamma = -0.079 \pm .012$. Therefore we find for $\alpha_\gamma = -0.69 \pm (0.11$ statistical) $\pm (0.11 \pm$ 0.11 systematic.) This is based on 37816 ± 261 events. We have performed only preliminary systematics studies therefore we are quoting a range of 0.00 to 0.22 for the systematic error. We believe this is our best present estimate of the systematic

error.

We find for the α parameter for $\Sigma^+ \to p\gamma$ a value of -0.69 ± (0.11 statistical) ± (0.11 ± 0.11 systematic.) This is a preliminary result. There are many improvements that we foresee. If we can reduce our systematic error to essentially zero and fully exploit the statistics of our sample the smallest statistical error we can expect is ±0.07.

This work was supported by the U. S. DOE under contract #DE-AC02-76CH03000.

REFERENCES

1. Members of the Fermilab E761 collaboration: R. Carrigan, P. S. Cooper, H. Gottschalk, J. Lach, A. Morelos (Graduate student from CINVESTAV-IPN) of Fermilab; Li Yunshan, Tang Fukun, Lang Pengfei, Li Chengze, Shi Huanzhang, Zhao Wenheng, Dai Lisheng, Zheng Shuchen, Zhong Yuanyuan, Yan Jie of Institute of High Energy Physics Beijing, PRC; N. F. Bondar, A. S. Denisov, V. L. Golovtsov, V. T. Grachev, A. V. Khanzadeev, V. M. Samsonov, N. K. Terentyev, I. I. Tkatch, L. N. Uvarov, A. A. Vorobyov of Leningrad Nuclear Physics Institute Leningrad, USSR;P. A. Goritchev, M. A. Kubantsev, V. N. Lebedenko of Institute of Theoretical and Experimental Physics Moscow, USSR; T. Dubbs, E. McCliment, C. Newsom of University of Iowa; I. F. Albuquerque, C. Escobar, P. Gouffon, J. Mahon of University of Sao Paulo, Brazil; M. Foucher of Yale University; A. M. F. Endler of Centro Brasileiro de Pesquisas Fisicas Rio de Janeiro, Brazil; M. C. Pommot Maia of Conselho Nacional De Pesquisa CNPq (on a leave of absence from UFRJ, Rio de Janeiro), Brazil; D. Chen of State University of New York; V. J. Smith of H. H. Wills Physics Laboratory University of Bristol, United Kingdom.
2. M. K. Gaillard, X. Q. Li, and S. Rudaz, Phys. Letters **158**B, 158(1985)
   I. I. Balitsky, V. M. Brawn, A. V. Kolesnichenko, Sov. J. Nucl. Phys. **44**, 1028(1986)
   D. Palle, Phys. Rev. D **36**, 2863(1987)
   Y. I. Kogan and M. A. Shifman, Sov. J. Nucl. Phys. **38**, 628(1983)
   F. J. Gilman and M. B. Wise, Phys. Rev. D **19** 976(1979)
   C. Goldman and C. O. Escobar, Phys. Rev. D **40** 106(1989)
   M. D. Scadron and M. Visinescu, Phys. Rev. D **28**, 1117(1983)
3. Particle Data Group: Phys. Letters B **239** II.22(1990)
4. M. Kobayashi et al, Phys. Rev. Letters **59**, 868(1987)
   A. Manz et al, Phys. Letters **96B**, 217(1980)
   L. K. Gershwin et al, Phys, Rev. **188**, 2077(1969)

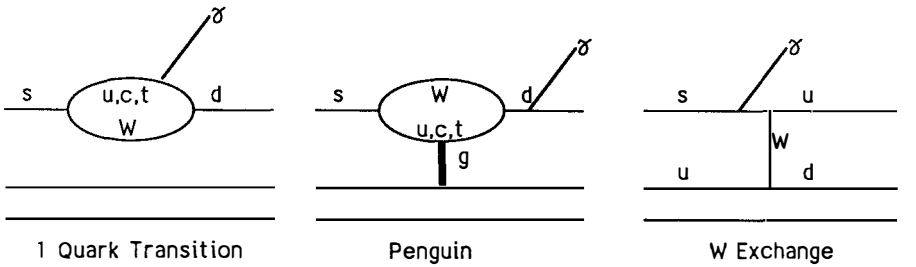

Figure 1: Diagrams contributing to hyperon radiative decays

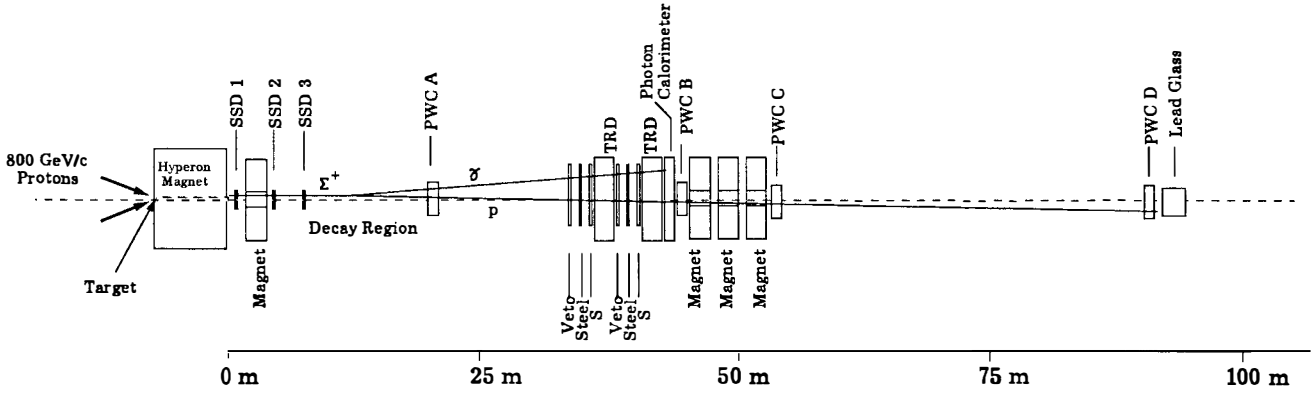

Figure 2: E761 experimental layout in Fermilab Proton Center Charged Hyperon Beam

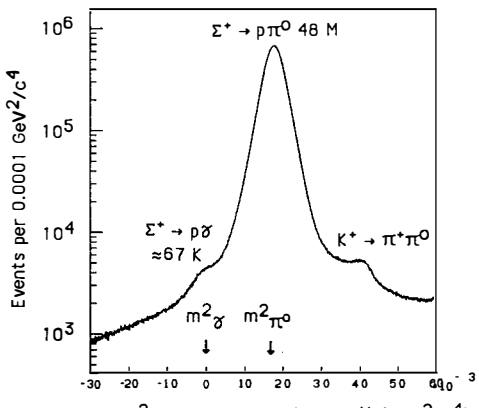

Figure 3: m^2_X distribution, $\Sigma^+ \to p + X$ (GeV^2/c^4)

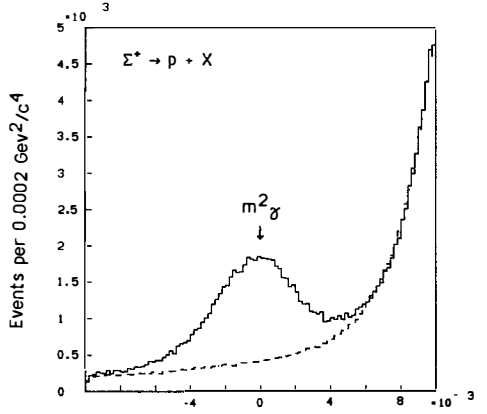

Figure 4: m^2_X (Gev^2/c^4) signal and background(dashed)

Study of $p\bar{p}$-Annihilations at Rest into Final States with Strange Mesons

Torsten Kiel

(1. Institut für Experimental Physik, U. Hamburg)
representing the Crystal Barrel Collaboration

Abstract

The Crystal Barrel detector is designed to detect neutral particles (calorimeter consisting of 1380 CsI(Tl)-crystals) and charged particles (jet drift chamber, solenoid 1.5 T) with good energy and momentum resolution covering $\approx 4\pi$ solid angle. It is the first detector of its kind used to study $p\bar{p}$-annihilations in the low energy region up to 2.4 GeV. The data taking started in the end of 1989. First results from $\pi^+\pi^- X$ and $K^+K^- X$ final states based on ≈ 1 million $p\bar{p}$-annihilations in liquid hydrogen are presented. The main emphasis is put on the discussion of the relative branching ratio of $p\bar{p} \to \phi\pi^\circ$ and $p\bar{p} \to \omega\pi^\circ$. The study of this ratio is related to the hadron structure at large distances (small momentum transfer q^2) and in particular to the question of a possible $s\bar{s}$-content of the proton.

Work supported in part by the BMFT

1 Detector

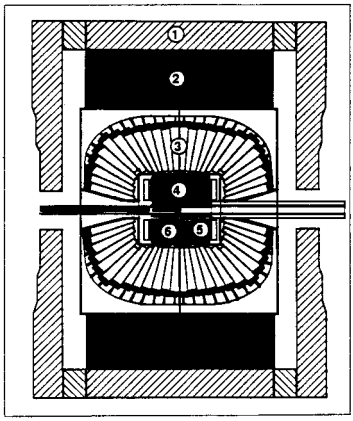

1. Iron Yoke
2. Magnet Coil (1.5T)
3. CsI(Tl)-Barrel
4. Jet-Drift-Chamber
5. Proportional-Wire-Chamber
6. Liquid-Hydrogen-Target

Figure 1: The Crystal Barrel detector

The Crystal Barrel detector, which is in operation since the end of 1989, is build up of the following components ordered from the inner side to the outer side: In the center of the detector the liquid hydrogen target is surrounded by a proportional wire chamber (PWC) and a jet drift chamber (JDC). The JDC is build of 23 layers of sense wires covering 92% of 4π solid angle, providing a momentum resolution of $\Delta P/P = 5\%$ at 1 GeV/c. The dE/dx information of the JDC allows a $\pi^{\pm}/K^{\pm}$ separation up to momenta of 500 MeV/c. The calorimeter consists of 1380 CsI(Tl)-crystals of 16 radiation lengths each read out by a photodiode connected via a wavelengthshifter to the crystal. The calorimeter covers 97% of 4π spatial angle, we observe an energy resolution of 2.7% at 1 GeV and a spatial resolution of 20 mrad. The whole apparatus is inside a 1.5T conventional magnet.
A detailed description of all components will be given in [CBA91] .

2 Motivation

In the constituent quark model (NQM) the proton wave function contains two u quarks and one d quark. Within this model and using the Okubo-Zweig-Iizuka (OZI) rule the branching ratio of $p\bar{p} \rightarrow \phi\pi^{\circ}$ should be suppressed compared to $BR(p\bar{p} \rightarrow \omega\pi^{\circ})$ by a factor of ≈ 240. Previous measurements (Tab.1) are indicating a suppression by a factor of ≈ 15. So far we do not understand why the OZI-rule is not working, one proposed way out of this situation is to add to the proton wave function a nonnegligible sea of $s\bar{s}$-quark pairs even for cases when the proton is probed in the low energy region. Additional hints that this seems to be necessary come from the measurement of the $\pi - N$ sigma term [GAS91] and from the measurement of deep inelastic polarized μp scattering [EMC88]. The aim of our measurements is to check the OZI-rule in $p\bar{p}$-annihilation at rest.

$BR(p\bar{p} \to \omega\pi^\circ)$	$= (4.9 \pm 3.6) * 10^{-3}$	liquid hydrogen	[CAR86]
	$= (5.2 \pm 0.5) * 10^{-3}$	liquid hydrogen	[CHI88]
$BR(p\bar{p} \to \omega\eta)$	$= (10.4^{+0.9}_{-1.0}) * 10^{-3}$	liquid hydrogen	[ADI89]
	$= (4.6 \pm 1.4) * 10^{-3}$	liquid hydrogen	[CHI89]
$BR(p\bar{p} \to \phi\pi^\circ)$	$= (0.33 \pm 0.15) * 10^{-3}$	liquid hydrogen	[CHI88]
	$= (0.35 \pm 0.09) * 10^{-3}$	liquid hydrogen	[BET69]
	$= (0.19 \pm 0.05) * 10^{-3}$	$(62 \pm 4)\%$ p-wave	[AST91]
	$= (0.03 \pm 0.03) * 10^{-3}$	$(92.5 \pm 0.1)\%$ p-wave	[AST91]
$BR(p\bar{p} \to \phi\eta)$	$< 2.8 * 10^{-3} (95\% CL)$	liquid hydrogen	[CHI89]
	$= (3.7 \pm 0.9) * 10^{-5}$	$(62 \pm 4)\%$ p-wave	[AST91]
	$= (4.1 \pm 1.6) * 10^{-5}$	$(92.5 \pm 0.1)\%$ p-wave	[AST91]

Table 1: previous measurements

3 Measurements

Until the end of 1990 about 10 million *minimum bias* events and 12 million *all-neutral* events of $p\bar{p}$-annihilations at rest are recorded. To take *minimum bias* data each event triggered by an incident $\bar{p}$ in a silicon beam counter placed in front of the target cell is recorded, for *all-neutral* data the JDC is used in addition as a veto trigger for charged particles. This preliminary analysis is based on $\approx$ 800k *minimum bias* events and $\approx$ 2 million *all-neutral* events. Except for $p\bar{p} \to K^0_L\pi^\circ\pi^\circ\pi^\circ$ all final states are detected exclusively. Energy and momentum conservation require that the total momentum is $\leq$ 200 MeV/c and the total energy is between 1642 MeV and 2042 MeV. This were the first cuts applied to our data set. π° and η are always detected in their decay into two photons.

The number of $p\bar{p} \to \omega\pi^\circ$ events is determined to 380, the number of $p\bar{p} \to \omega\eta$ to 391, the ω is detected for both channels in the $\pi^+\pi^-\pi^\circ$ final state (Fig.2).

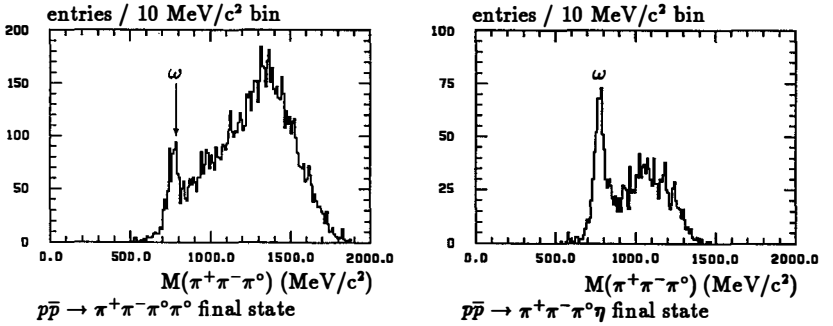

Figure 2: $\pi^+\pi^-\pi^\circ$ invariant mass distributions

$K^+K^-\pi^\circ$ final states were selected by calculating the total momentum and the total energy from a combination of two charged particles having the kaon rest mass assigned and a reconstructed π°. The remaining pion backround in the resulting data sample is suppressed by using the dE/dx information from the JDC (Fig.3). The sample of $p\bar{p} \to K^+K^-\pi^\circ$ candidates shows clear K^* and Φ signals (Fig.4).

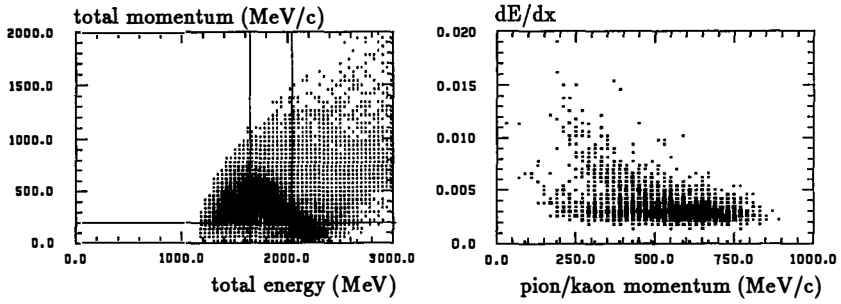

Figure 3: Selection of $p\bar{p} \to K^+K^-\pi^\circ$ final states

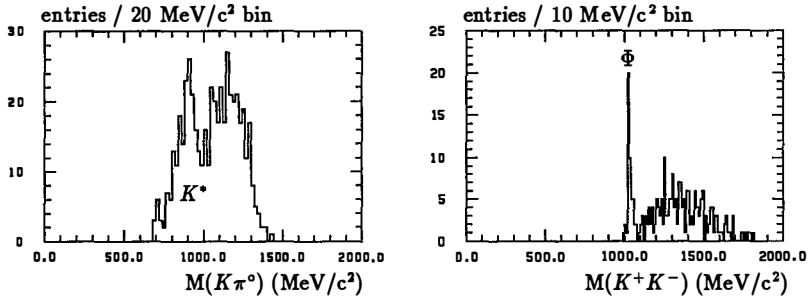

Figure 4: $p\bar{p} \to K^+K^-\pi^\circ$ final state

The width of the Φ signal gives an impression of the momentum resolution of the JDC (no kinematic fit applied). The number of $p\bar{p} \to \Phi\pi^\circ$ events with Φ decaying to K^+K^- is determined to 26-35 (depending on the description of the background under the Φ signal). In the $p\bar{p} \to K^+K^-\eta$ sample we observe 4 events with a K^+K^- invariant mass at the Φ mass region (Fig.5).

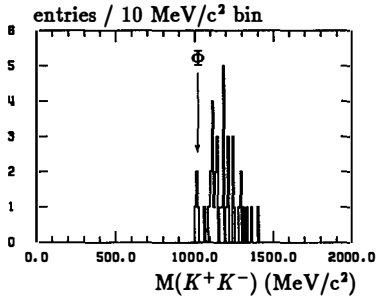

Figure 5: $p\bar{p} \to K^+K^-\eta$ final state

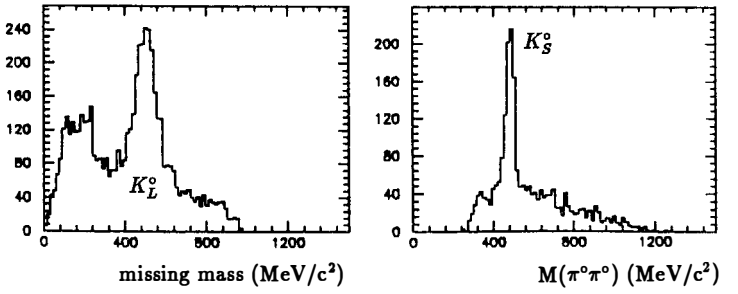

Figure 6: $p\bar{p} \to \pi^\circ\pi^\circ\pi^\circ X$ final state [DIE91]

In the *all-neutral* data sample collected with an online veto on charged events, $p\bar{p} \to K^0_L K^0_S \pi^\circ$ events are selected by requesting 6 photons reconstructed to be $3\pi^\circ$. The K^0_S decays then into $\pi^\circ\pi^\circ$, the K^0_L is observed in the missing mass spectrum (Fig.6). 4C kinematical fits are applied to the data. The resulting Dalitzplots show bands of the K^* and of the Φ. The number of $p\bar{p} \to \Phi\pi^\circ$ events with Φ decaying to $K^0_L K^0_S$ is determined to 330 (Fig.7).

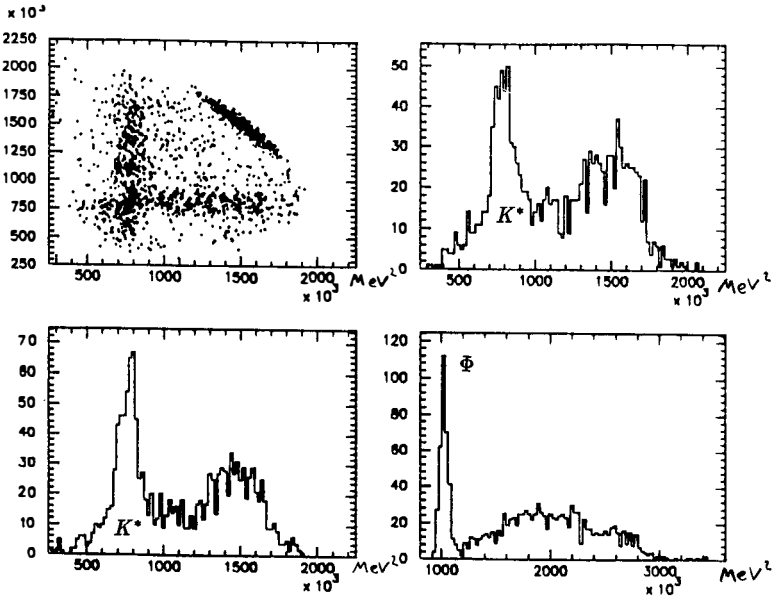

Figure 7: $p\bar{p} \to K^0_S K^0_L \pi^\circ$ final state [DIE91]

4 Summary

In this preliminary analysis of 800k *minimum bias* events we observe 380 $\omega\pi^\circ$, 391 $\omega\eta$, 26-35 $\Phi\pi^\circ$ and 4 $\Phi\eta$ events and out of 2 million *all-neutral* events we observe 330 $\Phi\pi^\circ$ events. As the determination of the corresponding efficiencies and systematic errors is not completely finished, no absolute branching ratio will be quoted. The relative branching ratios given in table 2 are determined using the numbers from the *minimum bias* data sample under the assumption that the detection efficiency for π° and η in the $\gamma\gamma$ decay is approximately the same. These preliminary results are compatible with previous measurements.

	this	previous measurements
$\frac{BR(p\bar{p}\to\omega\pi^\circ)}{BR(p\bar{p}\to\omega\eta)}$	0.38	$(0.47-1.13)$
$\frac{BR(p\bar{p}\to\phi\pi^\circ)}{BR(p\bar{p}\to\phi\eta)}$	$(2.56-3.45)$	$(5.14-9.19)$

Table 2: comparison of relative branching ratios

The statistic will be increased soon by analyzing the whole so far recorded data sample of 10 million *minimum bias* and 12 million *all-neutral* events.

References

[ADI89] L. Adiels et al., Z. Physik C42(1989)49.

[AST91] Φ Production in $\bar{p}p$ Annihilation at Rest, ASTERIX Collaboration, to be submitted.

[BET69] A. Bettini et al., Nuov. Cim. 63A(1969)1199.

[CAR86] LEAR PS182, S. Carius, PhD Thesis, Royal Institute of Technology, Stockholm, May 1986.

[CBA91] E. Aker et al., The Crystal Barrel Detector, in preparation.

[CHI88] M. Chiba et al., Phys. Lett. B202(1988)447.

[CHI89] M. Chiba et al., Phys. Rev. D39 (1989)3227.

[DIE91] H.-P. Dietz, Zerfall von Protonium in $\phi\pi^\circ$, Diplomarbeit, U München, January 1991, unpublished.

[ELL89] J. Ellis, E. Gabathuler, M. Karliner, Phys. Lett. B217(1989)173.

[EMC88] EMC collaboration, J. Ashman et al., Phys. Lett. B206(1988)364.; Nucl. Phys. B328(1990)1.

[GAS91] J. Gasser, H. Leutwyler, M. E. Sainio, Phys. Lett. B253(1991)252.; Phys. Lett. B253(1991)260.

Two Body $\bar{p}p$ Decays into All Neutral Final States

Gunter Folger
Universität München
representing the Crystal Barrel Collaboration

Abstract

The Crystal Barrel Collaboration is analyzing $\bar{p}p$-annihilation at rest in liquid hydrogen into two neutral mesons (π^0, η, ω, and η'). The status of the ongoing analysis is shown.

1 Introduction

The two main physics motivations to study $\bar{p}p$-annihilation at low energies and at rest are meson spectroscopy including the search for exotic states like glueballs and hybrid mesons, and a study of the annihilation dynamics itself. The latter is not well understood, as it involves non-perturbative QCD. In most models the $\bar{p}p$-annihilation into two or three mesons proceeds either via rearrangement of the constituent quarks (Fig 1a), or via annihilation of constituent quark antiquark pairs (Fig 1b). To decide which of the graphs dominates in $\bar{p}p$-annihilation many branching ratios for annihilation into two or three mesons need to be measured. Experimentally many of the branching ratios involving π°, η, ω, and η' are not well measured and some of the existing measurements are inconsistent, see table 1 or ref [1] for a review. The Crystal Barrel experiment has started a survey for $\bar{p}p$-annihilation into two mesons with the aim to measure many branching ratios with high accuracy.

Furthermore in both classes of models production of $s\bar{s}$ mesons (e.g. ϕ) together with non-strange mesons is suppressed. The experimental branching ratio for $\bar{p}p \to \phi\pi^\circ$ seems to violate this suppression by a factor of ten.

2 The Experiment

The Crystal Barrel detector covers nearly 4π sr and measures both charged particles and photons with good resolution. It consists of a liquid hydrogen target, two cylindrical proportional wire chambers (not installed for the data shown here), a cylindrical jet drift chamber of 30 sectors with 23 layers of sense wires each, and a barrel shaped electromagnetic calorimeter consisting of 1380 cesium iodide crystals, each 16 radiation length long. The chambers detect and measure charged particles in 92% of 4π sr. The electromagnetic calorimeter detects particles in 97% of 4π sr and measures photons with an energy resolution of $2.7\%/\sqrt[4]{E(\mathrm{GeV})}$. The angular resolution for photons varies with the photon energy from 20 mrad to 30 mrad. The detector is surrounded by a coil and iron return yoke for a homogeneous solenoidal field of up to 1.5 Tesla. For more details see [2].

The data shown here were taken with antiprotons stopping in the liquid hydrogen target. In 1989 and 1990 we recorded $8 \cdot 10^6$ minimum bias triggers and 10^7 zero prong triggers. The zero prong trigger selects events without hits in one of the inner four layers of the jet drift chamber. So far we have analyzed only (10-20)% of the recorded zero prong data.

Table 1: Branching ratios BR for $\bar{p}p$-annihilation at rest in liquid hydrogen.

Channel	BR				Ref
$\pi^\circ\pi^\circ$	2.06	$\pm$	0.14	10^{-4}	[6]
	1.4	$\pm$	0.3	10^{-4}	[7]
	2.5	$\pm$	0.3	10^{-4}	[8]
	4.8	$\pm$	1.0	10^{-4}	[9]
$\pi^\circ\eta$	4.6	$\pm$	1.3	10^{-4}	[10]
	1.33	$\pm$	0.27	10^{-4}	[11]
$\pi^\circ\omega$	5.2	$\pm$	0.5	10^{-3}	[10]

Channel	BR				Ref
$\pi^\circ\eta'$	5.0	$\pm$	1.9	10^{-4}	[10]
$\eta\eta$	8.1	$\pm$	3.1	10^{-5}	[11]
	1.6	$\pm$	0.8	10^{-3}	[12]
$\eta\omega$	1.0	$\pm$	0.1	10^{-2}	[11]
	4.4	$\pm$	1.4	10^{-3}	[12]
$\omega\omega$	1.4	$\pm$	0.6	10^{-2}	[7]

3 The Four Photon Final State

Here one can observe $\bar{p}p$-annihilation into $\pi^\circ\pi^\circ$, $\pi^\circ\eta$, $\pi^\circ\eta'$, $\eta\eta$, and $\eta\eta'$. To analyze the four photon events we select events with four photon candidates fully contained in the calorimeter and check for energy and momentum conservation by a 4-C kinematic fit. For the selected events we plot all possible combinations of $m_{\gamma\gamma}$ versus $m_{\gamma\gamma}$ of the four photons (Fig 2a). A signal for $\pi^\circ\pi^\circ$ events is evident. To enhance the other decay channels we remove $\pi^\circ\pi^\circ$ event candidates and plot for the remaining events $m_{\gamma\gamma}$ vs $m_{\gamma\gamma}$ (Fig 2b). Signals for $\pi^\circ\eta$, $\pi^\circ\eta'$, and $\eta\eta$ events are visible now.

Note that all the above decays are forbidden from atomic S-states (L=0). These decays stem from annihilation of $\bar{p}p$ in P-states (L=1). The $\pi^\circ\pi^\circ$ decay branching ratio is related to the well measured $BR_{L=1}(\bar{p}p\to\pi^+\pi^-) = (4.81 \pm 0.49)\cdot 10^{-3}$ from atomic P-states [3] by

$$B_{L=1}(\pi^+\pi^-) = 2B_{L=1}(\pi^\circ\pi^\circ) = 2f_P^{-1}B_{Liquid}(\pi^\circ\pi^\circ) \tag{1}$$

where f_P is the fraction of $\bar{p}p$-annihilation from atomic P-states in liquid hydrogen into any final state. A precise determination of the $\pi^\circ\pi^\circ$ rate in liquid hydrogen will yield f_P.

The above branching ratios also test the model of annihilation dominance (Fig 1a). There are relations for the phase space corrected branching ratios σ like [4]

$$\sigma(\eta\eta) = x^4\sigma(\pi^\circ\pi^\circ) \tag{2}$$

where x is related only to the pseudoscalar mixing angle Φ_{PS} and has a value of $x^2 = 0.72$ (0.51) for $\Phi_{PS} = -23^\circ$ (-10°). The existent measurements for $\pi^\circ\pi^\circ$ and $\eta\eta$ are, given the large errors, still consistent with the prediction of equ.2.

4 The Five Photon Final State

In this final state the dominant $\bar{p}p$ decays are $\pi^\circ\omega$ and $\eta\omega$. Similar to the four photon final state we select events with five photon candidates and check energy and momentum conservation by a 4-C kinematic fit. For all 15 combinations of $(\gamma\gamma)$ $(\gamma\gamma)$ γ of the five photons we plot the mass of one $(\gamma\gamma)$ pair vs. the other pair (Fig.3). There are two clear peaks of events for $\pi^\circ\pi^\circ\gamma$ and for $\pi^\circ\eta\gamma$. Using the events in the peaks to plot the $\pi^\circ\gamma$ invariant mass distribution, prominent signals for $\pi^\circ\omega$ and $\eta\omega$ show up (Figs.4a and 4b). A fit of the above signals yields, after detection efficiency correction, the preliminary ratio

$$r = \frac{BR(\bar{p}p\to\pi^\circ\omega)}{BR(\bar{p}p\to\eta\omega)} = 0.46 \pm 0.10 \tag{3}$$

Studies of systematic effects are still in progress.

Again the model of annihilation dominance predicts relations for the phase space corrected branching ratios [4]

$$x^2\sigma(\pi^\circ\rho^\circ) = \sigma(\eta\omega) \quad \text{and} \quad x^2\sigma(\pi^\circ\omega) = \sigma(\eta\rho^\circ) \tag{4}$$

In the ratios $\sigma(\pi^\circ\rho^\circ)/\sigma(\pi^\circ\omega)$ and $\sigma(\eta\omega)/\sigma(\eta\rho^\circ)$ the phase space correction factors cancel, as ρ° and ω have the same momenta. It then follows

$$\frac{BR(\bar{p}p\to\pi^\circ\rho^\circ)}{BR(\bar{p}p\to\pi^\circ\omega)} = \frac{BR(\bar{p}p\to\eta\omega)}{BR(\bar{p}p\to\eta\rho^\circ)} \tag{5}$$

The existing measurements have too big errors to draw conclusions on the validity of the model of annihilation dominance.

The ratio $BR(\bar{p}p\to\pi^\circ\phi)/BR(\bar{p}p\to\pi^\circ\omega)$ tests the quark line rule, for a discussion see [5].

5 The Six Photon Final State

In this channel there are in addition to the $\bar{p}p \rightarrow \omega\omega$ decay many three meson final states present. To measure the $\omega\omega$ branching ratio we use the sample of candidate six photon events, select events with two π°candidates and reject events compatible with $3\pi^\circ$ or $2\pi^\circ\eta$. For the events fulfilling these criteria we plot all combinations of $m_{\pi^\circ\gamma}$ versus $m_{\pi^\circ\gamma}$ (Fig.5). Events of type $\bar{p}p \rightarrow \omega\omega$ clearly are present, but to calculate the branching ratio further studies are necessary.

Here the annihilation dominance model predicts

$$BR(\bar{p}p \rightarrow \omega\omega) = BR(\bar{p}p \rightarrow \rho^\circ\rho^\circ) \tag{6}$$

which does not seem to be the case experimentally, even given the large uncertainty on the measured BR($\bar{p}p \rightarrow \omega\omega$).

6 Summary

An analysis of $\bar{p}p$ decays at rest into two neutral mesons (π°, η, ω, and η') is currently performed using the Crystal Barrel detector at LEAR. The large solid angle coverage and the excellent energy resolution for photons enable the full reconstruction of events containing several of these mesons. This will result in measurements of many branching ratios with small errors. These branching ratios will allow to constrain models describing $\bar{p}p$-annihilation .

References

[1] C.Amsler, F.Myhrer, CERN-PPE/91-29, to be published in Annual Review of Nuclear and Particle Science 41 (1991)

[2] E.Aker *et al.*, CERN/PSCC/P90, Experiment PS 197 (1985)

[3] M.Doser *et al.*, Nucl. Phys. A486 (1988) 493

[4] H.Genz *et al.*, Z. Phys. A335 (1990) 87

[5] T.Kiel, these proceedings.

[6] L.Adiels *et al.*, Z.Phys. C42 (1989) 15

[7] G.Bassompiere *et al.*, IV European Antiproton Symposium (1978), Vol.1, p. 139

[8] M.Chiba *et al.*, Phys. Lett. B202 (1988) 447

[9] S.Devons *et al.*, Phys. Rev. Lett. 27 (1971) 1614

[10] M.Chiba *et al.*, Phys. Rev. D38 (1988) 2021

[11] L.Adiels *et al.*, Z. Phys. C42 (1989) 49

[12] M.Chiba *et al.*, Phys. Rev. D39 (1989) 3227

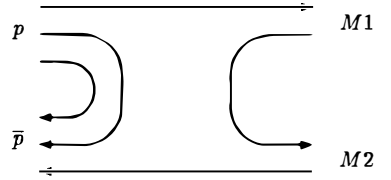

Fig. 1a

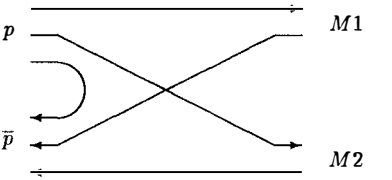

Fig. 1b

Figure 1: Annihilation (a) and rearrangement (b) diagrams of $\overline{p}p$-annihilation into two mesons.

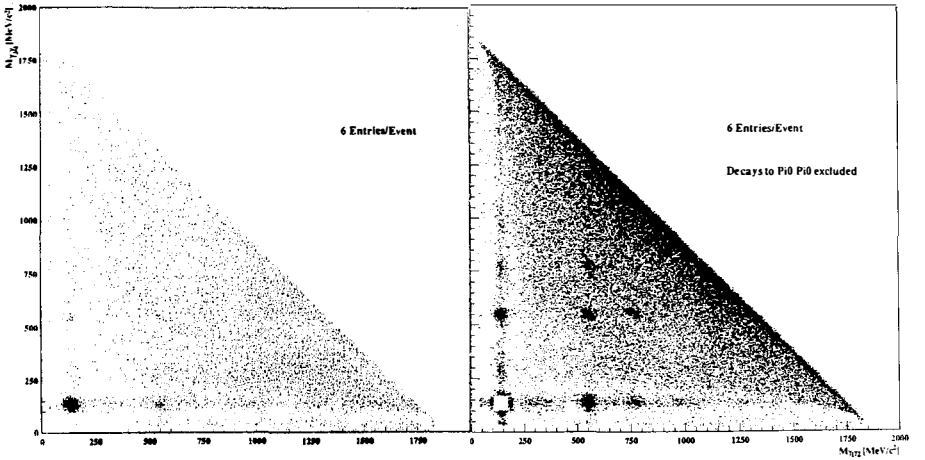

Figure 2: a) $m_{\gamma\gamma}$vs. $m_{\gamma\gamma}$for all four photon events, and 2b) as above but $\pi^\circ\pi^\circ$ events removed.

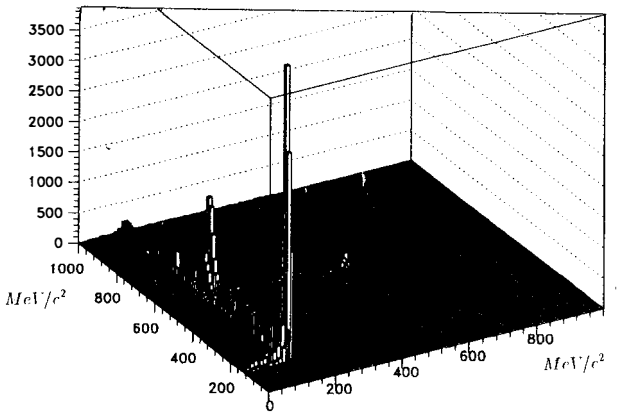

Figure 3: $m_{\gamma\gamma}$ vs. $m_{\gamma\gamma}$ for five photon events using all 15 combinations of $(\gamma\gamma)$ $(\gamma\gamma)$ γ. The entries are sorted such that the first pair always is the pair with the higher mass.

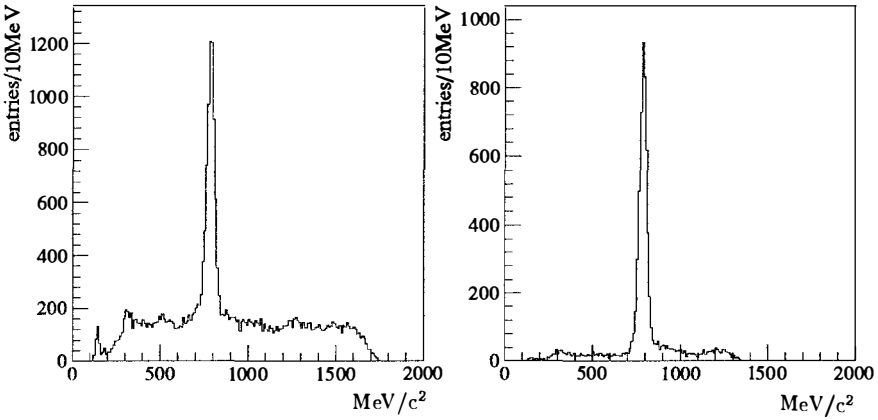

Figure 4: a) $m_{\pi^\circ\gamma}$ for $\pi^\circ\pi^\circ\gamma$ events. Two entries per event. Most of the events can be explained as $\pi^\circ\omega$.
b) $m_{\pi^\circ\gamma}$ for $\pi^\circ\eta\gamma$ events. One entry per event. Again most of the events can be explained as $\eta\omega$.

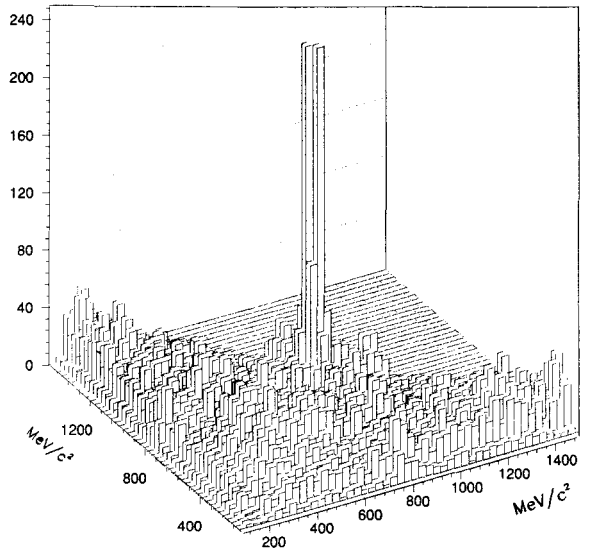

Figure 5: $m_{\pi^\circ\gamma}$ vs. $m_{\pi^\circ\gamma}$ for $\pi^\circ\pi^\circ\gamma\gamma$ events (six photon events).

SEARCH FOR GLUEBALLS IN Ω

presented by Antimo Palano
Dipartimento di Fisica and INFN, Bari, Italy

WA76 Collaboration

T.A. Armstrong[4], M. Benayoun[5], W. Beusch[4], I.J. Bloodworth[3], J.N. Carney[3], R. Childs[3], C. Evangelista[2], B.R. French[4], B. Ghidini[2], M. Girone[2], A. Jacholkowski[4], J. Kahane[5], J.B. Kinson[3], A. Kirk[4], K. Knudson[4], V. Lenti[2], Ph. Leruste[5], A. Malamant[5], J.L. Narjoux[5], F. Navach[2], A. Palano[2], E. Quercigh[4], N. Redaelli[4] L. Rossi[4], M. Sené[5], R. Sené[5], M. Stassinaki[1], M.T. Trainor[3], G. Vassiliadis[1], O. Villalobos Baillie[3], M.F. Votruba[3]

1) Athens University, Nuclear Physics Department, Athens, Greece
2) Dipartimento di Fisica dell'Universitá and Sezione INFN, Bari, Italy
3) University of Birmingham, Physics Department, Birmingham, U.K.
4) CERN, CH-1211 Geneva 23, Switzerland
5) Collège de France, F-75231 Paris, France

Abstract

Results are presented on a search for glueballs and hybrids centrally produced in the reaction $pp \rightarrow p_f(X^0)p_s$ at 85 and 300 GeV/c incident momentum using the CERN Ω spectrometer. In particular, contribution to the search for the scalar glueball is presented through the study of $\pi\pi$ and $K\bar{K}$ final states. New contribution to the E/ι puzzle are presented by studying the $\eta\pi\pi$ and $\rho^0\gamma$ final states.

1. Introduction

In this paper we describe the results from a search for gluonium and hybrid states centrally produced in the reaction $pp \rightarrow p_f(X^0)p_s$, where X=$\pi\pi$, $K\bar{K}$, $\eta\pi^+\pi^-$ and $\rho^0\gamma$, at 85 and 300 GeV/c incident beam momentum. At high centre of mass energies these double exchange processes are believed to be dominated by Double Pomeron Exchange (DPE). Since the Pomeron is thought to have a large gluonic content, Pomeron-Pomeron scattering could be a source of non $q\bar{q}$ states. The data come from the WA76 experiment performed at the CERN Ω spectrometer. Details of the layout of the apparatus, trigger conditions and data processing have been given in a previous publication [1].

2. Study of the $\pi\pi$ and $K\bar{K}$ systems

The scalar mesons are still a problem for hadron spectroscopy with the $S^*/f_0(975)$ resonance indicated as a possible glueball state [2] or a $K\bar{K}$ molecule [3]. A study of the $S^*/f_0(975)$ problem has been performed by using the centrally produced $\pi\pi$ and $K\bar{K}$ final states.

The reaction

$$pp \rightarrow p_f(\pi^+\pi^-)p_s$$

has been isolated from the sample of 4-prong events by requiring momentum and energy balance. The sample consists of 303K events whose $\pi^+\pi^-$ effective mass spectrum is shown in fig. 1a). We observe a small $\rho(770)$ signal, some $f_2(1270)$ and a sharp drop around 1 GeV due to the presence of the $S^*/f_0(975)$ resonance.

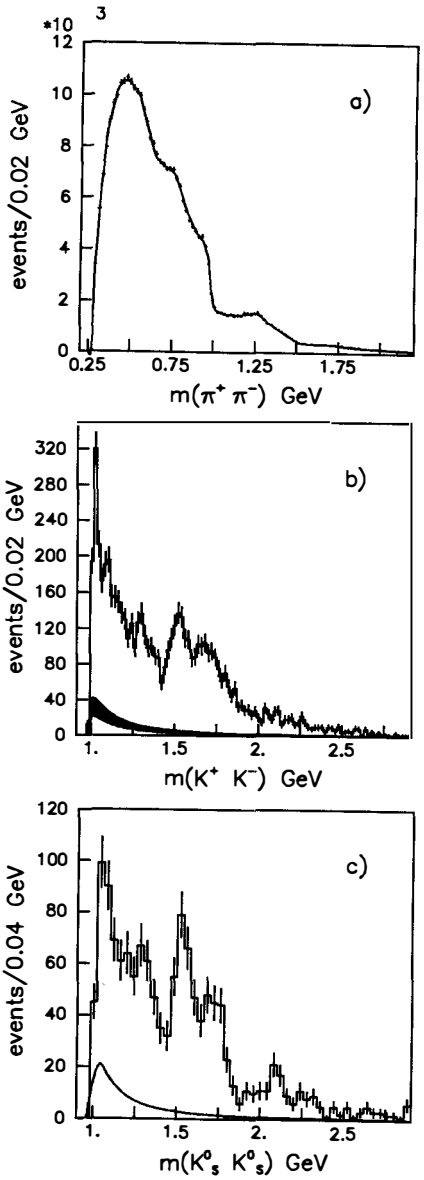

Figure 1
a) $\pi^+\pi^-$, b) K^+K^- and c) $K^0_SK^0_S$ mass distributions.

In order to extract the $S^*/f_0(975)$ parameters, a fit to the $\pi^+\pi^-$ mass spectrum has been performed using a coupled channel Breit-Wigner [4]

$$F_\pi(m) = \frac{m_0\sqrt{\Gamma_i}\sqrt{\Gamma_\pi}}{m_0^2 - m^2 - im_0(\Gamma_\pi + \Gamma_K)} \tag{1}$$

to describe the $S^*/f_0(975)$ region. In eq. (1), Γ_π and Γ_K are the partial widths of $S^*/f_0(975)$ to the $\pi\pi$ and $K\bar{K}$ systems. In order to have a satisfactory description of the $S^*/f_0(975)$ region it was found necessary to introduce an interference between the coupled channel Breit Wigner $F_\pi(m)$ and the background. The S-wave contribution then was parametrized as $B_s(m) = |1+A_sF_\pi(m)e^{i\delta}|^2$ where δ is a mass independent phase. The resulting $S^*/f_0(975)$ parameters are: $m_0 = 979\pm4$ MeV, $g_\pi = 0.28\pm0.04$, $g_K = 0.56\pm0.18$, $\delta = 23\pm4^0$, with a pole position on sheet II at $(1001\pm2) - i(36\pm4)$ MeV. The result of the fit is shown, as a curve superimposed on the data, in fig. 1a). We notice that, while the description of the $S^*/f_0(975)$ requires a large coupling to the $K\bar{K}$ system, the resulting parameters are quite different from what expected for a $K\bar{K}$ molecule [3].

Using the results from the fit to the $\pi^+\pi^-$ spectrum it is possible to have an absolute prediction of the expected number of events for the $S^*/f_0(975)$ in the K^+K^- and $K_S^0K_S^0$ spectra. The black band drawn in the threshold region of fig. 1b) and the curve drawn in the threshold region of fig. 1c), represent the predicted $S^*/f_0(975)$ contribution after having taken into account the different geometrical acceptance between the channels and Clebsch-Gordan coefficients. The band shows the prediction of $\pm1\sigma$ where σ is the statistical error. Such a contribution is easily accommodated in the threshold region of the $K\bar{K}$ mass spectra.

Thus it is possible to describe the $S^*/f_0(975)$ region of the centrally produced $\pi\pi$ and $K\bar{K}$ systems with a single resonance.

3. Study of the t dependence

It is interesting to compare the production characteristics of the centrally produced resonances observed in this experiment with what expected for production via DPE. Expected features of DPE are: i) a cross section constant or increasing with the centre of mass energy; ii) a simple exponential behaviour as a function of t ($1/t\ dN/dt \sim e^{-bt}$); iii) production of resonances with J^{PC} =even^{++}.

We have studied the t dependence (where $t = |t_1 + t_2|$ where t_1 and t_2 are the four-momentum transfer from the upper and lower protons vertices respectively) of the resonances observed in the $\pi^+\pi^-$ and K^+K^- mass spectra by dividing the data sample into different t regions. The corrected and uncorrected t distributions for $S^*/f_0(975)$, $f_2(1270)$, $\rho(770)$ $\phi(1020)$, $f_2'(1525)$ and $\theta/f_2(1720)$ are shown in fig. 2. It can be noticed

that, while the $S^*/f_0(975)$ and $\theta/f_2(1720)$ behave like simple exponentials having slopes of 8.7 ± 0.2 GeV^{-2} and 9.6 ± 0.4 GeV^{-2} respectively, the $\rho(770)$ $f_2(1270)$ and $\phi(1020)$ are consistent with zero in the first t interval suggesting a turn over at low t. Fitting the $f_2'(1525)$ with a simple exponential we obtain a slope of 6.1 ± 0.4 GeV^{-2}. Thus we observe enhanced production of $\theta/f_2(1720)$ at low t, in contrast with the behaviour of $f_2(1270)$ and $f_2'(1525)$.

It is interesting to compare the cross section for production of $\rho(770)$,$S^*/f_0(975)$ and $f_2(1270)$ in the 85 GeV/c and in the 300 GeV/c experiment. We obtain

$$\sigma(\rho(770))_{300}/\sigma(\rho(770))_{85} = 0.44 \pm 0.07$$
$$\sigma(S^*/f_0(975))_{300}/\sigma(S^*/f_0(975))_{85} = 3.12 \pm 1.00$$
$$\sigma(f_2(1270))_{300}/\sigma(f_2(1270))_{85} = 0.83 \pm 0.20$$

Thus, we observe a decrease of the $\rho(770)$ and an increase of the $S^*/f_0(975)$ cross sections as a function of energy. In conclusion, the production of $S^*/f_0(975)$ (and perhaps of the $\theta/f_2(1720)$) is consistent with what expected from DPE.

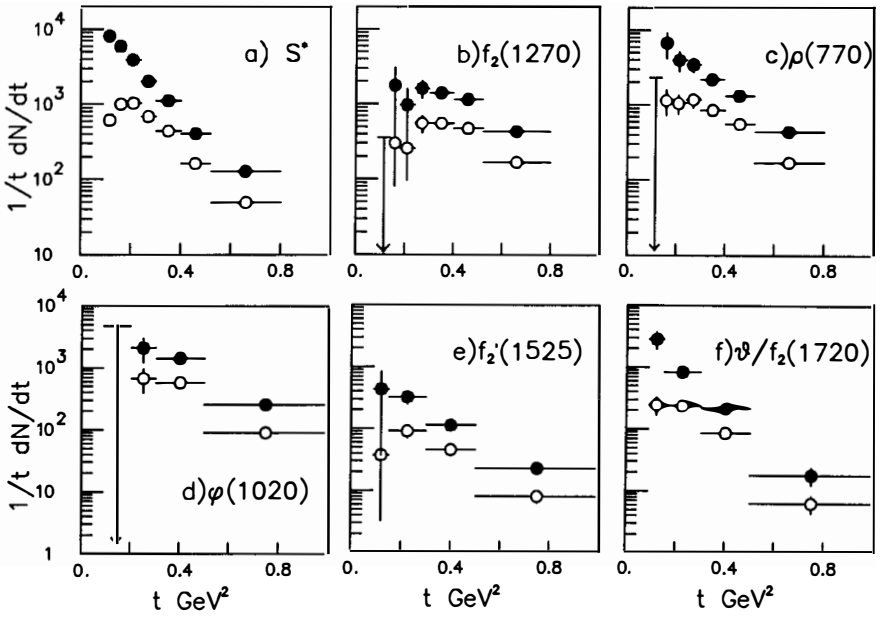

Figure 2
1/t dN/dt distributions (in arbitrary units) for: a) $S^*/f_0(975)$, b) $f_2(1270)$, c) $\rho(770)$, d) $\phi(1020)$, e) $f_2'(1525)$ and f) $\theta/f_2(1720)$. Open points: uncorrected data, black points: corrected data.

4. Study of the reactions $pp \to p_f(\eta\pi^+\pi^-)p_s$ and $pp \to p_f(\rho^0\gamma)p_s$

The $E/f_1(1420)$ meson is still a problem for hadron spectroscopy. It has been indicated as a possible hybrid [5] or a molecular state [6]. It has been observed in the reaction

$$pp \to p_f(K^0_S K^\pm \pi^\mp)p_s \qquad (2)$$

from the 85 GeV/c and 300 GeV/c runs of the WA76 experiment (see fig. 3a)). The $E/f_1(1420)$ meson has a dominant $K^*\bar{K}$ decay mode but other possible decays are not excluded. We have searched for $E/f_1(1420) \to 2\pi^+2\pi^-$ (fig. 3b)) but, instead, a different resonance is observed having a mass of 1449 ± 4 and $\Gamma = 78 \pm 18$ MeV [7].

The reaction

$$pp \to p_f(\eta\pi^+\pi^-)p_s$$

where $\eta \to \gamma\gamma$ and $\eta \to \pi^+\pi^-\pi^0$ have been selected from the sample of events balancing momentum and energy and having only two γ's reconstructed in the electromagnetic calorimeters. Showers in the calorimeters associated to charged tracks have been removed. The $\eta\pi^+\pi^-$ effective mass distribution is shown in fig. 3c). We observe clear peaks at the $\eta'(975)$ and $f_1(1285)$ masses and no evidence for structure in the E/ι region. No evidence is also seen for the new resonance X(1900) recently observed in the reaction $\gamma\gamma \to \eta\pi\pi$ [8]. Fitting the $\eta\pi^+\pi^-$ mass spectrum of fig. 3c) with a Breit-Wigner (Γ=25 MeV) convoluted with a Gaussian to describe the $f_1(1285)$ region we obtain $m_{f_1(1285)} = 1282 \pm 2$ MeV and $\sigma_{f_1(1285)} = 19 \pm 2$ MeV.

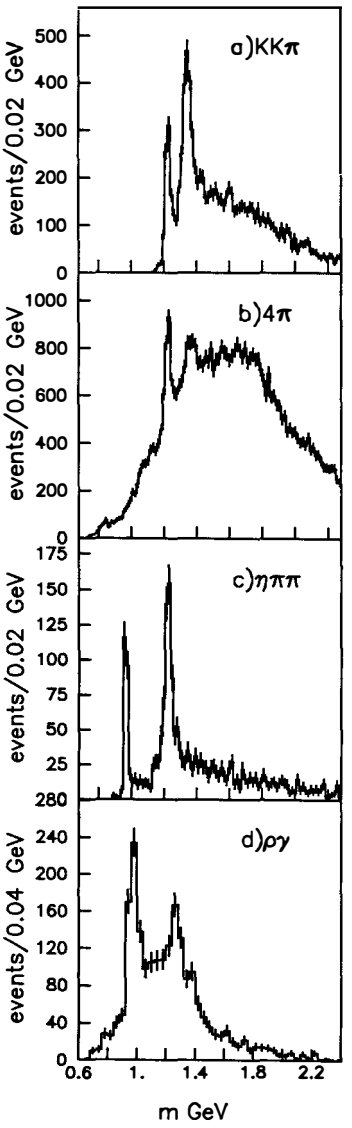

Figure 3
a) $K^0_S K^\pm \pi^\mp$ effective mass from the 85 GeV/c and 300 GeV/c data. b) $2\pi^+2\pi^-$, c) $\eta\pi^+\pi^-$ and d) $\rho^0\gamma$ mass spectra from the 300 GeV/c data.

Fig. 4 shows the $\eta\pi^{\pm}$ effective mass distribution after having removed the η' region (i.e. $m_{\eta\pi\pi} < 1.1$ GeV). The $\eta\pi^{\pm}$ mass spectrum shows a strong $\delta/a_0(980)$ along with some $a_2(1320)$. Describing the $\delta/a_0(980)$ by means of a relativistic S-wave Breit-Wigner convoluted with a Gaussian having a σ=20 MeV, we obtain $m(a_0) = 984 \pm 3$ MeV and $\Gamma(a_0) = 95 \pm 10$ MeV.

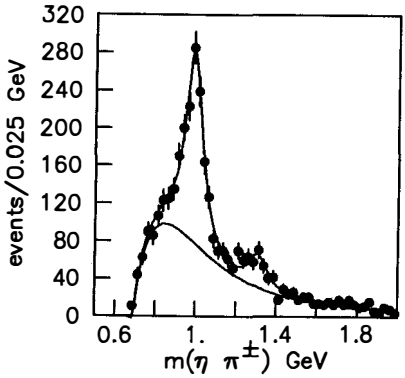

Figure 4
$\eta\pi^{\pm}$ mass spectrum from the $\eta\pi^{+}\pi^{-}$ final state.

A mass dependent spin parity analysis of the $\eta\pi^{+}\pi^{-}$ system has been performed in order to establish the nature of the structure observed in the 1.28 GeV region and search for other resonances. Maximum likelihood fits were performed on the Dalitz plot of the $\eta\pi\pi$ system using the Zemach tensor formalism. An isobar model is used assuming the $\delta/a_0(980)\pi$, $\epsilon/f_0(1400)\eta$ and $\rho(770)\eta$ intermediate states. Waves having small statistical significance have been removed from the fit.

The results are shown in fig. 5 and can be summarized as follows:

(a) The $J^{PC} = 1^{++}$ $\delta/a_0(980)\pi$ is the dominant wave and peaks at the $f_1(1285)$ mass. No evidence is seen for other resonant states; in particular, no evidence is seen for $E/f_1(1420)$ production. This confirms the results from the spin analysis of the centrally produced $K^0_S K^{\pm}\pi^{\mp}$ system [9] which gave a $\delta/a_0(980)\pi$ contribution consistent with zero in the $E/f_1(1420)$ region.

(b) The $J^{PC} = 0^{-+}$ waves are small and do not show resonant behaviour. In particular, no evidence is seen for $\eta(1270)$ or the pseudoscalar states observed in radiative J/ψ decay.

We have used the $K^0_S K^{\pm}\pi^{\mp}$ data from the 300 GeV/c experiment to compute an upper limit for the dacay $E/f_1(1420) \rightarrow \eta\pi\pi$. Taking as reference the presence of the $f_1(1285)$ in both the $\eta\pi\pi$ and $K^0_S K^{\pm}\pi^{\mp}$ mass spectra, and assuming an $f_1(1285)$ branching ratio to $K\bar{K}\pi$ of 12 %, we measure an upper limit for the decay of $E/f_1(1420)$ to $\eta\pi\pi$

$$B.R.(E/f_1(1420) \rightarrow \eta\pi\pi) < 0.1 \quad 95\% c.l.$$

The reaction

$$pp \rightarrow p_f(\pi^{+}\pi^{-}\gamma)p_s$$

has been selected from the sample of 4-prong events having only one γ reconstructed in the

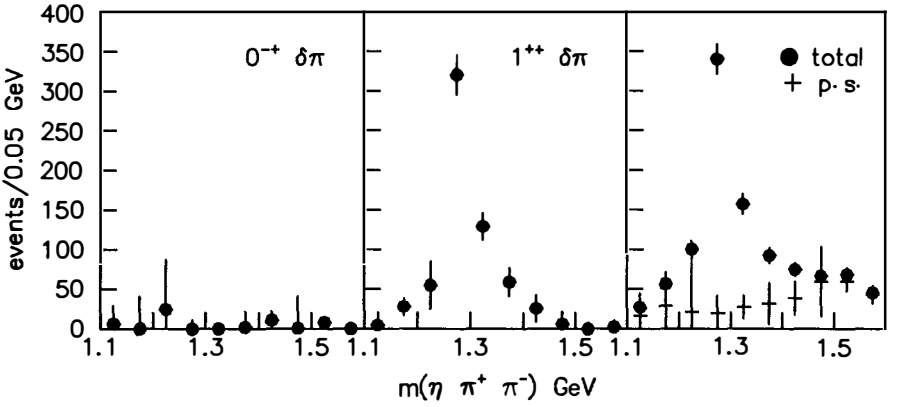

Figure 5
Results from the $\eta\pi^+\pi^-$ spin-parity analysis.

electromagnetic calorimeters and balancing momentum and energy. Requiring the $\pi^+\pi^-$ system to be in the ρ^0 band we obtain the mass spectrum shown in fig. 3d) where, above the η' a signal in the $f_1(1285)$ region can be seen. No signal is observed in the $E/f_1(1420)$ region.

In conclusion, no evidence is found for $E/f_1(1420)$ decay to $\eta\pi\pi$ or $\rho\gamma$. This result is particularly relevant in establishing the $E/f_1(1420)$ meson properties. The decay pattern observed in hadronic J/ψ decay to $\phi K\bar{K}\pi$ and $\omega K\bar{K}\pi$ [10] indicates a substantial $u\bar{u}$ and $d\bar{d}$ quark composition of the $E/f_1(1420)$ meson which would lead one to expect $\eta\pi\pi$, $\rho\gamma$ or 4π decay modes. However, this expectation is in contradiction with the non observation of the $E/f_1(1420)$ decay to other than the $K^*\bar{K}$ mode.

References

[1] T. Armstrong et al., Nucl. Instr. and Meth. A274 (1989) 165
[2] K.L. Au et al., Phys. Rev. D35 (1987) 1633.
[3] J. Weinstein and N. Isgur, Phys. Rev. D41 (1990) 2236.
[4] S.M. Flattè et al., Phys. Lett. 38B (1972) 232
[5] S. Ishida et al., Progress of Theoretical Phys. 82 (1989) 119
[6] D.O. Caldwell, Mod. Phys. Lett. A2 (1987) 771;
R.S. Longacre, Phys. Rev. D42 (1990) 874.
[7] T.A. Armstrong et al., Phys. Lett. 228B (1989) 536
[8] K. Karch et al., Phys. Lett. B249 (1990) 353.
[9] T.A. Armstrong et al., Phys. Lett. 221B (1989) 216
[10] L. Köpke and N. Wermes, Phys. Rep. 174 (1989) 67.

3-MESON FINAL STATES IN THE CRYSTAL BARREL

Norbert Winter
Institut für experimentelle Kernphysik
Universität Karlsruhe
Postfach 3640
D-75 Karlsruhe

representing the Crystal Barrel collaboration

Abstracts:

The Crystal Barrel experiment was designed to study antiproton proton annihilations up to center-of-mass energies of 2.43 GeV. In this report first results of $p\bar{p}$ annihilations at rest into 3 pseudoscalar mesons in the pure neutral final state are discussed. In particular the analysis chain of all neutral data , first results of the partial wave analysis of $\pi^0\pi^0\pi^0$ and the status of the analysis of the $\pi^0\pi^0\eta$ and $\pi^0\eta\eta$ final states will be presented.

Introduction

As previous talks showed the performance of the Crystal Barrel detector, I just want to recall, that this detector was designed for the detection of neutral and charged final states of the $p\bar{p}$ annihilation with high efficiency and good energy and angular resolution. Thus annihilation channels like $\pi^0\pi^0\pi^0$, $\pi^0\pi^0\eta$ and $\pi^0\eta\eta$ are easily accessible and their analysis will be described in this report.

The analysis chain of all neutral data

As all reactions of the types we are interested in this paper are very likely decaying into 6 γ, we have concentrated our selection on the all neutral data of the Crystal Barrel. The criteria, we use to isolate the 6 γ final state, are:

- no charged particle detected by the JDC
- 6 energy deposits in the calorimeter with an energy of at least 20 MeV in order to avoid the misinterpretation of shower fluctuations as γ candidates
- we look for complete events of the annihilation at rest, demanding energy and momentum conservation for the event:

$$\Sigma p_i < 200 \text{ MeV/c}$$

$$1675 \text{ MeV/c} < \Sigma E_i < 2075 \text{ MeV/c}$$

- with these preselected events we do a 4C fit, shifting the events energy sum to the exact value of 1876 MeV and its momentum to 0 MeV/c. These events can now be regarded as 6γ events and the invariant $\gamma\gamma$ masses (fig.1) show up the existence of π^0, η and η'. In addition we see a signal originating from the decay ω to π^0 γ with a missing low energetic γ. These fake ω's have to be removed from the data sample.

fig.1:

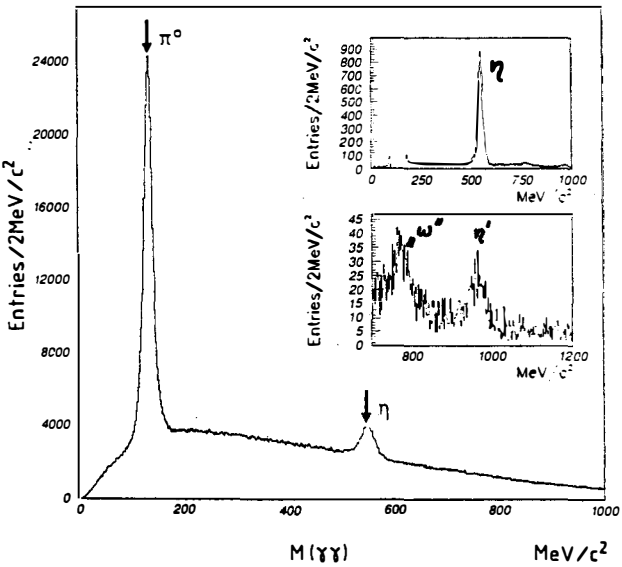

- The final step is the 7C fit, fitting as well the mesons nominal masses, in order to select certain channels and to remove background events.

The analysis of the $\pi^0\pi^0\pi^0$ final state:

A former analysis of this channel could not give a clear answer concerning a new structure in the $\pi^0\pi^0$ mass region of 1500MeV [1)-4)]. A $\pi^+\pi^-$ resonance of 1565 MeV and Spin 2 was observed by the ASTERIX experiment [5)] and it had to be tested, whether these both resonances could be identical. Using $1.2*10^6$ all neutral events of the CRYSTAL BARREL data, a sample of 54800 $\pi^0\pi^0\pi^0$ events could be extracted with hardly any background, using the selection criteria mentioned above. The Dalitzplot is shown in (fig.2). The partial wave analysis has been performed by K.PETERS [6)]. The results are summarized in table 1:

fig.2:

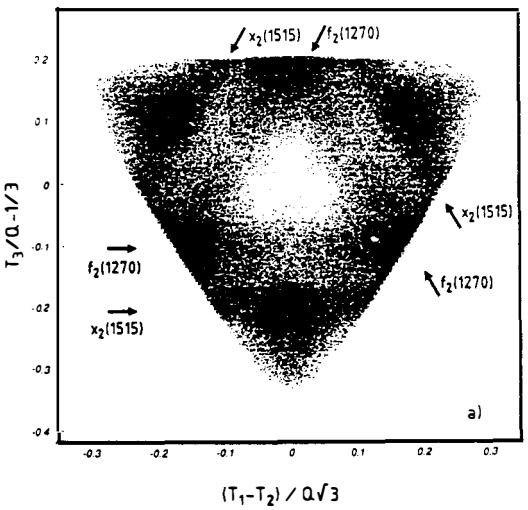

tab.1:

initial state	amplitude	fraction %	total %
$^1S_0$ (0^{-+})	$\pi^0\pi^0$ S-wave	28.3±1.8±1.7	
	$f_2(1270)$	2.9±0.5±1.0	40.7±1.2±1.7
	$X_2(1515)$	9.5±0.2±0.7	
$^3P_1$ (1^{++})	$f_2(1270)$	19.3±0.9±0.7	27.3±1.3±0.8
	$X_2(1515)$	8.0±0.4±0.3	
$^3P_2$ (2^{++})	$X_2(1515)$	8.8±0.9±0.7	32.0±1.3±0.7
	$f_2(1810)$	23.2±2.1±4.1	

For the $\pi^0\pi^0$ S-wave the parametrization of Au, Morgan and Pennington has been used [7]. The fit proofes the necessity for the introduction of a Spin-2 resonance with a mass of 1515±10 MeV and a width of 120±10 MeV. J^{PC} could be fixed to 2^{++}, the isospin is either 0 or 2. These quantum numbers suggest the new resonance to be identical to the ASTERIX state. For the description of higher masses the $f_2(1810)$ had to be introduced, which has to be verified in the future.

The status of the $\pi^0\pi^0\eta$ analysis

The probably most interesting point in the analysis of this final state is the search for the M(1405) with its exotic quantum numbers 1^{-+}, claimed by the GAMS collaboration [8]. Of further interest are any more informations on the $\pi^0\pi^0$ S-wave and on the unknown $\pi^0\eta$ S-wave including the $a_0(980)$. A sample of $1.2*10^6$ all neutral events contained 19690 $\pi^0\pi^0\eta$ events. The analysis is not yet completed and so only rough informations can be given. The Dalitzplot (fig.3) indicates very complicated interference patterns. However, at the present stage of the analysis, an interpretation in terms $\pi^0\pi^0$ S-wave, of $a_0(980)$, the $a_2(1320)$ and an approximately flat $\pi^0\eta$ S-wave seems possible. Maybe the $f_2(1270)$ will contribute by a small amount, but up to now no indication for the M(1405) or anything else is seen. (A small amount of M(1405) can however not yet be excluded).

fig.3:

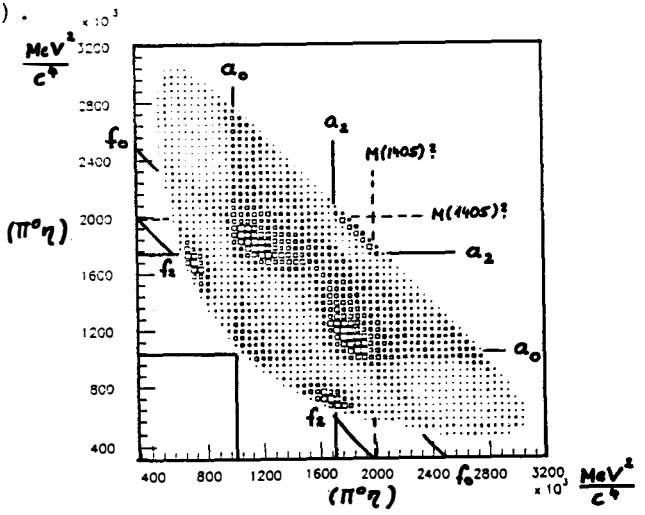

The status of the $\pi^0\eta\eta$ analysis

This channel can be used to answer the question on the isospin of the $X_2(1515)$. If the X_2 occurs in the $\eta\eta$ system, this would fix the isospin to 0. In this system one could look as well for the $f_2'(1525)$ and the $f_0(1590)$, claimed by GAMS, which is one of the most prominent glueball candidates. The Dalitzplot (fig.4) contains 3060 events,extracted from $1.2*10^6$ all neutral events. It suggests a $\pi\eta$ enhancement in the $a_0(980)$ mass region, a $\eta\eta$ enhancement in the $f_2(1270)$ mass region and a signal in the region between 1500 and 1600 MeV, which could be one (or more) of the resonances expected there.

fig.4:

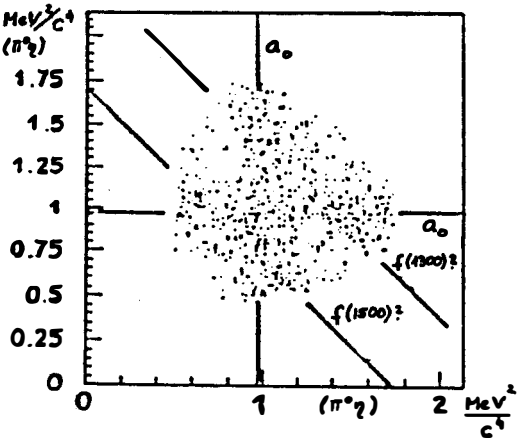

Outlook:

- the analysis discussed in this report is based on an all neutral data sample of $1.2*10^6$ events, but meanwhile a data sample of $10*10^6$ events has been acquired.

- thus a lot of interesting other 3 meson final states like $\pi\pi\eta'$, $\pi\eta\eta$, $\pi\pi\omega$, $\pi\eta\omega$ etc. can be studied, and the analysis has already started.

- in the near future data with annihilations at flight and with a deuterium target will be taken.

References:

1)	P.Anninos et al.	P.R.L. 20(68) 402
2)	S.Devons et al.	P.L. B47 (73) 271
3)	Kasper/ Opat	Univ.Melbourne report 1981 unpublished
4)	Gray et al.	P.R. D27 (83) 307
5)	May et al.	P.L. 225B (89) 450
		ZPHY. C46 (90) 191
		ZPHY. C46 (90) 203
6)	K.Peters	Diss.Univ. Mainz
	Aker et al.	to be publ. in P.L.
7)	Au, Morgan, Pennington	P.R. D35 (87) 1633
8)	Alde et al.	P.L. B205 (88) 397

SOME NEW ASPECTS OF THE UNITARY AND ANALYTIC VMD MODEL FOR ELECTROMAGNETIC STRUCTURE OF HADRONS

A.Z.DUBNIČKOVÁ and S.DUBNIČKA
Laboratory of Theoretical Physics, J.I.N.R., Dubna (USSR)

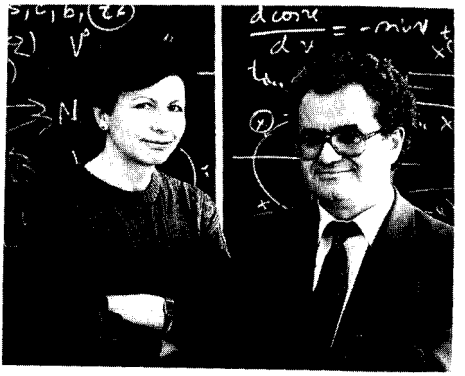

Abstract

Recent J/ $\psi \to \pi^+\pi^-$ data analysed along with all existing pion form factor data by means of the unitary and analytic VMD model manifest a strong evidence of the third excited state of the ρ (770) meson with resonance parameters $m_{\rho'''} = 2169 \pm 46$ MeV and $\Gamma_{\rho'''} = 319 \pm 136$ MeV.

A simultaneous analysis of all reliable proton and neutron form factor data in the space-like region along with data on the total cross section of electron - positron annihilation into a proton - antiproton pair by the same model predicts an unexpected inequality $\sigma_{tot}(e^+e^- \to n\bar{n}) \gg \sigma_{tot}(e^+e^- \to p\bar{p})$ just above the nucleon-antinucleon threshold and also surprisingly large one photon electromagnetic corrections to the strong $J/\psi \to p\bar{p}$ and $J/\psi \to n\bar{n}$ decay amplitudes. The calculated polar angle asymmetry parameter behaviour for $e^+e^- \to p\bar{p}$ and $e^+e^- \to n\bar{n}$ processes is asymptotically, however, in agreement with predictions following from QCD.

Dynamical description of the electromagnetic (e.m.) structure of hadrons is still one of the unsolved problems of particle physics. The perturbative QCD practicaly gives [1) 2)](due to the asymptotic freedom) a behaviour of coresponding e.m. form factors (ff's) only in the asymptotic region. The QCD sum rules predict [3) 4)] just a behaviour of e.m. ff's in a limited interval of the space-like momentum transfers squared. However in the finite energy time-like region, where ff's are complex functions of their argument and experiments on electron - positron annihilation into a hadron - antihadron pair manifest their nontrivial behaviour caused by a creation of various vector meson resonances, QCD gives no predictions up to now.

The latter shortage is partly compensated by the recently proposed unitary and analytic (UA) VMD model[5)–9)] which provides for every e.m. ff's of the hadron one real analytic function for the space-like and time-like region with the asymptotic behaviour to be consistend with QCD predictions and at the same time reflecting an experimental fact of a creation of unstable vector mesons in electron - positron annihilation processes, thus depending just on parameters with a clear physical meaning.

Here we present results:

- a strong evidence for $\rho'''(2150)$ by the data on $J/\psi \to \pi^+\pi^-$ decay
- a prediction of $\sigma_{tot}(e^+e^- \to n\bar{n}) \gg \sigma_{tot}(e^+e^- \to p\bar{p})$ just above the nucleon - antinucleon threshold
- surprisingly large one photon e.m. corrections to the strong $J/\psi \to p\bar{p}$ and $J/\psi \to n\bar{n}$ decay amplitudes
- the behaviour of the polar-angle asymmetry parameter α(t) for $e^+e^- \to p\bar{p}$ and $e^+e^- \to n\bar{n}$ processes

which have been obtained by utilizing the UA-VMD model for e.m. structure of pions and nucleons.

Unitary and analytic VMD model.

The UA-VMD model is obtained (for more detail see Refs. [5)–9)]) from a standard VMD parametrization of e.m. ff of the hadron

$$F(t) = \sum_{\nu} \frac{m_\nu^2 (f_{\nu hh}/f_\nu)}{m_\nu^2 - t} \tag{1}$$

by means of the following nonlinear transformation

$$t = t_0 - \frac{4(t_{in} - t_0)}{(\frac{1}{W} - W)^2} \tag{2}$$

which along with a correct making allovance for nonzero vector meson widths ($\Gamma_\nu \neq 0$) considers the two-cut approximation of the ff analytic properties and leads to the following factorized expression

$$F(t) = \left(\frac{1 - W^2}{1 - W_N^2}\right)^2 \left[\sum_r \frac{(W_N - W_r)(W_N - W_r^*)(W_N - \frac{1}{W_r})(W_N - \frac{1}{W_r^*})}{(W - W_r)(W - W_r^*)(W - \frac{1}{W_r})(W - \frac{1}{W_r^*})} (f_{rhh}/f_r) + \right.$$
$$\left. + \sum_s \frac{(W_N - W_s)(W_N - W_s^*)(W_N + W_s)(W_N + W_s^*)}{(W - W_s)(W - W_s^*)(W + W_s)(W + W_s^*)} (f_{shh}/f_s) \right] \tag{3}$$

where $t_0 < (m_r^2 - \frac{\Gamma_r^2}{4}) < t_{in}$; $(m_s^2 - \frac{\Gamma_s^2}{4}) > t_{in}$; W_r, W_s are the pole positions of vector mesons in the W-plane and W_N is the normalization point corresponding to t=0. The first term (that in front of square brackets) completely determines the asymptotic behaviour of F(t) and the second one (in the square brackets) describes the whole complicated ff resonant structure in the time-like region and for $t \to \pm\infty$ it becomes a finite real constant.

UA-VMD model for pions and an evidence of $\rho'''(2150)$ by $J/\psi \to \pi^+\pi^-$ decay.

The decay of $J/\psi \to \pi^+\pi^-$ is pure e.m. if G-parity is conserved by strong interactions and consequently one can extract an information on $|F_\pi(m_\psi^2)|$ from the latter by using the relation

$$\Gamma(J/\psi \to \pi^+\pi^-) = \frac{\pi\alpha^2 m_\psi}{3f_\psi^2}|F_\pi(t)|^2. \tag{4}$$

In an optimal description of all existing pion ff data by the UA-VMD model with $v = \rho, \rho', \rho''$ (all parameters are left to be free) an existence of two excited states of the $\rho(770)$ meson is demonstrated [5] (see Fig.1) to be simultaneously consistent with the space-like and time-like ff data unlike the results by A.Donnachie and H.Mirzaie [10] who have obtained the latter information just from the time-like $e^+e^- \to \pi^+\pi^-$ data. However, two DM2 points [11] and the last time-like point obtained [12] from $J/\psi \to \pi^+\pi^-$ decay are not described (see Fig.1) very well by the theoretical curve predicted by the pion ff UA-VMD model with $\rho(770)$, $\rho'(1450)$, $\rho''(1700)$ only, thus indicating that a higher mass isovector vector state cannot be neglected. Really, considering another vector meson in the pion ff UA-VMD model and repeating the analysis of the same data (again parameters are left to be free) one finds a strong evidence (see Fig.2) of the third excited state of the $\rho(770)$ meson with resonance parameters $m_{\rho'''} = 2169 \pm 46\ MeV$ and $\Gamma_{\rho'''} = 319 \pm 136\ MeV$. Moreover, the predicted value $|F_\pi(m_\psi^2)| = 0.1091$ by the UA-VMD model for the pion e.m. ff with three excited states of the $\rho(770)$ meson is through the relation

$$\Gamma(J/\psi \to \pi^+\pi^-) = \frac{1}{4}|F_\pi(m_\psi^2)|^2\Gamma(J/\psi \to \mu^+\mu^-) \tag{5}$$

in a perfect agreement with existing experimental $\Gamma(J/\psi \to \pi^+\pi^-)$ and $\Gamma(J/\psi \to \mu^+\mu^-)$.

Prediction of the inequality $\sigma_{tot}(e^+e^- \to n\bar{n}) \gg \sigma_{tot}(e^+e^- \to p\bar{p})$

The e.m. structure of nucleons is completely described [7] by the following four e.m. ff's

$$\begin{aligned} G_E^p(t) &= [F_1^s(t) + F_1^v(t)] + \frac{t}{4m_p^2}[F_2^s(t) + F_2^v(t)] \\ G_M^p(t) &= [F_1^s(t) + F_1^v(t)] + [F_2^s(t) + F_2^v(t)] \end{aligned} \tag{6}$$

$$\begin{aligned} G_E^n(t) &= [F_1^s(t) - F_1^v(t)] + \frac{t}{4m_n^2}[F_2^s(t) - F_2^v(t)] \\ G_M^n(t) &= [F_1^s(t) - F_1^v(t)] + [F_2^s(t) - F_2^v(t)] \end{aligned} \tag{7}$$

where $F_1^s(t)$, $F_2^s(t)$ and $F_1^v(t)$, $F_2^v(t)$ are isoscalar and isovector parts of the Dirac and Pauli nucleon e.m. ff's, respectively, to which directly the UA-VMD model (3), however with a changed asymptotic behaviour, can be applied. Unlike the analyses carried out in [7] here the OZI rule [13]-[15] is strictly taken into account and all ϕ-meson contributions are neglected. Consequently, the isoscalar e.m. ff's are saturated only with three ω-mesons [16] and the isovector e.m. ff's contain all known isovector vector mesons i.e. $\rho(770)$, $\rho'(1450)$, $\rho''(1700)$ and $\rho'''(2150)$.

Each free parameter of the model is fixed in an optimal description of 356 reliable experimental points on proton and neutron e.m. ff's for $t < 0$ and 12 data on $\sigma_{tot}(e^+e^- \to p\bar{p})$ for $3.610\ GeV^2 \leq t \leq 5.693 GeV^2$. Then, finally the behaviour of $\sigma_{tot}(e^+e^- \to n\bar{n})$, for which there is no experimental point at present, is predicted to be considerably larger (see Fig.3) than $\sigma_{tot}(e^+e^- \to p\bar{p})$ just above the nucleon-antinucleon threshold.

One photon e.m. corrections to strong $J/\psi \to N\bar{N}$ decay amplitudes.

The decay $J/\psi \to B\bar{B}$ (B being a member of the baryon octet) is currently assumed to proceed in the lowest-order approximation through the three graphs presented in Fig.4 and its integrated decay width is given [17] by the following relation

$$\Gamma(J/\psi \to B\bar{B}) = \frac{\beta N_B^2}{48\pi M_\psi}(2T + L) \tag{8}$$

where $\beta = (1 - (4m_B^2/M_\psi^2))^{1/2}$; $N_B = \frac{15}{6\sqrt{8}}(\frac{36\pi\alpha_s}{M_\psi^3})^3 f_\psi f_B^2$; $f_\psi \approx 0.26$ GeV is the decay constant of J/ψ; f_B an overall normalization constant to be calculated from the $J/\psi \to B\bar{B}$ data, and T, L are squares of helicity amplitudes for a polarized J/ψ having helicity $\Lambda = 0$ or $\Lambda = \pm 1$, respectively. Then an interesting question arises: what is the rate of a e.m. corrections represented by graphs (b) and (c) to the dominant direct hadronic decay given by graph (a).

Graph (b) gives [18]-[20] a contribution proportional to the leading amplitude (a), where the proportionality factor is

$$\delta = (-4/5)(\alpha_e/\alpha_s)Q_B \tag{9}$$

with Q_B defined as the charge of the final baryon B.

As for the one photon e.m. decay graph (c), it gives different contributions depending on whether T or L is involved. The corresponding ratios of amplitudes of graphs (c) to (a) are as follows

$$\delta_T = \frac{\alpha_e |G_M^B(M_\psi^2)|}{40\pi^2\alpha_s^3 3^6(1 + m_B^2/M_\psi^2)}\left(\frac{M_\psi^2}{f_B}\right)^2 \tag{10}$$

$$\delta_L = \frac{\alpha_e |G_E^B(M_\psi^2)|}{20\pi^2\alpha_s^3 3^6(1 + m_B^2/M_\psi^2)}\left(\frac{M_\psi^2}{f_B}\right)^2. \tag{11}$$

Now, using the overall normalization constants for protons and neutrons [17], f_p =0.00480 GeV^2; f_n =0.00488 GeV^2, the QCD running coupling constant $\alpha_s(M_\psi^2) \approx 0.25$ and values of the electric and magnetic nucleon ff's at $t=M_\psi^2$ as they are predicted by the UA-VMD model, one gets (see Table 1) surprisingly large one photon e.m. corrections to the $J/\psi \to p\bar{p}$ and $J/\psi \to n\bar{n}$ decay processes.

Table 1:

Author	$p\bar{p}$	$n\bar{n}$
CARIMALO[17]	δ_T=0.065; δ_L=0.047	δ_T=0.047; δ_L=0
OUR RESULTS	δ_T=0.104; δ_L=0.207	δ_T=0.303; δ_L=0.719

The polar angle asymmetry parameter behaviour for $e^+e^- \to N\bar{N}$.

Brodsky and Lepage [21], assuming in QCD the spin of the gluon to be 1 and using the helicity selection rule, have predicted the following angular distribution

$$\frac{d\sigma(e^+e^- \to N\bar{N})}{dcos\vartheta} \sim 1 + cos^2\vartheta \tag{12}$$

for nucleons in the asymptotic region of energies, where the quark and nucleon masses can be neglected. In the finite energy region relation (12) takes the form

$$\frac{d\sigma(e^+e^- \to N\bar{N})}{dcos\vartheta} \sim 1 + \alpha(t)cos^2\vartheta \tag{13}$$

where $\alpha(t)$ is called the polar angle asymmetry parameter.

Using the behaviour of the nucleon e.m. ff's predicted by the UA-VMD model, we show the $\alpha(t)$ behaviour in a perfect agreement with QCD predictions in the asymptotic region. Really, integratig over ϕ-angle in the relation

$$\frac{d\sigma(e^+e^- \to N\bar{N})}{d\Omega} = \frac{\alpha^2\beta_N}{4t}\left[\frac{4M^2}{t}|G_E|^2 sin^2\vartheta + |G_M|^2(1 + cos^2\vartheta)\right] \tag{14}$$

one gets

$$\frac{d\sigma(e^+e^- \to N\bar{N})}{dcos\vartheta} = \frac{2\pi\alpha^2\beta_N}{4t^2}(t|G_M|^2 + 4M^2|G_E|^2)[1 + \alpha(t)cos^2\vartheta] \tag{15}$$

where

$$\alpha(t) = \frac{t|G_M|^2 - 4M^2|G_E|^2}{t|G_M|^2 + 4M^2|G_E|^2} \tag{16}$$

The predicted behaviour of $\alpha(t)$ for protons and neutrons is given in Fig.5, from which one can see that first, $\alpha(t)$ asymptotically approaches unity as predicted by QCD and, second, just at that value the perturbative QCD starts to work as well.

References

1. G.P.Lepage and S.J.Brodsky, Phys. Rev. D22(1980) 2157.
2. V.L.Chernyak and A.R.Zhitnitsky, Phys. Rep. C112(1984) 173.
3. B.L.Ioffe and A.V.Smilga, Phys.Lett. 114B(1982) 353; Nucl.Phys. B216(1983) 373.
4. V.A.Nesterenko and A.V.Radyushkin, Phys.Lett. 115B(1982) 410.
5. S.Dubnička, I.Furdík and V.A.Meshcheryakov, Comm. of JINR, E2-88-521, Dubna(1988).
6. S.Dubnička, Comm. of JINR, E2-88-840, Dubna(1988).
7. S.Dubnička, Nuovo Cimento A100(1988) 1; ibid. A103(1990) 469 and 1417.
8. S.Dubnička, L.Lúčan, J.Phys. G15(1989) 1359.
9. M.E.Biagini, A.Castro, A.Z.Dubničková and S.Dubnička, Comm. of JINR, E2-90-396, Dubna(1990).
10. A.Donnachie and H.Mirzaie, Z.Phys. C33(1987) 407.
11. D.Bisello et al., Preprint LAL/85-15, ORSAY(1985).
12. R.M.Baltrusaitis et al., Phys. Rev. D32(1985) 566.
13. S.Okubo, Phys. Lett. 5(1963) 163.
14. G.Zweig, Report No.8419/TH 412, CERN(1964).
15. J.Iizuka, Progr. Theor. Phys., Suppl.No.37-38(1966) 21.
16. Particle Data Group, Phys.Lett. 239B, April (1990).
17. C.Carimalo, Int.J. of Modern Physics A2(1987) 249.
18. M.Claudson, S.L.Glashow, M.B.Wise, Phys.Rev. D25(1982) 1345.
19. V.L.Chernyak and I.R.Zhitnitsky, Nucl.Phys. B246(1984) 52.
20. J.-G.Kőrner, Z.Phys. C33(1987) 529.
21. S.J.Brodsky and G.P.Lepage, Phys.Rev. D24(1981) 2848.

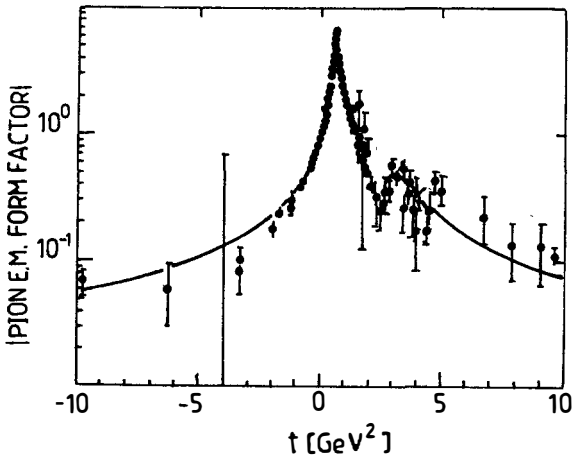

Fig.1. A demonstration of the existence of two excited states of the $\rho(770)$ meson in an optimal description of all existing pion e.m. ff data by the UA-VMD model.

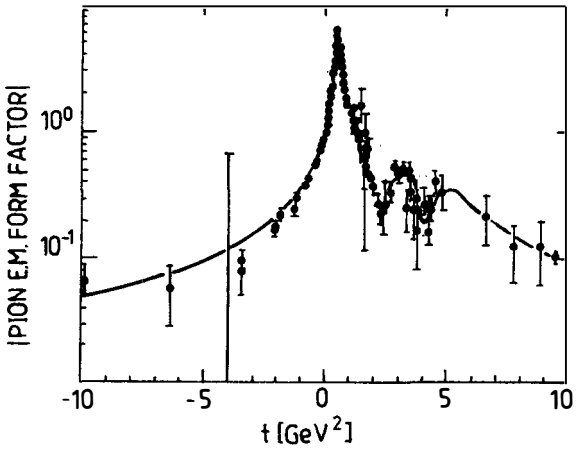

Fig.2. A strong evidence of the third excited state of the $\rho(770)$ meson in an optimal description of the same pion e.m. ff data by means of the UA-VMD model with four resonances, essentially by a perfect reproduction of the recent time-like experimental point obtained from $J/\psi \to \pi^+\pi^-$.

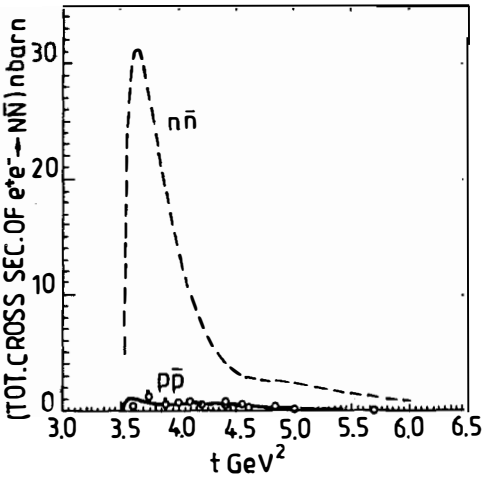

Fig.3. The nucleon e.m. structure UA-VMD model prediction for $\sigma_{tot}(e^+e^- \to n\bar{n}) \gg \sigma_{tot}(e^+e^- \to p\bar{p})$ just above the nucleon- antinucleon threshold.

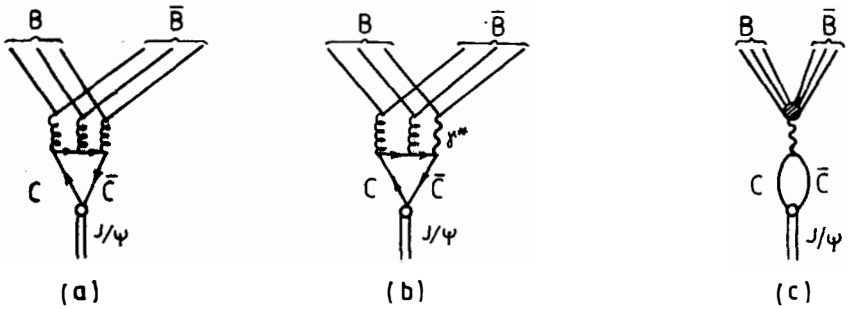

Fig.4. The lowest-order graphs for $J/\psi \to B\bar{B}$ decay. (a) a dominant direct hadronic decay. (b) the direct electromagnetic decay. (c) the one-photon electromagnetic decay.

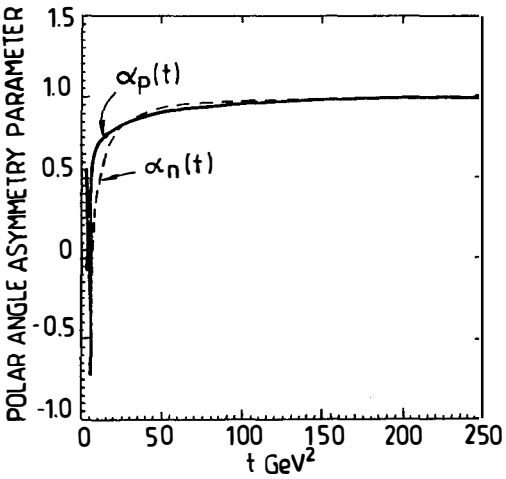

Fig.5. A prediction of the polar angle asymmetry parameter behaviour for $e^+e^- \to p\bar{p}$ and $e^+e^- \to n\bar{n}$ processes.

HIGH-PRECISION CHARMONIUM SPECTROSCOPY AT FERMILAB

T.Armstrong[6], D.Bettoni[2], V.Bharadwaj[1], C.Biino[7], G.Borreani[2], D.Brommelsiek[4], A.Buzzo[3], R.Calabrese[2], A.Ceccucci[7], R.Cester[7], M.Church[1], P.Dalpiaz[2], P.F.Dalpiaz[2], J.Fast[4], S.Ferroni[3], C.M.Ginsburg[5], K.Gollwitzer[4], A.Hahn[1], A.Hasan[6], S.Y.Hsueh[1], R.Lewis[6], E.Luppi[2], M.Macrí[3], A.Majewska[6], M.Mandelkern[4], F.Marchetto[7], M.Marinelli[3], J.Marques[4], W.Marsch[1], M.Martini[2], M.Masuzawa[5], E.Menichetti[7], A.Migliori[7], R.Mussa[7], S.Palestini[7], N.Pastrone[7], C.Patrignani[3], J.Peoples[1], L.Pesando[7], F.Petrucci[2], M.G.Pia[3], S.Pordes[1], P.Rapidis[1], R.Ray[5,1], J.Reid[6], G.Rinaudo[7], J.L.Rosen[5], A.Santroni[3], M.Sarmiento[5], M.Savrié[2], J.Schultz[4], K.Seth[5], G.A.Smith[6], L.Tecchio[7], F.Tommasini[3], S.Trokenheim[5], M.F.Weber[4], S.Werkema[1], J.L.Zhao[5], M.Zito[3].

[1]Fermilab, [2]INFN and University of Ferrara, [3]INFN and University of Genova, [4]University of California Irvine, [5]Northwestern University, [6]Pennsylvania State University, [7]INFN and University of Torino.

presented by Diego Bettoni
Istituto Nazionale di Fisica Nucleare - Ferrara, Italy

Abstract

Fermilab experiment E760 studies the direct formation of $c\bar{c}$ states in $p\bar{p}$ annihilations. In this paper we present new, high-precision measurements of the masses, total widths and branching ratios to $p\bar{p}$ of the χ_1 and χ_2 states, which represent a substantial improvement over existing data.

1 Introduction

In this paper we report the first results from Fermilab experiment E760, which studies the spectroscopy of $c\bar{c}$ states formed directly in $p\bar{p}$ interactions. In particular we shall report on the measurement of masses, total widths and widths to $p\bar{p}$ for the $^3P_1$ (χ_1) and $^3P_2$ (χ_2) states of charmonium via the reaction :

$$p\bar{p} \rightarrow \chi \rightarrow J/\psi\gamma \rightarrow e^+e^-\gamma \tag{1}$$

E760 is a fixed target experiment which uses the $\bar{p}$ beam circulating in the antiproton accumulator at Fermilab and an internal gas jet target. The parameters of the $c\bar{c}$ states are determined by studying the variation of the cross section for the process $p\bar{p} \rightarrow c\bar{c}$ with the energy of the $\bar{p}$ beam. The measurement is thus done by means of an energy scan across the resonance. This technique was first exploited at the CERN ISR by experiment R704 [1].

In this experiment the center of mass (CM) energy $W = \sqrt{s}$ is defined very precisely ($\Delta W \approx 250\ KeV$), because the antiproton beam is cooled down to $\Delta p/p \approx 2 \times 10^{-4}$. This makes it possible for the first time to measure directly resonance widths smaller than 1 MeV.

An accurate determination of masses and widths for the $c\bar{c}$ states depends crucially on the precise knowledge of the absolute energy scale, which is achieved by means of energy scans at the J/ψ and $\psi\prime$ [3].

2 The Detector

In the energy range of charmonium, the $p\bar{p}$ total cross section is several orders of magnitude larger then the $c\bar{c}$ formation cross section (10^6 at the χ states). Thus the study of $c\bar{c}$ resonances via their hadronic decay modes is contaminated by a very large background, which makes it extremely difficult to extract a clean signal. On the other hand a much better signal to noise ratio can be obtained if we limit our search to those decay modes of the $c\bar{c}$ states involving only electrons and photons in the final state (e.g. radiative decays).

For this reason the E760 detector has been designed to optimize the detection and the energy determination for electrons and photons. The layout of the detector is shown in fig. 1. It is a non-magnetic spectrometer with full azimuthal (ϕ) cov-

Figure 1: Layout of the E760 detector

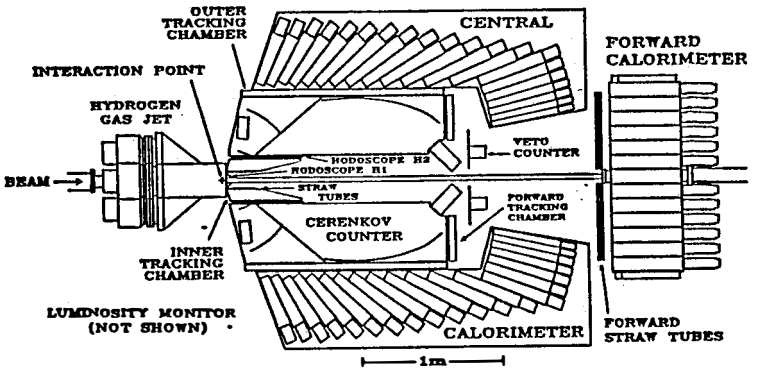

erage and polar angle (θ) acceptance ranging from 2° to 70°. The central detector ($12° < \theta < 70°$) has cylindrical symmetry around the beam axis and consists of : two scintillator hodoscopes (H1 and H2) ; a straw-tube drift chamber [4], a radial projection chamber and a multiwire proportional chamber [5] which provide the inner tracking ; a multicell threshold Čerenkov counter for electron/pion separation [6]; two planes of limited streamer tubes and a planar multiwire proportional chamber which provide the outer tracking [7]; an electromagnetic calorimeter consisting of 1280 lead-glass blocks pointing to the interaction region, with a 20-fold segmentation in θ and a 64-fold segmentation in ϕ [8]. The forward detector, extending the θ acceptance down to 2° consists of a veto hodoscope, a three-layer straw-tube drift chamber and a Pb/scintillator calorimeter [9]. The luminosity monitor is provided by a set of silicon detectors covering the polar angle region from 82° to 90°, which measure the direction and energy of the recoil proton from forward antiproton elastic scattering [10].

With this arrangement we achieve an angular resolution of 4 mrad in θ and 7 mrad in ϕ. The energy resolution $\Delta E/E$ is $0.06/\sqrt{E(GeV)}$ and $0.11/\sqrt{E(GeV)}$ for the central and forward calorimeter respectively.

3 Event Selection and Analysis

In the final state of reaction (1) the J/ψ is produced almost at rest in the CM frame and the e^+ and e^- momenta are nearly coplanar. The fast trigger logic, designed

Figure 2: e^+e^- invariant mass distributions (GeV)

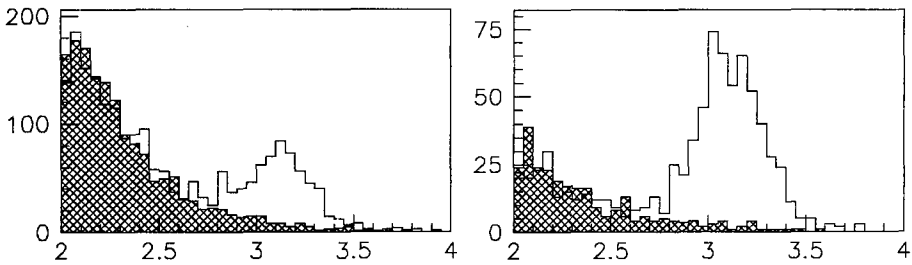

2a 2b

to select all $c\bar{c}$ resonances decaying either inclusively to J/ψ or exclusively to e^+e^-, uses the signals from the scintillator hodoscopes H1 and H2, the Čerenkov counter and a matrix of 5 × 8 analogue sums from the central calorimeter. The event trigger requires two loosely coplanar ($|\Delta\phi| > 163°$) electron tracks in the central detector (an electron track being defined as the coincidence between the appropriate elements of H1, H2 and the Čerenkov) and two energy depositions in the central calorimeter above a certain threshold and separated by at least 90° in ϕ. The measured efficiency for this trigger is $.87 \pm .02$.

At the offline level, a preliminary requirement of two electron candidates (defined as charged tracks with an associated cluster in the central calorimeter), of which at least one associated to a signal in the Čerenkov counter, with an invariant mass of least 2 GeV/c^2 selects 96% of the events from reaction (1).

A first analysis chain, called *inclusive* selection, is based on the requirement of two isolated electrons with an invariant mass m_{ee} equal to that of the J/ψ. The definition of an isolated electron is based on the pulse-height information from H2 and the Čerenkov and on the lateral dimensions of the central calorimeter shower, which are combined into an *electron quality index*. The cut on the electron quality index and the relative efficiency have been determined from a sample of approximately 4000 $J/\psi \rightarrow e^+e^-$ decays.

Fig. 2 shows, for the χ_2 data, the invariant mass distribution of the e^+e^- pair (a) for all events passing the preliminary cuts and (b) for those events in which

Figure 3: e^+e^- invariant mass distributions (GeV)

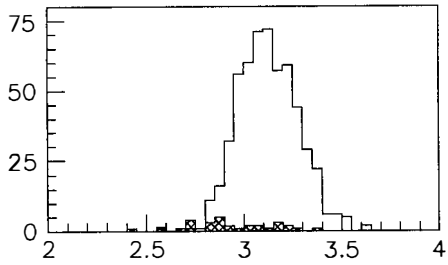

both electron candidates pass the cut on the electron quality index. The shaded areas represent an estimation of the background, obtained by applying the same analysis to a sample of events taken in an energy region away from resonances. Most of the residual background in fig. 2 (b) is eliminated by the requirement $m_{ee} > 2.75\ GeV/c^2$. The overall efficiency of this analysis, including the invariant mass cut, is $.833 \pm .007$.

A parallel analysis chain, performed on events passing the preliminary selection, is based on a kinematic fitting procedure, in which the conservation of four-momentum and the requirement $m_{ee} = m_{J/\psi}$ provide 5 constraints (2 for the case where the radiated γ in reaction (1) escaped detection). The fit is carried out with the method of Lagrangian multipliers ; events are rejected if the χ^2 probability is less than 10^{-4}. The efficiency of this selection is $.906 \pm .011$.

Fig. 3 shows the e^+e^- invariant mass distribution for the final sample, consisting of events which pass the selection based on the kinematic fit and with at least one electron passing the cut on the electron quality index. The shaded area is again an estimation of the background, which for this sample is found to be about 4%. The overall selection efficiency for the final sample is $.893 \pm .013$.

4 Results

The events in the final sample are grouped into energy bins corresponding to the points of the energy scan. Fig. 4 shows the measured cross section as a function of

Figure 4: Excitation curves for the χ states

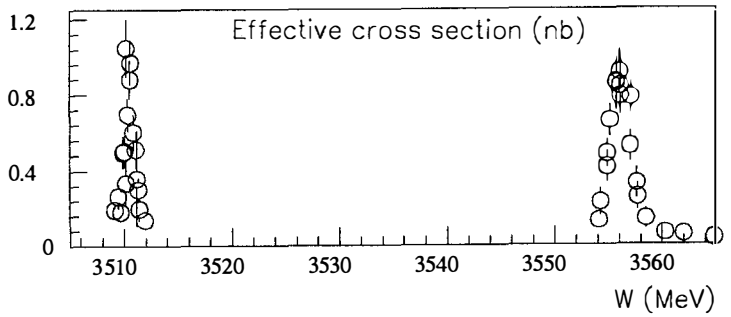

the CM energy for the χ_1 and the χ_2. The resonance parameters are determined by means of a maximum likelihood fit, in which these data points are fitted to the convolution of the Breit-Wigner cross section with the measured beam energy distribution, plus a constant background term. The fitted parameters are, for each resonance, its mass, total width and the product

$$\Gamma(\chi \to p\bar{p}) \times \Gamma(\chi \to J/\psi\gamma) \times \Gamma(J/\psi \to e^+e^-)$$

from which we can derive the value of the partial width into $p\bar{p}$ by using the world averages for the values of the partial widths in the final states.

The results of the fits are summarized in table 1, together with the values from the Particle Data Book [2]. The mass measurements are in good agreement with the existing ones, with errors which are smaller by a factor of 2. For the χ_1 we give the first measurements of the total width (for which previously only an upper limit existed) and of the branching ratio to $p\bar{p}$. The corresponding measurements for the χ_2 are given with a much smaller error ; in particular the error on the χ_2 total width has been reduced by a factor of about 4. These measurements are in good agreement with expectations based on perturbative QCD and on potential models [11].

To summarize, we have presented new measurements of the parameters of the χ states of charmonium, which represent a remarkable improvement over existing data. In particular, we have given the first direct measurement of the total width and branching ratio to $p\bar{p}$ for the χ_1.

Table 1: χ_1 and χ_2 parameters

State	Mass (MeV)	Width (MeV)	BR to $p\bar{p}$
χ_1, E760	$3510.53 \pm 0.04 \pm 0.12$	$0.88 \pm 0.11 \pm 0.08$	$(0.79 \pm 0.15) \times 10^{-4}$
χ_1, ref 2	3510.6 ± 0.5	< 1.3 MeV 95 % C.L.	$(0.54 - 12) \times 10^{-4}$
χ_2, E760	$3556.15 \pm 0.07 \pm 0.12$	$1.98 \pm 0.17 \pm 0.07$	$(0.87 \pm 0.15) \times 10^{-4}$
χ_2, ref 2	3556.3 ± 0.4	$2.6\ ^{+1.2}_{-0.9}$	$(.90\ ^{+0.45}_{-0.32}) \times 10^{-4}$

References

[1] C. Baglin et al., Nucl. Phys. **B286**(1987)592.

[2] Review of particle properties, Phys. Lett. **B239**(1990)1.

[3] T.A. Armstrong et al., Charmonium spectroscopy in Fermilab Pbar Accumulator Ring, to be submitted for publication to Physical Review D.

[4] C. Biino et al., Nucl. Instr. and Meth. **A271**(1988)417.

[5] R. Calabrese et al., Nucl Instr. and Meth. **A277**(1989)116.

[6] C. Biino et al., A large acceptance threshold Čerenkov counter for experiment E760 at Fermilab, to be submitted for publication to Nucl. Instr. and Meth.

[7] C. Barisone et al., INFN/AE-89/6(1989).

[8] L. Bartoszek et al., Nucl. Instr. and Meth. **A301**(1991)47.

[9] M.A. Hasan et al., Nucl. Instr. and Meth. **A295**(1990)73.

[10] M. Sarmiento et al., A luminosity monitor for FNAL experiment E760, to be submitted for publication to Nucl. Instr. and Meth.

[11] T.A. Armstrong et al., Determination of the parameters of χ_1 and χ_2 charmonium states formed in $p\bar{p}$ annihilations, to be submitted for publication to Nuclear Physics B, and references therein.

OVERVIEW AND CONCLUSIONS

CONFERENCE SUMMARY

Chris Quigg
Fermilab, Batavia, Illinois USA

ABSTRACT

I summarize the new results presented during the hadronic session of the XXVI Rencontre de Moriond.

1. INTRODUCTION

On this twenty-fifth anniversary of the Rencontres de Moriond, I want to begin my talk by saluting the marvelous spirit of common cause that has characterized this series of meetings. Again in this anniversary year, our friends—*gentils organisateurs*, conference staff, and *patron* Jean Trân Thanh Vân—have welcomed us with an inspired mixture of colleagues, topics, and entertainments. Diversity in the service of scientific excellence has been the hallmark of Moriond. Year after year, promising young physicists arrive in force to make their first presentations to an international audience that includes distinguished elders. Hot new subjects share the stage with old standbys. We participants are obliged to listen to—and even think about—research topics we didn't know could be interesting. Sometimes we find our prejudices confirmed, but sometimes we are treated to delicious surprises. To the pioneers of Moriond, to the veterans of many *Rencontres*, and to this year's first-time participants, I offer my thanks and congratulations for the atmosphere of support, encouragement, and curiosity about Nature that animates these encounters.

The Moriond years have spanned the development of the standard model: the establishment of quarks and leptons as basic constituents, the discovery of neutral weak currents, the proof that spontaneously broken gauge theories are renormalizable, the invention of asymptotic freedom, the rise of perturbative QCD, the discoveries of the ψ/J and charm, the tau lepton, the Υ and the b-quark, the $W^{\pm}$ and Z^0. Key experimental results have come from a succession of new machines: Serpukhov, SLAC, the ISR, Fermilab's Main Ring, CERN's SPS, the CEA Bypass, SPEAR, ADONE, ACO/DCI, DORIS, CESR, PETRA, PEP, the S$\bar{p}$pS collider, the Tevatron, TRISTAN, SLC, and LEP; from grand old machines like the AGS, the PS, and the KEK synchrotron; and from nonaccelerator experiments. Experimental techniques have ranged from emulsions and silicon microstrips to mammoth bubble chambers, water Cerenkov detectors, and 4π-solenoidal detectors. Theory has embraced the ancient wisdom of the complex angular momentum plane, the creation and application of the Lagrangian of the standard model, lattice gauge theory, supersymmetry, and dreams of superstrings. We have discovered common ground with cosmologists, astrophysicists,

and nuclear physicists. Moriond has provided a forum for all these developments and has helped nurture the new links with other fields.

2. Z^0 PHYSICS

The largest quantity of new results this year come from the four LEP experiments, summarized here in a talk by Klaus Tittel.[1] The principal parameters of the Z^0 resonance are summarized in Table 1.

Table 1. Z^0 Parameters determined by experiments at LEP.

Observable	LEP Average	Standard Model
$M(Z)$	91.174 ± 0.02 GeV/c^2	
$\Gamma(Z)$	2.485 ± 0.009 GeV	2.497 ± 0.025 GeV
σ^0(hadrons)	41.43 ± 0.25 nb	41.43 ±·0.07 nb
$\Gamma(Z\to$hadrons)	1740 ± 9 MeV	1744 ±18 MeV
$\Gamma(Z\to e^+e^-)$	83.2 ± 0.5 MeV	83.9 ± 0.8 MeV
$\Gamma(Z\to\mu^+\mu^-)$	83.5 ± 0.9 MeV	83.9 ± 0.8 MeV
$\Gamma(Z\to\tau^+\tau^-)$	83.1 ± 1.0 MeV	83.9 ± 0.8 MeV
$\Gamma(Z\to\ell^+\ell^-)$	83.31 ± 0.40 MeV	83.9 ± 0.8 MeV
$\Gamma(Z\to$hadrons)/$\Gamma(Z\to\ell^+\ell^-)$	20.90 ± 0.12	20.79 ± 0.08
$\Gamma(Z\to$invisible)	494 ± 8 MeV	502 ± 4 MeV
Number of neutrinos	2.97 ± 0.05 ± 0.05	3

One new measurement I greatly enjoyed seeing is the first determination of the polarization of fermions produced on the Z^0, using self-analyzing decays of the τ-lepton to infer the polarization $P(\tau)$. In terms of the chiral couplings of the electroweak theory,

$$\begin{aligned} L &= \tau_3 - 2Qx_W \\ R &= -2Qx_W \end{aligned} \qquad (1)$$

where τ_3 is the weak-isospin projection, $x_W = \sin^2\theta_W$ is the weak mixing parameter, and Q is the electric charge, we may express the polarization of the tau as

$$P = \frac{\sigma_R - \sigma_L}{\sigma_R + \sigma_L} = \frac{R^2 - L^2}{R^2 + L^2} = \frac{4x_W - 1}{1 - 4x_W + 8x_W^2}\,. \qquad (2)$$

The ALEPH Collaboration has measured the tau polarization in five decay modes, with the results shown in Table 2. The $\pi\nu_\tau$ and $\rho\nu_\tau$ channels have the greatest statistical weight. Within errors, all the channels give consistent determinations of the polarization. The mean value corresponds to a weak mixing parameter of $x_W = 0.2319 \pm 0.0057$, in good agreement with measurements by the L3 Collaboration ($x_W = 0.230 \pm 0.015$) and by the OPAL Collaboration ($x_W = 0.245 \pm 0.012$).

Table 2. ℵ Measurements of Tau Polarization on the Z^0 Peak.

Decay Mode	$P(\tau)$
$e\nu_e\nu_\tau$	$-0.193 \pm 0.162 \pm 0.061$
$\mu\nu_\mu\nu_\tau$	$-0.192 \pm 0.118 \pm 0.046$
$\pi\nu_\tau$	$-0.130 \pm 0.065 \pm 0.044$
$\rho\nu_\tau$	$-0.124 \pm 0.047 \pm 0.051$
$A_1\nu_\tau$	$-0.150 \pm 0.150 \pm 0.070$
Average	-0.143 ± 0.045

What is particularly noteworthy about the complex of measurements of Z^0 properties carried out at LEP is the consistency among the four experiments, and among many observables. This can be seen in the compilation[1] of ℵ measurements of the weak mixing parameter x_W shown in Table 3 and compared there with the overall LEP average. The LEP measurements significantly extend our tests of the standard model and enable us to place meaningful constraints on extensions to the standard model. Some of our colleagues are occasionally heard to claim that LEP is a disappointment because no "new" discoveries have been made and because the standard model has not (yet) been demolished. Let me be very clear: LEP is not a failure! Precisely these precision tests of standard-model predictions have been the stuff of our dreams for a decade. They will form a permanent part of the culture of our discipline.

Table 3. ℵ Measurements of the Weak Mixing Parameter.

Observable	$\sin^2\bar{\theta}_W$
Line shape, Γ_μ	0.2330 ± 0.0025
F-B asymmetry: leptons	0.2295 ± 0.0038
—: hadron charges	0.2300 ± 0.0052
—: $b\bar{b}$	0.2262 ± 0.0054
—: $c\bar{c}$	0.2310 ± 0.0110
Polarization: τ	0.2319 ± 0.0057
Average	0.2311 ± 0.0017
LEP Average	0.2320 ± 0.0017
	(0.0007 common systematics)

3. THE HIGGS BOSON

The Higgs boson arises naturally through the spontaneous breaking of electroweak symmetry in the minimal standard model. An important independent argument assures us that—in any acceptable theory—something like the Higgs boson must exist. Consider the role that the Higgs boson plays in the cancellation of high-energy divergences. An illuminating example is provided by the reaction

$$e^+e^- \to W^+W^- \ , \tag{3}$$

which is described in lowest order in the Weinberg-Salam theory by four Feynman graphs. The leading divergence in the $J=1$ amplitude of the t-channel neutrino-exchange diagram is cancelled by the contributions of the direct-channel γ- and Z^0-exchange diagrams. However, the $J=0$ scattering amplitude, which exists in this case because the electrons are massive and may therefore be found in the "wrong" helicity state, grows as $\sqrt{s}$ for the production of longitudinally polarized gauge bosons. The resulting divergence is precisely cancelled by the direct-channel Higgs-boson graph. From the point of view of S-matrix theory, the Higgs-electron-electron coupling must be proportional to the electron mass because the strength of "wrong-helicity" amplitudes is proportional to the fermion mass.

Let us summarize: Without spontaneous symmetry breaking in the standard model, there would be no Higgs boson, no longitudinal gauge bosons, and no extreme divergence difficulties. (Nor would there be a viable low-energy phenomenology of the weak interactions.) The most severe divergences are eliminated by the gauge structure of the couplings among gauge bosons and leptons. A lesser, but still potentially fatal, divergence arises because the electron has acquired mass—because of the Higgs mechanism. Spontaneous symmetry breaking provides its own cure by supplying a Higgs boson to remove the last divergence. A similar interplay and compensation must exist in any satisfactory theory.

The limited ability of the standard model to make definite predictions for the properties of the Higgs boson is well known. In the standard model, we expect a single, massive, spinless particle whose coupling to fermion-antifermion pairs is proportional to the fermion mass, but there is no definite prediction for the Higgs scalar's mass. Lower bounds on the Higgs mass can be derived by considering quantum corrections to the Higgs potential and requiring that the vacuum expectation value $\langle\phi\rangle_0$ of the Higgs field be nonzero and that the Higgs potential $V(\langle\phi\rangle_0)$ at that point be bounded from below. If $\langle\phi\rangle_0$ is not an absolute minimum of the potential, it is reasonable to require that its false-vacuum lifetime exceed the age of the universe. The resulting bounds[2] require that $M_H \gtrsim \sqrt{1 - (m_t/79.5\ \mathrm{GeV}/c^2)^4}$ or, for larger top-quark masses, that $M_H \gtrsim \frac{5}{3}(m_t - 95\ \mathrm{GeV}/c^2)$. The CDF Collaboration's limit on the mass of the top quark, $m_t > 89\ \mathrm{GeV}/c^2$, presented at this meeting by Rick Snider,[3] does not place a useful lower bound on the Higgs-boson mass.

Unitarity arguments lead to a conditional upper bound on the Higgs-boson mass.[4] It is straightforward to compute the s-wave amplitudes for scattering of the gauge-boson pairs $W_L^+W_L^-$, $Z_L^0Z_L^0$, HH, and HZ_L^0, where the subscript L denotes longitudinal gauge bosons, at high energies. All are proportional to $G_FM_H^2$ as $s \to \infty$. If we impose the minimal requirement of partial-wave unitarity that the magnitude of the s-wave amplitude be less than unity, an eigenchannel analysis leads to the constraint

$$M_H \lesssim \left(\frac{8\pi\sqrt{2}}{3G_F}\right)^{1/2} = 1 \text{ TeV}/c^2 \qquad (4)$$

If this "upper bound" is exceeded, the weak interactions among gauge bosons become strong on the 1-TeV scale. The triviality of strongly coupled scalar field theory on the lattice leads by a different path to an estimate[5] $M_H \lesssim 600\ \text{GeV}/c^2$.

Much effort has been devoted to searches for the standard-model Higgs boson in the fermion-antifermion, two-photon, and two-gauge-boson channels. A splendid survey of LEP searches in the process $e^+e^- \to HZ^*$, with the virtual Z tagged in lepton pairs, was presented by Ehud Duchovni.[6] The best current limit is

$$M_H > 48\ \text{GeV}/c^2 \ . \qquad (5)$$

If the Higgs boson is heavy ($M_H > 2M_W$), it will decay principally into pairs of gauge bosons. Strategies for detecting the "gold-plated" $ZZ \to \ell^+\ell^-\ell^+\ell^-$ signal in hadron supercolliders have been discussed in detail by Nigel Glover.[7] Giulia Pancheri[8] addressed the difficult region ($M_W \lesssim M_H \lesssim 2M_W$) in which rare decays seem the best bet for identifying a Higgs-boson peak. Although it will clearly be challenging to discover an intermediate-mass Higgs, we have reason to be optimistic about the prospects of high-luminosity pp colliders. The outstanding issues are the high resolution required to purify and reconstruct a $\gamma\gamma$ resonance and the fearsome interaction rates ($10^8 - 10^9$ Hz) a supercollider detector will have to survive. Finally, D. P. Roy[9] surveyed charged-Higgs-boson signatures and thereby reminded us that a single neutral Higgs scalar is but the simplest possibility.

4. STRONG INTERACTIONS AMONG GAUGE BOSONS[10]

We have seen that, in the standard model, the partial-wave amplitudes for gauge-boson scattering become large at high energies if the Higgs-boson mass is large. What might be the consequences of a strongly interacting gauge sector? How might we apply to this problem what Daniele Amati in his Moriond retrospective called the cultural capital of hadron physics? Can we give meaning to the mapping

$$\begin{array}{c} \pi \ \leftrightarrow\ W \\ \\ \text{GeV} \leftrightarrow \text{TeV} \end{array} \quad ? \qquad (6)$$

The beginning observation for all investigations is the low-energy behavior of the partial-wave amplitudes a_{ij} for gauge-boson scattering, which are determined by symmetry as

$$\begin{aligned} a_{00} &\sim G_F s/8\pi\sqrt{2} \quad \text{attractive} \\ a_{11} &\sim G_F s/48\pi\sqrt{2} \quad \text{attractive} \\ a_{20} &\sim -G_F s/16\pi\sqrt{2} \quad \text{repulsive} \end{aligned} \qquad (7)$$

Several approaches have been presented in talks at this meeting. Keiji Igi[11] showed us an N/D (elastic) unitarization of the low-energy amplitudes, an attempt to draw on the methods, as well as the intuition, of low-energy $\pi\pi$ scattering. His results give an example of a featureless amplitude that saturates unitarity. If you think about reasonable outcomes before doing a calculation, this is not the first possibility that comes to (my) mind. It seems to me more plausible, in light of the hadron spectrum, to anticipate a W^+W^- resonance as the means by which unitarity is preserved. How can we tell when a reasonable—but approximate and arbitrary—unitarization procedure gives us not just a possible answer, but the right one?

A second strategy is to construct explicit models of dynamical symmetry breaking, such as technicolor, and to solve these directly or by analogy with QCD. Kyungsik Kang[12] presented a variation on this theme in which the origin of electroweak symmetry breaking is the chiral phase transition in QCD with color-sextet or color-octet quarks.

The methods of chiral perturbation theory, or effective Lagrangians, which have enjoyed great recent popularity, were the topic of reports by R. Casalbuoni and Stefanie DeCurtis.[13] They emphasized the BESS (Breaking Electroweak Symmetry Strongly) approach, in which one supposes that the essential feature is an I=1, J=1 resonance decaying into a pair of gauge bosons. The more general applications of chiral perturbation theory endeavor to learn from the effective Lagrangian for $\pi\pi$ scattering, or to capture the essence of the full standard model. The appeal of these methods derives from the successful application of chiral Lagrangians to $\pi\pi$ scattering and from

the hope that symmetries might control gauge-boson dynamics at energies relevant to sorting out the nature of electroweak symmetry breaking.

Several problems arise in the application of chiral Lagrangians to gauge-boson scattering. First, the $O(s^2)$ effective Lagrangian necessarily produces featureless amplitudes and no longer makes sense in the interesting region around 1 TeV. Second, the results are highly sensitive to the unitarization procedure. This is clearly illustrated by the work of Dobado, Herrero, and Terron,[14] who compared K-matrix and Padé-approximant methods. For a Higgs-like model with $M_H \gg 1$ TeV/c^2, the Padé method may produce an s-wave resonance peak in the neighborhood of 1 TeV/c^2, while the K-matrix yields featureless amplitudes. Finally, everyone who has ever worked on technicolor will understand the appeal of capturing the essence of the idea without being burdened by the details of a flawed explicit model. But without a complete theory, how can we impose constraints from other data, such as the restrictions on new degrees of freedom from LEP observables? Although I like the economy and generality of the effective-Lagrangian approach, I wonder whether it is not time to move on—but where?

The last issue I want to raise concerns the criteria we set for a strongly interacting gauge sector. Consider for definiteness the $(I,J) = (2,0)$ partial wave, to be observed in the exotic W^+W^+ channel. To estimate the yield of W^+W^+ events in a strongly interacting gauge sector, many authors have extrapolated the threshold behavior (7) set by low-energy theorems up to the energy at which unitarity (in the form of $|a_{20}| < 1/2$) is saturated. Such a theory, which corresponds to $M_H \to \infty$ in the Lagrangian, is surely strongly interacting; but so is its counterpart with $M_H = 4$, or 2, or even 1 TeV/c^2. (I consider a theory in which $|a_{00}| = 1$, or $1/2$, strongly interacting.) The a_{20} partial-wave amplitude in a strongly interacting theory—by my definition—may be considerably smaller than extrapolation of the low-energy theorem would suggest, and the yield of W^+W^+ events will be correspondingly smaller. A large value of $|a_{20}|$ is therefore not an infallible diagnostic of a strongly interacting theory: it is sufficient, but not necessary. We have to aspire to a comprehensive study of the (0,0), (1,1), and (2,0) partial waves.

5. QCD STUDIES AT THE Z^0

The LEP experiments have carried out extensive fits to event shapes and kinematical distributions on the Z^0 resonance. The observations are consistent with the predictions of QCD and lead to determinations of the strong coupling constant at the Z^0 mass that are consistent among the experiments and the different observables. The best values are summarized in Table 4. Comparing with earlier work, it is possible to believe that measured values of α_s run, but belief is not yet obligatory.

Table 4. LEP Measurements of the strong coupling constant.

Experiment	$\alpha_S(M_Z^2)$
ℵ [15]	0.117 ± 0.005
DELPHI [16]	0.106 ± 0.005
L3 [17]	0.115 ± 0.004 (exp) $\pm$ 0.008 (theory)
OPAL [18]	0.120 ± 0.008

6. RUNNING TOWARD UNIFICATION

Why unify the gauge theories of the strong, weak, and electromagnetic interactions? We are motivated by the similarity of quarks and leptons as pointlike, Dirac particles, by the requirement of anomaly cancellation in the electroweak theory (which suggests a link between quarks and leptons), by the hope of understanding the equality of proton and positron charges, and by the running of the gauge couplings α_1, α_2, and α_3, which suggests that they might approach a common value at very high energy. The paradigm for unification is the SU(5) theory,[19] which breaks down according to $SU(5) \rightarrow SU(3)_c \otimes SU(2)_L \otimes U(1)_Y \rightarrow SU(3)_c \otimes U(1)_{em}$. Hermann Fürstenau[20] presented an analysis of the evolution of the coupling constants tied to the DELPHI determination of $\alpha_s(M_Z^2)$ that shows α_1 and α_2 crossing at 10^{13} GeV, but missing α_3 by many standard deviations. Going beyond the standard model by adding supersymmetric partners at around 1 TeV/c^2 changes the evolution so that all three coupling constants meet at around 10^{16} GeV. This has led some enthusiasts to announce that LEP has discovered supersymmetry!

Leaving aside the question of where the relevant knowledge of the coupling constants actually comes from, it strikes me that this is the sort of result that is really interesting only if it turns out to be true. Moreover, it is important to remember that nothing we know requires the $SU(3)_c$, $SU(2)_L$, and $U(1)_Y$ couplings to meet at a single point, even if the strong, weak, and electromagnetic interactions are unified without gravitation. I offer as a counterexample to the SU(5) paradigm the notion of petite unification advanced nearly a decade ago by Hung, Buras, and Bjorken.[21] In their scheme, electroweak unification is completed at an intermediate energy and the single electroweak coupling runs into the strong coupling at a higher energy.

7. HEAVY FLAVORS

New data were presented on the production and decay of charmed particles. Andrew Kirk[22] reported on the study of production dynamics and charm spectroscopy in the Ω-spectrometer experiment WA82 at CERN. Charm production is a difficult case for perturbative QCD, but the systematics of x-, $p_\perp$-, and energy-dependence are in reasonable agreement with experiment. Among the goals of WA82 are a study of the A-dependence of charm production, characterized by a power-law A^α, with $\alpha(D) = 0.88^{+0.04}_{-0.05}$ for charmed mesons produced with $\langle x \rangle = 0.24$, and an investigation of the leading-particle effect found in NA27. The theory of heavy-flavor production on complex targets was discussed by Kaidalov.[23] Laura Perasso showed lifetimes and branching ratios from E687 in the broadband photon beam at Fermilab.[24] Current data are comparable in statistics to E691 and NA32: a few thousand reconstructed events per decay mode for charmed mesons and about a hundred events per channel for the Λ_c. The 1990–1991 run is optimized (with an electron beam energy of 350 GeV) for the photoproduction of b-quarks, but will have a rich harvest of charms. I view the study of b-quarks in a photon beam as a long shot, because the high-energy cross section is expected to be quite small—perhaps a nanobarn at Fermilab energies[25] and no more than 75 nb at very high energies.[26]

New experimental results on b-quarks were presented in three talks to the conference. J. Gronberg[27] reported a new analysis of UA1 muon data. A Monte Carlo program based on the Nason-Dawson-Ellis calculation[28] accounts for the transverse-

momentum distribution of muons and leads to an inclusive cross section of $\sigma(\bar{p}p \to b + X) = 12.8^{+7.0}_{-5.4}$ nb. A study of same-sign and opposite-sign dimuons yields a measure of the average mixing parameter, $\chi \equiv f_d\chi_d + f_s\chi_s$, of $\chi = 0.148 \pm 0.029 \pm 0.017$. A. Sansoni, representing the CDF Collaboration, showed for the first time evidence for B-$\bar{B}$ mixing from like-sign $e\mu$ events.[29] CDF's preliminary result is $\chi = 0.176 \pm 0.049$. A. Stocchi[30] reported the DELPHI measurement of the average b-quark lifetime, $\tau_b = 1.31 \pm 0.13 \pm 0.12$ ps, which leads to an estimate of the quark-mixing matrix element $V_{bc} \approx 0.041$. DELPHI has also been able to estimate the partial widths for Z^0 decays into heavy flavors, $\Gamma(Z \to c\bar{c}) = 282 \pm 53 \pm 88$ MeV and $\Gamma(Z \to b\bar{b}) = 350 \pm 41$ MeV, in agreement with standard model expectations.

8. STRUCTURE FUNCTIONS

Theoretical and experimental work continues on the problem of nucleon structure. Antje Brüll[31] presented the NMC Collaboration's measurements of the ratio $F_2^{\mu n}/F_2^{\mu p}$ in the range $0.002 < x < 0.8$ and $0.1\ \text{GeV}^2 < Q^2 < 190\ \text{GeV}^2$, which are important for determining the relative importance of valence up and down quarks in the proton. Ewa Rondio[32] reported the extraction of the gluon distribution from NMC data on the reaction $\mu N \to \psi X$.

Jan Kwiecinski[33] discussed the behavior of parton distributions in the limit of small values of x and large values of Q^2. At very small values of x, the normal QCD evolution of the gluon distribution $G(x,Q^2)$ and the sea-quark distribution $q_s(x,Q^2)$ causes a rapid growth with Q^2 of the parton density that can be computed using the methods of Gribov, Levin, and Ryskin.[34] If the density becomes so large that partons overlap within the proton, the impulse approximation that is the basis of the (renormalization-group-improved) parton model becomes nonsensical. Where—in x and Q^2—this effect sets in depends on the x-dependence of the input structure functions at low Q^2. It may be possible to look for the breakdown of the impulse approximation in ep collisions at HERA and in the production of $W^{\pm}$ and Z^0 at supercollider energies. The rapid growth in the sea-quark distribution at small x significantly enhances the cross sections for ultrahigh-energy νN interactions.[35] Because of the damping effect of the W-propagator, the range $x \lesssim 10^{-4}$ becomes

extremely important for incident neutrino energies greater than about 10^{15} eV. Above this energy, the charged-current cross section may be boosted by more than an order of magnitude by the growth of the quark-antiquark sea.[36] It may be possible to measure these cross sections by instrumenting the ocean or the Antarctic ice.

9. HARD COLLISIONS / PERTURBATIVE QCD

The transverse-momentum distribution of gauge bosons produced in $\bar{p}p$ collisions has been the subject of very fruitful interplay between theory and experiment. J. Ng[37] showed the excellent agreement between the CDF measurements of the $p_\perp^W$-distribution and the beyond-leading-order calculation of Arnold and Kauffman.[38] The theory of gauge boson production was reviewed by Erwin Mirkes,[39] who emphasized the possibility of seeing the influence of higher-order contributions upon the $W^\pm$ polarization—hence the decay angular distribution. The UA2 analysis of W + jets was presented by Elisabetta Pennacchio.[40]

The data on direct photon production in hadron collisions from UA2,[41] CDF,[42] E706,[43] E705,[44] and UA6[45] are in good general agreement with the theory,[46,47] but the role of isolation cuts in defining the measured cross section needs continued careful attention, to ensure that theory and experiment are referring to the same quantity. P. Perez[48] reported the $\aleph$ studies of prompt photons at LEP.

"What is a jet?" is a question that can—and must be—asked with increasing precision, if we are to take best advantage of advances in higher-order calculations and improved experimental sensitivity. Dave Soper[49] presented the perturbative-QCD answer, while Naor Wainer[42] reported CDF's jet-shape studies and the dependence of $d\sigma/dE_T$ on jet definition. The measured cross section is in excellent agreement with QCD over nearly four decades. Patrizia Cenci[50] discussed the analysis-in-progress of UA2's 1990 jet sample and reviewed their current limit on quark compositeness, $\Lambda^* > 825$ GeV.

10. PARTICLE PRODUCTION

We heard many talks on particle production in hadron collisions and in electron-positron annihilations. I was particularly struck during Brigitte Buschbeck's talk on intermittency[51] and Wolfram Kittel's review of particle production[52] by the

continuing need to devise *differential* diagnostics of the production dynamics. In trying to make sense of multiplicity distributions and multiparticle correlation functions or rapidity-interval distributions, there is always a tension between the desire for a statistically sound result—which favors global, integrated quantities—and the hope for discrimination among competing dynamical ideas—which favors the most differential observables. It is important that we not neglect the lessons of the seventies, when it was found that two-particle correlations measured between particles of known charge could begin to distinguish among the many dynamical schemes that could reproduce topological cross sections. I am pleased to see critical examination of the methods used for the study of intermittency, so we can learn how best to unravel the dynamics of both commonplace and unusual events.

11. CONCLUDING REMARKS

At this twenty-fifth anniversary meeting, the traditions of Moriond have been much on the minds of all of us. With some embarrassment, I close my summary talk without reviewing all the contributions of this *Rencontre*. It is small comfort to know that I am following a well-established Moriond tradition that finds the haggard summary speaker in his room in a state of considerable panic, surrounded by photocopies of talks and little piles of incomplete transparencies, instead of attending the last sessions.

In thinking of what participation in Moriond conferences has meant to me over the years, I find myself returning to the notion of *une embellie*. The literal meaning is the calm after a storm, or between two storms, or what I think the English call a bright interval. Poetically, *l'embellie* evokes a moment of rest and repose away from workaday cares, a time for reflection and appreciation and metamorphosis. With its emphasis on lively participation, opportunity to spend a week with colleagues in informal settings, and focus on the excitement of trying to understand Nature, Moriond gives us all a moment to learn, to savor, to reflect. To the founders and their successors, I offer the heartfelt thanks of participants past, present, and future.

REFERENCES

1. K. Tittel, These Proceedings, p. .
2. A. D. Linde, *Pis'ma Zh. Eksp. Teor. Fiz.* **23,** 73 (1976) (*JETP Lett.* **23,** 64 (1976)); S. Weinberg, *Phys. Rev. Lett.* **36,** 294 (1976); Manfred Lindner, Marc Sher, and Helmut W. Zaglauer, *Phys. Lett.* **B228,** 139 (1989). For a review of electroweak Higgs potentials and vacuum stability, see M. Sher, *Phys. Rep.* **179,** 273 (1989). A recent discussion is given by J. Ellis, A. D. Linde, and M. Sher, *Phys. Lett.* **B252,** 303 (1990).
3. R. Snider, These Proceedings, p. . This applies if the top has normal semileptonic decays. A decay-independent lower bound of about 45 GeV/c^2 has been set by LEP experiments. During the next Tevatron run, it should be possible to infer a decay-mode independent lower bound approaching $m_t \gtrsim M_W - m_b$ from the W-boson width derived from the ratio $\sigma(W \to e\nu)/\sigma(Z \to ee)$.
4. B. W. Lee, C. Quigg, and H. B. Thacker, *Phys. Rev. Lett.* **38,** 883 (1977); *Phys. Rev. D***16,** 1519 (1977).
5. R. Dashen and H. Neuberger, *Phys. Rev. Lett.* **50,** 1897 (1983); M. P. Lüscher and P. Weisz, *Nucl. Phys.* **B318,** 705 (1989); J. Kuti, L. Lin, and Y. Shen, *Phys. Rev. Lett.* **61,** 678 (1988); G. Bhanot and K. Bitar, ibid. **61,** 798 (1988); A. Hasenfratz, et al., *Nucl. Phys.* **B317**, 81 (1989); Gyan Bhanot, Khalil Bitar, Urs M. Heller, Herbert Neuberger, *Nucl. Phys.* **B353**, 551 (1991).
6. E. Duchovni, These Proceedings, p. .
7. N. Glover, These Proceedings, p. .
8. G. Pancheri, These Proceedings, p. .
9. D. P. Roy, These Proceedings, p. .
10. For a recent review, see C. Quigg, "Gauge Boson Dynamics," Fermilab-Pub-91/58–T.
11. K. Igi, These Proceedings, p. .
12. K. Kang, These Proceedings, p. .
13. R. Casalbuoni, These Proceedings, p. ; S. DeCurtis, These Proceedings, p. .
14. A. Dobado, M. J. Herrero, and J. Terron, CERN-TH.5670/90.
15. R. St. Denis, These Proceedings, p. .
16. K. Hamacher, These Proceedings, p. .
17. S. Banerjee, These Proceedings, p. , and private communication.
18. G. Azuelos, These Proceedings, p. .
19. H. Georgi and S. L. Glashow, *Phys. Rev. Lett.* **32,** 438 (1974).
20. H. Fürstenau, These Proceedings, p. .
21. P. Q. Hung, A. J. Buras, and J. D. Bjorken, *Phys. Rev. D***25,** 805 (1982).
22. A. Kirk, These Proceedings, p. .
23. A. B. Kaidalov, These Proceedings, p. .
24. L. Perasso, These Proceedings, p. .
25. For a perturbative QCD estimate, see R. K. Ellis and P. Nason, *Nucl. Phys.* **B312,** 551 (1989).
26. C. Quigg and J. L. Rosner, *Phys. Rev. D***17,** 2364 (1978), use vector meson dominance and semiclassical sum rules to estimate the cross section far above threshold.
27. J. Gronberg, These Proceedings, p. .
28. P. Nason, S. Dawson, and R. K. Ellis, *Nucl. Phys.* **B303,** 607 (1988).
29. A. Sansoni, These Proceedings, p. .
30. A. Stocchi, These Proceedings, p. .
31. A. Brüll, These Proceedings, p. .
32. E. Rondio, These Proceedings, p. .
33. J. Kwiecinski, These Proceedings, p. .
34. L. V. Gribov, E. M. Levin, and M. G. Ryskin, *Phys. Rep.* **100,** 1 (1983).
35. Yu. M. Andreev, V. S. Berezinsky, and A. Yu. Smirnov, *Phys. Lett.* **84B,** 247 (1979).

36. D. MacKay and J. Ralston, *Phys. Lett.* **167B**, 103 (1986); C. Quigg, M. H. Reno, and T. P. Walker, *Phys. Rev. Lett.* **57**, 774 (1986); M. H. Reno and C. Quigg, *Phys. Rev. D***37**, 657 (1988).
37. J. Ng, These Proceedings, p. .
38. P. B. Arnold and R. B. Kauffman, *Nucl. Phys.* **B349**, 381 (1991).
39. E. Mirkes, These Proceedings, p. .
40. E. Pennacchio, These Proceedings, p. .
41. M. Primavera, These Proceedings, p. .
42. N. Wainer, These Proceedings, p. .
43. K. Hartman, These Proceedings, p. .
44. T. Murphy, These Proceedings, p. .
45. G. Ballocchi, These Proceedings, p. .
46. E. Pilon, These Proceedings, p. .
47. P. Aurenche, R. Baier, M. Fontennaz, and D. Schiff, *Nucl. Phys.* **B297**, 661 (1988); P. Aurenche, R. Baier, M. Fontennaz, *Phys. Rev. D***39**, 3275 (1989).
48. P. Perez, These Proceedings, p. .
49. D. Soper, These Proceedings, p. .
50. P. Cenci, These Proceedings, p. .
51. B. Buschbeck, These Proceedings, p.
52. W. Kittel, These Proceedings, p. .

LIST OF PARTICIPANTS

ALDE Douglas M.	Los Alamos National Laboratory MS-D449 LOS ALAMOS NM 87545 USA
AZUELOS Georges	Université de Montréal Centre de Rech. de Mathém. Appliquées MONTREAL Québec H3C 3J7 CANADA
BALLOCCHI Giuseppe	CERN Division PPE CH- 1211 GENEVE 23 SWITZERLAND
BANERJEE Sunanda	CERN Division PPE CH- 1211 GENEVE 23 SWITZERLAND
BARBERIS Dario	Universität Heidelberg Institut für Hochenergiephysik D- 6900 HEIDELBERG 1 FEDERAL REP. OF GERMANY
BARBERIS Dario	CERN Division PPE CH- 1211 GENEVE 23 SWITZERLAND
BARRING Olof	University of Lund Dept. of Particle Physics S- 223 62 LUND SWEDEN
BERAT Corinne	CERN Division PPE CH- 1211 GENEVE 23 SWITZERLAND
BETTONI Diego	I N F N Sezione di Ferrara FERRARA 44100 ITALY
BIENLEIN Johann	DESY Notkestrasse 85 D- 2000 HAMBURG 52 FEDERAL REP. OF GERMANY
BOPP Fritz Wilheim	Universität Gesamthochschule Siegen Fachbereich 7 - Physik D- 5900 SIEGEN FEDERAL REP. OF GERMANY
BORDES Gisèle	Collège de France Lab. de Physique Corpusculaire F- 75231 PARIS Cedex 05 FRANCE

BOSTJANCIC Bojan	Institut J. Stefan Jamova 39 61111 LJUBLJANA YUGOSLAVIA
BRAUN Mikhail	Universidad de Santiago de Compostela Faculdad de Fisica E- SANTIAGO DE COMPOSTELA SPAIN
BRULL Autje	University of Freiburg Hermann-Herder-Strasse 3 7800 FREIBURG FEDERAL REP. OF GERMANY
BUSCHBECK Brigitte	Oesterreich Akad. d. Wissensch. Inst. f. Hochenergiephysik (HEPHY) A- 1050 WIEN AUSTRIA
BUSSEY Peter	University of Glasgow Dept of Physics & Astronomy GLASGOW G12 8QQ UNITED KINGDOM
CAPELLA Alfons	Université Paris Sud LPTHE F- 91405 ORSAY Cedex FRANCE
CASALBUONI Roberto	Universita di Firenze Istituto di Fisica I- 50125 FIRENZE ITALY
CENCI Patrizia	INFN Sezione di Perugia I- 06100 PERUGIA ITALY
CHIBA Masami	Tokyo Metropolitan University High Energy Group - Dept of Physics 158 TOKYO JAPAN
COHEN-TANNOUDJI Gilles	CEN Saclay DPhPE F- 91191 GIF sur YVETTE Cedex FRANCE
CRUZ Andres	Universidad de Zaragoza Depto de Fisica Teorica E- 9 ZARAGOZA SPAIN
D'AGOSTINI Giulio	Universita di Roma "La Sapienza" Dipt di Fisica - INFN I- 00100 ROMA ITALY

DE CURTIS Stefania	Universita di Firenze Istituto di Fisica I- 50125 FIRENZE ITALY
DENEGRI Daniel	CEN Saclay DPhPE F- 91191 GIF sur YVETTE Cedex FRANCE
DHINA Mourad	Eidg. Technische Hochschule Institüt fur Hochenergiephysik CH- 8093 ZÜRICH SWITZERLAND
DRAPIER Olivier	IPN Lyon Institut de Physique Nucléaire F- 69622 VILLEURBANNE Cedex FRANCE
DREMIN Igor	Academic Science USSR (FIAN) P. N. Lebedev Inst. of Physics 117 924 MOSCOW U S S R
DUBNICKA Stanislav	Joint Inst. for Nuclear Research (JINR) Dubna, Head Post Office 101 000 DUBNA U S S R
DUCHOVNI Ehud	Weizmann Institut of Science Dept of Nuclear Physics 76100 REHOVOT ISRAEL
EBERT Dietmar	Joint Inst. for Nuclear Research (JINR) Dubna, Head Post Office 101 000 DUBNA U S S R
EVANS David	University of Birmingham School of Physics & Space Research BIRMINGHAM B15 2TT UNITED KINGDOM
FEINDT Michael	Universität Hamburg Kerntheorie u. II f. Theor. Physik D- 2000 HAMBURG 50 FEDERAL REP. OF GERMANY
FOLGER Gunter	CERN Division PPE CH- 1211 GENEVE 23 SWITZERLAND
FONTANNAZ Michel	Université Paris Sud LPTHE F- 91405 ORSAY Cedex FRANCE

FOUCHER Maurice	FERMILAB Dept of Physics BATAVIA IL 60510 USA
FÜRSTENAU Hermann	Univ. Karlsruhe Inst. fur Exp. Kernphysik D 7500 KARLSRUHE 1 FEDERAL REP. OF GERMANY
GABELLINI Yves	Université de Nice Inst. Non-Linéaire - UMR CNRS 129 F- 060034 NICE Cedex FRANCE
GALLO Elisabetta	Universita di Firenze Istituto di Fisica I- 50125 FIRENZE ITALY
GEDDES Neil	Rutherford and Appleton Lab. Chilton DIDCOT OX11 OQX UNITED KINGDOM
GLOVER Nigel	FERMILAB Dept of Physics BATAVIA IL 60510 USA
GOULIANOS Konstantin	Columbia University Dept of Physics NEW YORK NY 10027 USA
GRASSI Frédérique	Universidade de Sao Paulo Instituto di Fisica SP 05508 SAO PAULO BRAZIL
GRGIC Davorka	Filozofski Fakultet Zavod Za Fisiku 58000 SPLIT YUGOSLAVIA
GRONBERG Jeff	CERN Division PPE CH- 1211 GENEVE 23 SWITZERLAND
GUERIN Françoise	Université de Nice Lab. de Physique Théorique F- 060034 NICE Cedex FRANCE
GUERRA Catalina	CEN Saclay DPhPE F- 91191 GIF sur YVETTE Cedex FRANCE

GUSTAFSON Gösta	University of Lund Dept of Theor. Physics S- 223 62 LUND SWEDEN
HAMACHER Klaus	Bergische Universität Wuppertal Fachbereich Physik D- 5600 WUPPERTAL 1 GERMANY
HANSL-KOZANECKA Traudl	Max Planck Institut Physik und Astrophysik D- 8000 MUNCHEN 40 FEDERAL REP. OF GERMANY
HARTMAN Keith	Pennsylvania State University Lab. of Physics UNIVERSITY PARK PA 16802 USA
IGI Keiji	University of Tokyo Faculty of Science - ICEPP 113 TOKYO JAPAN
JACHOLKOWSKA Agnierka	Université Paris Sud LAL F- 91405 ORSAY Cedex FRANCE
JACQUET François	Ecole Polytechnique LPNHE F- 91128 PALAISEAU Cedex FRANCE
JAFFE David	University of Illinois at Chicago Dept of Physics CHICAGO IL 60680 USA
JEDICKE Robert	FERMILAB Dept of Physics BATAVIA IL 60510 USA
KAIDALOV Alexei	Université Paris Sud LPTHE F- 91405 ORSAY Cedex FRANCE
KAIDALOV Alexei	ITEP Inst. for Theor. and Exp. Physics 117259 MOSCOW U S S R
KANG Kyungsik	Brown University Dept of Physics PROVIDENCE RI 02912 USA

KAPUSTA Frédéric	Université Pierre et Marie Curie 4, Place Jussieu F- 75005 PARIS FRANCE
KARCH Karl-Heinz	DESY Notkestrasse 85 D- 2000 HAMBURG 52 FEDERAL REP. OF GERMANY
KIEL Torsten	Universität Hamburg II-Institut für Exp. Physik D- 2000 HAMBURG 52 FEDERAL REP. OF GERMANY
KIRK Andrew	CERN Division PPE CH- 1211 GENEVE 23 SWITZERLAND
KITTEL Wolfram	University of Nijmegen Fysisch Laboratorium NL- 6525 ED NIJMEGEN NETHERLANDS
KOWALSKI Marek	Max Planck Institut Physik und Astrophysik D- 8000 MUNCHEN 40 FEDERAL REP. OF GERMANY
KWIECINSKI Jan	Institut of Nuclear Physics Dept of Theoretical Physics PL- 31342 KRAKOW POLAND
LANARO Armando	CERN Division PPE CH- 1211 GENEVE 23 SWITZERLAND
LIU Keh-Fei	University of Kentucky Dept of Physics and Astronomy LEXINGTON KY 40506 USA
LODI-RIZZINI Evandro	Dipto Automazione Industriale Viale Europa 39 I- 25100 BRESCIA ITALY
MANI Sudhindra	University of California Dept of Physics DAVIS CA 95616 USA
MARTIN Cécile	Université Paris Sud Division de Physique Théorique-IPN F- 91406 ORSAY Cedex FRANCE

MEKHFI Mustapha	Université d'Oran Laboratoire de Physique Théorique ES-SENIA 31100 ALGERIA
MIRKES Erwin	Universität Karlsruhe Inst. f. Theoretische Kernphysik D- 7500 KARLSRUHE 1 FEDERAL REP. OF GERMANY
MONALDI Daniela	DESY Notkestrasse 85 D- 2000 HAMBURG 52 FEDERAL REP. OF GERMANY
MONALDI Daniela	Universita di Roma (INFN) Istituto di Fisica "La Sapienza" I- 00185 ROMA ITALY
MONTANET Lucien	CERN Division PPE CH- 1211 GENEVE 23 SWITZERLAND
MURPHY Thornton	FERMILAB Dept of Physics BATAVIA IL 60510 USA
NAGY Elemer	C P P M Faculté de Luminy 13288 MARSEILLE Cedex 09 FRANCE
NAVELET Henri	CEN Saclay DPhT F- 91191 GIF sur YVETTE Cedex FRANCE
NEUMEISTER Norbert	Oesterreich Akad. d. Wissensch. Inst. f. Hochenergiephysik (HEPHY) A- 1050 WIEN AUSTRIA
NG Johnny	University of Harvard High Energy Physics Laboratory CAMBRIDGE MA 02138 USA
OUVAROV Vladimir	CERN Division PPE CH- 1211 GENEVE 23 SWITZERLAND
PALANO Antonio	Universita di Bari INFN - Istituto di Fisica I- 70126 BARI ITALY

PANCHERI Giulia	Laboratorio Nazionale dell'INFN Via E. Fermi 40 I- 00044 FRASCATI ITALY
PENNACHIO Elisabetta	Universita di Pavia Istituto di Fisica Nucleare e Teorica I- 27100 PAVIA ITALY
PERALTA Luis	LIP - Lisbon Ave. Elias Garcia P- 1000 LISBOA PORTUGAL
PERASSO Laura	Universita di Milano Sezione dell' INFN - Dipto di Fisica I- 20133 MILANO ITALY
PEREZ Patrice	CEN Saclay DPhPE F- 91191 GIF sur YVETTE Cedex FRANCE
PIETRZYK Boleslaw	Faculté des Sciences Centre de Phys. des Particules F- 13288 MARSEILLE Cedex 02 FRANCE
PILON Eric	Université Paris Sud LPTHE F- 91405 ORSAY Cedex FRANCE
PODOBRIN Oliver	DESY Notkestrasse 85 D- 2000 HAMBURG 52 FEDERAL REP. OF GERMANY
PRIMAVERA Margherita	University of Cosenza Physics Dept I- 87036 RENDE ITALY
QUIGG Chris	FERMILAB Dept of Physics BATAVIA IL 60510 USA
ROBERTS Winston	Harvard University Department of Physics CAMBRIDGE MA 02138 USA
RONAN Michael	Lawrence Berkeley Laboratory Dept of Physics BERKELEY CA 94720 USA

RONDIO Ewa	Inst. f. Nuclear Studies IPJ High Energy Physics Lab. PL- 00681 WARSZAWA POLAND
RONDIO Ewa	CERN Division PPE CH- 1211 GENEVE 23 SWITZERLAND
ROTONDI Alberto	Universita di Pavia Istituto di Fisica Nucleare e Teorica I- 27100 PAVIA ITALY
ROY D.P.	CERN TH Division CH- 1211 GENEVE 23 SWITZERLAND
SACQUIN Yves	CEN Saclay DPhPE F- 91191 GIF sur YVETTE Cedex FRANCE
SAMOKHIN Anatoliy	IHEP Inst. for High Energy Physics 142 284 PROTVINO U S S R
SANSONI Andrea	Laboratorio Nazionale dell'INFN Via E. Fermi 40 I- 00044 FRASCATI ITALY
SEIBERT David	University of Jyvaskyla Dept of Physics SF- 40720 JYVASKYLA 72 FINLAND
SEIXAS Joao	CERN TH Division CH- 1211 GENEVE 23 SWITZERLAND
SHABELSKI Yuly	Leningrad Nuclear Physics Inst. High Energy Theory Dept 188350 GATCHINA U S S R
SINGOVCKY Sacha	IHEP Inst. for High Energy Physics 142 284 PROTVINO U S S R
SMIRNOVA Lidia	Nuclear Physics Institute Moscow State University 119899 MOSCOW U S S R

SNIDER Frederick	Johns Hopkins University Dept. of physics BALTIMORE MD 21218 USA
SOPER Dave	CERN TH Division CH- 1211 GENEVE 23 SWITZERLAND
ST DENIS Richard	CERN Division PPE CH- 1211 GENEVE 23 SWITZERLAND
STOCCHI Achille	Universita di Milano Istituto di Fisica I- 20133 MILANO ITALY
STUNDZIA Audrius B.	University of Toronto Dept of Physics TORONTO Ontario M5S 1A7 CANADA
TAN Chung I	Brown University Dept of Physics PROVIDENCE RI 02912 USA
TANNENBAUM Michael	CERN Division PPE CH- 1211 GENEVE 23 SWITZERLAND
THEWS Robert	University of Arizona Dept of Physics TUCSON AZ 85721 USA
TITTEL Klaus	Universität Heidelberg Institut für Hochenergiephysik D- 6900 HEIDELBERG 1 FEDERAL REP. OF GERMANY
TRAN THANH VAN Jean	Université Paris Sud LPTHE F- 91405 ORSAY Cedex FRANCE
UGOCCIONI Roberto	Dipartimento di Fisica Teorica I N F N 10125 TORINO ITALY
VAN MIDDELKOOP Ger	CERN Division PPE CH- 1211 GENEVE 23 SWITZERLAND

VAN MIDDELKOOP Ger	NIKHEF-H Kruislaan 409 1009 DB AMSTERDAM NETHERLANDS
VIRCHAUX Marc	CEN Saclay DPhPE F- 91191 GIF sur YVETTE Cedex FRANCE
VOLTOLINI Christian	Centre de Recherche Nucléaire Dept de Phys. Rayon. d'Electron. Nucl. F- 67037 STRASBOURG Cedex FRANCE
WAINER Naor	FERMILAB Dept of Physics BATAVIA IL 60510 USA
WINTER Norbert	Institut f. Kemphysik Univ. Karlsruhe D-75 KARLSRUHE FEDERAL REP. OF GERMANY